A Study on Influence of Control Parameters on Strength, Durability and Microstructure of Fly Ash-Ground Granulated Blast Furnace Slag based Geopolymer Mortar and Concrete

A thesis submitted in partial fulfillment of the requirements
for the award of

DOCTOR OF PHILOSOPHY

In

Civil Engineering

By

Jnyanendra Kumar Prusty

(Roll No. 156104033)

Under the supervision of

Prof. Bulu Pradhan

Department of Civil Engineering

Indian Institute of Technology Guwahati

Guwahati 781039

September 2022

This Ph.D. Thesis is dedicated

to

my parents

for their endless love, support and inspiration.

DEPARTMENT OF CIVIL ENGINEERING

INDIAN INSTITUTE OF TECHNOLOGY GUWAHATI

GUWAHATI - 781039, ASSAM, INDIA

Dr. Bulu Pradhan

Professor

Email: bulu@iitg.ac.in

Phone: +91-361-258-2425

CERTIFICATE

It is certified that the work contained in the thesis entitled "**A study on influence of control parameters on strength, durability and microstructure of fly ash-ground granulated blast furnace slag based geopolymer mortar and concrete**" submitted by **Mr. Jnyanendra Kumar Prusty (Roll No. 156104033)** to the Indian Institute of Technology Guwahati for the award of the degree of **Doctor of Philosophy** has been carried out under my supervision in the Department of Civil Engineering, Indian Institute of Technology Guwahati. This work has not been submitted elsewhere for the award of any other degree or diploma.

Place: IIT Guwahati **(Dr. Bulu Pradhan)**

ACKNOWLEDGEMENT

First of all, I would like to thank God, the source of all energy, for the unconditional guidance in achieving my goals in life. My life journey so far has developed a positive attitude in me that awakens inner strength, energy, discipline, and motivation.

Without the assistance and support of numerous people, this Ph.D. thesis could not have been finished. My gratitude to them is beyond description, but I will try to do it here.

I express my sincerest gratitude to my supervisor, *Prof. Bulu Pradhan*, for his invaluable support, guidance, and suggestions throughout this research work. I am deeply indebted to him for his encouragement and patience throughout this research journey. Without his robust input and constant support, this research would not have been completed.

I would also like to thank my doctoral committee: *Prof. Teiborlang L. Ryntathiang* (Chairman), *Dr. Kaustubh Dasgupta*, and *Prof. Tapas K. Mandal*, for their warm-hearted encouragement and advice in many ways to improve the quality of this research work.

This research work was carried out in the Concrete Technology Laboratory and Structural Engineering Laboratory, Department of Civil Engineering, Indian Institute of Technology Guwahati. I wish to express my sincere thanks to the Head of the Department, *Prof. Sharad Gokhale*, and all respected faculties of the Department of Civil Engineering. I express my appreciation to the technical officer/staff of the Structural Engineering and Concrete Technology Laboratory: *Dr. Arun Ch. Borsaikia*, *Mr. Pranab Hazarika*, and *Mr. Saurabh Kumar Mudoi*, for their timely help throughout this research work. I also thank *Mr. Omm Prakash Prasad* for supporting me while preparing the test specimens and many other experimental studies carried out in the laboratory.

I would like to acknowledge the "Central Instruments Facility" and "Department of Chemistry" of Indian Institute of Technology Guwahati for providing access to the instruments for carrying out the microstructure analyses of geopolymer mortar and concrete samples reported in this research work. I would also like to take this opportunity to thank the administrative staff of the Department of Civil Engineering, in particular *Juri Jyoti Hazarika*, and *Susanta Kumar Sarma*, for their assistance, and all the other departments, and administration of IIT Guwahati, for supporting me directly or indirectly in various aspects.

I want to thank my seniors, *Dr. Smrati Jain, Dr. Arya Anuj Jee, Dr. Jyotish Kumar Das, and Dr. Sritam Swapnadarshi Sahu*, for moral support and guidance during my Ph.D. journey. I also express thanks to my lab mates *Sathishraj Mani, Suresh Chandra Sarangi, Kunal Pradhan, Khwairakpam Selija, M. Leela Sai Rangarao, Arup Kumar Mohapatra, Shehnaazdeep Kaur*, and others from the Infrastructure Engineering and Management laboratory for sharing their quality time, and discussion regarding many aspects during my stay at IIT Guwahati.

My gratitude also goes to all my friends that I have earned during my Ph.D. journey at IIT Guwahati: *Dr. Pawan Kumar, Dr. Rajkumar Shufen, Chandrabhanu Gupt, Rajan Singh, Vijayan Chelliah, Himasmita Das, Chandrashekhar Wagh, Abhisekh Kammisetty, Uday Boddepalli, Rahul Das, Biswajit Nayak, Tushar Kanta Sahu, and* many others.

Finally, and importantly, I am very much thankful to my parents (*Mrs. Rajani Prusty and Mr. Arakshita Prusty*), my younger brother (*Mr. Surendra Prusty*), and other family members for their continuing support and their encouragement throughout my entire life. This research would not have been possible without unwavering support and love. I also wish to thank my childhood friends: *Munil Kumar Sahoo, Samaresh Mishra, Jagadish Sarangi, and Chinmaya Ranbirsingh*, for supporting me whenever needed.

Jnyanendra Ku. Prusty

Jnyanendra Kumar Prusty

ABSTRACT

Ordinary Portland cement (OPC) has been extensively used as the primary binding material in the preparation of concrete. However, over last few decades, Portland cement manufacturing industry has become one of the major contributors of emission of large volume of CO_2 during the manufacturing process. On the other hand, the management of industrial waste in limited landfill space creates a massive challenge for the developing countries. To mitigate these issues, since last few decades, extensive research work has been undertaken to explore new alternate and more sustainable construction materials. In this line, there is a widespread use of industrial wastes in the production of concrete. Geopolymer concrete (GPC) has gained popularity as a potential alternative of Portland cement concrete due to its better mechanical properties and environmental benefits. Different research works have been carried out on the development of geopolymer composites using various source materials namely fly ash, ground granulated blast furnace slag (GGBS), metakaolin, red mud, rice husk ash, silica fume, and palm oil fuel ash etc. However, the major challenges associated with the geopolymer composites are the variations in the physicochemical properties of precursor materials depending upon their sources, requirement of heat curing for the development of geopolymer composites with low calcium bearing precursor materials, limited availability of efficient and systematic mix design methodologies etc. Furthermore, the limited research works on durability performance of geopolymer composites in various aggressive environment is hindering the practical application of this material.

To address the aforementioned challenges associated with development of geopolymer composites, the present study aims to develop geopolymer mortar (GPM) and geopolymer concrete (GPC) by investigating the influence of wide range of control parameters on fresh, mechanical, microstructure, and various durability properties of fly ash-GGBS based geopolymer composites. In this study, Taguchi-Grey relational analysis (GRA) method was used to arrive at the optimal combination of control parameters (mix parameters) of geopolymer mortar and geopolymer concrete with respect to multiple properties simultaneously. In this research work, the materials used for preparation of geopolymer mortar and concrete mixes were class F fly ash and ground granulated blast furnace slag (GGBS) as precursor materials, a combination of sodium hydroxide (NaOH) solution (SH) and sodium silicate (Na_2SiO_3) solution (SS) as alkaline solution, river sand, and coarse aggregates of 20 mm MSA (maximum size of aggregate) and 10 mm MSA (in case of GPC mixes). Two types of sulfate solution such as sodium sulfate (Na_2SO_4) and magnesium sulfate ($MgSO_4$) solution and two types of acid solution such as sulfuric acid (H_2SO_4) and

hydrochloric acid (HCl) solution were used to investigate the resistance of geopolymer mortar (GPM) against sulfate and acid attack. Sodium chloride (NaCl) was used as the source of chloride ions while examining the effect of chloride ions on consistency, compressive strength, and steel rebar corrosion in geopolymer concrete (GPC).

The experimental program was carried out in two different series i.e., geopolymer mortar (GPM) series and geopolymer concrete (GPC) series, and in each series, various experiments were conducted in two different phases. In 1st phase of GPM series, Taguchi-Grey relational analysis (GRA) method was implemented to investigate and optimize the influence of control parameters on fresh (setting time, and flowability), mechanical (compressive strength), and durability properties (water absorption, apparent volume of permeable voids, sorptivity, and resistance against sulfate and acid attack) of geopolymer mortar mixes simultaneously. The considered control parameters and their levels were GGBS replacement level: 15%, 30%, and 45% (by mass of binder), water-to-geopolymer solids (W/GPS) ratio: 0.31, 0.33, and 0.35, molarity of NaOH solution: 10 M, 12 M, and 14 M, and sand-to-binder (S/B) ratio: 1.5, 2.0, and 2.5. Subsequently, the verification experiments were performed on the mix combination of optimized level of control parameters derived from the multi-response optimization by Taguchi-GRA method. The GPM cube specimens of size 50 mm were prepared for compressive strength test at the age of 7, 28, 90, and 180 days of ambient curing, water absorption and apparent volume of permeable voids (AVPV) test at 28 days, and sulfate and acid resistance test for an exposure period of 26 weeks. In addition, cylindrical GPM specimens of size 100 mm diameter × 50 mm height were prepared for sorptivity test at 28 days. All fly ash-GGBS based geopolymer mortar specimens were prepared under ambient condition. The resistance of GPM specimens against sulfate and acid attack was evaluated in terms of change in compressive strength after 26 weeks of immersion in different sulfate solutions (3% Na_2SO_4, 6% Na_2SO_4, 3% $MgSO_4$, 6% $MgSO_4$) and acid solutions (0.31 mol/l H_2SO_4, 0.62 mol/l H_2SO_4, 0.31 mol/l HCl, and 0.62 mol/l HCl). In 2nd phase of GPM series, another set of mix proportion of GPM was designed by varying two most influential control parameters i.e., GGBS replacement level and S/B ratio in the optimized GPM mix derived from the 1st phase of GPM series. Subsequently, all the experiments (except setting time), which were performed in the 1st phase of GPM series were carried out again on the mixes in 2nd phase of GPM series. It may be noted that in 2nd phase of GPM series, the resistance of GPM specimens against sulfate and acid attack was evaluated in terms of visual observation, change in weight, and change in compressive strength up to 26 weeks of immersion in different sulfate and acid solutions. In both phases of GPM series, the microstructural evolution of geopolymer mortar mixes during strength development at different ages of

ambient curing and after exposure against different sulfate and acid solutions were evaluated through X-ray diffraction (XRD), energy dispersive X-ray spectroscopy (EDS), field emission scanning electron microscope (FESEM), and Fourier transform infrared (FTIR) spectroscopy analyses.

In 1st phase of geopolymer concrete (GPC) series, Taguchi-Grey relational analysis (GRA) method was used to investigate and optimize the effect of different control parameters on fresh (setting time, and consistency), and mechanical (compressive strength) properties of GPC mixes simultaneously. The considered control parameters along with their individual levels were GGBS replacement level: 15%, 30%, 45%, and 60%, W/GPS ratio: 0.28, 0.29, 0.30, and 0.31, molarity of NaOH solution: 8 M, 10 M, 12 M, and 14 M, binder content: 375 kg/m^3, 400 kg/m^3, 425 kg/m^3, and 450 kg/m^3, and SS/SH ratio: 1.5, 1.75, 2.0, and 2.25. Afterward, the verification experiments were carried out on the optimized GPC mix. In 2nd phase of GPC series, the effect of chloride ions on consistency, compressive strength, corrosion behaviour of steel reinforcement, and chloride content of selected fly ash-GGBS based GPC mixes, and their corresponding fly ash based GPC mixes were examined. To investigate the effect of chloride ions, sodium chloride (NaCl) of different concentrations i.e., 1.5% and 3.5% by weight of geopolymer solids were added during the preparation of GPC mixes. The GPC cube specimens of size 150 mm were prepared for compressive strength test in both phases of GPC series. Further, cylindrical reinforced GPC specimens of size 72 mm diameter and 200 mm height with a centrally embedded steel bar were prepared for electrochemical measurements (corrosion potential and corrosion current density by linear polarization resistance measurement) in the 2nd phase of GPC series. All fly ash-GGBS based GPC specimens were prepared under ambient condition whereas the fly ash based GPC specimens, after preparation, were subjected to 48 hours of rest period followed by oven curing at temperature of 80° C for 48 hours. The microstructural changes (through XRD, EDS, FESEM, and FTIR analyses) in GPC mixes were evaluated and correlated with strength development as well as rebar corrosion in geopolymer concrete mixes.

From the obtained results, it is observed that GGBS replacement level and S/B ratio significantly influenced most of the studied properties of geopolymer mortar (GPM). The GPM prepared with higher GGBS replacement showed higher compressive strength under ambient condition, whereas the GPM prepared with lower GGBS replacement exhibited improved resistance against sulfate and acid attack. The results of multi-response optimization by Taguchi-GRA method indicated that the GPM mix made with GGBS replacement of 45%, molarity of NaOH solution of 14 M, S/B ratio of 2, and W/GPS ratio

of 0.31 showed better performance in relatively more number of properties simultaneously. The variations in peak intensity of the compounds related to N-A-S-H and N-(C)-A-S-H gels formed in this GPM mix were consistent with the variations in compressive strength with ambient curing age as well as with variations in compressive strength of GPM mix in case of exposure to different sulfate solutions. Furthermore, significant decrease in peak intensity of compounds related to aluminosilicate gels, and in atomic Na/Si ratio and Al/Si ratio are consistent with the significant reduction in compressive strength of GPM in case of exposure to acid solutions, which corroborates the depolymerization of aluminosilicate gels in acid exposure condition. From the results of Taguchi-GRA method, the mix parameters along with their individual levels of the optimized GPM mix based on maximum mean grey relational grade (GRG) were 45% GGBS, W/GPS ratio of 0.31, NaOH solution of 14 M and S/B ratio of 1.5. From the result of verification experiments, the optimized GPM mix showed adequate setting time, flow index, and water absorption properties, and higher compressive strength at all ages of ambient curing, and for exposure to different sulfate and acid solutions when compared with other GPM mixes.

The flowability of fresh GPM mixes decreased with increase in GGBS content from 15% to 45% in the mixes, whereas it increased with increase in sand-to-binder ratio from 1.5 to 2.5. The compressive strength of GPM mixes made from various fly ash/GGBS blends and S/B ratios mostly increased from 7 days to 180 days, which was supported by the formation of higher amount of N-A-S-H, N-(C)-A-S-H and C-S-H gel in the GPM mixes at later ages of ambient curing as indicated by the results of XRD analysis. The weight gain percentage of GPM mixes exposed to sulfate solutions mostly decreased with increase in GGBS content, whereas the weight loss percentage of the mixes exposed to acid solutions increased with increase in GGBS content and S/B ratio. The geopolymer mortar mix made with lower GGBS content, i.e., 15% showed maximum gain and minimum loss in compressive strength in case of exposure to sulfate and acid solutions respectively. These variations in compressive strength are consistent with the variations in peak intensity of aluminosilicate gels from XRD analysis, and atomic ratios obtained from EDS analysis of GPM mixes. The GPM mixes made with higher S/B ratio showed improved performance in offsetting the loss in compressive strength when exposed to sulfate and acid solutions. There was more formation of gypsum in geopolymer mortar mix made with higher GGBS content in case of exposure to sulfate and H_2SO_4 solutions as observed from XRD, EDS, and FESEM analyses. In case of exposure to acid solutions, the geopolymer mortar made with lower GGBS content showed improved stability of geopolymer gels as indicated by the variations in atomic Na/Si, Al/Si, and Ca/Si ratios obtained from EDS analysis.

From the obtained results of geopolymer concrete (GPC) mixes, it is observed that the GGBS replacement had dominant effect on setting time and compressive strength whereas W/GPS ratio significantly influenced the consistency of GPC mixes. The formation of N-(C)-A-S-H gel along with C-S-H gel in GPC mixes as indicated by the XRD patterns contributed to the development of compressive strength of GPC mixes. Based on the results of multi-response optimization by Taguchi-GRA method, the optimized level of control parameters of GPC mix were GGBS replacement of 45%, W/GPS ratio of 0.31, NaOH solution of 14 M, binder content of 450 kg/m^3 and SS/SH ratio of 1.5. The obtained results of verification experiments on the proposed optimized GPC mix confirmed the effectiveness of Taguchi-GRA approach for determining the optimal combination of mix parameters for the production of geopolymer concrete. The presence of NaCl improved the consistency of fly ash and fly ash-GGBS based geopolymer concrete (GPC) mixes. The fly ash and fly ash-GGBS based GPC mixes exhibited lower compressive strength with increase in concentration of NaCl, at all ages. However, the reduction in compressive strength of NaCl admixed GPC mixes decreased with increase in age, which indicates dominant effect of NaCl in hindering the geopolymerization reaction at early age. The fly ash-GGBS based GPC specimens mostly showed less negative corrosion potential (E_{corr}) and lower corrosion current density (I_{corr}) as compared to their corresponding fly ash based GPC specimens. In chloride admixed fly ash-GGBS based GPC mixes, the embedded steel bar mostly exhibited less negative E_{corr} and lower I_{corr} with increase in GGBS content as a result of availability of lower amount of chloride ions in the electrolytic pore solution of concrete surrounding the embedded rebar due to formation of denser microstructure in GPC mix made with higher GGBS content. The results of chloride analysis of GPC mixes at different ages and at rebar level of GPC specimens indicated very less extent of chloride binding in GPC mixes. The fly ash-GGBS based GPC mixes mostly showed higher chloride binding capacity as compared to their corresponding fly ash based GPC mixes at the age of 28 and 360 days and at rebar level of GPC specimens at the age of 600 days as a result of more physical adsorption of chloride ions on calcium bearing aluminosilicate gel (N-(C)-A-S-H) and C-S-H gel. The higher peak intensity of aluminosilicate gels and presence of C-S-H gel observed from XRD analysis, higher atomic Ca/Si ratio obtained from EDS analysis, comparatively denser microstructure observed from FESEM analysis, and shifting of wavenumbers of Si-O-Si(Al) bond toward lower magnitude in FTIR analysis corroborated the improved performance fly ash-GGBS based geopolymer concrete in terms of higher strength, lower corrosion activity and lower chloride content when compared with fly ash based geopolymer concrete.

TABLE OF CONTENTS

CHAPTER 3: Experimental Program

LIST OF FIGURES

LIST OF TABLES

LIST OF SYMBOLS AND ABBREVIATIONS

l	Number of levels
Y_{ij}	S/N ratio of i^{th} experiment for j^{th} response
v_{ijk}	Result of i^{th} experiment for j^{th} response in the k^{th} replication
r	Number of replications
Z_{ij}	Normalized S/N ratio of i^{th} experiment for j^{th} response
GRC_{0ij}	Grey relational coefficient of i^{th} experiment for j^{th} response
Z_{0j}	Ideal value of normalized S/N ratio
Δ_{0ij}	Deviation sequence (difference between Z_{0j} and Z_{ij})
Δ_{min}	$min_{\forall i} min_{\forall j} \Delta_{0ij}$
Δ_{max}	$max_{\forall i} max_{\forall j} \Delta_{0ij}$
ζ	Identification coefficient or distinguishing coefficient
GRG_{0i}	Grey relational grade of i^{th} experiment
ω_j	Normalized non-negative weight assigned to j^{th} response
γ	Predicted grey relational grade (GRG)
γ_m	Mean grey relational grade (GRG)
γ_n	Maximum mean grey relational grade (GRG) of a parameter
λ	Wave length of X-ray
θ	Diffraction angle of X-rays
W_D	Oven dry weight of specimen
W_S	Surface dry weight of specimen
W_B	Surface-dry weight of the specimen in air (after immersion and boiling)
W_{AP}	Apparent weight of specimen in water
S	Sorptivity coefficient
t	Time
I	Water absorption
m_t	Change in mass of the specimen in grams at time t
a	exposed area of the specimen in mm^2
d	density of water in g/mm^3
E_{corr}	Corrosion potential
I_{corr}	Corrosion current density
B	Stern-Geary constant
R_p	Polarization resistance of steel bar
B_c	Chloride binding capacity
C_f	Free chloride content

C_t	Total chloride content
FA	Fly ash
GGBS	Ground granulated blast furnace slag
GPM	Geopolymer mortar
GPC	Geopolymer concrete
OPC	Ordinary Portland cement
XRF	X-ray fluorescence
BET	Brunauer-Emmett-Teller
XRD	X-ray diffraction
EDS	Energy dispersive X-ray spectroscopy
FESEM	Field emission scanning electron microscope
FTIR	Fourier transform infrared
SH	Sodium hydroxide (NaOH) solution
SS	Sodium silicate (Na_2SiO_3) solution
MSA	Maximum size of aggregate
W/GPS	Water-to-geopolymer solids ratio
S/B	Sand-to-binder ratio
GRA	Grey relational analysis
S/N	Signal-to-noise ratio
ANOVA	Analysis of variance
DOF	Degree of freedom
SOS	Sum of square
MS	Mean square
OA	Orthogonal array
FI	Flow index
FD	Spread diameter
ID	Internal base diameter
AVPV	Apparent volume of permeable voids
LPR	Linear polarization resistance
WE	Working electrode
AE	Auxiliary electrode
RE	Reference electrode
SCE	Saturated calomel electrode
NC	Sodium chloride
TMT	Thermomechanically treated
Q	Quartz
M	Mullite
Mu	Muscovite

A	Albite
An	Anorthoclase
Ht	Hydrotalcite
S	Sodalite
N	Nepheline
C-S-H	Calcium silicate hydrate
N-A-S-H	Sodium aluminate silicate hydrate
N-(C)-A-S-H	Sodium (calcium) aluminate silicate hydrate
G	Gypsum
C	Calcite
H	Halite
IS	Indian standards
ASTM	American society for testing and materials
DF	Deterioration factor

Introduction

1.1 General

Ordinary Portland cement (OPC) is the primary binding material of concrete. It is estimated that the global demand of OPC will increase approximately to 200% by the year 2050 [1]. However, Portland cement industry consumes substantial amount of natural resources and energy, and contributes to high volume of carbon emission [1,2], which is against the philosophy of sustainable development in construction industry. According to International Energy Agency (IEA), the production of Portland cement releases around 6–7% of total CO_2 emissions into the atmosphere [1]. Hence, it is essential to find alternatives to make environment friendly concrete. In last few decades, several research works have been reported in the literature on the aspect of achieving sustainability in construction industry either by recycling the old materials or developing new sustainable binders. Cement manufacturing industries have been using natural pozzolans, and industrial by-products such as iron blast furnace slag, fly ash etc. to produce blended cements, which helps to achieve a minor reduction in CO_2 emission [3]. Some other attempts have also been made to reduce the consumption of Portland cement by partially replacing it with different supplementary cementitious materials related to industrial wastes [4–7] and agricultural wastes [8–10]. However, it could be realised that the current growth of global infrastructure needs a low-CO_2 binder in construction industry, which would completely replace OPC. Moreover, the idea of searching new sustainable binders is not only to replace the use of OPC but also to enhance the durability performance of concrete structures, which is a major drawback of OPC [1,11]. In recent years, researchers have found that geopolymer binders can be used as a potential alternative to Portland cement because of their low carbon footprint and it facilitates the use of wide variety of industrial waste materials [12].

1.2 Geopolymer and its reaction mechanism

In 1978, Prof. J. Davidovits coined the term “Geopolymer” to represent a family of mineral binders that can be produced from the polymerization reaction between the alkaline solution and aluminosilicate precursor materials [13]. In the geopolymerization process, the reaction of aluminosilicate precursor materials and alkaline solution results in the formation of geopolymer gel with three-dimensional polymeric structure consisting of Si–

O–Al–O bonds [14]. The mechanism of geopolymerization reaction can be divided in to three main stages as follows [15,16].

(1) Dissolution of aluminosilicate precursor materials in the presence of alkaline solution, which forms free silica and alumina tetrahedron unit.
(2) Transportation/orientation, followed by coagulation/gelation of the materials, and condensation reaction of alumina and silica hydroxyl to form the inorganic geopolymer gel phase.
(3) Polycondensation of gel phases to form three-dimensional network of aluminosilicate structures.

The aluminatosilicate structures can be in the form of poly(sialate) (–Si–O–Al–O–), poly(sialate-siloxo) (–Si–O–Al–O–Si–O–), and poly(sialate-disiloxo) (–Si–O–Al–O–Si–O–Si–O–), depending on the Si/Al ratio [16,17].

1.3 Geopolymer composites

Geopolymer composites (paste, mortar, and concrete) are the new class of construction materials, where the Portland cement is completely replaced with geopolymer binders. Various source materials such as fly ash, ground granulated blast furnace slag (GGBS), metakaolin, calcined clays, red mud, rice husk ash (RHA), and palm oil fuel ash (POFA) can be used for the manufacture of geopolymer composites [16]. Among the source materials, the use of fly ash and slag for the production of geopolymer composites has been increased significantly [18].

Fly ash is available abundantly worldwide with its annual production approximately 363 million tons [19,20]. However, the use of fly ash to date is limited [19]. The use of fly ash (class C or class F) for production of geopolymer concrete creates significant opportunity for environmental benefits and cost reduction [21]. In literature, it has been reported that fly ash shows significantly different particle morphology and chemistry, depending upon the source of fly ash that affects the mechanical properties of geopolymer. Therefore, it is difficult to predict the properties of fly ash based geopolymer [22]. Blast furnace slag is a byproduct formed in the production of pig iron in the blast furnace, which consists mainly of silica, calcium, aluminium, magnesium, and oxygen [23]. Ground granulated blast furnace slag (GGBS) is commonly used as a partial substitute to OPC due to its amorphous nature, high hardness and pozzolanic activity [15]. GGBS is also used as partial replacement of fly ash in geopolymer mortar and concrete [16]. The inclusion of calcium-

rich GGBS into fly ash based geopolymer may improve the setting time and compressive strength by forming geopolymer gel and aluminium-modified calcium silicate hydrate gel [24].

Strong alkalis are required to activate the aluminosilicate source materials that allows the transformation of glassy structure partially or fully into a compacted composite [25]. The common alkaline activators used to activate the aluminosilicate source materials are sodium hydroxide (NaOH), sodium silicate (Na_2SiO_3), potassium hydroxide (KOH), and potassium silicate (K_2SiO_3) solutions [26]. It is reported in the literature that KOH solution exhibits better alkalinity as compared to NaOH solution. However, NaOH solution shows greater capacity to liberate silicate and aluminate monomers [26]. The use of geopolymer composites is currently limited despite several research works conducted on this material [2]. The major challenges for the geopolymer composites remain with regard to the variations in the properties of precursor materials when obtained from different sources that may need different dosages of chemical activators and curing regimes to achieve a particular strength grade [27]. Moreover, the availability of limited research works on durability performance of geopolymer composites in various aggressive environment is also another reason for the limited implementation of this technology on a large industrial scale [28]. In recent years, different research works have been carried out to evaluate the performance of geopolymer concrete as an alternative to Portland cement concrete in specific applications such as precast concrete products, culverts, sewer pipes, railway sleepers, pre-fabricated units for housing construction, repair or retrofitting materials for existing concrete structures, as a repair coating or a construction material in marine environment [29].

1.4 Manufacturing process of geopolymer composites

The conventional techniques used in the production of Portland cement-based mortar and concrete can be implemented to manufacture the geopolymer mortar and concrete. Binder is the primary difference between Portland cement-based composites and geopolymer composites. Geopolymer paste (i.e., the mixture of alkaline solution and precursor materials) binds the loose fine and coarse aggregates together to form geopolymer concrete [30]. The manufacturing process of geopolymer concrete is divided into two types based on the state of the activators used during the preparation of geopolymer concrete. One is the preparation of one-part geopolymer and the other one is the preparation of two-part geopolymer [15]. In case of one-part geopolymer, all dry ingredients such as precursor

materials, solid alkali activators, and aggregates are mixed, and then water is gradually added to the dry mixture followed by further mixing to achieve a homogeneous geopolymer mortar or concrete mix [15]. In case of two-part geopolymer, the alkaline solution is prepared 24 hours prior to the mixing. The dry ingredients such as precursor materials and aggregates are mixed in dry condition and then the prepared alkaline solution is added to the dry mixture and the mixing is continued further to get a uniform geopolymer mortar or concrete mix. The common manufacturing process of geopolymer mortar and concrete followed by several researchers [14,31–35] is two-part geopolymer, which is presented in Fig. 1.1.

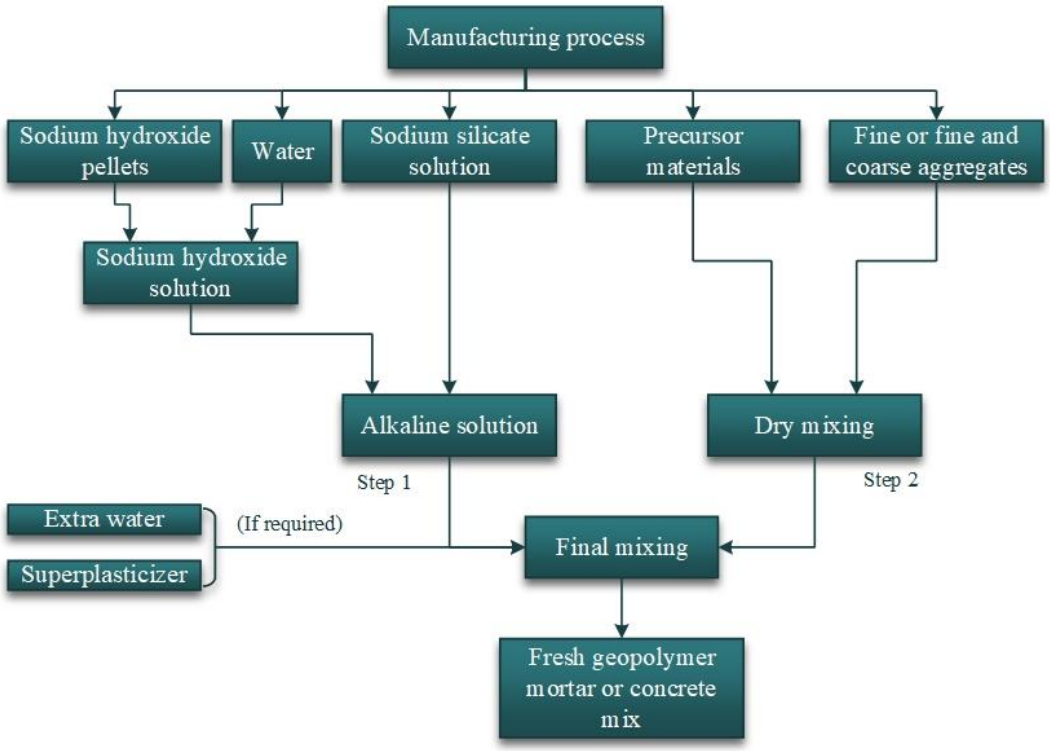

Fig. 1.1 Manufacturing process of geopolymer composites adopted in previous research works.

1.5 Properties of geopolymer composites

1.5.1 Fresh and mechanical properties

Setting time and consistency are the important fresh properties to be considered while deciding the mix parameters of the geopolymer composites. The low reactivity of fly ash results in slow setting of geopolymer composites, which has been a limiting factor [36]. Therefore, GGBS and silica fume have been used to increase the reactivity of precursors in geopolymer composites [15,36]. The use of sodium hydroxide (NaOH) solution as the only alkaline activator for preparation of geopolymer mortar showed delay in setting time [37].

However, the use of combination of sodium hydroxide (NaOH) solution and sodium silicate (Na_2SiO_3) solution as alkaline activator in geopolymer mortar resulted in shorter setting time [15].

The particle shape of the precursor materials is one of the factors that influence the consistency of geopolymer composites. Fly ash particles with spherical shape and smooth surface results in ball bearing effect, which increases the flow of the fresh geopolymer mixes without the requirement of additional water or water reducing admixture [16]. Besides, the consistency of geopolymer mixes has been observed to be significantly influenced by the alkaline liquid content and mass ratio of sodium silicate solution to sodium hydroxide solution used in the geopolymer mixes [38]. In case of alkali-activated slag (AAS) systems, quick setting time and poor workability are the limiting factors for its practical application. For this reason, various other precursor materials such as metakaolin, fly ash, rice husk ash, and palm oil fuel ash, and chemical admixtures are used to improve the setting time and workability of AAS systems [39].

Several research works evaluated the mechanical properties of geopolymer composites. It has been reported that the geopolymer materials showed better mechanical properties compared to traditional cement-based materials [2]. Despite showing excellent properties, geopolymer products are currently limited to the production of precast members [2]. Fly ash based geopolymers are developed under high temperature curing (40° C - 95° C), which promotes activation of fly ash, formation of aluminosilicate gels and early gain of high strength [40]. However, the requirement of high temperature curing for development of geopolymer products hinders its industrial application. Therefore, it is essential to avoid the use of high temperature curing, and to develop geopolymer materials in ambient condition [41].

1.5.2 Durability properties

For durability, there is a need to evaluate the behaviour of geopolymer composites exposed to different exposure environment including the aggressive exposure conditions such as sulfate, acid, and chloride-rich environment [16]. The durability performance of geopolymer composites in aggressive environment could be different from the Portland cement based composites due to its distinctive reaction products i.e., an amorphous aluminosilicate matrix [29]. As reported in different research works, the geopolymer composites exhibited good resistance against sulfate and acidic environment [42,43].

1.5.2.1 Sulfate resistance

Sulfate attack is an important durability issue regarding the performance of mortar and concrete, which results in expansion, cracking, and strength reduction [11,44,45]. In Portland cement based concrete, the reaction between sulfate ions and CH, C_3A, and C-S-H results in the formation of expansive compounds such as gypsum, ettringite and thaumasite, which cause expansion and cracking in concrete [43,46–48]. The strength reduction occurs due to loss of cohesion in the hydrated cement paste, and loss of adhesion between hydrated cement paste and aggregates [44]. Sulfate attack on concrete structures can occur either internally or externally [49,50]. It is classified as internal, when sulfate ions enter into the concrete through contamination of constituent materials, and it is classified as external, when sulfate ions penetrate into concrete structures in case of exposure to seawater, soil, and groundwater contaminated with sulfate salts [43,47,50]. Sulfate resistance of mortar and concrete is dependent on various factors such as cation type associated with sulfate ions in the exposure solution, concentration of sulfate solution, permeability of exposed mortar and concrete, paste chemistry, aggregate minerology, and nature of reaction products formed with the sulfates [47,49,50].

Different research works have been carried out in the literature on durability performance of geopolymer paste [50,51], mortar [29,42,45,48,49,52–54] and concrete [43,46,47] against sulfate solutions. In the reported literature, the research works have been carried out on sulfate resistance of low calcium alkali-activated systems (alkali-activated fly ash system) and high calcium alkali-activated systems (alkali-activated slag and alkali-activated slag/fly ash (slag content $\geq$ 50%) systems) [55]. The low calcium alkali-activated system generally shows better resistance against sulfate solutions as compared to high calcium alkali-activated system [43,55]. Further, studies in the literature reported about the superior performance of geopolymer composites against sulfate attack as compared to Portland cement-based composites [11,16,20,55,56]. From the review of literature, it is observed that the sulfate resistance of fly ash/slag based geopolymer composites containing slag content $\leq$ 50% and developed under ambient condition is less explored. Similar to conventional concrete, there is need to carry out a detailed investigation on sulfate resistance of geopolymer composites, which may depend on several factors including physicochemical properties of precursor materials, type and concentration of alkaline solutions, mixture design, curing regime, and type and concentration of sulfate solutions in the exposure environment.

1.5.2.2 Acid resistance

Acid resistance is another issue that significantly affects the durability property of concrete structures [57–59]. The concrete structures are exposed to acidic environment in many ways. Acids generated from industrial manufacturing processes, acid precipitation due to incomplete combustion of fuels, and industrial pollutants, acids present in ground water and sewer systems, and acid rain are the common sources of acid attack, which causes degradation of concrete structures [60–63]. The more rapid degradation of concrete structure occurs, when it is exposed to sewer collection systems, where the combination of bacteria, moisture, and oxygen in the atmosphere results in the production of biogenic sulphuric acid [62,64,65]. The existing concrete structures affected by acid attack results in increased expenditure on the repair works or complete replacement of structures that leads to huge economic loss [60,66]. Therefore, in recent years, research interest has been focussed on chemical resistance of alkali-activated composites as alternative to conventional cementitious composites. Investigations on the performance of alkali activated fly ash binders in acidic environment have reported that alkali activated fly ash binders may be a suitable alternative in the manufacture of acid resistant concrete because its reaction product consists mainly of sodium aluminosilicate hydrate gel, which is less susceptible to acid solutions than calcium silicate hydrate gel [59,67]. However, the requirement of high temperature curing for fly ash based geopolymer binder to achieve better or comparable properties as compared to conventional concrete is the major limitation that restricts its use in field applications [67]. A very few studies [59,60,62,68] have been carried out on performance evaluation of alkali activated pastes and mortars using blend of fly ash and slag as source materials against acidic environment. Further, in the literature, controversial outcomes were reported on acid resistance of alkali activated fly ash/slag binders due to different behaviour of N-A-S-H (sodium aluminosilicate hydrate) and C-A-S-H (calcium aluminosilicate hydrate) gels against acid solutions [68].

1.5.2.3 Corrosion of steel reinforcement

Apart from sulfate and acid attack, the durability behaviour of concrete structures is also largely dependent on the corrosion of steel reinforcement. Between the two causes of corrosion i.e., chloride ions and carbonation, the chloride ions are the primary cause of steel reinforcement corrosion in concrete. The chloride ions can enter into the concrete from external exposure environment through diffusion, wicking and absorption processes [69]. The penetration of chloride ions is the primary reason for long-term deterioration of

reinforced concrete structures in offshore locations, harbour, bridges, and pavements etc. [20]. Moreover, chloride ions can also be present in concrete as internal chloride during preparation of concrete mixes through the use of contaminated mixing water, aggregates, and admixtures [70]. Sodium chloride (NaCl), magnesium chloride ($MgCl_2$), potassium chloride (KCl), and calcium chloride ($CaCl_2$) are the main components of seawater environment [69]. Furthermore, the use of seawater, and sea sand in the preparation of concrete structures facilitates the presence of high concentration of chloride ions that can induce the corrosion of steel reinforcement, and significantly affects the durability of reinforced concrete structures [27,28].

Chloride-induced steel reinforcement corrosion is one of the major durability problems causing expenditure of billions of dollars globally in repair and maintenance of corrosion affected reinforced concrete structures [71,72]. Chloride ions destroy the protective passive layer, which is formed on the surface of the embedded steel reinforcement in concrete. The corrosion process proceeds in the presence of water and oxygen [44]. An electrochemical cell is build up when a difference in electrical potential along the embedded steel reinforcement in concrete occurs that consists of anodic and cathodic regions, which are connected by the electrolyte in the form of pore solution in the hardened cement paste [44]. The anodic and cathodic reactions involved in the process of corrosion of steel reinforcement in concrete are as follows [44]:

Anodic reaction: $Fe \rightarrow Fe^{++} + 2e^{-}$ (1.1)

Cathodic reaction: $4e^{-} + O_2 + 2H_2O \rightarrow 4(OH)^{-}$ (1.2)

Anodic reaction: $Fe^{++} + 2(OH)^{-} \rightarrow Fe(OH)_2$ (ferrous hydroxide) (1.3)

Anodic reaction: $4Fe(OH)_2 + 2H_2O + O_2 \rightarrow 4Fe(OH)_3$ (ferric hydroxide) (1.4)

When chloride-hydroxides ($[Cl^-]/[OH^-]$) ratio reduces, it causes the destruction of protective passive layer and the initiation of corrosion occurs [69]. The reactions involved during the initiation of steel reinforcement corrosion in the presence of chloride ions are as follows [44]:

$$Fe^{2+} + Cl^{-} \rightarrow [FeCl]^{+} \quad (1.5)$$

$$[FeCl]^{+} + 2OH^{-} \rightarrow Fe(OH)_2 + Cl^{-} \quad (1.6)$$

In order to overcome the durability issues related to chloride-induced steel reinforcement corrosion in Portland cement-based concrete, in last few years, some research works have

been carried out on the corrosion performance of steel reinforcement in geopolymer composites [21,34,71–76]. It was reported in the literature that fly ash-based geopolymer concrete can passivate the steel reinforcement as effectively as Portland cement concrete [72]. However, the corrosion performance of steel reinforcement in geopolymer mortar and concrete depends on many factors such as type of source materials, type and concentration of alkaline solution, curing temperature, and exposure conditions, which still need to be investigated comprehensively [72,76].

1.6 Organization of the thesis

The present research work has been organized in eight chapters as mentioned below.

Chapter 1

This chapter presents an overview about the development, manufacturing process and different properties of geopolymer composites. Further, Chapter 1 presents the organization of the thesis.

Chapter 2

This chapter presents the review of literature related to the present research work on geopolymer composites. The literature review related to the influence of various control parameters including source materials (especially fly ash and GGBS), curing temperature and duration, and type and concentration of alkaline solution on fresh, mechanical, and microstructure properties of geopolymer composites are presented. In addition, the review of literature on the effect of aforementioned control parameters on durability properties of geopolymer composites such as water absorption properties and resistance against sulfate, acid and chloride-rich environment are presented. The review of literature related to application of Taguchi method of design of experiment on development of geopolymer composites is also presented. This chapter also presents the summary of literature review, research gap, and the objectives of the present research work.

Chapter 3

This chapter presents the details of the experimental work performed to fulfil the objectives of the present research work. The details about the materials, mix design method, mix proportion, test specimens, exposure solutions, and various test methods conducted on geopolymer mortar (GPM) and geopolymer concrete (GPC) mixes are presented in this chapter.

Chapter 4

In this chapter, the results obtained from the experimental investigation and optimization of control parameters of geopolymer mortar (GPM) based on fresh, mechanical and durability properties are presented and discussed. The effect of control parameters namely GGBS replacement level, water-to-geopolymer solids (W/GPS) ratio, molarity of NaOH solution, and sand-to-binder (S/B) ratio on setting time, flowability, strength development, and various durability properties such as water absorption, apparent volume of permeable voids (AVPV), sorptivity, sulfate and acid resistance of geopolymer mortar are evaluated. The obtained results of microstructure study of GPM through XRD, EDS, FESEM and FTIR analyses are presented and discussed. Further, the results obtained from the verification experiments conducted on the optimized GPM mix are also discussed in this chapter.

Chapter 5

In this chapter, the effect of variations in fly ash/GGBS blends, and sand-to-binder (S/B) ratio on flowability, strength development, water absorption and apparent volume of permeable voids, sorptivity, sulfate and acid resistance, and microstructure evolution (through XRD, EDS, FESEM, and FTIR analyses) of the optimized geopolymer mortar (GPM) mix are analyzed and discussed. Further, the variations in compressive strength at different ages of ambient curing, and that obtained after exposure to different sulfate and acid solutions are analyzed with the changes in the microstructure of geopolymer mortar.

Chapter 6

This chapter presents the results obtained from the experimental investigation and optimization of control parameters of geopolymer concrete (GPC) based on fresh and mechanical properties. The influence of control parameters such as GGBS replacement level, water-to-geopolymer solids (W/GPS) ratio, molarity of NaOH solution, binder content, and sodium silicate solution to sodium hydroxide solution (SS/SH) ratio on variations in setting time, workability and compressive strength of fly ash-GGBS based GPC are evaluated and discussed in this chapter. In addition, the results obtained from the verification experiments conducted on the optimized GPC mix are presented and discussed. Further, in this chapter, the microstructure of optimized GPC mix was analyzed through the obtained results of XRD, EDS, FESEM and FTIR analyses.

Chapter 7

In this chapter, the results obtained from workability, compressive strength, and electrochemical measurements such as corrosion potential, and corrosion current density by linear polarization resistance (LPR) measurement on chloride admixed fly ash and fly ash-GGBS based geopolymer concrete (GPC) are presented and discussed. Further, the influence of fly ash/GGBS blends, and admixed NaCl concentration on obtained free chloride and total chloride contents, and chloride binding capacity at different ages, and at rebar level of cylindrical reinforced GPC specimens after electrochemical measurements are evaluated in this chapter. In addition, the effect of fly ash/GGBS blends, and admixed NaCl concentration on changes in microstructure (through XRD, EDS, FESEM and FTIR analyses) at different ages, and at rebar level of geopolymer concrete are analyzed in this chapter.

Chapter 8

This chapter presents the conclusions obtained from the present research work. In addition, the significance of research outcome, and the recommendations for future research work are also presented in this chapter.

Literature Review

2.1 General

This chapter presents the review of literature on fresh and mechanical properties of geopolymer composites i.e., paste, mortar, and concrete made with fly ash, and blend of fly ash and ground granulated blast furnace slag (GGBS). The review of literature related to durability properties namely water absorption properties, sulfate and acid attack, and chloride induced corrosion of steel reinforcement in fly ash and fly ash-GGBS based geopolymer composites is also presented in this chapter. In addition, the research work on microstructure analysis of fly ash and fly ash-GGBS based geopolymer composites are reviewed and presented in this chapter. The literature related to application of Taguchi method of design of experiment on development of geopolymer composites are also reviewed and presented. The summary of literature review and objectives of the present research work are also presented in this chapter.

2.2 Review of literature on fresh, mechanical, and microstructure properties of fly ash and fly ash-GGBS based geopolymer paste, mortar and concrete

Nath et al. [77] have investigated the effect of sodium hydroxide (NaOH) solution concentration (6 M, 8 M, and 10 M), and curing temperature (27° C, 45° C, and 60° C) on microstructural and morphological evolution of fly ash based geopolymer paste. The early reaction corresponding to dissolution and precipitation was monitored through Isothermal conduction calorimetry (ICC), whereas Thermo gravimetric analysis (TGA) was used to study the loss of structural water in final reaction product. Scanning electron microscopy (SEM), energy dispersive X-ray (EDX) spectrometer, X-ray diffraction (XRD), and Fourier transform infrared spectroscopy (FTIR) analyses were used for structural characterization and indexing of morphological features. Geopolymer paste samples were prepared by mixing fly ash and sodium hydroxide solution in 2:1 ratio. The Isothermal conduction calorimetry (ICC) results showed that the area under main reaction peak corresponding to geopolymerization increased with increase in NaOH concentration, but not with curing temperature. The maximum area under main reaction peak related to geopolymerization was obtained in the geopolymer paste sample synthesized at 45° C. This was also supported by TGA analysis with maximum weight loss in the sample cured at 45° C, which was due to formation of N-A-S-H gel with more OH^- molecules. Further, the TGA analysis revealed

that geopolymer paste samples made with NaOH solution concentration of 6 M exhibited low weight loss, which indicates low dissolution of silica and alumina, and resulted in formation of low quantity of reaction products. The effect of NaOH concentration, and curing temperature on structural re-organization was also evidenced by the changes in Si/Al ratio in the reaction products, shifting of Si-O-Si, and Al-O-Si spectrum, and formation of zeolite phases such as hydroxi-sodalite and zeolite ZK.

Durak et al. [78] have investigated the influence of pre-rest period under laboratory condition (1, 2, 3, 7, 14, and 28 days) before heat curing on various physical and mechanical properties and microstructure of fly ash based geopolymer mortars and pastes. After the pre-rest period, the mortar and paste samples were subjected to heat curing at 75° C for 48 hours. The obtained results were compared with the reference samples i.e., prepared without pre-rest period. The materials used were class F fly ash, sodium hydroxide solution, standard sand with maximum grain size of 2 mm, and water. The materials ratios of fly ash based geopolymer mortar were 3, 1, 0.29, and 0.1 by mass for sand, fly ash, water, and sodium hydroxide respectively. The alkaline solution and water binder ratio for geopolymer paste samples were kept same as geopolymer mortar samples. Prismatic mortar specimens of size 40 × 40 × 160 mm were used for determination of water absorption, porosity, unit weight, sorptivity, flexural strength, and compressive strength whereas cubic mortar specimens of size 71 mm were used for Bohme abrasion test. The reaction kinetics of geopolymer paste samples was evaluated using isothermal calorimeter. Further, X-ray diffraction (XRD), scanning electron microscopy (SEM), and energy dispersive X-ray (EDX) analyses were carried out on geopolymer paste samples for microstructural investigations. Test results indicated that with increase in pre-rest period, the unit weight of geopolymer mortar specimens increased whereas the water absorption, porosity and sorptivity decreased. The mechanical properties (compressive strength and flexural strength) of geopolymer mortar specimens increased with increase in pre-rest period. Further, the geopolymer mortar specimens subjected to longer pre-rest period exhibited higher abrasion resistance. The authors concluded that the pre-resting of geopolymer mortar specimens improved the strength, and durability related properties. From the results of reaction kinetics, it was observed that the pre-resting increased the cumulative heat of reaction of geopolymer pastes at the end of heat curing by approximately 45%. However, no significant difference in cumulative heat values was observed as the rest period increased from 1 to 28 days. The XRD analysis indicated that the pre-rest period before

heat curing resulted in dissolution of amorphous materials thereby leading to a more crystalline structure in the geopolymeric reaction. The pre-rest period allows more time for ion transfer between the alkaline solution (sodium hydroxide solution) and fly ash particles, which resulted in more compact microstructure as observed from the SEM analysis that led to better mechanical properties.

Chen et al. [79] have investigated the influence of CaO content (9%, 11%, 13%, and 15%) and SO_3 content (3.0%, 3.5%, 4.0%, 4.5%, and 5.0%) on flexural strength, compressive strength, water immersion expansion rate, drying shrinkage rate, and microstructure of fly ash based geopolymer mortar. The materials used were fly ash, $CaSO_4$ and $Ca(OH)_2$ as reagents, mixture of sodium hydroxide solution and sodium silicate solution as alkali activator, standard sand, and water. The modulus (SiO_2/Na_2O) of alkali activator, alkali content (Na_2O), and water-binder ratio used for the preparation of geopolymer mortar were 1.2, 16%, and 0.6 respectively. Prismatic specimens of size 40 × 40 × 160 mm were used for flexural and compressive strength test of geopolymer mortar at 3, 7, and 28 days. In addition, prismatic specimens of size 25 × 25 × 280 mm were used for water immersion expansion rate and drying shrinkage rate test up to 28 days. The microstructure of geopolymer mortar was analyzed through X-ray diffractography (XRD), scanning electron microscope (SEM), energy dispersive spectrometer (EDS), and ^{29}Si nuclear magnetic resonance (NMR) analyses. The test results showed that the flexural and compressive strength of fly ash based geopolymer mortar increased initially and then decreased with increase in CaO and SO_3 contents. The water immersion expansion rate of geopolymer mortar increased with increase in CaO and SO_3 content. However, the drying shrinkage rate of geopolymer mortar initially decreased and then increased with increase in CaO and SO_3 content. The optimum CaO and SO_3 contents of fly ash based geopolymer mortar were 11% and 4.0% respectively. The microstructure analysis showed that the addition of CaO and SO_3 in fly ash based geopolymer mortar promoted the geopolymerization reaction that resulted in formation of higher amount of gel products and generated ettringite, which improved the strength and compensated the shrinkage of geopolymer mortar.

Aliabdo et al. [80] have carried out a study to evaluate the effect of additional water content (10, 20, 30, and 35 kg/m^3), chemical admixture content (2.5, 5, 7.5, and 10.5 kg/m^3), molarity of sodium hydroxide solution (12 M, 16 M, and 18 M), alkaline solution to fly ash ratio (0.3, 0.35, 0.4, and 0.45), and sodium hydroxide solution to sodium silicate solution ratio (0.3, 0.4, and 0.5) on various properties of fly ash based geopolymer concrete. The

materials used for preparation of fly ash based geopolymer concrete were Class F fly ash, mixture of sodium hydroxide solution and sodium silicate solution as alkaline solution, sand, and limestone of 9.5 mm nominal maximum size, high range water reducer naphthalene-based admixture and additional water. The studied properties were workability, compressive strength, splitting tensile strength, modulus of elasticity, water absorption and porosity. Cube specimens of size 100 mm were prepared for compressive strength test at 7 and 28 days. Cylindrical specimens of size 75 mm diameter × 150 mm length, and 100 mm diameter × 200 mm length were prepared for 28 days splitting tensile strength and modulus of elasticity test respectively. Further, cube specimens of size 70 mm were prepared to measure absorption and porosity of fly ash based geopolymer concrete at 28 days. The test results revealed that with increase in additional water content and chemical admixture content in the mixes, the slump value, water absorption and porosity of fly ash based geopolymer concrete were increased whereas the opposite variation was observed in case of mechanical properties such as compressive strength, splitting tensile strength, and modulus of elasticity at all ages. Further, it was observed that the slump value of fly ash based geopolymer concrete decreased with increase in molarity of NaOH solution, and increased with increase in alkaline solution to fly ash ratio and sodium hydroxide solution to sodium silicate solution ratio. The increase in molarity of sodium hydroxide solution up to 16 M and alkaline solution to fly ash ratio up to 0.40 improved the mechanical properties, and reduced water absorption and porosity of fly ash based geopolymer concrete. Further, the decrease in sodium hydroxide solution to sodium silicate solution ratio resulted in better mechanical properties, and lower water absorption and porosity of fly ash based geopolymer concrete mixes.

Topark-Ngarm et al. [33] have investigated the effect of concentration of sodium hydroxide solution (10 M, 15 M, and 20 M), sodium silicate to sodium hydroxide solution ratio (S:H = 1.0, and 2.0), and curing regime (heat curing at 60 ± 2° C for 24 hours, and room temperature curing at 23 ± 2° C) on various properties of high calcium fly ash geopolymer concrete. The materials used for preparing the geopolymer concrete were high calcium fly ash, combination of sodium hydroxide (NaOH) and sodium silicate (Na_2SiO_3) solution as alkaline solution, river sand, and limestone with maximum size of 20 mm. The tests conducted were slump flow, setting time, compressive strength, splitting tensile strength, modulus of elasticity, and bond strength. Cylindrical specimens of size 100 (diameter) × 200 mm (length), and 150 (diameter) × 300 mm (length) were prepared for

compressive strength and splitting tensile strength tests at the age of 7 and 28 days, and modulus of elasticity test at the age of 28 days respectively. Further, cylindrical specimens of size 100 (diameter) × 150 mm (length) with a rebar placed vertically at the center were prepared for pullout bond strength test at the age of 7 days. The obtained results showed that for mixes with high NaOH content (S:H = 1.0), the flow values were decreased with increase in NaOH solution concentration. However, for mixes with low NaOH content (S:H = 2), the flow value remained relatively unaffected with change in NaOH solution concentration. The geopolymer concrete mixes showed shorter setting time of 28 to 58 min due to presence of high calcium content in fly ash. For mixes with high NaOH content (S:H = 1.0), the setting time decreased with increase in NaOH solution concentration. However, at low NaOH content (S:H = 2.0), the setting time slightly increased with increase in NaOH solution concentration. Geopolymer concrete mixes subjected to heat curing exhibited higher compressive strength than that subjected to room temperature curing. The optimum compressive strength of 54.4 MPa was obtained at 15 M NaOH solution for the geopolymer concrete mix made with S:H = 1.0. The splitting tensile strength, modulus of elasticity and bond strength were correlated with the compressive strength. Further, the bond strength between geopolymer concrete and rebar was significantly higher than that specified by the design code ACI 318 for normal Portland cement concrete.

Nagalia et al. [22] have carried out a study to investigate the effect of fly ash type (Class F and Class C), alkali hydroxide solutions (NaOH, KOH, $Ba(OH)_2$ and LiOH), combinations of hydroxide solutions (NaOH:KOH, NaOH:$Ba(OH)_2$, NaOH:LiOH, and NaOH:$Al(OH)_3$ at 9:1 and 5:5), molarity of NaOH solution (8 M, 12 M, and 14 M), coarse and fine aggregate combinations (16 mm, 9.5 mm and sand, and 9.5 mm and sand), curing temperature (oven-curing: 55°C and 70°C; steam-curing: 46°C and 100% humidity; and curing at room temperature: 25°C), and curing time (24 h and 48 h) on compressive strength and microstructure of fly ash based geopolymer concrete. Extra water and polycarboxylic ether based superplasticizer was used in the geopolymer concrete. The ratio of sodium silicate solution to hydroxide solution was fixed at 2.0 for all mixes. Cylindrical specimens with dimension of 100 × 200 mm were prepared for compressive strength test at the age of 1, 3, 7, and 28 days. The microstructure analyses were carried out through X-ray diffraction (XRD), scanning electron microscopy (SEM), and energy dispersive spectroscopy (EDS). The test results revealed that higher CaO content in fly ash (Class C) resulted in significantly higher compressive strength of geopolymer concrete. The use of any alkali

hydroxides or combination of any alkali hydroxides other than 100% NaOH solution significantly reduced the compressive strength of geopolymer concrete. Further, with increase in molarity of NaOH solution, the compressive strength was increased for geopolymer concrete mixes prepared with Class C fly ash whereas the compressive strength was decreased for geopolymer concrete mixes prepared with Class F fly ash. The geopolymer concrete mixes prepared with combination of coarse aggregate of size 9.5 mm and sand showed a decrease in compressive strength than that prepared with combination of 16 mm, 9.5 mm and sand. Among all curing conditions, the geopolymer concrete mixes subjected to higher curing temperature i.e., oven-curing at 70°C and curing time of 48 h resulted in higher compressive strength. The microstructure analyses indicated the formation of $NaAlSi_3O_8$ feldspar and an amorphous calcium silicate glassy matrix in the geopolymer concrete resulting an improvement in the compressive strength.

Saha and Rajasekaran [81] have studied the effect of ground granulated blast furnace slag (GGBFS) and molarity of NaOH solution on setting time and compressive strength of fly ash-GGBFS based geopolymer paste. The geopolymer pastes were prepared using Class F fly ash, GGBFS with replacement levels of 10%, 20%, 30%, 40%, and 50% (by total mass of binder), sodium silicate to sodium hydroxide solution ratio of 1.0, alkali solution to binder ratio of 0.4 and concentration of NaOH solution from 6 M to 16 M. The setting time test was conducted by Vicat apparatus method as described in IS 4031 (part 5). Cube specimens of size 50 mm were prepared for compressive strength test at the ages of 7, 28 and 56 days. From the results, it was observed that the setting time of geopolymer paste decreased with increase in GGBFS replacement level, whereas no significant variation was observed with respect to molarity of NaOH solution. The initial setting time of geopolymer paste with incorporation of GGBFS was reduced from 420-480 min to 25-130 min and final setting time from 1425-1600 min to 90-355 min. The compressive strength of geopolymer paste at different ages increased with increase in GGBFS content in the mixes. The mix with 16 M of NaOH solution and 50% GGBFS replacement showed the highest compressive strength of 66.4 MPa at 7 days, 78 MPa at 28 days and 78.2 MPa at 56 days. The SEM images showed that the geopolymer paste made with higher replacement of GGBFS had denser microstructure. The reason for shorter setting time and higher compressive strength of geopolymer paste made with higher GGBFS content was attributed to the formation of C-S-H gel due to high CaO content along with the formation of N-A-S-

H gel, which resulted in denser microstructure as evident from the SEM images of the mixes.

Ismail et al. [82] have investigated the microstructural evolution of alkali-activated slag/fly ash paste up to the age of 180 days using various analytical techniques namely X-ray diffraction (XRD), Fourier transform infrared (FTIR) spectroscopy, thermogravimetry (TG), and environmental scanning electron microscopy (ESEM) with energy dispersive X-ray (EDX) analyses. The materials used in this study were Class F fly ash and granulated blast furnace slag (GBFS) as precursor materials, and sodium metasilicate (Na_2SiO_3) at 8 wt.% or 12 wt.% (by total mass of precursor materials) as alkali activator. The alkali-activated paste samples were prepared with different slag/fly ash blends such as 100/0, 75/25, 50/50, 25/75, and 0/100. The alkali-activated paste samples prepared with slag/fly ash blends of 100/0, 75/25, and 50/50 were activated with 8 wt.% Na_2SiO_3 solution, and that prepared with slag/fly ash blends of 25/75, and 0/100 were activated with 12 wt.% Na_2SiO_3 solution. All the paste samples were prepared with water/binder ratio of 0.40 and cured at 30° C until the testing ages at 14, 28, 90, and 180 days. The obtained results indicated that the nature of alkali-activated slag/fly ash binder was strongly dependent on the slag/fly ash ratios. The alkali-activated paste made with 100% slag showed a structure dominated by a C-A-S-H type gel, while alkali-activated paste made with 100% fly ash exhibited a structure dominated by N-A-S-H type gel. A calcium silicate hydrate gel substituted with Al and Na (i.e., C-N-A-S-H) was identified as the main binding product in the mixes that made with slag ≥ 50 wt.% of the total binder. The alkali-activated slag/fly ash pastes made with higher content of fly ash (≥ 50 wt.%) composed mainly of hybrid binding phase i.e., N-C-A-S-H type gel, which had higher degree of crosslinking than that identified in C-A-S-H type gel formed in alkali-activated slag. Further, it was observed that an increase in fly ash content promotes the formation of zeolites in the hybrid gel system after 28 days.

Lee and Lee [83] have studied the microstructure, reaction products, and reactivity of alkali-activated fly ash/slag (AFS) paste synthesized at various slag replacement levels (10%, 30%, and 50%). Class F fly ash and blast furnace slag as binder materials, two types of alkali-activators such as sodium silicate powder with molar ratio (SiO_2/Na_2O) of 2.18, and sodium silicate liquid (combination of 4 M NaOH solution and water glass) with molar ratio of 1.0, and water were used in the preparation of paste samples. Cube specimens of size 50 mm were prepared and cured at room temperature (20° C, 50% relative humidity).

The AFS paste samples were analyzed by X-ray powder diffraction (XRD), scanning electron microscopy (SEM), energy-dispersive spectroscopy (EDS), thermogravimetric analysis (TGA), Inductively coupled plasma optical emission spectroscopy (ICP-OES), ^{29}Si nuclear magnetic resonance (NMR) spectroscopy, and Fourier transform infrared (FT-IR) spectroscopy analyses. The obtained results indicated that the total reactivity of AFS paste was strongly dependent on the mixture ratio of raw materials as well as type of alkali activator, while the degree of hydration was associated with the reactivity of alkali-activator. The total reactivity of AFS paste made with liquid activator was found much higher than that of solid activator. Further, it was observed that the reactivity of fly ash was significantly higher when mixed with liquid activator as compared to solid activator, whereas the reactivity of slag was comparable regardless of the activator type. When the amount of slag in AFS paste was increased, the amount of C-S-H gel increased, whereas the amount of aluminosilicate gel decreased. The reactivity (NMR analysis), weight loss (TGA) and extent of absorption (FTIR analysis) increased as the amount of slag increased in the AFS paste. Based on chemical composition and silicate structure, the aluminosilicate gel formed in AFS paste was similar to Ca-based geopolymer (N-C-A-S-H).

Phoo-ngernkham et al. [84] have investigated the effect of sodium hydroxide and sodium silicate solutions on compressive strength and shear bond strength of fly ash (FA)-ground granulated blast furnace slag (GBFS) geopolymer paste. Three types of geopolymer paste were prepared as per the binder type such as FA paste (100% FA), FA + GBFS paste (50% FA + 50% GBFS), and GBFS paste (100% GBFS). The geopolymer paste mixes were prepared with three types of alkaline solutions such as sodium hydroxide solution (NH) with concentration of 10 M, sodium silicate solution (NS), and sodium hydroxide solution (10 M) plus sodium silicate solution (NHNS) with NS/NH ratio of 2.0. All geopolymer paste mixes were prepared with a constant alkaline solution to binder ratio of 0.60. Cylindrical specimens of size 50 mm diameter × 100 mm height were prepared at ambient temperature for compressive strength test at the age of 7, 28, and 60 days. The shear bond strength was evaluated using slant shear test of concrete substrate and geopolymer paste at the age of 28 days. For slant shear test, the slant shear prisms of size 50 × 50 × 125 mm with interface line at 45° to the vertical were used. Microstructure analyses of geopolymer paste were carried out through X-ray diffraction (XRD) and scanning electron microscopy (SEM) at the age of 28 days. The test results showed that the compressive strength of geopolymer paste increased with increase in GBFS content for all types of alkaline

solutions (NH, NHNS, and NS). For the FA and FA + GBFS pastes, the use of NH solution or NS solution alone resulted in low compressive strength at ambient temperature. However, the use of NHNS solution showed better strength development in the geopolymer paste made with FA, and FA + GBFS. For GBFS paste, the presence of silicate enhanced the strength development. Therefore, the maximum compressive strength of 197.1 MPa at 60 days was obtained for GBFS paste activated with NS solution. The shear bond strength between concrete substrate and geopolymer paste was increased with increase in compressive strength and amount of N-A-S-H gel of geopolymer paste. The highest 28-day shear bond strength of 31 MPa was obtained for FA+GBFS paste activated with NHNS solution. The use of NH and NHNS solutions resulted in crystalline C-S-H, and amorphous gel whereas the use of NS solution resulted in mainly the amorphous products.

Yazdi et al. [85] have corelated the microstructural development and mechanical performance of geopolymer paste prepared from fly ash and ground granulated blast furnace slag (GGBS). The fly ash was partially replaced with GGBS at 30, 40, 50, 60, 70, and 100% by mass ratio. A mixture of sodium silicate solution and 10 M sodium hydroxide solution was used as alkaline solution for the preparation of geopolymer paste. Prismatic specimens of size 10 × 10 × 60 mm were cast and cured in room temperature until testing. The compressive and flexural strength tests were conducted at the age of 3, 7, and 28 days. The microstructure analyses such as thermogravimetrical analysis (TGA), X-ray diffraction (XRD) analysis, and environmental scanning electron microscope-energy dispersive X-ray spectroscopy (ESEM-EDX) were carried out on geopolymer pastes. In addition, the mercury intrusion porosity (MIP) measurement was also performed on geopolymer pastes. The effect of pre-conditioning drying method such as freeze-drying using liquid nitrogen, drying by acetone, and un-dried samples, were evaluated on microstructure analyses of geopolymer pastes. The obtained results showed that the compressive strength and flexural strength of geopolymer paste increased up to 100 MPa and 10 MPa respectively with increase in GGBS replacement in the mixes. However, for geopolymer paste prepared with greater than 50% GGBS content, the compressive strength and porosity were not changed significantly at the age of 28 days. The microstructure analyses indicated the presence of $CaCO_3$ in the form of calcite and vaterite as crystalline products as well as C-(A)-S-H and (N/K)-A-S-H gels as amorphous geopolymerization phases in case of geopolymer pastes containing high amount of GGBS, which resulted in higher mechanical strength and lower porosity. Among the pre-conditioning drying methods, the freeze-drying by liquid nitrogen

method was found to be a greater alternative to the conventional drying method for geopolymer samples.

Li and Liu [86] have investigated the effect of slag (4% by weight of dry powders) on compressive strength and microstructure of geopolymer paste made with fly ash, metakaolin, and slag. The materials used for preparation of geopolymer paste were class F fly ash, granulated blast furnace slag, metakaolin, water glass (Na_2SiO_3) with modulus of 3.3, and sodium hydroxide (NaOH) solution. Geopolymer paste samples were cast into 40 mm cubic moulds and demoulded after 24 h of casting. The specimens were subjected to two different curing temperatures such as at 30° C or 70° C for 14 days. The microstructure analysis was carried out through X-ray diffraction (XRD) analysis, Fourier transform infrared spectroscopy (FTIR), X-ray photoelectron spectroscopy (XPS), and mercury intrusion porosimetry (MIP). The test results showed that the compressive strength of geopolymer paste made with 4% slag was about 18 MPa higher than that of the paste made without slag at curing temperature of 30° C, whereas the increment of compressive strength was about 15 MPa at curing temperature of 70° C. The XRD and FTIR analyses indicated that the addition of slag in geopolymer paste and cured at 70° C resulted in formation of more amorphous products related to calcium silicate hydrate, and accelerated the rate of reaction. The results of MIP showed that the slag addition reduced the pore volume for geopolymer paste samples cured at both 30° C and 70° C. Further, the geopolymer paste samples made with slag and cured at 70° C resulted in finer pore size distribution. Thus, the reduced total pore volume and refined pore structure led to higher compressive strength of the geopolymer paste samples made with slag that was cured at 70° C. The decrease in binding energy due to addition of slag in geopolymer paste as observed from XPS analysis indicated more favourable to zeolite formation.

Chi and Huang [87] have carried out a study to evaluate the effect of fly ash/slag ratio (100/0, 70/30, 50/50, 30/70, and 0/100) and dosage of Na_2O (4% and 6% by weight of cementitious materials) on binding mechanism, and physical and mechanical properties of alkali-activated fly ash/slag (AAFS) mortars. The materials used in this study were class F fly ash, ground granulated blast furnace slag, sand, and combination of sodium hydroxide (NaOH) solution and sodium silicate (Na_2SiO_3) solution (modulus ratio, i.e., mass ratio of SiO_2 to Na_2O = 1) as the alkaline activator. The liquid/binder ratio was kept constant at 0.5 for all AAFS mortars. All the AAFS mortars after preparation were kept in a curing room at temperature 25° C and 80% relative humidity. The tests conducted in this study were

compressive strength, flexural strength, water absorption, drying shrinkage, scanning electron microscopy (SEM) and X-ray diffraction (XRD) analysis. The cube specimens of size 50 mm were used for compressive strength test at the ages of 7, 14, and 28 days and water absorption test. Further, the prismatic specimens of size 40 mm × 40 mm × 160 mm and 25 mm × 25 mm × 285 mm were prepared for determining flexural strength and drying shrinkage respectively, at the ages of 7, 14, and 28 days. The test results were compared with the results obtained from OPC mortars. From the test results, it was observed that both fly ash/slag ratio and dosage of Na_2O significantly influenced the binding mechanism and various properties of AAFS mortars. The maximum compressive and flexural strength were obtained in case of AAFS mortars prepared with fly ash/slag ratio of 50/50 whereas the maximum water absorption was observed in case of AAFS mortar made with 100% fly ash. Further, it was observed that the compressive and flexural strength increased, and water absorption decreased with increase in Na_2O concentration in AAFS mortars. From the drying shrinkage results, it was observed that the change in length of AAFS mortars decreased with increase in amount of fly ash. In addition, the change in length of AAFS mortars reduced with increase in Na_2O concentration. The AAFS mortars (except that prepared with 100% fly ash) exhibited higher compressive strength and flexural strength than OPC mortars. Furthermore, the water absorption of AAFS mortars was lower than that of OPC mortars. In addition, the change in length of AAFS mortar was higher than that of OPC mortar. From the microstructure analyses, it was observed that the hydration products of AAFS mortars are mainly amorphous alkaline aluminosilicate gel, and low crystalline calcium silicate hydrate gel.

Khan et al. [88] have investigated the influence of curing conditions (ambient air curing and water curing) on compressive strength, porosity, and microstructure of geopolymer mortar made with fly ash (FA), ultrafine fly ash (UFFA), and ground-granulated blast-furnace slag. Subsequently, the effect of two different sand-binder ratios (2 and 2.75), and the amount of FA replacement with UFFA (10%) and slag (30%, 40%, and 50%) were evaluated on workability, and compressive strength of geopolymer mortar. The materials used were Class F fly ash, ground-granulated blast-furnace slag, and ultrafine fly ash (UFFA) as source materials, combination of sodium silicate solution (Na_2SiO_3) and 12 M sodium hydroxide solution with mass ratio of 2.5 as alkaline solution, sand with maximum nominal size of 1.18 mm and polycarboxylate ether-based superplasticizer (1% by mass of binder). The alkaline liquid-to-binder ratio (L/B) of 0.60, and water-to-solids ratio (w/s) of

0.28 were used for all geopolymer mortar mixes. The geopolymer mortar mixes prepared with 100% fly ash were subjected to heat curing at 85° C for 24 h, whereas other mixes were prepared under room temperature. Cube specimens of size 50 mm were prepared for compressive strength test at the age of 3, 7, 14, and 28 days. Microstructure analysis of geopolymer mortar was carried out through scanning electron microscopy and energy-dispersive X-ray spectroscopy analysis, whereas the porosity of geopolymer mortar was determined by mercury intrusion porosimetry (MIP). The test results showed that the workability of geopolymer mortar decreased in the presence of UFFA and slag as additives. The ternary mix made with 60% FA, 30% slag, and 10% UFFA exhibited lowest workability among all the geopolymer mortar mixes. The geopolymer mortar mixes made with fly ash and slag blends and subjected to ambient air curing exhibited higher compressive strength than the water-cured counterparts. The geopolymer mortar made with 50% fly ash and 50% slag exhibited highest compressive strength of 103 MPa at 28 days of ambient curing. The geopolymer mortar samples cured in water medium exhibited higher porosity as compared to that cured in ambient air environment. Further, it was observed that the compressive strength of geopolymer mortar mixes decreased with increase in sand-binder ratio. Microstructure analysis of geopolymer mortar was found to be in good agreement with the observed compressive strength. Further, the microstructure analysis indicated the formation of crystalline C-S-H and/or C-A-S-H gel along with amorphous N-A-S-H gel products that improved the compressive strength of geopolymer mortar with age.

Lyu et al. [89] have studied the effect of different binders (fly ash + slag, fly ash + metakaolin), activators (liquid activator: combination of 12 M sodium hydroxide solution and sodium silicate solution, and solid activator: pentahydrate sodium metasilicate and anhydrous sodium metasilicate), sea sand, seawater, and curing condition (ambient condition and seawater curing) on various properties of geopolymer mortar. The tests conducted were slump and penetration test, unconfined compressive strength test (at the age of 3, 28, and 56 days), density test (at the age of 3, 28, and 56 days), sorptivity (at the age of 28 days), and nuclear magnetic resonance (NMR) test. Cube specimens of size 50 mm and cylindrical specimens of size 100 mm diameter × 50 mm thickness were prepared for compressive strength and sorptivity test respectively. The test results revealed that the use of fly ash (24% by weight of the mix) + slag (6% by weight of the mix) as binder improved the workability and compressive strength of geopolymer mortar as compared to

the use of fly ash (24%) + metakaolin (6%) as binder. Similarly, the geopolymer mortar made with liquid activator showed higher workability and compressive strength as compared to that made with solid activators. The use of fly ash + metakaolin as binder in geopolymer mortar resulted in higher sorptivity coefficient as compared to that made with fly ash + slag. Further, the use of anhydrous sodium metasilicate as activator exhibited lower sorptivity coefficient as compared to other activators when geopolymer mortar made with normal sand and tap water. The use of sea sand and seawater in geopolymer mortar exhibited lower workability and higher sorptivity coefficient than that prepared with normal silica sand. Further, the use of sea sand and seawater delayed the initial and final setting time and lower the density of geopolymer mortar as compared to that made with normal silica sand and tap water. The use of sea sand and seawater in geopolymer mortar made with fly ash + slag as binder did not show significant difference in compressive strength as compared to that made with normal sand and tap water. However, in case of geopolymer mortar made with fly ash + metakaolin, the use of sea sand and seawater improved the compressive strength as compared to that made with normal silica sand and tap water. The use of pentahydrate sodium metasilicate in geopolymer mortar reduced the compressive strength when compared with that made with anhydrous sodium metasilicate. The curing condition did not significantly affect the development of compressive strength of geopolymer mortar. The results obtained from NMR test indicated more rapid hydration processes when geopolymer mortar activated with liquid activator. In case of geopolymer mortar made with pentahydrate sodium metasilicate, the use of sea sand and seawater had a clear retardation effect on the geopolymer hydration process, whereas it had negligible influence on hydration rates of other geopolymer mortar mixes.

Nath and Sarker [38] have investigated the effect of different mix variables such as amount of ground granulated blast furnace slag (GGBFS) (10%, 20%, and 30%) in replacement of fly ash (Class F), amount of alkaline activator solution (35%, 40%, and 45% by mass of total binder), and ratio of sodium silicate to sodium hydroxide solution (SS/SH: 1.5, 2.0, and 2.5) on setting time, workability and compressive strength (at the age of 3, 7, 28, and 56 days) of geopolymer mortar and concrete cured under ambient condition. In order to evaluate the effect of curing temperature on compressive strength, geopolymer mortar and concrete mixes made with 10% GGBFS, alkaline activator solution of 40% and SS/SH ratio of 2.5 were subjected to oven curing at 60° C for 24 h, immediately after the preparation. The mixture of 14 M NaOH solution and Na_2SiO_3 solution was used as

activator solution. Sand with nominal maximum size of 1.18 mm, and coarse aggregates with nominal maximum size of 7, 10, and 20 mm were used in the mixes. Cube specimens of size 50 mm and cylindrical specimens of size 100 mm diameter × 200 mm height were prepared from geopolymer mortar and geopolymer concrete mixes respectively. The microstructure analyses through scanning electron microscope (SEM) and energy-dispersive X-ray spectroscopy (EDS) were carried out on geopolymer paste mixes made with 10% and 50% GGBFS replacement to fly ash, alkaline activator solution of 40% (of total binder), and SS/SH ratio of 2.5. The obtained results showed that increase in GGBFS content in geopolymer mortar and geopolymer concrete reduced the workability and setting time, and increased the compressive strength. The addition of GGBFS up to 30% exhibited maximum 28 days compressive strength of 63 MPa and 55 MPa for geopolymer mortar and geopolymer concrete respectively. The increase in activator solution content in the mixes increased the workability and setting time, and reduced the compressive strength. Further, the slump value, setting time, and compressive strength of geopolymer mortar and concrete mixes decreased with increase in SS/SH ratio from 1.5 to 2.5. The geopolymer mortar and concrete mixes developed under heat curing showed higher compressive strength than that developed under ambient condition, at all ages. Further, the strength development of geopolymer mixes was slower over age when developed under ambient condition. However, the mixes developed under heat curing showed high early compressive strength with insignificant increase over the ages. The microstructure analysis of fly ash-GGBFS blended geopolymer paste revealed the presence of mostly amorphous and calcium-containing hydration products that resulted in increased compactness of the gel at higher slag content. Authors have stated that the geopolymer concrete made with fly ash and GGBFS achieved setting time and compressive strength comparable to those of OPC concrete.

Deb et al. [90] have studied the effect of ground granulated blast-furnace slag (GGBFS) content (0%, 10%, and 20%) as a replacement of fly ash, alkaline activator content (35% and 40% by mass of total binder), and sodium silicate to sodium hydroxide solution (SS/SH) ratio (1.5 and 2.5) on workability, compressive strength, and splitting tensile strength of geopolymer concrete developed under ambient condition. For comparison purpose, OPC concrete mixtures were designed. The correlation of the splitting tensile strength with compressive strength of the ambient-cured geopolymer concrete was compared with that of heat-cured geopolymer concrete (reported in literature), and

conventional water-cured OPC concrete. The materials used for this study were Class F fly ash and GGBFS as binder, mixture of sodium silicate solution and 14 M sodium hydroxide solution as alkaline solution, fine and coarse aggregates, extra water, and naphthalene-based superplasticizer. The combined aggregate volume was a combination of 15% of 7 mm, 9% of 10 mm, 41% of 20 mm (coarse aggregate) and 35% of sand. Cylindrical specimens of size 100 × 200 mm and 150 × 300 mm were cast for compressive strength test (at 7, 28, 56, 90, and 180 days), and splitting tensile strength test (at 7, 28, and 90 days) respectively. The test results indicated that the increase in GGBFS content, and a reduction of alkaline activator content and SS/SH ratio resulted in decrease in slump value of geopolymer concrete. Further, the addition of extra water in geopolymer concrete improved the workability with a reduction in mechanical strength. The compressive strength of geopolymer concrete mixes increased with increase in GGBFS content, alkaline activator content, and decrease in SS/SH ratio in the mixes. The highest 28-day compressive strength of 51 MPa was achieved in the mix containing 20% GGBFS, SS/SH ratio of 1.5 and 40% alkaline activator content. The effect of mixture variables on the development of splitting tensile strength was similar to the development of compressive strength. The strength development of slag blended fly ash geopolymer concrete developed under ambient condition was similar as compared to water-cured OPC concrete. The method of estimating the splitting tensile strength from compressive strength of OPC concrete recommended in AS 3600 and ACI 318 design codes showed similar prediction for ambient cured geopolymer concrete and OPC concrete. However, the predictions were more conservative for heat-cured geopolymer concrete as compared to ambient-cured geopolymer concrete and OPC concrete.

Rafeet et al. [91] have carried out an investigation to study the effect of water/solids ratio (0.35 - 0.48), paste volume (30% - 33%) and fly ash/GGBS blends (100/0, 80/20, 60/40, and 30/70) on consistency (slump value), setting time and compressive strength of fly ash/GGBS based alkali-activated concrete (AAC). Further, the cost of AAC was compared with Portland cement concrete of similar compressive strength and consistency. AAC cube specimens of size 100 mm were used for compressive strength test. The obtained results showed that the paste volume in the range 30% - 33% (of total volume of AAC) did not affect the compressive strength of fly ash/GGBS based alkali-activated concrete (AAC). However, the consistency (slump value) of fresh AAC mixes significantly reduced with decrease in the paste volume from 33% to 30%. The compressive strength of fly ash/GGBS

based AAC increased as the GGBS content of the mixes increased. However, a higher GGBS content led to shorter setting time, and reduced consistency of fresh AAC mixes. A higher water/solids ratio in AAC resulted in longer initial and final setting time and improved the consistency. The water/solids ratio had influence on compressive strength, whereas its effect was reduced in case of AAC mixes prepared with higher GGBS content. Although, the authors have proposed a step-by-step procedure for determining the mix proportions based on required compressive strength, initial setting time and consistency class, this method has its own limitation as it was developed based on a specific alkali activator composition, and dosage, and one combination of fine and coarse aggregate of certain shape, texture, and grading. From the cost analysis, fly ash/GGBS based alkali-activated concrete (AAC) was found to be more expensive than Portland cement-based concrete, which can be reduced by using alternative alkali activators or adopting alternative production processes.

Fang et al. [92] have investigated the effect of ground granulated blast furnace slag (GGBS) content (10%, 15%, 20%, 25%, and 30%), molarity of sodium hydroxide solution (10 M and 12 M), sodium silicate to sodium hydroxide solution (SS/SH) ratio (1.5, 2.0, and 2.5) and alkaline activator to binder ratio (0.35 and 0.4) on various properties of alkali-activated fly ash-slag (AAFS) concrete. The studied properties were workability (AAFS paste and AAFS concrete), setting time (AAFS paste), compressive strength (at 1, 7, 14, 28, and 56 days), splitting tensile strength (at 7 and 28 days), flexural strength (at 28 days), and dynamic elastic modulus (at 7, 14, 21, and 28 days) of alkali-activated fly ash-slag concrete. The cube specimens of size 100 mm and cylinder specimens of size 100 × 200 mm were prepared for compressive strength test and splitting tensile strength test of AAFS concrete respectively. Further, the prismatic specimens of size 100 × 100 × 500 mm were prepared for flexural strength and dynamic elastic modulus test. From the test results, it was observed that the workability of AAFS paste and concrete decreased with increase in slag content, molarity of sodium hydroxide solution, SS/SH ratio, and decrease in alkaline activator to binder ratio. The AAFS paste exhibited shorter initial and final setting time with an increase in slag content, and a decrease in alkaline activator to binder ratio in the mixes. The compressive strength of AAFS concrete increased significantly with an increase in slag content, and molarity of sodium hydroxide solution. However, it decreased with an increase in alkaline activator to binder ratio. The authors suggested that the AAFS concrete mixes prepared with 20% to 30% slag replacement, alkali activator to binder ratio of 0.4,

10 M of sodium hydroxide solution, and SS/SH ratio in the range of 1.5 to 2.5 are the optimal mixtures based on the performance criteria of workability, setting time, and compressive strength.

Singh et al. [93] have investigated the effect of activator concentration (NaOH molarity: 10 M, 12 M, 14 M, and 16 M) on geopolymerization process, mechanical properties, and drying shrinkage of fly ash/slag geopolymer concrete. The materials used in this study were low calcium fly ash, ground granulated blast furnace slag, combination of sodium hydroxide (NaOH) solution and sodium silicate (Na_2SiO_3) solution as alkaline activator, sand, and coarse aggregate. Sodium silicofluoride, and polycarboxylic ether based superplasticizer were used for controlling the setting and consistency of the mixes. Geopolymer concrete mixes were prepared with fly ash and slag at ratio of 2:1 (by mass of total binder), water-geopolymer solid ratio of 0.19 and 0.21, and sodium silicate to sodium hydroxide solution ratio of 2.5. The heat flow rate during the alkaline activation of fly ash/slag geopolymer paste was evaluated through isothermal conduction calorimetry. The compressive strength test was conducted on cube specimens of size 100 mm and cylindrical specimens of size 150 mm diameter × 300 mm height. The modulus of elasticity of geopolymer concrete was calculated from the load-deflection curve of cylindrical specimens (size: 150 mm diameter × 300 mm height) subjected to compressive load. The splitting tensile strength test was carried out on cylindrical specimens of size 150 diameter × 300 mm height, whereas prismatic specimens of size 100 × 100 × 500 mm were used for modulus of rupture test. The drop weight impact test, and drying shrinkage test were carried out on geopolymer concrete specimens of size 150 mm diameter × 63.5 mm thickness, and 75 × 75 × 285 mm respectively. Further, the interfacial transition zone (ITZ) of fly ash-slag based geopolymer concrete was investigated by field emission scanning electron microscope (FESEM) attached with EDAX. From the obtained results, it was observed that the total heat release in the geopolymer paste increased with increase in activator concentration that resulted in rapid setting and hardening of geopolymer mixes. Geopolymer concrete prepared with 14 M NaOH solution showed maximum compressive strength with desired setting and hardening at room temperature. The compressive strength, elastic modulus and impact strength increased, and the Poisson's ratio decreased with increase in activator concentration. The drying shrinkage of fly ash-slag based geopolymer concrete was very small (~0.1%) after 6 months due to its dominant zeolitic characteristics. The microstructure analysis showed the presence of spongy amorphous geopolymer gel

extended onto the aggregates that supported improved aggregate-paste interface in the geopolymer concrete.

Wardhono et al. [94] have investigated the mechanical (density, compressive strength, tensile strength, and elastic modulus) and permeation properties (water absorption, apparent volume of permeable voids (AVPV), water permeability and ultrasonic pulse velocity (UPV)) of alkali activated slag (AAS) and fly ash based geopolymer (FAGP) concrete up to 540 days. The microstructural development of AAS and FAGP concrete was observed through scanning electron microscopy (SEM) and energy dispersive X-ray spectroscopy (EDS) analyses. The materials used in this study were class F fly ash, ground granulated blast-furnace slag (GGBS), a mixture of sodium silicate and sodium hydroxide solution (10 M for AAS and 15 M for FAGP) as alkaline activator, sand, crushed granite (7 mm and 10 mm size), and extra water. The activator modulus (SiO_2/Na_2O) was fixed at 1.0 of both concrete, while the Na_2O dosage (Na_2O in alkali activator/fly ash) was fixed at 5%, and 15% for AAS, and FAGP concrete respectively. A water solid ratio (w/s) of 0.44 and 0.37 was fixed for AAS and FAGP concrete respectively. The AAS concrete specimens were demoulded after one day, water cured for 6 days and then kept in room temperature until testing. However, the FAGP concrete specimens were subjected to heat curing at 80° C for 24 hours after one day of casting and then demoulded, and kept in room temperature until testing. The test results showed that the AAS and FAGP concrete exhibited less than 1% density increase during 28 to 540 days period. The AAS concrete performed better in terms of higher compressive strength, tensile strength and elastic modulus, and lower permeation properties than FAGP concrete in the initial 90 days. However, the performance of AAS concrete was reduced between 90 days and 540 days as compared to FAGP concrete. The microstructure analyses revealed the continuation of reaction after 90 days in AAS concrete producing excess C-S-H gel, which might be the reason for increased crack propagation and crack width at later ages due to the effect of disjoining pressure and self-desiccation.

Ravikumar et al. [95] have studied the effect of concentration of sodium hydroxide solution (4 M, 6 M, and 8 M) and activator-to-binder ratio (0.40, 0.50, and 0.60) on compressive strength, pore structure features, and microstructure of cement-free binder (CFB) concrete containing fly ash or ground granulated blast furnace slag (GGBFS) as sole binder. The materials used were Class F fly ash, ground granulated blast furnace slag (GGBFS), sodium hydroxide solution, fine aggregate, and coarse aggregate with nominal

maximum size of 9.5 mm. Cubic specimens of size 50 mm were prepared from CFB paste and concrete mixes. The tests conducted were compressive strength of CFB concrete, porosity of CFB concrete and paste from vacuum saturation method, porosity and pore size of CFB paste from image analysis, and microstructure analysis of CFB paste through scanning electron microscopy (SEM) coupled with energy dispersive X-ray analysis (EDX), and X-ray diffraction (XRD) analysis. Before investigating the effect of different concentrations of sodium hydroxide solution and activator-to-binder ratio, the binder contents (15%, 18%, 25%, and 30% by volume of concrete) and the curing parameters such as curing temperature (60° C, and 75° C) and curing duration (12 h, 24 h, and 48 h) were optimized to provide the highest compressive strength. The test results indicated that the CFB concrete made with 18% of fly ash or 25% GGBFS exhibited highest compressive strength at curing temperature of 75° C for 48 h. The curing temperature significantly influenced the compressive strength of CFB concrete containing fly ash as compared to that containing GGBFS. The compressive strength of CFB concrete increased with increase in activator concentration and decrease in activator-to-binder ratio. Further, the CFB concrete made with GGBFS exhibited higher compressive strength than that made with fly ash. From a statistical analysis, it was observed that the compressive strength of CFB concrete made with fly ash was influenced by the activator concentration to a greater degree whereas the activator-to-binder ratio had more influence on the compressive strength of CFB concrete made with GGBFS. The porosity of CFB concrete decreased with increase in activator concentration and decrease in activator-to-binder ratio. Further, the CFB concrete and paste made with fly ash were found to be more porous and contained large fraction of pores greater than 10 μm in size as compared that made with GGBFS. From microstructure analysis, the reaction product of CFB paste made with GGBFS indicated the presence of significant amount of calcium, in addition to sodium, alumina and silica phases that shows more homogeneous microstructure than that made with fly ash.

2.3 Review of literature on water absorption properties of geopolymer composites

Atabey et al. [96] have investigated the influence of activator type (sodium hydroxide solution, and combination of sodium silicate with sodium hydroxide solution) and Na dosage (6%, 9%, 12%, 15% by weight of fly ash) on transport properties of fly ash based geopolymer mortar. The materials used for preparation of geopolymer mortar were class F fly ash collected from two different sources (namely SG fly ash and CA fly ash), alkaline activators, standard sand and water. For all mixes, the sand/fly ash ratio and water/fly ash

ratio were taken as 3 and 0.3 respectively by mass. Prismatic specimens of size 40 × 40 × 160 mm were prepared for water absorption, volume of permeable voids (VPV), and sorptivity coefficient, and cube specimens of size 150 mm were prepared for test of water penetration depth within 24 h under pressure. Cylinder specimens of size 100 mm diameter × 200 mm height were prepared for chloride ion penetration depth test. Further, cylinders of size 100 mm diameter and 200 mm height with a reinforcing steel bar of 600 mm length and 16 mm diameter centrally embedded for a length of 175 mm were prepared for adherence test (pull out). This test was conducted to determine the adherence loss of steel reinforcement in the cylindrical specimen subjected to accelerated corrosion test. All the geopolymer mortar specimens were subjected to oven drying at 100° C for 24 hours. The obtained results showed that the grain size distribution of fly ash directly affects the permeability properties. The geopolymer mortar made with SG fly ash, which has low residue amount after passing through 45 µm sieve (19%) exhibited better properties than that made with CA fly ash (residue amount: 29%). Among the activator type, the geopolymer mortar activated with sodium hydroxide solution exhibited improved permeability properties that that activated with combination of sodium silicate and sodium hydroxide solution. Further, the geopolymer mortar made with Na dosage of 12% and 15% showed better results with respect to all permeability characteristics as compared to that made with Na dosage of 6% and 9%.

Hossain et al. [97] have examined the durability properties in terms of water absorption and sorptivity of two different mortars made with alkali activated binder (namely, AAB-1: 42% slag + 28% palm oil fuel ash + 30% rice husk ash; and AAB-2: 42% slag + 28% fly ash + 30% rice husk ash) and compared with reference OPC mortar. The materials used for preparation of AAB mortars were ground granulated blast furnace slag (GGBS), fly ash (FA), palm oil fuel ash (POFA), and rice husk ash (RHA) as binder, NaOH as alkaline solution, sand, and superplasticizer (Darex super 20). The AAB mortars were prepared with 2.5 M NaOH solution with alkaline solution to binder ratio of 0.55. The sand to binder ratio and superplasticizer content for AAB mortars were 3.0, and 4.5% (by weight of binder) respectively. The water to cement ratio for OPC mortar was 0.50. Mortar prism specimens of size 40 × 40 × 160 mm were prepared for water absorption test at 28, 90, 180, and 270 days of water curing and sorptivity test at 90, 180, and 270 days of water curing for AAB and OPC mortars. For correlation of durability properties, the authors have evaluated the 28 days compressive strength of AAB and OPC mortars and the compressive strength of

AAB-1, AAB-2, and OPC mortars were 37.7 MPa, 34.5 MPa, and 44.2 MPa respectively. The results of water absorption test showed that the AAB-1 and AAB-2 mortars exhibited 25% and 52% higher water absorption as compared to OPC mortar at the age of 270 days. Further, the AAB mortars showed comparatively higher sorptivity values than reference OPC mortar for all curing ages. The higher water absorption and sorptivity values of AAB mortars as compared to OPC mortar are due to the porous microstructure of pozzolans and lower compressive strength of AAB mortars than OPC mortar. The comparison between AAB mortars indicated that the AAB-2 mortar exhibited higher water absorption and sorptivity values than AAB-1 mortar, which was supported by the results of compressive strength. Thus, the authors suggested that the water transport properties of alkali activated binder (AAB) mortars can be improved by increasing the strength and making a denser microstructure by optimizing the properties of pozzolans and mixture composition of these mortars.

Ismail et al. [98] have investigated the compressive strength, and water absorption properties (volume of permeable voids (VPV) and capillary sorptivity) of alkali-activated mortar and concrete at the age of 28 and 90 days of curing. The chloride permeability by ponding test method was investigated on alkali-activated mortar specimens after 28 days of curing, and on alkali-activated concrete specimens after 28 and 90 days of curing. Further, the non-steady state chloride migration by NordTest method was conducted on alkali-activated concrete specimens after 28 and 90 days of curing. The chloride content analysis was performed on alkali-activated mortar and concrete at the end of ponding test (180 days) with 3.5% NaCl solution. The X-ray diffraction analysis (XRD) was conducted on alkali-activated mortar samples after ponding test. The obtained results were compared with the conventional mortar and concrete made with ordinary Portland cement (OPC). The materials used for preparation of alkali-activated mortar and concrete were Class F fly ash and granulated blast furnace slag (GBFS) as precursor materials, sodium metasilicate solution as alkali activator, sand and crushed gravel. For this study, five sets of alkali-activated mortar i.e., GBFS partially replaced with fly ash at 0%, 25%, 50%, 75%, and 100% by weight, and three sets of alkali-activated concrete i.e., GBFS partially replaced with fly ash at 0%, 25%, and 50% by weight were prepared. In case of alkali-activated mortar and concrete with 50% GBFS and more, the dosage of activator used was 8% of total precursor materials, whereas for alkali-activated mortar made with less than 50% GBFS, the dosage of activator used was 12% of total precursor materials. The alkali-

activated mortar mixes were prepared with constant water to binder ratio of 0.4 and constant sand to binder ratio of 2.75. The alkali-activated concrete mixes were prepared with water to binder ratios of 0.4, 0.38, and 0.36 respectively for GBFS partially replaced with fly ash at 0%, 25%, and 50%. Cube specimens of size 50 mm were prepared for compressive strength of alkali activated mortar whereas cylindrical specimens of size 100 mm diameter × 200 mm height were prepared for compressive strength of alkali-activated concrete. Rectangular prism specimens of size 160 mm length × 130 mm width × 60 mm height and cylindrical specimens of size 100 mm diameter × 200 mm height were prepared for ponding test on alkali-activated mortar, and alkali-activated concrete respectively. The non-steady state chloride migration by NordTest method was conducted on 50 mm thick alkali-activated concrete slices. The alkali-activated mortar specimens were kept in oven at 30° C until testing, whereas the alkali-activated concrete specimens were cured in a water bath at ambient temperature until testing. The test results revealed that the increase in fly ash addition led to formation of more porous N-A-S-H type gels that resulted in reduced compressive strength and increased water absorption properties. Further, the alkali-activated materials exhibited better performance against chloride ingress according to both NordTest method and ponding test method, despite showing higher porosity as compared to OPC counterparts. The alkali-activated materials made with higher amount of GBFS was dominated by C-A-S-H gels, which exhibited better durability performance in chloride environment as compared to alkali-activated materials made with higher amount of fly ash.

Noushini and Castel [14] have studied the influence of curing regime on mechanical properties (compressive strength, modulus of elasticity, Poisson's ratio, and ultrasonic pulse velocity (UPV) tests), and transport properties (water absorption, apparent volume of permeable voids (VPV), sorptivity, surface resistivity, and bulk resistivity) of geopolymer concrete (GPC) at the age of 28 days. The above properties of geopolymer concrete (GPC) were compared with that of conventional concrete made with OPC (OPCC). The materials used for the preparation of GPC were combination of 70% class F fly ash, 20% ultra-fine fly ash, and 10% ground granulated blast furnace slag (GGBFS) as aluminosilicate source materials, combination of sodium hydroxide solution (12 M) and sodium silicate solution as alkaline activator, free water, and fine and coarse aggregates. The OPCC specimens were cured in three different curing conditions such as lime-water curing (LWC), sealed ambient curing (SAC), and heat curing (HC), whereas the GPC specimens were cured in SAC and HC conditions. For the heat curing, three temperatures of 60 ºC, 75 ºC, and 90 ºC and four

curing periods of 8, 12, 18, and 24 h were studied to find out the optimum curing temperature and duration. The specimens of size 100 mm diameter × 50 mm thick were used for water absorption, VPV, and sorptivity test, while all other tests were carried out on the cylindrical specimens of size 100 mm diameter × 200 mm height. From the test results, it was observed that the performance of GPC was improved by the application of heat curing (HC) as compared to sealed ambient curing (SAC). The compressive strength and elastic modulus of GPC were increased with increase in curing temperature up to 75 ºC and curing duration up to 24 h. The optimum volume of permeable voids (VPV) of GPC was observed at 75 ºC and 90 ºC curing for 18–24 h. The GPC subjected to heat curing at 60 ºC showed higher sorptivity as compared to sealed ambient curing. However, GPC subjected to heat curing at 75 ºC and 90 ºC for 18–24 h resulted in lower sorptivity than ambient curing thereby indicating lower porosity or less interconnected pores. The highest surface resistivity, and bulk resistivity was observed when the GPC cured at 75 ºC for 18–24 h. The geopolymer concrete (GPC) subjected to heat curing at 75 ºC and 90 ºC exhibited higher compressive strength than OPC concrete. The volume of permeable voids of the properly heat cured fly ash based geopolymer concrete is similar to its counterpart Portland cement concrete subjected to lime-water curing. Based on the obtained results, the authors concluded that, similar to Portland cement concrete, the compressive strength can be a reasonable measure of the overall quality of GPC.

2.4 Review of literature on sulfate resistance of geopolymer composites

Bakharev [51] have investigated the sulfate resistance of geopolymer pastes made with class F fly ash and different alkaline solutions such as sodium hydroxide solution (8% Na), mixture of sodium and potassium hydroxide solution (8% Na+1% K), and sodium silicate solution (8% Na). The water/binder ratio of geopolymer paste mixes was fixed at 0.3. For comparison purpose, OPC and OPC + 20% fly ash pastes with water/binder ratio of 0.4 were prepared. Cylindrical specimens of size 25 mm diameter × 50 mm height were prepared for evaluating the resistance of geopolymer pastes against different sulfate solutions (5% sodium sulfate, 5% magnesium sulfate, and 5% sodium sulfate + 5% magnesium sulfate solutions) in terms of weight change, and change in compressive strength at 30, 60, 90, 120, and 150 days of exposure in sulfate solutions. The geopolymer paste specimens were kept for 24 h at room temperature followed by oven drying at 95° C for 24 h and then cured in room temperature for 2 days prior to test. The microstructure analysis was carried out by X-ray diffraction (XRD), Fourier transform infrared

spectroscopy (FTIR), and scanning electron microscopy (SEM) analyses. The obtained results indicated that the geopolymer paste made with sodium hydroxide solution exhibited best performance in different sulfate solutions with 4-12% increase in compressive strength as compared to other alkaline solutions. The geopolymer paste exhibited least weight change (0.4% to 2.1% weight gain) in sodium sulfate + magnesium sulfate solution as compared to sodium sulfate solution (1.3% to 4.7% weight gain) and magnesium sulfate solution (1.02% weight loss to 5.3% weight gain). In case of sodium sulfate solution, significant variation in strength occurred with 18% strength reduction in geopolymer paste made with sodium silicate solution, 65% strength reduction in geopolymer paste made with a mixture of sodium hydroxide and potassium hydroxide solution and a 4% strength increase in the geopolymer paste made with sodium hydroxide solution. The best performance of geopolymer paste made with sodium hydroxide solution was supported by the formation of more stable aluminosilicate polymer structure as evident from the results of microstructure analyses. The OPC and OPC+FA paste showed significant deterioration in terms of change in weight and change in strength in sodium sulfate + magnesium sulfate solution as compared to geopolymer paste.

Bascarevic et al. [99] have evaluated the effect of Na_2SO_4 solution (50 g/l) on durability performance of geopolymer mortar and paste made with two different fly ash (FA) samples (FA Svilajnac and FA Kolubara) over a period of 365 days. A mixture of sodium silicate solution and 10 M sodium hydroxide solution was used as the activator solution with modulus of 1.5. The activator solution to fly ash ratio was same for all the geopolymer mixes with 10% Na_2O content with respect to mass of fly ash. The water/FA ratio was 0.56 and 0.76 for geopolymer mortars made with FA Svilajnac and FA Kolubara respectively. The sand/FA ratio for all geopolymer mortar mixes was 3. The water/FA ratio was 0.49 and 0.69 for geopolymer paste made with FA Svilajnac and FA Kolubara respectively. The prismatic geopolymer mortar specimens of size 40 × 40 × 160 mm were prepared for compressive strength test. The prismatic geopolymer paste specimens of size 25 × 25 × 30 mm were prepared for microstructure analysis. The geopolymer mortar and paste samples were cured at 95° C for 24 hours. The tests conducted for this study were compressive strength, nitrogen adsorption-desorption isotherms, ion exchange between geopolymers and sodium sulfate solution by inductively coupled plasma optical emission spectrometer (ICP-OES), and evaluation of microstructure through XRD, SEM, EDS, and ^{29}Si MAS NMR analyses. The compressive strength of geopolymer mortar was conducted in three

groups of samples. In the first group, the initial compressive strength of geopolymer mortar was determined after heat curing at 95° C for 24 hours. Out of other two groups of samples, the compressive strength of one group of samples was determined after curing in humid chamber (20 ± 2° C, humidity ~98%) (as reference sample) for 28, 90, 180, and 365 days, and the compressive strength of other group of samples was determined after exposure to sodium sulfate solution for 28, 90, 180, and 365 days. The test results revealed that after 365 days, the compressive strength of reference geopolymer mortar samples were approximately 15% higher than the initial compressive strength. However, after 365 days, the geopolymer mortar samples exposed to sodium sulfate solution exhibited decrease in strength (about 12% in case of FA Svilajnac and 10% in case of FA Kolubara) as compared to the initial compressive strength. Further, the geopolymer mortar samples exposed to sodium sulfate solution exhibited lower compressive strength as compared to the reference samples up to 365 days. The ICP-OES analysis of sulfate solution after exposure of geopolymer samples indicated the leaching of Si from aluminosilicate gels to the sulfate solution. The microstructure analysis of geopolymer samples showed no new phases formed after exposure to sodium sulfate solution. Further, ^{29}Si MAS NMR analysis confirmed the breaking of -Si-O-Si- bonds and leaching of Si that resulted in increase in the pH value of sulfate solution.

Ismail et al. [50] have investigated the performance of alkali activated fly ash/slag geopolymer pastes subjected to different types of sulfate exposure, i.e., immersion in 5 wt% sodium sulfate solution and 5 wt% magnesium sulfate solution for 3 months. Alkali activated fly ash/slag geopolymer paste samples (size: 25 mm diameter × 25 mm height) were prepared using fly ash and slag with mass ratio of 1:1 as binder and water to binder (w/b) ratio of 0.40, 0.50, and 0.60. Sodium metasilicate (Na_2SiO_3) at 8 wt% of total binder (fly ash + slag) was dissolved in tap water for the preparation of alkaline activator. After 3 months of exposure, the alkali activated fly ash/slag paste samples were manually crushed and the analytical methods such as X-ray diffraction (XRD), Fourier transform infrared spectroscopy (FTIR), thermogravimetry (TGA/DTG), scanning electron microscopy (SEM) and energy dispersive X-ray (EDX) analyses were performed on the powder samples to understand the microstructural changes in alkali activated fly ash/slag geopolymer pastes under sulfate exposure. The obtained results indicated that the magnesium sulfate solution was more aggressive to geopolymer paste than sodium sulfate solution where the presence of magnesium led to decalcification of Ca-rich gel phases

present in geopolymer paste. This causes degradation of binder phase and precipitation of cohesive and expansive reaction product i.e., gypsum, which was confirmed by the XRD, FTIR, SEM, and EDX analyses. Further, the refinement of the pore system of geopolymer paste made with low w/b ratio densifies the binder and reduced the rate of sulfate attack on the binder system.

Dzunuzovic et al. [100] have examined the influence of 5% Na_2SO_4 solution on mechanical and microstructural properties of alkali-activated fly ash (FA)-blast furnace slag (BFS) binder during a period of 180 days. Further, the influence of Na_2SO_4 solution was estimated by comparison with reference samples simultaneously cured in humid chamber and with the benchmark material CEM II (Portland-composite cement). For this study, mortars and pastes of alkali-activated FA-BFS binder were prepared by mixing equal mass of fly ash (50%) and BFS (50%) and activated with combination of sodium silicate solution and sodium hydroxide solution (modulus, i.e., SiO_2/Na_2O mass ratio: 1.5). The concentration of activator was 10% Na_2O with respect to total mass of FA-BFS composite. The tests conducted were compressive and flexural strength, ion exchange by inductively coupled plasma optical emission spectrometer (ICP-OES), pH, XRD, ATR-FTIR, and SEM/EDS analyses. The mortar prisms of size 40 × 40 × 160 mm were prepared with binder (FA-BFS) to standard sand ratio of 1:3 and water/binder ratio of 0.39 for tests of mechanical properties (compressive and flexural strength) whereas paste samples (size: 25 × 25 × 30 mm) of alkali activated fly ash-BFS binder were prepared with water/binder ratio of 0.34 for investigation of microstructure properties. The results of ICP-OES analysis of Na_2SO_4 solution showed intense leaching of Na, Si, and Ca from the aluminosilicate structure that occured during the exposure of alkali activated FA-BFS mortar samples. However, it did not cause the strength deterioration. The external sulfate attack led only to slower the strength development of mortar in comparison with reference samples. The alkali activated FA-BFS binder showed slightly better resistance as compared to the benchmark CEM II with respect to compressive strength after exposure to sodium sulfate solution. The ATR-FTIR and SEM/EDS analysis of paste samples exposed to Na_2SiO_4 solution confirmed the reduction in Si/Al atomic ratio in the structure of the reaction product due to leaching of Si. However, no new phases due to reaction of alkali-activated FA-BFS binder with sulfates were identified from the XRD analysis.

Elyamany et al. [54] have investigated the effect of curing temperature (30 ºC, 60 ºC and 90 ºC), molarity of sodium hydroxide solution (10 M, 12 M, 14 M and 16 M), alkaline

solution to binder ratio (0.35, 0.40, 0.45 and 0.50) and binder type (class F fly ash, ground granulated blast furnace slag (GGBS), and silica fume) on resistance of geopolymer mortar against 10% magnesium sulfate solution for immersion period of 48 weeks. Three types geopolymer mortar mix (mix 1: 100% fly ash, mix 2: 50% of fly ash and 50% GGBS, and mix 3: 50% fly ash, 35% GGBS and 15% silica fume) were prepared and the test results were compared with OPC mortar made from water-cement ratio of 0.35. The combination of sodium hydroxide (NaOH) solution and sodium silicate (Na_2SiO_3) solution was used as the alkaline activator. The sodium silicate solution-to-sodium hydroxide solution ratio of 2, sand-to-binder ration of 3, extra water of 6% (by mass of binder), and high range water reducing naphthalene-based admixture of 3% (by mass of binder) were used for the preparation of geopolymer mortar mixes. The tests conducted were water absorption and voids ratio (before immersing in magnesium sulfate solution), weight change, residual compressive and flexural strength (at 12, 24, 36, and 48 weeks), expansion strain, scanning electron microscopy (SEM), X-ray diffraction (XRD) and thermogravimetry (TGA/DTG) analysis. Cubes specimens of size 70 × 70 × 70 mm were used to evaluate the water absorption and voids ratio whereas prisms of size 25 × 25 × 285 mm were used to evaluate expansion strain in each month till 48 weeks of exposure. The test results showed that increasing curing temperature and molarity of sodium hydroxide solution, and decreasing alkaline solution to binder ratio enhanced the resistance of geopolymer mortar against magnesium sulfate solution in terms of all studied properties. The increase in curing temperature from 30 ºC to 90 ºC, and molarity of sodium hydroxide solution from 10 M to 16 M led to a decrease in water absorption and voids ratio, and enhanced the magnesium sulfate resistance of geopolymer mortar mixes. However, the increase in alkaline solution to binder ratio from 0.35 to 0.50 increased the water absorption and voids ratio and thereby reduced the magnesium sulfate resistance of geopolymer mortar. The residual compressive and flexural strength increased with increase in curing temperature and molarity of sodium hydroxide solution, and with decrease in alkaline solution to binder ratio. Further, all geopolymer mortar mixes exhibited better performance in terms of resistance against magnesium sulfate solution as compared to OPC mortar. The geopolymer mortar mixes containing 50% fly ash, 35% GGBS, and 15% silica fume showed best performance against magnesium sulfate solution, which was confirmed by the microstructure analysis, showing dense microstructure and narrow micro cracks as compared to the mixes made with only fly ash, and combination of fly ash and GGBS.

Saavedra et al. [47] have studied the performance of geopolymer concrete made with blend of fly ash (FA) and ground granulated blast furnace slag (GBFS) with 80/20 ratio and exposed to 5% sodium sulfate solution and 5% magnesium sulfate solution for up to 360 days and compared the obtained results with conventional OPC concrete. A mixture of sodium silicate solution and sodium hydroxide solution (silicate modulus = 1.3) was used as activating agent. Parallel piped-shaped specimens (50.8 × 50.8 × 285 mm) and cubic specimens (50.8 × 50.8 × 50.8 mm) were prepared to determine the longitudinal expansion of concrete, and loss of compressive strength of concrete respectively after exposure to sulfate solution. The FA/GBFS geopolymer concrete specimens were cured for 28 days at room temperature and OPC based concrete specimens were cured for the same period by complete immersion in water before exposure to sulfate solutions. The microstructure analyses through X-ray diffraction (XRD), scanning electron microscopy (SEM), and energy dispersive X-ray (EDX) spectroscopy were carried out on paste samples after 180 days of exposure in sulfate solutions. The obtained results indicated that the geopolymer concrete is less susceptible to sulfate attack as compared to conventional OPC concrete. Magnesium sulfate solution indicated higher aggressiveness as compared to sodium sulfate solution with a loss in mechanical resistance (i.e., loss in compressive strength as compared to initial compressive strength measured before exposure to sulfate solution) by 33% for FA/GBFS geopolymer concrete and 44% for OPC concrete. Further, the expansion percentage of 0.041% and 0.086% were obtained for FA/GBFS geopolymer concrete and OPC concrete respectively in case of exposure to magnesium sulfate solution. In case of sodium sulfate solution exposure, the FA/GBFS geopolymer concrete showed increase in its mechanical resistance, whereas the OPC concrete exhibited loss in mechanical resistance by 30% and significantly higher expansion of 0.412% due to formation of expansive ettringite in OPC concrete. The microstructure analyses indicated the formation of gypsum in the FA/GBFS geopolymer concrete when exposed to magnesium sulfate solution whereas the formation of ettringite and gypsum in OPC concrete was observed when exposed to both sodium sulfate and magnesium sulfate solutions.

Karakoc et al. [43] have investigated the durability performance of ferrochrome slag (FS) based geopolymer concrete made with two types of aggregate (river sand and crushed sand aggregates with maximum size of 8 mm) after exposure to magnesium sulfate solution of different concentrations (3%, 5%, and 7%) for 180 days and compared with OPC based concrete. A mixture of sodium metasilicate (Na_2SiO_3) and sodium hydroxide (NaOH)

solution with silica modulus of 1.35 was used as the alkaline activator for the preparation of geopolymer concrete. Cube specimens of size 50 mm were prepared for compressive strength and weight change, whereas prismatic specimens of size 40 × 40 × 160 mm were prepared for length change after immersion in magnesium sulfate solutions. The geopolymer concrete specimens were cured at 75° C for 72 h. The resistance of geopolymer concrete against magnesium sulfate solution was evaluated through residual compressive strength (after 90 and 180 days), change in weight, change in length, and visual appearance after exposure to magnesium sulfate solutions. The obtained test results indicated that the compressive strength of geopolymer concrete and OPC concrete decreased as the concentration of magnesium sulfate solution and exposure duration increased. The geopolymer concrete prepared with crushed sand aggregate showed lower compressive strength loss after 180 days of exposure to magnesium sulfate solution as compared to the geopolymer concrete made with river sand aggregate and OPC based concrete. At the end of exposure, the weight of all geopolymer concrete and OPC based concrete specimens slightly increased due to absorption of exposure solution and formation of gypsum and ettringite on the exposed surface and within the pores of the specimens. The maximum gain in weight was observed in OPC based concrete when exposed to 3% and 5% magnesium sulfate solutions whereas geopolymer concrete mixes made with crushed sand aggregate showed maximum gain in weight after exposure to 7% magnesium sulfate solution. Further, the weight gain of geopolymer concrete and OPC based concrete specimens increased with increase in concentration of magnesium sulfate solution. The change in length of geopolymer concrete was less than that of OPC based concrete at the end of exposure in 7% magnesium sulfate solution. There was no change observed in the visual appearance i.e., no sign of surface erosion, and cracking or spalling of geopolymer concrete specimens after immersion in magnesium sulfate solutions for 24 weeks.

2.5 Review of literature on acid resistance of geopolymer composites

Bakharev [58] have evaluated the durability performance of class F fly ash based geopolymer paste after exposure to 5% acetic acid (pH: 2.4) and 5% sulfuric acid (pH: 0.8) solutions. In this study, fly ash was activated with three types of alkaline solution such as sodium hydroxide solution (8% Na), mixture of sodium hydroxide and potassium hydroxide solution (8% Na+1% K), and sodium silicate solution (8% Na). The water/binder ratio of mixes was fixed at 0.3. Cylindrical specimens of size 25 mm diameter × 50 mm height were prepared for evaluating the resistance of geopolymer paste against acid attack

through weight change after 2 months, and compressive strength after 30, 60, 90, 120, 150, and 180 days of exposure in acid solutions. For comparison purpose, OPC and OPC + 20% fly ash based pastes with water/binder ratio of 0.4 were prepared. After casting, the geopolymer paste specimens were kept in room temperature for 24 h followed by oven dry curing at 95° C for 24 h. The deterioration of paste samples was studied by X-ray diffraction (XRD), Fourier transform infrared spectroscopy (FTIR), and scanning electron microscopy (SEM) analyses. From the test results, it is observed that geopolymer paste samples activated by sodium hydroxide solution had more ordered structure and smallest average pore diameter than the samples activated by mixture of sodium hydroxide and potassium hydroxide solution, and sodium silicate solution. Thus, the geopolymer paste samples activated by sodium hydroxide solution showed lower weight loss after exposure to both acid solutions, and lower loss in compressive strength after exposure to sulfuric acid solution as compared to the geopolymer paste samples activated by mixture of sodium hydroxide and potassium hydroxide solution, and sodium silicate solution. The microstructure analyses revealed that geopolymer paste prepared with sodium hydroxide solution resulted in formation of more crystalline products, which were more stable in aggressive environment of sulfuric and acetic acid solutions than the amorphous gels in formed in geopolymer paste prepared with sodium silicate solution. The OPC and OPC + 20% fly ash based paste samples were severely deteriorated as compared to geopolymer paste samples after exposure to acid solutions.

Khan et al. [101] have studied the durability performance of low calcium fly ash based geopolymer mortar (FA-GPm) and sulfate resistant Portland cement mortar (SRPCm) exposed to natural sewer environment for 24 months and sulphuric acid solution for 6 months. The materials used for preparation of geopolymer mortar were low calcium fly ash, ground granulated blast furnace slag (GGBFS: 15% by weight of total source materials), a mixture of sodium silicate solution and 12 M sodium hydroxide solution with mass ratio of 2.5, free water, and fine aggregate. The water/binder ratio for FA-GPm and SRPCm mixes were 0.31 and 0.42 respectively. Cube specimens of size 50 mm were prepared from both types of mortar and placed in infield sewer chambers (Chamber 1: average concentration of H_2S = 53 ppm; and Chamber 2: average concentration of H_2S = 27 ppm) for natural sewer exposure, and in 1.5% sulphuric acid solution for acid resistance test. The tests conducted on the specimens in case of infield exposure were visual observation, loss in mass, failure load, compressive strength, and volume of permeable

voids after 24 months, and neutralization depth and pH profile after 12 and 24 months. The tests conducted in case of sulphuric acid attack were visual observation after 6 months, loss in mass, failure load and compressive strength up to 24 weeks at each 2 weeks interval and bulk porosity after 6 months, and neutralization depth and pH profile after 4 and 6 months. Further, the microstructure analyses (XRD, FTIR, and SEM with EDX) were conducted at the end of exposure period. The obtained results indicated that in both exposure condition, the SRPCm showed greater deterioration in terms of mass loss, porosity, compressive strength, and surface disintegration as compared to FA-GPm. However, the neutralization depth, corrosion depth (considering the loss of surface material and deterioration observed from microstructure analyses), and reduction in pH were greater in FA-GPm as compared to SRPCm under both exposure conditions (infield sewer exposure, and sulphuric acid solution exposure). The microstructure analyses indicated the formation of lower amount of gypsum in FA-GPm after infield exposure, but gypsum precipitation was not widespread due to low calcium content of FA-GPm. However, widespread crystallization of gypsum in SRPCm was responsible for higher micro-cracking, loss in mass and surface disintegration, and loss in compressive strength. The results of XRD and FTIR analyses indicated almost similar reaction products formed in both exposure conditions.

Lee and Lee [59] have investigated the effect of slag content (0%, 10%, 30%, and 50%) on sulfuric acid and chloride resistance of alkali-activated fly ash/slag (AFS) paste. The combination of sodium hydroxide (4 mol/L) solution and sodium silicate solution was used as alkaline solution for the preparation of AFS paste. For comparison, OPC paste samples were prepared using water to cement ratio of 0.4. For acid resistance test, after 28 days of curing in room temperature, the cube specimens of size 50 mm were immersed in 10% sulfuric acid solution for 28 days and 56 days. Tests such as mass change, and compressive strength test were conducted to investigate the physical changes of AFS paste samples after immersion in sulfuric acid solution. The residual compressive strength of AFS paste samples were measured by comparing with the results obtained from 28 days cured unexposed cube samples. Further, X-ray diffraction (XRD), Fourier transform infrared (FT-IR) spectroscopy, and ^{29}Si MAS NMR spectrometry analyses were conducted to observe the microstructural changes of AFS paste after immersion in sulfuric acid solution. For chloride penetration test, the 28 day cured cube specimens of size 50 mm were immersed in 10% sodium chloride solution for 28 days and 91 days and allowed the solutions to penetrate from bottom surface of the specimens (top and side surfaces sealed

with polymer sealant). Tests such as water absorption rate, volume of permeable voids, and acid-soluble and water-soluble chloride contents were measured to investigate the physical changes of AFS paste samples after immersion in sodium chloride solution. Further, XRD analysis, and ^{29}Si MAS NMR spectrometry were conducted to investigate the microstructure of AFS paste samples after immersion in sodium chloride solution. From the test results, it is observed that the AFS paste showed improved resistance to sulfuric acid attack than OPC paste. The OPC paste samples showed significantly higher mass loss as compared to AFS paste samples. Further, the mass of AFS paste made with 50% slag was slightly increased whereas the mass of other AFS paste samples were mostly remained unchanged up to 56 days of exposure in sulfuric acid solution. The AFS paste made with 30% slag exhibited highest rate of decrease in compressive strength whereas AFS paste made with 50% slag showed greater residual strength than OPC paste. The formation of gypsum and ettringite was the main cause for deterioration of OPC paste subjected to sulfuric acid solution, whereas the formation of ettringite was not found in the AFS paste due to lower Ca/Si ratio and lower Al content as observed from the microstructure analysis. The volume of permeable voids and chloride penetration depth decreased with increase in slag content in the AFS paste. The AFS paste showed a steep increase in rate of water absorption after the age of 28 days as compared to the OPC paste. It was observed that the chloride binding capacity of AFS paste decreased and the resistance to chloride penetration increased with increase in slag content in the AFS paste.

Aiken et al. [60] have carried out a study to evaluate the effect of slag content on acid resistance of geopolymer mortar and paste by replacing fly ash with slag at 0%, 20%, 40%, and 70%. A mixture of sodium silicate solution and sodium hydroxide solution was used as the alkaline solution for preparation of geopolymer mortar and paste samples. The Na_2O content and Na_2O/SiO_2 ratio of the mixes (slag: 20%, 40%, and 70%) were kept at 7.5% and 1.25 respectively. Further, the effect of activator dosage i.e., Na_2O content: 7.5% and 11.5%, and Na_2O/SiO_2 ratio of 1.25 and 0.95 on acid resistance of geopolymer mortar and paste made with 100% fly ash was evaluated. For comparison purpose, Portland cement (PC) based mortar and paste samples were prepared. Cube specimens of size 50 mm were prepared from all geopolymer, and PC mortar and paste mixes. Geopolymer mixes containing 100% fly ash were cured at 70° C for 7 days and then placed at 20 ± 1° C and 50% relative humidity. The fly ash and slag based gopolymer mixes and PC mixes were cured at 20 ± 1° C and relative humidity greater than 90%. After 28 days of curing, the

mortar samples were immersed in 1%, 3%, and 5% sulfuric acid solutions for 56 days, whereas the paste samples were immersed in 5% sulfuric acid solution for 21 days. Mortar samples were used for visual observation, mass change, compressive strength, alkalinity loss, and porosity. The paste samples were used to study the leaching behaviour by measurement of pH and inductively coupled plasma mass spectrometry (ICP) analysis of acid solutions. The microstructure investigation on paste samples was carried out by X-ray diffraction (XRD) analysis, thermogravimetric analysis (TGA), Fourier transform infrared spectroscopy (FTIR), scanning electron microscopy (SEM) and energy dispersive X-ray (EDX) analysis. The obtained results indicated that with increase in slag content in geopolymer mortar mixes, the porosity was decreased due to formation of space filling C-A-S-H gel, and alkalinity loss became smaller. However, the deterioration of geopolymer mortar against sulfuric acid solution was higher with increase in slag content due to greater decalcification of C-A-S-H gel and formation of higher amount of gypsum, which caused expansion in the geopolymer mortar mixes. The loss of strength and mass loss in geopolymer mortar and PC mortar due to acid exposure were increased with increase in concentration of sulfuric acid solution. The visual observation of PC mortar specimens indicated severe surface damage due to loss of cement paste whereas geopolymer mortar specimens had limited surface damage with almost no visible deterioration in case of geopolymer mortar made with 100% fly ash. Further, the PC mortar mixes showed higher mass loss as compared to geopolymer mortar mixes in 5% sulfuric acid solution. The cracks identified during visual appearance of geopolymer mortar specimens due to formation of gypsum was confirmed by XRD, TGA, FTIR, and EDX analyses. There was more formation of gypsum in PC mixes as a result of higher initial calcium content as compared to geopolymer mixes. The increase in activator dosage had very little effect on the sulfuric acid resistance of fly ash based geopolymer mortar. Based on the results, it was observed that the geopolymer mortar mixes showed superior sulfuric acid resistance than PC mortar mixes.

Ren et al. [68] have investigated the degradation of alkali activated slag/fly ash (AASF) mortars with different slag/fly ash ratios (80%/20%, 60%/40%, and 40%/60%) after immersion in three different types of aggressive acid solutions (phosphoric acid, sulfuric acid and a mixture of phosphoric acid and sulfuric acid) at constant pH value of 2.5 ± 0.5 for a period of 150 days. The AASF mortars were prepared with different water/binder ratios (0.40, 0.38, and 0.34), activator/binder ratios (7.0%, 7.5%, and 8.5%), and

sand/binder ratio of 2:1 to reach similar target compressive strength of around 60 ± 5 MPa at 56 days before immersion in acidic solutions. Solid anhydrous sodium metasilicate powder (Na_2SiO_3) with molar ratio of SiO_2/Na_2O = 1.0 was used to prepare the activator solution. The AASF mortars namely 80Slag_20FA and 60Slag_40FA were cured at room temperature (23°C ± 2°C) for 24 hours whereas the AAFS mortar 40Slag_60FA was cured under hydrothermal water bath conditions (70° C and RH = 95% ± 5%) in an oven for 7 days. Compressive strength test was performed on cubic mortar samples of size 50 mm after 56 days of curing prior to the acid exposure. Further, the initial water absorption, volume of permeable voids (VPV) and capillary sorptivity tests were conducted on cylindrical samples of size 27.5 mm diameter × 55 mm height after 56 days of curing prior to acid exposure. Degradation depth in the mortar samples using an optical microscope was measured after 7, 28, 56, 90, 120, and 150 days of exposure period. The numerical fitting and long-term prediction of degradation depth of AASF mortar was carried out using Hill function and Fick's second law of diffusion. The long-term prediction of degradation depth of AASF mortar was compared with OPC-based mortar. The test results showed that higher water absorption, volume of permeable voids (VPV), and capillary sorptivity were obtained for mix 80Slag_20FA followed by 60Slag_40FA and 40Slag_60FA. Among the acid solutions, the phosphoric acid caused most severe degradation in AASF mortars. The AASF mortar 60Slag_40FA showed best durability performance after immersion in all three types of acid solution for 150 days due to formation higher amount of C-A-S-H gel and relatively more densified structure. The results of the theoretical prediction indicated that the degradation depth of AASF mortar exposed to sulfuric acid (pH = 2.0) environment for 50 years could be reduced by about 52% to 60% as compared to OPC mortar.

Deb et al. [57] have investigated the effect of nano-silica on flowability, strength development, sorptivity and sulfuric acid resistance of geopolymer mortars made with three types of binder such as fly ash, fly ash blended with 15% ground granulated blast furnace slag (GGBFS), and fly ash blended with 10% OPC. In these mixes, fly ash was replaced by nano-silica at 1%, 2%, and 3% (by weight of binder). A combination of sodium silicate solution and 8 M sodium hydroxide solution with mass ratio of 2.0 was used as alkaline activator in the mixes. The alkaline activator to binder ratio was fixed at 0.4 for all mixes. The flowability and strength development were evaluated for geopolymer mortar mixes prepared with different percentages of nano-silica i.e., 0%, 1%, 2%, and 3%. However, the sorptivity and acid resistance test were performed on geopolymer mortar mixes made with

0% and 2% nano-silica. Cube specimens of size 50 mm were prepared for compressive strength test and acid resistance test, whereas cylinder specimens of size 100 mm diameter × 50 mm height were prepared for sorptivity test. The compressive strength test was performed at the age of 7, 28, 56, and 90 days of ambient curing. For sulfuric acid resistance test, the 28-day cured geopolymer mortar cube specimens were fully immersed in 3% sulfuric acid solution for 90 days. The changes in mass at every week, compressive strength loss after 28, 56 and 90 days of exposure period, and microstructural changes (through SEM, EDS, and XRD analyses) of the specimens before and after immersion in acid solution were evaluated. The test results revealed that the flow value was gradually decreased with increase in nano-silica in geopolymer mortars made with all three types of binder. Further, the flow value of geopolymer mortars containing GGBFS, and OPC were less than that of fly ash geopolymer mortar mixes. The inclusion of nano-silica improved the compressive strength of geopolymer mortar made with all three types of binder. The inclusion of nano-silica in geopolymer mortars made with fly ash and GGBFS blends, and fly ash and OPC blends increased the compressive strength by 40-64% as compared to the corresponding control mixes (without nano-silica). The highest compressive strength at all ages up to 90 days were found in the geopolymer mortar mixes containing 2% nano-silica for all three types of binder. The sorptivity coefficient of geopolymer mortar specimens made with 2% nano-silica was less than that of control geopolymer mortar specimens. Further, the acid resistance of geopolymer mortar specimens was significantly improved with the inclusion of 2% nano-silica due to formation of more compact microstructure as observed from the results of microstructure analysis when compared with the geopolymer mortar made without nano-silica.

Kuri et al. [102] have carried out a study to investigate the effect of ground ferronickel slag (GFNS: 0%, 25%, 50%, and 75%) on sulphuric acid resistance of GFNS blended fly ash geopolymer mortar. A mixture of solidum silicate solution and 8 M sodium hydroxide solution with mass ratio of 2.0 was used as alkali activator. For all mixes, the alkali activator content was 45% by mass of precursor materials. Mortar cube specimens of size 50 mm were prepared and cured at 60° C for 24 h. After heat curing, the geopolymer samples were cooled down to room temperature and then submerged in 3% sulphuric acid solution for up to one year. The tests conducted were visual appearance, mass change (at 1, 3, 6, 9, and 12 months of exposure), and residual compressive strength (at 1, 3, 6, 9, and 12 months of exposure). The microstructure analysis (SEM, EDX, and XRD) was carried on geopolymer

paste samples. The test results indicated that the use of GFNS as partial replacement of fly ash enhanced the resistance of geopolymer mortar against 3% sulphuric acid solution. The geopolymer mortar samples showed minor damages at surface after exposure to acid solution. Further, it was observed that the loss in compressive strength and mass loss of fly ash-GFNS geopolymer mortar were less than that of neat fly ash geopolymer mortar after exposure to sulphuric acid solution for 12 months. The lowest strength loss was observed in case of fly ash-GFNS geopolymer mortar mix prepared with 25% fly ash and 75% GFNS. The incorporation of GFNS resulted in a dense structure due to production of N-M-A-S-H gel, which is more stable than N-A-S-H gel of neat fly ash geopolymer mortar. The results obtained from the quantitative analysis of XRD patterns indicated the formation of higher amount of gypsum in neat fly ash geopolymer after acid exposure, which might have induced higher stresses that led to more cracks in neat fly ash geopolymer.

2.6 Review of literature on corrosion of steel reinforcement in geopolymer composites

Monticelli et al. [76] have investigated the corrosion behaviour of embedded steel reinforcement in class F fly ash based alkali-activated mortar (geopolymer mortar) cured at room temperature and traditional cement based mortar during wet and dry (w/d) exposure to 0.1 M NaCl solution. The materials used for preparation of geopolymer mortar were class F fly ash, combination of sodium silicate solution and 8 M sodium hydroxide solution and natural sand. The binder/sand ratio of 1: 2.7 and liquid/binder ratio of 0.52 were fixed for all mixes. Three different mixes of alkali-activated mortar were prepared with varying molar ratio (Na_2O/SiO_2) of activating solution such as 0.12, 0.14, and 0.16, and their performances were compared with traditional cement-based mortar. The tests conducted were compressive strength, bulk density, dynamic elastic modulus, shrinkage, microstructural characterization (pore size distribution) by mercury intrusion porosimetry (MIP), electrochemical tests such as potentiostatic polarization resistance measurement, electrochemical impedance spectroscopy measurement, polarization curves, and corrosion product analysis by visual observation and Raman analysis of surface corrosion products. Cylinders (size: 100 mm height and 35 mm diameter) with a centrally embedded rebar were prepared for electrochemical tests whereas unreinforced cylinders were prepared for chloride content and pH measurements. Prismatic specimens (size: 40 mm × 40 mm × 160 mm) were cast for mechanical tests after 28 days and microstructural characterization, and cube specimens (size: 100 mm) were cast for chloride diffusion test. The reinforced and unreinforced cylindrical samples were exposed to 11 weeks of w/d cycles with each cycle

consists of 4 days of immersion in 0.1 M NaCl solution and 3 days of drying under laboratory condition. The obtained test results indicated that the traditional cement-based mortar showed better performance in terms of higher compressive strength and dynamic elastic modulus, and lower shrinkage than geopolymer mortars. Further, the traditional cement-based mortar showed lower apparent chloride diffusion coefficient than geopolymer mortar, which was in good agreement with the total porosity values determined by MIP test. The use of low molar ratio (Na_2O/SiO_2) in activating solution while preparing geopolymer mortar exhibited more compact microstructure, higher compressive strength and dynamic elastic modulus, and lowest apparent chloride diffusion coefficient. The electrochemical measurements indicated that the traditional cement-based mortar showed highest corrosion protection to the reinforcement as compared to geopolymer mortar. The authors also reported that all geopolymer mortar samples suffered quick carbonation under wet and dry exposure condition, which was responsible for faster rebar depassivation, despite a lower total chloride concentration near rebar level.

Criado et al. [103] have studied the corrosion behaviour of carbon steel coated with hybrid organic-inorganic coatings in carbonated ordinary Portland cement (OPC) and alkali-activated fly ash (AAFA) mortars. The sol-gel coatings were prepared by condensation and polymerization of tetraethyl orthosilicate (TEOS, $Si(OCH_2CH_3)_4$) and 3-methacryloxy-propyl-trimethoxysilane (MPTS, $CH_2 = C(CH_3)COO(CH_2)_3Si(OCH_3)_3$); TEOS and methyl-triethoxysilane (MTES, $(CH_3)Si(OCH_2CH_3)_3$); tetramethyl orthosilicate (TMOS, $Si(OCH_3)_4$) and MPTS; or TMOS and MTES. The OPC and AAFA mortar specimens (size: 8 × 5.5 × 2 cm) embedded with two coated steel bars (10 mm diameter × 100 mm height) were prepared with type 1 (42.5 R) Portland cement, and Class F fly ash respectively. The AAFA mortar specimens were prepared with alkaline activator solution containing 85 wt.% 10 M NaOH solution and 15 wt.% sodium silicate solution. For both types of mortar, the liquid to binder ratio, and sand to binder ratio were 0.6 and 3 respectively. After preparation, the AAFA mortar specimens were subjected to oven drying for 24 hours at 85^o C and 100% relative humidity (RH), whereas the OPC mortar specimens were kept at room temperature and 100% RH for 24 hours. After 24 hours, all the mortar specimens (AAFA and OPC) were stored in a humidity chamber (98% RH, 20± 2^o C) for 28 days. Subsequently, the mortar specimens were stored in carbonation chamber at 43.2% RH in a K_2CO_3 solution for 60 days (with CO_2 saturation), prior to partial immersion in 3 wt.% NaCl solution for 240 days. The corrosion potential (E_{corr}), linear polarization resistance

(LPR), and electrochemical impedance spectroscopy (EIS) measurements were carried out after 1, 7, 30, 60, 90, 120, and 240 days of exposure. The obtained results indicated that the corrosion of coated rebar embedded in carbonated mortars in the presence of chloride ions was dependent on both cementitious system and nature of the reagents forming the coating on the steel bar. The coated steel bars embedded in AAFA mortar exhibited higher corrosion potential (less negative) and lower corrosion current density than that embedded in OPC mortar indicating better resistance against rebar corrosion than OPC mortar. Further, in AAFA mortar specimens, the rebars coated with hybrid organic-inorganic coatings synthesized with TEOS/MTES and TMOS/MTES showed lowest corrosion current density thereby indicating best protective properties over 240 days of exposure.

Kupwade-Patil and Allouche [21] have carried out an investigation to evaluate the corrosion behaviour of steel reinforcement in geopolymer concrete (GPC) made from Class F fly ash (two sources) and Class C fly ash (one source), and in ordinary Portland cement (OPC) concrete. The GPC mixes were prepared with the proportion of fly ash: sand: coarse aggregate of 1:1.5:2 by mass. The activator solution to pozzolanic materials ratio, and sodium silicate solution to 14 M of sodium hydroxide solution ratio were taken as 0.5 and 1.0 respectively. The GPC specimens were subjected to heat curing at 80° C for 72 hours. A high concentration of sodium chloride (7.5%) solution was used to simulate sever condition and to accelerate the corrosion, wet-dry cycle consisting of 14 days each was used over a period of 12 months. The test methods conducted were compressive strength at 28 days, electrochemical measurements through half-cell potential and corrosion current density by linear polarization resistance technique, chloride diffusion, chloride content (acid soluble) analysis, pore structure by mercury intrusion porosimetry (MIP), microstructure analyses (SEM, XRD, FTIR) at the rebar/binder interface, and visual examination. The concrete specimens of size 280 mm (length) × 114 mm (width) × 150 mm (height) (ASTM G109) were prepared with three embedded steel bars of size 10 mm in diameter and 381 mm in length in each specimen. Plexiglas dams of size 75 mm (wide) ×150 mm (long) × 75 mm (high) were fixed on top of the specimens to store salt water during the wet cycle. The obtained results indicated that the geopolymer concrete mixes made with Class C fly ash exhibited highest 28-day compressive strength followed by geopolymer concrete mixes made with Class F fly ash (both sources) and OPC concrete. Further, geopolymer concrete mixes exhibited lower chloride diffusion coefficient, chloride content, and porosity as compared to their OPC counterparts. The geopolymer

concrete specimens prepared with Class F fly ash (both sources) showed a significantly higher resistance to chloride ingress and rebar corrosion when compared with OPC specimens as well as the geopolymer concrete specimens prepared with Class C fly ash, possibly due to more complete geopolymerization process and formation of a denser matrix. The microstructure analysis revealed the formation of corrosion product in the form of akaganeite at the rebar/binder interface of geopolymer concrete, and OPC concrete.

Chindaprasirt and Chalee [73] have investigated the effect of sodium hydroxide (NaOH) concentration (8 M, 10 M, 12 M, 14 M, 16 M, and 18 M) on compressive strength, chloride penetration, chloride binding capacity, and steel corrosion in fly ash-based geopolymer concrete exposed to tidal zone of marine environment for 3 years. The materials used were class C fly ash, graded sand, crushed stone with maximum size of 19 mm, and combination of sodium silicate solution and sodium hydroxide solution. The liquid to binder ratio was kept constant at 0.6 for all geopolymer concrete mixes. Cylindrical specimens of size 100 mm diameter × 200 mm height were prepared for compressive strength test at 28 days, and at 3 years exposure in marine environment. For chloride penetration and steel corrosion test, cube specimens of size 200 mm were prepared and the steel bars of 12 mm diameter × 50 mm length were embedded at the corner of the cube specimens with cover depth of 20 mm, 50 mm, and 75 mm. The corrosion of embedded steel was measured in terms of percentage of rusted area, and percentage of weight loss. The percentage of rusted surface area was calculated by comparing it with the total surface area of the embedded steel bar and the percentage of weight loss was determined by comparing the weight loss of steel due to corrosion during the exposure period to the initial steel weight. The test results showed that the compressive strength of fly ash based geopolymer concrete increased with increase in concentration of NaOH solution. Further, geopolymer concrete at higher NaOH concentration gained compressive strength faster than that with a lower NaOH concentration during 3 years of exposure in seawater. The increase in NaOH concentration resulted in decrease in chloride diffusion coefficient, and steel corrosion, and increase in chloride binding capacity (% of total chloride) of geopolymer concrete.

Gunasekara et al. [71] have studied the corrosion behaviour of steel reinforcement embedded in fly ash based geopolymer concrete and Portland cement concrete admixed with different concentrations of NaCl. The materials used for preparation of geopolymer concrete were Class F fly ash (collected from three different sources: Gladstone, Pt. Augusta, and Collie), mixture of Na_2SiO_3 solution and 15 M NaOH solution as alkaline

activator, river sand as fine aggregate, and crushed granite with combination of 7 and 10 mm grain size as coarse aggregate. The water to solid ratio of all the mixes was fixed at 0.37. For all concrete types, cube specimen of size 150 mm with ribbed bars of size 10 mm diameter × 120 mm length were cast. For cast-in chloride specimens, the geopolymer and Portland cement concrete mixes were admixed with 0%, 0.25%, 0.5%, 1%, 2%, 3%, and 5% (by weight of binder) NaCl. Additional set of cubes with ribbed bars were prepared without NaCl addition for the ponding test. After casting, all geopolymer specimens were stored in room temperature for 1 day and then oven dried at 80° C for 24 h. All NaCl admixed concrete specimens were kept in a spray cabinet, and all concrete specimens prepared without admixed NaCl were kept under laboratory condition for 14 days before subjected to wetting/drying cycles up to 540 days in 3% NaCl solution. The wetting/drying cycles comprised of one week of ponding (wetting) and two weeks of drying. The tests conducted were compressive strength test at 28 and 540 days for concrete mixes admixed with 0%, 2%, and 5% NaCl, corrosion potential and corrosion rate by linear polarization resistance (LPR) measurement, chloride analysis, microstructure analysis through Fourier transform infrared (FT-IR), X-Ray diffraction (XRD), and scanning electron microscopy, and pore structure analysis by mercury intrusion porosimeter. The obtained results indicated that the addition of NaCl had no noticeable effect on the 28-day compressive strength of any of the mixes. However, all geopolymer and Portland cement concrete mixes with cast-in chloride showed a strength loss between 28 and 540 days. The maximum loss in strength was observed in the range of 19.8 – 23.2% when geopolymer and Portland cement concrete mixes added with 5% NaCl. The fly ash based geopolymer concrete showed significantly higher corrosion rate than Portland cement concrete admixed with the same concentration of NaCl. However, in case of ponded specimens, the formation of three-dimensional N-A-S-H and C-A-S-H cross linking in the gel matrix reduced the chloride diffusion, and resulted in lower corrosion rate of steel reinforcement in geopolymer concrete (made with Gladstone fly ash, and Pt. Augusta fly ash) than Portland cement concrete. Among the fly ash based geopolymer concrete mixes, the geopolymer concrete made with Gladstone fly ash showed higher compressive strength followed by that made with Pt. Augusta fly ash, and Collie fly ash. It was observed that the chloride binding capacity of low calcium fly ash based geopolymer concrete depends on the amount of CaO present in the precursor material. Therefore, the geopolymer concrete made with Pt. Augusta fly ash (CaO: 4.80%) showed highest chloride binding capacity followed by Gladstone fly ash (CaO: 3.81%) and Collie fly ash (CaO: 0.64%). The microstructure

analysis of rebar/binder interface indicated the formation of corrosion products in the form of hematite, akageneite, and lepidocrocite.

Nguyen et al. [104] have carried out a study to evaluate the effect of alkaline liquid to fly ash ratio, aggregate to fly ash ratio, and Si/Al ratio on mechanical properties of geopolymer concrete made with sea sand as fine aggregate, and compared with that prepared with river sand. The geopolymer concrete mixes were prepared with Class F fly ash. The alkaline liquid used was a combination of sodium silicate (Na_2SiO_3) solution and 12 M sodium hydroxide (NaOH) solution with mass ratio (Na_2SiO_3/NaOH) of 2.5. The alkaline liquid to fly ash ratios taken were 0.35, 0.4, 0.45, 0.5, 0.55, 0.6, and 0.65 by mass. The aggregate to fly ash ratios of geopolymer concrete were 3.5, 4.0, 4.5, and 5.0 by mass. To investigate the effect of Si/Al ratio, the fly ash in geopolymer concrete was partially replaced with micro-silica (0%, 10%, 15%, and 20%) with four different Si/Al ratios (1.16, 1.40, 1.52, and 1.67). The tests conducted were compressive strength, splitting tensile strength, scanning electron microscope (SEM) imaging and X-ray diffraction (XRD) analysis. The authors have also investigated the corrosion behaviour of steel bar embedded in sea sand geopolymer concrete under accelerated corrosion conditions during 252 wet/dry cyclic tests (30 min wetting in 0.0001 M and 0.001 M Na_2SO_4 solutions, and 60 min drying) using half-cell potential measurement and compared with the corrosion behaviour of steel bar embedded in OPC concrete. The cylindrical specimens of size 150 mm diameter and 300 mm height were prepared for determining the compressive strength, and splitting tensile strength of concrete at the age of 28 days. For the corrosion test of steel bar, the prismatic specimens of size 100 × 100 × 200 mm were embedded with two steel bars of 8 mm diameter (with concrete cover of 21 mm). The test results indicated that the strength difference between the geopolymer concrete made with sea sand and river sand was not significant. The sea sand geopolymer concrete exhibited highest compressive strength at alkaline liquid to fly ash ratio of 0.35 to 0.45. The geopolymer concrete showed higher compressive strength at lower aggregate to fly ash ratio and at higher Si/Al ratio. The half-cell potential results indicated that the rebar embedded in sea sand geopolymer concrete had higher potential (less negative) values than that in OPC concrete. This shows that the steel bar embedded in sea sand geopolymer concrete takes more time to corrode than the steel bar embedded in the OPC concrete.

Tennakoon et al. [34] have investigated the compressive strength, chloride diffusion rate, age factor, chloride permeability, and initiation of chloride induced steel bar corrosion in

blended fly ash and slag geopolymer concrete, and compared with OPC concrete. For this study, Class F fly ash with a 50/50 mixture of Gladstone fly ash and Callide fly ash, and ground granulated blast furnace slag (GGBS) were used as precursor materials with fly ash/slag ratio of 60/40, 50/50, and 40/60. Granular sodium metasilicate penta-hydrate (4% Na_2O by mass of precursor materials) was used as the solid activator. Cylindrical specimens of size 100 mm × 200 mm were cast for compressive strength test at 1, 7, 28, 90, 180, 365, and 600 days of curing. The chloride diffusion test was conducted on cylindrical specimens of size 100 mm diameter × 98 mm thick after 5 weeks of immersion in 2.826 M sodium chloride solution. The rapid chloride permeability test was conducted on cylindrical specimens of size 100 mm diameter × 51 mm thick at the age of 28 days, 180 days, and 500 days. For corrosion study, prismatic reinforced geopolymer concrete specimens of size 95 × 95 × 300 mm with a centrally embedded steel rebar of 20 mm diameter were partially immersed in 2.826 M and 0.6 M NaCl solutions up to 500 days. To evaluate the corrosion behaviour in contaminated concrete, blended fly ash/slag (50/50) geopolymer concrete specimens were admixed with 2% NaCl (by mass of binder) and partially immersed in water. The corrosion state of rebar was monitored by half-cell potential and linear polarization resistance measurements with $Cu/CuSO_4$ reference electrode. After 500 days, the chloride penetration depth was measured using $AgNO_3$ colorimetric method, and chloride content at the rebar level was measured using potentiometric titration method. The test results indicated that geopolymer concrete made with fly ash/slag ratio of 40/60 and 50/50 showed higher compressive strength than geopolymer concrete made with fly ash/slag ratio of 60/40 and OPC concrete. It was observed that the chloride diffusion coefficient decreased with increase in slag content in blended fly ash and slag geopolymer concrete. Further, the geopolymer concrete mixes showed lower chloride diffusion coefficient than OPC concrete. The geopolymer concrete mixes exhibited higher age factor than OPC concrete indicating better resistance to chloride ingress with time. The time taken for initiation of rebar corrosion in geopolymer concrete was significantly higher than OPC concrete. After 500 days, the amount of chloride present near the rebar level of geopolymer concrete was ten times lesser than that of OPC concrete, which was not sufficient to initiate the corrosion in geopolymer concrete. Blended fly ash and slag geopolymer concrete provided greater protection against rebar corrosion than OPC concrete when concrete was contaminated with chloride. The geopolymer concrete containing higher slag content produced higher amount of calcium bearing phases including calcium silicate hydrate phases as observed from the XRD analysis at 28 and 270 days.

2.7 Review of literature on application of Taguchi method for investigating and optimizing different properties of geopolymer composites

Panagiotopoulou et al. [105] have investigated the effect of alkali (R: Na, K) to aluminum ratio of starting mixture (R/Al: 0.50, 0.85, 1.20, and 1.50), alkali species in activation solution (Na/(Na + K): 0, 0.35, 0.70, and 1.0), and silicon content in activation solution (Si/R_2O: 0, 0.70, 1.35, and 2.0) on compressive strength of fly ash geopolymer paste using mean response data and ANOVA technique as per Taguchi method (L16 orthogonal array). The materials used for the preparation of geopolymer paste were fly ash and activation solution containing alkali (Na, K) hydroxide, and commercial water silica solution. The geopolymer paste mixes were prepared with solids to liquid ratio of 2.6 by mass. Cubic specimens of size 50 mm were prepared and left for 2 hours at ambient temperature before cured at 70° C for 48 hours. After that, the specimens were left for 24 hours to cool down. Compressive strength test was conducted on paste specimens 7 days after thermal curing (i.e., 10 days after the mixture preparation) and the microstructure of geopolymer paste was examined through XRD, FTIR, and SEM analyses. From the obtained results, it was observed that the optimal combination of parameters for achieving highest compressive strength was R/Al of 0.85, Na/(Na + K) of 0, and Si/R_2O of 1.35. Among the factors, the R/Al ratio significantly influenced the compressive strength of geopolymer paste with a contribution of 88.2%. The confirmatory experiment on the optimal combination of parameters resulted a compressive strength of 43.1 MPa, which was within the predicted range (42.6 ± 3.1 MPa). The results of XRD and SEM analyses indicated that the use of activation solution with high alkali and low silicon content resulted in formation of zeolitic phases in the mixes, which led to higher compressive strength.

Yuan et al. [106] have investigated the effect of sodium carbonate content (wt.% of Na_2O: 3.0%, 4.0%, and 5.0%), water to solid ratio (0.40, 0.45, and 0.50), waterglass modulus (1.1, 1.3, and 1.5), and waterglass content (wt.% of Na_2O: 0.5%, 1.5%, and 2.5%) on reaction kinetics, and compressive strength of ternary activators activated slag paste using Taguchi method (L9 orthogonal array). Sodium hydroxide was used to modify the waterglass modulus to obtain the desired values. For comparison purpose, sodium carbonate activated slag pastes were prepared as reference samples. To validate the results, three mixes were further designed and their performance was evaluated through reaction kinetics and compressive strength. The reaction kinetics of the paste mixes were measured by isothermal calorimeter up to 168 h. The compressive strength test was conducted on prismatic

specimens of size 40 × 40 × 160 mm at the age of 7 and 28 days after casting. The microstructure of 28 days samples was characterized by X-ray diffraction (XRD) and Fourier transform infrared spectroscopy (FTIR) analyses. The test results revealed that the ternary activators significantly accelerated the reaction of slag as compared only sodium carbonate. Among all the factors, waterglass content had the most significant effect on reaction kinetics and compressive strength, whereas the effect of waterglass modulus on reaction kinetics and compressive strength was not prominent. Based on the results, the optimal proportion of ternary alkali activators was sodium carbonate content of 4%, water to solid ratio of 0.4, waterglass modulus of 1.1 to 1.5, and waterglass content of 2.5%. The XRD analysis indicated the presence of amorphous structure of $CaO\text{-}Al_2O_3\text{-}MgO\text{-}SiO_2$ centred at 25° to 35° 2θ and the formation of new phases related to calcite, hydrotalcite and C-(A)-S-H gel in the mixes. Further, it was observed that sodium carbonate had dominant role on the gel structure of the reaction products.

Hadi et al. [107] have studied the influence of binder content (400 kg/m^3, 450 kg/m^3, and 500 kg/m^3), alkaline activator to binder content (Al/Bi) ratio (0.35, 0.45, and 0.55), sodium silicate solution to sodium hydroxide solution (SS/SH) ratio (1.5, 2.0, and 2.5), and sodium hydroxide concentration (10 M, 12 M, and 14 M) on compressive strength of geopolymer concrete made with ground granulated blast furnace slag (GGBFS) using Taguchi method (L9 orthogonal array). Cylindrical specimens of size 100 mm diameter × 200 mm length were prepared for compressive strength test at the age of 7 and 28 days. The obtained results indicated that the compressive strength of geopolymer concrete mixes increased with increase in age from 7 to 28 days. Based on the results of 7-day compressive strength, optimum levels of each parameter were evaluated, and then the setting time and compressive strength tests were conducted on the optimized mix. The obtained optimum levels of the considered parameters (based on 7-day compressive strength) were binder content of 450 kg/m^3, Al/Bi ratio of 0.35, SS/SH ratio of 2.5, and 14 M of sodium hydroxide solution. The geopolymer concrete mix prepared with the optimum levels of the considered parameters showed highest 7-day compressive strength of 60.4 MPa, however, shorter setting time i.e., initial setting time of 25 min and final setting time of 55 min were obtained. Therefore, the GGBFS was replaced with fly ash (FA), metakaolin (MK) and silica fume (SF) in the range of 10% to 60% (by mass of total binder) each to investigate the setting time, workability and 7 day-compressive strength of geopolymer concrete. The inclusion of FA, MK, and SF as partial replacement of GGBFS in geopolymer concrete increased the

setting time (initial setting time up to 55 min to 75 min and final setting time up to 90 min to 105 min) and workability, and decreased the compressive strength (up to 41% to 58%). Among the combination of source materials, the mixture of fly ash and GGBFS was found to be a suitable binder for geopolymer concrete mixes.

Shojaei et al. [108] have proposed a method for selecting the mix proportions of alkali-activated slag (AAS) concrete for application in the manufacture of prestressed concrete railway sleepers. The considered factors affecting the properties of AAS concrete were concentration of sodium hydroxide (NaOH) solution (4 M, 6 M, and 8 M), alkaline liquid to slag ratio (0.4, 0.45, and 0.5), NaOH to sodium silicate solution (Na_2SiO_3) ratio (1, 3, and 5), and aggregate content (1800 kg/m^3, 1848 kg/m^3, 1896 kg/m^3). The materials used for the preparation of AAS concrete were ground granulated blast furnace slag (GGBFS), a combination of sodium silicate solution and sodium hydroxide solution as alkaline liquid, crushed sand as fine aggregate, crushed stone with maximum nominal size of 12 mm as coarse aggregate and extra water. The optimal mix proportions based on maximum compressive strength (7 and 28 days) were identified by Taguchi method of experimental design. Subsequently, prestressed concrete sleeper (type B70) was prepared using the optimal mixture design and then the flexural strength of railway sleeper was investigated. Further, the efficiency of the optimal mixture was evaluated through eco-mechanical indicator i.e., ratio between the quantity of CO_2 released by the production of binder materials and compressive strength, and compared with the value calculated for ordinary concrete used for railway sleepers. The obtained results showed that the optimal combination of parameters for obtaining the highest compressive strength was 6 M NaOH solution, alkaline liquid to slag ratio of 0.5, NaOH to Na_2SiO_3 solution ratio of 1 and aggregate content of 1800 kg/m^3. The proposed AAS concrete railway sleeper (based on optimal mixture design) satisfied the minimum flexural strength requirement in terms of negative bending moment for railway sleepers as per EN 13230 standard. Further, the eco-mechanical performance of AAS concrete was superior with 29% less CO_2 footprint than the ordinary concrete.

2.8 Summary of literature review and research gap

From the review of literature, it is observed that in recent years, different studies have been conducted on the influence of various parameters such as combination of different binders, concentration of alkaline solution, alkaline solution to binder ratio, and sand-to-binder ratio etc., on various properties of geopolymer composites developed under ambient condition.

It is reported in the literature that the incorporation of GGBS in fly ash based geopolymer concrete (GPC) significantly improved the setting time and compressive strength under ambient curing condition with reduced workability. The addition of extra water somewhat helped to increase the workability but resulted in a strength reduction. Therefore, an optimum balance is required amongst the amount of GGBS, alkaline solution content and sodium silicate solution to sodium hydroxide solution ratio to achieve the desired setting time, workability and compressive strength of fly ash-GGBS based GPC.

From the review of literature, different studies reported about the mechanical and durability properties of geopolymer paste, mortar, and concrete made from fly ash and GGBS as precursor materials. Further, a few studies discussed about the microstructural development of fly ash/GGBS based geopolymer mortar and concrete developed under ambient condition, and after exposure to aggressive environment especially acidic exposure condition. It may be noted that most of the previous research works reported about the effect of binder type, alkali activator type and concentration, W/GPS ratio, and SS/SH ratio on compressive strength of geopolymer mortar. Further, some research works are reported in the literature on the influence of binder type, and alkali activator type and concentration on the performance of geopolymer mortar against exposure to sulfuric acid solution. However, the research works on the performance evaluation of fly ash-GGBS based geopolymer mortar in case of exposure to hydrochloric acid (HCl) solution are scanty.

In addition to the proportion of source materials, and concentration of alkaline solution, sand-to-binder ratio can also be directly related to the pore structure of geopolymer mortar. The review of the literature found little research work on the influence of sand-to-binder ratio and source materials on resistance against sulfate and acid attack and on the microstructural changes of geopolymer mortar. It is also reported in the literature that alkali activated binders made with different source materials such as rice husk ash, fly ash, palm oil fuel ash, and slag exhibited higher sorptivity as compared to OPC, which can be minimized by improving the compressive strength and making a dense microstructure by optimizing the properties of source materials and the mixture compositions of alkali activated binders. Therefore, it is essential to investigate the sorptivity of geopolymer mortar and concrete, which indicates the pore structure of the materials and its connectivity, and that influences the penetration of aggressive ions into the mortar and concrete to a greater extent, when exposed to aggressive environment.

In recent years, few research works in the literature reported about the durability performance of geopolymer composites in chloride-rich environment. As observed from the literature, for external exposure, geopolymer composites showed better performance with respect to chloride diffusion resistance and chloride-induced steel reinforcement corrosion in comparison to conventional concrete. Furthermore, the durability of geopolymer composites in chloride-rich environment is largely dependent on the aluminosilicate source materials, type and concentration of alkaline solution, and severity of exposure environment. From the available literature, it is noted that most of the research studies focused on chloride diffusion resistance and corrosion of steel bar due to ingress of chloride ions into geopolymer composites from external exposure environment. However, there are very few research works reported in the literature on the corrosion behaviour of steel reinforcement in geopolymer mortar or concrete admixed with chloride ions. Furthermore, the available research works on fresh and hardened properties, and microstructure of chloride admixed geopolymer concrete are scanty. It is reported in the literature that the combination of fly ash and slag in geopolymer composites alters the reaction phases, and microstructure, which exhibits different level of chloride binding and corrosion behaviour in comparison to the geopolymer composites made from only fly ash or slag. Therefore, there is a need to investigate the corrosion behaviour of steel reinforcement in geopolymer concrete prepared from varying combinations of fly ash and ground granulated blast furnace slag (GGBS) in the presence of chloride ions.

Keeping in view the aforementioned research gap in the literature, there is a need to investigate the effect of wide range of control parameters on fresh, mechanical, and various durability properties, and microstructure of fly ash-GGBS based geopolymer composites. To evaluate the effect of a wide range of control parameters at their different levels on the properties of geopolymer composites, a large number of experiments are required as per the traditional experimental design method, which consumes more time, and is expensive. However, an appropriate method of design of experiment can be selected to evaluate the influence of these parameters with a reduced number of experiments. Taguchi method is an efficient experimental design method for designing the parameters with a minimum number of test series. The optimum combination of different parameters to achieve an individual property (response) can be obtained by analysing the results using Taguchi method. In addition, Taguchi-Grey relational analysis (GRA) method can be used to achieve a single set of optimized level of different parameters for various properties

(responses) simultaneously. A very few studies have been undertaken in the literature on Taguchi method to optimize the mix parameters with respect to different properties of fly ash-GGBS based geopolymer composites. Further, the studies on multi-response optimization approach using Taguchi-GRA method to arrive at a single set of optimized level of mix parameters to achieve different properties of fly ash-GGBS based geopolymer composites simultaneously are scanty. Therefore, in the present research work, Taguchi method of design of experiment was used to design the mix compositions of fly ash-GGBS based geopolymer mortar and concrete mixes incorporating different control parameters (mix parameters) with their individual levels. Further, Taguchi-Grey relational analysis (GRA) method was used in the present research work to arrive at the optimal combination of mix parameters of geopolymer mortar and concrete with respect to multiple properties simultaneously.

In the present study, for the development of fly ash-GGBS based geopolymer mortar (GPM) under ambient curing condition, a wide range of control parameters namely GGBS replacement level, water-to-geopolymer solids (W/GPS) ratio, molarity of NaOH solution, and sand-to-binder (S/B) ratio were considered, and their effect on setting time, flowability, strength development, and various durability properties such as water absorption, apparent volume of permeable voids (AVPV), sorptivity, sulfate and acid resistance were evaluated. In addition, the microstructure evolution of geopolymer mortar at different ages and after exposure to different sulfate and acid solutions were analysed through XRD, EDS, FESEM, and FTIR analyses. Similarly, for the development of fly ash-GGBS based geopolymer concrete (GPC) under ambient curing condition, the control parameters considered were GGBS replacement level, water-to-geopolymer solids (W/GPS) ratio, molarity of NaOH solution, binder content, and sodium silicate solution to sodium hydroxide solution (SS/SH) ratio. Further, the influence of these control parameters on setting time, workability, and compressive strength of fly ash-GGBS based geopolymer concrete were evaluated. In addition, the effect of admixed chloride on workability, strength development, free and total chloride, and rebar corrosion in fly ash and fly ash-GGBS based geopolymer concrete (GPC) were investigated. The effect of fly ash/GGBS blends, and admixed chloride on microstructural changes at different ages, and at rebar level of geopolymer concrete were analyzed through XRD, EDS, FESEM and FTIR analyses.

2.9 Objectives of the present research work

The objectives of the present research work are as follows.

i. To design and develop fly ash-GGBS based geopolymer mortar (GPM) and geopolymer concrete (GPC) under ambient curing condition by Taguchi-Grey relational analysis (GRA) method.

ii. To study the influence of various control parameters such as GGBS replacement level, water-to-geopolymer solids ratio, molarity of NaOH solution, and sand-to-binder ratio on fresh, mechanical and durability properties of fly ash-GGBS based geopolymer mortar.

iii. To investigate the effect of GGBS replacement level, water-to-geopolymer solids ratio, molarity of NaOH solution, binder content, and mass ratio of sodium silicate to sodium hydroxide solution on fresh and mechanical properties of fly ash-GGBS based geopolymer concrete.

iv. To evaluate the influence of admixed chloride on workability, strength development, and corrosion behaviour of steel reinforcement in fly ash and fly ash-GGBS based geopolymer concrete.

v. To examine the effect of control parameters on variations in the microstructure of geopolymer mortar and concrete through XRD, EDS, FESEM and FTIR analyses, and to correlate the strength development and durability properties with changes in microstructure.

Experimental Program

3.1 General

This chapter describes about the materials used for preparation of geopolymer mortar (GPM) and geopolymer concrete (GPC) mixes, mix design methods, mix proportions of ingredients, details of specimens prepared and different test methods performed on geopolymer mortar and geopolymer concrete mixes. In this study, the experiments were conducted in two different series. In series 1, fly ash-GGBS based geopolymer mortar (GPM) mixes were designed and in series 2, fly ash-GGBS based geopolymer concrete (GPC) mixes were designed. In each series, various experiments were performed in two different phases.

3.2 Materials

3.2.1 Precursor materials

In this study, class F fly ash as per ASTM C618-2019 [109] and ground granulated blast furnace slag (GGBS) were used as precursor materials for the preparation of geopolymer mortar (GPM) and geopolymer concrete (GPC) mixes. The chemical composition of precursor materials (fly ash and GGBS) determined by X-ray fluorescence (XRF) technique are presented in Table 3.1.

Table 3.1 Chemical composition of precursor materials (fly ash and GGBS)

Source material	SiO_2	Al_2O_3	CaO	Fe_2O_3	MgO	K_2O	Na_2O	TiO_2	LOI*
Fly ash	48.96	24.48	2.69	4.59	0.81	1.03	0.03	1.9	0.43
GGBS	34.48	14.54	27.83	1.01	7.26	0.56	0	0.5	1.14

*Loss on ignition

The measured specific surface area of fly ash and GGBS based on Brunauer-Emmett-Teller (BET) method are 878 m^2/kg and 3066 m^2/kg respectively. The specific gravity of fly ash and GGBS measured as per IS 4031 (Part 11)-2019 [110] are 2.14 and 2.78 respectively. The particle size (d_{50}) of fly ash and GGBS measured using particle size analyser (Mastersizer 2000) are 24.98 µm and 23.89 µm respectively.

The micrographs of precursor materials obtained from the FESEM analysis are illustrated in Fig. 3.1 (a, b). The particles of fly ash are spherical and have smooth surface whereas the particles of GGBS are angular in shape and more irregular as evident from Fig. 3.1 (a, b). The XRD patterns of fly ash and GGBS are illustrated in Fig. 3.2. The fly ash consists

mainly of amorphous phases with some crystalline phases i.e., quartz, and mullite as evident from Fig. 3.2. The XRD patterns of GGBS indicated that it consists primarily of amorphous phases with a detectable crystalline peak of quartz and calcite. The elemental composition of precursor materials determined by EDS analysis are shown in Fig. 3.3 (a, b). The major elements found in fly ash are oxygen (O), silicon (Si), and aluminium (Al) whereas GGBS mostly contains oxygen (O), silicon (Si), aluminium (Al), calcium (Ca), and magnesium (Mg). The chemical bonds in precursor materials identified by FTIR analysis are shown in Fig. 3.4. A broad spectrum was observed in fly ash, which might be because of the glassy nature of this material [105]. The main vibration band was at 1090 cm^{-1} for fly ash and at 996 cm^{-1} for GGBS, which is attributed to the asymmetric stretching vibration of Si-O-Si(Al) bonds [40,111]. The difference in the main band can be expected because of different glassy network of fly ash and GGBS [112]. In fly ash, peak at 694 cm^{-1} is ascribed to the symmetric stretching of Si-O-Si whereas peak at 518 cm^{-1} is associated with bending vibration of Si-O [40]. These bands indicate that quartz and mullite are present in fly ash [40,112]. Similarly, in GGBS, the bands at 713 cm^{-1} indicate Al-O bonds in the AlO_4 group [106] and the peak at 461 cm^{-1} is due to the bending vibration of Si-O-Si bonds [111]. The band at 1492 cm^{-1} in GGBS is ascribed to the CO_3^{2-} groups, which may be due to calcium carbonate in the form of calcite [106]. Calcite was also identified in the XRD pattern of GGBS (Fig. 3.2). The band at 1620 cm^{-1} for fly ash and at 1640 cm^{-1} for GGBS are ascribed to the bending vibration of H-O-H group, whereas the band at 3430 cm^{-1} for fly ash and at 3425 cm^{-1} for GGBS are ascribed to the stretching vibration of -OH group of adsorbed water [113].

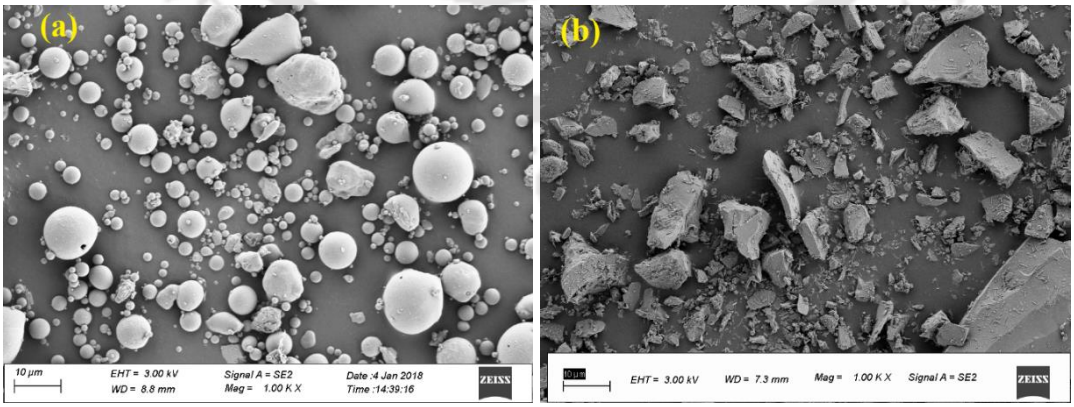

Fig. 3.1 FESEM micrographs of (a) fly ash and (b) GGBS.

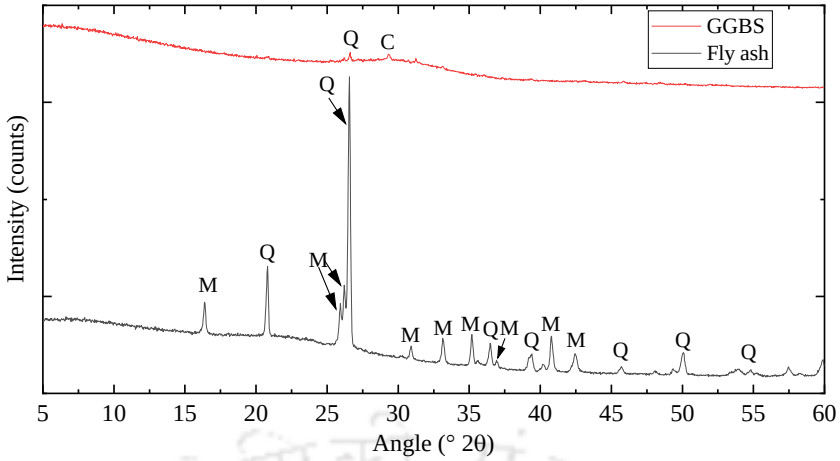

Fig. 3.2 XRD patterns of fly ash and GGBS (Q: Quartz, C: Calcite, M: Mullite).

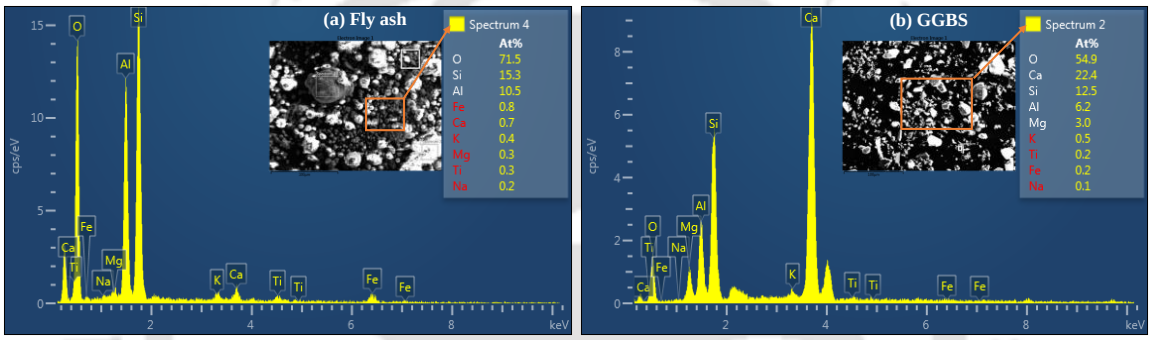

Fig. 3.3 EDS spectra of (a) fly ash and (b) GGBS.

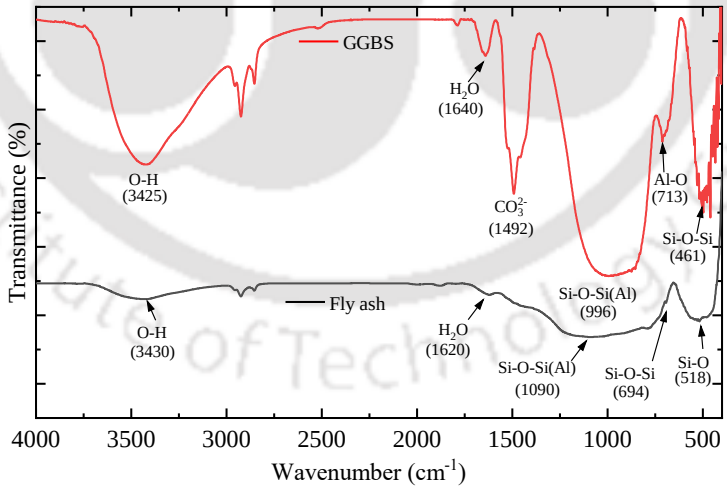

Fig. 3.4 FTIR spectra of fly ash and GGBS.

3.2.2 Alkaline solution

The combination of sodium hydroxide (NaOH) solution (SH) and sodium silicate (Na_2SiO_3) solution (SS) was used as alkaline solution for the preparation of GPM and GPC mixes. Commercially available sodium hydroxide pellets and sodium silicate solution were

used in the present work. The sodium silicate solution contained 26.5% SiO_2, and 8% Na_2O. The sodium hydroxide solution was prepared 48 hours before the preparation of GPM and GPC mixes as per the required molarity by dissolving NaOH pellets in potable water available in the laboratory. Sodium silicate solution was added with sodium hydroxide solution, 24 hours prior to the preparation of mixes, based on the alkaline solution content and SS/SH of the mixes.

3.2.3 Fine and coarse aggregates

Locally available river sand confirming to grading zone II as per the specification mentioned in IS 383-2021 [114] was used as fine aggregate in the preparation of GPM and GPC mixes. The particle size distribution curve of sand is shown in Fig. 3.5 (a). The measured values of specific gravity and fineness modulus of sand were 2.62, and 2.46 respectively. Coarse aggregates of 20 mm MSA (maximum size of aggregate) and 10 mm MSA were used for the preparation of GPC mixes. The measured values of specific gravity of 10 mm MSA and 20 mm MSA coarse aggregates were 2.65 each. The particle size distribution curves of 10 mm MSA and 20 mm MSA coarse aggregates are shown in Fig. 3.5 (b), and Fig. 3.5 (c) respectively.

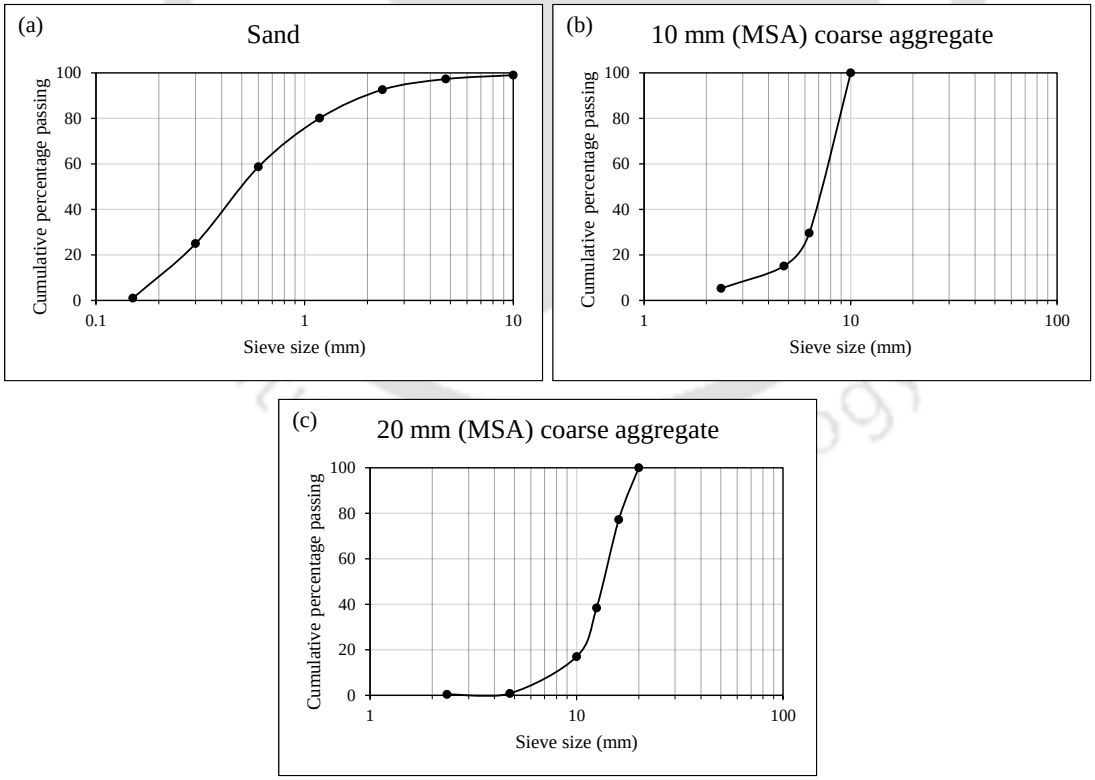

Fig. 3.5 Particle size distribution curve of (a) sand, (b) 10 mm (MSA) coarse aggregate, and (c) 20 mm (MSA) coarse aggregate.

3.2.4 Sulfate solutions, acid solutions, and chloride ions

In the present study, two types of sulfate solution such as sodium sulfate (Na_2SO_4) and magnesium sulfate ($MgSO_4$) solutions, and two types of acid solution such as sulfuric acid (H_2SO_4) and hydrochloric acid (HCl) solutions were used to investigate the resistance of geopolymer mortar (GPM) against sulfate and acid exposure environment. Sodium chloride (NaCl) was used as the source of chloride ions to examine its influence on workability, compressive strength and steel reinforcement corrosion in GPC mixes.

3.2.5 Steel bar for reinforced GPC specimens

Tempcore TMT (Thermomechanically treated) steel bar of diameter 12 mm was used as the steel reinforcement for making cylindrical reinforced geopolymer concrete (GPC) specimens. The elemental composition of steel reinforcement measured by EDS analysis is presented in Table 3.2.

Table 3.2 Elemental composition of steel reinforcement

Element	C	S	Fe	Si	Cu
Wt. %	52.4	30.2	13.1	3.2	1.1

3.3 Fly ash-GGBS based geopolymer mortar (GPM) mixes (Series 1)

The layout of experimental program for fly ash-GGBS based geopolymer mortar (GPM) is illustrated in Fig. 3.6. In 1st phase of fly ash-GGBS based geopolymer mortar (GPM) series, the mix design of GPM was carried out by Taguchi method of design of experiment (L_9 orthogonal array) by considering four control parameters namely GGBS replacement level (%), water-to-geopolymer solids (W/GPS) ratio, molarity of NaOH solution, and sand-to-binder (S/B) ratio with three levels each as mentioned in Fig. 3.6. After conducting various tests (as mentioned in Fig. 3.6) on the GPM mixes derived from Taguchi method of design of experiment, the studied parameters were optimized by Taguchi-Grey relational analysis (GRA) method. Further, the verification experiments were conducted on the GPM mix with optimized level of control parameters. In 2nd phase of GPM series, another set of mix proportion was formulated by considering the most influential parameters evaluated in the 1st phase of GPM series, and the experiments (except setting time) conducted in 1st phase of GPM series were carried out again in the 2nd phase of GPM series. The microstructure analysis was conducted on GPM mixes in 1st phase as well as in 2nd phase of GPM series (Fig. 3.6).

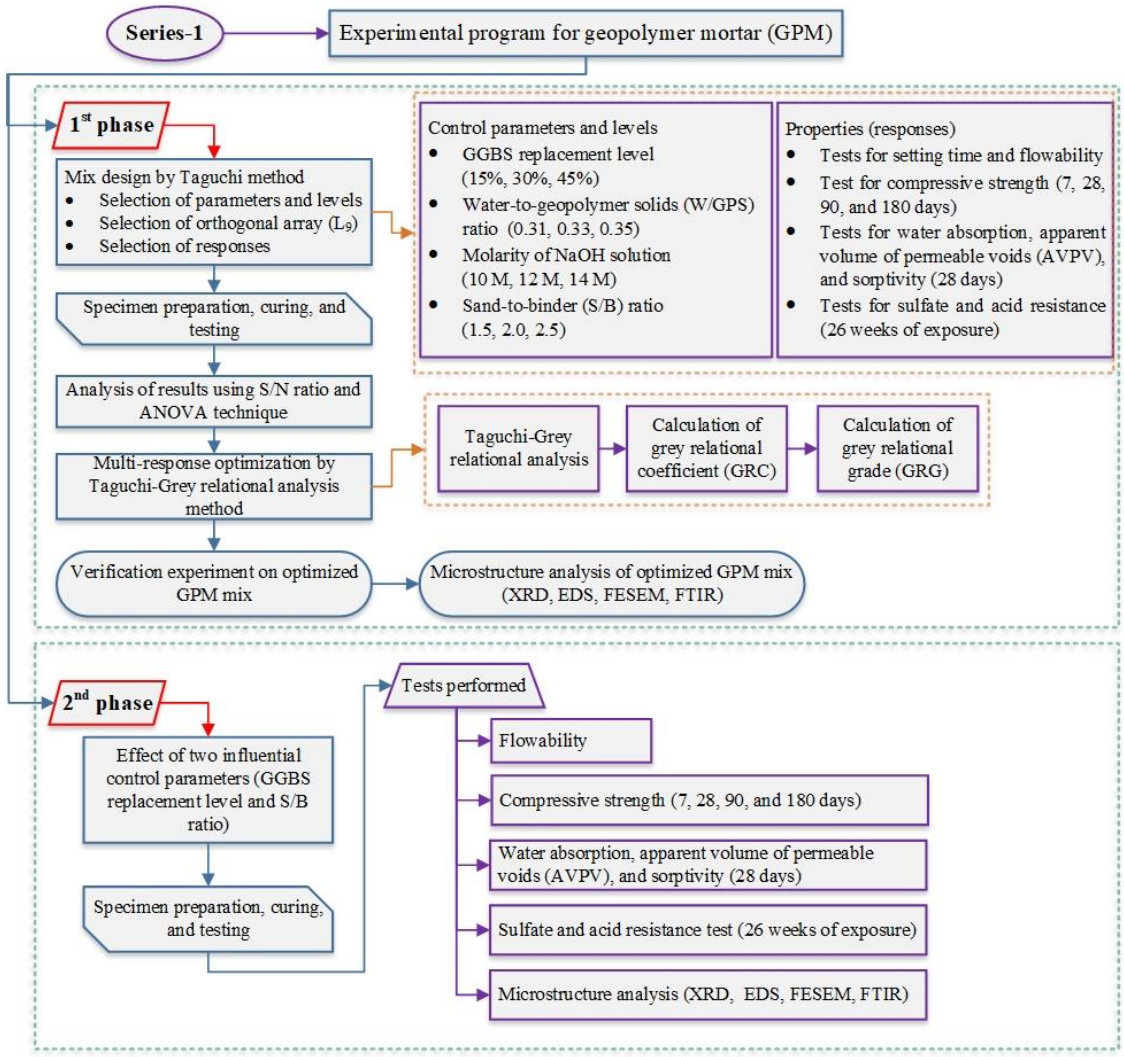

Fig. 3.6 Layout of experimental program for fly ash-GGBS based geopolymer mortar (GPM).

3.3.1 Design of experiment

The steps involved in the Taguchi method of design of experiment are as follows;

(1) Selection of parameters and their corresponding levels.

(2) Selection of appropriate orthogonal array by Taguchi method and the arrangement of selected parameters and their levels.

(3) Conducting the experiments on geopolymer mixes selected as per the Taguchi method of experimental design.

(4) Calculation of signal-to-noise (S/N) ratio of the experimental results and analysis using ANOVA (Analysis of variance) technique.

(5) Adopting Taguchi-GRA (Grey relational analysis) method to optimize the multiple properties simultaneously.

(6) Conducting verification experiments on the optimized geopolymer mixes.

Keeping in view the dependence of fly ash-GGBS based GPM properties on different parameters, GGBS replacement level (% by mass of total binder content), water-to-geopolymer solids (W/GPS) ratio, molarity of NaOH solution (M), and sand-to-binder (S/B) ratio were selected for the experimental design. For geopolymer mortar (GPM) mixes, three levels were selected for each parameter. As per the full factorial design method, a total of 81 (i.e., $Level^{Parameter}$: 3^4) experimental combinations are required to investigate the effect of each parameter, which is certainly a time-consuming process and not economical. Therefore, in this investigation, Taguchi method [115] of experimental design was adopted to examine the influence of varying levels of mix parameters on the properties (responses) of GPM with reduced number of experiments and to arrive at the best possible combination of these parameters to achieve the optimum result.

In Taguchi method, the orthogonal array can be selected as per the total degrees of freedom of all parameters, which depends on the levels of each parameter and is calculated using the following equation [115];

$$DOF = l - 1 \tag{3.1}$$

Where *DOF* and *l* represent the degree of freedom and number of levels of each parameter respectively. In the present study, four parameters with three levels each were considered. Thus, each parameter has a degree of freedom equal to two with total degrees of freedom of all the parameters equal to 8. Keeping this in view, a design of L_9 orthogonal array (OA) as per Taguchi method was considered for the experiment, which has the same degree of freedom (i.e., 8). The selected parameters and their corresponding levels used in Taguchi method of experimental design for GPM mixes are presented in Fig. 3.6. The experimental series for GPM mixes as per L_9 orthogonal array is presented in Table 3.3.

Table 3.3 Experimental series for fly ash-GGBS based GPM as per L_9 orthogonal array (Taguchi method)

Mix	GGBS replacement level (%)	W/GPS ratio	Molarity of NaOH solution	Sand-to-binder (S/B) ratio
M1	15	0.31	10 M	1.5
M2	15	0.33	12 M	2
M3	15	0.35	14 M	2.5
M4	30	0.31	12 M	2.5
M5	30	0.33	14 M	1.5
M6	30	0.35	10 M	2
M7	45	0.31	14 M	2
M8	45	0.33	10 M	2.5
M9	45	0.35	12 M	1.5

The properties such as setting time, flowability, compressive strength, water absorption, apparent volume of permeable voids (AVPV), sorptivity, sulfate and acid resistance of fly ash-GGBS based GPM were studied. In Taguchi approach, the results were analyzed by the signal-to-noise (S/N) ratio and ANOVA technique. The S/N ratio is a performance characteristics, which considers both the average value and standard deviation of the experimental results, instead of only the average value [116]. There are three categories of performance characteristics such as "larger-the-better", "smaller-the-better" and "nominal-the-better". An appropriate category of performance characteristics must be selected depending on the objective of the properties to be studied [115,117]. In the present study, the S/N ratio of "larger-the-better" performance characteristics was selected for flowability, compressive strength at different ages of ambient curing, and compressive strength after exposure to sulfate and acid solutions whereas "smaller-the-better" performance characteristics was selected for setting time, water absorption, apparent volume of permeable voids (AVPV), and sorptivity of geopolymer mortar. It is to be noted that, based on the obtained results of initial and final setting time, "smaller-the-better" performance characteristics was selected for setting time of GPM. The S/N ratio for "larger-the-better" and "smaller-the-better" performance characteristics were calculated by using the following equations [118].

Larger-the-better, $Y_{ij} = -10 \times \log\left[\frac{1}{r}\sum_{k=1}^{r}\frac{1}{v_{ijk}^2}\right]$ (3.2)

Smaller-the-better, $Y_{ij} = -10 \times \log\left[\frac{1}{r}\sum_{k=1}^{r} v_{ijk}^2\right]$ (3.3)

Where Y_{ij} represents the S/N ratio of i^{th} experiment for j^{th} response, v_{ijk} denotes the result of i^{th} experiment for j^{th} response in the k^{th} replication, and r denotes number of replications. Analysis of variance (ANOVA) was conducted on the obtained S/N ratio to evaluate the influence of the parameters on each response. Since the F-value could not be calculated because of over fitted design (i.e., the degree of freedom of error was zero) [115], the contribution of each parameter on various properties of GPM was estimated by calculating the percentage of sum of squares of the studied parameter with respect to the total sum of squares of all the parameters [105]. Further, the mean S/N ratio for each response (property) with respect to a given level of a parameter was calculated to arrive at a set of optimal combination of the parameters for individual properties. Subsequently, Taguchi-GRA method was used to achieve a single optimal combination of the parameters with respect to

multiple responses. Firstly, the S/N ratio of each response was transformed into a normalized value using the following equation [117,119].

$$Z_{ij} = \frac{Y_{ij} - \min(Y_{ij})}{\max(Y_{ij}) - \min(Y_{ij})} \; ; \quad i = 1, 2, \ldots, m \quad j = 1, 2, \ldots, n \tag{3.4}$$

Where Z_{ij} is the normalized S/N ratio of i^{th} experiment for j^{th} response [118–120].

Then, the grey relational coefficient was computed using the following equation [117–119].

$$GRC_{0ij} = \frac{\Delta_{min} + \zeta \Delta_{max}}{\Delta_{0ij} + \zeta \Delta_{max}} \tag{3.5}$$

Where GRC_{0ij} represents the grey relational coefficient of i^{th} experiment for j^{th} response.

Δ_{0ij}= difference between the ideal value of normalized S/N ratio (Z_{0j}) and the normalized S/N ratio (Z_{ij})

$\Delta_{min} = min_{\forall i} min_{\forall j} \Delta_{0ij}$ and $\Delta_{max} = max_{\forall i} max_{\forall j} \Delta_{0ij}$

ζ = identification coefficient or distinguishing coefficient that ranges between 0 and 1, and is usually set as 0.5 [117,118,120].

Finally, the grey relational grade was computed using the equation below.

$$GRG_{0i} = \sum_{j=1}^{n} \omega_j GRC_{0ij} \; ; \; i = 1,2, \ldots, m \tag{3.6}$$

Where GRG_{0i} represents the grey relational grade of i^{th} experiment, ω_j represents the normalized non-negative weight assigned to j^{th} response, and $\sum_{j=1}^{n} \omega_j$ is equal to 1 [118,120]. In the present research work, equal weight was assigned to all the properties (responses) considered in the study.

3.3.2 Mix proportions and preparation of specimens in 1st phase of experiment on fly ash-GGBS based geopolymer mortar (GPM)

The mix quantities of ingredients of fly ash-GGBS based geopolymer mortar (GPM) mixes prepared in 1st phase of experiment are presented in Table 3.4. The SS/SH ratio (sodium silicate solution to sodium hydroxide solution ratio) was kept constant at 1.5 for all geopolymer mortar mixes. Based on the combination of W/GPS ratio, molarity of NaOH solution, and S/B ratio obtained from the Taguchi method of experimental design at constant SS/SH ratio, the quantity of total binder content of each mix was calculated. Subsequently, the quantities of fly ash and GGBS based on GGBS replacement level (%),

NaOH solution, Na_2SiO_3 solution, and sand content of each GPM mix were calculated. A planetary mixer (4.75 l capacity) was used to prepare geopolymer mortar mixes. The mixing procedure of mortar was completed in about 7 minutes as shown in Fig. 3.7. First, the precursor materials (fly ash and GGBS) were mixed for 2 minutes in dry condition in the mixer followed by mixing with sand for another 2 minutes. Then, the alkaline solution, which was prepared 24 hours prior to mixing, was added gradually to the dry mixture in the mortar mixer and the mixing was continued for 3 minutes till a homogeneous mix was obtained. Immediately after preparation, the flow table test was conducted on the fresh GPM mix as per ASTM C1437-2020 [121]. Subsequently, the fresh mortar mix was poured into cube (50 mm size), and cylindrical (100 mm diameter × 200 mm height) moulds. The fresh mortar was poured into cube moulds in two layers while compacting each layer for 30 seconds on a vibrating table. Similarly, the fresh mortar was poured into cylindrical moulds in three layers with each layer compacted for 30 seconds on the vibrating table. From a given geopolymer mortar mix, three replicate cube specimens (50 mm size) each were prepared for compressive strength test at different ages of ambient curing, water absorption and AVPV tests, sulfate and acid resistance tests. For sorptivity test, one cylindrical specimen (100 mm diameter × 200 mm height) was prepared from each mix. After 24 hours of casting, all the specimens were demoulded and kept in ambient laboratory condition until testing. After 28 days of ambient curing, the cylindrical specimens were cut into four pieces of size 100 mm diameter × 50 mm height, out of which 3 pieces were used for sorptivity test. The details of specimens prepared for different tests conducted in 1st phase of experiment for geopolymer mortar are presented in Table 3.5.

Table 3.4 Mix quantities of ingredients of GPM prepared in 1st phase of experiment

Mix	Binder content (kg/m^3)		Fine aggregate (kg/m^3)	Alkaline solution (kg/m^3)	
	Fly ash	GGBS		NaOH solution	Na_2SiO_3 solution
M1	599.31	105.76	1057.60	154.93	232.40
M2	504.90	89.10	1187.99	147.21	220.81
M3	435.46	76.85	1280.78	142.76	214.15
M4	369.38	158.30	1319.20	121.25	181.87
M5	478.18	204.93	1024.67	176.89	265.33
M6	414.01	177.43	1182.87	150.28	225.42
M7	328.52	268.79	1194.62	143.23	214.84
M8	288.99	236.45	1313.61	124.38	186.57
M9	373.51	305.60	1018.67	180.89	271.33

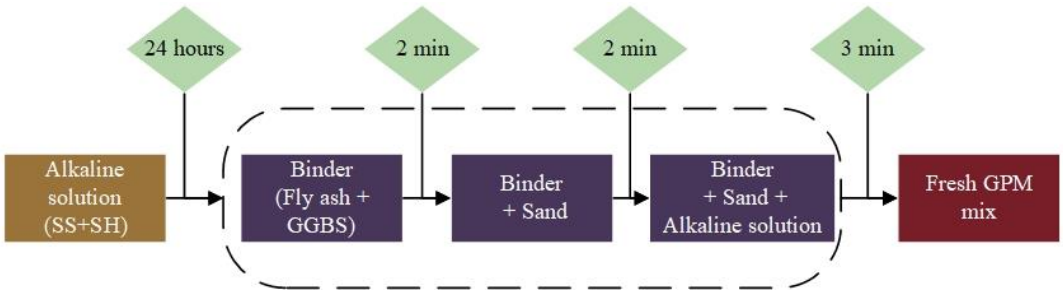

Fig. 3.7 Mixing sequence of ingredients of geopolymer mortar.

Table 3.5 Details of specimens prepared for different tests conducted in 1st phase of experiment on geopolymer mortar

Test details	Specimen	Testing age/exposure period	No. of specimens
Compressive strength	Cube specimen of size 50 mm	7, 28, 90, and 180 days	108
Water absorption and AVPV	Cube specimen of size 50 mm	28 days	27
Sorptivity	Cylindrical specimen of size 100 mm diameter × 50 mm height	28 days	27
Sulphate and acid resistance test	Cube specimen of size 50 mm	Exposure period: 26 weeks (182 days) Exposure solutions: Na_2SO_4 solution (3% and 6%), $MgSO_4$ solution (3% and 6%), H_2SO_4 solution (0.31 mol/l and 0.62 mol/l), HCl solution (0.31 mol/l and 0.62 mol/l), and Normal water	243
Total specimens	Cube specimen of size 50 mm		378
	Cylindrical specimen of size 100 mm diameter × 50 mm height		27

3.3.3 Tests performed in 1st phase of experiment on fly ash-GGBS based geopolymer mortar (GPM)

3.3.3.1 Setting time of GPM

The penetration resistance method described in ASTM C403/C403M-2016 [122] was used to determine the initial and final setting time of geopolymer mortar. The fresh geopolymer mortar mix was poured into 150 mm size cube mould. To obtain the penetration resistance of mortar, at least six penetration readings were taken on the specimen using the loading apparatus and different penetration needles with bearing surface area of 645 mm^2, 323 mm^2, 161 mm^2, 65 mm^2, 32 mm^2, and 16 mm^2. The force required to penetrate the specimen up

to 25 mm and the corresponding elapsed time (measured after initial contact of binder with the alkaline solution till the time of application of penetration needle) were recorded. The penetration resistance at a given time was calculated by dividing the recorded force by the bearing surface area of the needle. Then, the initial and final setting time of each mortar mix were determined as the time corresponding to the penetration resistance of 500 psi (3.5 MPa) and 4000 psi (27.6 MPa) respectively.

3.3.3.2 Flowability of GPM

Flowability of fresh GPM mix was measured by flow table test in accordance with ASTM C1437-2020 [121]. In the present study, flow table test was conducted three times for each mix and the average flow index value was reported. The fresh GPM mix was placed into the flow mould in two layers while tamping 20 times each layer. Then, the mould was lifted and immediately, the flow table was dropped 25 times in 15 seconds. The spread diameter along the four lines inscribed on top of the flow table was measured and the average value was reported.

The flow index of geopolymer mortar was computed as follows:

$$FI\ (\%) = \frac{FD-ID}{ID} \times 100 \qquad (3.7)$$

Where, *FI*: flow index expressed in %, *FD*: average of four spread diameter in mm, and *ID*: internal base diameter of the mould, in mm.

3.3.3.3 Compressive strength of GPM

The compressive strength of GPM was measured at the ages of 7, 28, 90, and 180 days of ambient curing from the day of preparation in a compression testing machine as per ASTM C109/C109M-2021 [123]. For each mix, three replicate cubes were tested at a given age.

3.3.3.4 Water absorption and apparent volume of permeable voids (AVPV) of GPM

Tests for water absorption and apparent volume of permeable voids (AVPV) were conducted on 28 days ambient cured GPM cube specimens as per the procedure described in ASTM C642-2013 [124]. For each mix, the average value of three replicate cube specimens was reported as the water absorption and apparent volume of permeable voids. The cube specimens were first kept in an oven at 110°C for 48 hours and after that, the oven dry weight (W_D) was measured. Subsequently, the cube specimens were immersed in water at ambient temperature for 48 hours. After removing from water, the surface moisture

of cube specimen was wiped with a towel and the surface dry weight (W_S) was measured. The water absorption (WA) value was calculated as follows:

$$WA\ (\%) = \frac{W_S - W_D}{W_D} \times 100 \quad (3.8)$$

In order to determine the apparent volume of permeable voids, the same cube specimens (saturated cube specimens from water absorption test) after measuring W_S were subjected to boiling in water for 5 hours and subsequently left in air for 24 hours to cool down to room temperature by natural loss of heat. Subsequently, the surface-dry weight (W_B) of the specimen in air (after immersion and boiling) was measured. After that, the cube specimen was suspended in water by a wire and the apparent weight (W_{AP}) of cube specimen in water was measured. The apparent volume of permeable voids ($AVPV$) was calculated as follows:

$$AVPV\ (\%) = \frac{W_B - W_D}{W_B - W_{AP}} \times 100 \quad (3.9)$$

3.3.3.5 Sorptivity of GPM

The sorptivity test was carried out on three cylindrical specimens (100 mm diameter and 50 mm height) of a given GPM mix after 28 days of ambient curing following the guidelines mentioned in ASTM C1585-2020 [125] and the average value of three cylindrical specimens was reported as the sorptivity coefficient. Three replicate specimens from each GPM mix were dried in an oven at 50°C for 3 days. After 3 days, the specimens were cooled down to room temperature and subsequently, the specimens were placed in airtight polyethylene storage containers and left again in room temperature for 15 days for equilibration of moisture distribution within the specimen. After that, the specimens were removed from the storage containers and the side surface of each specimen was sealed with non-absorbent vinyl tape in order to allow the absorption of water only through the bottom surface of the specimen. The top surface of the specimen was covered with a plastic sheet. The initial weight of the sealed specimen was measured before immersing it partially into water in a pan with water level of 2 - 3 mm above the base of the specimen. The photographs during oven drying, pre-conditioning, and sorptivity test of GPM specimens are shown in Fig. 3.8. Further, the schematic diagram of test setup for sorptivity test is shown in Fig. 3.9. The capillary water absorption was determined at specific time intervals as mentioned in ASTM C1585-2020 [125] up to 8 days by measuring the weight of the specimen. During each weight measurement, the specimens were removed from the pan and surface was

wiped off by cloth and the weight was measured with the whole operation completed within 30 seconds. The sorptivity coefficient was calculated as follows:

$$S = \frac{I}{t^{1/2}} \tag{3.10}$$

Where, S = sorptivity coefficient, t = time, and I = water absorption, which is calculated as follows:

$$I = \frac{m_t}{a \times d} \tag{3.11}$$

Where, m_t = change in mass of the specimen in grams at time t, a = exposed area of the specimen in mm^2, and d = density of water in g/mm^3.

Fig. 3.8 Photographs during (a) oven drying, (b) pre-conditioning, and (c) sorptivity test of GPM specimens.

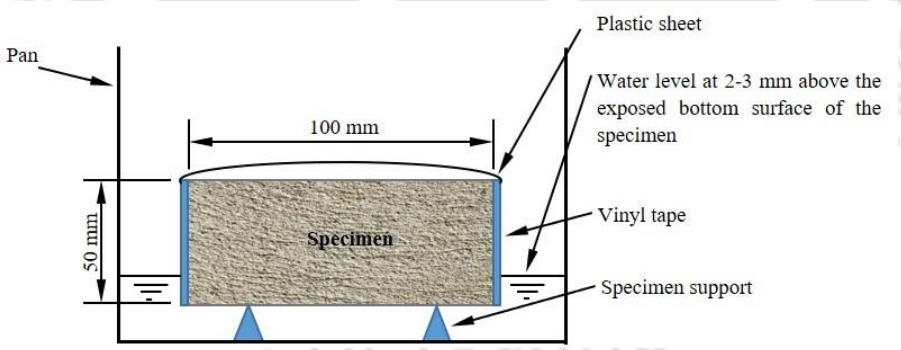

Fig. 3.9 Schematic diagram of test setup for sorptivity test on geopolymer mortar (GPM).

3.3.3.6 Sulfate and acid resistance of GPM

For sulfate resistance test, the GPM cube specimens (size 50 mm) cured in ambient condition for 28 days were immersed fully in different concentrations (3 wt.% and 6 wt.%) of Na_2SO_4, and $MgSO_4$ solutions for a period of 26 weeks. For acid resistance test, the GPM cube specimens were immersed fully in different concentrations (0.31 mol/l, and 0.62 mol/l) of H_2SO_4, and HCl solutions for a period of 26 weeks. For comparison purpose, the companion cube specimens from each GPM mix were immersed in water. In order to

maintain the concentration, the exposure solutions were replenished at every two weeks interval till the end of exposure period of 26 weeks. From each GPM mix, three replicate cube specimens were immersed in each type of exposure solution. The photograph of GPM cube specimens immersed in different sulfate and acid solutions are shown in Fig. 3.10. The compressive strength of GPM specimens immersed in different sulfate and acid solutions were determined at the end of exposure period of 26 weeks. Subsequently, the changes in compressive strength of the GPM specimens exposed to these solutions were calculated with respect to the compressive strength of GPM specimens exposed to water to evaluate the sulfate and acid resistance of geopolymer mortar.

(a)

(b)

Fig. 3.10 Photograph of GPM specimens immersed in different (a) sulfate and (b) acid solutions.

3.3.3.7 Microstructure analysis of GPM

The microstructure analyses such as X-ray diffraction (XRD), energy-dispersive X-ray spectroscopy (EDS), field emission scanning electron microscope (FESEM), and Fourier-transform infrared (FTIR) spectroscopy analyses were conducted on the optimized GPM mix. The XRD and FTIR analyses were carried out on GPM powder samples collected after compressive strength test on cube specimens. After completion of compressive strength test, the crushed samples of GPM mixes were further pulverized in a jaw crusher. Subsequently, the crushed materials were passed through a sieve having 75 µm square openings, and the sieved material was then kept inside air tight plastic bags in a desiccator. The FESEM and EDS analyses were carried out on the GPM chunk samples of approximate size of 3 mm × 3 mm collected after compressive strength test. It may be noted that in case

of exposure of GPM specimens to sulfate and acid solutions, the EDS analysis (elemental compositions) and FESEM analysis (morphology) were conducted on the chunk samples collected from the deteriorated surfaces of the specimens after compressive strength test. The procedure followed for microstructure analysis of GPM mix is discussed below.

3.3.3.7.1 XRD analysis

The XRD analysis was performed on the GPM powder samples using Rigaku SmartLab 9 kW model X-ray diffractometer with CuKα radiation (λ = 1.5405 Å). The powder samples were analyzed from 5º to 60º 2θ at step size of 0.03º 2θ. The phases obtained from the XRD analysis were identified on the basis of the match score of peak intensity and peak position using the standard database.

3.3.3.7.2 EDS analysis

The EDS analysis was conducted to identify the elemental composition of GPM mixes. For EDS analysis, FESEM (ZEISS Gemini) coupled with Oxford EDS instrument was used with an accelerating voltage of 15 kV. The elemental compositions (atomic %) of GPM mixes were collected from five locations (areas selected within the paste regions, which mostly exclude sand and unreacted precursor particles) to analyze the gel composition of GPM mixes at different ambient curing ages as well as for different exposure environment.

3.3.3.7.3 FESEM analysis

The morphology of GPM mixes was examined using the FESEM instrument: ZEISS (model: Gemini). The chunk sample collected from GPM specimen was mounted on a stub over carbon tape. Subsequently, the mortar chunk was coated with a thin layer of gold by sputtering method. The morphology of GPM sample was observed with in-lens mode.

3.3.3.7.4 FTIR analysis

The functional groups related to the compounds formed in the GPM mix were characterized by FTIR analysis. The FTIR analysis was carried out using PerkinElmer Spectrum Two FTIR spectrometer in transmission mode with wavenumber ranging from 400 cm^{-1} to 4000 cm^{-1} at a scan resolution of 5 scans per spectrum. The sample for FTIR analysis was prepared using KBr pellet method where 3 mg of GPM powder (after passing through 75 µm sieve) was mixed with 250 mg of potassium bromide (KBr).

3.3.4 Mix proportions, and preparation of specimens in 2nd phase of experiment on fly ash-GGBS based geopolymer mortar (GPM)

After 1st phase of experiment on GPM mixes, it was observed that most of the studied properties were significantly influenced by two parameters such as GGBS replacement

level and sand-to-binder (S/B) ratio. Therefore, the effect of these two parameters were further studied in the 2nd phase of the experiment by preparing the GPM mixes where the GGBS replacement level and sand-to-binder (S/B) ratio were varied in the optimized mix (obtained from 1st phase of experiment). The mix quantities of ingredients of GPM mixes prepared in 2nd phase of experiment are presented in Table 3.6. The same type of test specimens as used in the 1st phase of experiment were prepared separately from the above GPM mixes. The details of specimens prepared for different tests conducted in 2nd phase of experiment for GPM are presented in Table 3.7.

Table 3.6 Mix quantities of ingredients of GPM prepared in 2nd phase of experiment

Mix	Binder content (kg/m^3)		Fine aggregate (kg/m^3)	Alkaline solution (kg/m^3)	
	Fly ash	GGBS		NaOH solution	Na_2SiO_3 solution
M1 (FA85/G15, S/B1.5)	589.6	104.1	1040.5	166.3	249.5
M2 (FA70/G30, S/B1.5)	485.6	208.1	1040.5	166.3	249.5
M3 (FA55/G45, S/B1.5)	381.5	312.2	1040.5	166.3	249.5
M4 (FA55/G45, S/B2.0)	286.1	234.1	1040.5	166.3	249.5
M5 (FA55/G45, S/B2.5)	228.9	187.3	1040.5	166.3	249.5

Table 3.7 Details of specimens prepared for different tests conducted in 2nd phase of experiment on geopolymer mortar

Test details	Specimen	Testing age/exposure period	No. of specimens
Compressive strength	Cube specimen of size 50 mm	7, 28, 90, and 180 days	60
Water absorption and apparent volume of permeable voids (AVPV)	Cube specimen of size 50 mm	28 days	15
Sorptivity	Cylindrical specimen of size 100 mm diameter × 50 mm height	28 days	15
Sulphate and acid resistance test	Cube specimen of size 50 mm	Exposure period: 26 weeks (182 days) Exposure solutions: Na_2SO_4 solution (3% and 6%), $MgSO_4$ solution (3% and 6%), H_2SO_4 solution (0.31 mol/l and 0.62 mol/l), HCl solution (0.31 mol/l and 0.62 mol/l), and Normal water	135
Total specimens	Cube specimen of size 50 mm		210
	Cylindrical specimen of size 100 mm diameter × 50 mm height		15

3.3.5 Tests performed in 2nd phase of experiment on fly ash-GGBS based geopolymer mortar (GPM)

The tests such as flowability, compressive strength, water absorption, apparent volume of permeable voids (AVPV), sorptivity, sulfate and acid resistance test, and microstructure analyses as mentioned in 1st phase of experiment (Section 3.3.3) were also performed on the GPM mixes prepared in 2nd phase of experiment. It may be noted that in 2nd phase of experiment, the sulfate and acid resistance of geopolymer mortar were evaluated in terms of visual observation, change in weight, and change in compressive strength of the specimens immersed in different exposure solutions. The initial weight of each specimen was recorded before immersion in the exposure solution. At the end of every two weeks, the specimens were removed from the exposure solution and were visually observed to check the surface deterioration of the specimens if any followed by wiping the surface with a towel. After that, the specimens were kept for one hour in ambient condition for drying followed by measuring the weight of the specimens. The percentage change in weight of the specimen was calculated with respect to its initial weight.

3.4 Fly ash-GGBS based geopolymer concrete (GPC) mixes (Series 2)

The layout of experimental program for fly ash-GGBS based geopolymer concrete (GPC) is illustrated in Fig. 3.11. In 1st phase of fly ash-GGBS based geopolymer concrete (GPC) series, the mix design of GPC mixes was carried out by Taguchi method of design of experiment. Keeping in view the dependence of fly ash-GGBS based geopolymer concrete properties on different parameters, the GGBS replacement level (% by mass of total binder content), W/GPS ratio, molarity of NaOH solution (M), binder content (kg/m^3), and SS/SH ratio were selected for the experimental design. In this study, for each parameter, four levels were selected. The same procedure as followed in case of geopolymer mortar (Section 3.3.1) was used for selection of orthogonal array for GPC in Taguchi method of design of experiment. Based on the parameters and levels, a design of L_{16} orthogonal array as per Taguchi method was considered for the experiment. The selected parameters and their corresponding levels used in Taguchi method of experimental design for geopolymer concrete (GPC) are presented in Fig. 3.11. The experimental series for GPC as per L_{16} orthogonal array (Taguchi method) is presented in Table 3.8.

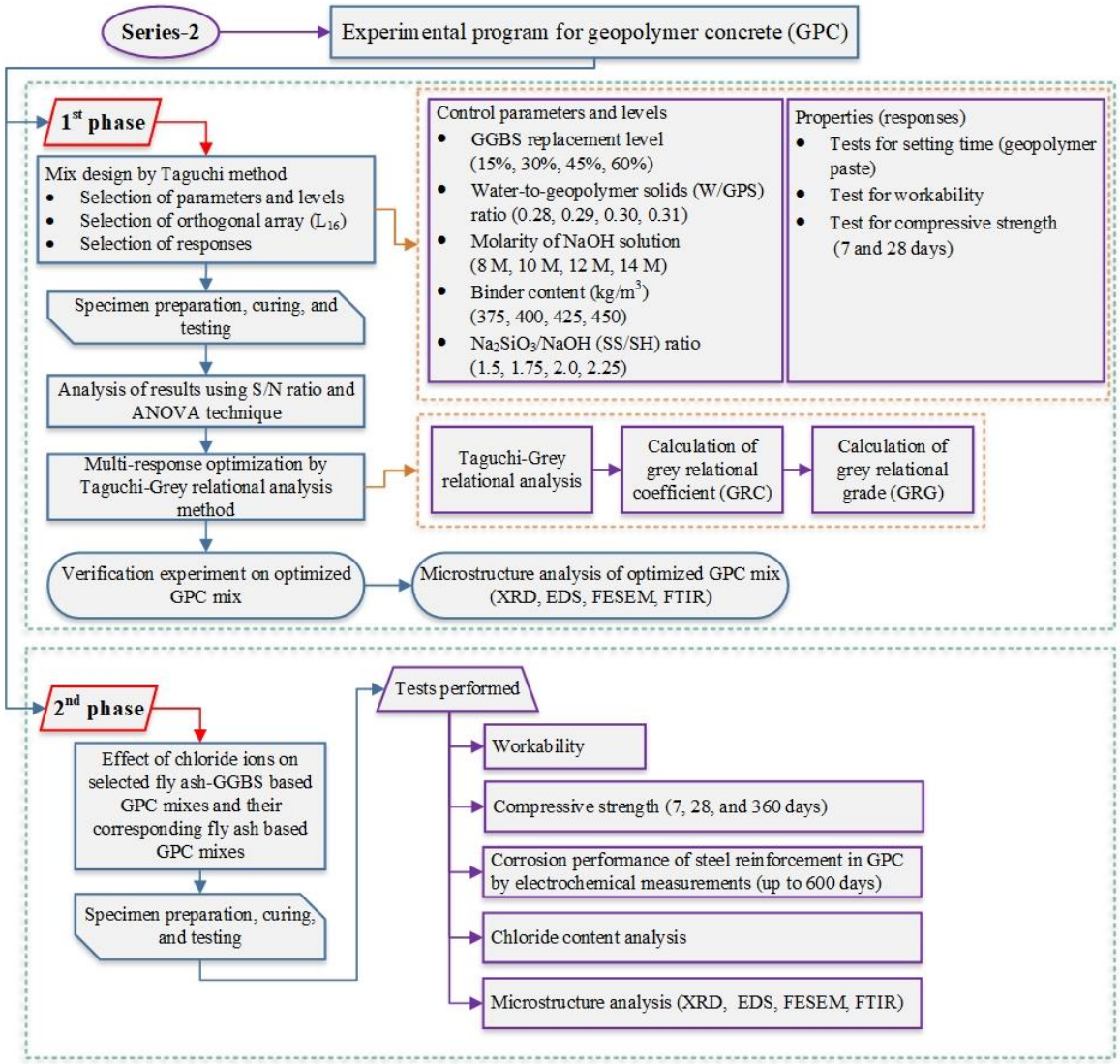

Fig. 3.11 Layout of experimental program for fly ash-GGBS based geopolymer concrete (GPC).

The quick setting time and poor workability have become the most challenging issues for the development of GPC incorporating GGBS [107]. Therefore, in addition to compressive strength, the properties such as setting time, and slump value for workability (consistency) were selected for the study. After conducting various tests such as setting time, workability, and compressive strength on the fly ash-GGBS based GPC mixes (derived from Taguchi method of design of experiment), the studied parameters were optimized by Taguchi-Grey relational analysis method and the verification experiments were conducted on the GPC mix with optimized level of control parameters. Since, longer setting time, higher workability and higher compressive strength are the requirements of fly ash-GGBS based GPC, the S/N ratio of the response (property) was calculated based on "larger-the-better" performance characteristics using equation 3.2. The procedure for optimization of

parameters for geopolymer concrete with respect to multiple responses as per Taguchi-GRA method was same as that followed during the optimization of parameters for geopolymer mortar. In 2nd phase of GPC series, the influence of chloride ions on workability, compressive strength, corrosion behaviour of embedded steel reinforcement, and chloride content of selected fly ash-GGBS based GPC mixes (based on grey relational grade: GRG), and their corresponding fly ash based GPC mixes were investigated. The microstructure analysis was performed on the GPC mixes both in the 1st phase and 2nd phase of GPC series (Fig. 3.11).

Table 3.8 Experimental series for fly ash-GGBS based GPC as per L_{16} orthogonal array (Taguchi method)

Mix	GGBS replacement level (%)	W/GPS ratio	Molarity of NaOH solution	Binder content (kg/m^3)	SS/SH ratio
M1	15	0.28	8 M	375	1.5
M2	15	0.29	10 M	400	1.75
M3	15	0.3	12 M	425	2
M4	15	0.31	14 M	450	2.25
M5	30	0.28	10 M	425	2.25
M6	30	0.29	8 M	450	2
M7	30	0.3	14 M	375	1.75
M8	30	0.31	12 M	400	1.5
M9	45	0.28	12 M	450	1.75
M10	45	0.29	14 M	425	1.5
M11	45	0.3	8 M	400	2.25
M12	45	0.31	10 M	375	2
M13	60	0.28	14 M	400	2
M14	60	0.29	12 M	375	2.25
M15	60	0.3	10 M	450	1.5
M16	60	0.31	8 M	425	1.75

3.4.1 Mix proportions and preparation of specimens in 1st phase of experiment on fly ash-GGBS based geopolymer concrete (GPC)

The mix quantities of ingredients of GPC mixes prepared in 1st phase of experiment are presented in Table 3.9. Coarse aggregates of maximum size 20 mm and 10 mm were used in a combination of 60% and 40% respectively by mass of total coarse aggregate. The proportions of coarse and fine aggregates were 65% and 35% respectively by mass of total aggregate. The alkaline solution content of each GPC mix was calculated based on the combination of W/GPS ratio, molarity of NaOH solution, binder content and SS/SH ratio obtained from the Taguchi method of experimental design (Table 3.8). The mixing of geopolymer concrete was carried out in a laboratory drum mixer. The mixing sequence of

the ingredients of GPC is shown in Fig. 3.12. First, the precursor materials were thoroughly mixed by a trowel in a container for 1 minute. After that, the fine and coarse aggregates were placed into the concrete mixer and mixed for 2 minutes. Subsequently, the binder (fly ash plus GGBS) was introduced into the mixer and the mixing of binder and aggregates was continued for 2 minutes. The mixing was done for another 5 minutes after adding the alkaline solution, to obtain the fresh GPC mix. Immediately after preparation, slump test was performed on the fresh GPC mixes. Subsequently, the fresh GPC mix was placed into cube moulds (150 mm size) in three layers with each layer compacted for 30 seconds on a vibrating table. The cube specimens were demoulded after 24 hours of casting and kept under ambient laboratory condition until testing. A total of 96 cube specimens of size 150 mm with three replicates each at the age of 7 and 28 days were prepared for compressive strength test of 16 GPC mixes (Table 3.8) as per L_{16} orthogonal array. Similarly, 6 cube specimens with three replicates each at the age of 7 and 28 days were prepared for compressive strength test of the optimized GPC mix.

Table 3.9 Mix quantities of ingredients of GPC mixes prepared in 1st phase of experiment

Mix	Binder content (kg/m^3)		Fine aggregate (kg/m^3)	Coarse aggregate (kg/m^3)		Alkaline solution (kg/m^3)	
	Fly ash	GGBS		10 mm MSA*	20 mm MSA	NaOH solution	Na_2SiO_3 solution
M1	318.75	56.25	612.59	455.07	682.60	69.90	104.84
M2	340	60	593.71	441.04	661.56	74.07	129.62
M3	361.25	63.75	574.30	426.63	639.94	78.04	156.09
M4	382.5	67.5	554.37	411.82	617.73	81.87	184.21
M5	297.5	127.5	583.26	433.28	649.92	64.17	144.38
M6	315	135	570.17	423.55	635.33	73.65	147.30
M7	262.5	112.5	598.55	444.64	666.96	78.13	136.73
M8	280	120	584.58	434.26	651.39	91.91	137.86
M9	247.5	202.5	567.46	421.54	632.31	83.16	145.53
M10	233.75	191.25	574.01	426.40	639.61	93.99	140.99
M11	220	180	593.17	440.64	660.96	63.15	142.08
M12	206.25	168.75	601.30	446.68	670.02	69.00	138.00
M13	160	240	591.49	439.39	659.08	70.01	140.03
M14	150	225	604.37	448.96	673.44	60.99	137.24
M15	180	270	564.26	419.16	628.74	95.13	142.70
M16	170	255	577.77	429.20	643.80	81.54	142.69

*MSA: Maximum size of aggregate

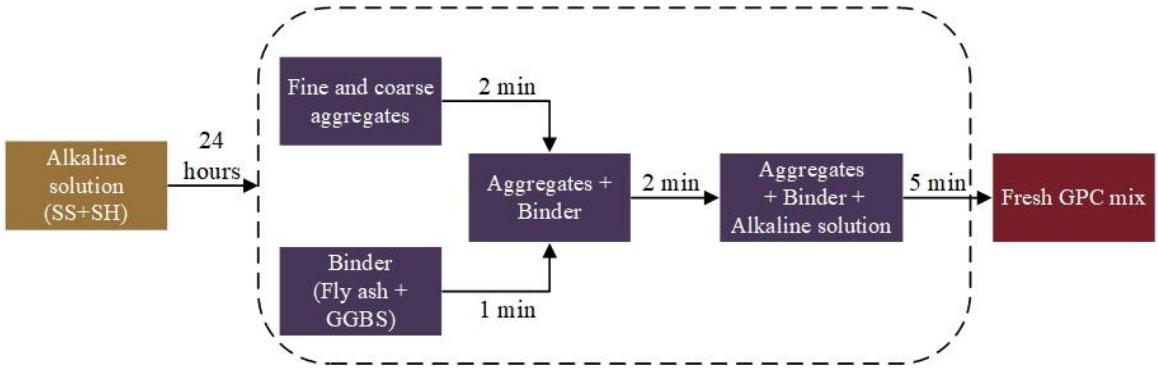

Fig. 3.12 Mixing sequence of ingredients of geopolymer concrete (GPC).

3.4.2 Tests performed in 1st phase of experiment on fly ash-GGBS based geopolymer concrete (GPC)

3.4.2.1 Setting time and workability of GPC

The tests for setting time were conducted on paste samples of GPC mixes as per IS 4031 (Part 5)-2019 [126] and ASTM C191-2019 [127]. The paste of GPC mixes (presented in Table 3.8) was made by mixing the alkaline solution with binder of respective mixes. The slump test was performed on fresh GPC mixes in accordance with IS 1199 (Part 2)-2018 [128], and ASTM C143-2020 [129] to measure the consistency (workability) of the mixes.

3.4.2.2 Compressive strength of GPC

The compressive strength test on GPC mixes was performed at the age of 7 and 28 days of ambient curing from the day of preparation as per IS 516 (Part 1/Sec 1)-2021 [130]. The compressive strength test was carried out on three replicate cube specimens (150 mm size) of a given GPC mix in a compression testing machine, and the average value of three replicates was reported.

3.4.2.3 Microstructure analysis of GPC

Out of sixteen fly ash-GGBS based GPC mixes (Table 3.8), the microstructure study was carried out on the selected mixes (based on grey relational grade: GRG). After completion of compressive strength test on cube specimens, the crushed samples of selected GPC mixes were further pulverized in a jaw crusher. Subsequently, the crushed materials were passed through a sieve having 75 µm square openings, and the sieved materials were then kept in air tight plastic containers inside a desiccator. The XRD, EDS, FESEM, and FTIR analyses were conducted on the GPC powder samples. The procedures followed for microstructure analyses in case of geopolymer concrete (GPC) were same as that used in case of geopolymer mortar (GPM) as mentioned in Section 3.3.3.6.

3.4.3 Mix proportions, and preparation of specimens in 2nd phase of experiment on geopolymer concrete (GPC)

As stated earlier, in 2nd phase of experiment on GPC, the influence of chloride ions on different properties (i.e., workability, compressive strength, corrosion behaviour of steel reinforcement, chloride content, and microstructure) of selected fly ash-GGBS based GPC mixes and their corresponding fly ash based GPC mixes were studied. For this purpose, one GPC mix was selected for each GGBS replacement level (%) based on grey relational grade (GRG) from the GPC mixes formulated in 1st phase of experiment of GPC series. The mix proportion of selected fly ash-GGBS based GPC mixes for the 2nd phase of experiment and their corresponding fly ash based GPC mixes are presented in Table 3.10. Further, the mix quantities of ingredients of GPC mixes prepared in 2nd phase of experiment are presented in Table 3.11.

Table 3.10 Mix proportion of fly ash-GGBS based GPC mixes and their corresponding fly ash based GPC mixes

Mix	Fly ash (%)	GGBS (%)	Water-to-geopolymer solids (W/GPS) ratio	Molarity of NaOH solution	Binder content (kg/m^3)	SS/SH ratio
M3: FA85/G15	85	15	0.3	12 M	425	2
M8: FA70/G30	70	30	0.31	12 M	400	1.5
M10: FA55/G45	55	45	0.29	14 M	425	1.5
M15: FA40/G60	40	60	0.3	10 M	450	1.5
M3: FA100	100	-	0.3	12 M	425	2
M8: FA100	100	-	0.31	12 M	400	1.5
M10: FA100	100	-	0.29	14 M	425	1.5
M15: FA100	100	-	0.3	10 M	450	1.5

Table 3.11 Mix quantities of ingredients of GPC mixes prepared in 2nd phase of experiment

Mix	Binder content (kg/m^3)		Fine aggregate (kg/m^3)	Coarse aggregate (kg/m^3)		Alkaline solution (kg/m^3)	
	Fly ash	GGBS		10 mm MSA	20 mm MSA	NaOH solution	Na_2SiO_3 solution
M3: FA85/G15	361.25	63.75	574.30	426.63	639.94	78.04	156.09
M8: FA70/G30	280	120	584.58	434.26	651.39	91.91	137.86
M10: FA55/G45	233.75	191.25	574.01	426.40	639.61	93.99	140.99
M15: FA40/G60	180	270	564.26	419.16	628.74	95.13	142.70
M3: FA100	425	-	574.30	426.63	639.94	78.04	156.09
M8: FA100	400	-	584.58	434.26	651.39	91.91	137.86
M10: FA100	425	-	574.01	426.40	639.61	93.99	140.99
M15: FA100	450	-	564.26	419.16	628.74	95.13	142.70

To evaluate the effect of chloride ions on workability, compressive strength and corrosion behaviour of steel reinforcement in fly ash and fly ash-GGBS based GPC mixes, sodium chloride (NaCl) of different concentrations such as 1.5% and 3.5% (by mass of geopolymer solids) were added in alkaline solution at the time of preparation of GPC mixes. Two types of specimens were prepared from each GPC mix. Cube specimens of size 150 mm were prepared for compressive strength test. Cylindrical reinforced GPC specimens of size 72 mm diameter and 200 mm height with a centrally embedded steel bar were prepared for electrochemical measurements such as corrosion potential and corrosion current density by linear polarization resistance (LPR) measurement. The Tempcore TMT steel bars of diameter 12 mm to be embedded in the cylindrical specimens were cleaned with wire brush, and insulating tape followed by epoxy coating was applied at specific locations, where there is a discontinuity of steel bar with surrounding concrete to prevent crevice corrosion. The schematic diagram of steel bar is shown in Fig. 3.13 (a). The fly ash-GGBS based GPC specimens were demoulded after 24 hours of preparation. However, the fly ash based GPC specimens were subjected to 48 hours of rest period after preparation followed by 48 hours of oven drying at 80° C before demoulding. After demoulding, the GPC specimens were kept in ambient laboratory condition until testing. The schematic diagram of cylindrical reinforced GPC specimen is shown in Fig. 3.13 (b). The photograph of cube specimens and cylindrical reinforced specimens prepared in the 2nd phase of experiment of GPC series is shown in Fig. 3.14. The details of cube and cylindrical reinforced GPC specimens prepared in 2nd phase of experiment are presented in Table 3.12.

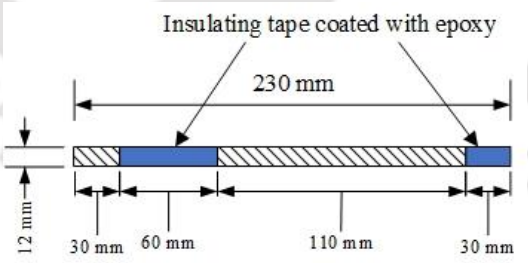

(a)

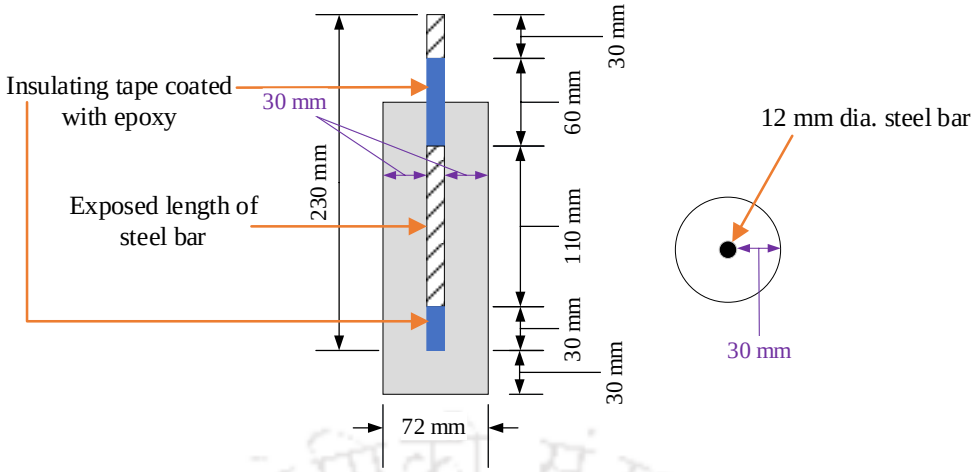

(b)

Fig. 3.13 Schematic diagram of (a) steel bar and (b) cylindrical reinforced GPC specimen.

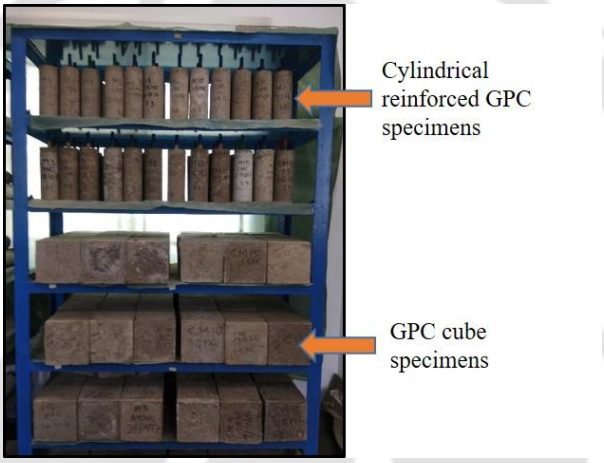

Fig. 3.14 Photograph of cubes and cylindrical reinforced specimens prepared in 2nd phase of experiment of GPC series.

Table 3.12 Details of specimens prepared for different tests conducted in 2nd phase of experiment on GPC

Mix	Number of cube specimens (age: 7, 28, and 360 days)			Number of cylindrical reinforced specimens		
	Admixed NaCl concentration			Admixed NaCl concentration		
	0%	1.5%	3.5%	0%	1.5%	3.5%
M3: FA85/G15	3*	9	9	3	3	3
M8: FA70/G30	3	9	9	3	3	3
M10: FA55/G45	3	9	9	3	3	3
M15: FA40/G60	3	9	9	3	3	3
M3: FA100	9	9	9	3	3	3
M8: FA100	9	9	9	3	3	3
M10: FA100	9	9	9	3	3	3
M15: FA100	9	9	9	3	3	3
Total	48	72	72	24	24	24

Note: *Remaining 6 cube specimens of control fly ash-GGBS based GPC mixes (without NaCl) for the age of 7 and 28 days were already prepared in the 1st phase of experiment of GPC series.

3.4.4 Tests performed in 2nd phase of experiment on geopolymer concrete (GPC)

3.4.4.1 Workability and compressive strength of GPC

The same procedure as followed in the 1st phase of experiment in GPC series was used for conducting slump test and compressive strength test on GPC mixes in the 2nd phase of experiment. The compressive strength test was conducted on GPC cube specimens of size 150 mm at the age of 7, 28, and 360 days from the day of preparation.

3.4.4.2 Electrochemical measurements

The corrosion potential (E_{corr}), and corrosion current density (I_{corr}) of steel reinforcement by linear polarization resistance (LPR) technique were measured using a corrosion monitoring instrument (make: ACM, Gill AC serial no. 1836-sequencer) at the age of 60, 150, 240, 330, 420, 510, and 600 days. The schematic diagram of experimental setup for electrochemical measurements is shown in Fig. 3.15. The corrosion monitoring tests were carried out using a three-electrode arrangement, which comprises of working electrode (WE) (i.e., the steel bar embedded in cylindrical GPC specimen), auxiliary electrode (AE) (a pair of stainless steel plates) and reference electrode (RE) (SCE: saturated calomel electrode). The photograph of the experimental setup for electrochemical measurements is shown in Fig. 3.16. During the electrochemical measurements, the cylindrical reinforced GPC specimen (size: 72 mm diameter and 200 mm height) was partially immersed in the test solution in a plastic container. The concentration of NaCl in the test solution was same as that admixed during the preparation of GPC mixes. The E_{corr} value of the steel reinforcement in the cylindrical specimen was measured with reference to saturated calomel electrode, and the probability of steel reinforcement corrosion in GPC was evaluated as per ASTM C876-15 [131]. The I_{corr} value was determined by polarizing the reinforcing steel bar to ± 20 mV from the equilibrium potential at scan rate of 6 mV/minute. The I_{corr} of steel bar was calculated using the Stern-Geary equation [70,72] and is given by:

$$I_{corr} = \frac{B}{R_p} \tag{3.12}$$

Where B is Stern-Geary constant, which was considered as 26 mV in the present study for reinforcing steel bar in active condition, and R_p is polarization resistance of steel bar [70].

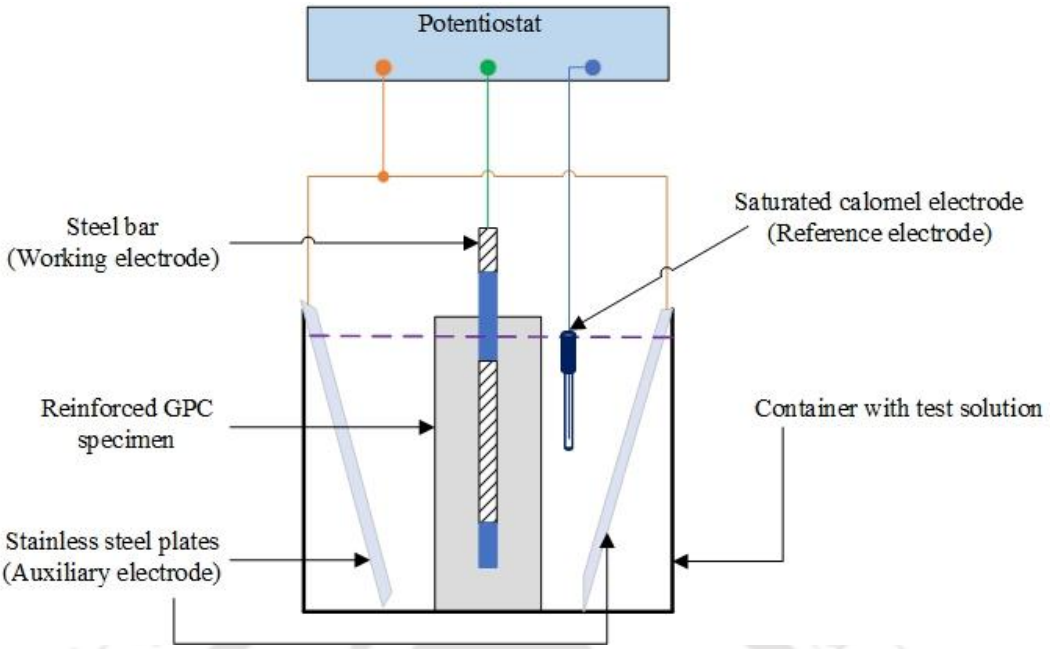

Fig. 3.15 Schematic diagram of experimental setup for electrochemical measurements.

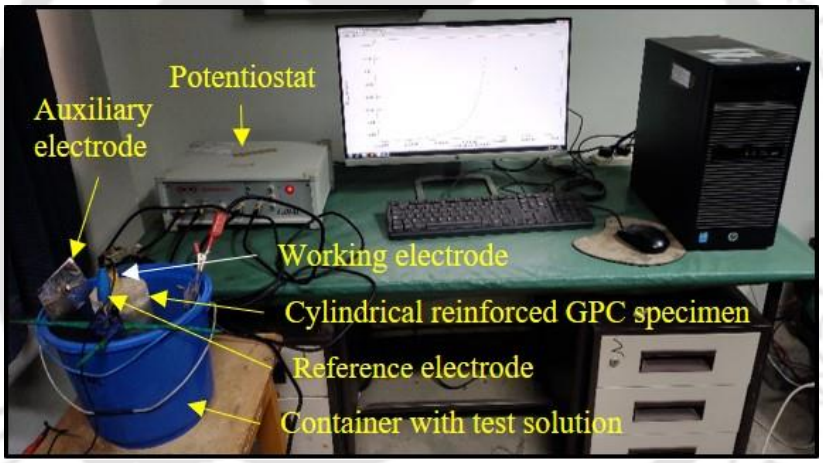

Fig. 3.16 Photograph of experimental setup for electrochemical measurements.

3.4.4.3 Chloride content analysis

For chloride analysis, the free chloride (C_f) and total chloride (C_t) contents of powder samples collected from the chloride admixed GPC cube specimens and rebar level of chloride admixed cylindrical reinforced GPC specimens were measured. The same procedure as mentioned in Section 3.4.2.3 was followed for obtaining the powder samples from chloride admixed GPC cube specimens after completion of compressive strength test at the ages of 7, 28, and 360 days. After completion of electrochemical measurements, i.e., after 600 days, the powder samples near the rebar level i.e., in the depth interval of 25-30 mm from the surface of cylindrical reinforced GPC specimens were collected by drilling. The collected powder samples were subsequently passed through a sieve having 75 µm

square openings, and were kept in airtight plastic containers inside a desiccator. The free chloride (C_f) and total chloride (C_t) contents of GPC powder samples were determined using a potentiometric titrator (make: Metrohm, model: 848 Titrino Plus). In order to determine the free chloride (C_f) and total chloride (C_t) contents, 3 g of GPC powder sample was added with 50 ml of respective solvent (i.e., distilled water in case of free chloride, and concentrated nitric acid (1 N) in case of total chloride) in a 100 ml beaker. For free chloride content, the powder solution was thoroughly mixed and heated gradually up to boiling on a hot plate with magnetic stirrer and continued for boiling for about one minute. After that, the powder solution was cooled to the room temperature, and then titrated against 0.1 M $AgNO_3$ solution. For total chloride content, the powder solution was thoroughly mixed by stirring without heating and then titrated 0.1 M $AgNO_3$ solution. The free chloride and total chloride contents were expressed as percentage by mass of geopolymer concrete (GPC). The photographs of drilled cylindrical reinforced specimens, collected GPC powder samples, and chloride content analysis of GPC powder samples using potentiometric titrator are shown in Fig. 3.17.

Fig. 3.17 Photographs of drilled cylindrical reinforced specimens, GPC powder samples, and chloride analysis using potentiometric titrator.

3.4.4.4 Microstructure analysis

For microstructure analysis on GPC mixes, XRD, EDS, FESEM, and FTIR analyses were performed on GPC powder samples (Section 3.4.4.3) collected after compressive strength test on cube specimens, and from near the rebar level of cylindrical reinforced specimens after completion of electrochemical measurements. The procedures followed for microstructure analyses were same as that used in case of geopolymer mortar (GPM).

3.5 Summary

In this experimental program, the geopolymer mortar and concrete mixes were prepared using fly ash and ground granulated blast furnace slag (GGBS) as precursor materials, and combination of sodium hydroxide solution and sodium silicate solution as alkaline solution. Geopolymer mortar and concrete mixes were designed in two different series. In each series, various experiments were performed in two different phases. In 1st phase of geopolymer mortar (GPM) series, the mix design of fly ash-GGBS based geopolymer mortar was carried out by Taguchi method of design of experiment (L_9 orthogonal array) by considering four control parameters with three levels each. The control parameters considered were GGBS replacement level, water-to-geopolymer solids (W/GPS) ratio, molarity of NaOH solution, and sand-to-binder (S/B) ratio. After conducting experiments for fresh (setting time, and flowability), mechanical (compressive strength), and durability properties (water absorption, apparent volume of permeable voids, sorptivity, and resistance against sulfate and acid attack) of geopolymer mortar mixes derived from Taguchi method of design of experiment, the control parameters were optimized by Taguchi-Grey relational analysis (GRA) method. Subsequently, the verification experiments were conducted on the optimized GPM mix. In 2nd phase of geopolymer mortar series, the mix proportions of geopolymer mortar mixes were designed by considering the most influential parameters evaluated in the 1st phase of geopolymer mortar series such as GGBS replacement level and sand-to-binder (S/B) ratio. The experiments (except setting time) that were conducted in 1st phase of geopolymer mortar series were performed again in the 2nd phase of geopolymer mortar series. Cube specimens of size 50 mm were prepared for compressive strength, water absorption, apparent volume of permeable voids, and sulfate and acid resistance tests, whereas cylindrical specimens of size 100 mm diameter × 50 mm height were prepared for sorptivity test in both phases of geopolymer mortar series.

In 1st phase of geopolymer concrete (GPC) series, the mix proportioning of geopolymer concrete mixes was carried out by Taguchi method of design of experiment (L_{16} orthogonal array) by considering five control parameters with four levels each. The considered control parameters were GGBS replacement level, W/GPS ratio, molarity of NaOH solution, binder content, and SS/SH ratio. After conducting setting time, workability, and compressive strength tests on geopolymer concrete mixes derived from Taguchi method of design of experiment, the control parameters were optimized by Taguchi-GRA method.

After that, verification experiments were conducted on the mix combination of optimized level of control parameters. In 2nd phase of geopolymer concrete series, the effect of chloride ions on different properties namely workability, compressive strength, corrosion behaviour of embedded steel reinforcement, and chloride content of selected fly ash-GGBS based geopolymer concrete mixes, and their corresponding fly ash based geopolymer concrete mixes were evaluated. Geopolymer concrete cube specimens of size 150 mm, and cylindrical reinforced specimens of size 72 mm diameter and 200 mm height with a centrally embedded steel bar were prepared for compressive strength test and electrochemical measurements (corrosion potential and corrosion current density by linear polarization resistance measurement) respectively. The microstructure of geopolymer mortar and concrete were studied through X-ray diffraction (XRD), energy dispersive X-ray spectroscopy (EDS), field emission scanning electron microscope (FESEM), and Fourier transform infrared (FTIR) spectroscopy analyses.

Optimizing the Performance of Geopolymer Mortar Based on Fresh, Hardened and Durability Properties

4.1 General

In this chapter, the Taguchi-Grey relational analysis was used to investigate and optimize the effect of various control parameters such as GGBS replacement level, water-to-geopolymer solids (W/GPS) ratio, molarity of NaOH solution, and sand-to-binder (S/B) ratio on fresh (setting time, and flowability), hardened (compressive strength at different ages of ambient curing), and durability (water absorption, apparent volume of permeable voids (AVPV), sorptivity, sulfate and acid resistance) properties of fly ash-GGBS based geopolymer mortar. The microstructure of the geopolymer mortar mix with highest grey relational grade (GRG) was analyzed through XRD, FESEM, EDS, and FTIR analyses. Based on the results obtained from Taguchi-Grey relational analysis, the optimal combination of mix parameters was proposed and the obtained results of verification experiments conducted on the proposed optimized geopolymer mortar mix were discussed.

4.2 Setting time

The initial and final setting time of geopolymer mortar (GPM) mixes determined by penetration resistance method are presented in Fig. 4.1. From Fig. 4.1, it is observed that the initial setting time of geopolymer mortar mixes ranges from 47 minutes to 780 minutes and the final setting time ranges from 150 minutes to 919 minutes. Among all the GPM mixes, M1 (GGBS replacement: 15%, W/GPS ratio: 0.31, NaOH solution: 10 M and S/B ratio: 1.5) exhibited longer initial and final setting time whereas the mix M4 (GGBS replacement: 30%, W/GPS ratio: 0.31, NaOH solution: 12 M and S/B ratio: 2.5) showed quick initial and final setting time. From Fig. 4.1, while comparing the mixes M1, M2 and M3, it is noted that the initial and final setting time of GPM decreased with increase in NaOH solution molarity and S/B ratio. This indicated that at GGBS replacement level of 15% (M1, M2, and M3), the combined effect of NaOH solution molarity and S/B ratio dominated the effect of W/GPS ratio on setting time. However, for GGBS replacement levels of 30% (M4, M5, and M6) and 45% (M7, M8, and M9), the W/GPS ratio had dominant effect on setting time of GPM irrespective of NaOH solution molarity and S/B ratio.

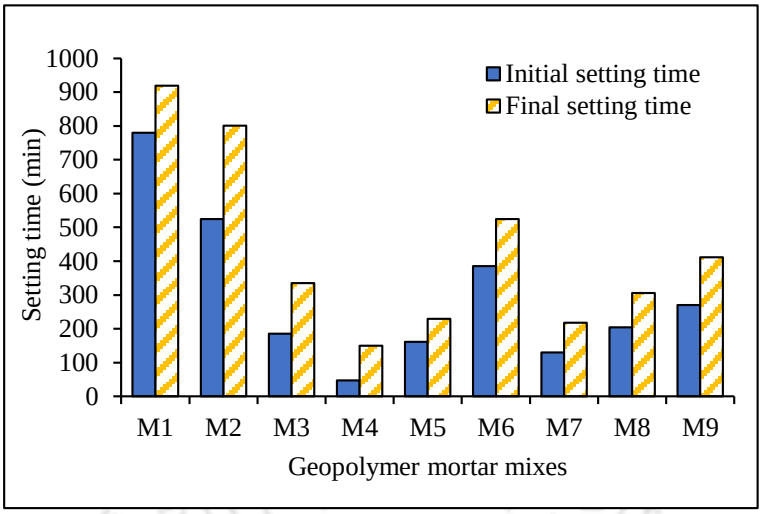

Fig. 4.1 Initial and final setting time of geopolymer mortar mixes.

The signal-to-noise (S/N) ratio for setting time was calculated as per "smaller-the-better" function (Equation 3.3) and is presented in Table 4.1. The performance statistics (mean S/N ratio) of setting time (initial and final) for different control parameters of GPM mixes are shown in Fig. 4.2. For a given level of a parameter, the performance statistics value of a given response (i.e., setting time) was calculated as the average of S/N ratio of that response for the GPM mixes made with same level of the parameter. The higher performance statistics value indicates the best level of each parameter. The combination of these optimal levels of the parameters was considered as the best possible combination to achieve the desired property i.e., lower setting time. From Fig. 4.2, it is observed that the shorter initial and final setting time for GPM mixes were achieved due to increase in GGBS replacement level (from 15% to 30%), NaOH solution molarity (from 10 M to 14 M) and sand to binder (S/B) ratio (from 1.5 to 2.5). The setting time (initial and final) of GPM increased with increase in W/GPS ratio of the mixes. With increase in GGBS replacement level from 15% to 30%, the decrease in setting time may be ascribed to effect of higher calcium oxide (CaO) content of GGBS that increased the rate of geopolymerization process of the GPM mixes and formed calcium aluminosilicate hydrate gel [132]. At 45% GGBS replacement level, the increase in setting time of GPM mixes may be due to the combined effect of higher W/GPS ratio and lower S/B ratio that resulted in higher paste content of the GPM mix. With increase in molarity of NaOH solution, the sodium content in the mixes increased, which accelerated the geopolymerization process and resulted in significant decrease in setting time. The decrease in setting time with increase in S/B ratio is attributed to the effect of lower paste content of the GPM mix at higher S/B ratio. The water content in the alkaline solution increased at higher W/GPS ratio of the mix and led to retardation

of the reaction process [91]. Thus, longer setting time was achieved when the GPM mix was prepared with higher W/GPS ratio. The results of ANOVA of S/N ratio for setting time of geopolymer mortar are presented in Table 4.2. From this table, it is observed that except W/GPS ratio, other parameters such as GGBS replacement level (%), NaOH solution molarity and S/B ratio substantially influenced the setting time (both initial and final) of GPM. The order of contribution (%) of parameters to achieve lower initial setting time was GGBS replacement (34.35%) > S/B ratio (32.41%) > molarity of NaOH solution (25.94%) > W/GPS ratio (7.3%). Similarly, the order of contribution (%) of parameters to achieve lower final setting time was GGBS replacement (44.99%) > molarity of NaOH solution (26.95%) > S/B ratio (23.42%) > W/GPS ratio (4.64%).

Table 4.1 Signal-to-noise (S/N) ratio of setting time, flow index, and compressive strength of GPM mixes

Mix	Setting time		Flow index	Compressive strength			
	Initial setting time	Final setting time		7 days	28 days	90 days	180 days
M1	-57.84	-59.27	39.34	27.97	32.16	32.17	32.19
M2	-54.40	-58.07	35.95	26.01	30.70	31.37	31.86
M3	-45.34	-50.50	27.86	26.02	30.52	30.71	30.95
M4	-33.44	-43.52	12.02	28.83	30.09	30.73	31.95
M5	-44.14	-47.20	40.88	28.59	31.48	31.86	32.52
M6	-51.71	-54.40	35.38	27.65	30.95	31.18	31.89
M7	-42.28	-46.77	30.21	30.18	32.86	33.18	33.77
M8	-46.19	-49.71	16.79	30.02	31.22	31.89	33.04
M9	-48.63	-52.28	42.01	30.75	31.75	32.03	32.65

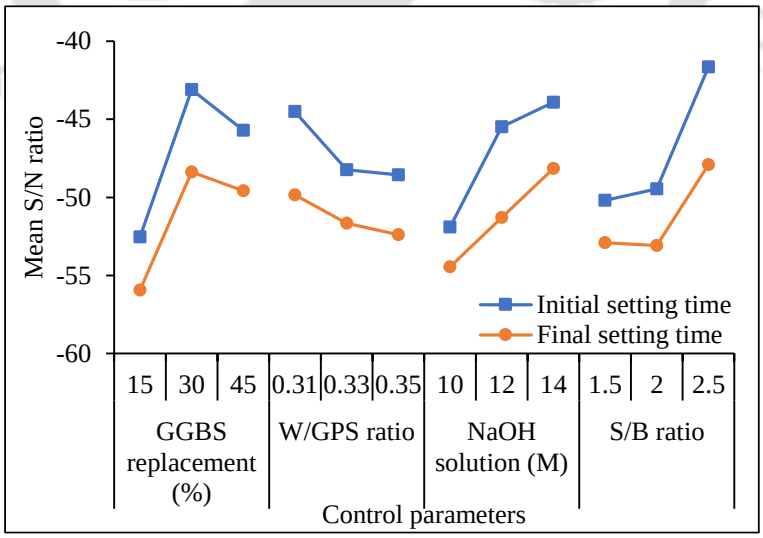

Fig. 4.2 Performance statistics (mean S/N ratio) of setting time for different control parameters of GPM mixes.

Table 4.2 ANOVA results of signal-to-noise (S/N) ratio for setting time of geopolymer mortar

Parameter	DOF	SOS	MS	Contribution (%)
Initial setting time				
GGBS replacement level	2	142.33	71.17	34.35
W/GPS ratio	2	30.26	15.13	7.3
NaOH molarity	2	107.52	53.76	25.94
Sand-to-binder (S/B) ratio	2	134.32	67.16	32.41
Error	-			
Total	8	414.44		100
Final setting time				
GGBS replacement level	2	99.39	49.7	44.99
W/GPS ratio	2	10.26	5.13	4.64
NaOH molarity	2	59.54	29.77	26.95
Sand-to-binder (S/B) ratio	2	51.76	25.88	23.42
Error		-		
Total	8	220.95		100

Note: DOF: Degree of freedom, SOS: Sum of square, MS: Mean square

4.3 Flowability

The obtained flow table test results are illustrated in Fig. 4.3. The flowability of GPM mixes was evaluated in terms of flow index (%). From Fig. 4.3, it is observed that the GPM mix M4 (prepared with GGBS replacement of 30%, W/GPS ratio of 0.31, 12 M NaOH solution, and S/B ratio of 2.5) showed the lowest flow index of 4% whereas the mix M9 (prepared with GGBS replacement of 45%, W/GPS ratio of 0.35, 12 M NaOH solution, and S/B ratio of 1.5) showed the highest flow index of 127%. Further, the geopolymer mortar mixes M1 and M5 prepared with S/B ratio of 1.5 showed comparatively higher flow index of 93% and 111% respectively. The GPM mixes M3 and M8 prepared with S/B ratio of 2.5 showed comparatively poor flowability with flow index of 29% and 7% respectively. The GPM mixes made with S/B ratio of 2 i.e., M2, M6 and M7 showed intermediate flow index of 63%, 59% and 33% respectively when compared with GPM mixes made with S/B ratio of 1.5 and 2.5. From these observations, it can be noticed that the flowability of geopolymer mortar was significantly influenced by sand to binder (S/B) ratio.

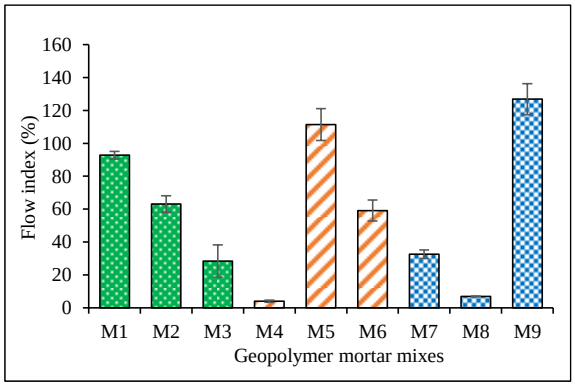

Fig. 4.3 Flow index (%) of geopolymer mortar mixes.

The S/N ratio of flow index of GPM are presented in Table 4.1. The performance statistics (mean S/N ratio) of flow index for different control parameters of GPM mixes are shown in Fig. 4.4. From Fig. 4.4, it is observed that flowability of fresh GPM mixes decreased significantly with increase in S/B ratio, which may be ascribed to the dominant effect of increase in sand content, and decrease in binder and alkaline solution contents. From Fig. 4.4, it was noticed that the performance statistics of flow index increased with increase in W/GPS ratio. When GPM mixes prepared with higher W/GPS ratio, the water content of the mixes increased, which improved the particle mobility of the precursor materials in the GPM mixes. Further, the performance statistics value of flow index decreased significantly with increase in GGBS replacement level from 15% to 30% followed by a small increase at GGBS replacement level of 45%. The significant decrease in flow index with increase in GGBS replacement level from 15% to 30% may be ascribed to the dominant effect of angular particles of GGBS that might have increased the friction among the fly ash particles [38]. The small increase in flow index of GPM mixes with increase in GGBS replacement level from 30% and 45% may be due to the dominant effect of S/B ratio (over the effect of angular particles of GGBS), which did not vary with increase in GGBS replacement level from 30% to 45%. From Fig. 4.4, it is noted that the performance statistics value of flow index decreased slightly with increase in molarity of NaOH solution from 10 M to 12 M followed by an increase at 14 M. This variation in flow index with molarity of NaOH solution may be ascribed to the dominant effect of variation in S/B ratio of the GPM mix although the paste content of the mix increased with increase in molarity of NaOH solution. The results of ANOVA of S/N ratio for flow index of geopolymer mortar are presented in Table 4.3. From the table, it is observed that S/B ratio has highest contributing effect (82.81%) followed by W/GPS ratio (10.19%), GGBS replacement (5.28%) and molarity of NaOH solution (1.72%) on flow index of GPM mixes.

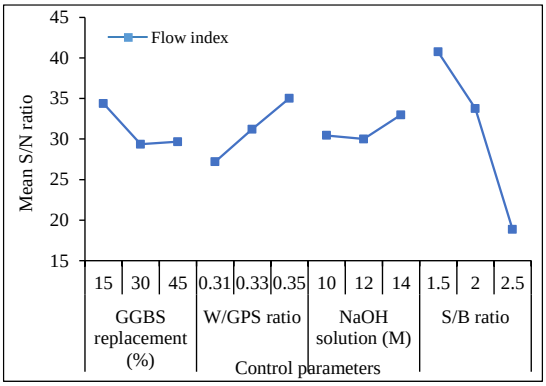

Fig. 4.4 Performance statistics (mean S/N ratio) of flow index for different control parameters of GPM mixes.

Table 4.3 ANOVA results of signal-to-noise (S/N) ratio for flow index of geopolymer mortar

Parameter	DOF	SOS	MS	Contribution (%)
GGBS replacement level	2	47.68	23.84	5.28
W/GPS ratio	2	91.99	45.99	10.19
NaOH molarity	2	15.53	7.76	1.72
Sand-to-binder (S/B) ratio	2	747.58	373.79	82.81
Error	-	-	-	
Total	8	902.76		100.00

Note: DOF: Degree of freedom, SOS: Sum of square, MS: Mean square

4.4 Compressive strength

The results obtained from compressive strength test of GPM mixes (M1 - M9) at 7, 28, 90, and 180 days of ambient curing are illustrated in Fig. 4.5. From this figure, it is observed that the mixes M2 (15% GGBS) and M3 (15% GGBS) achieved lowest 7 days compressive strength of 20 N/mm^2 each, and mix M9 (45% GGBS) achieved the highest 7 days compressive strength of 34.67 N/mm^2. This variation in early age compressive strength is attributed to the effect of GGBS content in the GPM mixes. At 7 days of ambient curing, all the GPM mixes prepared with 45% GGBS replacement (M7, M8, and M9) showed higher compressive strength as compared to the GPM mixes prepared with other replacement levels. With increase in GGBS replacement level, the calcium oxide content of the GPM mixes increased, which resulted in relatively greater extent of geopolymerization process as well as in the formation of more amount of C-S-H gel. Therefore, the coexistence of geopolymer gels (N-A-S-H and N-(C)-A-S-H) and C-S-H gel increased the compressive strength of GPM made with higher GGBS replacement level at early age of ambient curing [81]. From Fig. 4.5, it is noticed that the compressive strength of GPM mixes increased with increase in ambient curing age i.e., from 7 days to 180 days through 28 days and 90 days. The increase in compressive strength of GPM mixes at later

age of curing is due to the effect of delayed reactivity of fly ash in GPM mixes under ambient condition that improved the compressive strength at later age. However, the improvement in compressive strength of GPM mixes after 28 days was observed to be very less as 86.4% to 93.5% of 180 days compressive strength was achieved at 28 days of ambient curing for all the GPM mixes. It can also be noted that the strength enhancement of GPM mixes with age i.e., from 7 to 180 days was reliant on the quantity of fly ash present in the mix. The GPM mixes (M1 - M3) prepared with 85% fly ash (and 15% GGBS) had highest average compressive strength enhancement of 79.5% from 7 to 180 days as compared to the GPM mixes (M4 - M6) prepared with 70% fly ash (and 30% GGBS) with average compressive strength enhancement of 54.44% followed by the GPM mixes (M7 - M9) prepared with 55% fly ash (and 45% GGBS) with average compressive strength enhancement of 38.62%.

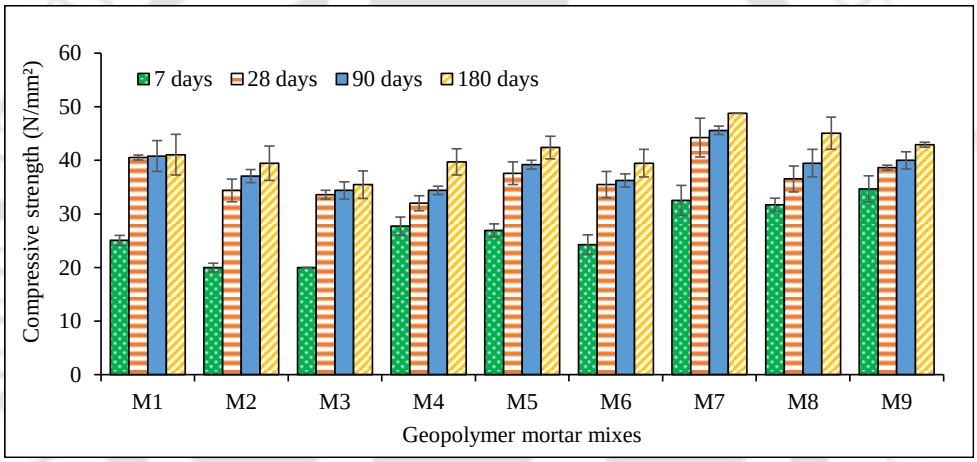

Fig. 4.5 Compressive strength of geopolymer mortar mixes at different ages of ambient curing.

The S/N ratio of compressive strength of GPM mixes at 7, 28, 90 and 180 days are presented in Table 4.1. The performance statistics of compressive strength for different control parameters of GPM mixes are shown in Fig. 4.6. From Fig. 4.6, it is observed that performance statistics value of 7 days and 180 days compressive strength increased with increase in GGBS replacement. Further, at the ages of 28 days and 90 days, the performance statistics of compressive strength decreased slightly at 30% GGBS replacement followed by a relatively significant increase at 45% GGBS replacement when compared with 15% GGBS replacement. This indicates that the compressive strength of GPM mostly increased with increase in GGBS replacement level at all ambient curing ages. The minor reduction in compressive strength of GPM mix made with 30% GGBS replacement at 28 and 90 days of ambient curing may be attributed to the effect of alterations in the extent of

geopolymerization reaction in the GPM mix. The performance statistics of compressive strength decreased with increase in W/GPS ratio as shown in Fig. 4.6. This may be ascribed to the effect of increase in porosity of the GPM mix in the presence of higher amount of water at higher W/GPS ratio. The performance statistics for 7 days compressive strength decreased slightly with increase in molarity of NaOH solution as observed from Fig. 4.6. However, at later ages (28, 90 and 180 days), the variation in performance statistics for compressive strength was unsystematic with increase in molarity of NaOH solution with higher value for the GPM mix prepared with 14 M NaOH solution. At the early age (7 days), the effect of NaOH solution molarity on compressive strength was not reflected because of comparatively lower extent of geopolymerization process. However, at later ages, there is greater extent of geopolymerization process of the precursor materials at higher molarity of NaOH solution (14 M) that resulted in higher compressive strength. The variation in performance statistics for compressive strength with S/B ratio was not systematic at the early age (7 days) as observed from Fig. 4.6. However, at later ages (28, 90 and 180 days), the performance statistics for compressive strength of GPM mixes mostly decreased with increase in S/B ratio. The decrease in compressive strength with increase in S/B ratio may be ascribed to the effect of formation of porous microstructure due to reduced binder content and alkaline solution content in the GPM mix at higher S/B ratio. The results of ANOVA of S/N ratio for compressive strength of geopolymer mortar are presented in Table 4.4. From the table, it is observed that for different ages of ambient curing, GGBS replacement has highest contributing effect (32.74 - 84.75%) followed by S/B ratio (8.86 - 38.29%), W/GPS ratio (5.72 - 21.28%), and molarity of NaOH solution (0.67 - 16.8%) on compressive strength of GPM mixes.

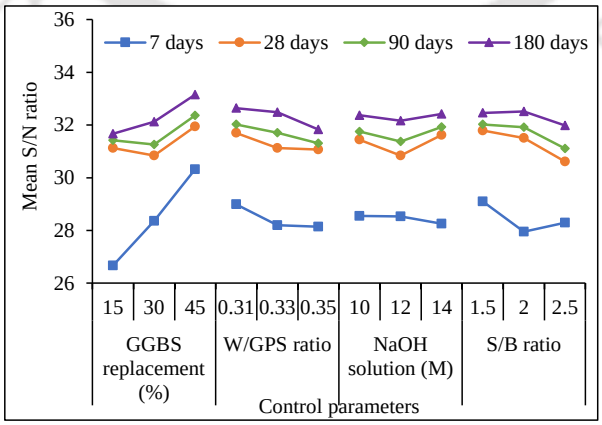

Fig. 4.6 Performance statistics (mean S/N ratio) of compressive strength for different control parameters of geopolymer mortar mixes.

Table 4.4 ANOVA results of signal-to-noise (S/N) ratio for compressive strength of geopolymer mortar

Parameter	DOF	SOS	MS	Contribution (%)
7 days compressive strength				
GGBS replacement level	2	20.02	10.01	84.75
W/GPS ratio	2	1.35	0.68	5.72
NaOH molarity	2	0.16	0.08	0.67
Sand-to-binder (S/B) ratio	2	2.09	1.05	8.86
Error	-	-	-	-
Total	8	23.62		100.00
28 days compressive strength				
GGBS replacement level	2	1.95	0.98	32.74
W/GPS ratio	2	0.73	0.36	12.17
NaOH molarity	2	1	0.50	16.80
Sand-to-binder (S/B) ratio	2	2.28	1.14	38.29
Error	-	-	-	-
Total	8	5.96		100.00
90 days compressive strength				
GGBS replacement level	2	2.12	1.06	43.83
W/GPS ratio	2	0.76	0.38	15.72
NaOH molarity	2	0.48	0.24	9.84
Sand-to-binder (S/B) ratio	2	1.48	0.74	30.61
Error	-	-	-	-
Total	8	4.84		100.00
180 days compressive strength				
GGBS replacement level	2	3.45	1.73	66.73
W/GPS ratio	2	1.10	0.55	21.28
NaOH molarity	2	0.11	0.06	2.13
Sand-to-binder (S/B) ratio	2	0.51	0.26	9.86
Error	-	-	-	-
Total	8	5.17		100.00

Note: DOF: Degree of freedom, SOS: Sum of square, MS: Mean square

4.5 Water absorption and apparent volume of permeable voids (AVPV)

The results obtained from water absorption and apparent volume of permeable voids (AVPV) of fly ash-GGBS based GPM at 28 days of ambient curing are presented in Fig. 4.7 (a) and (b) respectively. From Fig. 4.7, it is observed that the GPM mixes (M1, M2, and M3) prepared with 15% GGBS replacement exhibited higher water absorption value (6.08% - 6.59%) and higher volume of permeable voids (6.44% - 6.87%) as compared to the GPM mixes made with other GGBS replacement levels. Further, the GPM mixes prepared with 30% GGBS (M4, M5, and M6) showed water absorption, and volume of permeable voids of 5.18% - 5.72%, and 5.23% - 5.86% respectively. Similarly, the GPM mixes made with 45% GGBS replacement (M7, M8, and M9) exhibited water absorption and volume of permeable voids of 5.2% - 5.62%, and 5.29% - 5.81% respectively. This

indicates that the variations in water absorption, and volume of permeable voids of GPM mixes between 30% and 45% GGBS replacement levels are less. A linear relationship (with $R^2 = 0.974$) was observed between water absorption and volume of permeable voids for all the GPM mixes as shown in Fig. 4.8.

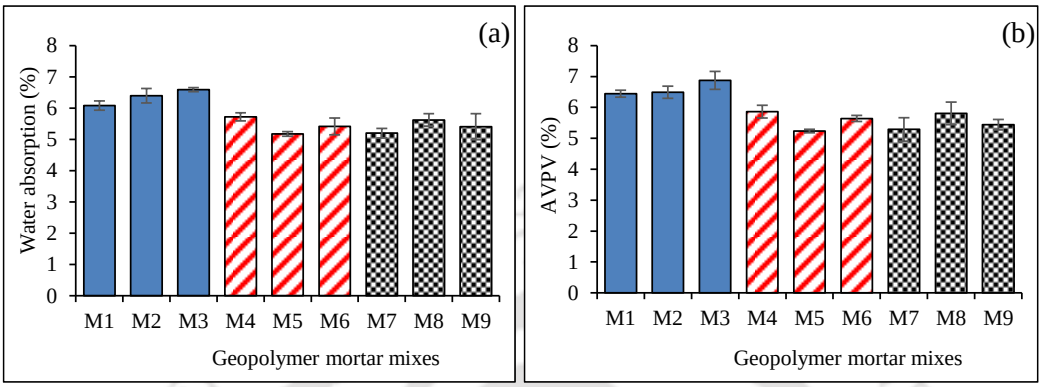

Fig. 4.7 (a) Water absorption (%) and (b) apparent volume of permeable voids (%) of geopolymer mortar mixes at 28 days of ambient curing.

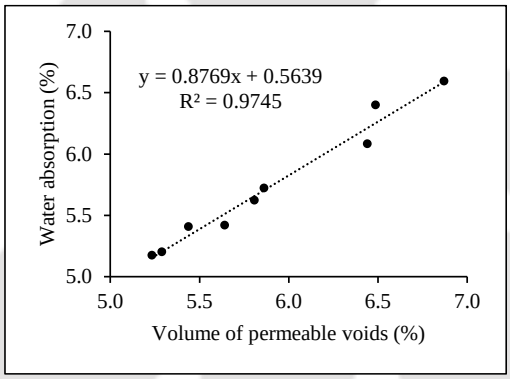

Fig. 4.8 Relationship between water absorption (%) and volume of permeable voids (%) of GPM mixes.

The S/N ratio of water absorption and volume of permeable voids of GPM mixes at 28 days of ambient curing are presented in Table 4.5. The performance statistics of water absorption and volume of permeable voids of GPM mixes are presented in Fig. 4.9. From Fig. 4.9, it can be observed that GGBS replacement level had significant influence on water absorption and volume permeable voids of GPM as compared to other control parameters. The water absorption and volume of permeable voids of GPM mixes decreased (i.e., performance statistics (mean S/N ratio) increased) significantly with increase in GGBS replacement from 15% to 30% followed by a small variation (i.e., small increase in performance statistics) from 30% to 45%. This may be ascribed to the effect of type of geopolymer gel formed in the GPM mixes [98], wherein the formation of more amount of calcium rich gels (N-(C)-A-S-H and C-S-H gels) in the GPM mixes made with higher GGBS content (and

lower fly ash content) resulted in a denser microstructure thereby decreasing the water absorption and volume of permeable voids of GPM mixes. The water absorption of GPM mixes increased (i.e., performance statistics value decreased) with increase in W/GPS ratio and S/B ratio as observed from Fig. 4.9. Further, the performance statistics of volume of permeable voids of GPM mixes mostly decreased with increase in W/GPS ratio. Similarly, the volume of permeable voids of GPM mixes increased (i.e., performance statistics value decreased) with increase in S/B ratio as observed from Fig. 4.9. When W/GPS ratio increased, the water content of the mixes increased thereby resulting in more pores in the GPM mixes. With increase in S/B ratio, the dominant effect of reduced binder content led to a porous microstructure thereby resulting in higher water absorption and volume of permeable voids in the GPM mixes made with higher S/B ratio. From Fig. 4.9, mostly there was unsystematic variation in the performance statistics of water absorption of GPM mixes with molarity of NaOH solution, however, lower water absorption (i.e., higher value of performance statistics) was observed at higher molarity of NaOH solution i.e., 14 M. Further, the volume of permeable voids of GPM mixes decreased (i.e., performance statistics value increased) with increase in molarity of NaOH solution as observed from Fig. 4.9. This may be attributed to the effect of relatively greater extent of polycondensation process in the geopolymer mortar made with higher molarity of NaOH solution that resulted in lower volume of permeable voids in the mixes.

Table 4.5 Signal-to-noise (S/N) ratio of water absorption, apparent volume of permeable voids (AVPV), and sorptivity of geopolymer mortar mixes

Mix	Water absorption	Apparent volume of permeable voids (AVPV)	Sorptivity coefficient
M1	-15.68	-16.18	37.73
M2	-16.12	-16.24	36.15
M3	-16.38	-16.74	32.03
M4	-15.15	-15.37	33.97
M5	-14.28	-14.38	38.48
M6	-14.68	-15.03	33.17
M7	-14.32	-14.48	38.78
M8	-15.00	-15.30	32.11
M9	-14.68	-14.71	36.70

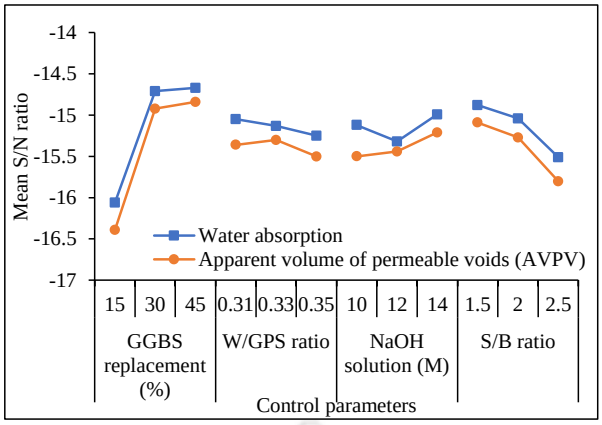

Fig. 4.9 Performance statistics (mean S/N ratio) of water absorption and apparent volume of permeable voids (AVPV) of GPM mixes.

The results of ANOVA of S/N ratio for water absorption and apparent volume of permeable voids of geopolymer mortar are presented in Table 4.6. From this table, it is observed that GGBS replacement dominated the influence of other parameters with highest contributing effect of 81.19% for water absorption, and 81.73% for volume of permeable voids. The S/B ratio (contribution: 13.91% for water absorption, and 14.62% for volume of permeable voids) was the second-best influential parameter after GGBS replacement level followed by molarity of NaOH solution (contribution: 3.59% for water absorption, and 2.52% for volume of permeable voids) and W/GPS ratio (contribution: 1.31% for water absorption, and 1.13% for volume of permeable voids).

Table 4.6 ANOVA results of signal-to-noise (S/N) ratio for water absorption and apparent volume of permeable voids (AVPV) of geopolymer mortar

Parameter	DOF	SOS	MS	Contribution (%)
Water absorption				
GGBS replacement level	2	3.76	1.88	81.19
W/GPS ratio	2	0.06	0.03	1.31
NaOH molarity	2	0.17	0.08	3.59
Sand-to-binder (S/B) ratio	2	0.64	0.32	13.91
Error	-	-	-	-
Total	8	4.63		100.00
Apparent volume of permeable voids (AVPV)				
GGBS replacement level	2	4.57	2.28	81.73
W/GPS ratio	2	0.06	0.03	1.13
NaOH molarity	2	0.14	0.07	2.52
Sand-to-binder (S/B) ratio	2	0.82	0.41	14.62
Error	-	-	-	-
Total	8	5.59		100.00

Note: DOF: Degree of freedom, SOS: Sum of square, MS: Mean square

4.6 Sorptivity

The sorptivity of GPM provides information about the pore structure and its connectivity [98]. Sorptivity curves of fly ash-GGBS based GPM are presented in Fig. 4.10. Sorptivity curves of GPM consist of two stages such as a sharp linear increase, which is called initial rate of water absorption followed by secondary rate of water absorption. In the initial rate of water absorption stage, the capillary pores dominate the sorption process whereas the secondary absorption is dominated by the gel pores, which limit the rate of absorption [14]. As observed from Fig. 4.10, the fly ash-GGBS based GPM did not reach the saturation limit even after 8 days (corresponding to 831.38 $s^{1/2}$ on *x*-axis of Fig. 4.10), which shows a low rate of capillary absorption. The mix M7 (45% GGBS replacement, W/GPS ratio of 0.31, NaOH solution molarity of 14 M, and S/B ratio of 2) showed the lowest rate of water absorption among all the GPM mixes, which indicates a comparatively denser microstructure. It may be noted that the mix M7 exhibited highest 28 days compressive strength as compared to other GPM mixes (Fig. 4.5). The initial slope of the sorptivity curves measured up to 6 hours of water absorption for GPM mixes are shown in Fig. 4.11. The correlation coefficient (R^2) of linear relationship for all the GPM mixes was greater than 0.98 as evident from Fig. 4.11.

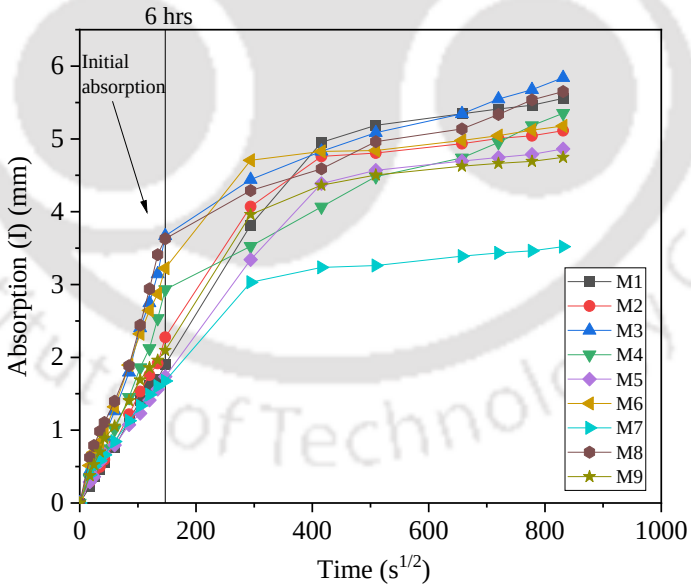

Fig. 4.10 Sorptivity of geopolymer mortar mixes.

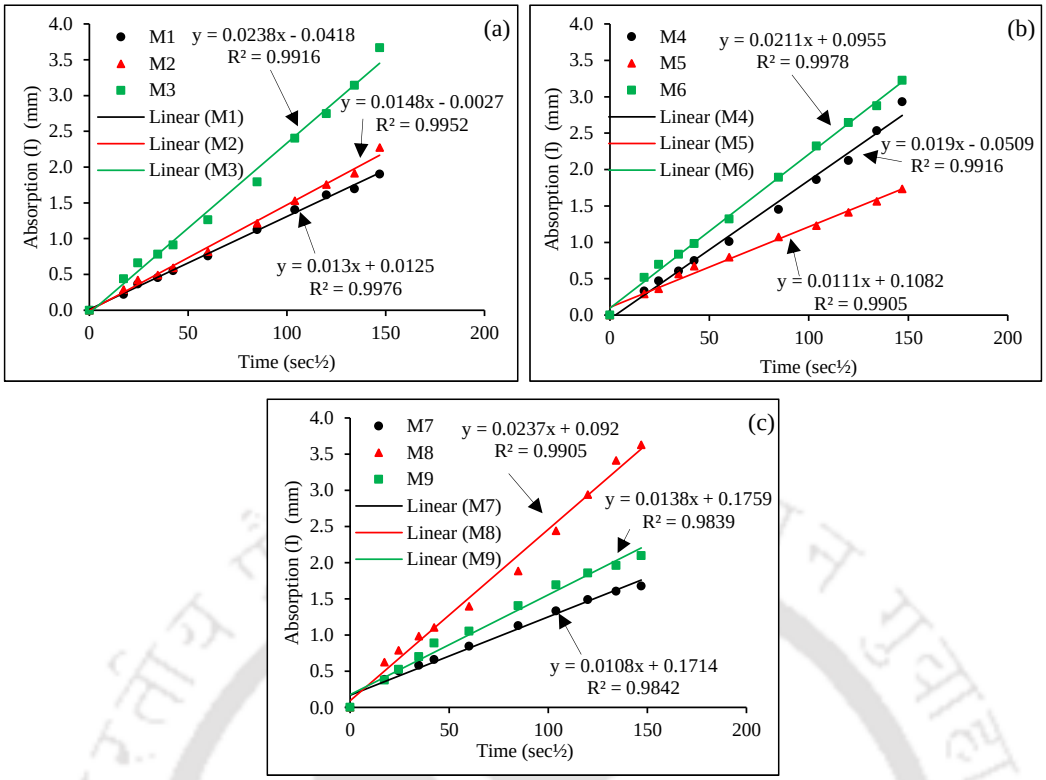

Fig. 4.11 Initial sorptivity of GPM mixes made with (a) 15% GGBS (M1, M2, and M3), (b) 30% GGBS (M4, M5, and M6), and (c) 45% GGBS (M7, M8, and M9).

The sorptivity coefficient (S) of initial absorption of GPM mixes, which was calculated using equation 3.10 is illustrated in Fig. 4.12. From Fig. 4.12, it is observed that the mix M3 (GGBS replacement of 15%, W/GPS ratio of 0.35, NaOH solution molarity of 14 M, and S/B ratio of 2.5) exhibited highest sorptivity coefficient of 24.97 × 10^{-3} mm/$s^{1/2}$, whereas the mix M7 (45% GGBS replacement, W/GPS ratio of 0.31, NaOH solution molarity of 14 M, and S/B ratio of 2) exhibited lowest sorptivity coefficient of 11.4 × 10^{-3} mm/$s^{1/2}$. The S/N ratio of sorptivity coefficient of GPM mixes are presented in Table 4.5. The performance statistics of sorptivity coefficient of fly ash-GGBS based GPM mixes are shown in Fig. 4.13. From this figure, it is observed that the sorptivity of fly ash-GGBS based GPM is primarily controlled by S/B ratio followed by W/GPS ratio. The performance statistics value of sorptivity coefficient of the GPM mixes decreased with increase in S/B ratio and W/GPS ratio as observed from Fig. 4.13. In other words, the sorptivity of GPM mixes increased with increase in S/B ratio and W/GPS ratio, which may be ascribed to the effect of increase in porosity of GPM mixes with increase in S/B ratio and W/GPS ratio. The effects of molarity of NaOH solution and GGBS replacement level were comparatively less significant on the sorptivity of GPM, which may be due to the dominant effect of S/B ratio and W/GPS ratio. The results of ANOVA of S/N ratio for sorptivity coefficient of

geopolymer mortar are presented in Table 4.7. From this table, it is observed that S/B ratio has highest contributing effect of 65.69%. The W/GPS ratio was the second-best influential parameter with contributing effect of 21.43% followed by molarity of NaOH solution (11.58%) and GGBS replacement level (1.30%).

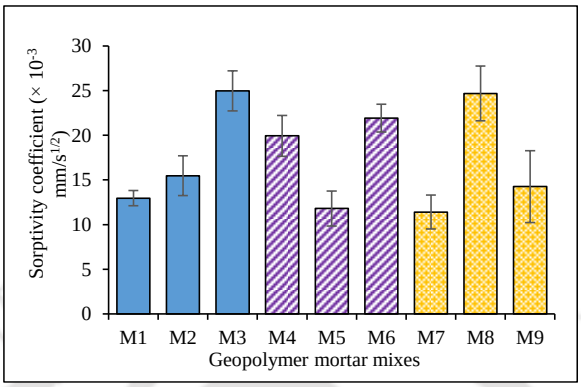

Fig. 4.12 Sorptivity coefficient of geopolymer mortar mixes.

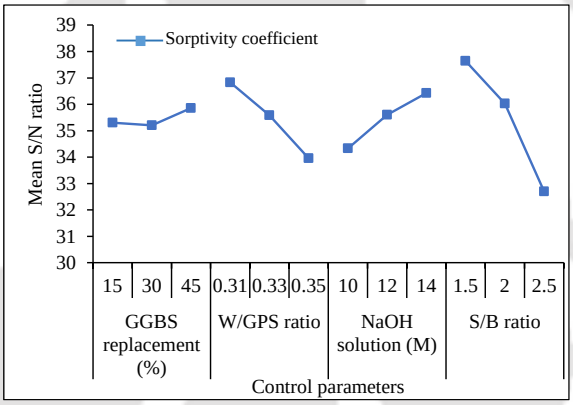

Fig. 4.13 Performance statistics (mean S/N ratio) of sorptivity coefficient of geopolymer mortar mixes.

Table 4.7 ANOVA results of signal-to-noise (S/N) ratio for sorptivity coefficient of geopolymer mortar

Parameter	DOF	SOS	MS	Contribution (%)
GGBS replacement level	2	0.76	0.38	1.30
W/GPS ratio	2	12.42	6.21	21.43
NaOH molarity	2	6.71	3.36	11.58
Sand-to-binder (S/B) ratio	2	38.08	19.04	65.69
Error	-	-	-	-
Total	8	57.98		100.00

Note: DOF: Degree of freedom, SOS: Sum of square, MS: Mean square

4.7 Sulfate and acid resistance

4.7.1 Change in compressive strength (%)

The compressive strength of GPM mixes (L_9) measured after 26 weeks of immersion in different exposure solutions are shown in Fig. 4.14 and Fig. 4.15. The change in

compressive strength of GPM mixes after exposure to different sulfate and acid solutions with respect to control mixes (i.e., GPM mixes immersed in normal water) are shown in Fig. 4.16 and Fig. 4.17 respectively. From Fig. 4.14, it is observed that the GPM mixes prepared with 15% GGBS (M1 - M3) and 30% GGBS (M4 - M6) exhibited highest compressive strength when immersed in 6% Na_2SO_4 solution whereas the GPM mixes prepared with 45% GGBS (M7 - M9) exhibited highest compressive strength when immersed in normal water as compared to other exposure solutions. From Fig. 4.16, it is observed that the GPM mixes prepared with 15% GGBS (M1 - M3) showed maximum strength gain in the range of 3.51% to 32.73%, and 6.14% to 25.45% when immersed in Na_2SO_4 solution (3% and 6%) and $MgSO_4$ solution (3% and 6%) respectively with respect to control mixes (i.e., specimens immersed in water). Similarly, the compressive strength gain for the GPM mixes prepared with 30% GGBS (M4 - M6) with respect to control mixes are in the range of 0.65% to 13.93% when immersed in Na_2SO_4 solution (3% and 6%), and 0.65% to 5.93% when immersed in $MgSO_4$ solution (3% and 6%). However, the GPM mixes prepared with 45% GGBS (M7 - M9) showed loss of compressive strength in the range of 0.63% to 10.37%, and 4.14% to 15.85% in case of exposure to Na_2SO_4 (3% and 6%) solution and $MgSO_4$ solution (3% and 6%) respectively when compared with control mixes. The increase in compressive strength of GPM mixes (M1 - M6: prepared with comparatively lower GGBS replacement levels) in case of exposure to Na_2SO_4 and $MgSO_4$ solutions may be attributed to the formation of lower amount of gypsum in the presence of sulfate ions that might have filled the pores in the matrix. Further, the main geopolymerization product of fly ash or fly ash-GGBS (lower GGBS replacement) based geopolymer i.e., a stable three-dimensional alkaline aluminosilicate gel is less susceptible to sulfate attack [43]. The reason for strength loss in GPM mixes prepared with 45% GGBS (M7 - M9) for exposure against sulfate solutions (Na_2SO_4 solution and $MgSO_4$ solution) may be attributed to the effect of decalcification of calcium enriched gels (N-(C)-A-S-H and C-S-H gels) to a comparatively higher extent that promoted the formation of more amount of gypsum in the geopolymer matrix [47]. Further, it is observed that the GPM mixes M1 - M6 mostly exhibited higher gain in compressive strength when exposed to 6% Na_2SO_4 and 6% $MgSO_4$ solutions as compared to 3% Na_2SO_4 and 3% $MgSO_4$ solutions respectively. However, the GPM mixes made with higher GGBS replacement i.e., M7 - M9 exhibited higher loss in compressive strength in case of exposure to 6% Na_2SO_4 and 6% $MgSO_4$ solutions when compared with 3% Na_2SO_4 and 3% $MgSO_4$ solutions respectively.

From Fig. 4.15, it is noticed that the compressive strength of GPM mixes immersed in H_2SO_4 solutions (0.31 mol/l and 0.62 mol/l) and HCl solutions (0.31 mol/l and 0.62 mol/l) decreased significantly as compared to the control GPM mixes. As evident from Fig. 4.17, the maximum compressive strength loss was observed in the GPM mixes prepared with 45% GGBS (M7 - M9) and it varied from 55.49% to 72.56%, and 53.66% to 73.17% for exposure against H_2SO_4 and HCl solutions respectively. Similarly, the GPM mixes prepared with 15% of GGBS exhibited minimum strength loss in the range of 25.45% to 47.37% when immersed in H_2SO_4 solutions, and 27.27% to 48.25% when immersed in HCl solutions. The significant strength loss in the GPM mixes immersed in acid solutions may be attributed to the effect of depolymerization of the aluminosilicate gels. The oxy-aluminum bridge (-Al-Si-O) of geopolymer gel may get destroyed in the acidic media thereby resulting in reduction of compressive strength of GPM mixes [57]. While comparing the strength loss of GPM mixes (M1 - M9), it is observed that there is no systematic variation in strength loss between 0.31 mol/l H_2SO_4 and 0.31 mol/l HCl solutions. However, all the GPM mixes immersed in 0.62 mol/l H_2SO_4 solution exhibited less strength loss (35.45% to 72.56%) as compared to that immersed in 0.62 mol/l HCl solution (40.91% to 73.17%) as observed from Fig. 4.17. This may be attributed to the fact that the presence of Na-rich gel in the GPM mix neutralizes the effect of sulfuric acid to a comparatively higher extent and mitigates its destructive effect on the geopolymer gel structures [133] as compared to the effect of hydrochloric acid. Further, from Fig. 4.17, it is observed that the GPM mixes exhibited more strength loss when immersed in higher concentration of H_2SO_4 and HCl solutions as compared to lower concentration. This may be due to the effect of increase in the extent depolymerization of aluminosilicate gels in the presence of higher concentration of acid solutions.

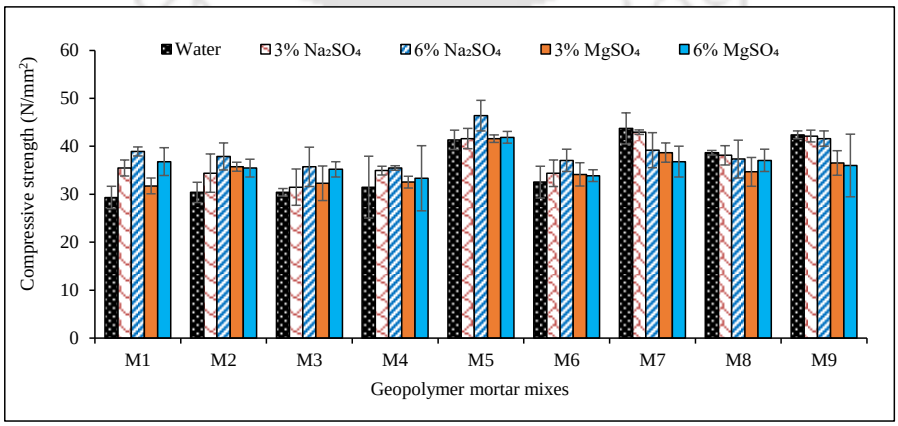

Fig. 4.14 Compressive strength of GPM mixes after 26 weeks of exposure to water and different sulfate solutions.

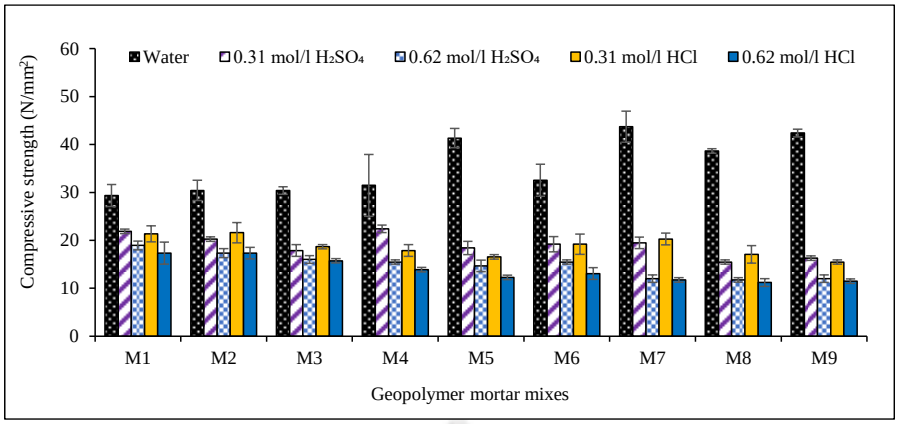

Fig. 4.15 Compressive strength of GPM mixes after 26 weeks of exposure to water and different acid solutions.

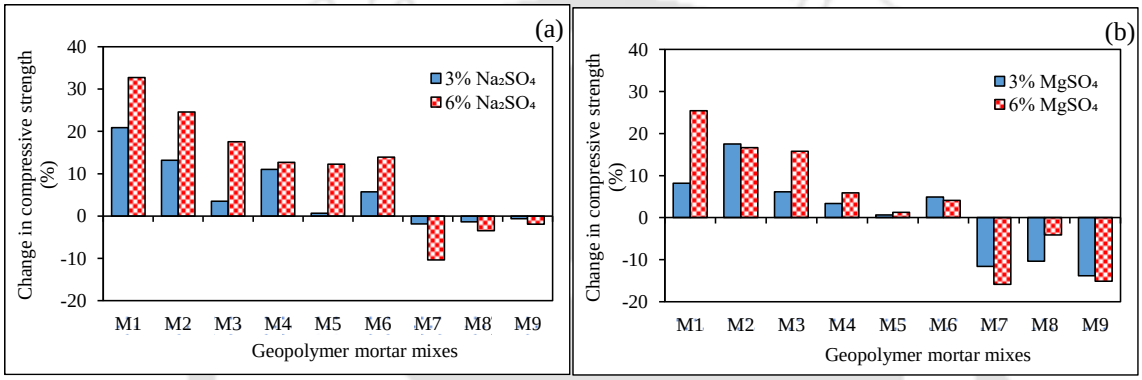

Fig. 4.16 Change in compressive strength of GPM mixes after 26 weeks of exposure to (a) Na_2SO_4 solutions and (b) $MgSO_4$ solutions in comparison to exposure to water.

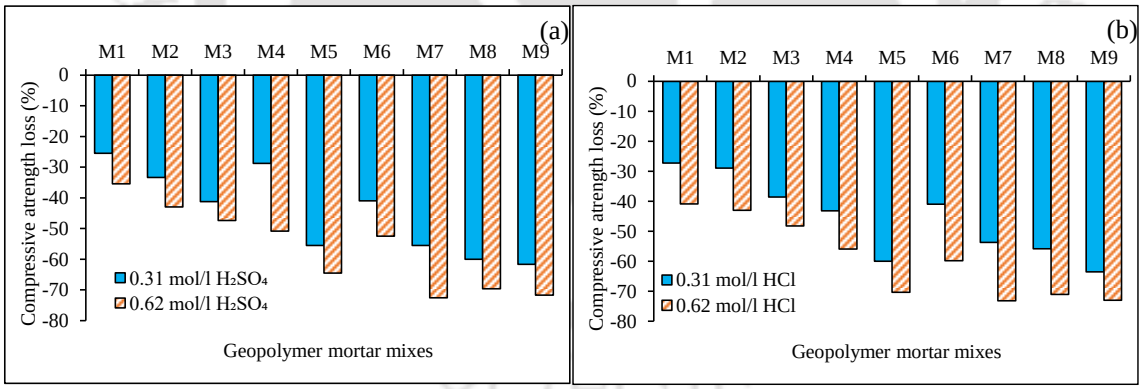

Fig. 4.17 Change in compressive strength of GPM mixes after 26 weeks of exposure to (a) H_2SO_4 solutions and (b) HCl solutions in comparison to exposure to water.

The S/N ratio of compressive strength of GPM mixes after immersion in different solutions for 26 weeks of exposure period are presented in Table 4.8. The performance statistics of compressive strength of GPM mixes after immersion in different solutions for 26 weeks are shown in Fig. 4.18 (a - e). From Fig. 4.18 (a - c), it is observed that the optimal level of control parameters for better performance (in terms of compressive strength) of GPM mixes immersed in water, Na_2SO_4 and $MgSO_4$ solutions are GGBS replacement of 45% (except

the GPM mixes immersed in 6% Na_2SO_4 solution, where the optimum GGBS replacement was 30%), W/GPS ratio of 0.33, NaOH solution of 14 M, and S/B ratio of 1.5. Similarly, from Fig. 4.18 (d and e), it can be noted that the optimal level of control parameters for better performance of GPM mixes immersed in H_2SO_4 and HCl solutions are GGBS replacement of 15%, W/GPS ratio of 0.31, NaOH solution of 10 M and 12 M, and S/B ratio of 1.5 and 2.0. It can be observed from Fig. 4.18 (a) that the GGBS replacement had significant influence on compressive strength of GPM mixes immersed in water as compared to other parameters. The performance statistics of compressive strength of control GPM mixes (specimens immersed in water) increased with increase in GGBS replacement level and molarity of NaOH solution as observed from Fig. 4.18 (a). The effect of GGBS replacement level on compressive strength was less significant for the GPM mixes immersed in sulfate solutions except 3% Na_2SO_4 solution (Fig. 4.18 (b and c)). The performance statistics of compressive strength of GPM mixes increased slightly with increase in molarity of NaOH solution in case of exposure to 3% and 6% Na_2SO_4 solution, and 3% $MgSO_4$ solution whereas there was unsystematic variation in performance statistics of compressive strength with increase in molarity of NaOH solution in case of exposure to 6% $MgSO_4$ solution. Further, the performance statistics of compressive strength of GPM mixes immersed in water, and both concentrations of Na_2SO_4 and $MgSO_4$ solutions decreased with increase in S/B ratio of the mixes as observed from Fig. 4.18 (a - c). This indicates that the effect of formation of porous matrix as a result of comparatively lower extent of geopolymerization process due to lower paste content in the GPM mixes made with higher S/B ratio was dominant in reducing the compressive strength of GPM mixes exposed to water and sulfate solutions. Further, there was unsystematic variation in performance statistics of compressive strength with W/GPS ratio for the GPM mixes immersed in water, and both concentrations of Na_2SO_4 and $MgSO_4$ solutions.

From Fig. 4.18 (d and e), it is observed that the effects of W/GPS ratio, molarity of NaOH solution and S/B ratio on variations in compressive strength were less significant for the GPM mixes immersed in acid solutions except in case of exposure to 0.31 mol/l H_2SO_4 solution. However, the performance statistics of compressive strength decreased with increase in GGBS replacement level of the GPM mixes immersed in acid solutions as evident from Fig. 4.18 (d and e) with significant decrease with increase in GGBS replacement level in case of exposure to 0.62 mol/l H_2SO_4 and 0.62 mol/l HCl solutions. This may be ascribed to the effect of depolymerization of aluminosilicate gels to a greater

extent in case of exposure to both the acid solutions as well as formation of higher amount of gypsum in case of exposure to sulfuric acid solution for the GPM mixes made with higher GGBS content. The percentage of contribution of control parameters on compressive strength of GPM mixes immersed in different exposure solutions determined from ANOVA technique are presented in Table 4.9 and Table 4.10. From Table 4.9, it is observed that GGBS replacement level had dominant effect on compressive strength of GPM mixes followed by S/B ratio in case of exposure against water, and sulfate solutions. Similarly, in case of exposure against acid solutions, the compressive strength was significantly influenced by GGBS replacement level as compared to other control parameters.

Table 4.8 Signal-to-noise (S/N) ratio of compressive strength of geopolymer mortar mixes after immersion in water, and different sulfate and acid solutions

Mix	Water	Sulfate solutions				Acid solutions			
		3% Na_2SO_4	6% Na_2SO_4	3% $MgSO_4$	6% $MgSO_4$	0.31 mol/l H_2SO_4	0.62 mol/l H_2SO_4	0.31 mol/l HCl	0.62 mol/l HCl
M1	29.30	30.98	31.80	30.01	31.26	26.79	25.52	26.53	24.64
M2	29.61	30.61	31.52	31.06	30.97	26.13	24.75	26.61	24.73
M3	29.65	29.82	30.94	30.07	30.91	25.00	24.06	25.42	23.93
M4	29.60	30.86	30.99	30.23	30.04	26.99	23.78	25.00	22.83
M5	32.31	32.36	33.29	32.38	32.43	25.24	23.27	24.36	21.76
M6	30.15	30.67	31.34	30.62	30.58	25.61	23.78	25.55	22.25
M7	32.77	32.65	31.79	31.72	31.25	25.75	21.54	26.10	21.37
M8	31.75	31.60	31.34	30.73	31.34	23.78	21.37	24.55	20.94
M9	32.54	32.49	32.37	31.21	30.86	24.22	21.54	23.78	21.18

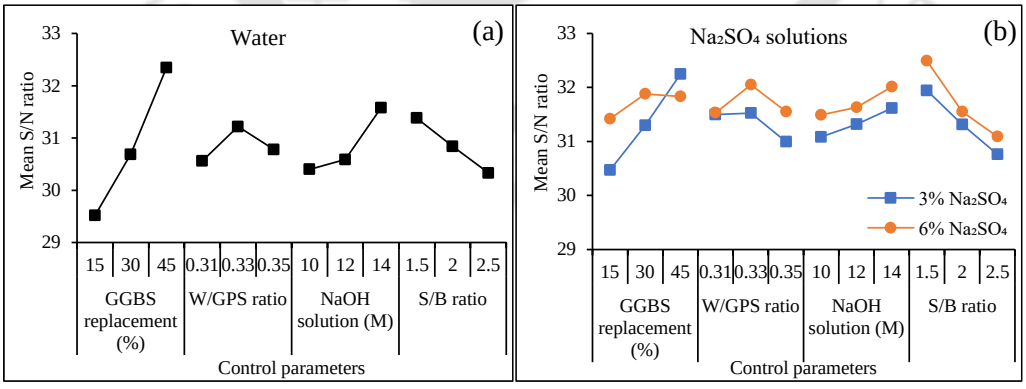

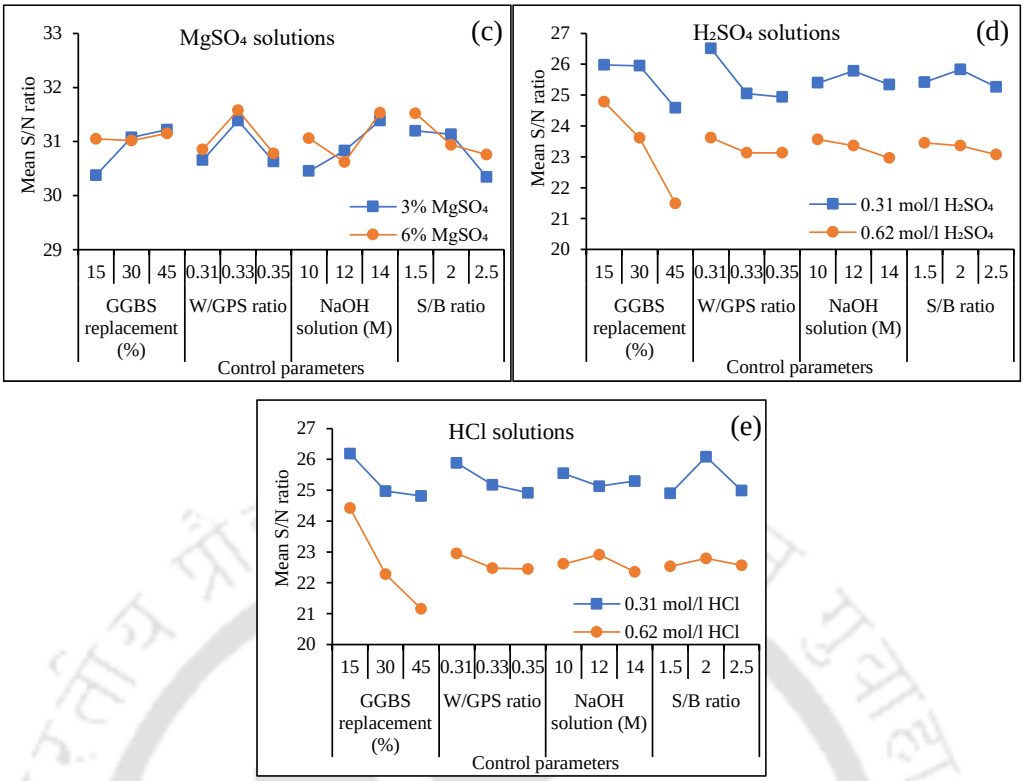

Fig. 4.18 Performance statistics (mean S/N ratio) of compressive strength of GPM mixes after 26 weeks of immersion in different exposure solutions: (a) water, (b) Na_2SO_4 solutions, (c) $MgSO_4$ solutions, (d) H_2SO_4 solutions, (e) HCl solutions.

Table 4.9 ANOVA results of signal-to-noise (S/N) ratio for compressive strength of geopolymer mortar after exposure to water and different sulfate solutions

Parameter	DOF	SOS	MS	Contribution (%)
Compressive strength after exposure to water				
GGBS replacement level	2	12.13	6.07	71.91
W/GPS ratio	2	0.68	0.34	4.02
NaOH molarity	2	2.41	1.2	14.27
Sand-to-binder (S/B) ratio	2	1.65	0.83	9.80
Error	-	-	-	-
Total	8	16.87		100.00
Compressive strength after exposure to 3% Na_2SO_4 solution				
GGBS replacement level	2	4.74	2.73	60.85
W/GPS ratio	2	0.54	0.27	6.91
NaOH molarity	2	0.42	0.21	5.41
Sand-to-binder (S/B) ratio	2	2.09	1.05	26.83
Error	-	-	-	-
Total	8	7.80		100.00
Compressive strength after exposure to 6% Na_2SO_4 solution				
GGBS replacement level	2	0.38	0.19	8.70
W/GPS ratio	2	0.52	0.26	11.86
NaOH molarity	2	0.43	0.22	9.89
Sand-to-binder (S/B) ratio	2	3.06	1.53	69.55
Error	-	-	-	-

Total	8	4.39		100.00
Compressive strength after exposure to 3% $MgSO_4$ solution				
GGBS replacement level	2	1.22	0.61	24.32
W/GPS ratio	2	1.11	0.55	22.04
NaOH molarity	2	1.34	0.67	26.58
Sand-to-binder (S/B) ratio	2	1.36	0.68	27.06
Error	-	-	-	-
Total	8	5.03		100.00
Compressive strength after exposure to 6% $MgSO_4$ solution				
GGBS replacement level	2	0.03	0.01	0.82
W/GPS ratio	2	1.18	0.59	34.70
NaOH molarity	2	1.24	0.62	36.60
Sand-to-binder (S/B) ratio	2	0.95	0.47	27.88
Error	-	-	-	-
Total	8	3.39		100.00

Note: DOF: Degree of freedom, SOS: Sum of square, MS: Mean square

Table 4.10 ANOVA results of signal-to-noise (S/N) ratio for compressive strength of geopolymer mortar after exposure to different acid solutions

Parameter	DOF	SOS	MS	Contribution (%)
Compressive strength after exposure to 0.31 mol/l H_2SO_4 solution				
GGBS replacement level	2	3.80	1.90	40.87
W/GPS ratio	2	4.61	2.31	49.68
NaOH molarity	2	0.36	0.28	3.84
Sand-to-binder (S/B) ratio	2	0.52	0.12	5.61
Error	-	-	-	-
Total	8	9.29		100.00
Compressive strength after exposure to 0.62 mol/l H_2SO_4 solution				
GGBS replacement level	2	16.69	8.34	92.89
W/GPS ratio	2	0.48	0.24	2.67
NaOH molarity	2	0.56	0.28	3.12
Sand-to-binder (S/B) ratio	2	0.24	0.12	1.32
Error	-	-	-	-
Total	8	17.96		100.00
Compressive strength after exposure to 0.31 mol/l HCl solution				
GGBS replacement level	2	3.39	1.69	43.47
W/GPS ratio	2	1.49	0.75	19.12
NaOH molarity	2	0.26	0.13	3.33
Sand-to-binder (S/B) ratio	2	2.66	1.33	34.08
Error	-	-	-	-
Total	8	7.80		100.00
Compressive strength after exposure to 0.62 mol/l HCl solution				
GGBS replacement level	2	16.57	8.28	94.07
W/GPS ratio	2	0.47	0.24	2.68
NaOH molarity	2	0.46	0.23	2.58
Sand-to-binder (S/B) ratio	2	0.12	0.06	0.67
Error	-	-	-	-
Total	8	17.61		100.00

Note: DOF: Degree of freedom, SOS: Sum of square, MS: Mean square

4.8 Optimization of GPM mixes using Taguchi-GRA method

In the present study, different properties such as setting time (initial and final), flowability, compressive strength (7, 28, 90, and 180 days), water absorption (28 days), volume of permeable voids (28 days), sorptivity (28 days), and sulfate and acid resistance (26 weeks of exposure) of GPM mixes designed by Taguchi method were studied. Further, the optimum combination of different control parameters to obtain a given property (response) as per the appropriate function such as "larger-the-better", and "smaller-the-better" were determined by Taguchi method. The optimal combination of control parameters for individual properties of geopolymer mortar mixes corresponding to maximum performance statistics are presented in Table 4.11. This table provides information about the selection of appropriate levels of control parameters to achieve the optimum value of an individual property of the geopolymer mortar. However, to optimize the control parameters for multiple properties simultaneously, Taguchi-GRA (Grey relational analysis) method was implemented (already stated in Chapter 3).

As stated earlier in Chapter 3, the obtained results of different properties (responses) of GPM mixes (L_9 OA) were converted to S/N ratio using the appropriate functions. Grey relational analysis was then carried out wherein the normalized S/N ratio, deviation sequence (difference between ideal value of normalized S/N ratio and the normalized S/N ratio), grey relational coefficient (GRC) and grey relational grade (GRG) were calculated. It may be noted that the grey relational grade (GRG) for a given GPM mix was calculated by assigning equal weightage to each response (property). The calculated values of normalized S/N ratio, deviation sequence (Δ_{0ij}), and GRC and GRG for all the GPM mixes are presented in Table 4.12, Table 4.13, and Table 4.14 respectively. From Table 4.14, it is observed that the GPM mix M7 showed highest value of grey relational coefficient (GRC) for compressive strength at 28, 90, and 180 days of ambient curing, sorptivity, and compressive strength after exposure to water and 3% Na_2SO_4 solution thereby indicating better performance with respect to these properties as compared to other mixes. Similarly, the GPM mix M5 showed better performance with respect to water absorption, apparent volume of permeable voids (AVPV), and compressive strength after exposure to 6% Na_2SO_4, 3% $MgSO_4$, and 6% $MgSO_4$ solutions as compared to other mixes. The GPM mix M4 showed better performance from view point of setting time (both initial and final) and compressive strength after exposure to 0.31 mol/l sulfuric acid solution as observed from Table 4.14. Similarly, the GPM mix M9 exhibited better performance with respect to flow

index, and compressive strength at 7 days of ambient curing. Further, the GPM mix M2 showed better performance with respect to compressive strength after exposure to 0.31 mol/l and 0.62 mol/l hydrochloric acid solution, and GPM mix M1 showed better performance with respect to compressive strength after exposure to 0.62 mol/l sulfuric acid solution when compared with other mixes as evident from Table 4.14. Since, the GPM mix M 7 (prepared with 45% GGBS, W/GPS ratio of 0.31, NaOH solution of 14 M and S/B ratio of 2) showed highest grey relational coefficient (GRC) for relatively more number of properties as compared to other GPM mixes, it achieved the highest grey relational grade (GRG) of 0.74 among all the GPM mixes. However, the optimal combination of these parameters may change, if different weightages are assigned to the considered responses (properties). For example, if a design of GPM mix is required with greater emphasis on its durability performance against acidic environment with adequate flowability and strength, in that scenario, while calculating the grey relational grade (GRG), higher weightage will be assigned to the compressive strength of GPM after exposure to acid solutions as compared to other properties. Accordingly, in that case, a different combination of the control parameters could be achieved with a highest GRG value. Further, if the number of studied properties (responses) is changed, then, a different combination of control parameters could be obtained with a highest GRG value.

To obtain the overall optimal GPM mix, the mean GRG for all the parameters were calculated. The level of a parameter with maximum mean GRG is the optimal one among all the levels of that parameter, as it will have highest main effect on the responses [112]. The mean GRG for a given level of a parameter was found out by calculating the average of the GRG for the mixes made with that level of the parameter. Table 4.15 presents the calculated values of mean GRG for all the parameters. From Table 4.15, it was noted that the highest values of mean GRG were obtained for the following combination of parameters: GGBS replacement of 45% (Level-3), W/GPS ratio of 0.31 (Level-1), NaOH solution of 14 M (Level-3), and S/B ratio of 1.5 (Level-1). The higher mean GRG indicates that the mix prepared with these levels of the mix parameters would perform better with respect to all the studied properties of geopolymer mortar.

Table 4.11 Optimal mix proportions for different properties of geopolymer mortar corresponding to maximum performance statistics

Optimized Mix	GGBS replacement level (%)	Water-to-geopolymer solids (W/GPS) ratio	NaOH (M)	Sand to binder (S/B) ratio
M_{IST}	30	0.31	14	2.5
M_{FST}	30	0.31	14	2.5
$M_{Flowability}$	15	0.35	14	1.5
$M_{7\ days\text{-}CS}$	45	0.31	10	1.5
$M_{28\ days\text{-}CS}$	45	0.31	14	1.5
$M_{90\ days\text{-}CS}$	45	0.31	14	1.5
$M_{180\ days\text{-}CS}$	45	0.31	14	2.0
$M_{Water\ absorption}$	45	0.31	14	1.5
M_{AVPV}	45	0.33	14	1.5
$M_{Sorptivity}$	45	0.31	14	1.5
$M_{Water\ exposure}$	45	0.33	14	1.5
$M_{3\%\ sodium\ sulfate\ exposure}$	45	0.33	14	1.5
$M_{6\%\ sodium\ sulfate\ exposure}$	30	0.33	14	1.5
$M_{3\%\ magnesium\ sulfate\ exposure}$	45	0.33	14	1.5
$M_{6\%\ magnesium\ sulfate\ exposure}$	45	0.33	14	1.5
$M_{0.31\ mol/l\ sulfuric\ acid\ exposure}$	15	0.31	12	2.0
$M_{0.62\ mol/l\ sulfuric\ acid\ exposure}$	15	0.31	10	1.5
$M_{0.31\ mol/l\ hydrochloric\ acid\ exposure}$	15	0.31	10	2.0
$M_{0.62\ mol/l\ hydrochloric\ acid\ exposure}$	15	0.31	12	2.0

Note: IST= Initial setting time; FST= Final setting time; CS= Compressive strength; AVPV= Apparent volume of permeable voids.

Table 4.12 Normalized S/N ratio of different properties (responses) of geopolymer mortar mixes

Mix	Normalized S/N ratio of setting time		Normalized S/N ratio of flow index	Normalized S/N ratio of compressive strength				Normalized S/N ratio of water absorption	Normalized S/N ratio of AVPV	Normalized S/N ratio of sorptivity coefficient	Normalized S/N ratio of compressive strength after immersion in different exposure solutions								
	IST	FST		7 days	28 days	90 days	180 days				Water	3% Na_2SO_4	6% Na_2SO_4	3% $MgSO_4$	6% $MgSO_4$	0.31 mol/l H_2SO_4	0.62 mol/l H_2SO_4	0.31 mol/l HCl	0.62 mol/l HCl
M1	0.00	0.00	0.91	0.41	0.74	0.59	0.44	0.33	0.24	0.84	0.00	0.41	0.37	0.00	0.51	0.94	1.00	0.97	0.97
M2	0.14	0.08	0.80	0.00	0.22	0.27	0.32	0.12	0.21	0.61	0.09	0.28	0.25	0.44	0.39	0.73	0.81	1.00	1.00
M3	0.51	0.56	0.53	0.00	0.16	0.00	0.00	0.00	0.00	0.00	0.10	0.00	0.00	0.03	0.37	0.38	0.65	0.58	0.79
M4	1.00	1.00	0.00	0.59	0.00	0.01	0.35	0.58	0.58	0.29	0.09	0.37	0.02	0.10	0.00	1.00	0.58	0.43	0.50
M5	0.56	0.77	0.96	0.54	0.50	0.47	0.56	1.00	1.00	0.96	0.87	0.90	1.00	1.00	1.00	0.46	0.46	0.20	0.22
M6	0.25	0.31	0.78	0.35	0.31	0.19	0.33	0.81	0.72	0.17	0.25	0.30	0.17	0.26	0.23	0.57	0.58	0.63	0.35
M7	0.64	0.79	0.61	0.88	1.00	1.00	1.00	0.98	0.95	1.00	1.00	1.00	0.36	0.72	0.51	0.61	0.04	0.82	0.11
M8	0.48	0.61	0.16	0.84	0.41	0.48	0.74	0.66	0.61	0.01	0.71	0.63	0.17	0.30	0.55	0.00	0.00	0.27	0.00
M9	0.38	0.44	1.00	1.00	0.60	0.53	0.60	0.81	0.86	0.69	0.94	0.94	0.61	0.51	0.34	0.14	0.04	0.00	0.06

Note: IST= Initial setting time; FST= Final setting time; AVPV= Apparent volume of permeable voids.

Table 4.13 Deviation sequence (Δ_{0ij}) values of different properties (responses) of geopolymer mortar mixes

Mix	Δ_{0ij} of setting time		Δ_{0ij} of flow index	Δ_{0ij} of compressive strength				Δ_{0ij} of water absorption	Δ_{0ij} of AVPV	Δ_{0ij} of sorptivity coefficient	Δ_{0ij} of compressive strength after immersion in different exposure solutions								
	IST	FST		7 days	28 days	90 days	180 days				Water	3% Na_2SO_4	6% Na_2SO_4	3% $MgSO_4$	6% $MgSO_4$	0.31 mol/l H_2SO_4	0.62 mol/l H_2SO_4	0.31 mol/l HCl	0.62 mol/l HCl
M1	1.00	1.00	0.09	0.59	0.26	0.41	0.56	0.67	0.76	0.16	1.00	0.59	0.63	1.00	0.49	0.06	0.00	0.03	0.03
M2	0.86	0.92	0.20	1.00	0.78	0.73	0.68	0.88	0.79	0.39	0.91	0.72	0.75	0.56	0.61	0.27	0.19	0.00	0.00
M3	0.49	0.44	0.47	1.00	0.84	1.00	1.00	1.00	1.00	1.00	0.90	1.00	1.00	0.97	0.63	0.62	0.35	0.42	0.21
M4	0.00	0.00	1.00	0.41	1.00	0.99	0.65	0.42	0.42	0.71	0.91	0.63	0.98	0.90	1.00	0.00	0.42	0.57	0.50
M5	0.44	0.23	0.04	0.46	0.50	0.53	0.44	0.00	0.00	0.04	0.13	0.10	0.00	0.00	0.00	0.54	0.54	0.80	0.78
M6	0.75	0.69	0.22	0.65	0.69	0.81	0.67	0.19	0.28	0.83	0.75	0.70	0.83	0.74	0.77	0.43	0.42	0.37	0.65
M7	0.36	0.21	0.39	0.12	0.00	0.00	0.00	0.02	0.05	0.00	0.00	0.00	0.64	0.28	0.49	0.39	0.96	0.18	0.89
M8	0.52	0.39	0.84	0.16	0.59	0.52	0.26	0.34	0.39	0.99	0.29	0.37	0.83	0.70	0.45	1.00	1.00	0.73	1.00
M9	0.62	0.56	0.00	0.00	0.40	0.47	0.40	0.19	0.14	0.31	0.06	0.06	0.39	0.49	0.66	0.86	0.96	1.00	0.94

Note: IST= Initial setting time; FST= Final setting time; AVPV= Apparent volume of permeable voids.

Table 4.14 Grey relational coefficient (GRC) and grey relational grade (GRG) of geopolymer mortar mixes

Mix	GRC of setting time		GRC of flow index	GRC of compressive strength				GRC of water absorption	GRC of AVPV	GRC of sorptivity coefficient	GRC of compressive strength after immersion in different exposure solutions									Grey relational grade (GRG)
	IST	FST		7 days	28 days	90 days	180 days				Water	3% Na_2SO_4	6% Na_2SO_4	3% $MgSO_4$	6% $MgSO_4$	0.31 mol/l H_2SO_4	0.62 mol/l H_2SO_4	0.31 mol/l HCl	0.62 mol/l HCl	
M1	0.33	0.33	0.85	0.46	0.66	0.55	0.47	0.43	0.40	0.76	0.33	0.46	0.44	0.33	0.51	0.89	1.00	0.95	0.95	0.58
M2	0.37	0.35	0.71	0.33	0.39	0.41	0.43	0.36	0.39	0.56	0.35	0.41	0.40	0.47	0.45	0.65	0.73	1.00	1.00	0.51
M3	0.51	0.53	0.51	0.33	0.37	0.33	0.33	0.33	0.33	0.33	0.36	0.33	0.33	0.34	0.44	0.45	0.59	0.54	0.70	0.42
M4	1.00	1.00	0.33	0.55	0.33	0.33	0.44	0.55	0.54	0.41	0.35	0.44	0.34	0.36	0.33	1.00	0.54	0.47	0.50	0.52
M5	0.53	0.68	0.93	0.52	0.50	0.48	0.53	1.00	1.00	0.92	0.79	0.83	1.00	1.00	1.00	0.48	0.48	0.39	0.39	0.71
M6	0.40	0.42	0.69	0.43	0.42	0.38	0.43	0.72	0.64	0.38	0.40	0.42	0.38	0.40	0.39	0.54	0.54	0.57	0.43	0.47
M7	0.58	0.71	0.56	0.81	1.00	1.00	1.00	0.96	0.92	1.00	1.00	1.00	0.44	0.64	0.50	0.56	0.34	0.74	0.36	**0.74**
M8	0.49	0.56	0.37	0.76	0.46	0.49	0.66	0.59	0.56	0.34	0.63	0.57	0.38	0.42	0.52	0.33	0.33	0.41	0.33	0.48
M9	0.45	0.47	1.00	1.00	0.55	0.52	0.56	0.73	0.78	0.62	0.89	0.89	0.56	0.50	0.43	0.37	0.34	0.33	0.35	0.60

Note: IST= Initial setting time; FST= Final setting time; AVPV= Apparent volume of permeable voids.

Table 4.15 Mean grey relational grade for each level of all the mix parameters

Parameter	Level-1	Level-2	Level-3
GGBS replacement level	0.51	0.57	**0.61***
W/GPS ratio	**0.62***	0.57	0.50
Molarity of NaOH solution	0.51	0.54	**0.62***
Sand-to-binder (S/B) ratio	**0.63***	0.58	0.47

*Optimum level

4.9 Microstructure study

The microstructure of the GPM mix M7 that showed highest grey relational grade was studied through XRD, EDS, FESEM and FTIR analyses.

4.9.1 XRD analysis

The XRD patterns of GPM mix M7 at 7, 28, 90 and 180 days of ambient curing are shown in Fig. 4.19 (a). From the obtained XRD patterns, it is observed that the crystalline peaks of quartz and mullite indicated the presence of unreacted fly ash particles in the GPM mix. The main crystalline peaks formed during the geopolymerization reaction at all ambient curing ages were related to sodium (and calcium) aluminosilicate complex (N-(C)-A-S-H) such as albite ((Na, Ca)Al(Si Al)$_3$O$_8$), anorthoclase ((Na$_{0.85}$ K$_{0.15}$)(AlSi$_3$O$_8$)), and nepheline (NaAlSiO$_4$). The albite peaks at 22.1º 2θ, 24.1º 2θ and 28.0º 2θ; anorthoclase peaks at 23.7º 2θ, 27.5º 2θ and 35.3º 2θ; and nepheline peak at 27.1º 2θ were identified in the XRD patterns of the GPM mix at all ages of ambient curing (Fig. 4.19 (a)). A less intense peak of muscovite (KAl$_3$Si$_3$O$_{10}$(OH)$_2$) and hydrotalcite (Mg$_6$-Al$_2$(CO$_3$)(OH)$_{16}$.4H$_2$O) were identified at 8.8º 2θ, and 10.5º 2θ respectively in the XRD patterns of the GPM mix as observed from Fig. 4.25 (a). A peak corresponding to C-S-H gel or calcite (CaCO$_3$) was identified at 29.4º 2θ in the XRD patterns of the GPM mix M7 at all ages of ambient curing. The peak intensity of anorthoclase, albite, and nepheline mostly increased with increase in ambient curing age, which indicates continuation of geopolymerization reaction with age in the GPM mix.

The XRD patterns of GPM mix (M7) exposed to water, 6% Na$_2$SO$_4$ and 6% MgSO$_4$ solutions for 26 weeks are shown in Fig. 4.19 (b). From Fig. 4.19 (b), it is observed that in addition to the peaks identified in Fig. 4.19 (a), a new peak related to anorthite ((Ca, Na)(Si, Al)$_4$O$_8$), an aluminosilicate complex was identified at 28.1º 2θ in the GPM mix exposed to water, 6% Na$_2$SO$_4$ and 6% MgSO$_4$ solutions. Further, sodalite (Na$_8$Al$_6$Si$_6$O$_{24}$ (OH)$_2$ (H$_2$O)$_2$), a zeolite product was identified at 14.1º 2θ and 24.5º 2θ in case of exposure to water and 6% Na$_2$SO$_4$ solution. The peak intensity of anorthite was higher in case of exposure to 6% Na$_2$SO$_4$ solution as compared to water followed by 6% MgSO$_4$ solution. However, the peak intensity of albite, anorthoclase, sodalite, and nepheline were mostly lower in case of exposure to 6% Na$_2$SO$_4$ and 6% MgSO$_4$ solutions as compared to water, which indicates presence of comparatively lower amount of geopolymer gels that resulted in lower compressive strength of GPM mix (M7) immersed in 6% Na$_2$SO$_4$ and 6% MgSO$_4$ solutions as compared to that immersed in water (Fig. 4.14). Further, the decalcification of

calcium enriched gels (N-(C)-A-S-H and C-S-H gels) in the geopolymer mortar mix exposed to sulfate solutions (6% Na_2SO_4 and 6% $MgSO_4$ solutions) resulted in the formation of gypsum ($CaSO_4.2H_2O$), which was identified at 31.1º 2θ in the XRD patterns of the GPM mix (M7) immersed in 6% Na_2SO_4 and 6% $MgSO_4$ solutions (Fig. 4.19 (b)). While comparing the XRD patterns of GPM mix (M7) exposed to 6% Na_2SO_4 and 6% $MgSO_4$ solutions, the peak intensity of albite, anorthoclase, anorthite, sodalite, and nepheline were lower in case of exposure to 6% $MgSO_4$ solution as compared to 6% Na_2SO_4 solution (Fig. 4.19 (b)). This can be correlated with the results of compressive strength of GPM mix (M7) after 26 weeks of exposure (Fig. 4.14) where the GPM mix exposed to 6% $MgSO_4$ solution exhibited lower compressive strength as compared to that exposed to 6% Na_2SO_4 solution.

The XRD patterns of GPM mix exposed to water, 0.62 mol/l H_2SO_4 and 0.62 mol/l HCl solutions for 26 weeks are shown in Fig. 4.19 (c). The compounds related to N-A-S-H and N-(C)-A-S-H gels i.e., nepheline, albite, anorthoclase, anorthite, and sodalite; and C-S-H were more susceptible to H_2SO_4 and HCl attack as their peak intensity reduced significantly or disappeared (in case of sodalite, anorthite, and C-S-H) in the XRD patterns (Fig. 4.19 (c)) of GPM mix (M7) exposed to 0.62 mol/l H_2SO_4 and 0.62 mol/l HCl solutions as compared to that exposed to water. Further, the peaks related to hydrotalcite, and muscovite in the XRD patterns disappeared in case of exposure to acid solutions. These observations indicate depolymerization of aluminosilicate gels in the GPM mix exposed to sulfuric acid and hydrochloric acid solutions that resulted in significant reduction of compressive strength as compared to the GPM mix exposed to water as evident from Fig. 4.15. The peaks related to gypsum ($CaSO_4.2H_2O$) were identified at 11.6º 2θ, 29.1º 2θ, 31.1º 2θ, 32.1º 2θ, 33.35º 2θ, 40.58º 2θ, 43.34º 2θ, and 56.78º 2θ in the XRD patterns of GPM mix (M7) exposed to 0.62 mol/l H_2SO_4 solution [60].

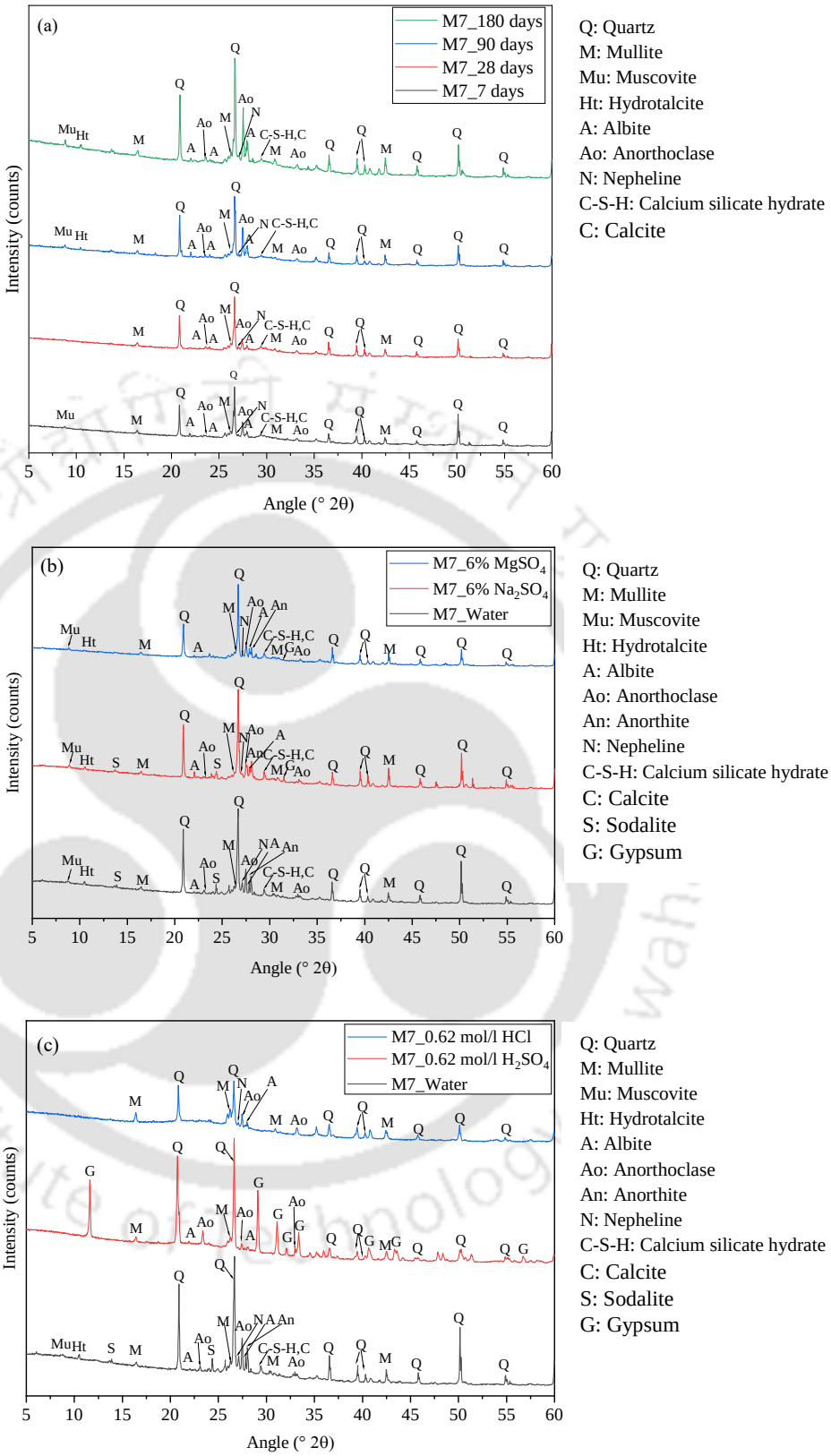

Fig. 4.19 XRD patterns of GPM mix M7: (a) at different ages of ambient curing (7, 28, 90 and 180 days), (b) exposure to water, 6% Na_2SO_4 solution, and 6% $MgSO_4$ solution, and (c) exposure to water, 0.62 mol/l H_2SO_4 solution, and 0.62 mol/l HCl solution for 26 weeks.

4.9.2 FESEM analysis

The FESEM images of GPM mix (M7) at different ages of ambient curing are shown in Fig. 4.20. From Fig. 4.20, it can be observed that the microstructure of GPM mix became denser at later ages (90 days and 180 days) of ambient curing. This may be ascribed to the effect of continued geopolymerization reaction, which resulted in formation of more amount of geopolymer gels (N-A-S-H and N-(C)-A-S-H gel), and C-S-H gel leading to higher compressive strength at later ages. Partially reacted fly ash and GGBS particles were observed at ambient curing age of 7 days as evident from the FESEM image shown in Fig. 4.20 (a), which indicates lower extent of geopolymerization reaction at early age. From the FESEM image of GPM mix at the age of 28 days (Fig. 4.20 (b)), although partially reacted precursor materials were not observed, however, some loosely distributed geopolymer gels were identified in the GPM mix.

The FESEM images of GPM mix (M7) after immersion in water, 6% Na_2SO_4 solution, 6% $MgSO_4$ solution, 0.62 mol/l H_2SO_4 solution, and 0.62 mol/l HCl solution are shown in Fig. 4.21. From Fig. 4.21, significant differences were observed in the morphology of GPM mix (M7) immersed in different exposure solutions. The FESEM image of GPM mix (M7) immersed in water (Fig. 4.21 (a)) indicated relatively more compacted microstructure than that immersed in 6% Na_2SO_4 solution, (Fig. 4.21 (b)), 6% $MgSO_4$ solution (Fig. 4.21 (c)), 0.62 mol/l H_2SO_4 solution (Fig. 4.21 (d)), and 0.62 mol/l HCl solution (Fig. 4.21 (e)). The less compacted microstructure of the GPM mix exposed to sulfate and acid solutions is ascribed to the effect of decalcification, and depolymerization of the geopolymer gels that resulted in lower compressive strength when exposed to these solutions as compared to exposure to water (Fig. 4.14 and Fig. 4.15). From Fig. 4.21 (b) and (c), gypsum crystals were observed in the GPM mix (M7) exposed to 6% Na_2SO_4 and 6% $MgSO_4$ solutions, which is responsible for reduction in compressive strength than exposure to water. Larger amount of gypsum crystals were observed in the FESEM image of GPM mix immersed in 0.62 mol/l H_2SO_4 solution (Fig. 4.21 (d)), which resulted in volumetric expansion [134], thereby significantly reducing the compressive strength of the GPM mix (M7) as evident from Fig. 4.15. The FESEM image of the GPM mix immersed in 0.62 mol/l HCl (Fig. 4.21 (e)) showed comparatively porous and disintegrated geopolymer gels. This is attributed to the leaching of sodium (Na), calcium (Ca), and aluminum (Al) into the HCl solution [134] that resulted in microcracks to a greater extent in the GPM mix and eventually resulting in significant reduction of compressive strength (Fig. 4.15).

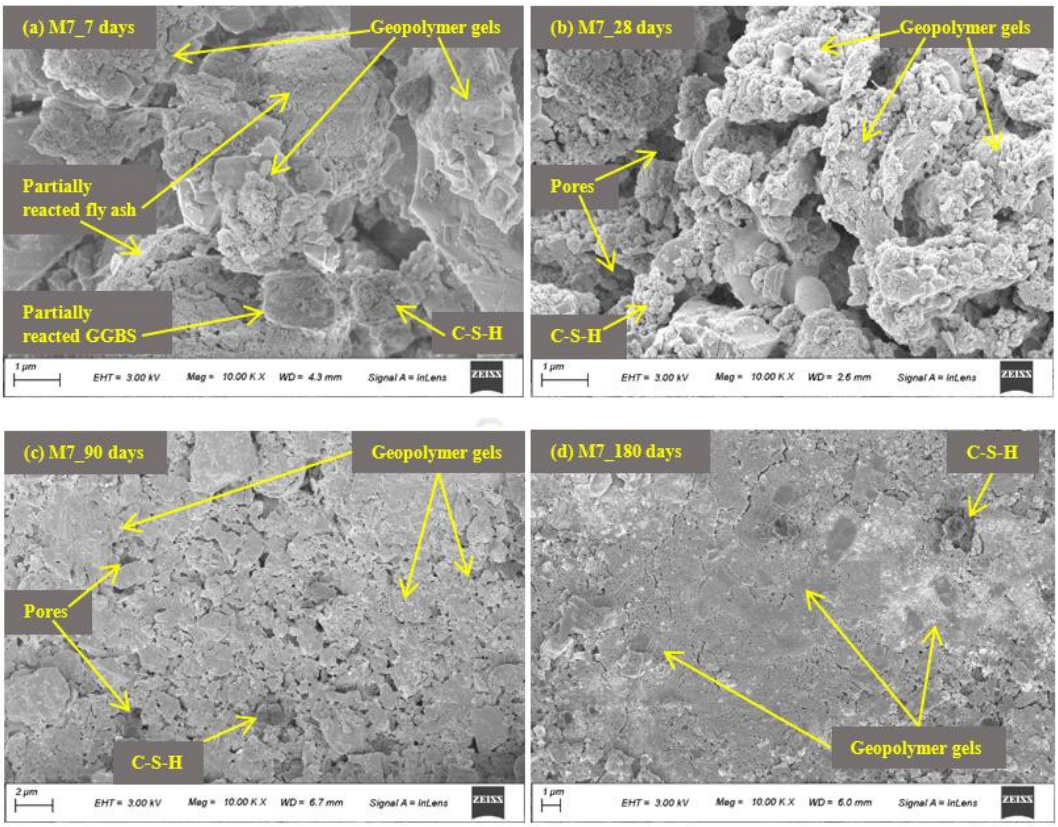

Fig. 4.20 FESEM images of GPM mix M7 at ambient curing age: (a) 7 days, (b) 28 days, (c) 90 days, and (d) 180 days.

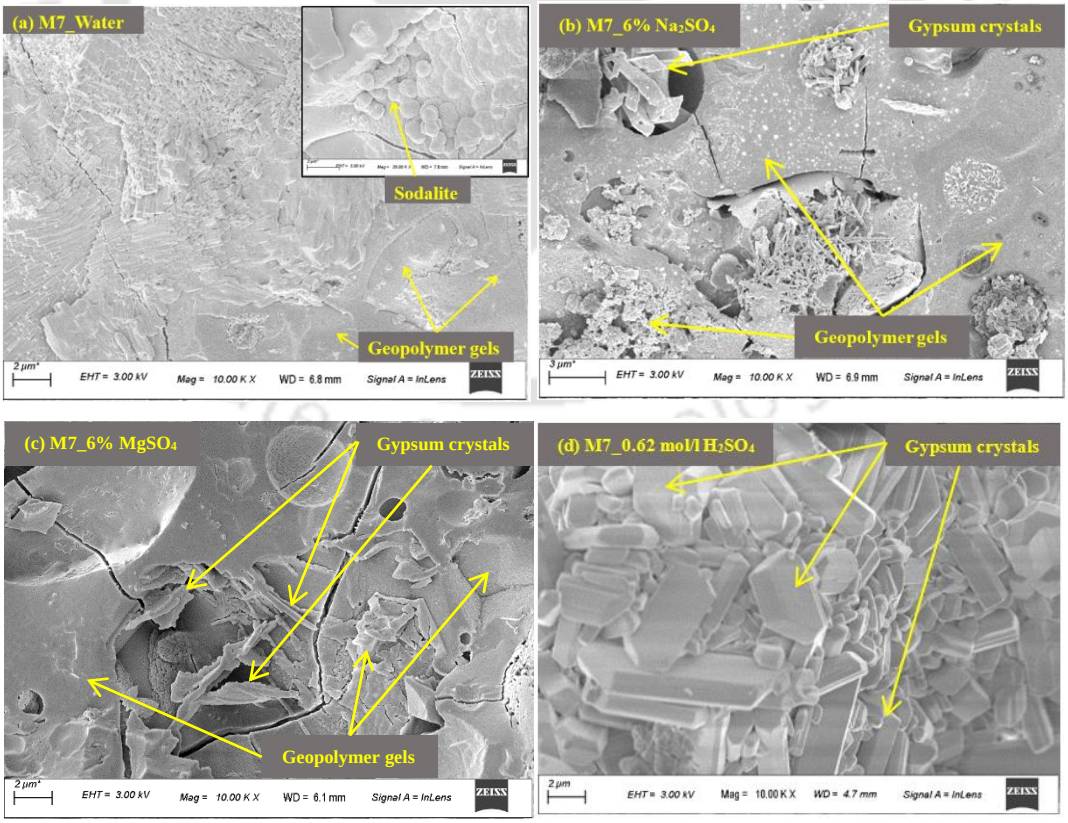

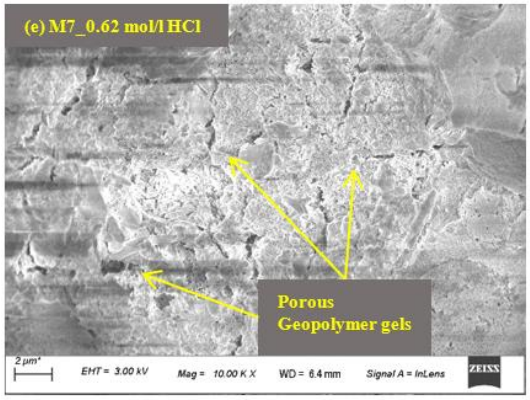

Fig. 4.21 FESEM images of GPM mix M7 exposed to: (a) water, (b) 6% Na_2SO_4 solution, (c) 6% $MgSO_4$ solution, (d) 0.62 mol/l H_2SO_4 solution, and (e) 0.62 mol/l HCl solution for 26 weeks.

4.9.3 EDS analysis

Typical EDS spectra of GPM mix (M7) at different ages of ambient curing are shown in Fig. 4.22. From this figure, it is observed that the major elements of gel phase of GPM mix (M7) include oxygen (O), silicon (Si), aluminum (Al), calcium (Ca), and sodium (Na). The average atomic Na/Si ratio vs. Al/Si ratio, and Ca/Si ratio vs. Al/Si ratio are illustrated in Fig. 4.23. From Fig. 4.23, the average atomic Na/Si ratio, Al/Si ratio and Ca/Si ratio were observed in the range of 0.27-3.08, 0.34-0.77 and 0.12-2.72 respectively. These obtained values of atomic ratios indicate the coexistence of N-A-S-H gel, N-(C)-A-S-H gel and C-S-H gel in the GPM mix. Similar results were also reported in the literature where Al/Si ratio in the range of 0.08-1.0 indicated the formation of N-A-S-H or N-(C)-A-S-H gel, and Ca/Si ratio in the range of 0.6 to 1.4 indicated the formation of C-S-H gel in the geopolymer mixes [41,82,83,85,95,135,136]. From Fig. 4.23 (a), there was no systematic variation in the atomic ratios of Na/Si and Al/Si with ambient curing age. However, Ca/Si ratio (Fig. 4.23 (b)) of the GPM mix (M7) at 90 days and 180 days of ambient curing were higher as compared to that at 7 days and 28 days of ambient curing, which indicates formation of more amount of N-(C)-A-S-H gel and C-S-H gel that resulted in higher compressive strength of the GPM mix at later ages as observed from Fig. 4.5. Further, the presence of potassium (K), and magnesium (Mg) in the geopolymer mortar mix (Fig. 4.22) may influence its rate of hardening [85].

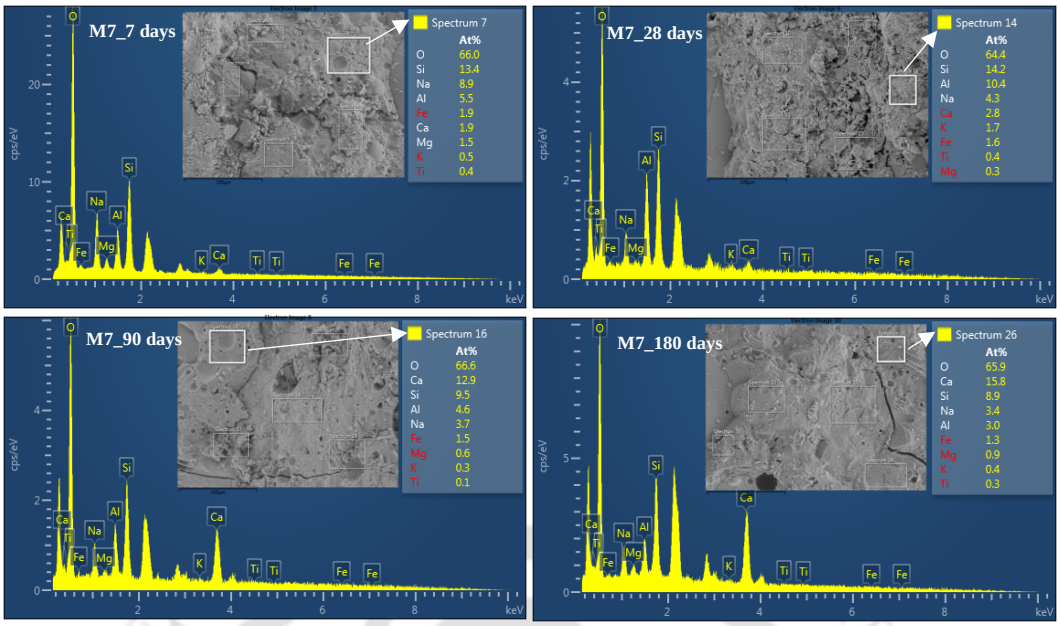

Fig. 4.22 EDS Spectra of GPM mix M7 at different ages of ambient curing.

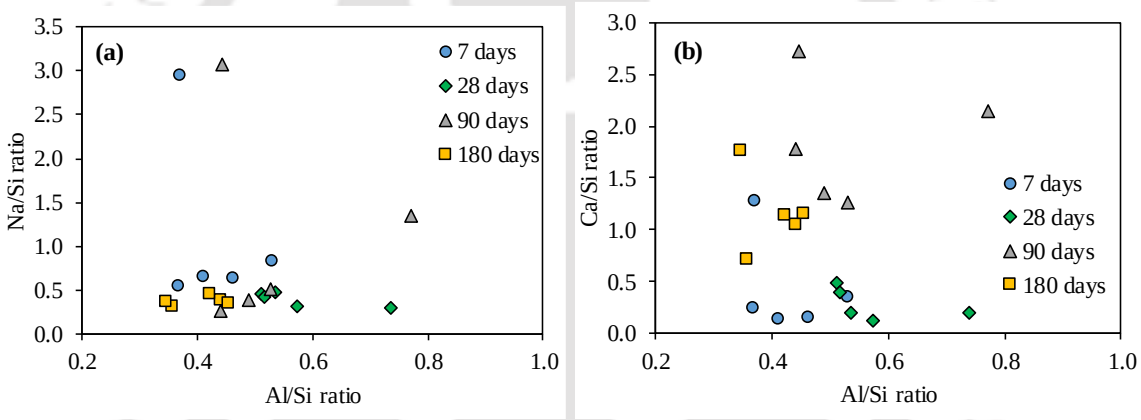

Fig. 4.23 EDS analysis of GPM mix M7 at 7, 28, 90 and 180 days of ambient curing: (a) Atomic Na/Si ratio versus Al/Si ratio, and (b) Atomic Ca/Si ratio versus Al/Si ratio.

Typical EDS spectra of the GPM mix (M7) exposed to water, 6% Na_2SO_4 solution, 6% $MgSO_4$ solution, 0.62 mol/l H_2SO_4 solution, and 0.62 mol/l HCl solution for 26 weeks are presented in Fig. 4.24. The atomic Na/Si ratio vs. Al/Si ratio, and Ca/Si ratio vs. Al/Si ratio for the mix M7 exposed to water, sulfate and acid solutions are illustrated in Fig. 4.25. From Fig. 4.25, it is observed that the GPM mix (M7) exhibited higher Na/Si ratio (0.21-0.32), Al/Si ratio (0.51-0.81), and Ca/Si ratio (0.38-0.93) when exposed to water followed by exposure to 6% Na_2SO_4 solution (Na/Si ratio: 0.18-0.34; Al/Si ratio: 0.41-0.51; and Ca/Si ratio: 0.06-0.39), and 6% $MgSO_4$ solution (Na/Si ratio: 0.10-0.16; Al/Si ratio: 0.36-0.54; and Ca/Si ratio: 0.07-0.34). The lower values of these atomic ratios in case exposure to sulfate solutions is attributed to the dominant effect of decalcification as well as due to depolymerization of aluminosilicate gels in the GPM mix. This observation is in line with

the results of compressive strength (Fig. 4.14), XRD analysis (Fig. 4.19 (b)) and FESEM analysis (Fig. 4.21). Further from Fig. 4.25, it is observed that the atomic Na/Si ratio, and Al/Si ratio of the GPM mix (M7) decreased significantly in case of exposure to 0.62 mol/l H_2SO_4, and 0.62 mol/l HCl solutions, which indicates dominant effect of depolymerization of the aluminosilicate gels thereby resulting in significant reduction of compressive strength as evident from Fig. 4.15. The EDS spectra of GPM mix (M7) exposed to 0.62 mol/l H_2SO_4 solution showed higher content of O (70.5-76.3 At%), Ca (0.5-8.9 At%) and S (0.9-9.7 At%) that indicates the formation of gypsum ($CaSO_4.2H_2O$) in the GPM mix as observed from the results of XRD analysis (Fig. 4.19 (c)) and FESEM analysis (Fig. 4.21). Similarly, the EDS spectra of the GPM mix (M7) exposed to 0.62 mol/l HCl solution showed lower content of Ca, Na and Al as compared to exposure to water, which indicates leaching of these elements into the acidic solution that led to disintegrated geopolymer matrix and showed significantly lower compressive strength [137].

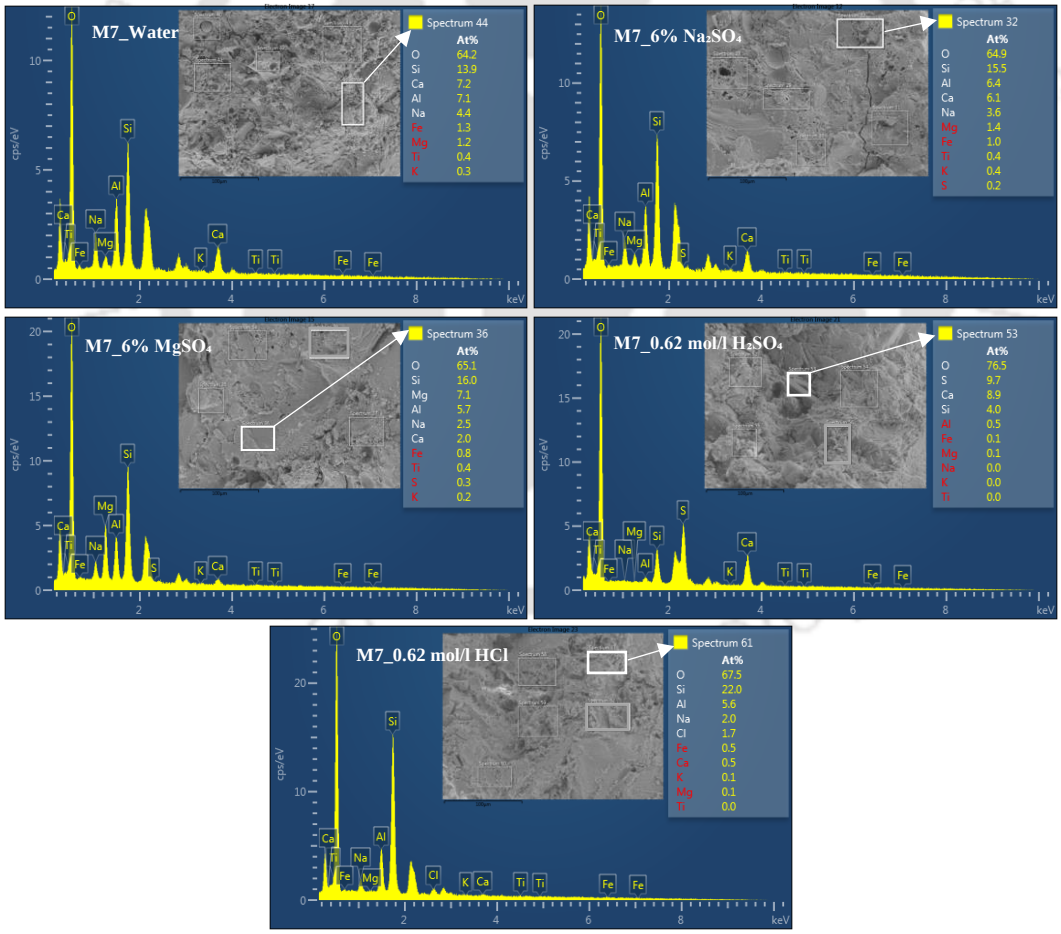

Fig. 4.24 EDS spectra of GPM mix M7 exposed to water, 6% Na_2SO_4 solution, 6% $MgSO_4$ solution, 0.62 mol/l H_2SO_4 solution, and 0.62 mol/l HCl solution for 26 weeks.

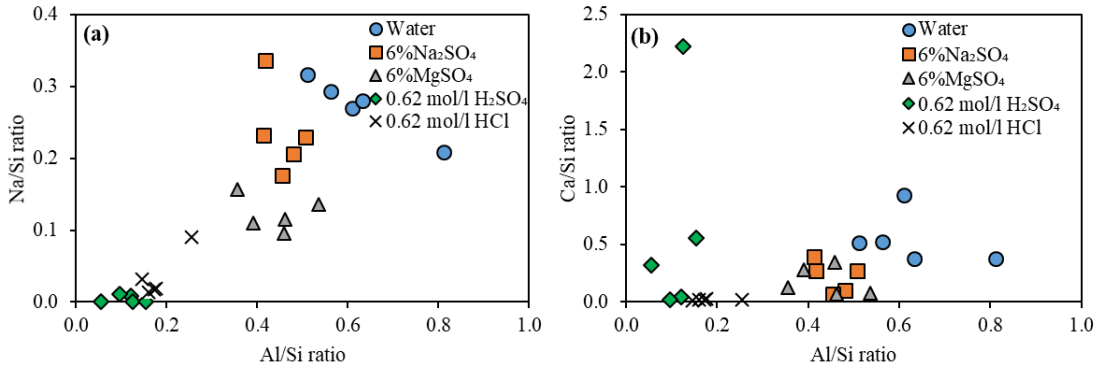

Fig. 4.25 EDS analysis of GPM mix M7 exposed to different exposure solutions: (a) Atomic Na/Si ratio versus Al/Si ratio, and (b) Atomic Ca/Si ratio versus Al/Si ratio.

4.9.4 FTIR analysis

The FTIR spectra of geopolymer mortar mix M7 at different ages of ambient curing are shown in Fig. 4.26 (a). From this figure, it is observed that the peaks related to asymmetric bending vibration of Si-O-Si bond (465 cm^{-1} - 472 cm^{-1}) and Al-O bond (779 cm^{-1}) indicate the presence of unreacted/partially reacted precursor materials in the GPM mix. The peak centered around 1034 cm^{-1} - 1035 cm^{-1} is ascribed to the asymmetric stretching vibration of Si-O-Si(Al) bond, which indicates the coexistence of geopolymer gels (N-A-S-H and N-(C)-A-S-H), and C-S-H gel in the GPM mix [138]. The appearance of absorption band ranging from 1426 cm^{-1} to 1448 cm^{-1} corresponds to the stretching vibration of carbonate groups (CO_3^{2-}) in the GPM mix [106]. The peak ranging from 1639 cm^{-1} to 1641 cm^{-1}, and the band ranging from 3432 cm^{-1} to 3480 cm^{-1} in the GPM mix (Fig. 4.26 (a)) correspond to the bending vibration of H-O-H group, and stretching vibration of –OH group respectively.

The FTIR spectra of GPM mix M7 exposed to water, 6% Na_2SO_4 and 6% $MgSO_4$ solutions for 26 weeks are shown in Fig. 4.26 (b). The asymmetric stretching vibration of Si-O-Si(Al) bond appeared at 1034 cm^{-1} in the FTIR spectra of GPM mix exposed to water was not altered when compared with exposure to 6% Na_2SO_4 solution (1035 cm^{-1}), and 6% $MgSO_4$ solution (1033 cm^{-1}). Further, the bending vibration of H-O-H group (1637 cm^{-1} - 1639 cm^{-1}), and stretching vibration of –OH group (3434 cm^{-1} - 3445 cm^{-1}) were not altered significantly among water, 6% Na_2SO_4 solution, and 6% $MgSO_4$ solution as observed from Fig. 4.26 (b). The FTIR spectra of GPM mix (M7) exposed to water, 0.62 mol/l H_2SO_4 solution, and 0.62 mol/l HCl solution for 26 weeks are shown in Fig. 4.26 (c). From this figure, it is observed that in case of exposure to water, the main band attributed to asymmetric stretching vibration of Si-O-Si(Al) bond appeared at 1034 cm^{-1} was shifted

toward higher wavenumbers i.e., 1140 cm^{-1} and 1088 cm^{-1} when exposed to 0.62 mol/l H_2SO_4 solution, and 0.62 mol/l HCl solution respectively. This indicates increase in atomic Si/Al ratio due to weaker Al-O bonds in the aluminosilicate network, which is replaced by Si-O bonds during acid exposure condition [60,137,139]. Therefore, the GPM mix (M7) exhibited significant decrease in compressive strength in case of exposure to acid solutions as compared to exposure to water (Fig. 4.15). This observation can also be correlated with the atomic Al/Si ratio obtained in the EDS analysis (Fig. 4.25), which showed a significant decrease in the atomic Al/Si ratio in case of exposure to 0.62 mol/l H_2SO_4 and 0.62 mol/l HCl solutions. Further, the peaks identified at 602 cm^{-1} and 669 cm^{-1} are attributed to the formation of gypsum [60] in the GPM mix (M7) exposed to 0.62 mol/l H_2SO_4 solution, which in agreement with the results obtained from XRD, FESEM and EDS analyses. In addition, the shifting of stretching vibration of –OH group from 3435 cm^{-1} (in case of exposure to water) to 3406 cm^{-1} (in case of exposure to 0.62 mol/l H_2SO_4 solution), and shifting of bending vibration of H-O-H group from 1639 cm^{-1} (in case of exposure to water) to 1623 cm^{-1} (in case of exposure to 0.62 mol/l H_2SO_4 solution) also indicate the formation of gypsum crystals in the GPM mix exposed to 0.62 mol/l H_2SO_4 solution [60,137,139]. The band at 1483 cm^{-1}, which corresponds to the stretching vibration of carbonate groups (CO_3^{2-}) in the GPM mix exposed to water disappeared when exposed to 0.62 mol/l H_2SO_4 solution and 0.62 mol/l HCl solution, which indicates dissolution of carbonate compounds during acid exposure [137].

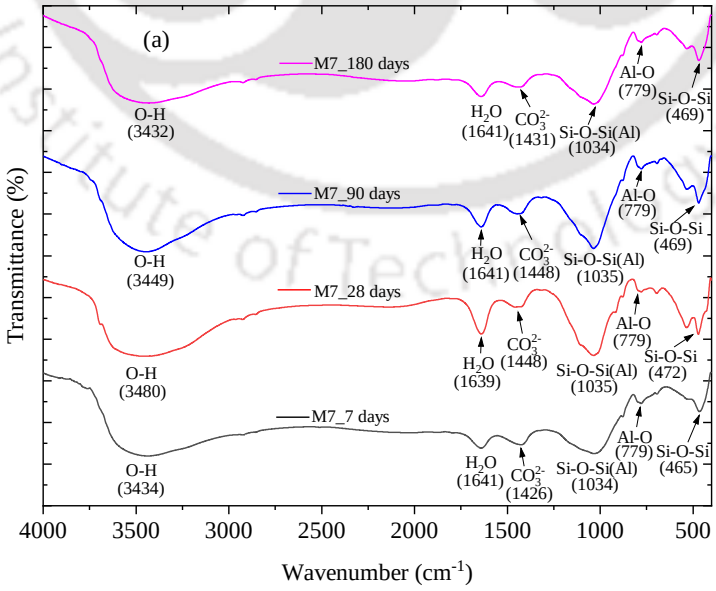

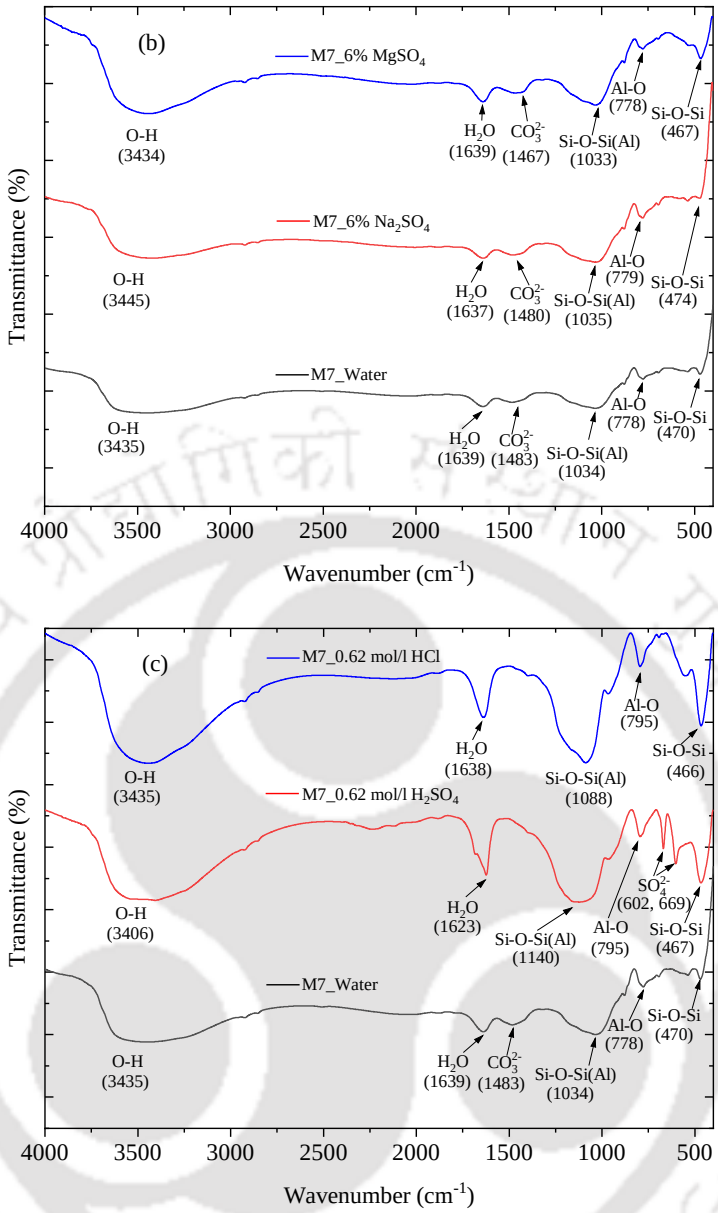

Fig. 4.26 FTIR spectra of GPM mix M7: (a) at different ages of ambient curing, (b) exposure to water, 6% Na_2SO_4 solution, and 6% $MgSO_4$ solution, and (c) exposure to water, 0.62 mol/l H_2SO_4 solution, and 0.62 mol/l HCl solution for 26 weeks.

4.10 Verification experiments

The verification experiments were conducted on the optimized fly ash-GGBS based GPM mix (GGBS 45%_W/GPS 1.5_14 M NaOH_S/B 1.5) as proposed in Section 4.8. Tests for setting time, flowability, compressive strength at different ages of ambient curing, water absorption, apparent volume of permeable voids (AVPV), sorptivity, and compressive strength after 26 weeks of immersion in different exposure solutions (i.e., water, 3% and 6% Na_2SO_4 solutions, 3% and 6% $MgSO_4$ solutions, 0.31 mol/l and 0.62 mol/l H_2SO_4 solutions, and 0.31 mol/l and 0.62 mol/l HCl solutions) were carried out on the optimized

GPM mix. The results of studied properties are presented in Table 4.16. From Table 4.16, it is observed that the optimized GPM mix showed adequate setting time and flow index when compared with the GPM mixes M1 – M9 as per L_9 orthogonal array. Further, the optimized GPM mix exhibited highest compressive strength at all ages of ambient curing, and after 26 weeks of immersion in water, different sulfate solutions, and HCl solutions as compared to the GPM mixes M1 – M9. The optimized GPM mix showed adequate water absorption and AVPV, and lowest sorptivity coefficient when compared with the GPM mixes as per L_9 orthogonal array. Besides, the optimized GPM mix showed adequate compressive strength after 26 weeks of immersion in different H_2SO_4 solutions as compared to the GPM mixes M1 – M9.

Table 4.16 Results of the proposed optimized GPM mix

Responses (Properties)		Result
Initial setting time (minute)		154
Final setting time (minute)		273
Flow index (%)		108
Compressive strength (N/mm^2)	7 days	37.60
	28 days	44.53
	90 days	48.53
	180 days	56.00
Water absorption (%)	28 days	5.85
AVPV (%)	28 days	6.07
Sorptivity coefficient ($\times 10^{-3}$ $mm/s^{1/2}$)	28 days	0.011
Compressive strength after 26 weeks of immersion in different exposure solutions (N/mm^2)	Water	52.80
	3% Na_2SO_4	53.87
	6% Na_2SO_4	50.93
	3% $MgSO_4$	46.67
	6% $MgSO_4$	45.60
	0.31 mol/l H_2SO_4	22.13
	0.62 mol/l H_2SO_4	14.93
	0.31 mol/l HCl	29.60
	0.62 mol/l HCl	21.07

The grey relational grade (GRG) of the optimized GPM mix based on the obtained results of setting time, flowability, compressive strength at different ages of ambient curing, water absorption, AVPV, sorptivity, and compressive strength after 26 weeks of immersion in different exposure solutions was calculated using equation 3.2, to 3.6 and the calculated value is 0.87. The predicted grey relational grade (GRG) of the optimized GPM mix was calculated using the following equation [120].

$$\gamma = \gamma_m + \sum(\gamma_n - \gamma_m) \quad (4.1)$$

Where γ is the predicted GRG of the optimized GPM mix, γ_m is the mean GRG of all the GPM mixes as per L_9 orthogonal array (Table 4.14) and γ_n is the maximum mean GRG of a parameter (Table 4.15). The calculated value of the predicted grey relational grade (GRG) of the optimized GPM mix from equation 4.1 is 0.80. The GRG of the optimized GPM mix based on the experimental results (responses) is highest (0.87) as compared to the GPM mixes as per L_9 orthogonal array (Table 4.14). The higher value of grey relational grade (GRG) of the optimized GPM mix when compared with the predicted GRG, and that of the GPM mixes as per L_9 orthogonal array indicates that the optimized GPM mix performed excellently with respect to the studied properties simultaneously.

4.11 Summary

This chapter presents application of Taguchi-Grey relational analysis (GRA) to investigate effect of control parameters on setting time, flowability, compressive strength at different ages of ambient curing, water absorption, apparent volume of permeable voids (AVPV), sorptivity, sulfate and acid resistance of fly ash-GGBS based geopolymer mortar (GPM) simultaneously. Control parameters selected were GGBS replacement level (15%, 30%, 45%), water-to-geopolymer solids (W/GPS) ratio (0.31, 0.33, 0.35), molarity of NaOH solution (10 M, 12 M, 14 M) and sand-to-binder (S/B) ratio (1.5, 2, 2.5). From the obtained results, GGBS replacement level, and S/B ratio significantly influenced most of the studied properties of geopolymer mortar. Geopolymer mortar (GPM) prepared with higher GGBS replacement level showed higher compressive strength under ambient condition whereas GPM prepared with lower GGBS replacement level exhibited improved resistance against sulfate and acid attack. From the results of multi-response optimization by Taguchi-GRA method, the GPM mix M7 made with higher level of GGBS replacement (45%), and molarity of NaOH solution (14 M), medium level of S/B ratio (2) and lower level of W/GPS ratio (0.31) exhibited better performance in relatively more number of properties simultaneously. The variations in peak intensity of compounds related to aluminosilicate gels i.e., N-A-S-H and N-(C)-A-S-H gels formed in geopolymer mortar mix M7 were consistent with the variations in compressive strength with ambient curing age as well as with variations in compressive strength of geopolymer mortar exposed to sulfate solutions. Further, the significant decrease in peak intensity of compounds related to aluminosilicate gels, and in atomic Na/Si ratio and Al/Si ratio are in line with the significant reduction in compressive strength of geopolymer mortar when exposed to acid solutions that

substantiates the depolymerization of aluminosilicate gels in the acidic environment. The obtained GRG of the optimized geopolymer mortar mix (with combination of parameters i.e., GGBS replacement of 45%, W/GPS ratio of 0.31, NaOH solution of 14 M, and S/B ratio of 1.5) based on the experimental results was 0.87, which is greater than the predicted GRG (0.80) as well as that of the GPM mixes as per L_9 orthogonal array thereby indicating better overall performance among all the GPM mixes.

Effect of Fly Ash/GGBS Blends and Sand-to-Binder Ratio on Flowability, Strength, Durability and Microstructure of Geopolymer Mortar

5.1. General

In this chapter, the effect of fly ash/GGBS blends, and sand-to-binder (S/B) ratio on flowability, strength development, water absorption and apparent volume of permeable voids, sorptivity, sulfate and acid resistance, and microstructure evolution of geopolymer mortar (GPM) have been investigated. The results obtained from compressive strength at different ages of ambient curing (7, 28, 90, and 180 days) are corelated with the microstructure evolution of geopolymer mortar. The resistance of geopolymer mortar specimens was evaluated in terms of visual observation, and change in weight and compressive strength after immersion in different sulfate and acid solutions for 26 weeks. Further, the changes in compressive strength of geopolymer mortar specimens after immersion in different sulfate and acid solutions were correlated with the changes in microstructure analyzed through XRD, EDS, FESEM, and FTIR analyses.

5.2 Flowability of fresh geopolymer mortar (GPM) mixes

The flow index (%) of fly ash-GGBS based geopolymer mortar (GPM) made with different fly ash/GGBS blends and S/B ratios are shown in Fig. 5.1. From Fig. 5.1, it is noted that the flow index indicating the flowability of fresh GPM mixes decreased from 126% to 108% with increase in GGBS content from 15% to 45% in the GPM mixes at constant S/B ratio of 1.5. This is attributed to the fact that the particle mobility of freshly prepared GPM reduced due to increase in the angular shape particles of GGBS in the mixes. The decrease in flowability of GPM made with higher amount of GGBS may also be related to higher reactivity of GGBS with the alkaline solution compared to fly ash due to increased calcium content in the mixes that affected the rate of solidification [2,88]. Further, from Fig. 5.1, it is observed that the flow index of GPM mixes increased from 108% to 146% with increase in S/B ratio of the mixes from 1.5 to 2.5 at constant fly ash/GGBS blend (FA55/G45). This is ascribed to the fact that the binder content in the GPM made with higher S/B ratio decreased at constant alkaline solution and sand content that leads to availability of comparatively more amount of alkaline solution for lower amount of binder thereby resulting in higher flow index for the geopolymer mortar. It may be noted that, as discussed

earlier in Section 4.3 (Chapter 4), the performance statistics (mean S/N ratio) of flow index indicated significant decrease in flowability of fresh GPM mixes with increase in S/B ratio, which was attributed to the dominant effect of increase in sand content, and decrease in binder and alkaline solution contents. Thus, the opposite variation in flow index (%) with change in S/B ratio in these two cases is ascribed to the inconsistent variations in alkaline solution and sand content.

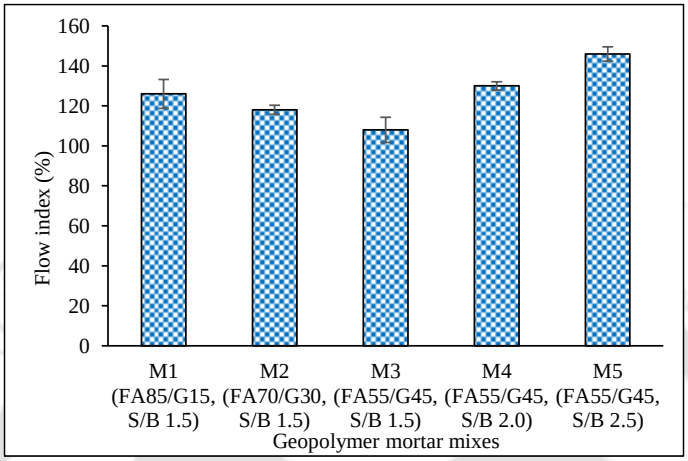

Fig. 5.1 Flow index of geopolymer mortar (GPM) made with different fly ash/GGBS blends and S/B ratios.

5.3 Compressive strength of geopolymer mortar (GPM) mixes

The compressive strength of fly ash-GGBS based geopolymer mortar (GPM) made with various fly ash/GGBS blends and S/B ratios at the ambient curing age of 7, 28, 90, and 180 days are presented in Fig. 5.2. From Fig. 5.2, it is observed that the compressive strength of geopolymer mortar (GPM) made with various fly ash/GGBS blends and S/B ratios mostly increased as ambient curing age increased from 7 to 180 days. This is attributed to the continuation of geopolymerization reaction in the GPM with increase in curing age. The delay in dissolution of silica and alumina species due to lower reactivity of fly ash particles in alkaline solution resulted in formation of higher amount of N-A-S-H gel at later age of ambient curing that ensures higher strength of fly ash-GGBS based geopolymer mortar (GPM) [2]. From Fig. 5.2, it is noted that the strength enhancement of geopolymer mortar (GPM) varied in the range of 18.4% to 38.0% from 7 to 28 days, followed by in the range of 7.5% to 25.4% from 28 to 90 days, and in the range of -4.5% to 15.4% from 90 to 180 days, irrespective of fly ash/GGBS blend and S/B ratio in the mixes. This indicates that the rate of strength enhancement of GPM was higher in the early age of ambient curing (i.e., from 7 to 28 days), and then it was gradually reduced as the age increased from 28 to 180 days. This is attributed to comparatively higher dissolution of calcium (Ca) as well as

silica (Si), and alumina (Al) species due to higher reactivity of GGBS with alkaline solution that resulted in formation of higher amount of sodium (and calcium) aluminosilicate gels and C-S-H gel in GPM during the period of 7 to 28 days. However, the rate of dissolution was decreased from 28 to 180 days.

While comparing the effect of fly ash/GGBS blends, from Fig. 5.2, it is noted that the strength of geopolymer mortar (GPM) increased from 0.6% to 24.0% and 4.6% to 18.6% with increase in the amount of GGBS from 15% to 30% and 30% to 45% respectively in the geopolymer mortar (GPM), irrespective of ambient curing age. This may be ascribed to the effect of higher amount of GGBS in the GPM mixes that provided additional silica (Si), alumina (Al), and calcium (Ca) in the fly ash-GGBS based geopolymer system, which greatly altered the nature of the binding gels due to higher extent of reaction of calcium and formed more amount of hybrid binding gels. These binding gels consist of sodium (and calcium) aluminosilicate gels, and C-S-H gel [88] that resulted in higher strength development. Further, from Fig. 5.2, it is observed that the compressive strength of geopolymer mortar (GPM) mixes decreased in the range of 23.6% to 35.7%, and 10.1% to 18.6% with increase in S/B ratio from 1.5 to 2.0, and 2.0 to 2.5 respectively in the GPM mixes irrespective of ambient curing age. This may be ascribed to the effect of significant decrease in binder content in the mixes that resulted in lower formation of binding gels due to lower extent of geopolymerization reaction and exhibited poor bonding between the binding gels and fine aggregate present in the geopolymer mortar (GPM) made with higher S/B ratio [88].

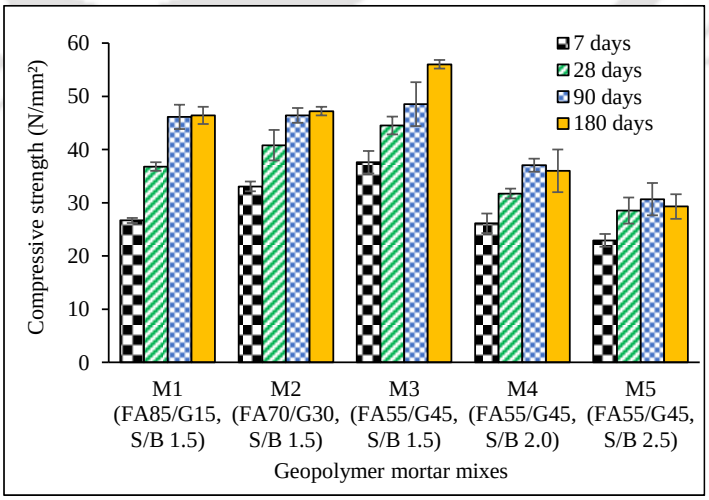

Fig. 5.2 Compressive strength of geopolymer mortar (GPM) made with different fly ash/GGBS blends and S/B ratio at different ages of ambient curing.

5.4 Water absorption and apparent volume of permeable voids (AVPV) of geopolymer mortar (GPM) mixes

Water absorption and apparent volume of permeable voids (AVPV) of geopolymer mortar (GPM) determined at 28 days are presented in Fig. 5.3. It is noted that the water absorption of GPM made with different fly ash/GGBS blends (M1, M2, and M3) varied from 5.85% to 6.57%, and AVPV varied from 6.07% to 7.60% as observed from Fig. 5.3. While comparing the effect of fly ash/GGBS blends on the water absorption of GPM, it is observed that the water absorption was slightly lower for the GPM made with higher amount of GGBS. From Fig. 5.3, it is noted that the GPM made with 30% GGBS (M2) exhibited slightly higher AVPV value compared to the mix made with 15% GGBS (M1). Further, the GPM made with 45% GGBS (M3) exhibited lower AVPV value as compared to that made with 15% and 30% GGBS (M1, M2). This is ascribed to the effect of development of relatively higher amount of calcium-rich gels in the geopolymer mortar (GPM) made with higher amount of GGBS that resulted in denser microstructure, thereby reducing the water absorption and AVPV values [59]. In addition, the pores of GPM made with higher amount of GGBS might have been filled due to finer particle size of GGBS and resulted in decrease in water absorption and AVPV values [87]. The water absorption and AVPV values were slightly higher for GPM made with higher S/B ratio as seen from Fig. 5.3. This may be ascribed to the effect of presence of lower amount of binder content in the mixes made with higher S/B ratio that resulted in lower formation of aluminosilicate gels, which leads to comparatively higher water absorption and AVPV. The obtained results of water absorption and AVPV of geopolymer mortar (GPM) can be correlated with the compressive strength of GPM as observed from Fig. 5.2, where the mixes with lower water absorption and AVPV values exhibited higher 28 days compressive strength.

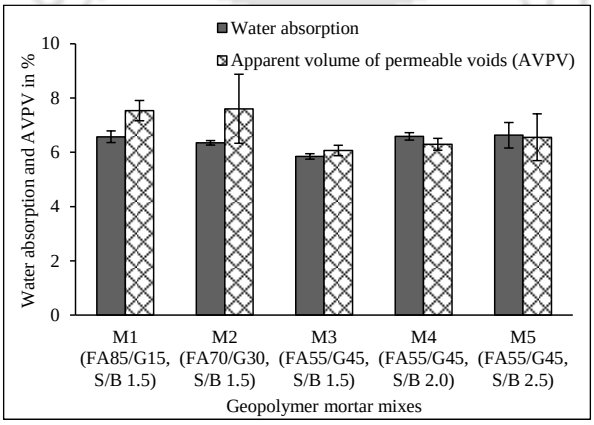

Fig. 5.3 Water absorption and apparent volume of permeable voids (AVPV) of geopolymer mortar (GPM) made with different fly ash/GGBS blends and S/B ratio.

5.5 Sorptivity of geopolymer mortar (GPM) mixes

Sorptivity tests were conducted to measure the tendency of geopolymer mortar (GPM) made with different fly ash/GGBS blends and S/B ratios to absorb and transmit water through the capillary pores. The sorptivity curves of geopolymer mortar (GPM) mixes made with different fly ash/GGBS blends and S/B ratios are shown in Fig. 5.4. The GPM mix M3 (FA55/G45, S/B 1.5) had a lower rate of water absorption than the other mixes (M1, M2, M4, and M5) (Fig. 5.4). This indicates the formation of denser microstructure in the GPM mix made with 45% GGBS content and S/B ratio of 1.5 when compared with other mixes. Furthermore, the rate of water absorption of GPM mixes significantly decreased after the first 6 hours. The slope of the sorptivity curves of initial absorption measured up to 6 hours of water absorption for GPM mixes are shown in Fig. 5.5. All the GPM mixes exhibited linear curves with a correlation coefficient greater than 0.98. Therefore, the sorptivity coefficient can be obtained for all the GPM mixes from the initial rate of water absorption (i.e., after 6 hours of water absorption). The sorptivity coefficient (S) of initial absorption of GPM mixes calculated using equation 3.10 is shown in Fig. 5.6. The sorptivity coefficient of geopolymer mortar (GPM) mix decreased significantly with increase in the GGBS content in the mix at a constant S/B ratio (Fig. 5.6). The GPM mixes M2 (FA70/G30, S/B 1.5) and M3 (FA55/G45, S/B 1.5) had 14.5% and 48.0% lower sorptivity coefficient than GPM mix M1 (FA85/G15, S/B 1.5). This may be ascribed to the effect of increased GGBS content in the mix, which has finer particle size than fly ash that enhanced the geopolymerization reaction and resulted in a decrease in the porosity of the mixes. Furthermore, the sorptivity coefficient of GPM mixes increased with increase in S/B ratio of the mixes. The GPM mixes M4 (FA55/G45, S/B 2.0) and M5 (FA55/G45, S/B 2.5) had 153% and 255% higher sorptivity coefficient than that of the mix M3 (FA55/G45, S/B 1.5). This may be attributed to the effect of significant increase in the porosity of the GPM mixes made with higher S/B ratio.

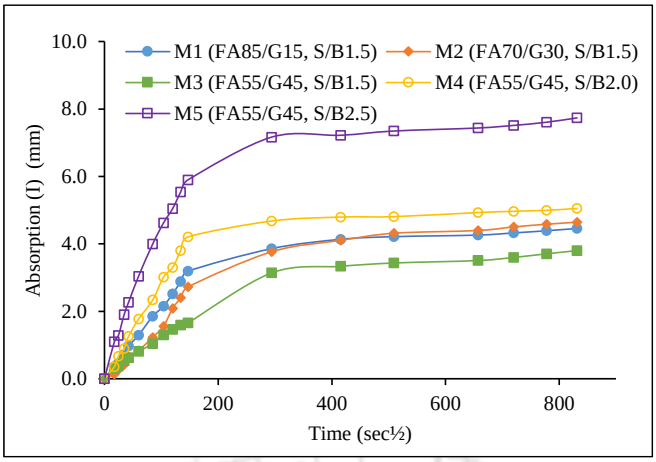

Fig. 5.4 Sorptivity curves of geopolymer mortar (GPM) mixes made with different fly ash/GGBS blends and S/B ratios.

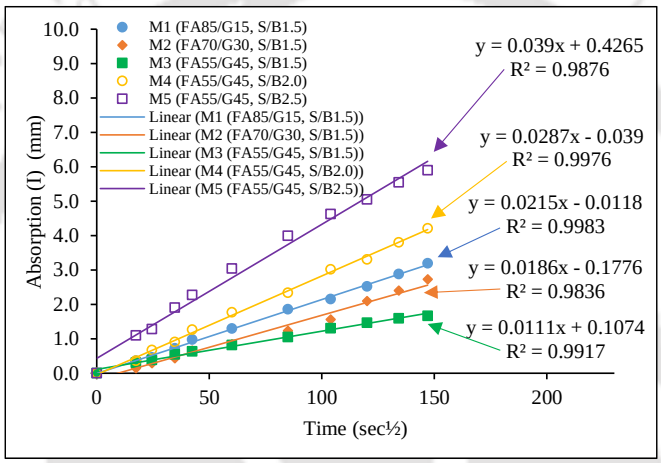

Fig. 5.5 Slope of the sorptivity curves of initial absorption (up to 6 hours of water absorption) for geopolymer mortar (GPM) mixes made with different fly ash/GGBS blends and S/B ratios.

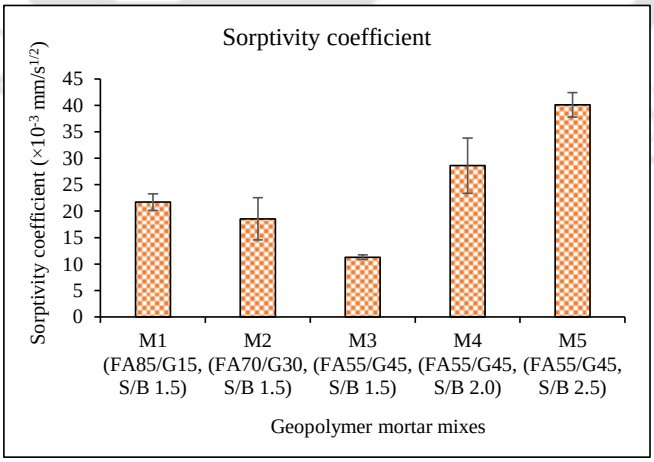

Fig. 5.6 Sorptivity coefficient of geopolymer mortar (GPM) mixes made with different fly ash/GGBS blends and S/B ratios.

5.6 Resistance of geopolymer mortar (GPM) specimens against sulfate and acid solutions

5.6.1 Visual observation of geopolymer mortar (GPM) specimens

The visual appearance of geopolymer mortar (GPM) specimens after 26 weeks of exposure to water, and different sulfate solutions (3% Na_2SO_4, 6% Na_2SO_4, 3% $MgSO_4$, and 6% $MgSO_4$) are shown in Fig. 5.7. Similarly, the visual appearance of geopolymer mortar (GPM) specimens after 26 weeks of exposure to water, and different acid solutions (0.31 mol/l H_2SO_4, 0.62 mol/l H_2SO_4, 0.31 mol/l HCl, and 0.62 mol/l HCl) are shown in Fig. 5.8. As observed from Fig. 5.7, there was no significant changes appeared on the surface of the GPM specimens exposed to water, 3% Na_2SO_4 and 6% Na_2SO_4 solutions, and 3% $MgSO_4$ solution for a period of 26 weeks. However, some white deposits were observed on the surface of GPM specimens made with 45% GGBS and S/B ratios of 2.0 and 2.5 (M4 and M5) in case of exposure to 6% $MgSO_4$ solution. This may be attributed to the formation of reaction product, i.e., gypsum on the surface of GPM after exposure to 6% $MgSO_4$ solution. Furthermore, small cracks were formed on the edges of GPM specimen made with 45% GGBS and S/B ratio of 2.5 (M5) after exposure to 6% $MgSO_4$ solution. This may be ascribed to the effect of formation of a comparatively higher amount of reaction products (gypsum) in the pores of GPM specimens made with higher S/B ratio (2.5), which led to the formation of cracks on the surface of specimens. In case of GPM mixes prepared with S/B ratio 1.5 (M1, M2 and M3), no significant changes were observed on the surface of the specimens exposed to 6% $MgSO_4$ solution for a period of 26 weeks.

Visual observation of GPM specimens exposed to acid solutions indicated that GPM mix M1 (FA85/G15, S/B 1.5) had better resistance against H_2SO_4 and HCl solutions than other mixes. No deterioration was identified on the surface of GPM mix M1 after 26 weeks of immersion in H_2SO_4 and HCl solutions (Fig. 5.8). This indicates the development of a strong cross-linking three-dimensional polymerization network in GPM made with a lower GGBS content (15%). However, the formation of expansion cracks was identified on the edges of the GPM specimens made with 30% and 45% GGBS content (M2, M3, M4, and M5) after exposure to 0.31 mol/l H_2SO_4 and 0.62 mol/l H_2SO_4 solutions for 26 weeks. This may be ascribed to the effect of more formation of reaction products (i.e., gypsum, as identified in the microstructure analysis, discussed later in Section 5.7) in the pores of the specimens during sulfuric acid attack, which caused expansion around the edges of the GPM specimens. The expansion cracks were more prominent in the GPM specimens made

with higher GGBS content (i.e., 45% GGBS). This may be due to the availability of comparatively higher amount of calcium in the GPM made with 45% GGBS, which reacted with H_2SO_4 solution and formed more amount of gypsum that led to expansion cracks to a greater extent around the edges of the GPM specimens. No significant difference was observed in the appearance of GPM specimens exposed to 0.62 mol/l H_2SO_4 solution with increase in sand-to-binder (S/B) ratio. However, in case of exposure to 0.31 mol/l H_2SO_4 solution, relatively more prominent expansion cracks were observed on the GPM specimens made with lower S/B ratio. The GPM specimens after exposure to water and HCl solutions were compared, and no sign of surface deterioration was found in the GPM specimens made with 15% and 30% GGBS (M1 and M2) in case of exposure to HCl solutions. However, damage was observed on surfaces and edges of all the GPM specimens made with 45% GGBS (M3, M4, and M5) after exposure to 0.31 mol/l HCl and 0.62 mol/l HCl solutions. The visible damage occurred due to loss in geopolymer paste from the edges and surfaces of GPM specimens that exposed the sand particles. Mostly no significant difference was observed in the appearance of GPM specimens exposed to HCl solutions with increase in sand-to-binder (S/B) ratio. Comparing the effect of acid solutions on the visual appearance of GPM specimens showed that the GPM specimens exposed to H_2SO_4 solutions had more-intense surface damage due to the formation of gypsum crystals, which led to significant volumetric expansion in the GPM specimens.

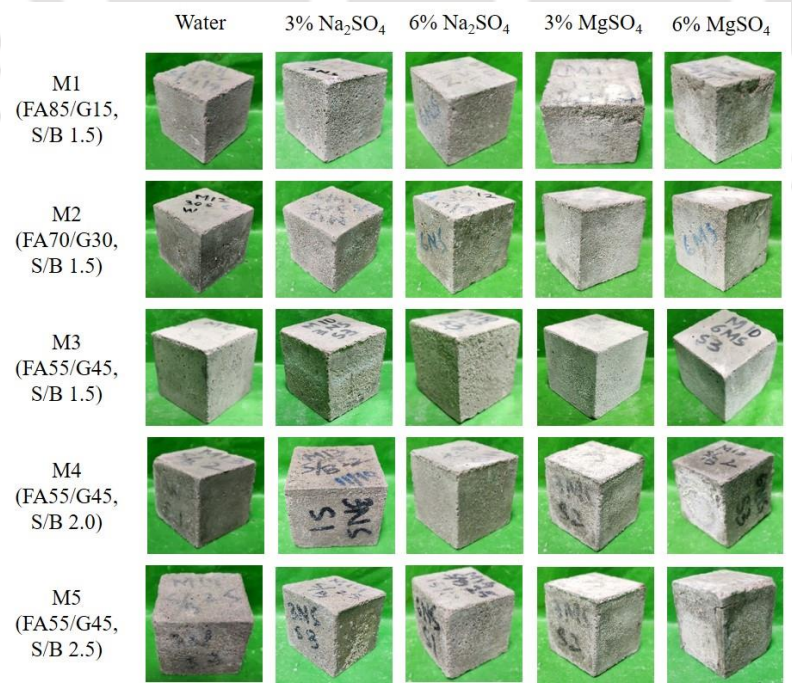

Fig. 5.7 Visual appearance of geopolymer mortar (GPM) specimens after exposure to water, and different sulfate solutions for a period of 26 weeks.

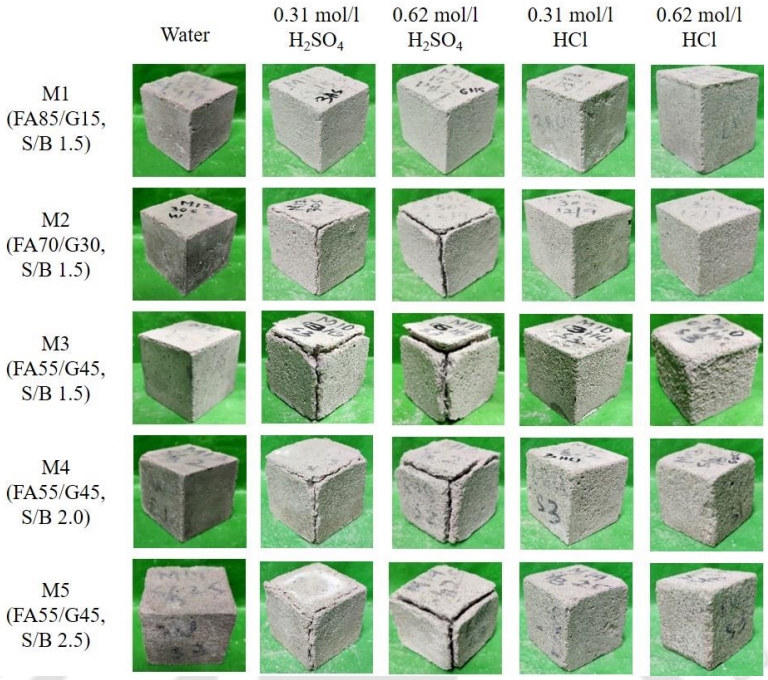

Fig. 5.8 Visual appearance of geopolymer mortar (GPM) specimens after exposure to water, and different acid solutions for a period of 26 weeks.

5.6.2 Change in weight of geopolymer mortar (GPM) specimens

5.6.2.1 Geopolymer mortar specimens exposed to water and sulfate solutions

The percentage change in weight of geopolymer mortar (GPM) specimens exposed to water and different sulfate solutions (i.e., 3% Na_2SO_4, 6% Na_2SO_4, 3% $MgSO_4$, and 6% $MgSO_4$) for a period of 26 weeks are shown in Fig. 5.9. The GPM specimens gained weight after exposure to water and different sulfate solutions (Fig. 5.9). The weight gain of the GPM specimens may be ascribed to the effect of absorption of water and sulfate solutions into the pores of the specimens [29,139]. The weight gain percentage for the GPM specimens increased with increase in the exposure duration, i.e., up to 12-14, 12-18, 6-10, 8-12 and 8-16 weeks for GPM mixes M1, M2, M3, M4, and M5 respectively, irrespective of water and sulfate solutions followed by decrease in weight gain thereafter (Fig. 5.9). The weight gain percentage for GPM mix M3 (FA55/G45, S/B 1.5) decreased much earlier than that of the other mixes. Furthermore, at the end of exposure period, the weight gain percentage of the GPM mixes mostly decreased with increase in GGBS content in the mixes, whereas no systematic variations were observed in the weight gain percentage with increase in S/B ratio of the mixes. This may be ascribed to the effect of presence of a higher GGBS content in the mixes, which enhanced the geopolymerization reaction and resulted in a denser microstructure of the geopolymer mortar.

Comparing the effect of exposure solutions, i.e., water and different sulfate solutions on weight gain percentage of GPM specimens indicated that the GPM specimens exposed to 3% and 6% $MgSO_4$ solutions had higher weight gain (0.16%–2.54%), followed by the GPM specimens exposed to 3% and 6% Na_2SO_4 solutions (0.03%–1.48%) and water (0.02%–0.58%). Gopalkrishnan and Chinaraju [46] reported similar observations in case of fly ash-GGBS based geopolymer concrete where the geopolymer concrete specimens immersed in 5% $MgSO_4$ solution for 180 days had higher weight gain percentage than those immersed in 5% Na_2SO_4 solution. The reason for higher weight gain percentage for the GPM specimens immersed in $MgSO_4$ solutions may be due to the effect of formation of some reaction products, i.e., gypsum, on the surface and within the pores of the GPM specimens [54]. This can be corroborated by the visual observation of the appearance of white deposits on the surface of the geopolymer mortar (GPM) specimens subjected to 6% $MgSO_4$ solution (Fig. 5.7).

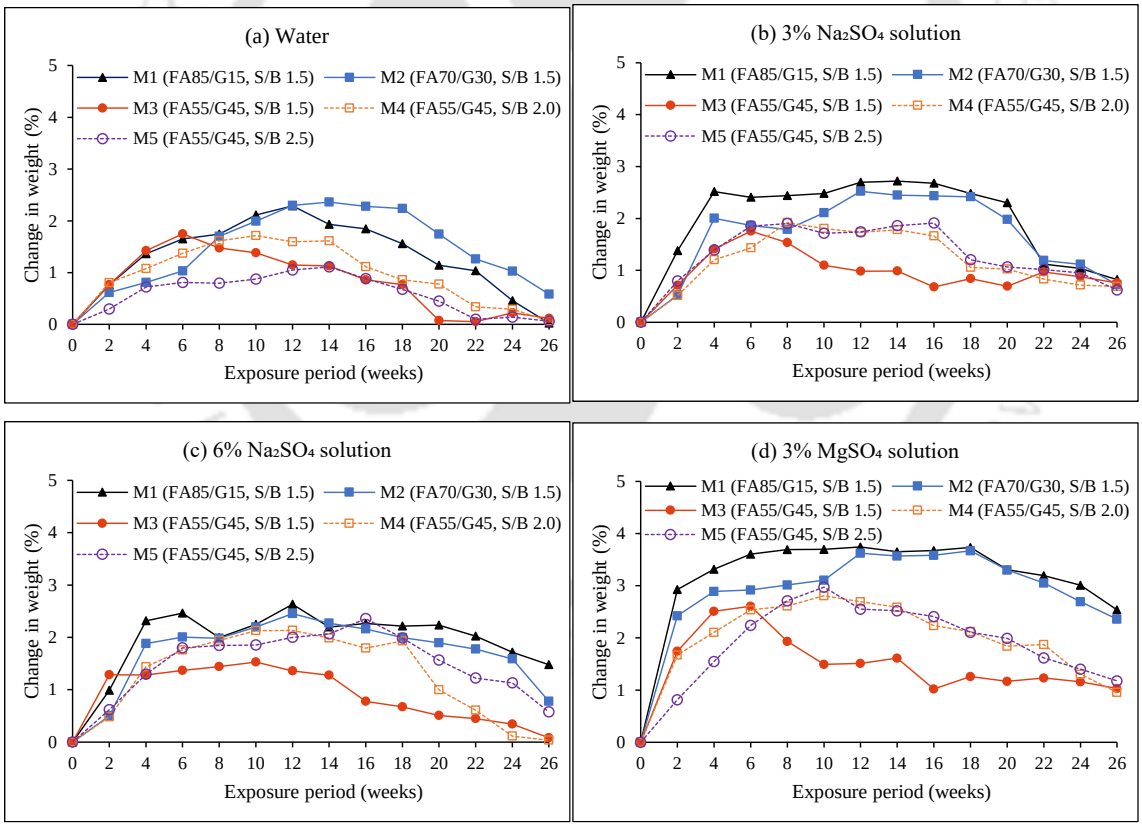

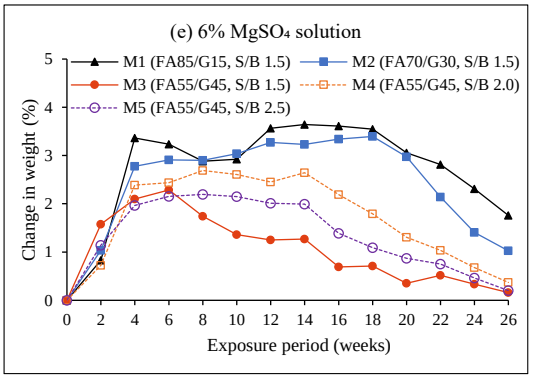

Fig. 5.9 Percentage change in weight of geopolymer mortar (GPM) specimens exposed for 26 weeks to (a) water, (b) 3% Na_2SO_4, (c) 6% Na_2SO_4, (d) 3% $MgSO_4$, and (e) 6% $MgSO_4$ solutions.

5.6.2.2 Geopolymer mortar specimens exposed to acid solutions

The percentage change in weight of GPM specimens exposed to different acid solutions (i.e., 0.31 mol/l H_2SO_4, 0.62 mol/l H_2SO_4, 0.31 mol/l HCl, and 0.62 mol/l HCl solutions) are presented in Fig. 5.10. Some of the GPM specimens slightly gained weight (i.e., as much as 1.59%) during initial weeks of exposure to different acid solutions, i.e., up to 12 weeks in case of H_2SO_4 solutions and 6 weeks in case of HCl solutions. This may be attributed to the effect of initial absorption of acid solutions in the pores of the GPM specimens. Further, in case of exposure to H_2SO_4 solution, the formation of reaction products such as gypsum may initially fill the pores, which resulted an increase in the weight of the specimens during initial weeks of exposure. In literature, some researchers also reported the weight gain (%) of alkali-activated fly ash/slag (AFS) paste [59], and fly ash/GGBFS based geopolymer mortar [101] specimens during initial few weeks of exposure to sulfuric acid solution. In alkali-activated fly ash/slag (AFS) paste made with different slag contents (0%, 10%, 30%, 50%) and 4 mol/L NaOH solution, Lee and Lee [59] reported that the mass of AFS paste specimens made with 0%, 10%, and 30% slag mostly remained unchanged, whereas the AFS paste specimens made with 50% slag showed a gain in mass approximately 6% after immersion in 10% sulfuric acid solution for 56 days. In another study, Khan et al. [101] reported that fly ash/GGBFS (85%/15%) based geopolymer mortar specimens made with 12 M NaOH solution showed a maximum gain in mass up to 2% during the initial 6 weeks of exposure to 1.5% sulfuric acid solution. In the present study, after a few weeks of exposure, the weight of the GPM specimens decreased and significant weight loss was observed toward the end of exposure duration, i.e., in the range of 1.32% to 7.93% in case of H_2SO_4 solutions, and in the range of 5.66% to 14.32% in case of HCl solutions. This may be ascribed to the effect of depolymerization

of geopolymer matrix in the presence of acid solutions, which led to dissolution of Si, Al, Ca and Na species and destroyed the aluminosilicate gel networks as well as C-S-H gel. A similar observation was reported by Aiken et al. [60], in which fly ash and slag based geopolymer mortars exposed to 5% H_2SO_4 solution for a period of 56 days had mass loss in the range of 3.4% to 7.6%.

Comparing the effect of GGBS content on the weight loss of the GPM specimens exposed to acid solutions indicated that the weight loss percentage increased with increase in the GGBS content in the mixes. The weight loss in the GPM specimens subjected to H_2SO_4 solutions may be ascribed to the effect of decalcification of geopolymer matrix, which eventually caused a loss of the binder phases. Furthermore, the effect of decalcification occurred to a greater extent in the GPM mixes made with higher GGBS content. The calcium reacted with the sulfur present in the H_2SO_4 solution and formed expansive reaction products, i.e., gypsum ($CaSO_4.2H_2O$), on the surface of the GPM specimens [139]. Therefore, cracks developed on the edges of the specimens and reduced their original weight. This result can be corroborated with the formation of cracks due to volumetric expansion as observed during the visual inspection of the GPM specimens (Fig. 5.8). In case of HCl solution, the effect of depolymerization of GPM specimens made with higher GGBS content leads to more leaching of silica (Si), alumina (Al), calcium (Ca) and sodium (Na) species that destroyed the aluminosilicate gel networks and C-S-H gel. Hence, maximum loss in binder phases was observed on the surface of GPM specimens made with higher amount of GGBS despite having lower volume of permeable voids (Fig. 5.3), which exposed the sand particles, and resulted in loss of original weight of the GPM specimens. Comparing the effect of S/B ratio on weight loss of the GPM specimens immersed in H_2SO_4 and HCl solutions indicated that the weight loss percentage increased with increase in S/B ratio of the mixes. The more weight loss at higher S/B ratio may be attributed to the presence of lower binder content at constant alkaline solution and sand content that led to higher water-to-geopolymer solids ratio, which caused higher volume of permeable voids in the mortar matrix (as seen in Fig. 5.3). This resulted in penetration of comparatively more acid solutions into the pores of the GPM specimens made with higher S/B ratio and deteriorated the surface of the specimens to a greater extent. Furthermore, the weight loss of the GPM specimens increased with increase in concentration of acid solutions (Fig. 5.10). This may be ascribed to the effect of greater deterioration of geopolymer matrix at higher concentration of acid solutions.

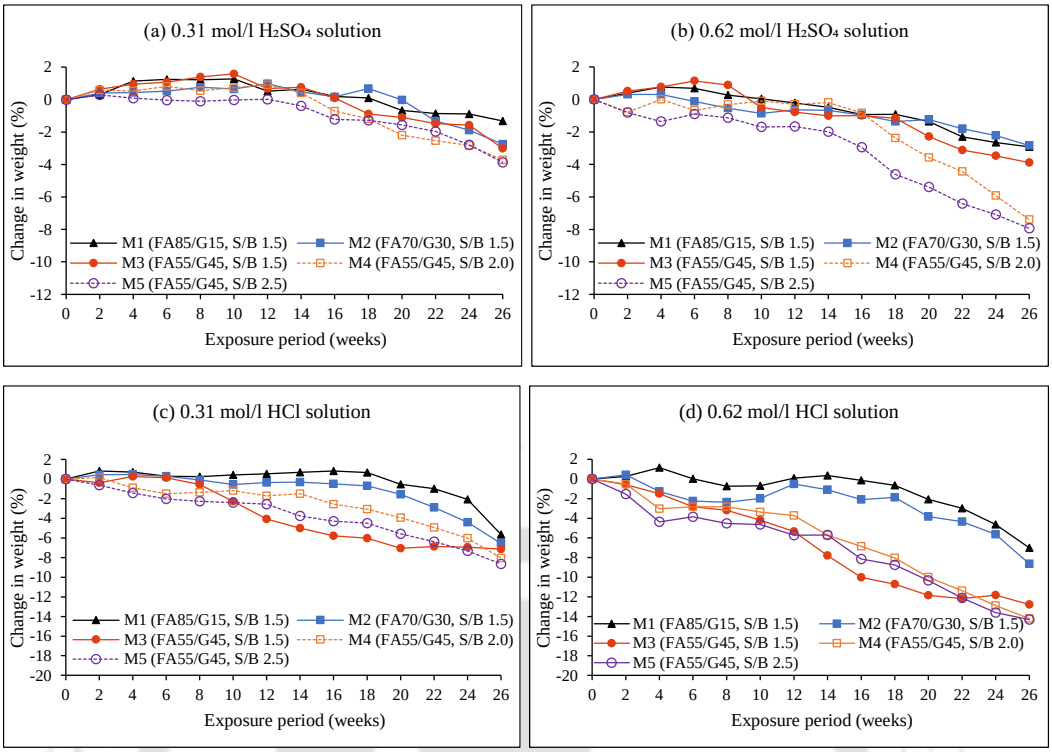

Fig. 5.10 Percentage change in weight of geopolymer mortar (GPM) specimens exposed for 26 weeks to (a) 0.31 mol/l H_2SO_4, (b) 0.62 mol/l H_2SO_4, (c) 0.31 mol/l HCl, and (d) 0.62 mol/l HCl solutions.

5.6.3 Change in compressive strength of geopolymer mortar (GPM) specimens

5.6.3.1 Geopolymer mortar (GPM) specimens exposed to different sulfate solutions

The compressive strength of geopolymer mortar (GPM) mixes made with different fly ash/GGBS blends and S/B ratio after 26 weeks of exposure to water, and different sulfate solutions (3% Na_2SO_4, 6% Na_2SO_4, 3% $MgSO_4$, and 6% $MgSO_4$ solutions) are illustrated in Fig. 5.11. The compressive strength of GPM mixes after 26 weeks of exposure to water and sulfate solutions increased with increase in GGBS content in the mixes (Fig. 5.11). This may be ascribed to the effect of higher extent of geopolymerization reaction in the presence of higher GGBS content in the mix. In GPM mixes made with higher GGBS content (M3: FA55/G45, S/B 1.5), a certain amount of calcium incorporated in to the N-A-S-H gels (the primary reaction product in fly ash-based geopolymer) and formed N-(C)-A-S-H type gels [59]. In addition, C-S-H gel may be formed due to presence of higher amount of calcium in the GGBS, resulting in higher compressive strength for GPM mixes made with more GGBS content [81]. The compressive strength of GPM mixes after exposure to water and different sulfate solutions decreased with increase in S/B ratio of the mixes. This is attributed to the fact that as the S/B ratio increased in the GPM mixes, the binder content of the mixes decreased at constant alkaline solution and sand content in the mixes, which

resulted in a decrease in the polymerization reaction in the mixes that led to formation of a porous microstructure in the mixes. Thus, there may be more penetration of sulfate solutions in the porous microstructure, which breaks the aluminosilicate network of GPM mixes.

The percentage change in compressive strength of GPM mixes exposed to different sulfate solutions with respect to reference mixes (i.e., the mortar specimens exposed to water) are presented in Fig. 5.12. The GPM mix M1 (FA85/G15, S/B 1.5) exhibited a gain in compressive strength after exposure to sulfate solutions i.e., 2.61% (3% Na_2SO_4), 1.96% (6% Na_2SO_4), 7.84% (3% $MgSO_4$), and 10.46% (6% $MgSO_4$) when compared with the reference mix i.e., the mix exposed to water. This may be ascribed to the effect of presence of a lower amount of calcium in the GPM mix M1 (FA85/G15, S/B 1.5), which resulted in formation of lower amount of gypsum in the presence of sulfate ions that might have filled the pores of the GPM mix. Furthermore, the main geopolymerization reaction product formed in the GPM mixes made with a lower amount of GGBS is a stable three-dimensional aluminosilicate gel, which is less vulnerable to sulfate solutions. Saavedra et al. [47] reported that 80%/20% fly ash/GGBS based geopolymer concrete exhibited 2.65% and 4.03% loss in compressive strength after 180 days of immersion in 5% Na_2SO_4 and 5% $MgSO_4$ solutions respectively, compared with the reference geopolymer concrete immersed in water. Similarly, in the present research work, GPM mixes M2 (FA70/G30, S/B 1.5) and M3 (FA55/G45, S/B 1.5) exhibited a loss in compressive strength when exposed to 6% Na_2SO_4 solution [i.e., 1.67% (M2), 3.54% (M3)], 3% $MgSO_4$ solution [i.e., 6.11% (M2), 11.62% (M3)], and 6% $MgSO_4$ solution [i.e., 7.78% (M2), 13.64% (M3)] as compared to the mixes exposed to water. This may be due to the effect of decalcification of calcium enriched gels (N-(C)-A-S-H and C-S-H gels) in GPM mixes M2 and M3 that promoted the formation of more gypsum in the geopolymer matrix [47]. The GPM mix M4 (FA55/G45, S/B 2.0) gained compressive strength after exposure to 3% Na_2SO_4 solution (2.92%), 6% Na_2SO_4 solution (2.19%) and 3% $MgSO_4$ solution (7.30%). Further, GPM mix M5 (FA55/G45, S/B 2.5) gained compressive strength after exposure to 6% Na_2SO_4 solution (1.74%) and 3% $MgSO_4$ solution (4.35%) compared with the reference mix (exposed to water). However, GPM mixes M4 and M5 lost compressive strength after exposure to 6% $MgSO_4$ solution (i.e., 5.84% for M4 and 5.22% for M5) compared with the reference mix. Further, the GPM mix M5 showed slight loss (0.87%) in compressive strength after exposure to 3% Na_2SO_4 solution. The reason for gain in compressive strength

of GPM mixes made with S/B ratios of 2.0 and 2.5 may be due to the filling of pores (formed due to comparatively lower binder content) by the formation of adequate amount of gypsum. However, the loss in compressive strength of GPM mixes (M4 and M5) exposed to 6% $MgSO_4$ solution may be due to the formation of comparatively more amount of gypsum in the geopolymer matrix, which promoted cracks on the surface of the specimens (Fig. 5.7). Comparing the effect of sulfate solutions indicated that the GPM mix M1 (FA85/G15, S/B 1.5) had the maximum gain in compressive strength and GPM mix M3 (FA55/G45, S/B 1.5) had the maximum loss in compressive strength when exposed to $MgSO_4$ solutions compared with Na_2SO_4 solutions. This may be ascribed to the fact that the formation of gypsum in case of exposure to $MgSO_4$ solutions may be higher than Na_2SO_4 solutions. As observed from Fig. 5.12, the loss in compressive strength of GPM mixes mostly increased with increase in concentration of both sulfate solutions. This may be due to the effect of decalcification of calcium enriched gels in GPM mixes to a comparatively greater extent at higher concentration of sulfate solutions.

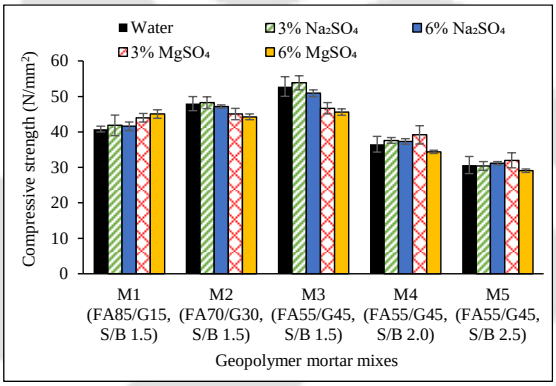

Fig. 5.11 Compressive strength of geopolymer mortar (GPM) mixes after exposure to water, and different sulfate solutions (3% Na_2SO_4, 6% Na_2SO_4, 3% $MgSO_4$, 6% $MgSO_4$ solutions) for 26 weeks.

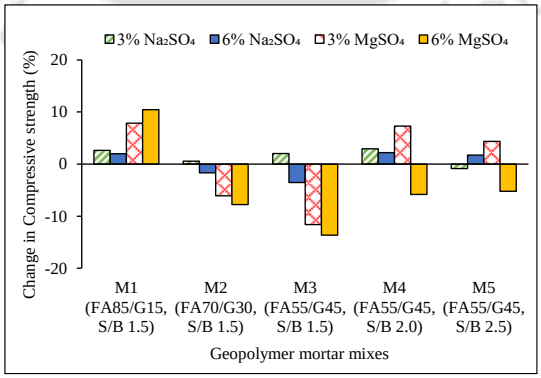

Fig. 5.12 Percentage change in compressive strength of geopolymer mortar (GPM) mixes after exposure to different sulfate solutions (3% Na_2SO_4, 6% Na_2SO_4, 3% $MgSO_4$, 6% $MgSO_4$ solutions) for 26 weeks.

5.6.3.2 Geopolymer mortar (GPM) specimens exposed to different acid solutions

The compressive strength of GPM mixes made with different fly ash/GGBS blends and S/B ratio after 26 weeks of exposure to water and acid solutions (0.31 mol/l H_2SO_4, 0.62 mol/l H_2SO_4, 0.31 mol/l HCl, and 0.62 mol/l HCl solutions) are presented in Fig. 5.13. Further, the percentage change in compressive strength (strength loss) of GPM mixes exposed to different acid solutions with respect to reference mixes (i.e., GPM mixes exposed to water) is shown in Fig. 5.14.

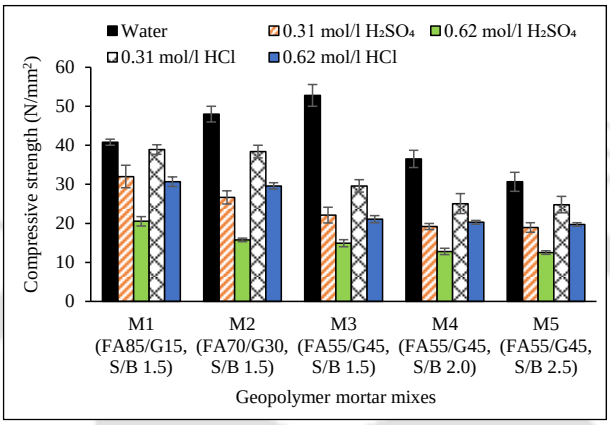

Fig. 5.13 Compressive strength of geopolymer mortar (GPM) mixes after exposure to water, and different acid solutions (0.31 mol/l H_2SO_4, 0.62 mol/l H_2SO_4, 0.31 mol/l HCl, and 0.62 mol/l HCl solutions for 26 weeks.

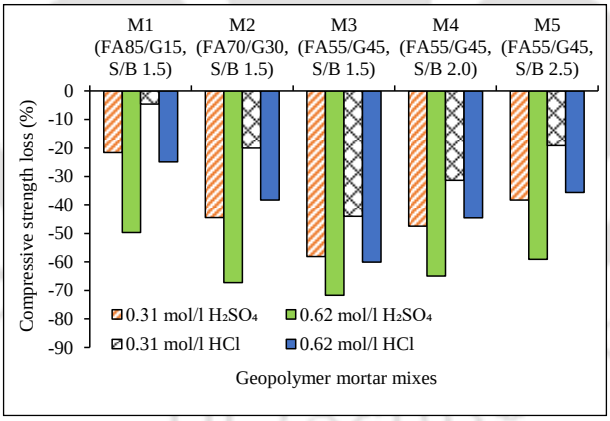

Fig. 5.14 Strength loss percentage in geopolymer mortar (GPM) mixes after exposure to different acid solutions (0.31 mol/l H_2SO_4, 0.62 mol/l H_2SO_4, 0.31 mol/l HCl, and 0.62 mol/l HCl solutions for 26 weeks.

The GPM specimens immersed in acid solutions exhibited lower compressive strength as compared to the specimens immersed in water as observed from Fig. 5.13. The strength loss was found in the range of 21.57% to 71.72%, and 4.58% to 60.10% in case of H_2SO_4, and HCl solutions respectively. This may be ascribed to the effect of depolymerization of aluminosilicate gels in GPM mixes in the presence of acid solutions [58]. In the literature,

similar results were reported by Aiken et al. [60], where the loss in compressive strength of fly ash/slag (100/0, 80/20, 60/40, 30/70) based geopolymer mortar was observed in the rage of 23% to 52%, 51% to 60%, and 61% to 67% after exposure to 1%, 3%, and 5% H_2SO_4 solutions respectively for a period of 56 days. The authors also observed that increase in the slag content decreased the porosity but the geopolymer mortar made with higher slag content became more susceptible to sulfuric acid attack due to decalcification of calcium-enriched gels and formation of more amount of gypsum. Further, the authors did not observe significant difference in the strength loss when the alkaline activator dosage in fly ash based geopolymer mortar increased from 7.5% to 11.5%. In another study, Khan et al. [101] reported that in case of geopolymer mortar made with 85% fly ash and 15% GGBFS, and activated with 12 M NaOH solution, a strength loss of 25% was observed after exposure to 1.5% H_2SO_4 solution for a period of 24 weeks when compared with the strength of geopolymer mortar specimens measured before exposure to H_2SO_4 solution. While comparing this with the results obtained in the present research work, the geopolymer mortar mix M1, which was prepared with a blend of 85% fly ash and 15% GGBS and NaOH solution of 14 M exhibited a comparatively lower strength loss of 21.57% after immersion in 0.31 mol/l H_2SO_4 solution for a period of 26 weeks. In the present research work, the lower strength loss after immersion in comparatively higher concentration of H_2SO_4 solution i.e., 0.31 mol/l H_2SO_4 solution (3% H_2SO_4 solution) when compared with that reported by Khan et al. [101] where geopolymer mortar specimens were exposed to 1.5% H_2SO_4 solution may be attributed to the effect of formation of denser geopolymer matrix due to the combined effect of higher binder content, and higher molarity of NaOH solution (in the present research work) as compared to that prepared with lower binder content and lower molarity of NaOH solution by Khan et al. [101].

While comparing the effect of fly ash/GGBS blends on compressive strength of GPM specimens immersed in acid solutions, it is observed that the compressive strength of GPM mixes decreased with increase in GGBS content in the mixes. This may be due to the decalcification of calcium enriched gels (N-(C)-A-S-H and C-S-H) to a greater extent at higher GGBS content in the GPM mixes. The maximum loss in compressive strength was observed in the mix M3 (FA55/G45, S/B 1.5) i.e., 58.08% in the 0.31 mol/l H_2SO_4 solution, 71.72% in the 0.62 mol/l H_2SO_4 solution, 43.94% in the 0.31 mol/l HCl solution, and 60.10% in the 0.62 mol/l HCl solution. The GPM mix M1 (FA85/G15, S/B 1.5) exhibited lower strength loss after immersion in H_2SO_4 solutions (21.57% in case of 0.31 mol/l H_2SO_4

solution and 49.67% in case of 0.62 mol/l H_2SO_4 solution), and HCl solutions (4.58% in case of 0.31 mol/l HCl solution and 24.84% in case of 0.62 mol/l HCl solution) as compared to other GPM mixes despite having relatively higher water absorption and permeable voids (as evident from Fig. 5.3). The reason for comparatively better performance of GPM mix M1 may be due to the relatively higher chemical stability of the aluminosilicate molecular structure compared with that of calcium-enriched gels, which formed in higher amount in GPM mix M3 [137].

While investigating the effect of S/B ratio, it is noted that the GPM mixes made with higher S/B ratio showed lower compressive strength, when immersed in acid solutions. However, the strength loss after immersion in acid solutions was reduced at higher S/B ratio as observed from Fig. 5.14. As stated earlier, the decrease in binder content in the mixes made with higher S/B ratio resulted in formation of lower amount of aluminosilicate gels leading to poor bonding between the aluminosilicate gels and fine aggregate, and resulted in lower compressive strength for the GPM mixes made with higher S/B ratio.

Further, the leaching of lower amount of Si, Al, and Ca species into the acid solutions due to lower availability of aluminosilicate gels may reduce the strength loss of the GPM mixes made with higher S/B ratio. In addition, the lower formation of gypsum in GPM specimens made with higher S/B ratio in case of immersion in H_2SO_4 solution might have filled the pores in the specimens, which resulted in lower strength loss as compared to that made with lower S/B ratio (Fig. 5.14). The loss in compressive strength was higher for GPM mixes immersed in H_2SO_4 solutions than HCl solutions (Fig. 5.14). In case of GPM specimens immersed in H_2SO_4 solution, the deposition of gypsum crystals leads to increase in the structural degradation of the specimens that resulted in higher strength loss in comparison to immersion in HCl solution [137]. Furthermore, the strength loss of GPM mixes increased with increase in concentration of both acid solutions. This may be ascribed to the effect of increase in the degree of deterioration of geopolymer matrix at higher concentration of acid solutions.

5.6.3.2.1 Deterioration factor of GPM mixes exposed to different acid solutions

The deterioration factor (DF) of GPM mixes immersed in acid solutions was evaluated with respect to the GPM mixes cured under ambient condition at the age of 28 and 180 days. For a given GPM mix immersed in acid solution, the deterioration factor greater than 1 indicates loss in compressive strength when compared with the compressive strength measured at 28 and 180 days. The deterioration factor of GPM mixes immersed in acid

solutions are presented in Table 5.1. From Table 5.1, it is noted that the DF_{28}, and DF_{180} of all GPM mixes immersed in H_2SO_4 solution varied from 1.15 to 2.94, and 1.45 to 3.70 respectively. Similarly, in case of HCl solution, the DF_{28}, and DF_{180} of all GPM mixes varied from 0.95 to 1.86, and 1.18 to 2.35 respectively. This indicates that all GPM specimens immersed in acid solutions exhibited strength loss as compared to that measured at 28 days and 180 days of ambient curing. Further, from Table 5.1, it can be observed that the GPM mix M1 (FA85/G15, S/B 1.5) exhibited lowest deterioration factor, whereas the GPM mixes M3 (FA55/G45, S/B 1.5) and M5 (FA55/G45, S/B 2.5) showed higher deterioration factor against acid solutions.

Table 5.1 Deterioration factor of geopolymer mortar (GPM) mixes after immersion in acid solutions

GPM mixes	Deterioration Factor (DF_{28}) *				Deterioration Factor (DF_{180}) **			
	0.31 mol/l H_2SO_4	0.62 mol/l H_2SO_4	0.31 mol/l HCl	0.62 mol/l HCl	0.31 mol/l H_2SO_4	0.62 mol/l H_2SO_4	0.31 mol/l HCl	0.62 mol/l HCl
M1 (FA85/G15, S/B 1.5)	1.15	1.79	0.95	1.20	1.45	2.26	1.19	1.51
M2 (FA70/G30, S/B 1.5)	1.53	2.34	1.06	1.24	1.77	2.95	1.23	1.57
M3 (FA55/G45, S/B 1.5)	2.01	2.46	1.50	1.75	2.53	3.11	1.89	2.20
M4 (FA55/G45, S/B 2.0)	1.65	2.88	1.27	1.82	1.88	3.63	1.44	2.29
M5 (FA55/G45, S/B 2.5)	1.51	2.94	1.15	1.86	1.55	3.70	1.18	2.35

*DF_{28}: Ratio of compressive strength of geopolymer mortar (GPM) measured at 28 days of ambient curing to that measured after 26 weeks of immersion in acid solutions.

**DF_{180}: Ratio of compressive strength of geopolymer mortar (GPM) measured at 180 days of ambient curing to that measured after 26 weeks of immersion in acid solutions.

5.7 Microstructure analysis

5.7.1 Correlation of microstructure with strength development of geopolymer mortar (GPM) at different ages of ambient curing

5.7.1.1 XRD analysis

The XRD patterns of geopolymer mortar (GPM) mixes made with various fly ash/GGBS blends and S/B ratio at 7, 28, 90, and 180 days of ambient curing are shown in Fig. 5.15 (a - e). From these figures, the crystalline peaks related to quartz (SiO_2) and mullite

($Al_{4.75}Si_{1.25}O_{9.63}$) were found in all GPM mixes, which indicates the presence of unreacted/partially reacted fly ash in the GPM mixes. Further, the amorphous to semi-crystalline phases related to the reaction products formed during the alkali activation of precursor materials were identified. The peaks related to albite ((Na, Ca)Al(Si Al)$_3O_8$) at 22.1º 2θ, and 28.0º 2θ, nepheline ($NaAlSiO_4$) at 27.1º 2θ, and anorthoclase (($Na_{0.85}$ $K_{0.15}$)($AlSi_3O_8$)) at 23.7º 2θ, 27.5º 2θ and 35.3º 2θ were identified in the XRD patterns of GPM mixes at all ages of ambient curing. Further, sodalite ($Na_8Al_6Si_6O_{24}(OH)_2(H_2O)_2$) was found at 24.5º 2θ in the XRD patterns of some GPM mixes. The peaks related to poorly ordered C-S-H and calcite was identified at 29.4º 2θ in all GPM mixes. From the XRD patterns, it is found that the intensity of peaks related to anorthoclase mostly reduced in all GPM mixes as the curing age increased from 7 to 180 days. Further, the intensity of peaks related to albite, nepheline, and C-S-H were mostly higher in the GPM mixes at later ages of ambient curing. Thus, the dominant effect of more formation of albite, nepheline, and C-S-H gel improved the strength of geopolymer mortar (GPM) at later ages. From Fig. 5.15 (a - c), it is observed that the geopolymer mortar (GPM) mixes made with higher amount of GGBS exhibited mostly higher peak intensity related to nepheline, albite, and C-S-H at all ages. This indicates the formation of higher amount of calcium-rich gels (N-(C)-A-S-H and C-S-H gel) and N-A-S-H gel that resulted in higher compressive strength for the GPM mixes made with higher amount of GGBS as observed from Fig. 5.2. While observing the XRD patterns of GPM mixes made with different S/B ratios (Fig. 5.15 (c - e)), it is noted that the GPM mixes made with higher S/B ratio exhibited mostly lower intensity of peaks related to anorthoclase. However, there was no systematic variation in the intensity of peaks related to nepheline, albite, and C-S-H gel. Thus, the dominant effect less formation of anorthoclase over the unsystematic variation in the formation of nepheline, albite, and C-S-H gel as indicated by the peak intensity in the XRD patterns led to lower compressive strength of GPM mixes made with relatively higher S/B ratio (M4 and M5) when compared with that made with lower S/B ratio (M3) (Fig. 5.2).

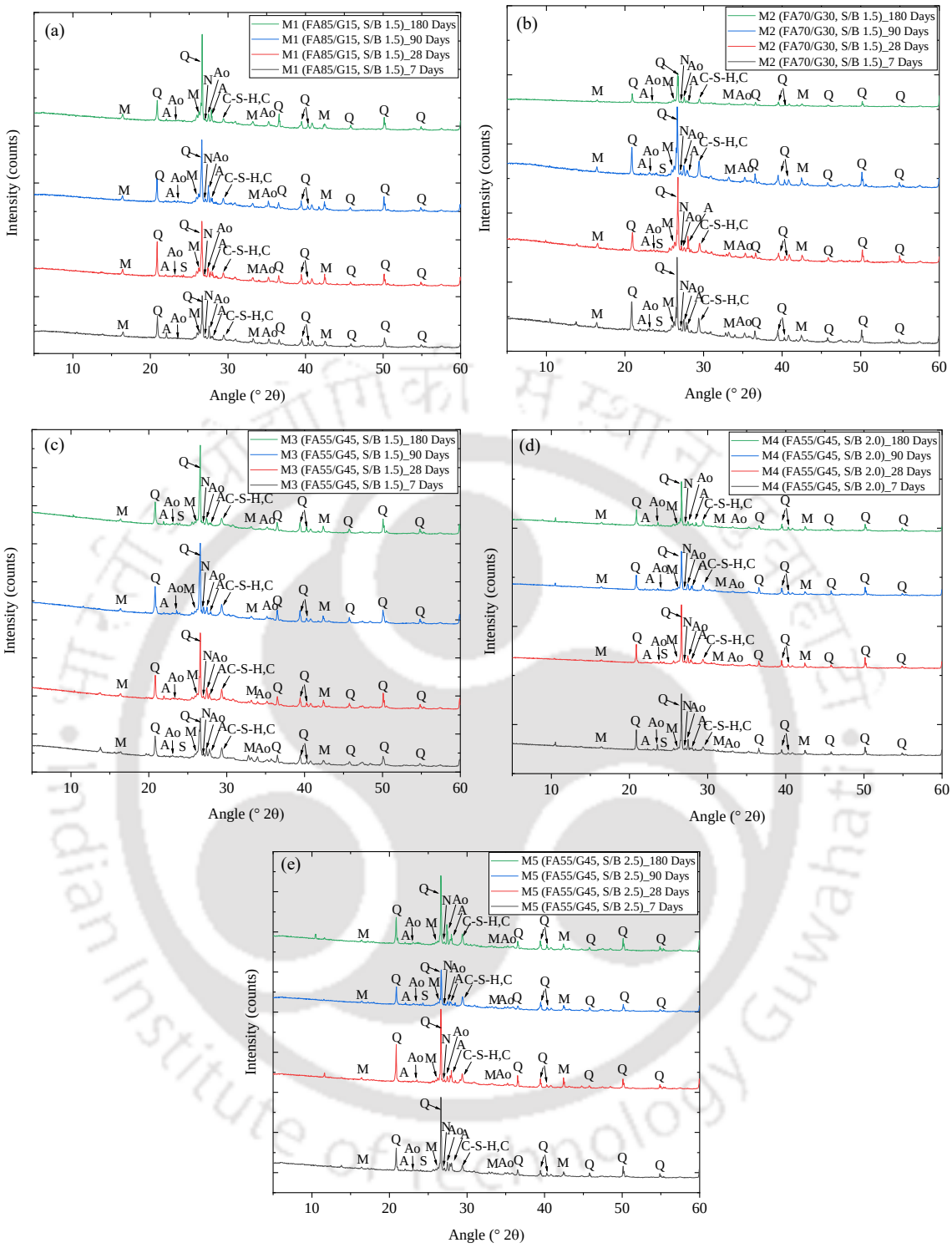

(Q: Quartz, M: Mullite, A: Albite, Ao: Anorthoclase, N: Nepheline, S: Sodalite, C-S-H: Calcium silicate hydrate, C: Calcite)

Fig. 5.15 XRD patterns of geopolymer mortar (GPM) mixes at different ages of ambient curing: (a) M1 (FA85/G15, S/B 1.5), (b) M2 (FA70/G30, S/B 1.5) (c) M3 (FA55/G45, S/B 1.5), (d) M4 (FA55/G45, S/B 2.0), (e) M5 (FA55/G45, S/B 2.5).

5.7.1.2 EDS analysis

Typical EDS spectra of geopolymer mortar (GPM) mixes at various ages of ambient curing are illustrated in Fig. 5.16 and Fig. A1 to Fig. A4 (in Appendix section). Further, the obtained elemental ratios such as atomic Na/Si, Al/Si, and Ca/Si ratios are presented in Fig. 5.17. From Fig. 5.17, it is noted that the GPM mixes exhibited atomic Na/Si, Al/Si, and Ca/Si ratios in the range of 0.20 - 1.66, 0.32 - 0.86, and 0.07 - 0.97 respectively. The atomic ratios were mostly increased with increase in ambient curing age for GPM mix M1. However, in case of other mixes, the variations in atomic ratios were mostly unsystematic with ambient curing age. This may be ascribed to the effect of differences in the enhancement of compressive strength of GPM mixes at various ages of ambient curing as observed from Fig. 5.2. The atomic Na/Si, Al/Si, and Ca/Si ratios increased from 7 days (Na/Si: 0.27 - 1.08, Al/Si: 0.32 - 0.86, Ca/Si: 0.08 - 0.70) to 28 days (Na/Si: 0.36 - 1.66, Al/Si: 0.43 - 0.86, Ca/Si: 0.19 - 0.97), and then it decreased from 28 to 90 days (Na/Si: 0.23 - 1.30, Al/Si: 0.42 - 0.62, Ca/Si: 0.07 - 0.75) followed by a decrease mostly from 90 to 180 days (Na/Si: 0.20 - 1.0, Al/Si: 0.33 - 0.69, Ca/Si: 0.11 - 0.45) irrespective of fly ash/GGBS blends and S/B ratio. This can be corroborated with the results obtained from compressive strength enhancement of GPM mixes, where the rate of strength enhancement was observed to be higher from 7 to 28 days (18.4% to 38.0%) and then it gradually decreased from 28 to 90 days (7.5% to 25.4%), followed by a decrease from 90 to 180 days (-4.5% to 15.4%) as discussed in section 5.3.

From Fig. 5.17, it is observed that the variations in atomic Na/Si, and Ca/Si ratios were dependent on the fly ash/GGBS blends of GPM. The GPM mix M3 exhibited higher atomic Na/Si ratio (0.32 - 0.58) as compared to mix M1 (0.23 - 0.55), and M2 (0.20 - 0.54). Similarly, the GPM mix M3 exhibited higher atomic Ca/Si ratio (0.36 - 0.91) followed by mix M2 (0.21 - 0.52) and M1 (0.07 - 0.19). However, there was no systematic variation in the atomic Al/Si ratio among the GPM mixes M1, M2, and M3. The higher atomic Na/Si and Ca/Si ratios in the GPM made with more amount of GGBS indicates the formation of higher amount of sodium (and calcium) aluminosilicate gels and C-S-H gel that resulted in higher strength development in the mixes as inferred from Fig. 5.2. Similar observations related to the variations in the atomic ratios with respect to fly ash/GGBS blends were also reported in the literature [82,140]. While evaluating the influence of S/B ratio on atomic ratios of GPM mixes, it is noted that the atomic Na/Si ratio was mostly higher for GPM mixes made with higher S/B ratio (M4, M5) whereas the atomic Al/Si and Ca/Si ratios

exhibited mostly unsystematic variations in the GPM mixes made with different S/B ratios. The GPM mix M5 (S/B ratio of 2.5) exhibited significantly higher atomic Na/Si ratio (1.0 to 1.66) as compared to GPM mix made with S/B ratio of 2.0 (M4, Na/Si ratio: 0.36 to 0.49), and S/B ratio of 1.5 (M3, Na/Si ratio: 0.32 to 0.58). This may be ascribed to the fact that the availability of lower binder content in the GPM made with higher S/B ratio at constant alkaline solution and sand content led to decrease in the silica content in the mixes. This was also identified from the EDS analysis where the GPM mix M5 exhibited lower silica content (average atomic percent of Si varied in the range of 7.6 - 11.8) as compared to the mix M3 (10.5 - 15.9) and M4 (11.3 - 16.1). Therefore, the GPM mix made with higher S/B ratio (M5) exhibited lower compressive strength (Fig. 5.2) despite showing higher atomic Na/Si ratio.

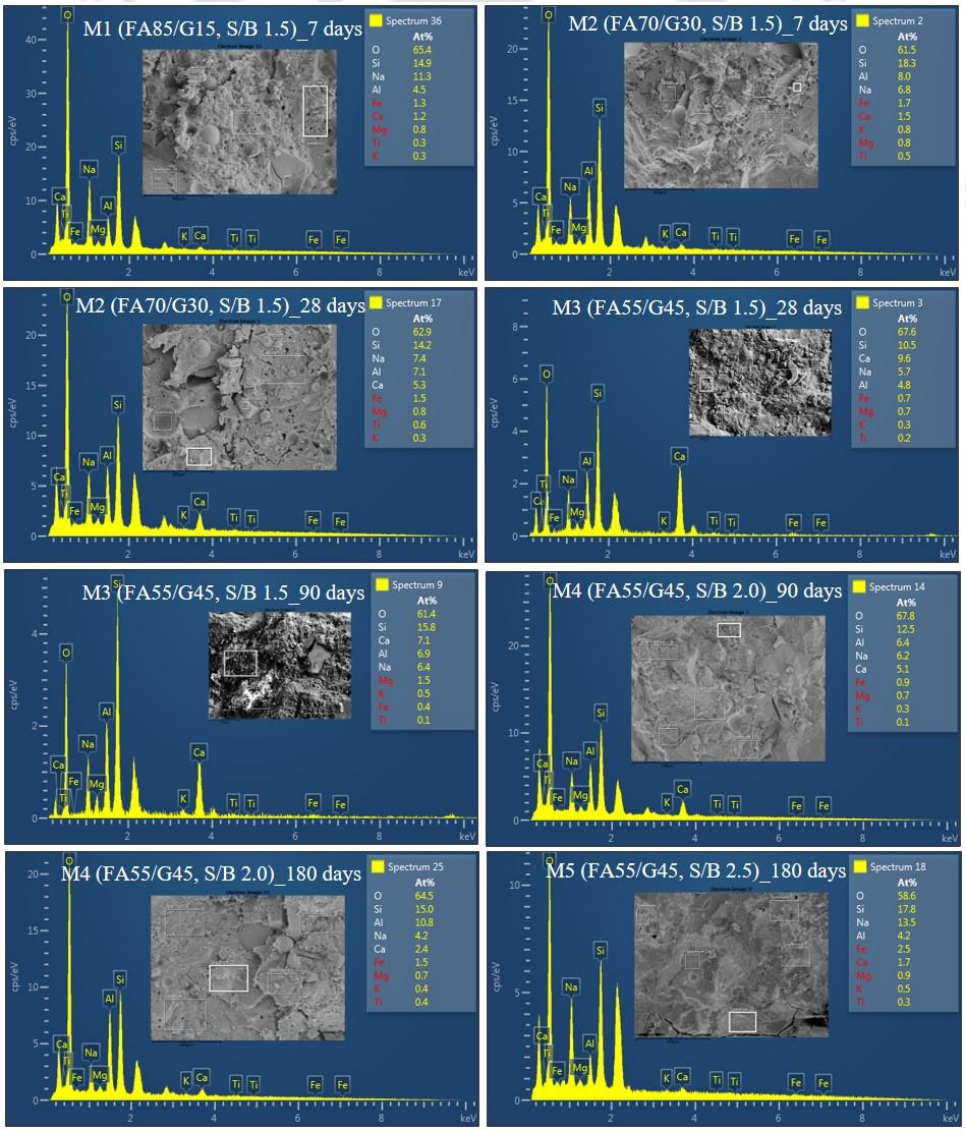

Fig. 5.16 EDS spectra of geopolymer mortar (GPM) mixes at different ages of ambient curing.

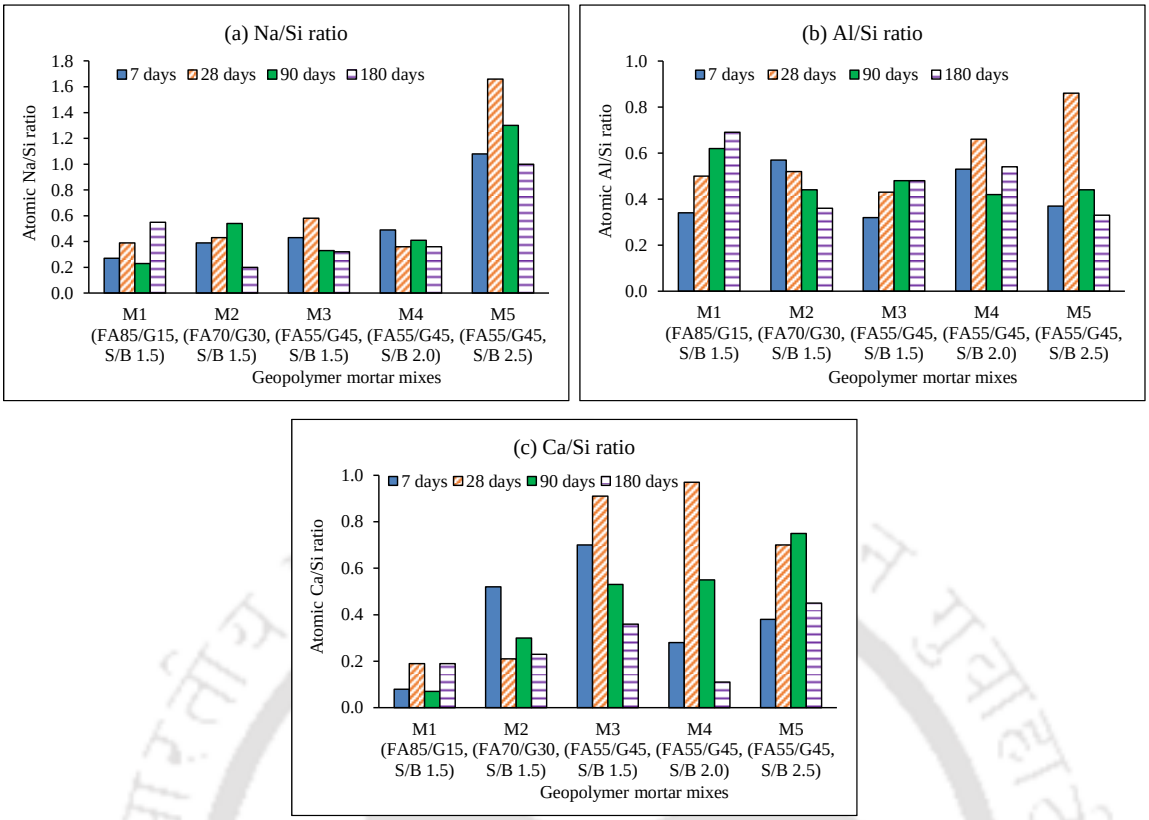

Fig. 5.17 Atomic (a) Na/Si ratio, (b) Al/Si ratio, and (c) Ca/Si ratio obtained from EDS analysis of geopolymer mortar (GPM) mixes at different ages of ambient curing.

5.7.1.3 FESEM analysis

The FESEM images of geopolymer mortar (GPM) mixes at ambient curing ages of 7 and 180 days are presented in Fig. 5.18. In addition, the FESEM images of GPM mixes at ambient curing ages of 28 and 90 days are presented in Fig. A5 (in Appendix section). From these figures, it is observed that the morphology of GPM mixes mainly consists of unreacted/partially reacted fly ash particles with different shape, and geopolymer gels. The unreacted/partially reacted GGBS particles were found in the GPM mix M4 at the age of 180 days and M5 at the age of 7 days. The presence of unreacted/partially reacted fly ash and GGBS particles indicates incomplete reaction of precursor materials, even after 180 days of ambient curing. Similar observation was also observed by Zhang et al. [20] in case of alkali activated cements developed under ambient curing condition. From Fig. 5.18, and Fig. A6, it is observed that the morphology of GPM mixes obtained at the age of 180 days exhibited slightly more homogeneous and denser microstructure in comparison with that at the age of 7, 28 and 90 days. This may be ascribed to the fact that as the reaction process progressed from 7 to 180 days, higher amount of geopolymer gels formed and that surrounded the unreacted/partially reacted fly ash particles (as seen in the morphology of GPM mixes M1 and M2). This enhanced the interphase bond between the unreacted fly ash

particles and geopolymer matrix leading to higher compressive strength at later age as evident from Fig. 5.2 [85]. While comparing the influence of fly ash/GGBS blends on morphology of GPM mixes, it is observed from Fig. 5.18, and Fig. A5 that the GPM mix made with higher amount of GGBS (M3) resulted in more compact microstructure as compared to that made with lower amount of GGBS (M1 and M2). This may be attributed to the formation of more amount of calcium-rich gels due to increase in the extent of geopolymerization reaction in the presence of higher amount of GGBS that leads to increase in the compressive strength of GPM mixes. The partially reacted fly ash particles leave some heterogeneously dispersed cavities and also developed some pores (as observed on the morphology of GPM mix M1_180 days, M2_7 days and M2_90 days) that caused the microstructure more porous thereby leading to lower compressive strength for the GPM made with lower amount of GGBS. Further, from Fig. 5.18, and Fig. A5, no significant differences were observed in the morphology of GPM made with different S/B ratios (M3, M4, and M5). However, there was mostly higher formation of geopolymers gels in the GPM mix made with lower S/B ratio as compared to that made with higher S/B ratio as observed from Fig. 5.18, and Fig. A5.

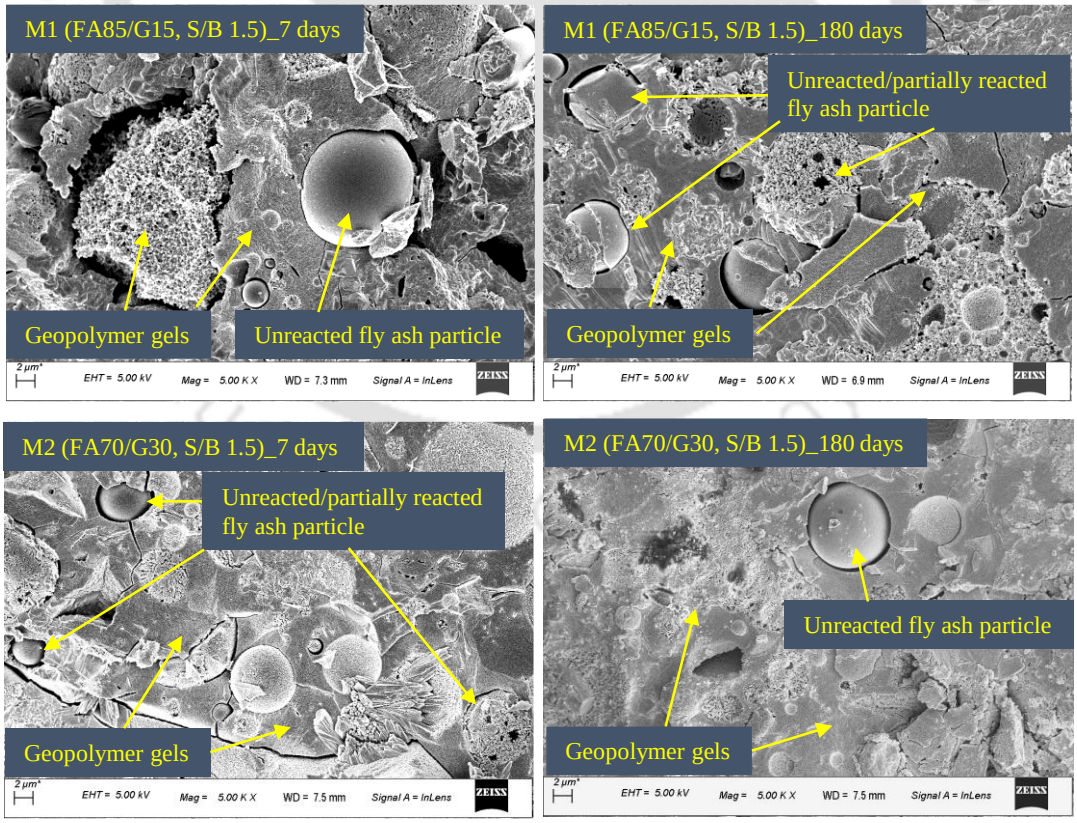

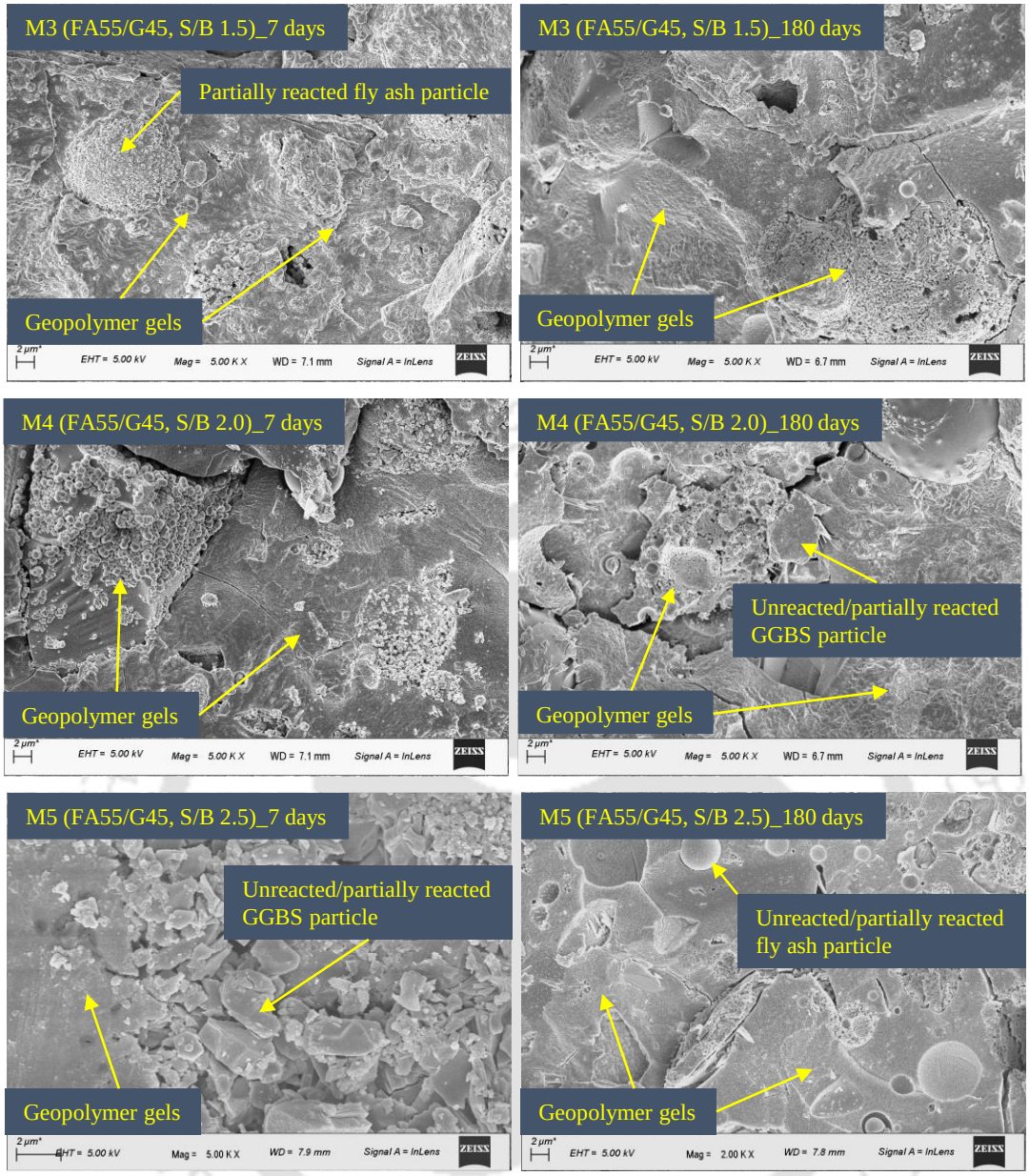

Fig. 5.18 FESEM images of geopolymer mortar (GPM) mixes at 7 and 180 days of ambient curing.

5.7.1.4 FTIR analysis

The FTIR spectra of geopolymer mortar (GPM) mixes made with different fly ash/GGBS blends and S/B ratio at the ambient curing ages of 7, 28, and 180 days are shown in Fig. 5.19 (a - e). From these figures, the peaks related to asymmetric bending vibration of Si-O-Si bond, and Al-O bond were identified in the range of 465 cm^{-1} to 472 cm^{-1}, and 695 cm^{-1} to 779 cm^{-1} respectively, which indicate the presence of unreacted/partially reacted precursor materials in the GPM mixes. The peaks related to asymmetric stretching vibration of Si-O-Si(Al) bond found in the range of 1028 cm^{-1} to 1040 cm^{-1} indicate the coexistence of geopolymer gels (N-A-S-H and N-(C)-A-S-H) and C-S-H gel in the GPM mix. The

stretching vibration of carbonate groups (CO_3^{2-}) were identified in the range of 1426 cm^{-1} to 1458 cm^{-1}. Further, the bending vibration of H-O-H group, and stretching vibration of -OH group were identified in the range of 1638 cm^{-1} to 1645 cm^{-1}, and 3429 cm^{-1} to 3462 cm^{-1} respectively. From Fig. 5.19 (a - e), it is observed that the peaks related to Si-O-Si(Al) bond mostly shifted towards higher wavenumbers as the ambient curing age increased from 7 to 180 days. This indicates the initial formation of C-S-H gel followed by N-(C)-A-S-H gels gradually over time [40,82]. While evaluating the effect of GGBS content, and S/B ratio, there was no systematic variation in the peaks related to Si-O-Si(Al) bond with increase in GGBS content and S/B ratio in the GPM mixes as observed from Fig. 5.19 (a - e).

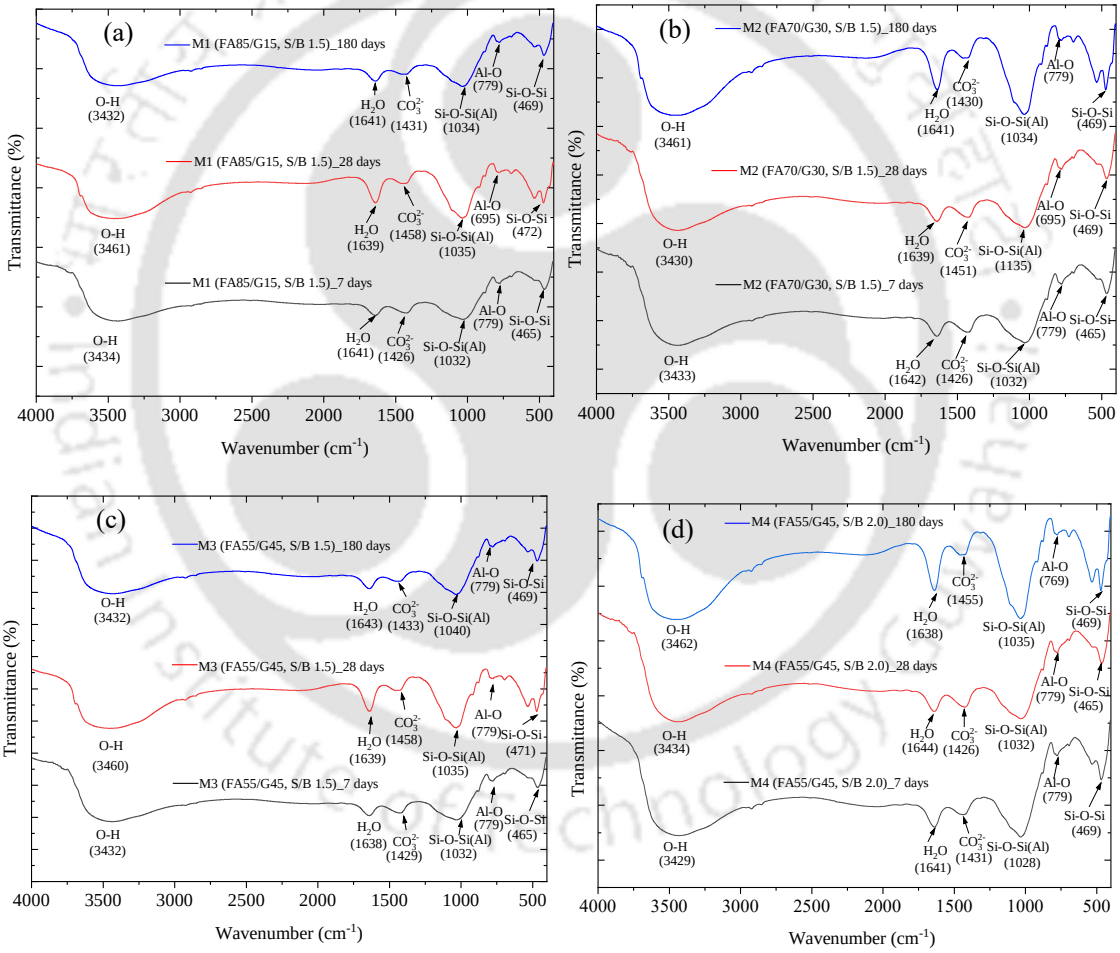

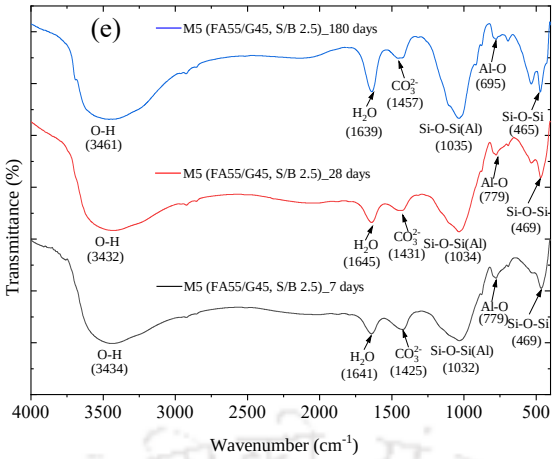

Fig. 5.19 FTIR spectra of geopolymer mortar (GPM) mixes at different ages of ambient curing: (a) GPM mix M1 (FA85/G15, S/B 1.5), (b) GPM mix M2 (FA70/G30, S/B 1.5) (c) GPM mix M3 (FA55/G45, S/B 1.5), (d) GPM mix M4 (FA55/G45, S/B 2.0), (e) GPM mix M5 (FA55/G45, S/B 2.5).

5.7.2 Correlation of microstructure with compressive strength of geopolymer mortar (GPM) mixes after immersion in different exposure solutions

5.7.2.1 XRD analysis

5.7.2.1.1 Geopolymer mortar (GPM) exposed to water and sulfate solutions

The XRD patterns of geopolymer mortar (GPM) mixes exposed to water, and different sulfate solutions (3% Na_2SO_4, 6% Na_2SO_4, 3% $MgSO_4$, and 6% $MgSO_4$ solutions) for 26 weeks are presented in Fig. 5.20 to Fig. 5.22. From these figures, it is observed that the peak intensity of nepheline, anorthoclase, albite, sodalite, and C-S-H gel mostly increased with increase in GGBS content from 15% to 45% in the GPM mixes exposed to water and different sulfate solutions for 26 weeks. Furthermore, a peak related to anorthite ((Ca, Na)(Si, Al)$_4O_8$) i.e., a calcium and sodium aluminosilicate complex was identified at 28. 1º 2θ in the XRD pattern of GPM mix made with 45% GGBS (M3: FA55/G45, S/B 1.5) and exposed to water, which indicates the formation of higher amount of calcium-rich gels in the mix. The presence of higher amount of GGBS enhanced the geopolymerization reaction in the GPM mixes exposed to water and different sulfate solutions, which led to formation of higher amount of N-A-S-H, N-(C)-A-S-H and C-S-H gels, and resulted in increase in compressive strength of GPM mix M3 (Fig. 5.11).

The peak intensity of albite and C-S-H decreased with increase in S/B ratio of the GPM mixes exposed to water (Fig. 5.20). Furthermore, the peak intensity of nepheline, anorthoclase, albite, and C-S-H mostly decreased with increase in S/B ratio of the GPM mixes exposed to different sulfate solutions (Fig. 5.21 and Fig. 5.22). This may be ascribed

to the formation of a comparatively lower amount of geopolymer gels and C-S-H gel due to presence of a lower amount of binder in the GPM mixes made with higher S/B ratio (M4, and M5), which resulted in a decrease in compressive strength of GPM mixes made with higher S/B ratio in case of exposure to water and different sulfate solutions (Fig. 5.11).

Comparing the XRD patterns of GPM mixes exposed to water and sulfate solutions (Fig. 5.20 to Fig. 5.22) indicated that the peak intensity of nepheline, anorthoclase, albite and C-S-H gel were mostly higher for the GPM mixes exposed to Na_2SO_4 solutions followed by exposure to water and $MgSO_4$ solutions. This may be attributed to the formation of more geopolymer gels and C-S-H gel in the GPM mixes due to a comparatively higher extent of polymerization reaction in the presence of Na_2SO_4 solution. Therefore, increase in compressive strength was observed in most of the cases in case of exposure to Na_2SO_4 solutions as compared to water (Fig. 5.12). Similarly, strength loss was observed in most of the cases in case of exposure to $MgSO_4$ solutions as compared to Na_2SO_4 solutions when compared with exposure to water (Fig. 5.12). Although, the peak intensity of geopolymer gels and C-S-H gel were mostly higher in the GPM mix M2 and M3 in case of exposure to 6% Na_2SO_4 solution than water, the lower compressive strength when exposed to 6% Na_2SO_4 solution as compared to water (Fig. 5.12) may be ascribed to the dominant effect of formation of gypsum, which was identified at 31.1º 2θ in the XRD patterns (Fig. 5.21 (b)). The formation of gypsum might have caused the reduction in compressive strength of the GPM mix M2 and M3 in case of exposure to 6% Na_2SO_4 solution. The gypsum formation was indicated by a small peak in the XRD patterns of GPM mixes in case of exposure to 6% Na_2SO_4 solution (Fig. 5.21 (b)).

Although the peak intensity related to geopolymer gels and C-S-H gel were mostly lower in the GPM mixes exposed to 3% $MgSO_4$ and 6% $MgSO_4$ solutions, the GPM mix made with 15% GGBS content (M1) in case of exposure to both $MgSO_4$ solutions (3% and 6%) gained compressive strength when compared with that exposed to water (Fig. 5.12). This indicates that the formation of gypsum in the pores was not sufficient to deteriorate the geopolymer matrix due to formation of more stable aluminosilicate gels in the GPM mix M1 made with lower amount of GGBS i.e., 15%. The formation of lower amount of gypsum in the presence of lower amount of calcium in GPM mix M1 in case of exposure to sulfate solution might have filled the pores in the mix. For the GPM mix made with higher GGBS content (M2, M3, M4, and M5) in case of exposure to 3% and 6% $MgSO_4$ solutions, the peak intensity of albite, and C-S-H gel were mostly lower as compared to exposure to water,

which may be ascribed to the decalcification of these calcium enriched gels. The decalcification of calcium enriched gels resulted in formation of more amount of gypsum, which deteriorated the geopolymer matrix to a greater extent and led to loss in compressive strength in case of exposure to $MgSO_4$ solutions (mix M2 and M3: exposure to 3% $MgSO_4$ solution, and mix M2, M3, M4, and M5: exposure to 6% $MgSO_4$ solution) as compared to that exposed to water (Fig. 5.12). The formation of gypsum was identified by a small peak in the XRD patterns of GPM mixes exposed to 6% $MgSO_4$ solution (Fig. 5.22 (b)).

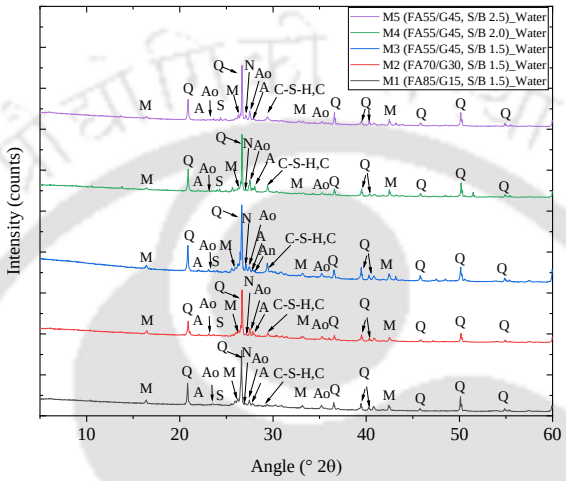

Fig. 5.20 XRD patterns of geopolymer mortar (GPM) mixes exposed to water for a period of 26 weeks.

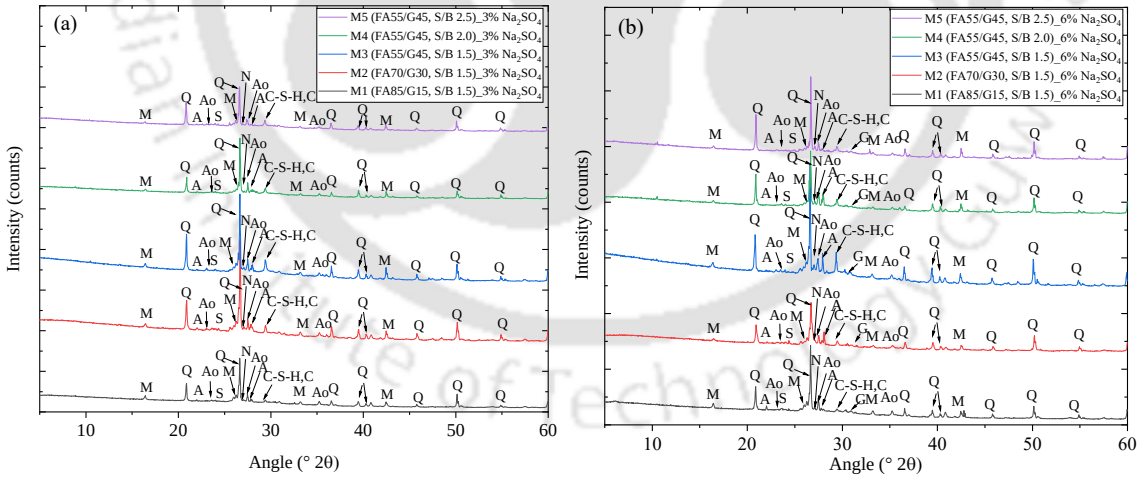

(Q: Quartz, M: Mullite, A: Albite, Ao: Anorthoclase, N: Nepheline, S: Sodalite, C-S-H: Calcium silicate hydrate, C: Calcite, G: Gypsum)

Fig. 5.21 XRD patterns of geopolymer mortar (GPM) mixes exposed to: (a) 3% Na_2SO_4 solution, and (b) 6% Na_2SO_4 solution, for a period of 26 weeks.

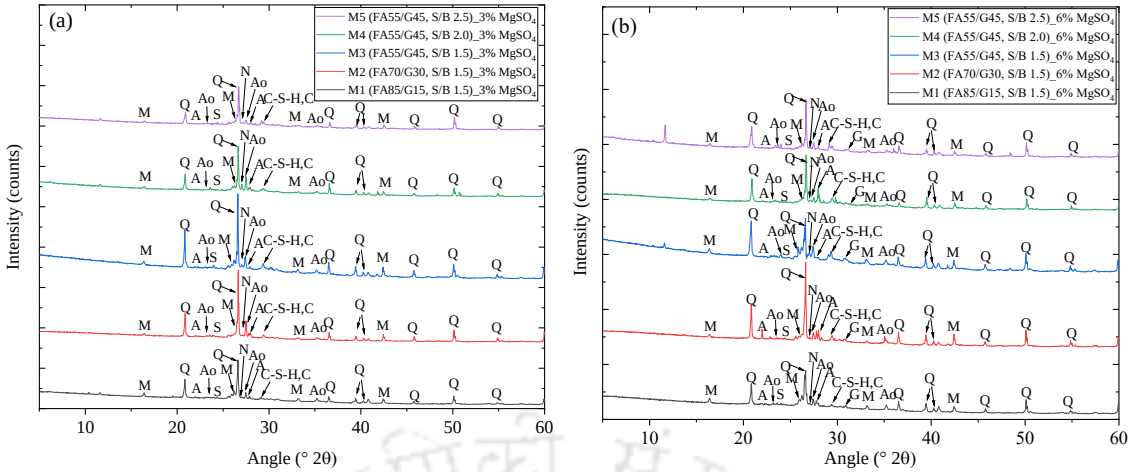

Fig. 5.22 XRD patterns of geopolymer mortar (GPM) mixes exposed to: (a) 3% $MgSO_4$ solution, and (b) 6% $MgSO_4$ solution, for a period of 26 weeks.

5.7.2.1.2 Geopolymer mortar (GPM) exposed to acid solutions

The XRD patterns of geopolymer mortar (GPM) mixes exposed to different acid solutions (0.31 mol/l H_2SO_4, 0.62 mol/l H_2SO_4, 0.31 mol/l HCl, and 0.62 mol/l HCl solutions) for 26 weeks are shown in Fig. 5.23 and Fig. 5.24. Comparison of the XRD patterns of GPM mixes exposed to water (Fig. 5.20) and acid solutions (Fig. 5.23 and Fig. 5.24) indicated that the peak intensity of anorthoclase and albite decreased in the GPM mixes exposed to both H_2SO_4 solutions and HCl solutions than that exposed to water. Furthermore, the peak intensity of nepheline, sodalite and C-S-H gel disappeared in the XRD patterns of GPM mixes exposed to both types of acid solutions. This indicates that the phases related to N-A-S-H and N-(C)-A-S-H gels, and C-S-H gel are more susceptible to H_2SO_4 and HCl solutions, which caused depolymerization of the aluminosilicate gels and resulted in a significant reduction in compressive strength of GPM mixes exposed to H_2SO_4 and HCl solutions when compared with that exposed to water. The peaks associated with gypsum ($CaSO_4.2H_2O$) were identified at 11.6º 2θ, 29.1º 2θ, 31.1º 2θ, 32.1º 2θ, 33.35º 2θ, 40.58º 2θ, 43.34º 2θ, and 56.78º 2θ in the XRD patterns of all GPM mixes exposed to 0.31 mol/l H_2SO_4 and 0.62 mol/l H_2SO_4 solutions (Fig. 5.23 (a and b)).

The peak intensity of anorthoclase, albite, and gypsum increased with increase in GGBS content in the GPM mixes exposed to H_2SO_4 solutions (Fig. 5.23 (a, b)). This indicates that although a higher amount of N-A-S-H and N-(C)-A-S-H gels were formed in the GPM mixes made with higher GGBS content, the dominant effect of formation of more amount of gypsum caused deterioration of aluminosilicate gels to a higher extent. This observation can be corroborated with the results obtained from the compressive strength of GPM mixes

made with higher GGBS content, which exhibited higher loss in compressive strength compared with the GPM mixes made with lower GGBS content (Fig. 5.14). The peak intensity of anorthoclase, albite, and gypsum mostly decreased with increase in S/B ratio in the GPM mixes exposed to H_2SO_4 solutions (Fig. 5.23 (a, b)), which indicates presence of less amount of aluminosilicate gels and gypsum in the GPM mixes made with higher S/B ratio. This is attributed to the fact that the binder content of the GPM mixes decreased with increase in the S/B ratio, which resulted in the formation of lower amount of aluminosilicate gels. This led to lower dissolution of Si, Al, Na, and Ca species from the aluminosilicate gels in the presence of H_2SO_4 solution thereby forming lower amount of gypsum as a result of lower extent of reaction of calcium with H_2SO_4 solution. Thus, the dominant effect of formation of lower amount of gypsum in the GPM mixes made with higher S/B ratio resulted in less compressive strength loss as compared to that made with lower S/B ratio (Fig. 5.14). The XRD patterns of GPM mixes exposed to 0.31 mol/l and 0.62 mol/l HCl solutions (Fig. 5.24 (a and b)) indicated that although the peak intensity of anorthoclase and albite mostly increased with increase in GGBS content, the compressive strength reduced with increase in GGBS content. This may be due to the dominant effect of disappearance of phases related to nepheline, sodalite, and C-S-H gel in the GPM mixes. Furthermore, the peak intensity of albite decreased with increase in S/B ratio in the GPM mixes exposed to HCl solutions. This can be corroborated with the decrease in compressive strength of GPM with increase in S/B ratio in case of exposure to HCl solutions (Fig. 5.13). However, comparatively lower dissolution of Si, Al, and Ca species from the aluminosilicate gels in the presence of HCl solution due to presence of lower amount of aluminosilicate gels as indicated by XRD patterns resulted in less strength loss in the GPM made with higher S/B ratio than that made with lower S/B ratio (Fig. 5.14). While comparing the XRD patterns of GPM exposed to H_2SO_4 and HCl solutions (Fig. 5.23 and Fig. 5.24), the intensity of peaks related to anorthoclase and albite were mostly higher in case of GPM mixes exposed HCl solutions as compared to that exposed to H_2SO_4 solutions. This indicates comparatively less dissolution of aluminosilicate gels in case of exposure to HCl solutions than H_2SO_4 solutions. This is in line with the variation in loss in compressive strength of GPM mixes where the strength loss was lower in case of exposure to HCl solutions than H_2SO_4 solutions (Fig. 5.14). Further, the peak intensity of anorthoclase and albite in the XRD patterns mostly decreased with increase in concentration of both acid solutions (Fig. 5.23 and Fig. 5.24), which shows presence of less amount of aluminoslilicate

gels in the GPM mixes in case of exposure to acid solutions of higher concentration. It may be noted that the loss in compressive strength of GPM mixes was higher at higher concentration of both acid solutions than that at lower concentration (Fig. 5.14).

While comparing the XRD patterns of GPM obtained at 28 and 180 days of ambient curing with that of GPM immersed in H_2SO_4, and HCl solutions, it is noted that the GPM mixes immersed in H_2SO_4 solutions exhibited lower intensity of peaks related to anorthoclase and albite in comparison to that obtained at 28 and 180 days of ambient curing. However, there was no systematic variation in the peak intensity of anorthoclase and albite of GPM mixes immersed in HCl solutions when compared with that obtained at 28 and 180 days of ambient curing. Further, the intensity of peaks related to sodalite, nepheline, and C-S-H gel were disappeared in the XRD patterns of GPM mixes immersed in both types of acid solution as compared to that obtained at 28 and 180 days of ambient curing. Therefore, all the GPM mixes immersed in acid solutions mostly exhibited higher deterioration factor (i.e., greater than 1).

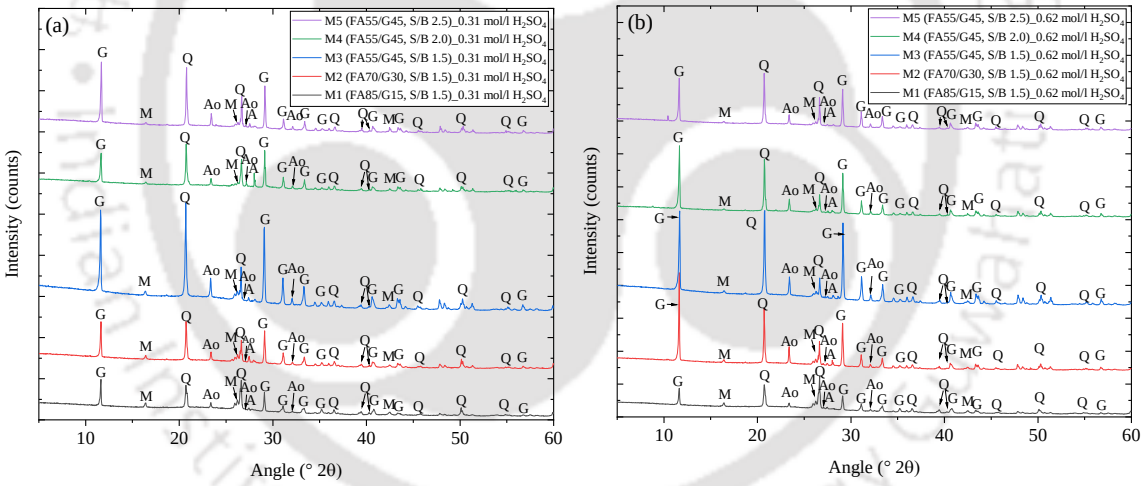

Fig. 5.23 XRD patterns of geopolymer mortar (GPM) mixes exposed to: (a) 0.31 mol/l H_2SO_4 solution, and (b) 0.62 mol/l H_2SO_4 solution, for a period of 26 weeks.

.

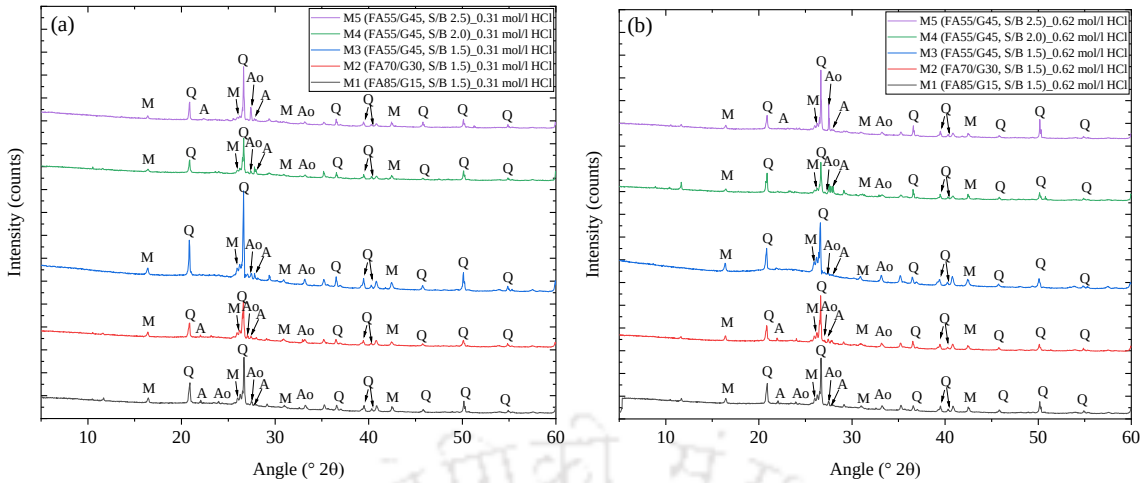

Fig. 5.24 XRD patterns of geopolymer mortar (GPM) mixes exposed to: (a) 0.31 mol/l HCl solution, and (b) 0.62 mol/l HCl solution, for a period of 26 weeks.

5.7.2.2 EDS analysis

5.7.2.2.1 Geopolymer mortar (GPM) exposed to water and sulfate solutions

Typical EDS spectra of geopolymer mortar (GPM) mixes exposed to water and to different sulfate solutions for 26 weeks are shown in Fig. 5.25 to Fig. 5.29. The elemental ratios (average atomic Na/Si, Al/Si, and Ca/Si ratios) obtained from EDS analysis of GPM mixes are shown in Fig. 5.30. The GPM mixes exposed to water had average atomic Na/Si ratio, Al/Si ratio, and Ca/Si ratio in the range 0.19-0.28, 0.39-0.52 and 0.06-0.65, respectively, irrespective of the GGBS content and S/B ratio (Fig. 5.30). These values of atomic ratios indicate the presence of N-A-S-H gel and N-(C)-A-S-H gel in the GPM mixes [41,82,85,95]. The GPM mix made with 45% GGBS content (M3) exhibited higher atomic Al/Si ratio (0.52), and moderate Na/Si ratio (0.24) after immersion in water. Furthermore, the GPM mix made with 45% GGBS content (M3) had atomic Ca/Si ratio of 0.65, which is significantly higher than the mixes made with 15% GGBS content (Ca/Si ratio = 0.06) and 30% GGBS content (Ca/Si ratio = 0.14). This indicates the coexistence of C-S-H gel along with N-A-S-H and N-(C)-A-S-H gels in the mix M3 that resulted in highest compressive strength among all the GPM mixes exposed to water (Fig. 5.11). Similar observations were reported in literature about the formation of C-S-H gel when the atomic Ca/Si ratio in the mixes was in the range 0.6 to 1.4 [41,82,83,85,95,135,136]. The variations in atomic ratios (Na/Si, Al/Si, and Ca/Si ratios) were not systematic with increase in GGBS content from 15% to 45% in the GPM mixes after exposure to 3% Na_2SO_4, 6% Na_2SO_4, and 3% $MgSO_4$ solutions (Fig. 5.30). The atomic Na/Si ratio, Al/Si ratio, and Ca/Si ratio decreased with increase in GGBS content in the GPM mixes exposed to 6% $MgSO_4$ solution. However, the compressive strength of GPM mixes after exposure to different

sulfate solutions were mostly increased with increase in GGBS content from 15% to 45%. This may be attributed to the effect of inconsistent variation between the extent of formation of different binding gels in the GPM mixes with increase in GGBS content in the presence of sulfate solutions that led to inconsistent variations in the atomic ratios.

The GPM mix M1 (FA85/G15, S/B 1.5) exposed to Na_2SO_4 and $MgSO_4$ solutions exhibited higher atomic ratios (Na/Si, Al/Si, and Ca/Si ratios) than in case of exposure to water (Fig. 5.30). This is in line with the variation in compressive strength of GPM mix M1 between exposure to sulfate solutions and water (Fig. 5.11). As already discussed in Section 5.7.2.1.1, there was comparatively lower formation of binding gels in GPM mix M1 in case of exposure to $MgSO_4$ solutions when compared with that exposure to water as indicated by the peak intensity in the XRD patterns. The gain in strength of GPM mix M1 (15% GGBS) in case of exposure to $MgSO_4$ solutions when compared with water was attributed to the formation of more stable aluminosilicate gels in the GPM, and pore filling effect of gypsum due to its lower formation in the presence of lower calcium content in the mix M1. Thus, the higher atomic ratios in GPM mix M1 may ascribed to the effect of inconsistent variation among silica, alumina, sodium, and calcium species in the GPM mix M1 exposed to $MgSO_4$ solutions. In case of GPM mix M2 (FA70/G30, S/B 1.5), the variations in atomic ratios were not systematic with respect to different exposure solutions (Fig. 5.30). However, GPM mix M3 (FA55/G45, S/B 1.5) exposed to $MgSO_4$ solutions had lower atomic Na/Si, Al/Si, and Ca/Si ratios than that exposed to water and Na_2SO_4 solutions. This can be correlated with the results obtained from the compressive strength where GPM mix M3 exposed to $MgSO_4$ solutions had lower compressive strength than that exposed to water and Na_2SO_4 solutions (Fig. 5.11).

The GPM mix made with S/B ratio of 2.5 (M5) had a lower atomic Na/Si ratio than those made with lower S/B ratios (M3 and M4) when exposed to water (Fig. 5.30). However, there was less difference in atomic Na/Si ratio between mixes M3 and M4. Furthermore, the atomic Al/Si ratio and Ca/Si ratio of GPM mixes decreased with increase in S/B ratio in case of exposure to water. This may be attributed to the less paste content in the GPM mixes made with higher S/B ratio, which led to lower extent of geopolymerization reaction and resulted in lower compressive strength of the GPM mixes made with higher S/B ratio (Fig. 5.11). In case of GPM mixes exposed to Na_2SO_4 and $MgSO_4$ solutions, no systematic variations were observed in atomic ratios with increase in S/B ratio of the mixes. Further, in GPM mixes M4 (FA55/G45, S/B 2.0) and M5 (FA55/G45, S/B 2.5), there was no

systematic variation in atomic Na/Si, Al/Si, and Ca/Si ratios among different exposure environment i.e., water, Na_2SO_4, and $MgSO_4$ solutions. The presence of calcium and sulfur in the GPM mixes exposed to sulfate solutions (Fig. 5.26-5.29, and Table 5.2) indicates the formation of gypsum in the mixes. The formation of comparatively more amount of gypsum in GPM mixes M2 and M3 in case of exposure to 6% Na_2SO_4, 3% $MgSO_4$, and 6% $MgSO_4$ solutions, M4 in case of exposure to 6% $MgSO_4$ solution, and M5 in case of exposure to 6% $MgSO_4$ solution might have resulted in the propagation of expansion cracks in the mixes, which led to a decrease in compressive strength (Fig. 5.11). However, the formation of gypsum to a certain amount in case of GPM mix M1 exposed to all solutions; M2 and M3 exposed to 3% Na_2SO_4 solution; M4 exposed to 3% Na_2SO_4, 6% Na_2SO_4, and 3% $MgSO_4$ solutions; and M5 exposed to 6% Na_2SO_4, and 3% $MgSO_4$ solutions might have filled the pores in the mixes, thereby resulting in comparatively higher compressive strength in comparison to exposure to water (Fig. 5.11).

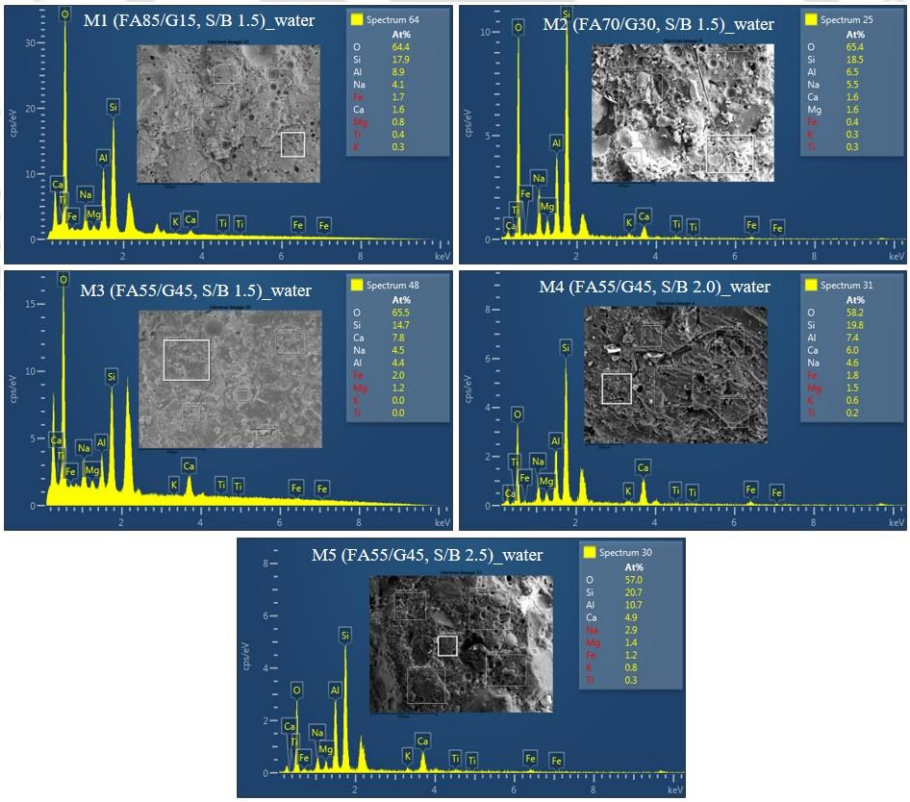

Fig. 5.25 EDS spectra of geopolymer mortar (GPM) mixes exposed to water for 26 weeks.

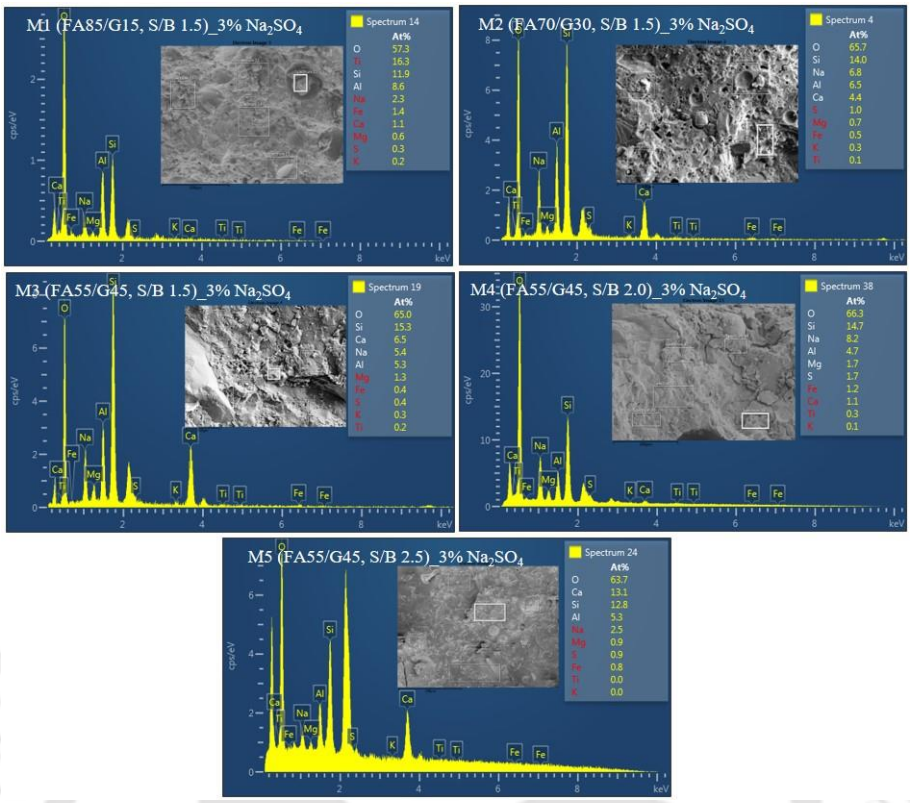

Fig. 5.26 EDS spectra of geopolymer mortar (GPM) mixes exposed to 3% Na_2SO_4 solution for 26 weeks.

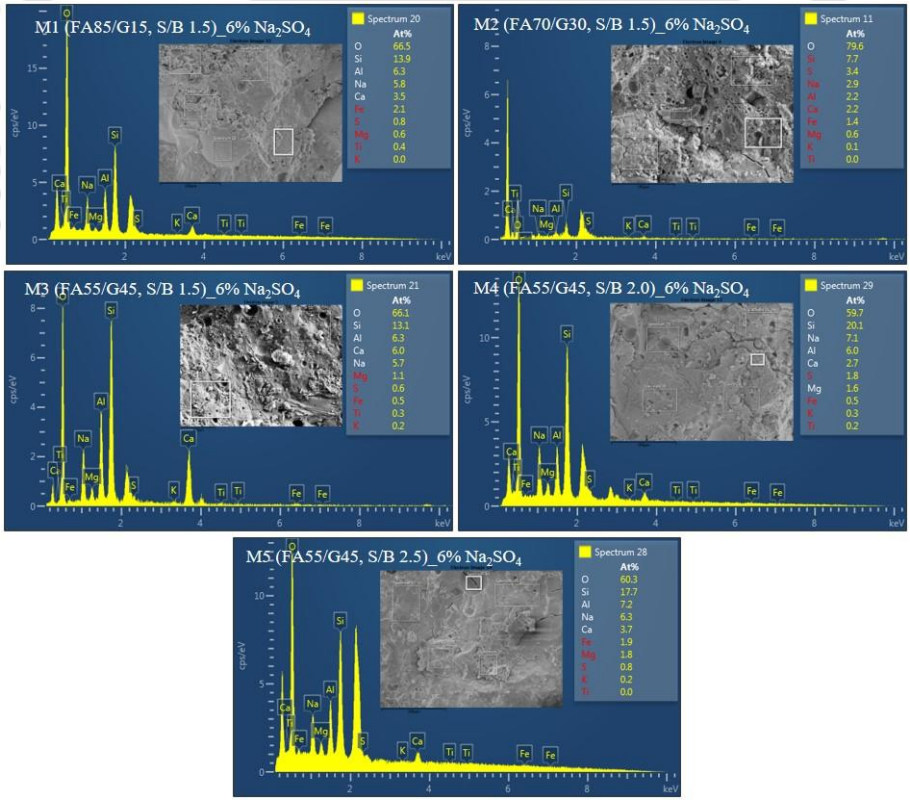

Fig. 5.27 EDS spectra of geopolymer mortar (GPM) mixes exposed to 6% Na_2SO_4 solution for 26 weeks.

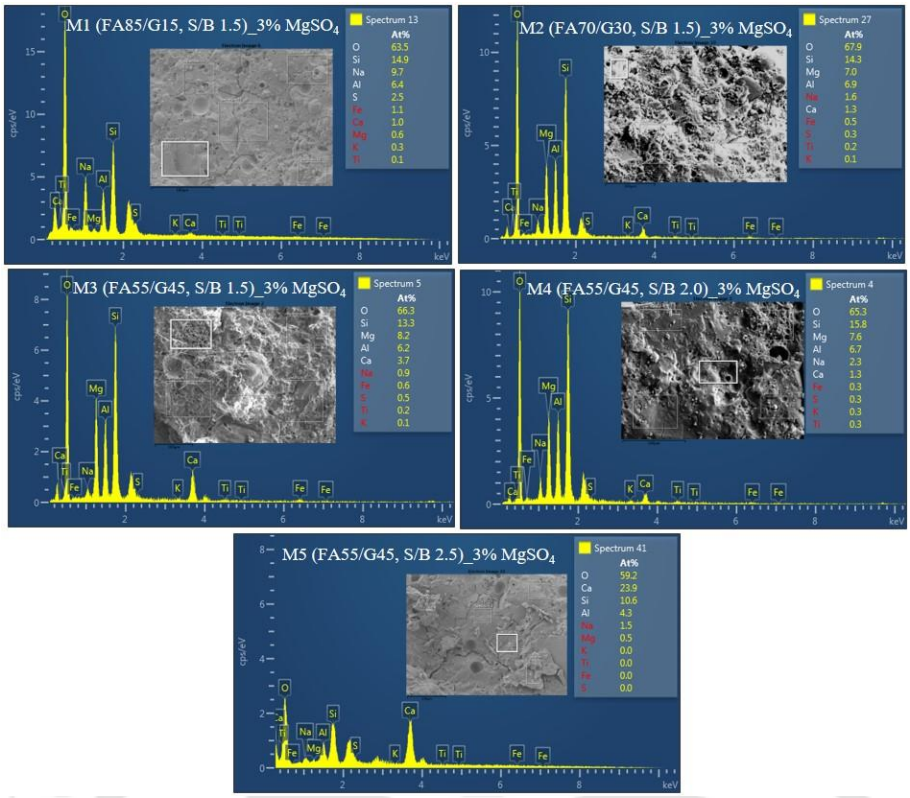

Fig. 5.28 EDS spectra of geopolymer mortar (GPM) mixes exposed to 3% $MgSO_4$ solution for 26 weeks.

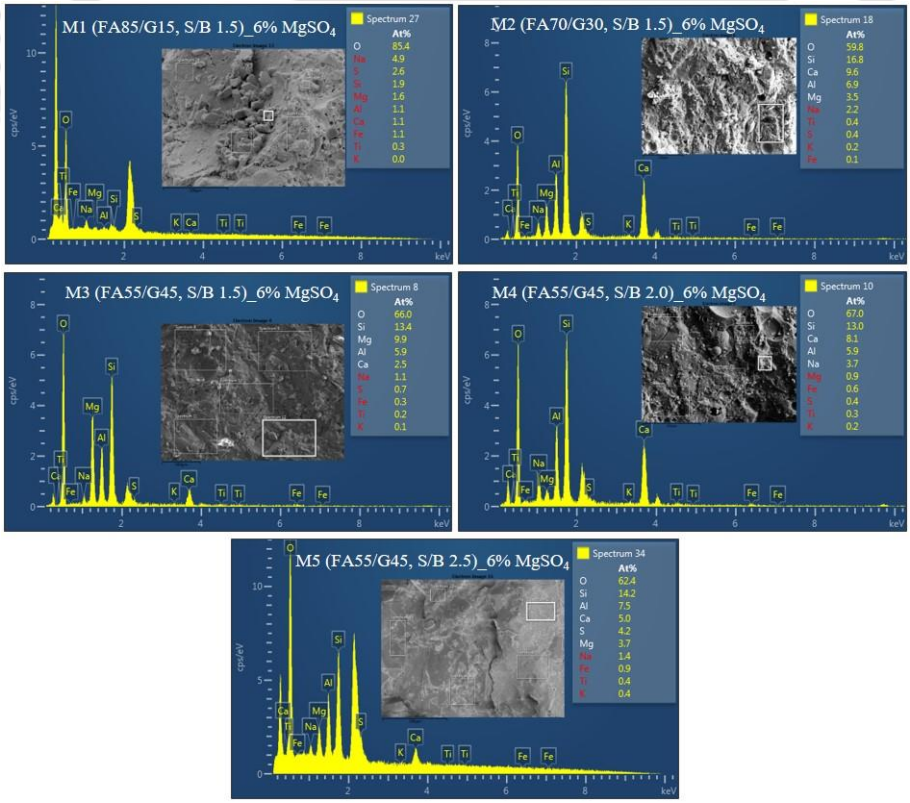

Fig. 5.29 EDS spectra of geopolymer mortar (GPM) mixes exposed to 6% $MgSO_4$ solution for 26 weeks.

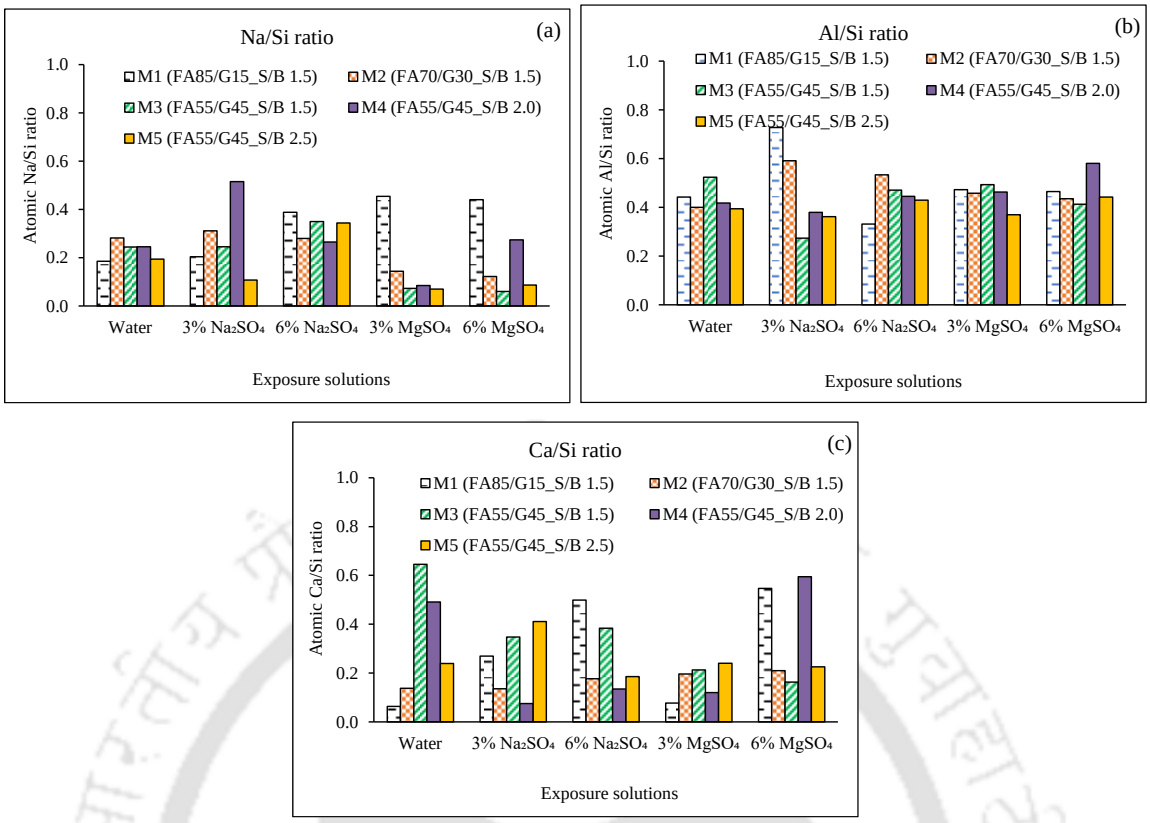

Fig. 5.30 Atomic ratios obtained from EDS analysis of geopolymer mortar (GPM) mixes exposed to water and different sulfate solutions: (a) Na/Si ratio, (b) Al/Si ratio, and (c) Ca/Si ratio.

Table 5.2 Average atomic percent of Ca and S in geopolymer mortar (GPM) mixes exposed to different sulfate solutions for 26 weeks

Mix	Na_2SO_4 solutions	Calcium (Ca)	Sulfur (S)	$MgSO_4$ solutions	Calcium (Ca)	Sulfur (S)
M1 (FA85/G15, S/B 1.5)	3% Na_2SO_4	2.08	0.12	3% $MgSO_4$	1.22	1.36
	6% Na_2SO_4	6.90	0.60	6% $MgSO_4$	5.46	0.90
M2 (FA70/G30, S/B 1.5)	3% Na_2SO_4	2.18	0.66	3% $MgSO_4$	2.92	0.16
	6% Na_2SO_4	2.94	1.28	6% $MgSO_4$	3.80	0.18
M3 (FA55/G45, S/B 1.5)	3% Na_2SO_4	6.06	0.28	3% $MgSO_4$	2.96	0.36
	6% Na_2SO_4	5.68	0.36	6% $MgSO_4$	2.38	0.52
M4 (FA55/G45, S/B 2.0)	3% Na_2SO_4	1.10	1.70	3% $MgSO_4$	2.04	0.20
	6% Na_2SO_4	2.64	0.96	6% $MgSO_4$	7.20	0.20
M5 (FA55/G45, S/B 2.5)	3% Na_2SO_4	7.02	0.56	3% $MgSO_4$	3.40	0.16
	6% Na_2SO_4	3.32	0.60	6% $MgSO_4$	3.16	2.84

5.7.2.2.2 Geopolymer mortar (GPM) exposed to acid solutions

Typical EDS spectra of GPM mixes exposed to different acid solutions (H_2SO_4, and HCl solutions) for 26 weeks are shown in Fig. 5.31 to Fig. 5.34. The elemental ratios (atomic

Na/Si, Al/Si, and Ca/Si ratios) obtained from EDS analysis of GPM mixes are shown in Fig. 5.35.

The atomic Na/Si ratio and Al/Si ratio mostly decreased in GPM mixes in case of exposure to 0.31 mol/l and 0.62 mol/l H_2SO_4 solutions when compared with the reference mix i.e., exposure to water (Fig. 5.35). Furthermore, the GPM mixes exposed to 0.31 mol/l and 0.62 mol/l H_2SO_4 solutions had mostly higher atomic Ca/Si ratio than the reference mix exposed to water. A higher atomic mass of calcium (Ca) and sulfur (S) were observed in the GPM mixes exposed to 0.31 mol/l and 0.62 mol/l H_2SO_4 solutions (Table 5.3). The decrease in atomic Na/Si ratio, and Al/Si ratio; and increase in atomic mass of calcium (Ca) and sulfur (S) indicates the simultaneous effect of leaching of Na, Al and Ca from N-A-S-H, N-(C)-A-S-H, and C-S-H gels, and formation of gypsum crystals in the GPM mixes exposed to H_2SO_4 solutions. The calcium ions present in GPM mixes diffuse toward H_2SO_4 solution and react with counter-diffusing sulfate anions present in H_2SO_4 solution, which resulted in the formation, and deposition of gypsum crystals in the pores of GPM specimens [57]. Furthermore, the GPM mixes exposed to 0.31 mol/l and 0.62 mol/l HCl solutions had mostly lower atomic Na/Si ratio, and Ca/Si ratio as compared to the reference mix i.e., exposure to water (Fig. 5.35). This may be ascribed to the effect of significant leaching of Na and Ca ions from the binding gels in GPM mixes in the presence of HCl solution. Thus, the GPM mixes exposed to both HCl solutions had lower compressive strength (Fig. 5.13) than that exposed to water. The highly vulnerable nature of calcium enriched binding gels in HCl solution also are reported in the literature [137]. Further, the GPM mixes exposed to 0.31 mol/l and 0.62 mol/l HCl solutions had Cl ions in the range of 0.38 - 2.48 atomic % (Table 5.3), which might have deteriorated the geopolymer gels in the GPM mixes. Comparison of the effect of acid solutions indicated no systematic variations in the atomic Na/Si and Al/Si ratios of the GPM mixes between exposure to H_2SO_4 and HCl solutions. However, the GPM mixes exposed to H_2SO_4 solutions had significantly higher Ca/Si ratio than the GPM mixes exposed to HCl solutions. This indicates that a higher amount of calcium might have reacted with the sulfur present in the H_2SO_4 solution and formed higher amount of gypsum in the GPM mixes exposed to H_2SO_4 solution. This caused volumetric expansion of the GPM specimens and resulted in lower compressive strength as compared to the GPM specimens exposed to HCl solution (Fig. 5.13).

The GPM mix M1 (FA85/G15, S/B 1.5) had mostly higher atomic Na/Si ratio, Al/Si ratio and Ca/Si ratio than the GPM mix M2 (FA70/G30, S/B 1.5) and M3 (FA55/G45, S/B 1.5)

in case of exposure to different H_2SO_4 and HCl solutions (Fig. 5.35). This indicates the stability of geopolymer gels (N-A-S-H and N-(C)-A-S-H) formed in the GPM mix (M1) made with lower GGBS content, which were comparatively less susceptible to both acid solutions. This observation can be corroborated with the results obtained from the visual appearance of the specimens (Fig. 5.8), compressive strength (Fig. 5.13), and XRD analysis (Fig. 5.23 and Fig. 5.24) of GPM mix M1. The atomic Na/Si ratio, and Al/Si ratio mostly increased with increase in S/B ratio of the GPM mixes after exposure to H_2SO_4 and HCl solutions (Fig. 5.35). It may be noted that the GPM mixes made with higher S/B ratio exhibited lower compressive strength in case of exposure to acid solutions (Fig. 5.13). This may be due to the dominant effect of acid solutions on the GPM mixes, which deteriorated the GPM specimens significantly as a result of lower formation of aluminosilicate gels at lower binder content in the mixes made with higher S/B ratio. However, the loss in compressive strength after immersion in acid solutions was lower at higher S/B ratio than that at lower S/B ratio (Fig. 5.14), which is line with the variations in the atomic ratios of GPM mixes with increase in S/B ratio. The GPM mixes exposed to H_2SO_4 and HCl solutions had significantly lower atomic Na/Si ratio, and mostly lower atomic Al/Si and Ca/Si ratios as compared to that obtained at 28 and 180 days of ambient curing. The lower atomic ratios in GPM mixes immersed in acid solutions indicate the depolymerization of aluminosilicate gels in the presence of acid solutions that resulted in significant decrease in compressive strength when compared with that obtained at 28 and 180 days of ambient curing (Table 5.1, where DF_{28} and DF_{180} values were greater than 1, indicating strength loss in case of exposure to acid solutions).

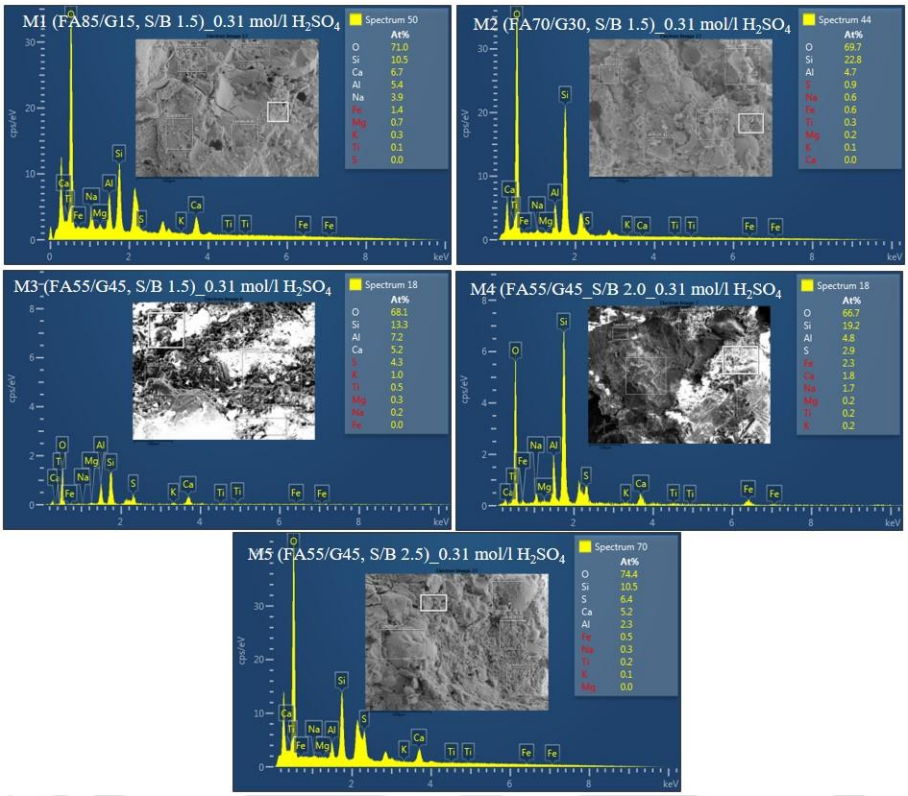

Fig. 5.31 EDS spectra of geopolymer mortar (GPM) mixes exposed to 0.31 mol/l H_2SO_4 solution for 26 weeks.

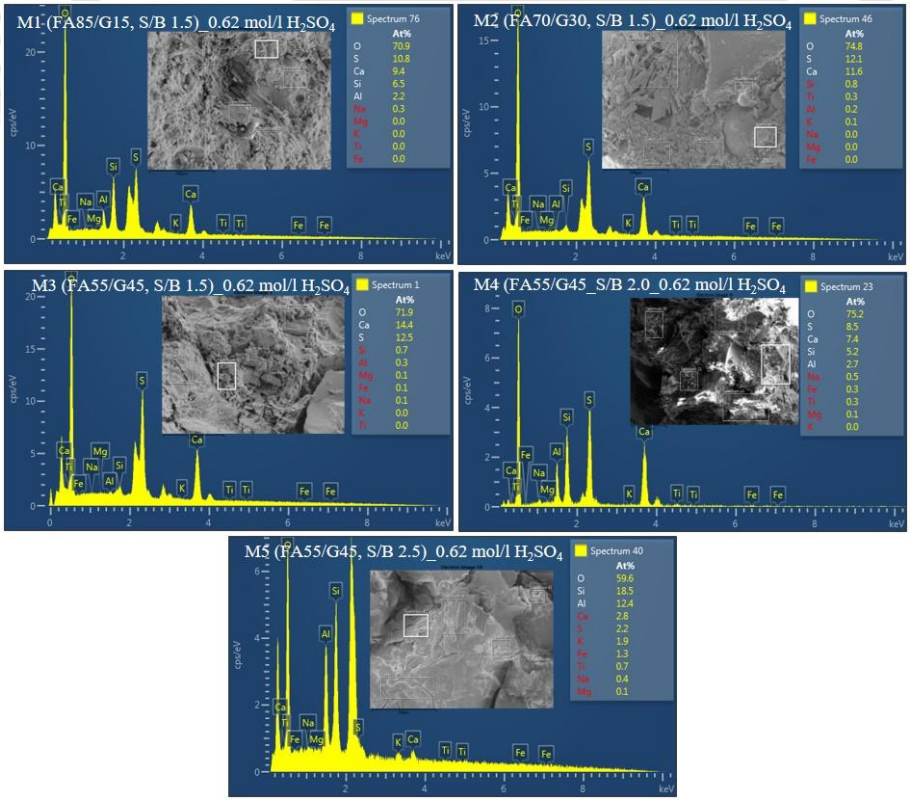

Fig. 5.32 EDS spectra of geopolymer mortar (GPM) mixes exposed to 0.62 mol/l H_2SO_4 solution for 26 weeks.

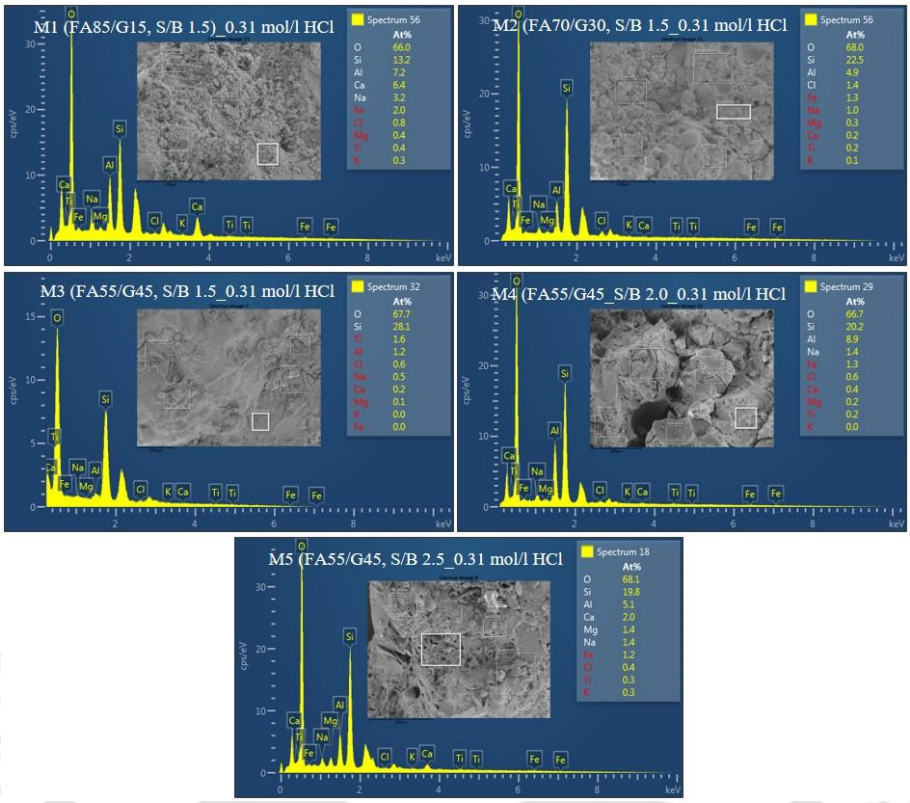

Fig. 5.33 EDS spectra of geopolymer mortar (GPM) mixes exposed to 0.31 mol/l HCl solution for 26 weeks.

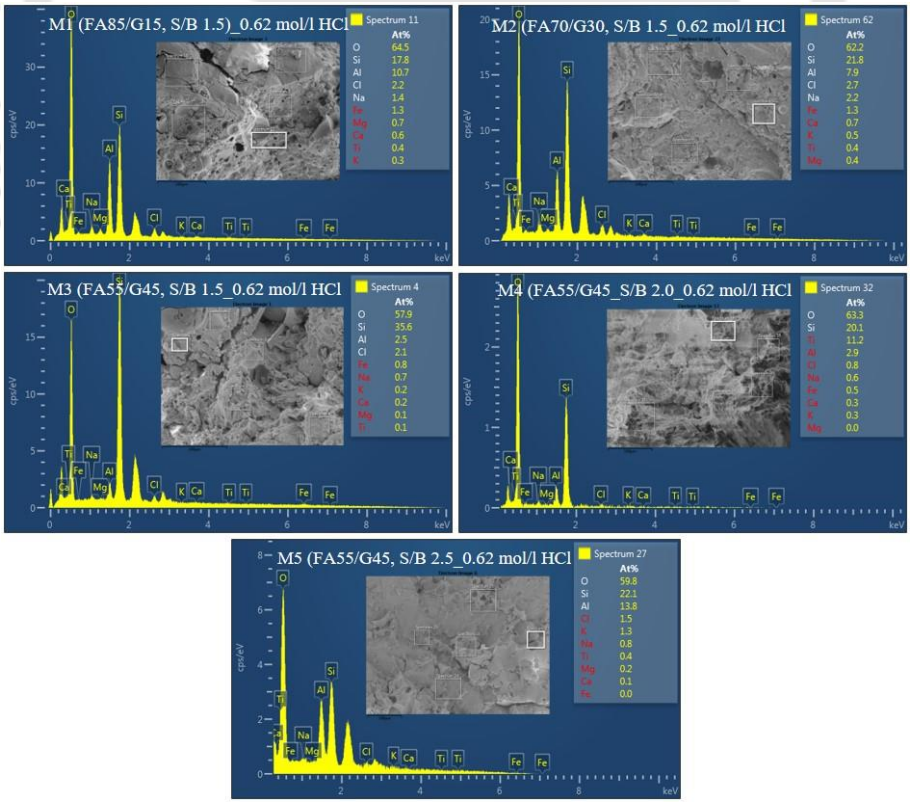

Fig. 5.34 EDS spectra of geopolymer mortar (GPM) mixes exposed to 0.62 mol/l HCl solution for 26 weeks.

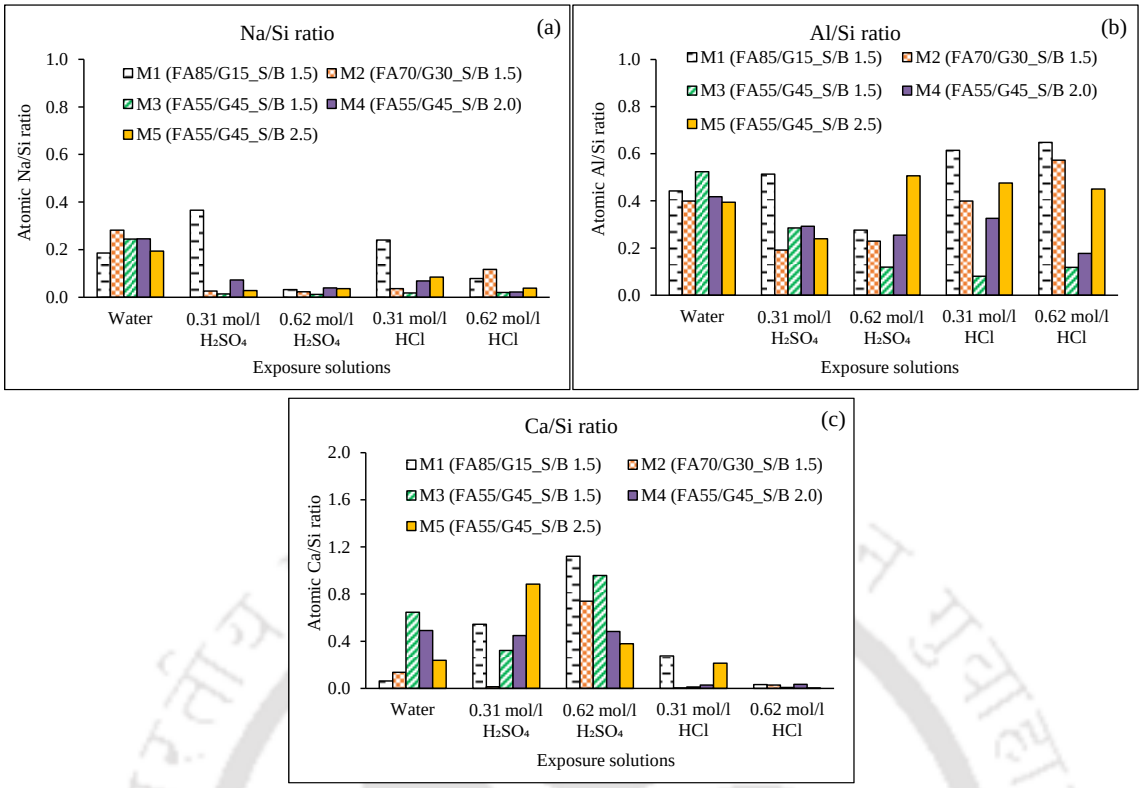

Fig. 5.35 Atomic ratios obtained from EDS analysis of geopolymer mortar (GPM) mixes exposed to water and different acid solutions: (a) Na/Si ratio, (b) Al/Si ratio, and (c) Ca/Si ratio.

Table 5.3 Average atomic percent of Ca, S, and Cl in geopolymer mortar (GPM) mixes exposed to different acid solutions for 26 weeks

Mix	H_2SO_4 solutions	Calcium (Ca)	Sulfur (S)	HCl solutions	Calcium (Ca)	Chloride (Cl)
M1 (FA85/G15, S/B 1.5)	0.31 mol/l H_2SO_4	6.42	0	0.31 mol/l HCl	4.24	0.92
	0.62 mol/l H_2SO_4	7.62	8.76	0.62 mol/l HCl	0.58	2.48
M2 (FA70/G30, S/B 1.5)	0.31 mol/l H_2SO_4	0.34	1.24	0.31 mol/l HCl	0.06	1.10
	0.62 mol/l H_2SO_4	7.82	8.56	0.62 mol/l HCl	0.52	2.0
M3 (FA55/G45, S/B 1.5)	0.31 mol/l H_2SO_4	5.0	4.84	0.31 mol/l HCl	0.34	0.38
	0.62 mol/l H_2SO_4	9.64	8.08	0.62 mol/l HCl	0.28	1.52
M4 (FA55/G45, S/B 2.0)	0.31 mol/l H_2SO_4	6.06	5.88	0.31 mol/l HCl	0.68	1.14
	0.62 mol/l H_2SO_4	5.24	6.3	0.62 mol/l HCl	0.58	0.60
M5 (FA55/G45, S/B 2.5)	0.31 mol/l H_2SO_4	6.94	8.20	0.31 mol/l HCl	3.50	0.46
	0.62 mol/l H_2SO_4	5.26	5.84	0.62 mol/l HCl	0.02	1.28

5.7.2.3 FESEM analysis

Typical FESEM images of GPM mixes (M1, M3 and M5) exposed to water, different sulfate solutions (6% Na_2SO_4 and 6% $MgSO_4$ solutions), and acid solutions (0.62 mol/l H_2SO_4 and 0.62 mol/l HCl solutions) for 26 weeks are shown in Fig. 5.36 to Fig. 5.40. In addition, the FESEM images of GPM mixes (M1, M3 and M5) exposed to 3% Na_2SO_4, 3%

$MgSO_4$, 0.31 mol/l H_2SO_4 and 0.31 mol/l HCl solutions for 26 weeks are presented in Fig. A6 to Fig. A9 (Appendix section). Similarly, the FESEM images of GPM mixes i.e., M2 and M4 exposed to water, and different sulfate and acid solutions for 26 weeks are presented in Fig. A10 to Fig. A14. The GPM mixes exposed to water and different sulfate solutions had comparatively denser microstructure than the mixes exposed to acid solutions (Fig. 5.36 to Fig. 5.40). This may be attributed to the effect of continuation of geopolymerization reaction when immersed in water and sulfate solutions that resulted in formation of more geopolymer gels (N-A-S-H and N-(C)-A-S-H gel) in the mixes, which led to higher compressive strength when compared with the mixes exposed to acid solutions. The FESEM image of GPM mix M1 (FA85/G15, S/B 1.5) exposed to water shows partially reacted fly ash particle, which may be due to the presence of higher amount of fly ash in the mix whereas the FESEM image of GPM mix M3 (FA55/G45, S/B 1.5) exhibited more compact microstructure as a result of more calcium-rich gel formation at higher amount of GGBS in the mix immersed in water (Fig. 5.36). This is supported by the higher intensity of peaks related to aluminosilicate gels and C-S-H gel as observed from the XRD analysis (Fig. 5.20) and higher atomic Ca/Si ratio (0.65) as observed from EDS analysis (Fig. 5.30 (c)) of the GPM mix M3 in case of immersion in water. The morphology of GPM mix M5 (FA55/G45, S/B 2.5) shows relatively less homogenous microstructure as compared to the GPM mix M3 (Fig. 5.36), which may be due to lower extent of geopolymerization reaction in the presence of lower amount of binder in the mix M5 that led to reduction in strength as observed from Fig. 5.11. This can be corroborated with the results obtained from XRD analysis (Fig. 5.20) and EDS analysis (Fig. 5.30), where the intensity of peaks related to albite and C-S-H gel, and the atomic Al/Si and Ca/Si ratios in the GPM were lower at higher S/B ratio.

The FESEM images of GPM mix M1 exposed to Na_2SO_4 and $MgSO_4$ solutions indicated the presence of geopolymer gels and some partially reacted fly ash particles surrounded by the geopolymer gels (Fig. 5.37: 6% Na_2SO_4; Fig. 5.38: 6% $MgSO_4$). In addition, the development of some microcracks (Fig. 5.37: 6% Na_2SO_4) and pores (Fig. A7: 3% $MgSO_4$) were also observed in the GPM mix M1. The development of microcracks in the GPM mix may be due to the internal stresses exerted during the partial reaction of fly ash particles in the mix as a result of continuation of geopolymerization reaction. However, the development of microcracks did not affect the strength of GPM mix M1 after exposure to sulfate solutions as there was gain in compressive strength after exposure to sulfate

solutions, and the reason for the strength gain is already stated in Section 5.6.3.1. Similarly, the FESEM images of GPM mix M2 exposed to 3% Na_2SO_4 (Fig A11), and 3% and 6% $MgSO_4$ solutions (Fig. A12) indicate the presence of some partially reacted fly ash particles surrounded by the geopolymer gels. Although, the GPM mixes exposed to sulfate solutions had comparatively denser microstructure, the formation of gypsum crystals in some of the GPM mixes made with 30% and 45% GGBS contents as evident from the FESEM images (Fig. 5.37: M3_6% Na_2SO_4, Fig. 5.38: M3_6% $MgSO_4$, M5_6% $MgSO_4$, Fig. A11: M2_6% Na_2SO_4, and Fig. A12: M2_3% $MgSO_4$, M2_6% $MgSO_4$, M4_6% $MgSO_4$) might have caused expansion in the GPM mixes, which led to lower compressive strength than the mixes exposed to water.

The FESEM images of GPM mixes exposed to H_2SO_4 solutions (Fig. 5.39, Fig. A8, Fig. A13) showed more amount of gypsum crystals, which was formed due to severe decalcification of GPM mixes in H_2SO_4 solutions that resulted in significant loss of compressive strength as compared to the GPM mixes exposed to water. Further, it is noted that a higher amount of gypsum crystals was formed in the GPM mixes made with 30% and 45% GGBS (M2, M3, M4, and M5) as compared to that made with 15% GGBS (M1) (Fig. 5.39, Fig. A8, Fig. A13). This indicates greater aggressiveness of H_2SO_4 solutions on GPM mixes made with higher GGBS content, thereby resulting in higher decalcification than that made with lower GGBS content. This can be correlated with the results obtained from compressive strength (Fig. 5.13), XRD analysis (Fig. 5.23) and EDS analysis (Fig. 5.35). The presence of a comparatively porous and disintegrated geopolymer matrix in GPM mixes immersed in HCl solutions as observed from the FESEM images (Fig. 5.40, Fig. A9, Fig. A14) may be due to the effect of depolymerization of geopolymer gels in HCl solution. In case of exposure of GPM mixes to HCl solution, the significant leaching of sodium, calcium, and aluminum from the paste region of the mixes into the HCl solution [134] resulted in pores and microcracks to a greater extent in the GPM mixes and eventually resulted in significant reduction of compressive strength (Fig. 5.13).

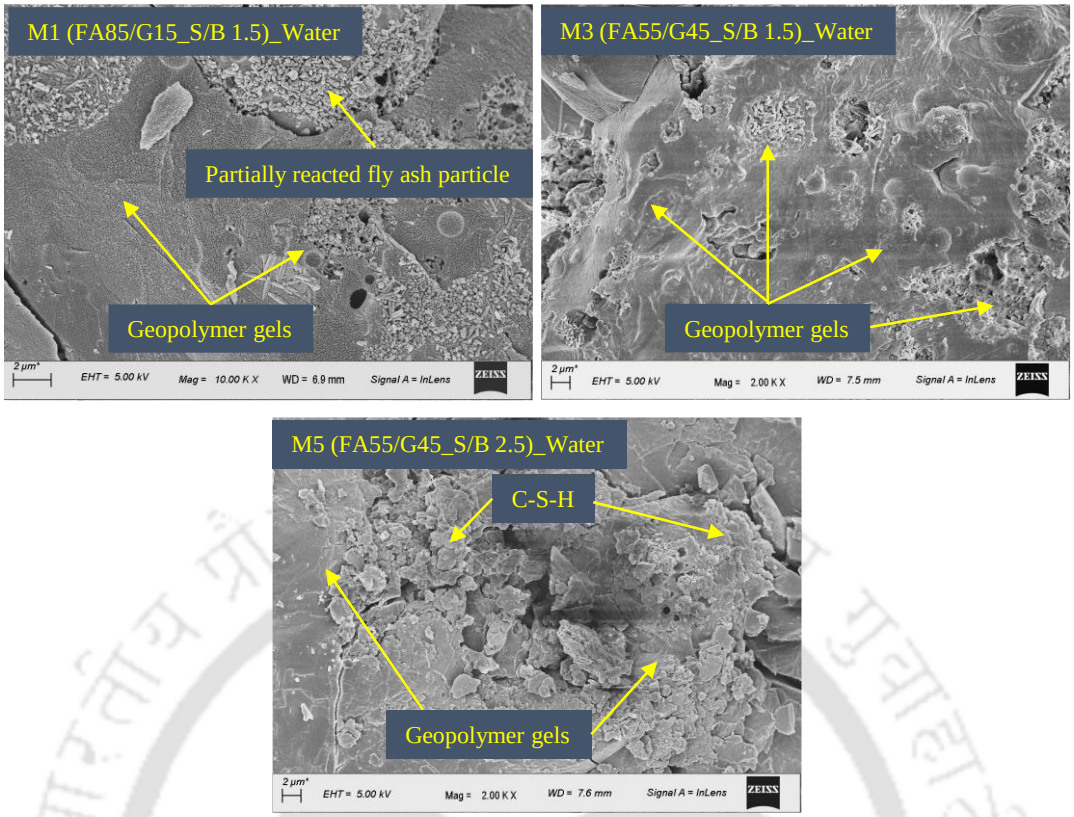

Fig. 5.36 FESEM images of geopolymer mortar (GPM) mixes exposed to water for 26 weeks.

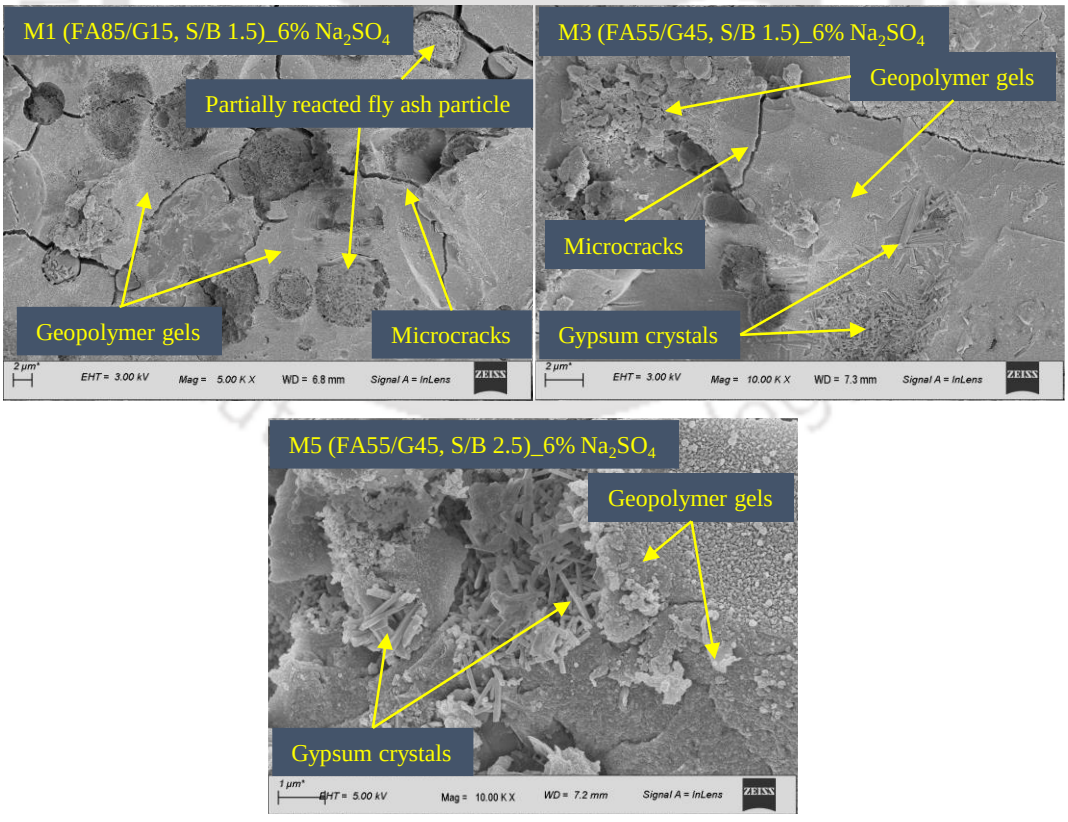

Fig. 5.37 FESEM images of geopolymer mortar (GPM) mixes exposed to 6% Na_2SO_4 solution for 26 weeks.

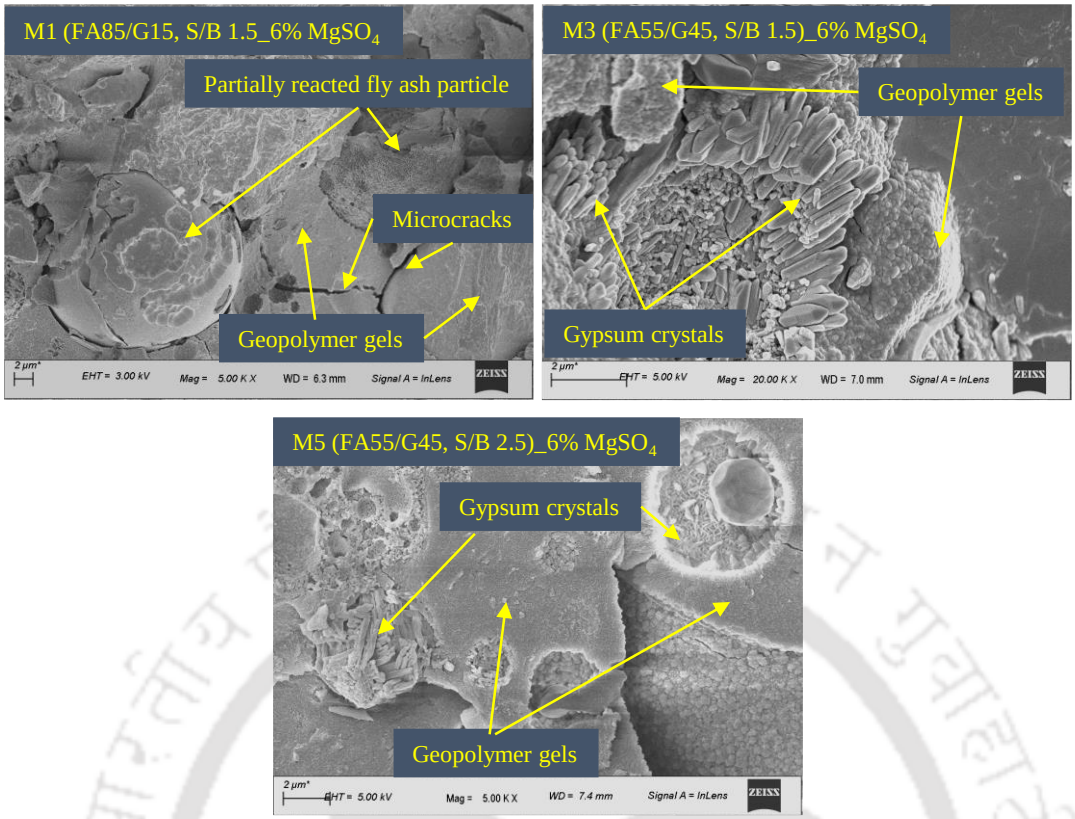

Fig. 5.38 FESEM images of geopolymer mortar (GPM) mixes exposed to 6% $MgSO_4$ solution for 26 weeks.

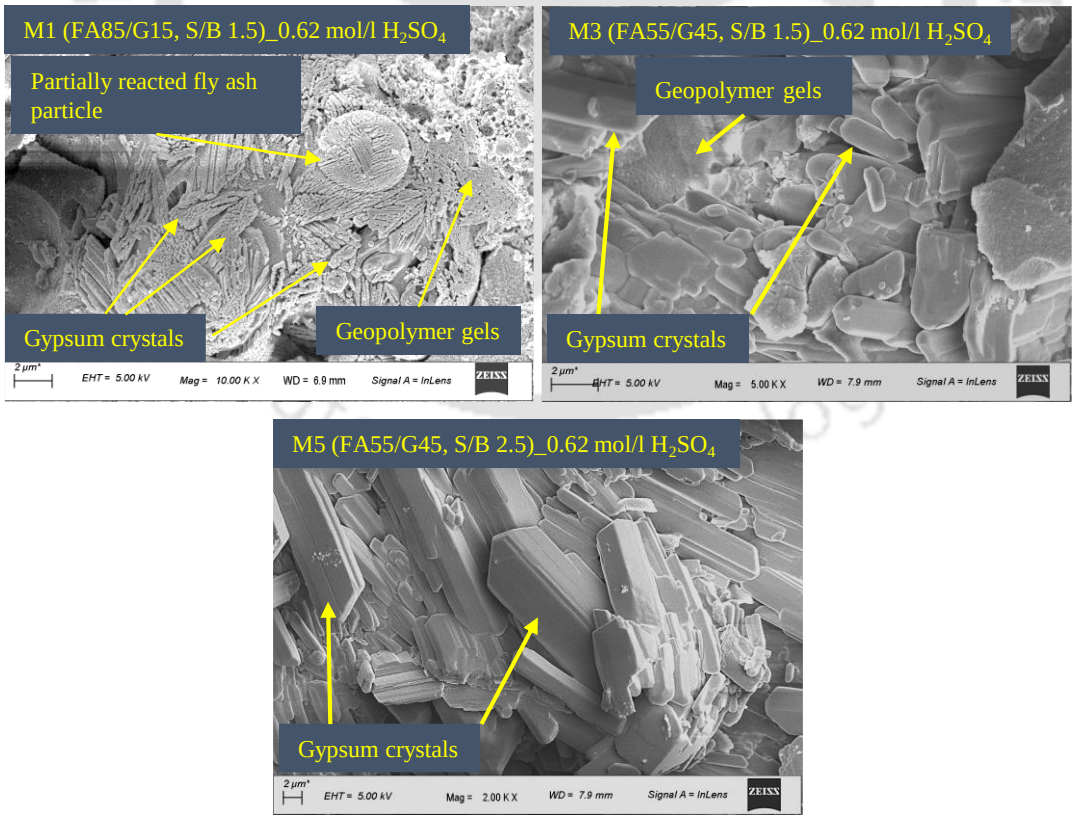

Fig. 5.39 FESEM images of geopolymer mortar (GPM) mixes after 26 weeks of immersion in 0.62 mol/l H_2SO_4 solution.

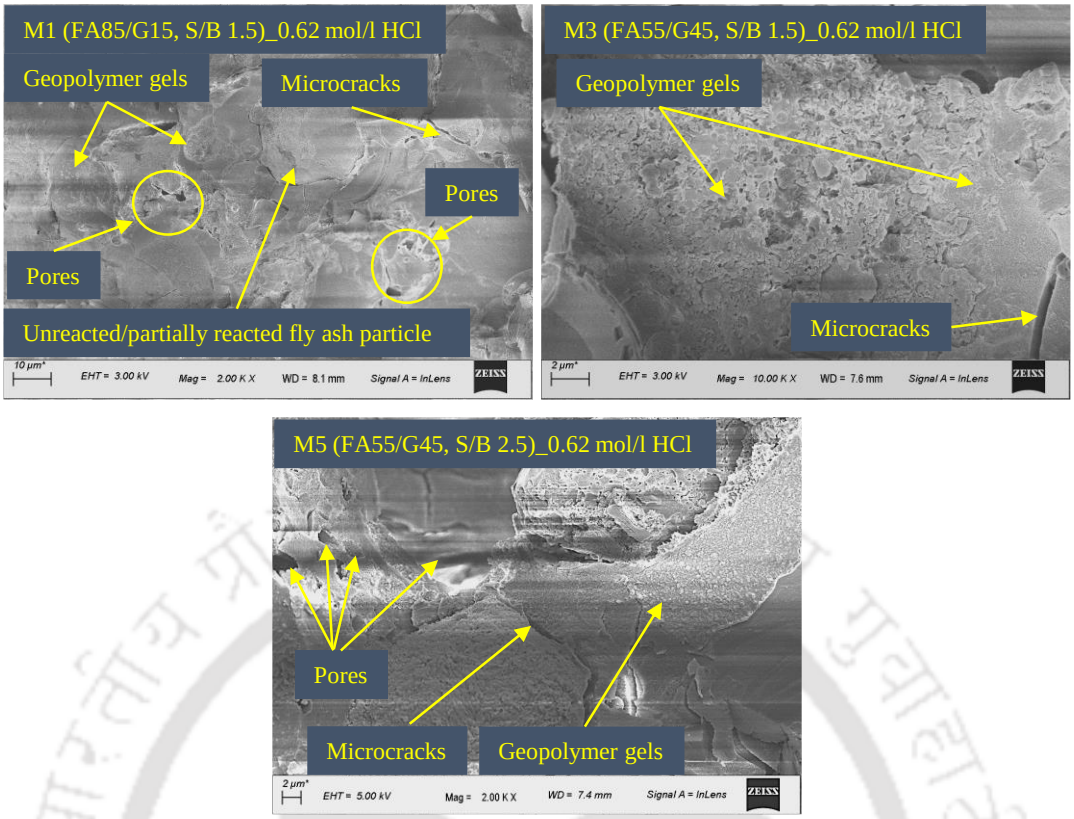

Fig. 5.40 FESEM images of geopolymer mortar (GPM) mixes after 26 weeks of immersion in 0.62 mol/l HCl solution.

5.7.2.4 FTIR analysis

The FTIR spectra of geopolymer mortar (GPM) mixes exposed to water, different sulfate (6% Na_2SO_4 and 6% $MgSO_4$) and acid (0.62 mol/l H_2SO_4 and 0.62 mol/l HCl) solutions for 26 weeks are shown in Fig. 5.41 to Fig. 5.43. There was no significant change in the asymmetric stretching vibration of Si-O-Si(Al) bond identified in the FTIR spectra of GPM mixes exposed to water (1031 cm^{-1} to 1035 cm^{-1}) when compared with that exposed to 6% Na_2SO_4 solution (1029 cm^{-1} to 1036 cm^{-1}), and 6% $MgSO_4$ solution (1026 cm^{-1} to 1034 cm^{-1}) (Fig. 5.41 and Fig. 5.42). However, the asymmetric stretching vibration of Si-O-Si(Al) bond was shifted toward higher wavenumbers after exposure to 0.62 mol/l H_2SO_4 solution (1120 cm^{-1} to 1125 cm^{-1}) and 0.62 mol/l HCl solution (1039 cm^{-1} to 1090 cm^{-1}) when compared with exposure to water (1031 cm^{-1} to 1035 cm^{-1}) (Fig. 5.41 and Fig. 5.43). This indicates the increase in atomic Si/Al ratio due to weaker Al-O bonds in the aluminosilicate network, which is replaced by Si-O bonds in acid exposure condition [60,137,139]. Therefore, the geopolymer mortar (GPM) mixes exhibited significantly lower compressive strength after exposure to 0.62 mol/l H_2SO_4 solution and 0.62 mol/l HCl solution than the mixes exposed to water (Fig. 5.13). This observation can be corroborated with the atomic Al/Si ratio obtained in the EDS analysis (Fig. 5.35), where the GPM mixes exposed to 0.62

mol/l H_2SO_4 solution mostly showed lower atomic Al/Si ratio than that exposed to water. The bending vibration of H-O-H group (1629 cm^{-1} to 1644 cm^{-1}), and stretching vibration of –OH group (3415 cm^{-1} to 3436 cm^{-1}) identified in the FTIR spectra were not altered significantly among the GPM mixes exposed to water, 6% Na_2SO_4 solution, and 6% $MgSO_4$ solution. The bending vibration of H-O-H group in the FTIR spectra varied from 1622 cm^{-1} to 1642 cm^{-1} irrespective of exposure to acid solution. The stretching vibration of –OH group varied from 3406 cm^{-1} to 3434 cm^{-1} in case of exposure to 0.62 mol/l H_2SO_4 solution whereas it varied from 3420 cm^{-1} to 3632 cm^{-1} in case of exposure to 0.62 mol/l HCl solution. This may be ascribed to the alterations in the extent of water adsorbed in the rings of geopolymer gels between different acid solutions. From Fig. 5.43, the peaks identified at 602 cm^{-1} and 669 cm^{-1} in the FTIR spectra indicate the formation of gypsum [60] in all the GPM mixes exposed to 0.62 mol/l H_2SO_4 solution. This is confirmed with the results obtained from XRD, EDS, and FESEM analyses of the GPM mixes exposed to H_2SO_4 solution. Further, it is noted that the band corresponding to the stretching vibration of carbonate groups (CO_3^{2-}) in the GPM mixes exposed to water (1430 cm^{-1} to 1484 cm^{-1}) disappeared when exposed to 0.62 mol/l H_2SO_4 solution and 0.62 mol/l HCl solution, which indicates dissolution of carbonate compounds during acid exposure [137]. While evaluating the effect of GGBS content and S/B ratio on the FTIR spectra of GPM mixes exposed to water, different sulfate (6% Na_2SO_4 and 6% $MgSO_4$) and acid (0.62 mol/l H_2SO_4 and 0.62 mol/l HCl) solutions, no systematic variation was observed in the Si-O-Si(Al) bond with increase in GGBS content and S/B ratio in the geopolymer mortar mixes.

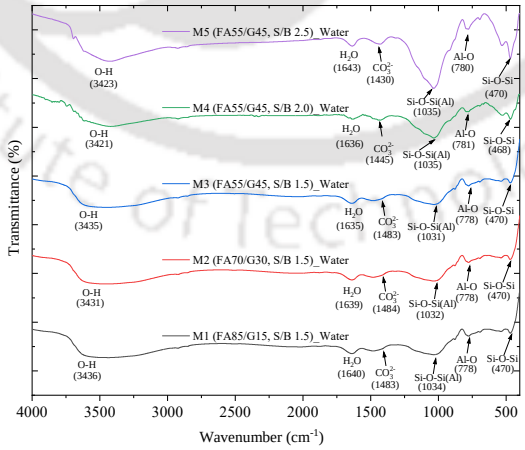

Fig. 5.41 FTIR spectra of geopolymer mortar (GPM) mixes exposed to water for 26 weeks.

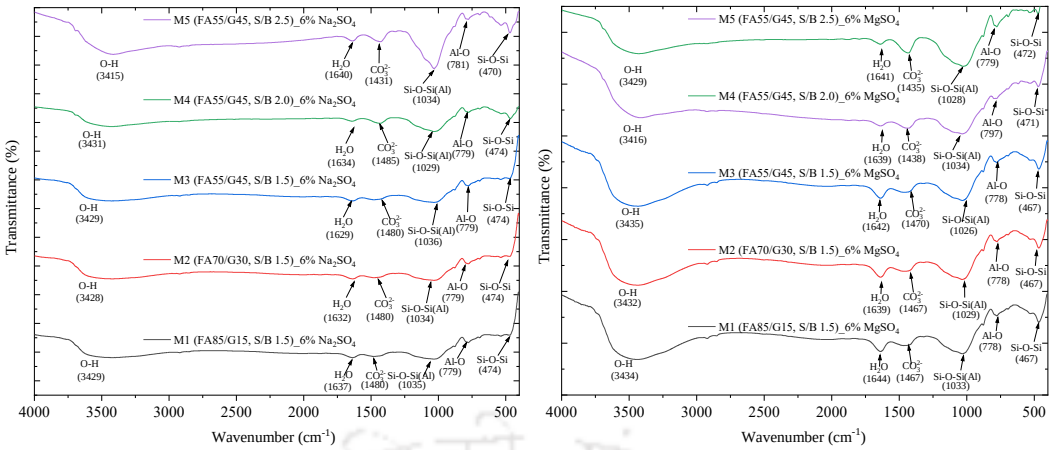

Fig. 5.42 FTIR spectra of geopolymer mortar (GPM) mixes exposed to 6% Na_2SO_4 and 6% $MgSO_4$ solutions for 26 weeks.

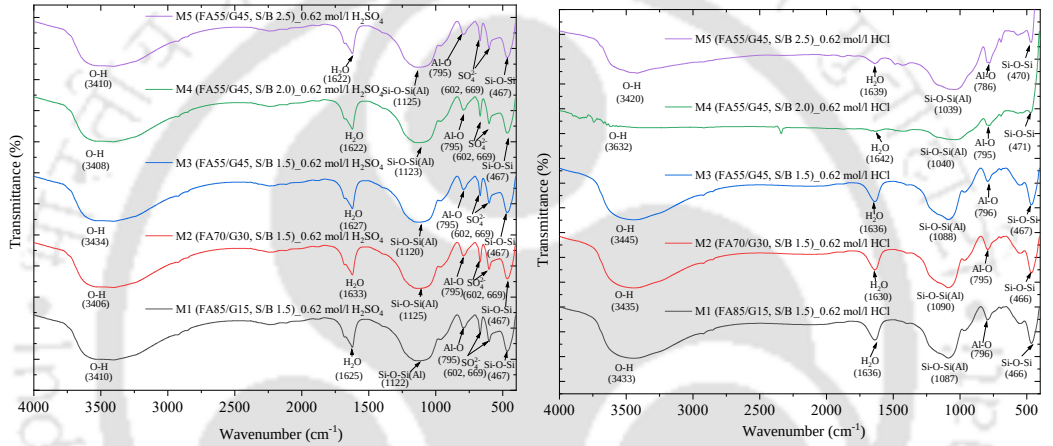

Fig. 5.43 FTIR spectra of geopolymer mortar (GPM) mixes exposed to 0.62 mol/l H_2SO_4 and 0.62 mol/l HCl solutions for 26 weeks.

5.8 Summary

In this chapter, the effect of fly ash/GGBS blends and sand-to-binder (S/B) ratio on behaviour of fly ash-GGBS based geopolymer mortar (GPM) in terms of flowability, strength development in ambient condition, water absorption properties, resistance against sulfate and acidic environment, and microstructural changes were investigated. The durability performance of geopolymer mortar against exposure to different concentrations of sulfate (Na_2SO_4, $MgSO_4$) and acid (H_2SO_4, and HCl) solutions for a period of 26 weeks was investigated through visual observation, change in weight, and change in compressive strength. The deterioration factor of GPM specimens exposed to acidic environment were determined for different fly ash/GGBS blends and sand-to-binder (S/B) ratios. From the obtained results, it is observed that the GPM mix made with 45% GGBS content exhibited: lower flow index; higher compressive strength at different ages of ambient curing; and lower water absorption, apparent volume of permeable voids, and sorptivity coefficient as

compared to the GPM mixes made with 15% and 30% GGBS contents at constant S/B ratio of 1.5. Similarly, the GPM mixes made with higher S/B ratio (2.5) showed higher flow index, lower compressive strength at different ages of ambient curing, and higher water absorption properties when compared with the GPM mixes made with S/B ratio of 1.5 and 2.0 at constant GGBS content of 45%. The weight gain percentage of the GPM mixes at the end of exposure period mostly decreased with increase in GGBS content, however there was no systematic variation in weight gain percentage with increase in S/B ratio in the GPM mixes exposed to sulfate solutions. In case of exposure to acid solutions, the weight loss percentage of the mixes increased with an increase in GGBS content and S/B ratio. The GPM mix made with lower GGBS content, i.e., 15% had maximum gain and minimum loss in compressive strength when exposed to sulfate and acid solutions respectively, which is in line with the variations in the peak intensity of aluminosilicate gels observed from XRD analysis, and atomic ratios obtained from the EDS analysis. The GPM mixes made with higher S/B ratio performed better in offsetting the loss in compressive strength in sulfate and acidic environment. The GPM specimens showed higher deterioration factor in case exposure to acidic environment when compared with the compressive strength obtained at 28 days and 180 days of ambient curing. The results of XRD, EDS, and FESEM analyses indicated more formation of gypsum in the geopolymer mortar mixes made with higher GGBS content when exposed to sulfate and H_2SO_4 solutions. The atomic Na/Si ratio, Al/Si ratio, and Ca/Si ratio obtained from EDS analysis indicated comparatively improved stability of geopolymer gels in the mortar made with lower GGBS content when exposed to acid solutions.

Multi-response Optimization for Composition of Fly Ash-Ground Granulated Blast Furnace Slag Based Geopolymer Concrete

6.1 General

In this chapter, the Taguchi-Grey relational analysis was used to investigate and optimize the effect of ground granulated blast furnace slag (GGBS) replacement, water-to-geopolymer solids (W/GPS) ratio, molarity of NaOH solution, binder content and Na_2SiO_3 to NaOH solution ratio on setting time, workability and compressive strength of fly ash-GGBS based geopolymer concrete (GPC). After arriving at the optimal combination of mix parameters, verification experiments were conducted on the proposed optimized GPC mix with respect to setting time, workability and compressive strength. The microstructural studies on selected fly ash-GGBS based GPC mixes at each GGBS replacement level and the proposed optimized GPC mix were conducted through X-ray diffraction (XRD), Fourier transform infrared (FTIR) spectroscopy, and Field emission scanning electron microscope (FESEM) analyses. Further, Energy dispersive X-ray spectroscopy (EDS) analysis was also conducted on the proposed optimized geopolymer concrete mix.

6.2 Fresh properties

6.2.1 Setting time

The obtained results of initial setting time and final setting time of the geopolymer mixes (M1 - M16 as per Taguchi method) are shown in Fig. 6.1. From Fig. 6.1, it can be noticed that setting time of geopolymer pastes decreased due to increase in GGBS replacement in the mix. Among all the GPC mixes, the mix M4 prepared with 85% of fly ash and 15% of GGBS, W/GPS ratio of 0.31, 14 M NaOH solution, 450 kg/m^3 of binder and SS/SH ratio of 2.25 showed longer initial setting time (590 min) and final setting time (960 min). The reason for longer setting time can be elucidated from the view point that higher content of fly ash delayed the reaction process of geopolymer paste [81]. In addition, higher W/GPS ratio (i.e. 0.31), and higher binder content (450 kg/m^3) also delayed the setting time of geopolymer paste [91,141]. The mixes M11 and M16 showed lower initial setting time (50 min), which may be ascribed to the effect of relatively higher GGBS replacement level (45% in M11 and 60% in M16) [141]. The lowest final setting time of 90 min was observed in case of mix M14, which is due to the dominant effect of highest GGBS content (60%)

followed by relatively lower W/GPS ratio (0.29) and lowest binder content (375 kg/m^3) in the mix.

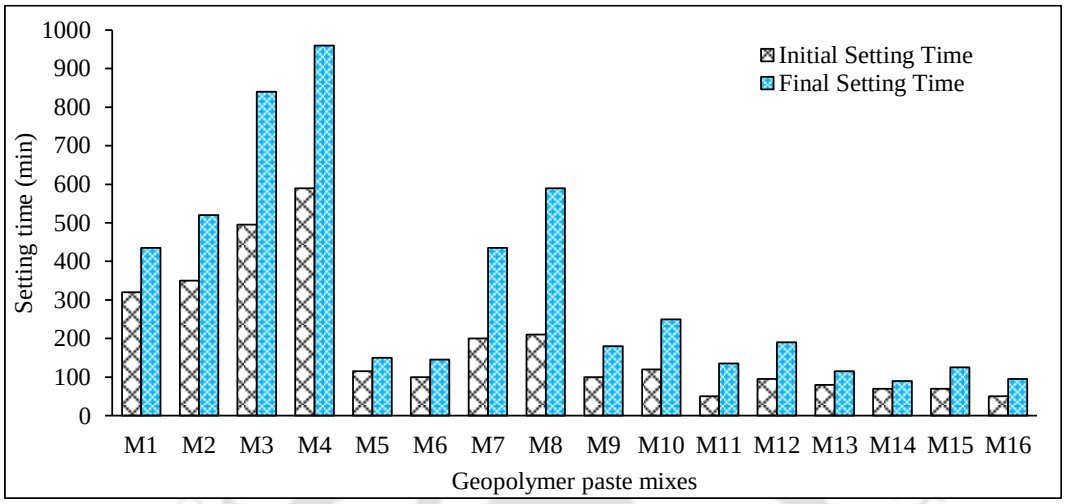

Fig. 6.1 Initial and final setting time of geopolymer paste.

The S/N ratio of initial and final setting time calculated using "larger-the-better" function (Equation 3.2, Chapter 3) are presented in Table 6.1. The performance statistics (mean S/N ratio) of initial and final setting time of geopolymer pastes for different parameters i.e. GGBS replacement level (%), W/GPS ratio, molarity of NaOH solution (M), binder content and Na_2SiO_3 to NaOH solution (SS/SH) ratio are illustrated in Fig. 6.2. The performance statistics (mean S/N ratio) for a given response (i.e. setting time) with respect to a given level of a parameter is found out by calculating the average of the S/N ratio of that response for the mixes made with that level of the parameter. The higher performance statistics signifies the best level of each parameter. The combination of those optimal levels of the parameters was considered as the best possible combination to achieve the desired property i.e. longer setting time.

The performance statistics (mean S/N ratio) for setting time (both initial and final) decreased when the GGBS content of the mixes increased from 15% to 60% as observed from Fig. 6.2. The reason for reduced setting time at higher GGBS content can be ascribed to the presence of more amount of calcium, which enhanced the reactivity of geopolymer paste by forming calcium aluminosilicate hydrate gel [107]. However, the performance statistics (mean S/N ratio) increased with increase in W/GPS ratio, and molarity of NaOH solution indicating longer setting time of the geopolymer paste. The obtained results are in line with the research work reported by other researchers [91,141,142]. The increase in setting time with increase in W/GPS ratio may be attributed to the dominant effect of

increase in water content at higher W/GPS ratio that diluted the alkaline solution present in the geopolymer mix, which slowed down the reaction process [91]. The increase in setting time with increase in NaOH solution molarity may be ascribed to the increase in alkaline solution content in the geopolymer paste. Further, the performance statistics (mean S/N ratio) of setting time decreased due to increase in SS/SH ratio as observed from Fig. 6.2. This may be due to the dominant effect of Na_2SiO_3 solution, which increased with increase in SS/SH ratio and that resulted an increase in soluble silica content leading to faster polymerization process of geopolymer paste [38]. Further, From Fig. 6.2, it was inferred that change in binder content of the mixes had no systematic variation on mean S/N ratio of setting time.

The results of ANOVA of S/N ratio for setting time of geopolymer paste are presented in Table 6.2. From this table, it is evident that GGBS replacement level (%) is the most significant parameter influencing the setting time (both initial and final) of geopolymer paste as it has higher percentage contribution i.e., 86.71% for initial setting time and 75.76% for final setting time as compared to other parameters. The molarity of NaOH solution was the second most influential parameter for both initial (contribution = 11.15%) and final (contribution = 12.74%) setting time. The W/GPS ratio had less effect (7.77%) in case of final setting time whereas it had negligible effect on initial setting time. Further, the binder content and SS/SH ratio had negligible effects on setting time as the percentage contributions of these parameters were less as observed from Table 6.2. This may be ascribed to the fact that the effect of these parameters on setting time might have been dominated by the effect of GGBS replacement level in the mix.

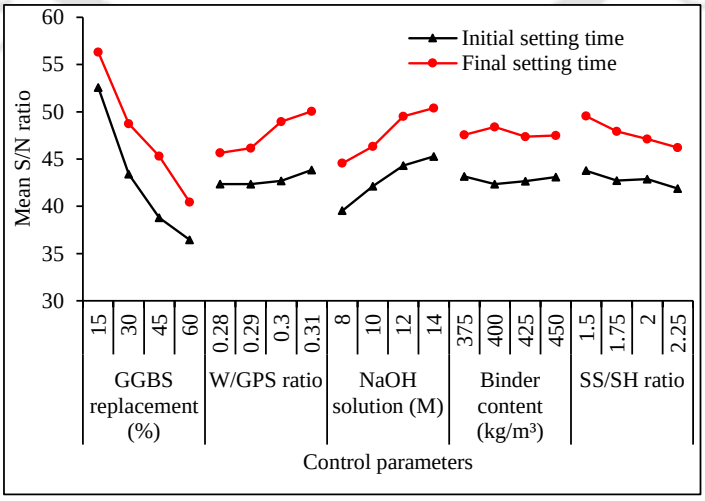

Fig. 6.2 Mean S/N ratio of setting time for different parameters.

Table 6.1 Signal-to-noise (S/N) ratio of properties of geopolymer concrete mixes based on Taguchi method of design of experiment

Mix	GGBS replacement level (%)	W/GPS ratio	Molarity of NaOH solution	Binder content (kg/m^3)	SS/SH ratio	Signal-to-noise (S/N) ratio (Y_{ij})				
						Setting time		Slump	Compressive strength	
						Initial	Final		7 days	28 days
M1	15	0.28	8 M	375	1.5	50.10	52.77	29.54	27.92	32.23
M2	15	0.29	10 M	400	1.75	50.88	54.32	32.04	27.28	33.46
M3	15	0.3	12 M	425	2	53.89	58.49	43.52	28.02	34.15
M4	15	0.31	14 M	450	2.25	55.42	59.65	44.61	29.48	33.99
M5	30	0.28	10 M	425	2.25	41.21	43.52	32.04	32.17	35.03
M6	30	0.29	8 M	450	2	40.00	43.23	36.90	30.95	34.66
M7	30	0.3	14 M	375	1.75	46.02	52.77	42.28	32.75	35.94
M8	30	0.31	12 M	400	1.5	46.44	55.42	44.61	32.39	35.75
M9	45	0.28	12 M	450	1.75	40.00	45.11	36.90	34.32	37.98
M10	45	0.29	14 M	425	1.5	41.58	47.96	42.28	34.85	37.75
M11	45	0.3	8 M	400	2.25	33.98	42.61	42.28	34.71	36.71
M12	45	0.31	10 M	375	2	39.55	45.58	42.61	33.99	36.98
M13	60	0.28	14 M	400	2	38.06	41.21	29.54	35.56	37.29
M14	60	0.29	12 M	375	2.25	36.90	39.08	27.96	35.75	36.65
M15	60	0.3	10 M	450	1.5	36.90	41.94	40.00	36.61	37.72
M16	60	0.31	8 M	425	1.75	33.98	39.55	38.06	36.52	37.34

Table 6.2 ANOVA results of signal-to-noise (S/N) ratio for setting time of geopolymer paste

Parameter	DOF	SOS	MS	Contribution (%)
Initial setting time				
GGBS replacement level	3	608.77	202.92	86.71
W/GPS ratio	3	6.14	2.05	0.88
NaOH molarity	3	78.30	26.10	11.15
Binder content	3	1.72	0.57	0.25
SS/SH ratio	3	7.12	2.37	1.01
Error	-	-	-	-
Total	15	702.05		100.00
Final setting time				
GGBS replacement level	3	533.87	177.96	75.76
W/GPS ratio	3	54.76	18.25	7.77
NaOH molarity	3	89.75	29.92	12.74
Binder content	3	2.60	0.87	0.37
SS/SH ratio	3	23.66	7.89	3.36
Error	-	-	-	-
Total	15	704.64		100.00

Note: DOF: Degree of freedom, SOS: Sum of square, MS: Mean square

6.2.2 Workability

The obtained slump values of fly ash-GGBS based GPC mixes are illustrated in Fig. 6.3. From Fig. 6.3, it is noticed that both the mixes M4 and M8 exhibited the highest slump value of 170 mm whereas the mix M14 exhibited the lowest slump value of 25 mm. The reason of this variation in slump value is ascribed to the dominant effect of alkaline solution content as the mixes M4 and M8 had higher alkaline solution content when compared with the mix M14 as observed from Table 3.11 (Chapter 3).

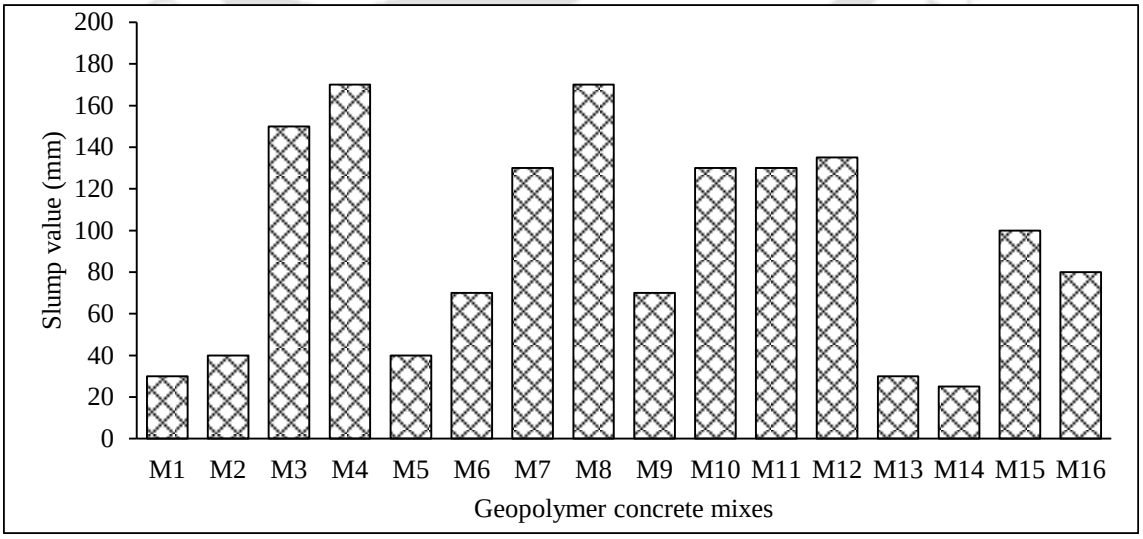

Fig. 6.3 Slump values of geopolymer concrete mixes.

The S/N ratio of slump of GPC mixes are presented in Table 6.1. The performance statistics (mean S/N ratio) of slump value for different parameters are illustrated in Fig. 6.4. The effects of W/GPS ratio and binder content on slump value were consistent with the findings of other researchers [91]. From Fig. 6.4, it is observed that the mean S/N ratio of slump value of GPC mixes significantly increased with a small increase in W/GPS ratio. This is ascribed to more amount of water present in the GPC mixes made with higher W/GPS ratio. Usually, the alkaline solutions used for the preparation of GPC mixes are more viscous, which makes the fresh GPC mix more cohesive and sticky [90]. However, when the water content in the mix is increased due to increase in alkaline solution content, it increases the particle mobility of the source materials, and hence the workability of the GPC mix. From Fig. 6.4 it is observed that the mean S/N ratio for slump increased with increase in binder content. This is ascribed to higher paste content with increase in binder content that improves the lubrication effect in the mix and thus, the workability increases [91].

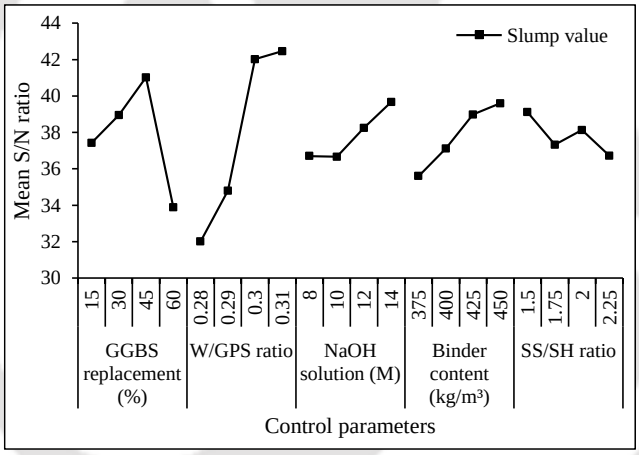

Fig. 6.4 Mean S/N ratio of slump value for different parameters.

As reported in literature, the slump value of GPC mix decreases with increase in GGBS replacement and NaOH solution molarity used in the mix [38,90,107]. However, in the present research work, an increasing trend of mean S/N ratio was observed when GGBS replacement increased from 15% to 45% by mass of total binder, and molarity of NaOH solution increased from 8 M to 14 M. This may be ascribed to the dominating effect of W/GPS ratio on slump of GPC mixes as compared to these parameters. However, at 60% GGBS content, the performance statistics (mean S/N ratio) of slump value drastically reduced, which may be due to the significant effect of higher GGBS content that reduced the particle mobility in the fresh GPC mix. From past research work [38,80,90], no consistent results were observed about the influence of SS/SH ratio on the workability of GPC mix. Aliabdo et al. [80] reported that when SS/SH ratio decreased, the slump value of

mixes increased. Nath and Sarker [38] reported that with increase in amount of Na_2SiO_3 solution in the alkaline solution, the cohesiveness of the GPC mixes increased and resulted in poor workability. However, they had not observed any significant change in slump value with increase in SS/SH ratio. In another study, Deb et al. [90] found a decreasing trend of slump value with decrease in SS/SH ratio of geopolymer concrete mixes. In present research work, there was no systematic variation in performance statistics (mean S/N ratio) of slump with increase in SS/SH ratio as observed from Fig. 6.4.

From ANOVA results (Table 6.3), it was observed that W/GPS ratio had significant effect on slump of GPC mixes when compared with other parameters as it has the highest contributing effect (63.84%) followed by GGBS replacement (21.09%), binder content (7.72%), molarity of NaOH solution (4.84%) and SS/SH ratio (2.51%) on slump value of GPC mixes.

Table 6.3 ANOVA results of signal-to-noise (S/N) ratio for slump value of GPC

Parameter	DOF	SOS	MS	Contribution (%)
GGBS replacement level	3	108.55	36.18	21.09
W/GPS ratio	3	328.55	109.52	63.84
NaOH molarity	3	24.89	8.30	4.84
Binder content	3	39.73	13.24	7.72
SS/SH ratio	3	12.90	4.30	2.51
Error	-	-	-	-
Total	15	514.62		100.00

Note: DOF: Degree of freedom, SOS: Sum of square, MS: Mean square

6.3 Hardened properties

6.3.1 Compressive strength

The compressive strength results of GPC mixes (M1 - M16 as per Taguchi method) are illustrated in Fig. 6.5. From this figure, it is seen that among all the GPC mixes, mix M2 (15% GGBS replacement) exhibited lowest compressive strength of 23.11 N/mm^2 at 7 days of ambient curing whereas the mix M15 (60% GGBS replacement) showed highest 7 days compressive strength of 67.7 N/mm^2. Similarly, at 28 days of ambient curing, mix M1 (15% GGBS replacement) showed lowest compressive strength (40.89 N/mm^2) whereas mix M9 (45% GGBS replacement) exhibited highest compressive strength (79.26 N/mm^2). The large difference in compressive strength of GPC mixes at a particular age can be attributed to the significant effect of GGBS replacement level. Further, it was inferred that the compressive strength enhancement from 7 to 28 days of ambient curing was dependent on the amount of fly ash present in the mix. The GPC mixes made with higher fly ash and lower GGBS contents showed comparatively higher strength enhancement from 7 to 28

days as compared to those made with lower fly ash and higher GGBS contents as observed from Fig. 6.5. Therefore, a suitable proportion of fly ash and GGBS is essential for better strength development of GPC mixes.

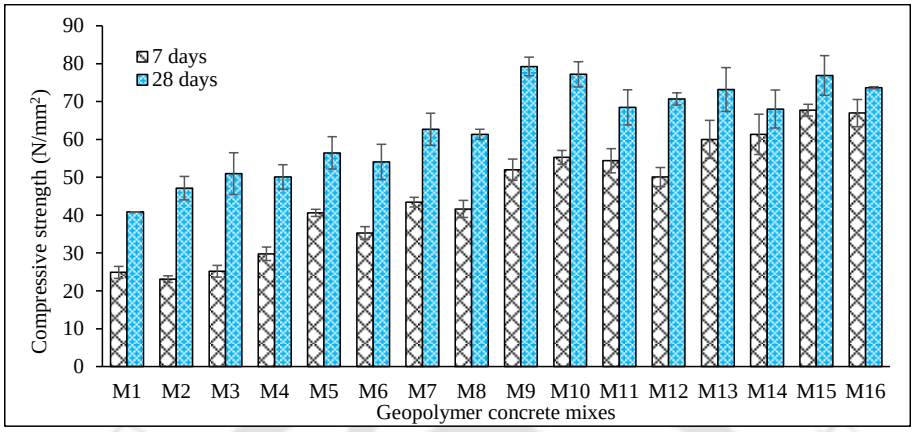

Fig. 6.5 Compressive strength of geopolymer concrete mixes.

The S/N ratio of compressive strength of GPC mixes at 7 and 28 days are presented in Table 6.1. The mean S/N ratio of compressive strength of GPC mixes at 7 and 28 days for various parameters are illustrated in Fig. 6.6. The mean S/N ratio of early age (7 days) compressive strength of GPC mixes increased significantly with increase in GGBS replacement level. Several researchers have reported similar observation about the early age compressive strength of GPC mixes [38,81,86,90,91,132,143]. The high calcium content in GGBS might have improved the compressive strength of GPC mixes [90,141]. The rate of geopolymerization process is increased due to increase in GGBS replacement in the GPC mix [132]. In addition, higher amount of calcium in GGBS resulted in formation of C-S-H gel, which contributed to compressive strength development of GPC mixes [81]. The GGBS replacement level of 45% showed the highest mean of S/N ratio for 28 days compressive strength of GPC mixes. Further, the increase in mean S/N ratio from 7 to 28 days decreased with increase GGBS replacement level as observed from Fig. 6.6. This shows that the presence of higher amount of fly ash in GPC mixes enhanced the strength development at 28 days. This is ascribed to the increase in rate of dissolution process of fly ash at later age.

The variation in mean of S/N ratio for compressive strength with W/GPS ratio was not systematic at both ages as observed from Fig. 6.6. The unsystematic variation in compressive strength with increase in W/GPS ratio may be ascribed to the dominant effect of variations in fly ash and GGBS contents in the GPC mixes. The mean S/N ratio for compressive strength increased with NaOH solution molarity, although the increase is not

significant as in case of GGBS replacement level as evident from Fig. 6.6. At lower NaOH solution molarity, the lower extent of polycondensation process resulted in less compressive strength of GPC mixes [93]. However, higher molarity of NaOH solution results in dissolution of Al, Si, and Ca species to a greater extent thereby increasing the extent of geopolymerization process. This results in formation of a stable aluminosilicate network along with C-S-H gel in the mix that led to higher compressive strength of the mixes [81].

The variation in mean S/N ratio for compressive strength at 7 days was mostly not systematic with increase in binder content however, the performance statistics (mean S/N ratio) for compressive strength at 28 days increased with increase in binder content as observed from Fig. 6.6. It may be noted that the mean S/N ratio for compressive strength at both 7 and 28 days was maximum at binder content of 450 kg/m^3 as observed from Fig. 6.6. The unsystematic variation in 7 days compressive strength with binder content may be ascribed to the variations in the extent of geopolymerization process at the early age. Further, the increase in compressive strength with increase in binder content at 28 days may be due to greater dissolution of Al, Si and Ca species, which increased the extent of geopolymerization process.

The variation in mean S/N ratio for compressive strength was not systematic with SS/SH ratio at both ages as observed from Fig. 6.6. Various researchers have reported contradicting results about the influence of SS/SH ratio on compressive strength of GPC [38,90,107,108,144–146]. Some of the researchers [107,108,144,146] have reported that the compressive strength of GPC mixes increased due to increase in SS/SH ratio. Olivia et al. [144] reported that in fly ash based GPC, higher content of Na_2SiO_3 had a positive influence on early age strength development. Shojaei et al. [108] and Hadi et al. [107] also observed the similar variation in compressive strength with SS/SH ratio for alkali-activated slag concrete. Mijarsh et al. [146] stated that the higher silica content due to more amount of Na_2SiO_3 in the alkaline solution enhanced the geopolymerization process and led to higher compressive strength of GPC. In contrary, some other researchers [38,90] have stated that the compressive strength of GPC mixes decreased with increase in SS/SH ratio. Nazari et al. [145] reported that the type of aluminosilicate source material is an important factor while selecting the NaOH solution molarity and SS/SH ratio to achieve better compressive strength of GPC mixes. In the present research work, the mean S/N ratio for 28 days compressive strength was maximum at a comparatively lower value of SS/SH ratio

i.e., 1.75. At lower SS/SH ratio, the availability of comparatively more quantity of NaOH solution and lower quantity of Na_2SiO_3 solution along with Al, Si and Ca species present in precursor materials might have increased the extent of polycondensation process thereby resulting in higher strength development of GPC at 28 days. From ANOVA results presented in Table 6.4, it was inferred that the GGBS replacement level had considerably higher contributing effect on compressive strength of GPC at both 7 days (96.15%) and 28 days (88.95%) as compared to other parameters.

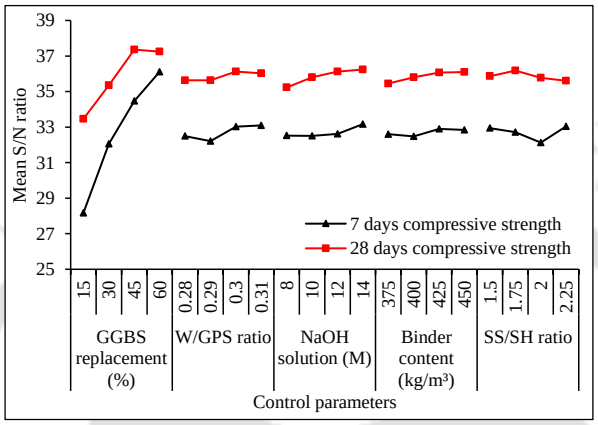

Fig. 6.6 Mean S/N ratio of compressive strength for different parameters.

Table 6.4 ANOVA results of signal-to-noise (S/N) ratio for compressive strength of GPC

Parameter	DOF	SOS	MS	Contribution (%)
7 days compressive strength				
GGBS replacement level	3	142.77	47.59	96.15
W/GPS ratio	3	2.15	0.72	1.45
NaOH molarity	3	1.15	0.38	0.77
Binder content	3	0.46	0.15	0.31
SS/SH ratio	3	1.97	0.66	1.32
Error	-	-	-	-
Total	15	148.49		100.00
28 days compressive strength				
GGBS replacement level	3	40.81	13.60	88.95
W/GPS ratio	3	0.82	0.27	1.78
NaOH molarity	3	2.47	0.82	5.38
Binder content	3	1.07	0.36	2.34
SS/SH ratio	3	0.71	0.24	1.55
Error	-	-	-	-
Total	15	45.88		100.00

Note: DOF: Degree of freedom, SOS: Sum of square, MS: Mean square

6.4 Multi-response optimization by Taguchi-Grey relational analysis (GRA) method

The combinations of optimum level of parameters corresponding to maximum performance statistics (mean S/N ratio) indicating better performance in terms of setting time (both

initial and final), slump, and compressive strength (at both ages) of fly ash-GGBS based GPC are presented in Table 6.5. From Table 6.5, one can obtain the optimum combination of different parameters to achieve a given property with respect to "larger-the-better" function. However, in order to arrive at a single set of optimized level of parameters for all the properties simultaneously, Taguchi- GRA method was used in the present work.

Table 6.5 Optimal mix proportions for different properties of GPC corresponding to maximum mean signal-to-noise (S/N) ratio

Optimized Mix	GGBS (%)	W/GPS ratio	NaOH (M)	Binder content (kg/m^3)	SS/SH ratio
M_{IST}	15	0.31	14	375	1.5
M_{FST}	15	0.31	14	400	1.5
M_{Slump}	45	0.31	14	450	1.5
$M_{7\ days\text{-}CS}$	60	0.31	14	425	2.25
$M_{28\ days\text{-}CS}$	45	0.3	14	450	1.75

Note: IST: Initial setting time, FST: Final setting time, CS: Compressive strength

The expressions for determining; Z_{ij}, Δ_{0ij}, GRC_{0ij} and GRG_{0i} are already presented in Section 3.3.1 (Chapter 3). The calculated values of these factors for all the sixteen geopolymer concrete mixes are presented in Table 6.6. From Table 6.6, mix M4 (proportioned with 85% fly ash, 15% GGBS, W/GPS ratio of 0.31, NaOH solution of 14 M, binder content of 450 kg/m^3 and SS/SH ratio of 2.25) showed the highest grey relational grade (GRG) of 0.76, as it exhibited higher setting time (Fig. 6.1), and slump value (Fig. 6.3). However, it may not be the optimal mix as it showed lower compressive strength (Fig. 6.5). Thus, to obtain the overall optimal GPC mix, the mean GRG for all the parameters were calculated. The level of a parameter with maximum mean GRG is the optimal one among all the levels of that parameter, as it will have highest main effect on the responses [118]. The mean GRG for a given level of a parameter was found out by calculating the average of the GRG for the mixes made with that level of the parameter. Table 6.7 presents the calculated values of mean GRG for all the parameters. From Table 6.7, it was noted that the highest values of mean GRG were obtained for the following combination of parameters: GGBS replacement of 45% (Level-3), W/GPS ratio of 0.31 (Level-4), NaOH solution of 14 M (Level-4), binder content of 450 kg/m^3 (Level-4) and SS/SH ratio of 1.5 (Level-1). The higher mean GRG indicates that the mix prepared with these levels of the mix parameters would perform better with respect to all the studied properties of geopolymer concrete (GPC).

Table 6.6 Grey relational grade of each GPC mix obtained from Taguchi-Grey relational analysis method

Mix	Normalized S/N ratio (Z_{ij})					Δ_{0ij}					Grey relational coefficient (GRC_{0ij})					Grey relational grade (GRG_{0i})
	IST	FST	Slump	7D CS	28D CS	IST	FST	Slump	7D CS	28D CS	IST	FST	Slump	7D CS	28D CS	
M1	0.75	0.67	0.10	0.07	0.00	0.25	0.33	0.90	0.93	1.00	0.67	0.60	0.36	0.35	0.33	0.46
M2	0.79	0.74	0.25	0.00	0.21	0.21	0.26	0.75	1.00	0.79	0.70	0.66	0.40	0.33	0.39	0.50
M3	0.93	0.94	0.93	0.08	0.33	0.07	0.06	0.07	0.92	0.67	0.88	0.90	0.88	0.35	0.43	0.69
M4	1.00	1.00	1.00	0.24	0.31	0.00	0.00	0.00	0.76	0.69	1.00	1.00	1.00	0.40	0.42	0.76
M5	0.34	0.22	0.25	0.52	0.49	0.66	0.78	0.75	0.48	0.51	0.43	0.39	0.40	0.51	0.49	0.44
M6	0.28	0.20	0.54	0.39	0.42	0.72	0.80	0.46	0.61	0.58	0.41	0.39	0.52	0.45	0.46	0.45
M7	0.56	0.67	0.86	0.59	0.65	0.44	0.33	0.14	0.41	0.35	0.53	0.60	0.78	0.55	0.58	0.61
M8	0.58	0.79	1.00	0.55	0.61	0.42	0.21	0.00	0.45	0.39	0.54	0.71	1.00	0.52	0.56	0.67
M9	0.28	0.29	0.54	0.75	1.00	0.72	0.71	0.46	0.25	0.00	0.41	0.41	0.52	0.67	1.00	0.60
M10	0.35	0.43	0.86	0.81	0.96	0.65	0.57	0.14	0.19	0.04	0.44	0.47	0.78	0.73	0.93	0.67
M11	0.00	0.17	0.86	0.80	0.78	1.00	0.83	0.14	0.20	0.22	0.33	0.38	0.78	0.71	0.69	0.58
M12	0.26	0.32	0.88	0.72	0.83	0.74	0.68	0.12	0.28	0.17	0.40	0.42	0.81	0.64	0.74	0.60
M13	0.19	0.10	0.10	0.89	0.88	0.81	0.90	0.90	0.11	0.12	0.38	0.36	0.36	0.82	0.81	0.54
M14	0.14	0.00	0.00	0.91	0.77	0.86	1.00	1.00	0.09	0.23	0.37	0.33	0.33	0.84	0.68	0.51
M15	0.14	0.14	0.72	1.00	0.95	0.86	0.86	0.28	0.00	0.05	0.37	0.37	0.64	1.00	0.92	0.66
M16	0.00	0.02	0.61	0.99	0.89	1.00	0.98	0.39	0.01	0.11	0.33	0.34	0.56	0.98	0.82	0.61

Note: IST: Initial setting time, FST: Final setting time, 7D CS: Compressive strength at 7 days, 28D CS: Compressive strength at 28 days

Table 6.7 Mean grey relational grade for each level of all the mix parameters

Parameter	Level-1	Level-2	Level-3	Level-4
GGBS replacement level	0.60	0.54	**0.61***	0.58
W/GPS ratio	0.51	0.53	0.63	**0.66***
Molarity of NaOH solution	0.52	0.55	0.62	**0.64***
Binder content	0.55	0.57	0.60	**0.62***
SS/SH ratio	**0.61***	0.58	0.57	0.57

*Optimum level

6.5 Microstructure analysis of GPC mixes

Out of the sixteen GPC mixes, for microstructure study, the mix from each GGBS replacement level having the highest grey relational grade was selected except for 15% GGBS replacement where the mix with second highest grey relational grade (GRG) i.e. mix M3 was selected because it exhibited higher enhancement of compressive strength from 7 days to 28 days as compared to the mix with highest GRG i.e. mix M4, and also, mix M3 exhibited satisfactory setting time and workability. The mixes M3, M8, M10, and M15 with GRG of 0.69, 0.67, 0.67, and 0.66 respectively were selected for the microstructure study.

6.5.1 XRD analysis

The XRD patterns of GPC mixes (M3, M8, M10, and M15) at 7 and 28 days of ambient curing are shown in Fig. 6.7 and Fig. 6.8 respectively. From the XRD patterns, two types of peak were identified. The main crystalline phases of fly ash such as quartz (SiO_2) and mullite ($Al_{4.75}Si_{1.25}O_{9.63}$) (shown in Fig. 3.2) were still present in the GPC mixes, which indicated unreacted fly ash particles in the GPC mixes. Some new crystalline peaks were identified in the XRD patterns, which are formed during the geopolymerization process. A broadly diffused amorphous halo between 20º 2θ to 35º 2θ was identified in GPC mixes when compared with the raw fly ash and GGBS as shown in Fig. 6.9, which indicates the formation of alkaline aluminosilicate geopolymer gels [22]. The new crystalline phases in the XRD patterns correspond to the sodium (or calcium) aluminosilicate complex (N-(C)-A-S-H), which contributes to compressive strength development of GPC mixes. Among the newly formed crystalline phases, muscovite ($KAl_3Si_3O_{10}(OH)_2$) at 8.8º 2θ, and 25.7º 2θ, nepheline ($NaAlSiO_4$) at 23.1º 2θ, 27.1º 2θ and 30.3º 2θ, anorthoclase (($Na_{0.85}K_{0.15}$)($AlSi_3O_8$)) at 23.7º 2θ, 27.5º 2θ and 35.3º 2θ, albite ((Na, Ca)Al(Si Al)$_3O_8$) at 22.1º 2θ, 24.1º 2θ and 28.0º 2θ, and sodalite ($Na_8Al_6Si_6O_{24}(OH)_2(H_2O)_2$) at 24.5º 2θ were identified in the XRD patterns of GPC mixes at both ages of 7 and 28 days.

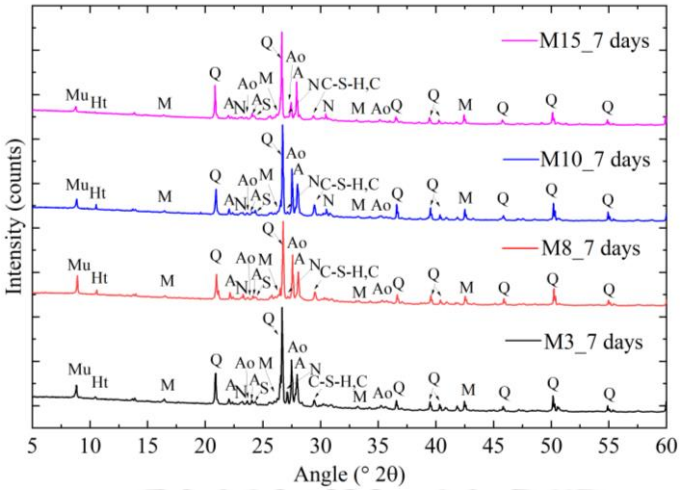

(Q: Quartz, M: Mullite, Mu: Muscovite, A: Albite, Ao: Anorthoclase, N: Nepheline, Ht: Hydrotalcite, C-S-H: Calcium silicate hydrate, C: Calcite)

Fig. 6.7 XRD patterns of GPC mixes (M3, M8, M10, M15) at 7 days of ambient curing.

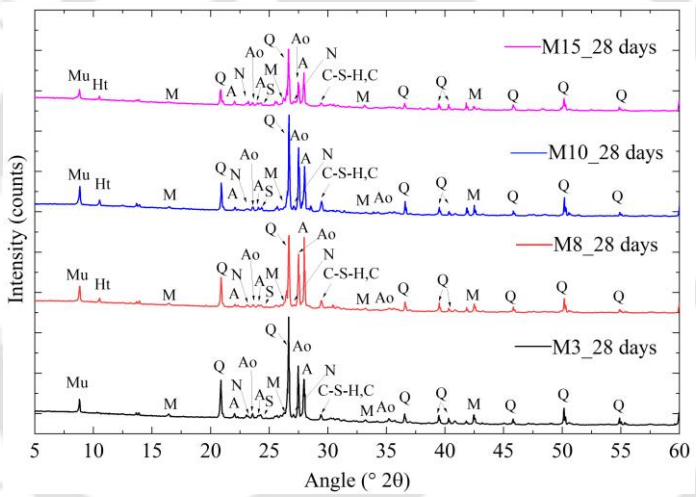

Fig. 6.8 XRD patterns of GPC mixes (M3, M8, M10, M15) at 28 days of ambient curing.

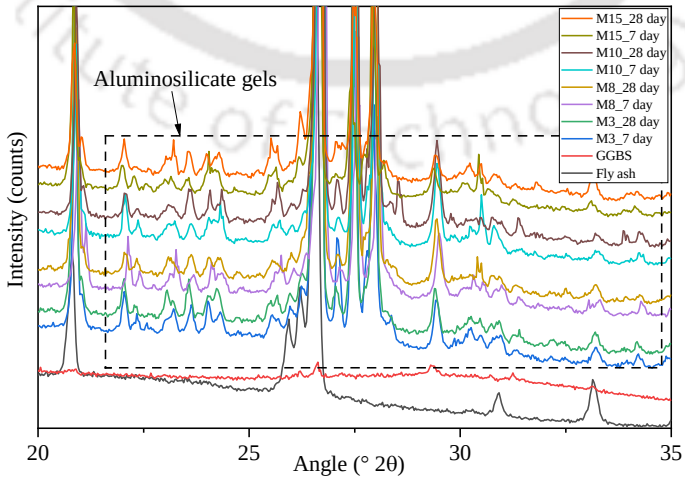

Fig. 6.9 XRD patterns of fly ash, GGBS and GPC mixes (M3, M8, M10, M15) at angle 20 º2θ to 35 º2θ.

From Fig. 6.7 and 6.8, it was observed that there is an increase in the peak intensity of muscovite, anorthoclase and albite from 7 days to 28 days, which indicates the continuation of geopolymerization process in the GPC mixes leading to compressive strength enhancement from 7 to 28 days. A peak at 29.4º 2θ was identified in the GPC mixes at all replacement levels of GGBS, which is associated with C-S-H gel or calcite ($CaCO_3$) [83]. The calcium oxide in GGBS contributes to C-S-H gel formation in the GPC mixes [83]. A less intense peak of hydrotalcite (Mg_6-$Al_2(CO_3)(OH)_{16}.4H_2O$) was identified at 10.5º 2θ in all the GPC mixes [41,135]. The peak intensity of albite mostly increased whereas that of anorthoclase and nepheline mostly decreased with increase in GGBS replacement level in the GPC mixes at 7 days of ambient curing as observed from Fig. 6.7. This indicates that as the GGBS replacement in the GPC mix is increased, the calcium oxide present in GGBS is incorporated into the geopolymerization process by reacting with N-A-S-H type gels (anorthoclase and nepheline) to a greater extent and forms more amount of N-(C)-A-S-H type gel (albite). Therefore, highest 7 days compressive strength was achieved for mix M15, which was made with 60% GGBS replacement level.

From Fig. 6.8, it is noticed that the peak intensity of albite, anorthoclase, nepheline and C-S-H gel were mostly higher for the mix M10 when compared with the mixes M3, M8, and M15 at 28 days of ambient curing. This is ascribed to the dissolution of precursor materials to a greater extent due to higher molarity of NaOH solution (14 M) that resulted in the formation of more amount of N-A-S-H, N-(C)-A-S-H, and C-S-H gels. Thus, the mix M10 showed higher compressive strength at 28 days of ambient curing when compared with the mixes M3, M8, and M15.

6.5.2 FTIR analysis

FTIR analysis was performed to analyze the chemical bonds in GPC mixes. Fig. 6.10 and 6.11 show the FTIR spectra of the GPC mixes (M3, M8, M10, and M15) at the ages of 7 and 28 days. Some major changes were observed between the FTIR spectra of precursor materials (Fig. 3.4, Chapter 3), and GPC mixes. The asymmetric bending vibration of Si-O-Si ranging from 453 cm^{-1} to 467 cm^{-1}, and Al-O bond at 778 cm^{-1} in GPC mixes at both 7 and 28 days are attributed to the unreacted precursor materials [147]. The broad peak centred around 1090 cm^{-1} in the spectra of raw fly ash, attributed to the asymmetric stretching vibration of Si-O-Si(Al) bonds (Fig. 3.4) shifted to lower wavenumbers ranging from 1011 cm^{-1} - 1018 cm^{-1} in the spectra of GPC mixes (Fig. 6.10 and 6.11). This indicates the occurrence of geopolymerization of precursor materials leading to formation of

geopolymer gel [40,113,148]. The exact shifting of wavenumbers and the span of shifting are dependent on the Si/Al ratio of the precursor materials and the reaction conditions [113]. When Al substitutes for Si in the Si-O-Si(Al) bond, its angle reduces and the main band of geopolymer system shifts to a lower wavenumber because the bond force constant of Si-O-Al bond is smaller as compared to that of Si-O-Si bond [113,148–150]. For the raw GGBS, the main band at 996 cm^{-1} (Fig. 3.4) was shifted to higher wavenumbers i.e., 1011 cm^{-1} - 1018 cm^{-1} in the spectra of GPC mixes (Fig. 6.10 and 6.11), which shows more formation of polymerized Si-O-Si(Al) structure [111,112]. From Fig. 6.10 and 6.11, it was observed that the peaks attributed to Si-O-Si(Al) bond shifted slightly towards higher wavenumbers in the GPC mixes from 7 days of ambient curing (1016 cm^{-1} in M3, 1011 cm^{-1} in M8, 1013 cm^{-1} in M10 and 1011 cm^{-1} in M15) to 28 days of ambient curing (1018 cm^{-1} in M3, 1015 cm^{-1} in M8, 1016 cm^{-1} in M10, and 1017 cm^{-1} in M15). This indicates the formation of C-S-H gel initially followed by the formation of N-(C)-A-S-H gel gradually over time [40,82]. The band ranging from 1413 cm^{-1} to 1480 cm^{-1} corresponds to the stretching vibration of CO_3^{2-} that is associated with carbonate group in the GPC mixes [40,77,106,113,147,149,151,152]. The broad band ranging from 3418 cm^{-1} to 3460 cm^{-1}, and the peak from 1637 cm^{-1} to 1640 cm^{-1} observed in the GPC mixes at both ages of ambient curing are ascribed to the stretching vibration of -OH group, and bending vibration of H-O-H group respectively. These bands are attributed to the water adsorbed in the rings of geopolymeric products [40,153].

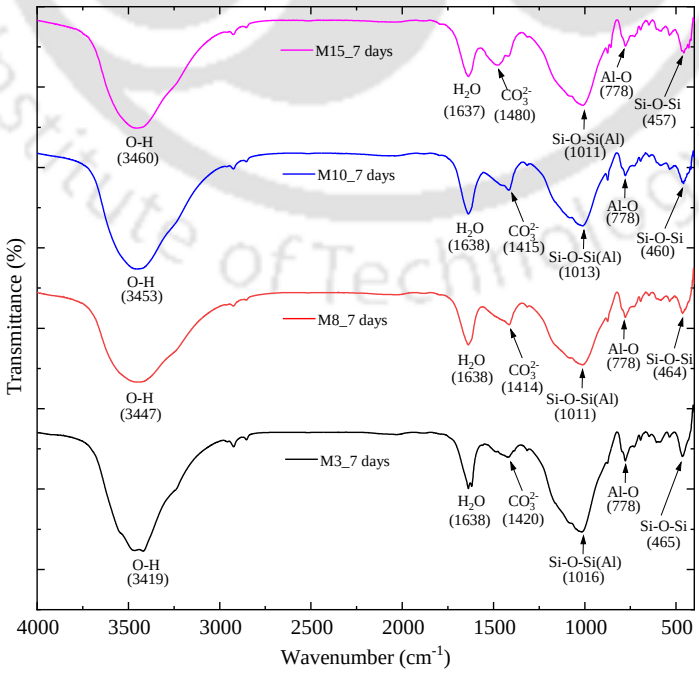

Fig. 6.10 FTIR spectra of GPC mixes (M3, M8, M10, M15) at 7 days of ambient curing.

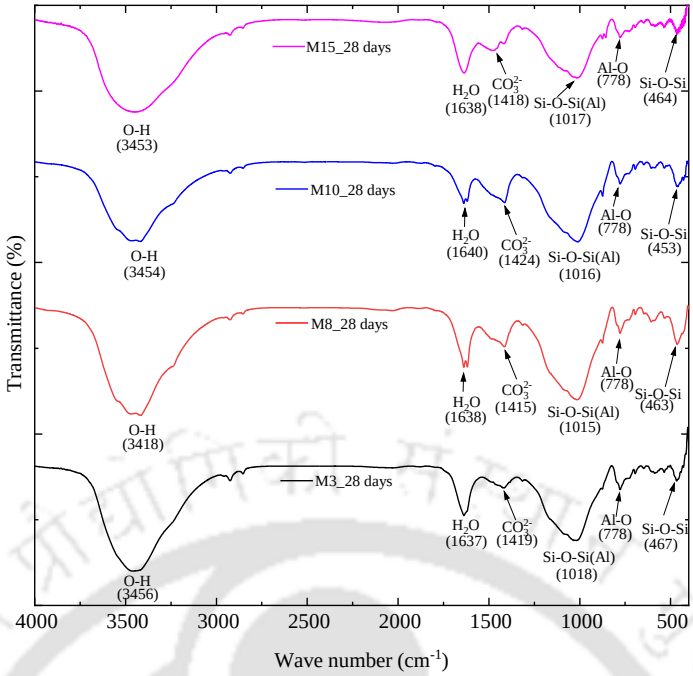

Fig. 6.11 FTIR spectra of GPC mixes (M3, M8, M10, M15) at 28 days of ambient curing.

6.5.3 FESEM analysis

The obtained FESEM micrographs of GPC mixes (M3, M8, M10 and M15) are presented in Fig. 6.12. From the micrographs, it was observed that the main binding phase shows the dense morphology indicating the presence of C-S-H gel, N-A-S-H and N-(C)-A-S-H gel [2,154], which is also evident from XRD and FTIR analyses. At 7 days of ambient curing, unreacted and partially reacted fly ash and GGBS particles are present in the GPC mixes along with binding phase as observed from Fig. 6.12. The presence of pores is also observed in the GPC mixes at 7 days of ambient curing. The combination of unreacted or partially reacted source materials and presence of pores resulted in lower initial compressive strength of GPC mixes [94]. When the GGBS replacement is increased in the GPC mixes (M3: 15% GGBS, M8: 30% GGBS, M10: 45% GGBS and M15: 60% GGBS), it enhanced the geopolymerization process and formed more amount of C-S-H and C-A-S-H type gel, leading to denser microstructure and exhibited higher compressive strength [38,84].

The micrographs of GPC mixes at 28 days of ambient curing showed more densely distributed aluminosilicate geopolymer gel as compared to that at 7 days of ambient curing. During early age, fly ash present in GPC mixes under ambient condition slows down the formation of geopolymer gel, however at later age, the Si and Al species in fly ash participates in the dissolution process thereby forming more N-A-S-H gel [2]. Further, needle-shaped crystalline phases were also identified in some of the GPC mixes (Fig. 6.12)

that indicates the presence of mullite, which remain after the dissolution of glass phase of fly ash [154].

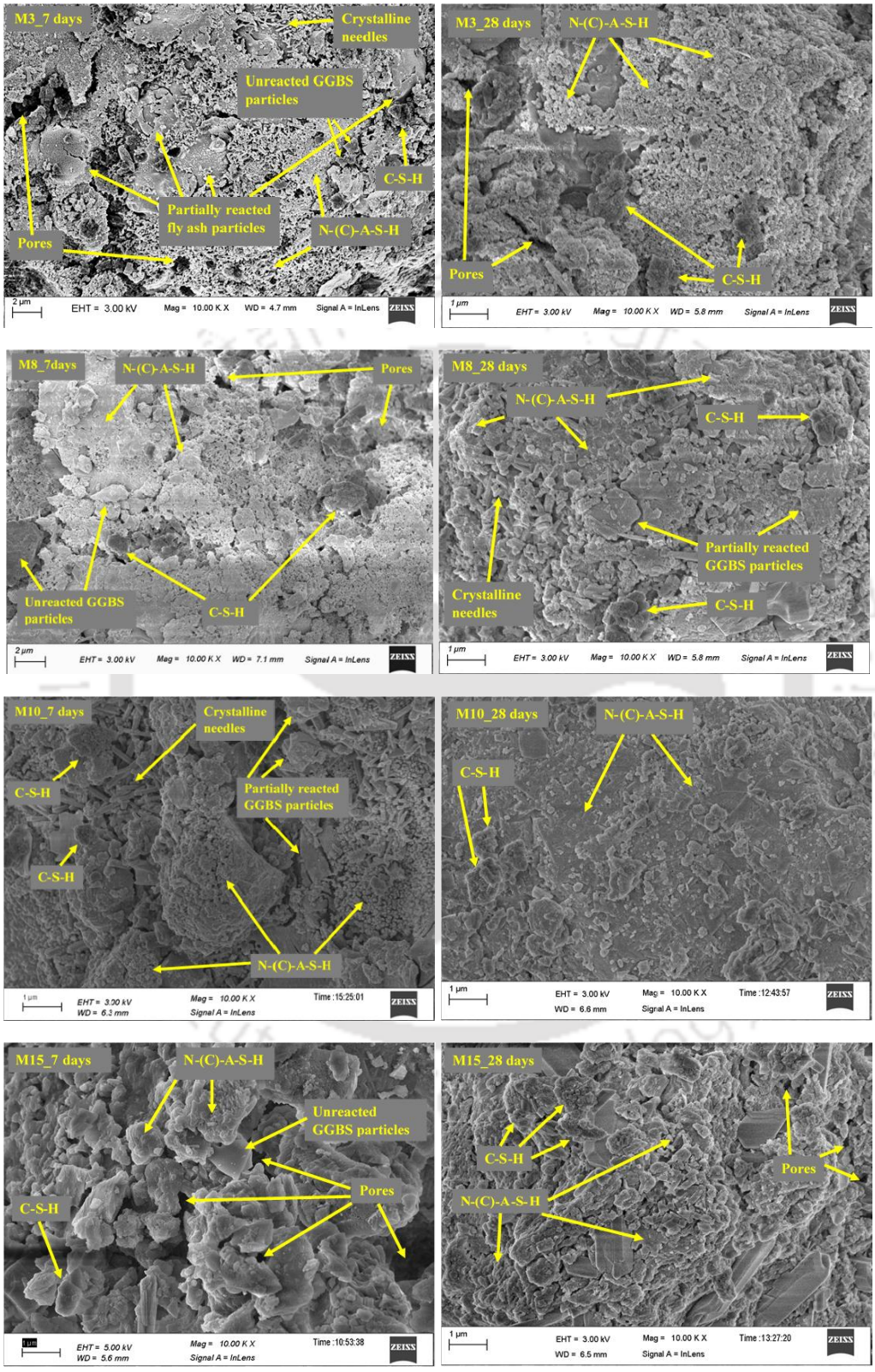

Fig. 6.12 FESEM micrographs of GPC mixes (M3, M8, M10, and M15) at 7 and 28 days of ambient curing.

6.6 Verification experiment

The verification experiments were conducted on the optimized fly ash-GGBS based GPC mix (designated as M17) as proposed in Section 6.4. Tests for setting time, workability, and compressive strength were carried out on the optimized GPC mix (M17). In addition, the microstructure studies such as XRD, FTIR spectroscopy, FESEM, and EDS analyses were also performed on this mix. The results of setting time, workability, and 7 days and 28 days compressive strength along with the calculated S/N ratio for each property are presented in Table 6.8. From Table 6.8, it was observed that the optimized GPC mix (M17) showed adequate setting time and highest slump value when compared with the GPC mixes as per L_{16} orthogonal array. Similarly, the optimized GPC mix exhibited adequate 7 days compressive strength and highest 28 days compressive strength.

Table 6.8 Results of the proposed optimized GPC mix

Responses	Result
Initial setting time (minute)	210
Final setting time (minute)	360
Slump value (mm)	200
7 days compressive strength (N/mm^2)	56.15
28 days compressive strength (N/mm^2)	79.70

The XRD patterns and FTIR spectra of the optimized GPC mix (M17) at 7 and 28 days of ambient curing are shown in Fig. 6.13 and Fig. 6.14 respectively. From Fig. 6.13, it was observed that the peak intensity of albite, and anorthoclase increased with increase in ambient curing age from 7 days to 28 days, which indicates the continuation of geopolymerization process in the GPC mix leading to compressive strength enhancement from 7 to 28 days. In addition, the peak intensity of C-S-H gel increased with increase in curing age from 7 to 28 days. From the FTIR spectra of optimized GPC mix shown in Fig. 6.14, it was observed that the asymmetric stretching vibration of Si-O-Si(Al) bonds shifted to lower wavenumbers i.e., 1005 cm^{-1} at 7 days, and 1009 cm^{-1} at 28 days with respect to the raw fly ash (1090 cm^{-1}), and shifted to higher wavenumbers with respect to raw GGBS (996 cm^{-1}). This indicates the occurrence of geopolymerization of precursor materials leading to the formation of geopolymer gel. Further, the Si-O-Si(Al) bond shifted slightly towards higher wavenumbers in the optimized GPC mix from 7 days of ambient curing (1005 cm^{-1}) to 28 days of ambient curing (1009 cm^{-1}), which indicates the formation of C-

S-H, and N-(C)-A-S-H gels gradually over time resulting in higher mechanical strength at the age of 28 days. The FESEM micrographs of the optimized GPC mix at 7 and 28 days of ambient curing are shown in Fig. 6.15. The micrographs indicated the presence of unreacted GGBS particles, N-(C)-A-S-H gel, and C-S-H gel. The presence of pores was observed in the mix at 7 days of ambient curing. Further, the micrographs indicated denser microstructure of the GPC mix at 28 days of ambient curing as compared to that at 7 days of ambient curing. The EDS spectra of the optimized GPC mix (M17) at 7 and 28 days of ambient curing are shown in Fig. 6.16. The atomic ratios such as Na/Si, and Al/Si ratios calculated from the elemental composition of the GPC mix decreased from 0.35 to 0.27, and 0.47 to 0.36 respectively with increase in ambient curing age from 7 to 28 days. However, the atomic Ca/Si ratio increased from 0.67 to 0.71 with increase in age from 7 to 28 days. The increase in atomic Ca/Si ratio with increase in age is in line with the formation of calcium enriched gels as indicated by the results of XRD analysis where the peak intensity of albite and C-S-H gel increased with increase in age from 7 to 28 days. The formation of higher amount of binding gels with increase in curing age is also corroborated with the results of FTIR spectroscopy, and FESEM analyses of the optimized GPC mix.

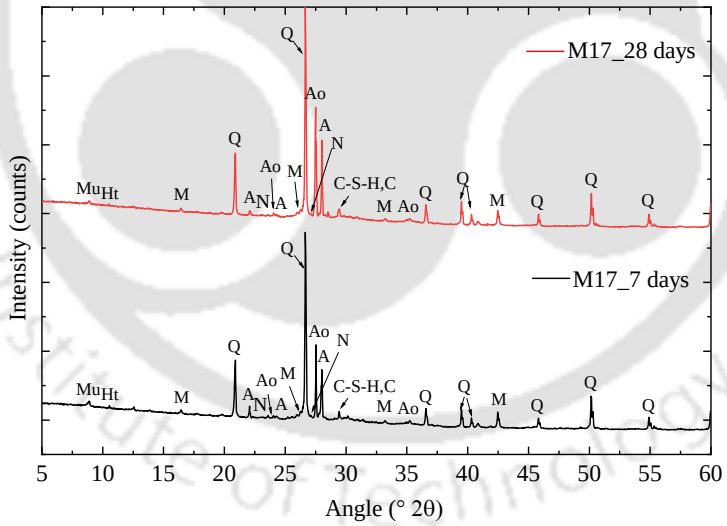

(Q: Quartz, M: Mullite, Mu: Muscovite, A: Albite, Ao: Anorthoclase, N: Nepheline, Ht: Hydrotalcite, C-S-H: Calcium silicate hydrate, C: Calcite)

Fig. 6.13 XRD patterns of optimized GPC mix (M17) at 7 days and 28 days of ambient curing.

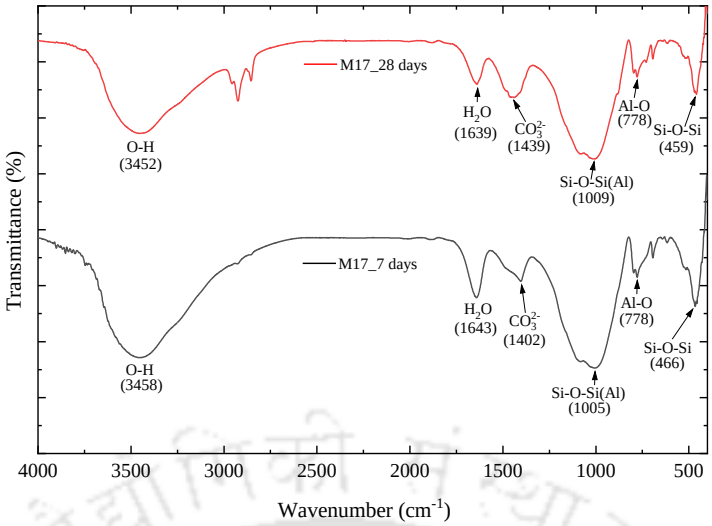

Fig. 6.14 FTIR spectra of optimized GPC mix (M17) at 7 days and 28 days of ambient curing.

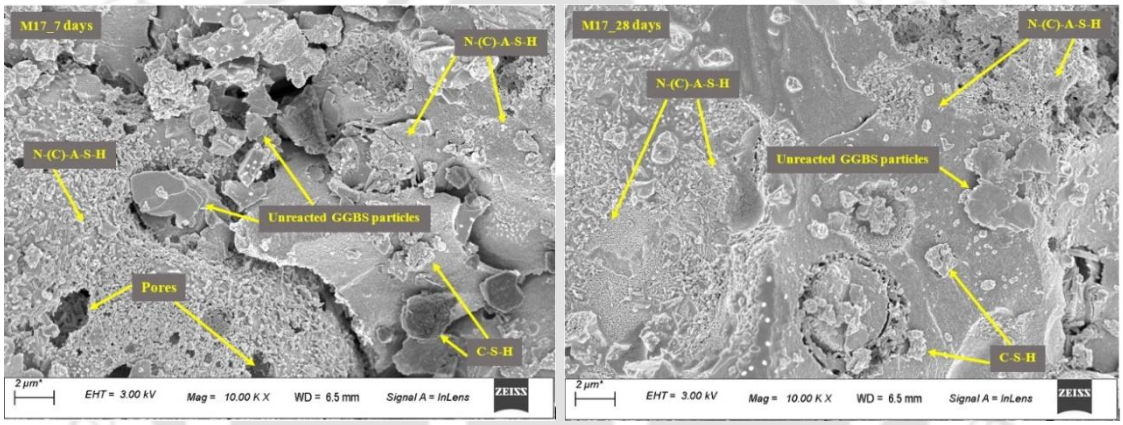

Fig. 6.15 FESEM micrographs of optimized GPC mix (M17) at 7 days and 28 days of ambient curing.

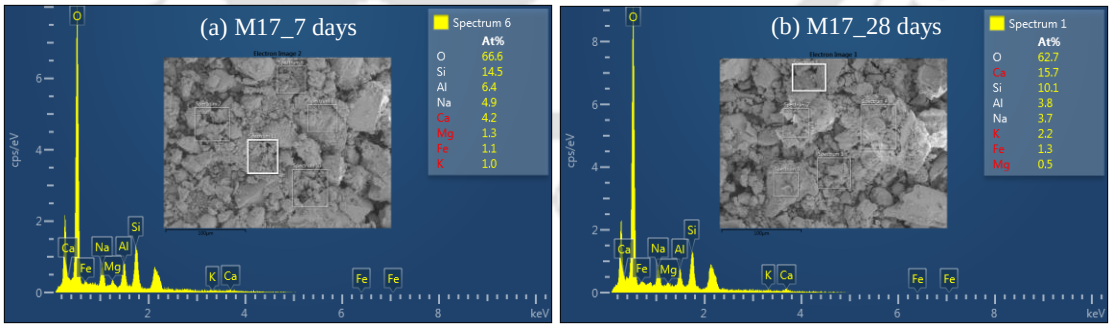

Fig. 6.16 EDS spectra of GPC mix (M17) at 7 and 28 days of ambient curing.

The grey relational grade (GRG) of the optimized GPC mix (M17) based on the obtained results of setting time, workability, and compressive strength was calculated using equation 3.2, 3.4, 3.5, and 3.6 (Chapter 3), and the calculated value is 0.81. The predicted grey

relational grade (GRG) of the optimized GPC mix (M17) was calculated using equation 4.1 (Chapter 4).

The calculated value of the predicted grey relational grade (GRG) of the optimized GPC mix (M17) is 0.82, which is close to the calculated GRG based on the experimental results. The GRG of the optimized GPC mix (M17) is highest (0.81) when compared with the GPC mixes as per L_{16} orthogonal array (Table 6.6). This indicates that the optimized GPC mix M17 performed better among all the GPC mixes with respect to setting time, workability, and compressive strength simultaneously.

6.7 Summary

This chapter presents application of Taguchi-Grey relational analysis (GRA) method to evaluate the influence of various parameters such as GGBS replacement level (15%, 30%, 45%, 60%), W/GPS ratio (0.28, 0.29, 0.30, 0.31), molarity of NaOH solution (8 M, 10 M, 12 M, 14 M), binder content (375 kg/m^3, 400 kg/m^3, 425 kg/m^3, 450 kg/m^3), and SS/SH ratio (1.5, 1.75, 2, 2.25) on setting time, workability and compressive strength of fly ash-GGBS based geopolymer concrete (GPC) mixes and to arrive at a single set of optimized level of these parameters with respect to all properties simultaneously. After arriving at the optimal combination of mix parameters, verification experiments were conducted on the proposed optimized GPC mix to evaluate its fresh and hardened properties, and the overall performance was predicted through grey relational analysis method. The microstructural studies on selected fly ash-GGBS based GPC mixes (one mix from each GGBS replacement level) and the proposed optimized GPC mix were conducted through XRD, FTIR, and FESEM analyses. In addition, EDS analysis was also carried out on the proposed optimized GPC mix. The experimental results showed that GGBS replacement level had dominant effect on initial and final setting time and compressive strength whereas W/GPS ratio significantly influenced the workability of GPC. Variations in formations of N-(C)-A-S-H and C-S-H gels in geopolymer concrete (GPC) were confirmed from the obtained results of microstructural analyses. Based on the results of multi-response optimization approach, the optimized mix prepared with 55% fly ash, 45% GGBS, W/GPS ratio of 0.31, NaOH solution of 14 M, binder content of 450 kg/m^3, and SS/SH ratio of 1.5 in the verification experiment exhibited better performance with respect to setting time, workability and compressive strength simultaneously as compared to the GPC mixes as per L_{16} orthogonal array.

Influence of Chloride Ions on Workability, Compressive Strength, Rebar Corrosion, and Microstructure Evolution in Fly Ash and Fly Ash-GGBS Based Geopolymer Concrete

7.1 General

In this chapter, the results obtained from the experimental investigation on the effect of admixed NaCl on workability, strength development, rebar corrosion evaluated through corrosion potential and corrosion current density by linear polarization resistance (LPR) measurement, chloride content analysis, and microstructural evolution in fly ash and fly ash-GGBS based geopolymer concrete (GPC) are presented and discussed. For this study, the fly ash-GGBS based geopolymer concrete (GPC) mixes (M3, M8, M10, and M15) derived from multi-response optimization by Taguchi-GRA method (Chapter 6: Section 3.5) were selected. Further, the obtained results of fly ash-GGBS based geopolymer concrete mixes were compared with their corresponding fly ash based geopolymer concrete mixes.

7.2 Workability of fresh geopolymer concrete (GPC) mixes

As stated earlier in Chapter 3, the slump test was carried out to measure the workability of fresh geopolymer concrete mixes. The measured slump values obtained from control (0% NaCl) and chloride (1.5% and 3.5% NaCl) admixed fly ash and fly ash-GGBS based geopolymer concrete (GPC) mixes are presented in Fig. 7.1 (a - d). As observed from Fig. 7.1, all the GPC mixes exhibited satisfactory workability with slump value in the range of 150 mm to 220 mm for fly ash based GPC mixes (M3: FA100, M8: FA100, M10: FA100, M15: FA100) and in the range of 100 mm to 175 mm for fly ash-GGBS based GPC mixes (M3: FA85/G15, M8: FA70/G30, M10: FA55/G45, and M15: FA40/G60). The fly ash-GGBS based GPC mixes exhibited lower slump value as compared to the corresponding fly ash based GPC mixes. Further, the slump value of GPC mixes mostly decreased with increase in GGBS content in the mixes. The decrease in slump value due to addition of GGBS in geopolymer concrete (GPC) mixes was observed in the range 2.8% to 9.1%, 5.9% to 8.1%, 9.1% to 13.3%, and 44.4% to 50.0% for mix M3, M8, M10, and M15 respectively. The influence of GGBS on reduction in consistency of GPC was more significant for the mix M15, which was prepared with 40% fly ash and 60% GGBS. The reason for lower slump value in fly ash-GGBS based GPC mixes may be ascribed to influence of angular

shape of particles of GGBS that reduced the mobility of fly ash particles in the freshly prepared fly ash-GGBS based GPC mixes. Further, the water demand of GGBS in fly ash-GGBS based GPC mixes may be higher due to its larger surface area and angular particle shape as compared to fly ash [112]. In addition, the higher reactivity of GGBS in alkaline solution in comparison to fly ash leads to rapid formation of geopolymer gels and reduced the workability of fly ash-GGBS based GPC mixes [2]. As observed from Fig. 7.1, the slump value of fly ash and fly ash-GGBS based GPC mixes slightly improved with increase in admixed NaCl concentration in the mixes, which may be ascribed to the effect of decrease in viscosity of fresh fly ash and fly ash-GGBS based GPC mixes in the presence of NaCl.

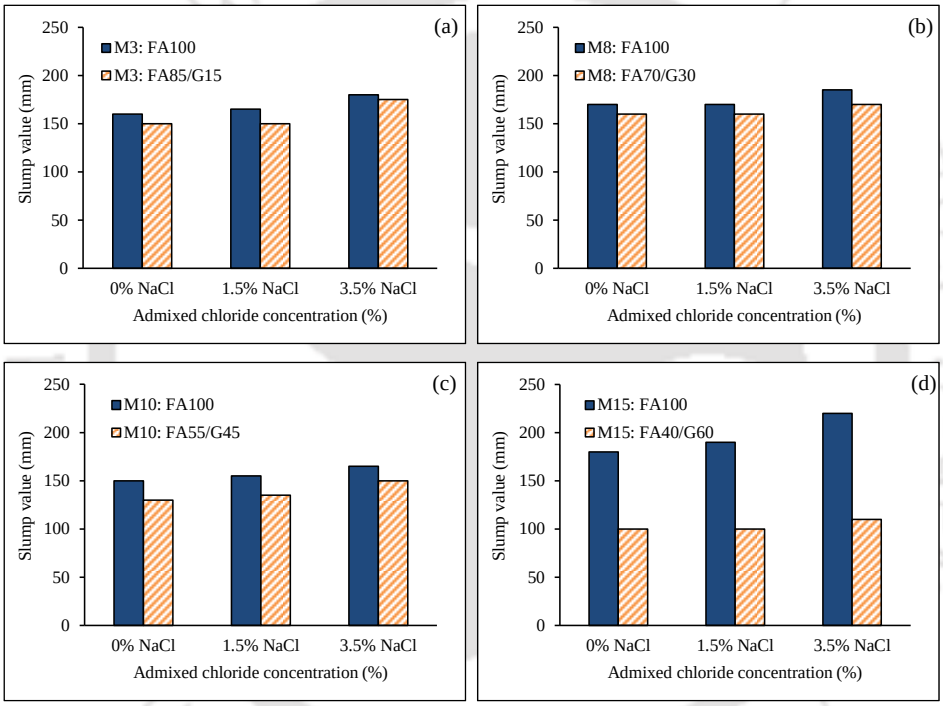

Fig. 7.1 Slump value of control (0% NaCl) and chloride (1.5% and 3.5% NaCl) admixed fly ash and fly ash-GGBS based GPC mixes: (a) M3: FA100; FA85/G15, (b) M8: FA100; FA70/G30, (c) M10: FA100; FA55/G45, (d) M15: FA100; FA40/G60.

7.3 Compressive strength of geopolymer concrete (GPC) mixes

The compressive strength of fly ash and fly ash-GGBS based geopolymer concrete (GPC) mixes at the age of 7, 28 and 360 days are presented in Fig. 7.2 to Fig. 7.5. As observed from these figures, the fly ash-GGBS based GPC mixes exhibited higher compressive strength as compared to the corresponding fly ash based GPC mixes (except for mix M3 at 7 days) at all ages. The presence of higher calcium oxide (CaO) content in GGBS in fly ash-GGBS based GPC mixes enhanced the formation of calcium-rich gels i.e., N-(C)-A-S-H and C-S-H gels along with formation of N-A-S-H gel [41,83,155]. Further, the formation

of calcium-rich gels improved the alkalinity of fly ash-GGBS based GPC mixes, which leads to dissolution of alumina and silica to a greater extent that helps to attain the geopolymerization process at ambient temperature and improves the compressive strength of fly ash-GGBS based GPC mixes [155]. The reason for decrease in 7 days compressive strength of GPC mix M3: FA85/G15 as compared to its corresponding fly ash based GPC mix M3: FA100 may be due to the effect of slower geopolymerization reaction in the mix M3: FA85/G15 in the presence of lower amount of GGBS content (15%) during early age of ambient curing. From Fig. 7.2 to Fig. 7.5, it is observed that the compressive strength of fly ash-GGBS based GPC mixes mostly increased with increase in GGBS replacement level in the mixes from 15% to 60%, at all ages. This may be ascribed to the effect of increase in degree of geopolymerization reaction in the presence of higher GGBS content, which leads to formation of more homogeneous and denser geopolymer matrix and resulted in higher compressive strength of GPC mixes made with higher GGBS replacement level [81,90,140,156].

While comparing the effect of NaCl, it is observed that the compressive strength of NaCl admixed fly ash and fly ash-GGBS based GPC mixes decreased in the range from 3.3% to 41.9%, and 0.6% to 30.2% as compared to control (without admixed NaCl) fly ash and fly ash-GGBS based GPC mixes respectively (Fig. 7.2 to Fig. 7.5). Further, the compressive strength of NaCl admixed GPC mixes decreased with increase in admixed NaCl concentration, at all ages (7, 28, and 360 days). The reduction in compressive strength may be attributed to the effect of NaCl in the GPC mixes that hindered the polycondensation process to certain extent. Furthermore, it is observed that the reduction in compressive strength of NaCl admixed fly ash and fly ash-GGBS based GPC mixes decreased with increase in age. The reduction in strength was found in the range of 3.6% to 41.9% at 7 days, followed by 6.1% to 34.9% at 28 days, and 0.6% to 24.3% at 360 days. This indicates that the effect of NaCl in hindering the geopolymerization process was significant at early ages. It is also noted that, in the presence of NaCl, the reduction in compressive strength of fly ash based GPC mixes was higher (3.3% to 41.9%) in comparison to fly ash-GGBS based GPC mixes (0.6% to 30.2%). This may be ascribed to the effect of crystallization of NaCl in the pores of GPC mixes to a comparatively higher extent in case of fly ash based GPC mixes as compared to fly ash-GGBS based GPC mixes. Further, the fly ash and fly ash-GGBS based GPC mixes exhibited higher compressive strength during later ages. This may

be due to the influence of higher extent of polycondensation reaction in GPC mixes at later ages.

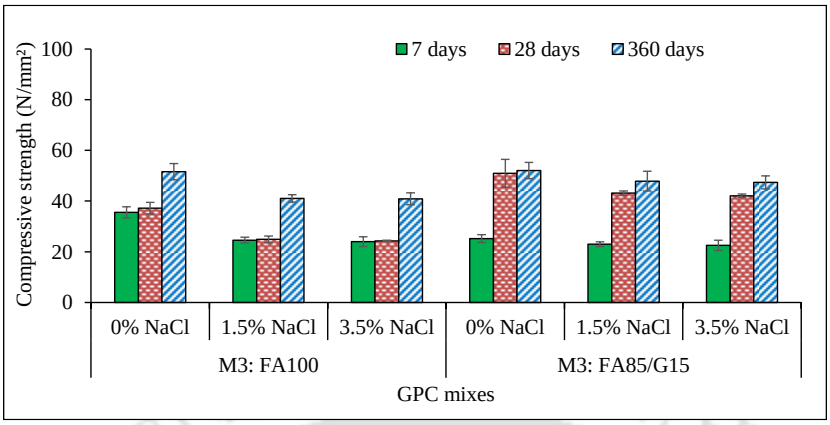

Fig. 7.2 Compressive strength of control (0% NaCl) and chloride (1.5% and 3.5% NaCl) admixed fly ash and fly ash-GGBS based GPC mixes (M3: FA100; FA85/G15) at the age of 7, 28, and 360 days.

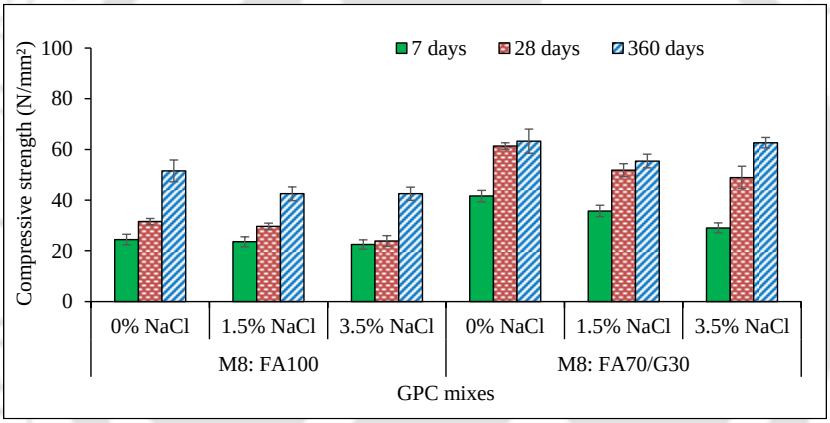

Fig. 7.3 Compressive strength of control (0% NaCl) and chloride (1.5% and 3.5% NaCl) admixed fly ash and fly ash-GGBS based GPC mixes (M8: FA100; FA70/G30) at the age of 7, 28, and 360 days.

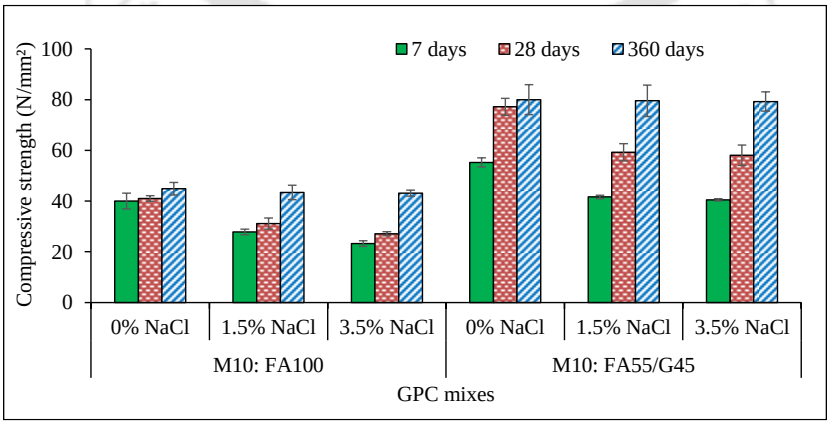

Fig. 7.4 Compressive strength of control (0% NaCl) and chloride (1.5% and 3.5% NaCl) admixed fly ash and fly ash-GGBS based GPC mixes (M10: FA100; FA55/G45) at the age of 7, 28, and 360 days.

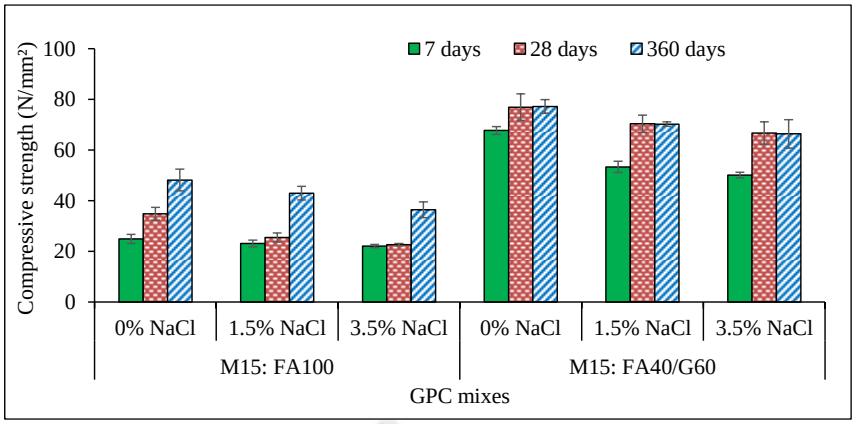

Fig. 7.5 Compressive strength of control (0% NaCl) and chloride (1.5% and 3.5% NaCl) admixed fly ash and fly ash-GGBS based GPC mixes (M15: FA100; FA40/G60) at the age of 7, 28, and 360 days.

7.4 Electrochemical measurements

7.4.1 Corrosion potential (E_{corr})

The corrosion potential (E_{corr}) of steel bar embedded in cylindrical fly ash and fly ash-GGBS based GPC specimens are depicted in Fig. 7.6 to Fig. 7.9. Each value of corrosion potential shown in these figures is the average value of three replicate cylindrical reinforced specimens of a given GPC mix. As observed from these figures, the E_{corr} values of steel bar in control fly ash and fly ash-GGBS based GPC mixes (M3, M8, M10, and M15) were mostly less negative than -270 mV (SCE) at all ages. This shows lower probability of occurrence of steel bar corrosion as per ASTM C876-15 [131]. Furthermore, the E_{corr} of embedded steel bar in NaCl admixed fly ash and fly ash-GGBS based GPC mixes were more negative than -270 mV (SCE) at all ages, thereby indicating greater than 90% probability of occurrence of reinforcing steel corrosion. This may be attributed to the effect of alteration in the passivity of steel bar in the presence of Cl^- ions in the vicinity of the steel bar in NaCl admixed GPC mixes.

While comparing the E_{corr} of steel bar embedded in fly ash and fly ash-GGBS based GPC mixes, it is noted that the embedded rebar in control fly ash-GGBS based GPC specimens mostly exhibited less negative E_{corr} values in comparison to corresponding control fly ash based GPC specimens at all ages. Similarly, in the presence of NaCl, the steel bar embedded in fly ash-GGBS based GPC specimens mostly showed less negative E_{corr} values as compared to corresponding fly ash based GPC specimens at all ages, except for GPC mix M3: FA85/G15 admixed with 1.5% NaCl. The mostly less negative corrosion potential of reinforcing steel in fly ash-GGBS based GPC mixes may be ascribed to the effect of presence of higher calcium oxide content in GGBS in fly ash-GGBS based GPC mixes that

enhanced the geopolymerization reaction in ambient condition and resulted in formation of comparatively denser microstructure and thereby reduced the availability of chloride ions in the vicinity of steel bar in NaCl added fly ash-GGBS based GPC specimens. In case of fly ash-GGBS based GPC mix i.e., M3: FA85/G15 admixed with 1.5% NaCl, the more negative corrosion potential as compared to corresponding fly ash based GPC mix may be attributed to the dominant effect of alteration in the amount of oxygen near steel reinforcement. Further, the steel bar embedded in fly ash-GGBS based GPC specimens mostly exhibited less negative E_{corr} values with increase in GGBS content in the mixes at all ages. This may be attributed to the effect of formation of more amount of calcium-rich gels at higher GGBS content that led to formation of comparatively denser microstructure. This resulted in availability of comparatively lower amount of chloride ions near steel bar embedded in fly ash-GGBS based GPC specimens made with higher GGBS content.

From Fig. 7.6 to Fig. 7.9, it is noted that the steel bar embedded in fly ash and fly ash-GGBS based GPC specimens exhibited mostly more negative E_{corr} values with increase in admixed NaCl concentration except in case of fly ash based GPC mix i.e., M10: FA100. The mostly more negative corrosion potential with increase in admixed NaCl concentration may be ascribed to the effect of presence of higher amount of chloride ions in the vicinity of steel bar in GPC specimens admixed with higher NaCl concentration that might have altered its passivity. In case of fly ash based GPC mix M10, the more negative corrosion potential at lower concentration of admixed NaCl may be ascribed to the effect of variation in oxygen content in the vicinity of steel reinforcement. From Fig. 7.6 and Fig. 7.7, it is inferred that there is no systematic variation in E_{corr} of steel bar with age in control fly ash-GGBS based GPC specimens made with 15% and 30% GGBS (M3: FA85/G15 and M8: FA70/G30) and their corresponding fly ash based GPC specimens (M3: FA100 and M8: FA100). Furthermore, from Fig. 7.8 and Fig. 7.9, it is noted that the E_{corr} of steel bar embedded in control fly ash-GGBS based GPC specimens made with 45% and 60% GGBS ((M10: FA55/G45 and M15: FA40/G60) and their corresponding fly ash based GPC specimens (M10: FA100 and M15: FA100) mostly became less negative at later ages. This can be attributed to the effect of improved passivity of reinforcing steel bar in control fly ash and fly ash-GGBS based GPC mixes during later ages. Further, unsystematic variation was observed in E_{corr} of embedded rebar with age in NaCl admixed fly ash and fly ash-GGBS based GPC specimens. This can be attributed to the effect of variations in the

conductivity of electrolytic pore solution of GPC mixes surrounding the steel reinforcement with age.

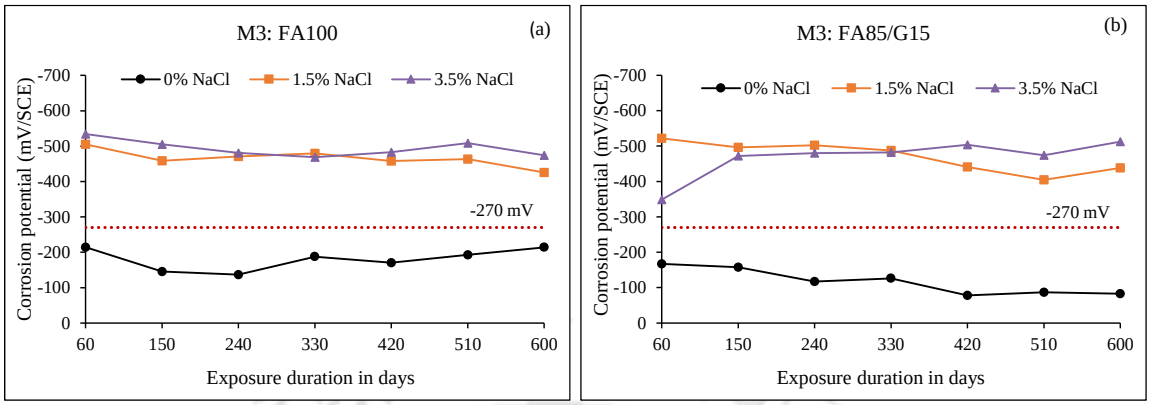

Fig. 7.6 Corrosion potential (E_{corr}) of steel bar embedded in control (0% NaCl) and chloride (1.5% and 3.5% NaCl) admixed fly ash and fly ash-GGBS based GPC specimens: (a) M3: FA100, and (b) M3: FA85/G15.

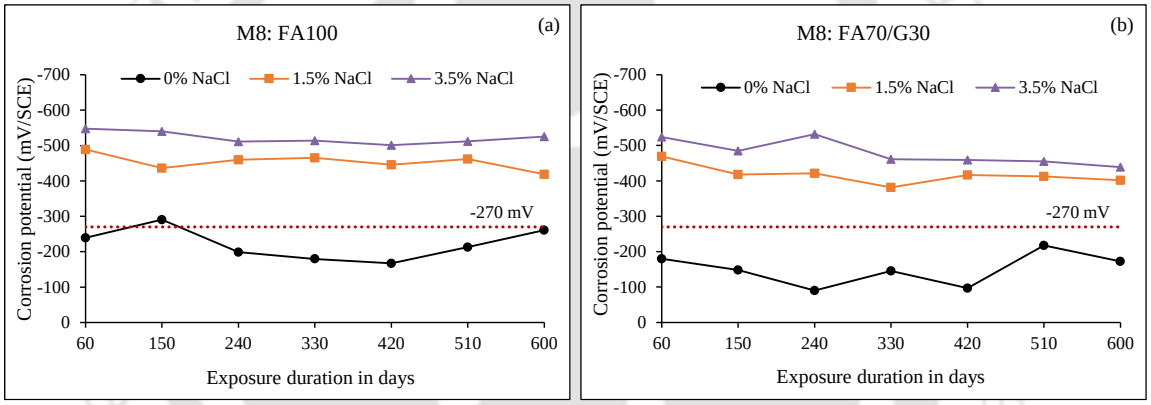

Fig. 7.7 Corrosion potential (E_{corr}) of steel bar embedded in control (0% NaCl) and chloride (1.5% and 3.5% NaCl) admixed fly ash and fly ash-GGBS based GPC specimens: (a) M8: FA100, and (b) M8: FA70/G30.

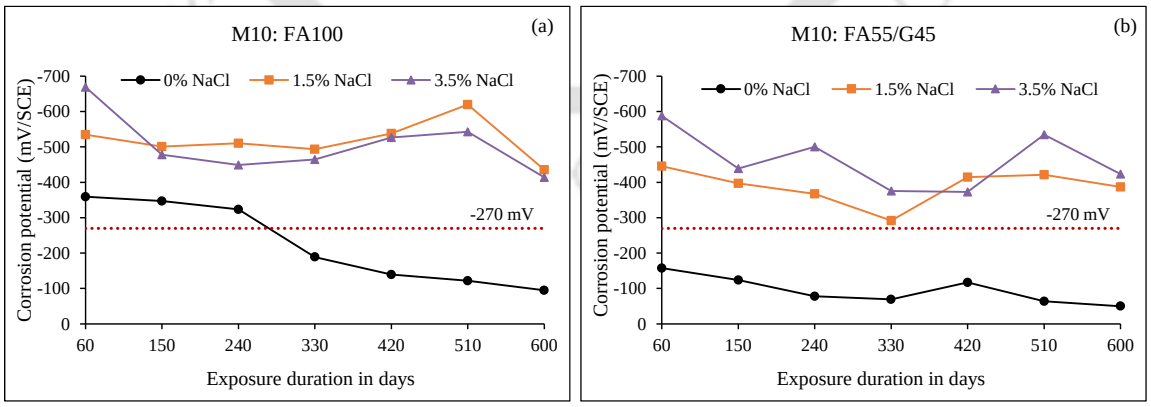

Fig. 7.8 Corrosion potential (E_{corr}) of steel bar embedded in control (0% NaCl) and chloride (1.5% and 3.5% NaCl) admixed fly ash and fly ash-GGBS based GPC specimens: (a) M10: FA100, and (b) M10: FA55/G45.

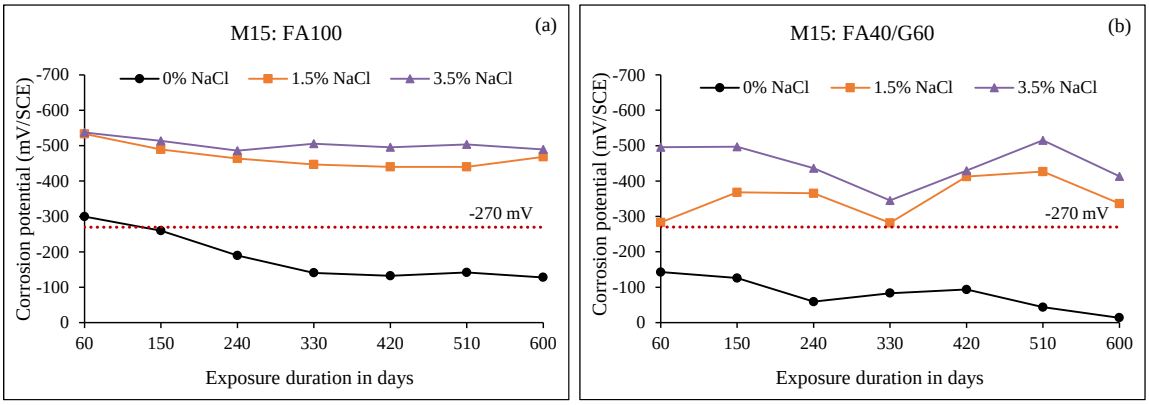

Fig. 7.9 Corrosion potential (E_{corr}) of steel bar embedded in control (0% NaCl) and chloride (1.5% and 3.5% NaCl) admixed fly ash and fly ash-GGBS based GPC specimens: (a) M15: FA100, and (b) M15: FA40/G60.

7.4.2 Corrosion current density (I_{corr})

The corrosion current density (I_{corr}) of embedded steel bar in cylindrical fly ash and fly ash-GGBS based GPC specimens are illustrated in Fig. 7.10 to Fig. 7.13. Each value of corrosion current density shown in these figures is the average value of three replicate cylindrical reinforced specimens of a given GPC mix. As observed from Fig. 7.10 to 7.13, the corrosion current density (I_{corr}) values of embedded steel bar in control GPC specimens were significantly lower as compared to chloride admixed GPC mixes. The I_{corr} varied in the range of 0.02 to 0.12 µA/cm^2 for control fly ash-GGBS based GPC mixes (M3, M8, M10, and M15), and in the range of 0.04 to 0.28 µA/cm^2 for their corresponding fly ash based GPC mixes. In case of chloride (1.5% and 3.5% NaCl) admixed GPC mixes, the corrosion current density (I_{corr}) of embedded steel bar varied in the range of 0.19 µA/cm^2 to 4.34 µA/cm^2 for fly ash-GGBS based GPC mixes (M3, M8, M10, and M15) and in the range of 1.18 µA/cm^2 to 13.59 µA/cm^2 for their corresponding fly ash based GPC mixes, irrespective of concentration of admixed NaCl and age. The higher rate of rebar corrosion in NaCl admixed fly ash and fly ash-GGBS based GPC specimens can be attributed to the effect of increase in conductivity of GPC in the presence of chloride ions.

While comparing the I_{corr} of steel bar embedded in fly ash-GGBS based GPC specimens with their corresponding fly ash based GPC specimens, it is observed that the rebar in control fly ash-GGBS based GPC specimens mostly showed lower I_{corr} as compared to their corresponding fly ash based GPC specimens. Similarly, it is noted that the embedded rebar in chloride admixed fly ash-GGBS based GPC specimens mostly exhibited lower I_{corr} when compared with their corresponding fly ash based GPC specimens, except for the GPC mix M3: FA85/G15 admixed with 1.5% NaCl. The lower corrosion current density in chloride

admixed fly ash-GGBS based GPC mixes is attributed to the effect of greater extent of polycondensation reaction in the presence of GGBS in the GPC mixes that resulted in higher amount of geopolymer gels. This led to comparatively denser microstructure in fly ash-GGBS based GPC mixes thereby leading to availability of less amount of Cl^- ions near embedded steel bar, which resulted in lower I_{corr} values. The mostly higher corrosion current density in fly ash-GGBS based GPC mix i.e., M3: FA85/G15 admixed with 1.5% NaCl as compared to the corresponding fly ash based GPC mix may be due to the effect of variations in oxygen and moisture content near rebar in GPC mixes. It may be noted that the corrosion potential was also mostly more negative in fly ash-GGBS based GPC mix M3 as compared to its corresponding fly ash based mix at NaCl concentration of 1.5% (Fig. 7.6).

The corrosion current density (I_{corr}) of embedded rebar in control fly ash-GGBS based GPC mixes mostly increased with increase in GGBS content. The higher I_{corr} in control GPC mixes at higher GGBS content may be attributed to the effect of alterations in the electrolytic pore solution, and variations in the availability of oxygen and moisture near steel reinforcement. In case of chloride admixed fly ash-GGBS based GPC mixes, the corrosion current density (I_{corr}) mostly decreased with increase in GGBS content (Fig. 7.10 to Fig. 7.13). The lower I_{corr} in chloride admixed GPC mixes made with higher GGBS content may be due to the effect of comparatively higher resistivity as a result of formation of denser microstructure in the mixes made with higher GGBS content that resulted in availability of lower amount of chloride ions in the electrolytic pore solution of concrete surrounding embedded steel bar.

The I_{corr} of rebar in fly ash and fly ash-GGBS based GPC mixes mostly increased with increase in admixed NaCl concentration (Fig. 7.10 to Fig. 7.13). This is due to the effect of higher conductivity of GPC in the presence of more amount of chloride ions. Further, from Fig. 7.10 to Fig. 7.13, it can be noted that there was mostly unsystematic variation in I_{corr} of embedded steel bar with age in control as well as chloride admixed fly ash and fly ash-GGBS based GPC mixes. The unsystematic variation in I_{corr} with age in GPC mixes may be ascribed to the dominant effect of variations in oxygen and moisture content surrounding the steel bar as well as changes in chloride ion concentration in electrolytic pore solution of NaCl admixed GPC mixes.

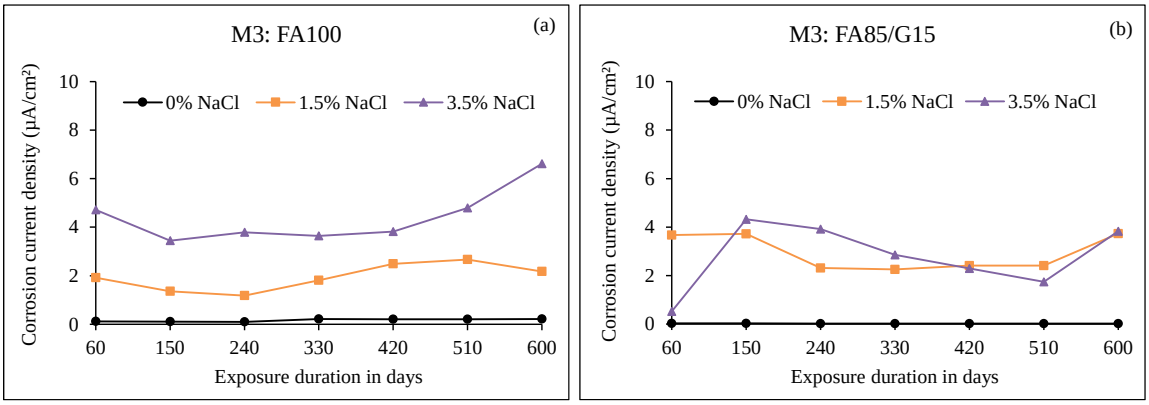

Fig. 7.10 Corrosion current density (I_{corr}) of steel bar embedded in control (0% NaCl) and chloride (1.5% and 3.5% NaCl) admixed fly ash and fly ash-GGBS based GPC specimens: (a) M3: FA100, and (b) M3: FA85/G15.

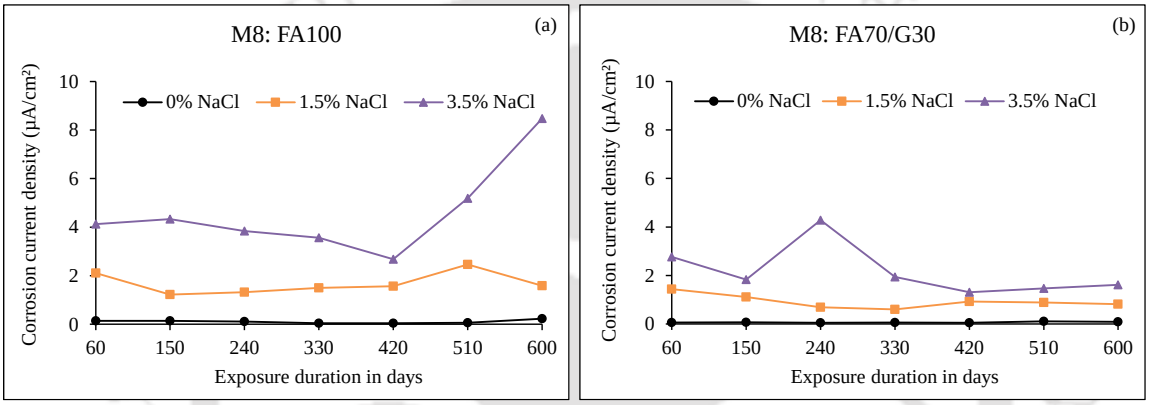

Fig. 7.11 Corrosion current density (I_{corr}) of steel bar embedded in control (0% NaCl) and chloride (1.5% and 3.5% NaCl) admixed fly ash and fly ash-GGBS based GPC specimens: (a) M8: FA100, and (b) M8: FA70/G30.

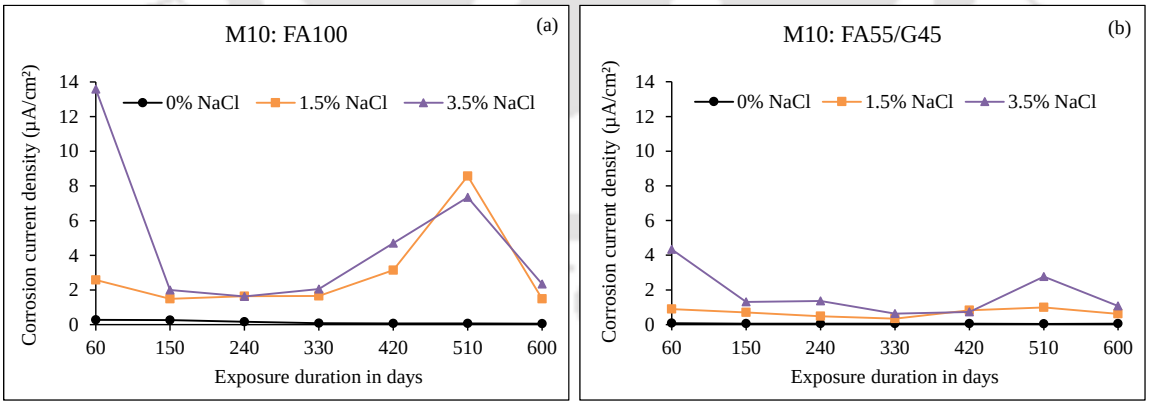

Fig. 7.12 Corrosion current density (I_{corr}) of steel bar embedded in control (0% NaCl) and chloride (1.5% and 3.5% NaCl) admixed fly ash and fly ash-GGBS based GPC specimens: (a) M10: FA100, and (b) M10: FA55/G45.

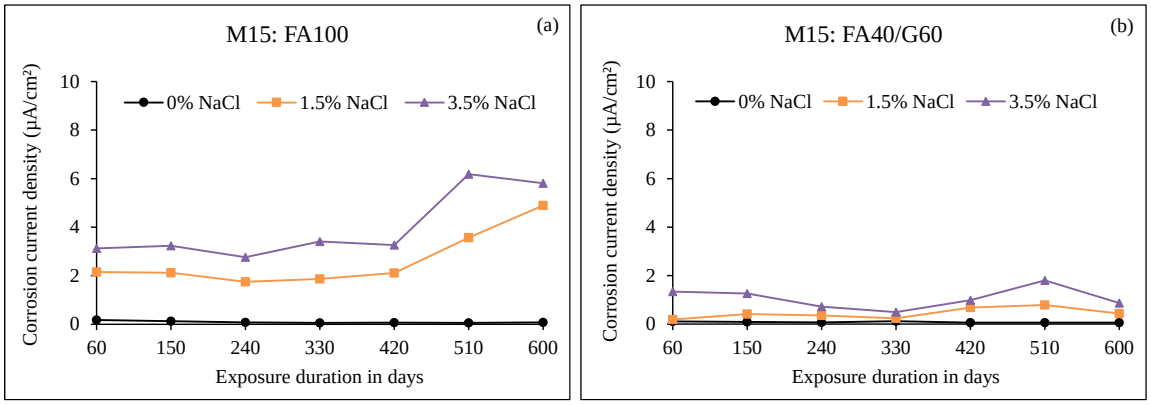

Fig. 7.13 Corrosion current density (I_{corr}) of steel bar embedded in control (0% NaCl) and chloride (1.5% and 3.5% NaCl) admixed fly ash and fly ash-GGBS based GPC specimens: (a) M15: FA100, and (b) M15: FA40/G60.

7.5 Chloride content analysis of geopolymer concrete (GPC) mixes

7.5.1 Chloride content of GPC mixes at different ages

The results obtained from the chloride content (free and total chloride) measurement of GPC powder samples collected after compressive strength test at the age of 7, 28 and 360 days are presented in Fig. 7.14 to Fig. 7.17. From these figures, it is observed that the total chloride content of GPC mixes were higher than free chloride content. However, the difference between total and free chloride content was very less, thereby indicating very less extent of chloride binding ability of both fly ash and fly ash-GGBS based GPC mixes. The lower extent of chloride binding in GPC mixes may be attributed to the effect of physical adsorption of chloride ions on geopolymer gels. The fly ash-GGBS based GPC mixes exhibited lower free chloride content as compared to their corresponding fly ash based GPC mixes at all ages, except mix M3: FA85/G15 at 7 and 28 days (Fig. 7.14 a and b). This is attributed to the effect of formation of higher amount of calcium-rich gels (N-(C)-A-S-H and C-S-H gels) in fly ash-GGBS based GPC mixes as compared to their corresponding fly ash based GPC mixes, which resulted in denser microstructure, thereby resulting in availability of lower amount of chloride ions in the electrolytic pore solution of fly ash-GGBS based GPC mixes. This observation is in line with the results obtained from compressive strength as evident from Fig. 7.2 to Fig. 7.5, where chloride admixed fly ash-GGBS based GPC mixes exhibited higher compressive strength than chloride admixed fly ash based GPC mixes. The higher free chloride content in fly ash-GGBS based GPC mix M3: FA85/G15 as compared to fly ash based GPC mix M3: FA100 at the age of 7 and 28 days may be ascribed to the lower extent of competing effect of hydroxyl ions with chloride ions thereby resulting in higher amount of chloride ions in the pore solution.

Further, the total chloride content was mostly lower in fly ash-GGBS based GPC mixes as compared to fly ash based GPC mixes.

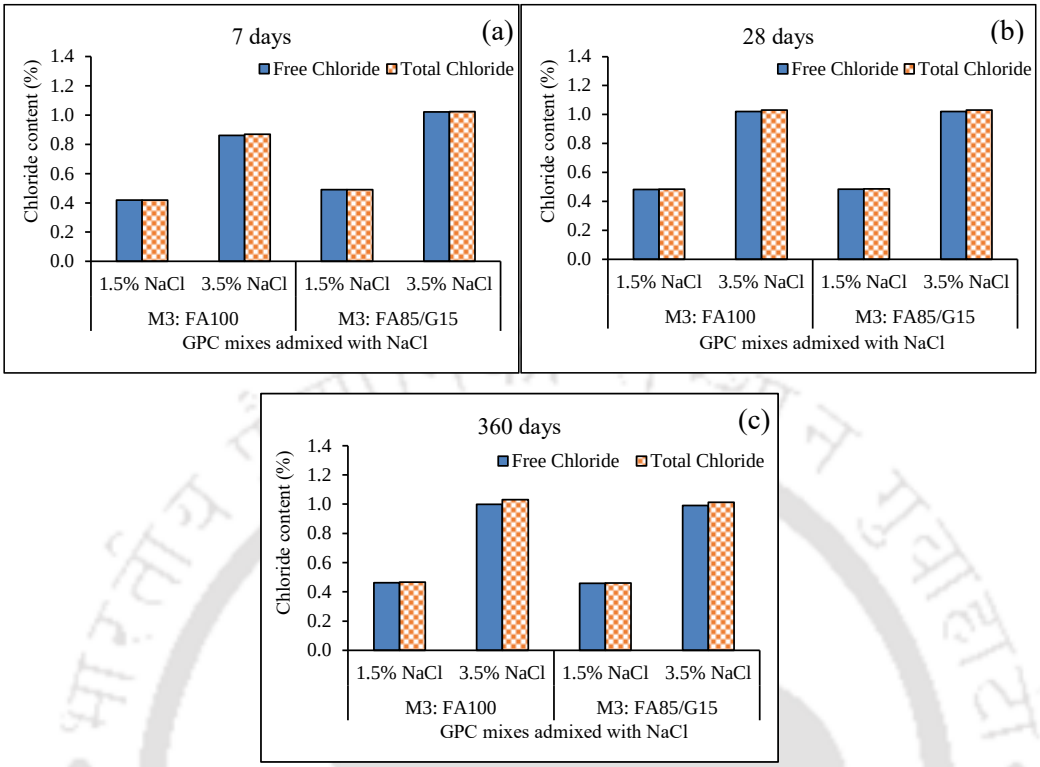

Fig. 7.14 Chloride content (%) of fly ash and fly ash-GGBS based GPC mixes (M3: FA100; FA85/G15) at the age of (a) 7 days, (b) 28 days, and (c) 360 days.

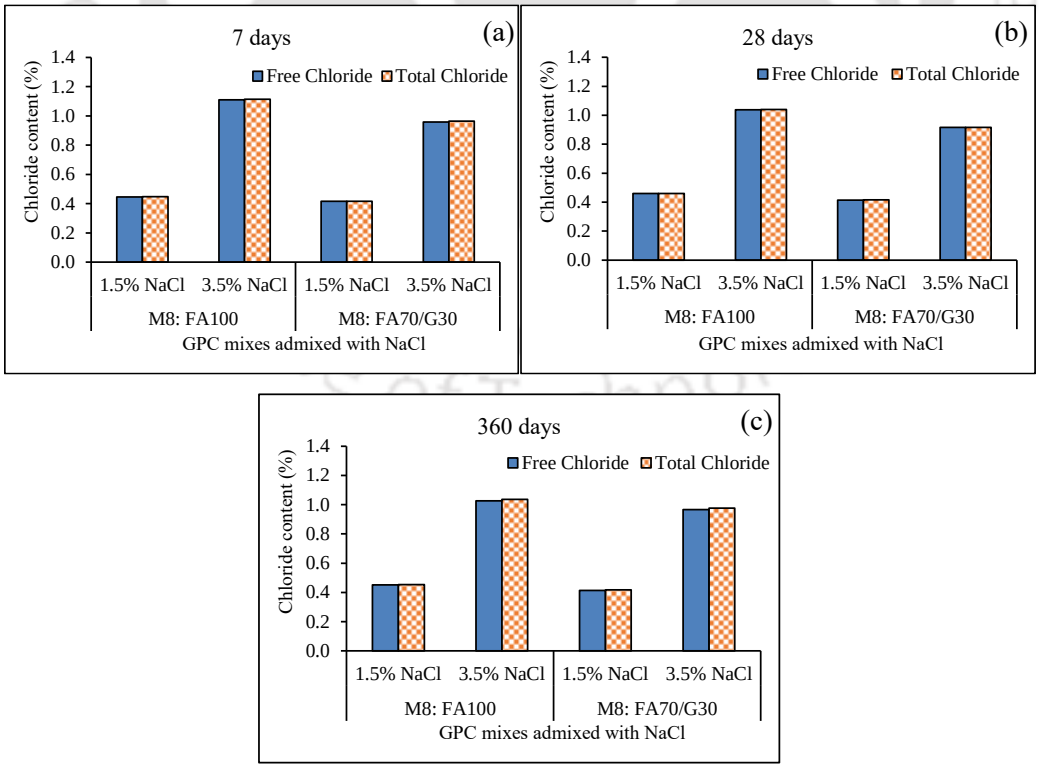

Fig. 7.15 Chloride content (%) of fly ash and fly ash-GGBS based GPC mixes (M8: FA100; FA70/G30) at the age of (a) 7 days, (b) 28 days, and (c) 360 days.

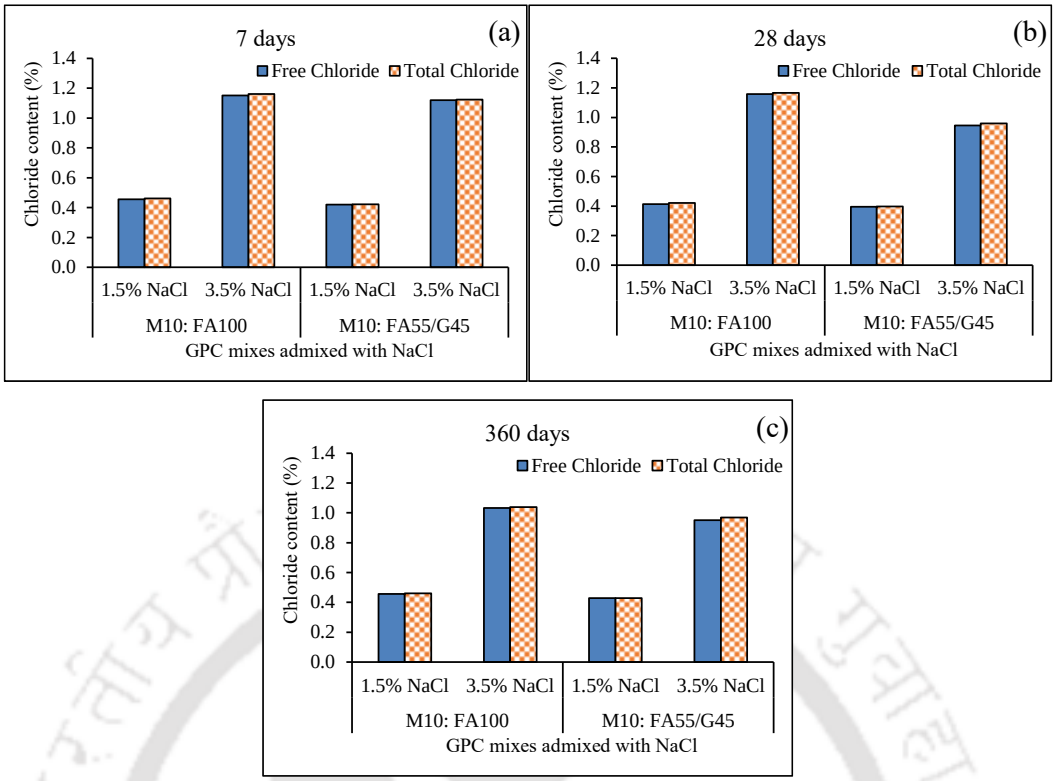

Fig. 7.16 Chloride content (%) of fly ash and fly ash-GGBS based GPC mixes (M10: FA100; FA55/G45) at the age of (a) 7 days, (b) 28 days, and (c) 360 days.

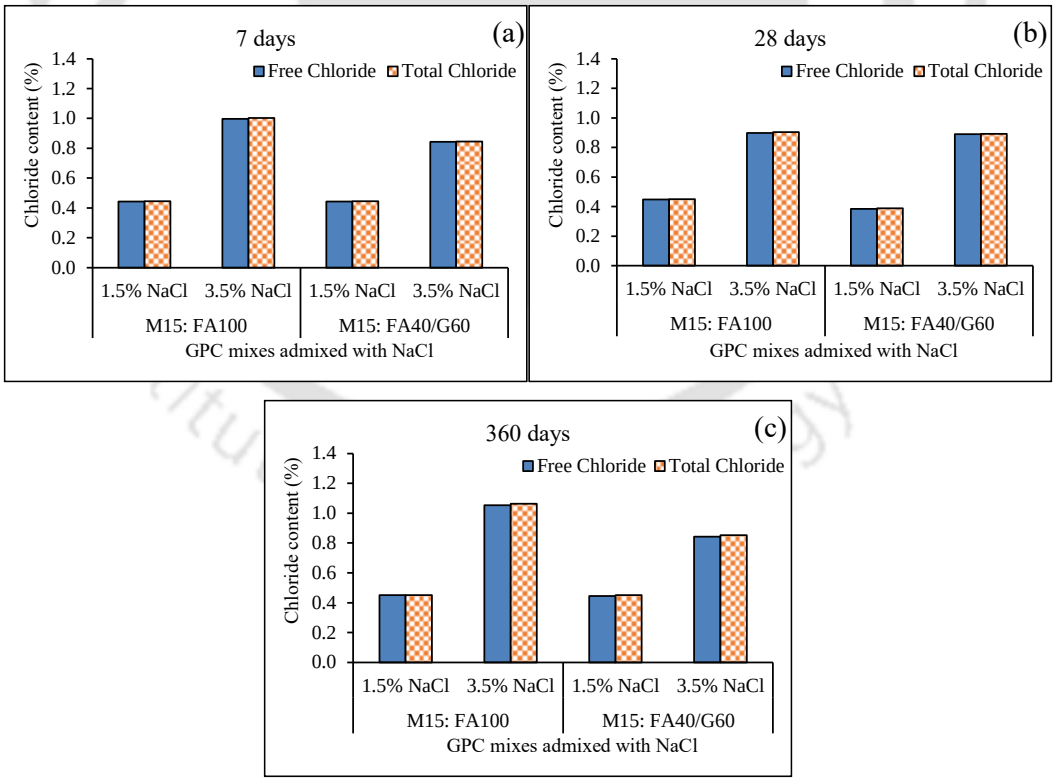

Fig. 7.17 Chloride content (%) of fly ash and fly ash-GGBS based GPC mixes (M15: FA100; FA40/G60) at the age of (a) 7 days, (b) 28 days, and (c) 360 days.

While comparing the effect of GGBS replacement level on chloride content of GPC mixes at various ages, it is observed that the free chloride content of GPC mixes at 7 days varied unsystematically with increase in GGBS replacement level, which may be ascribed to the inconsistent variation between the extent of geopolymerization reaction and the interaction of chloride ions with geopolymer gels at early age. However, the free chloride content of GPC mixes at the age of 28 and 360 days mostly decreased with increase in GGBS replacement level in the mixes. This may be ascribed to the fact that when GGBS content increased in the GPC mixes, the extent of calcium bearing gels (N-(C)-A-S-H, C-S-H) formation increased, which resulted in denser microstructure in the GPC mixes made with higher GGBS content during later age thereby resulting in lower availability of chloride ions in the pore solution. Similarly, there was unsystematic variation in total chloride content with GGBS content in GPC mixes at the age of 7 days, however, the total chloride content mostly decreased with increase in GGBS content in the mixes at the age of 28 and 360 days. From Fig. 7.14 to Fig. 7.17, it is observed that free and total chloride content of fly ash and fly ash-GGBS based GPC mixes increased with increase in admixed NaCl concentration from 1.5% to 3.5%. This may be attributed to the effect of presence of higher amount of chloride ions in the GPC mixes made with higher concentration of NaCl. This can be correlated with the results obtained from compressive strength of chloride admixed GPC mixes (Fig. 7.2 to Fig. 7.5) where the presence of higher amount of chloride hindered the geopolymerization reaction to a greater extent and resulted in lower compressive strength at all ages in the GPC mixes admixed with higher concentration of NaCl. Further, it can be noted that there was unsystematic variation in free and total chloride content of fly ash and fly ash-GGBS based GPC mixes with age (Fig. 7.14 to Fig. 7.17).

Although, the extent of chloride binding was significantly lower in the GPC mixes, the chloride binding capacity of the NaCl added GPC mixes was calculated to evaluate the relative variation in the extent of chloride binding with GGBS content, admixed NaCl concentration and age. The chloride binding capacity of chloride admixed GPC was calculated using the following equation [73];

$$B_c\ (\%) = \frac{(C_t - C_f)}{C_t} \times 100 \qquad (7.1)$$

Where, B_c = chloride binding capacity, C_t = total chloride content, and C_f = free chloride content.

The obtained chloride binding capacity of GPC mixes are illustrated in Fig. 7.18. From this figure, it is observed that the Cl^- binding capacity of fly ash-GGBS based GPC mixes at the age of 7 days were mostly lower than their corresponding fly ash based GPC mixes whereas at the age of 28 and 360 days, the fly ash-GGBS based GPC mixes mostly exhibited higher Cl^- binding capacity as compared to their corresponding fly ash based GPC mixes. The lower extent of chloride binding in fly ash-GGBS based GPC mixes at the age of 7 days may be ascribed to the alteration in the extent of physical adsorption of chloride ions on geopolymer gels during early age, although there was mostly higher formation of geopolymer gels in fly ash-GGBS based GPC mixes as indicated by compressive strength at the early age of 7 days when compared with fly ash based GPC mixes. The higher chloride binding capacity of fly ash-GGBS based GPC mixes at the age of 28 and 360 days may be ascribed to the formation of more amount of calcium bearing aluminosilicate gels (N-(C)-A-S-H) along with C-S-H gel that resulted in more physical adsorption of Cl^- ions [73].

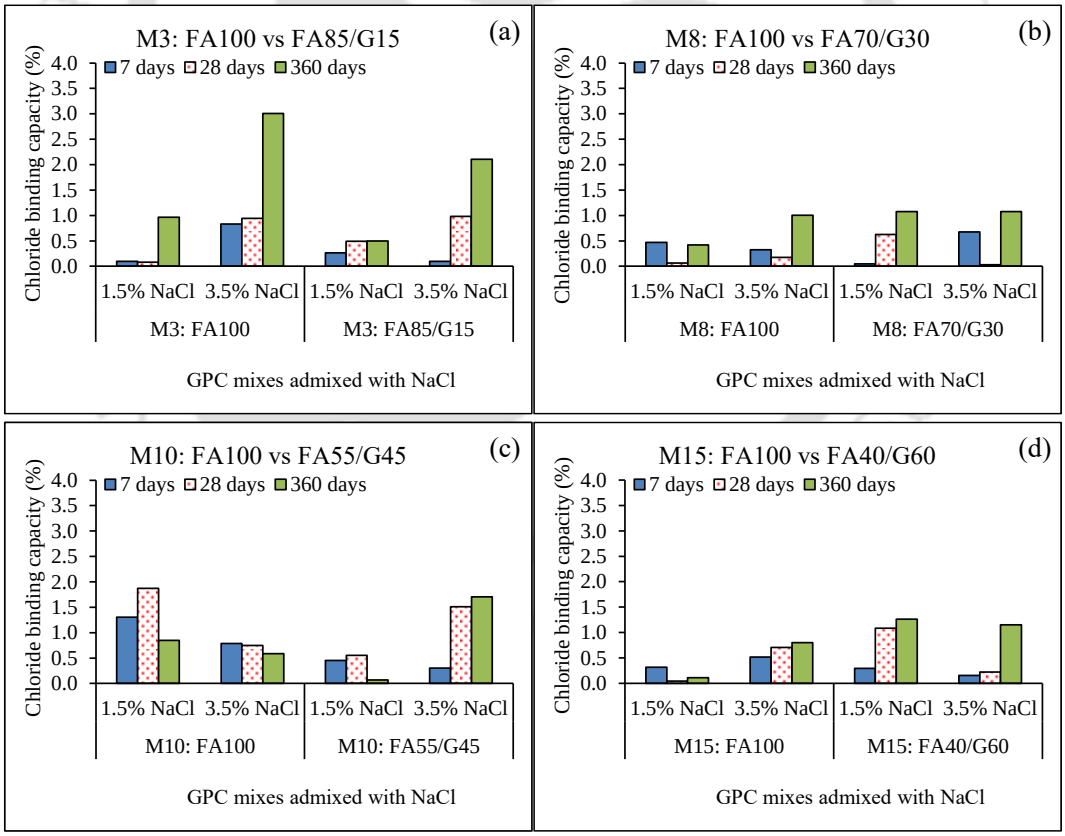

Fig. 7.18 Chloride binding capacity of fly ash and fly ash-GGBS based GPC mixes at different ages: (a) M3: FA100 vs. FA85/G15, (b) M8: FA100 vs. FA70/G30, (c) M10: FA100 vs. FA55/G45, and (d) M15: FA100 vs. FA40/G60.

From Fig. 7.18, it is inferred that there was unsystematic variation in Cl^- binding capacity with increase in GGBS replacement level from 15% to 60% in the fly ash-GGBS based GPC mixes. This can be inferred to the effect of inconsistent variation between free and total chloride content with increase in GGBS content as a result of alterations in the interaction of chloride ions with the binding gels in GPC mixes. Further, the Cl^- binding capacity of fly ash and fly ash-GGBS based GPC mixes varied unsystematically with NaCl concentration (Fig. 7.18). This may be ascribed to the effect of variations in the physical adsorption of chloride ions with geopolymer gels at different NaCl concentrations. There was mostly unsystematic variation in chloride binding capacity of fly ash based GPC mixes with age. However, the chloride binding capacity of fly ash-GGBS based GPC mixes mostly increased with age. The formation of higher amount of binding gels in fly ash-GGBS based GPC mixes may be responsible for higher Cl^- binding capacity at later ages.

7.5.2 Chloride content of GPC at rebar level

The results obtained from chloride content (%) measurement of GPC powder near steel bar embedded in cylindrical fly ash and fly ash-GGBS based GPC specimens at the age of 600 days are depicted in Fig. 7.19. As observed from this figure, there is no significant difference between free and total chloride content of both fly ash and fly ash-GGBS based GPC mixes. This indicates chloride binding ability of GPC mixes to a significantly lower extent, which resulted in availability of higher amount of free chloride in the pore solution of NaCl admixed GPC mixes. This led to more negative E_{corr} (Fig. 7.6 to Fig. 7.9) and higher I_{corr} values (Fig. 7.10 to Fig. 7.13) of steel bar embedded in NaCl admixed fly ash and fly ash-GGBS based GPC specimens. From Fig. 7.19, it is also noted that the fly ash-GGBS based GPC mixes exhibited lower free chloride content as compared to their corresponding fly ash based GPC mixes at both NaCl concentrations. This is attributed to the effect of availability comparatively lower amount of chloride ions near rebar level due to formation of compacted microstructure in fly ash-GGBS based GPC mixes, which led to mostly less negative E_{corr} values (Fig. 7.6 to Fig. 7.9) and lower I_{corr} values (Fig. 7.10 to Fig. 7.13) in NaCl added fly ash-GGBS based GPC specimens as compared to NaCl added fly ash based GPC specimens. The total chloride content was also lower in NaCl admixed fly ash-GGBS based GPC mixes as compared to their corresponding fly ash based GPC mixes. From Fig. 7.19, it is observed that the free chloride content near steel reinforcement in fly ash-GGBS based GPC specimens mostly decreased with increase in GGBS content in the mixes. This result is in line with the results obtained from corrosion potential (Fig.

7.6 (b), Fig. 7.7 (b), Fig. 7.8 (b), Fig. 7.9 (b)) and corrosion current density (Fig. 7.10 (b), Fig. 7.11 (b), Fig. 7.12 (b), Fig. 7.13 (b)), where the rebar embedded in fly ash-GGBS based GPC specimens mostly exhibited less negative E_{corr} and lower I_{corr} values with increase in GGBS content in the GPC mixes. The total chloride content near steel reinforcement in fly ash-GGBS based GPC specimens mostly decreased with increase in GGBS content. Further, the measured free and total chloride content near rebar level of fly ash and fly ash-GGBS based GPC specimens increased with NaCl concentration. This is in line with the variations in E_{corr} and I_{corr} of steel reinforcement with increase in NaCl concentration in the GPC mixes (Fig. 7.10 to Fig. 7.13).

The Cl^- binding capacity of GPC mixes calculated using equation 7.1 are illustrated in Fig. 7.20. The fly ash-GGBS based GPC mixes mostly showed higher Cl^- binding capacity at rebar level as compared to their corresponding fly ash based GPC mixes. In addition, the Cl^- binding capacity at rebar level of fly ash-GGBS based GPC mixes mostly increased as the GGBS replacement increased from 15% to 60% in the mixes. This can be attributed to the effect of formation of higher amount of calcium bearing aluminosilicate gels and C-S-H gel in fly ash-GGBS based GPC mixes with higher GGBS content that led to more physical adsorption of chloride ions at rebar level in GPC specimens. The Cl^- binding capacity at rebar level of fly ash-GGBS based GPC specimens made with comparatively lower GGBS content (M3: FA85/G15 and M8: FA70/G30), and all fly ash based GPC specimens mostly decreased with increase in NaCl concentration. However, the Cl^- binding capacity at rebar level of fly ash-GGBS based GPC specimens made with comparatively higher GGBS content (M10: FA55/G45 and M15: FA40/G60) increased with NaCl concentration. The lower Cl^- binding capacity of fly ash based GPC mixes, and fly ash-GGBS based GPC mixes made with comparatively lower GGBS content can be attributed to the formation of lower amount of N-A-S-H and N-(C)-A-S-H gels, and C-S-H gel (in case of fly ash-GGBS based GPC mixes) at higher concentration of NaCl (3.5%) that resulted in physical adsorption of chloride ions on binding gels to a lower extent. It may be noted that, as stated earlier, the increase in concentration of admixed NaCl reduced the compressive strength of all GPC mixes at the age of 7, 28 and 360 days (Fig. 7.2 to Fig. 7.5). In fly ash-GGBS based GPC mixes made with comparatively higher GGBS content, the more chloride binding capacity at higher NaCl concentration may be attributed to the effect of physical adsorption of chloride ions on the binding gels to a comparatively higher extent in the presence of higher amount of chloride ions although there might be formation

of comparatively lower amount of binding gels in the presence of higher NaCl concentration. This indicates the dominant effect of higher calcium content of GGBS that might have favoured comparatively higher extent of physical adsorption of chloride ions.

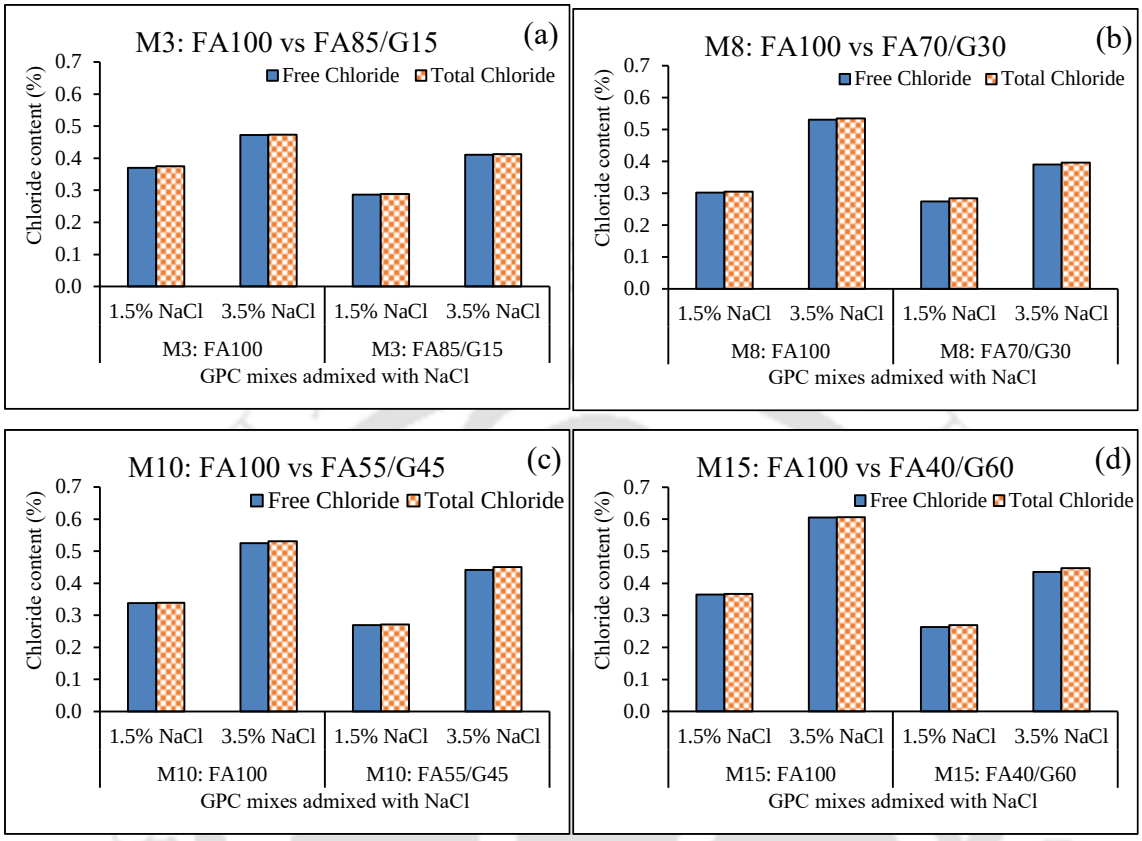

Fig. 7.19 Chloride content (%) at rebar level of fly ash and fly ash-GGBS based GPC specimens: (a) M3, (b) M8, (c) M10, and (d) M15.

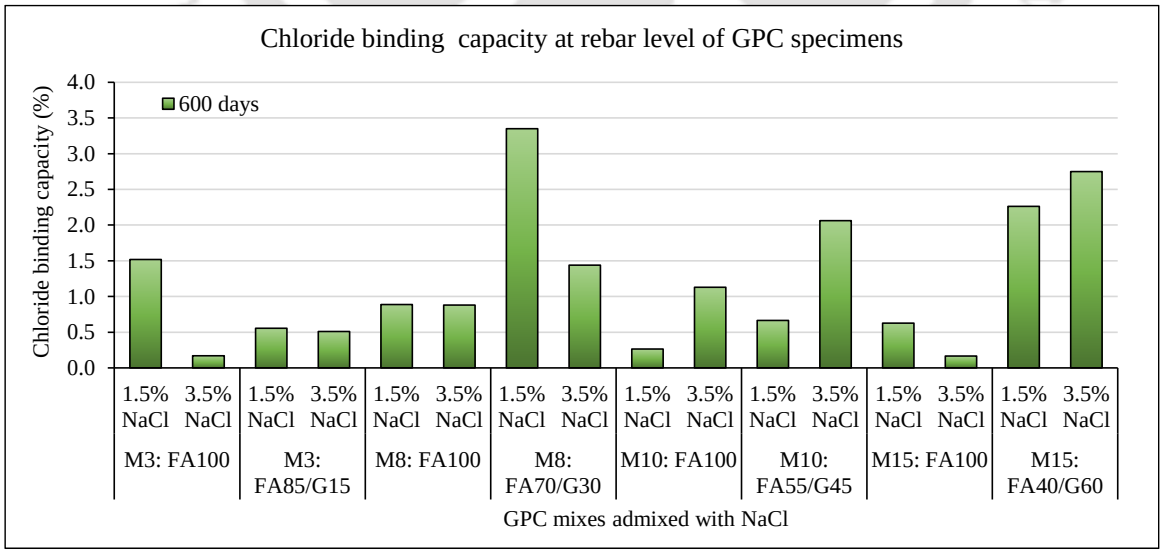

Fig. 7.20 Chloride binding capacity at rebar level of fly ash and fly ash-GGBS based GPC specimens.

7.6 Microstructure analysis of geopolymer concrete (GPC) mixes

7.6.1 XRD analysis of GPC mixes

7.6.1.1 XRD analysis of GPC mixes at different ages

The XRD patterns of control and NaCl admixed fly ash and fly ash-GGBS based GPC mixes at the age of 7, 28, and 360 days are illustrated in Fig. 7.21 to Fig. 7.28. From the XRD patterns of GPC mixes, the crystalline peaks related to quartz and mullite were identified. The amorphous to semi-crystalline phases formed during geopolymerization process in fly ash and fly ash-GGBS based GPC mixes were muscovite ($KAl_3Si_3O_{10}(OH)_2$) at 8.8° 2θ, sodalite ($Na_8Al_6Si_6O_{24}(OH)_2(H_2O)_2$) at 24.5° 2θ, nepheline ($NaAlSiO_4$) at 27.1° 2θ, anorthoclase ($(Na_{0.85}K_{0.15})(AlSi_3O_8)$) at 27.5° 2θ, and albite ((Na, Ca)Al(Si Al)$_3O_8$) at 28.0° 2θ. These compounds indicate the formation of aluminosilicate gels (N-A-S-H and N-(C)-A-S-H), which are mainly responsible for the compressive strength development of GPC mixes. A poorly ordered semi-crystalline peak related to C-S-H gel along with calcite was identified at 29.5º 2θ in the XRD patterns of fly ash-GGBS based GPC mixes. The C-S-H gel is formed due to higher calcium content in GGBS [83,157].

While comparing the XRD patterns of fly ash-GGBS based GPC mixes and their corresponding fly ash based GPC mixes (control and NaCl admixed) at different ages, it is observed that the peak intensity of sodalite, nepheline, anorthoclase and albite were mostly lower in the GPC mix M3: FA85/G15 as compared to its corresponding fly ash based GPC mix (M3: FA100). The peak intensity of albite in GPC mix M8: FA70/G30 was mostly higher as compared to its corresponding fly ash based GPC mix (M8: FA100). In case of GPC mixes M10: FA55/G45 and M15: FA40/G60, the peak intensity of anorthoclase and albite were mostly higher as compared to their corresponding fly ash based GPC mixes (M10: FA100 and M15: FA100). The formation of C-S-H gel along with formation of more amount of geopolymer gels (N-A-S-H and N-(C)-A-S-H) in the GPC mixes made with relatively higher GGBS replacement (30%, 45%, and 60%) exhibited higher compressive strength as compared to their corresponding fly ash based GPC mixes as evident from Fig. 7.3 to Fig. 7.5. In case of GPC mix made with 15% GGBS (M3: FA85/G15), the formation of C-S-H gel may be the primary cause for higher compressive strength at the age of 28 and 360 days when compared with its corresponding fly ash based GPC mix as evident from Fig. 7.2. It may be noted that the 7 day compressive strength of fly ash-GGBS based GPC mix M3: FA85/G15 was lower as compared to its corresponding fly ash based GPC mix M3: FA100 (Fig. 7.2).

From Fig. 7.22, Fig. 7.24, Fig. 7.26, and Fig. 7.28, it is observed that the variations in peak intensity of nepheline, sodalite, anorthoclase and albite were mostly unsystematic, and the peak intensity of C-S-H gel mostly increased with increase in GGBS replacement level in the GPC mixes. The formation of more amount of C-S-H gel in the GPC mixes made with higher GGBS content contributed toward mostly higher compressive strength irrespective of age and admixed NaCl concentration. While comparing the XRD patterns of control and NaCl admixed GPC mixes, It is observed that in case of fly ash-GGBS based GPC mixes such as M3:FA85/G15 (Fig. 7.22), M8: FA70/G30 (Fig. 7.24), and M15: FA40/G60 (Fig. 7.28), and their corresponding fly ash based GPC mixes (Fig. 7.21, Fig. 7.23, Fig. 7.27), there was no systematic variation in the peak intensity related to aluminosilicate gels and C-S-H gel (in fly ash-GGBS based GPC) with increase in admixed NaCl concentration. In case of GPC mix M10: FA100 (Fig. 7.25), it is noted that the peak intensity corresponding to anorthoclase and albite were mostly decreased with increase in admixed NaCl concentration from 0% to 3.5%. However, there was unsystematic variation in peak intensity related to sodalite and nepheline with increase in NaCl concentration. In case of GPC mix M10: FA55/G45 (Fig. 7.26), the peak intensity related to nepheline, anorthoclase, albite, sodalite, and C-S-H gel mostly decreased with increase in NaCl concentration. This indicates formation of lower amount of aluminosilicate gels in NaCl admixed fly ash based GPC mixes, and lower amount of aluminosilicate gels and C-S-H gel in NaCl admixed fly ash-GGBS based GPC mixes, which resulted in lower strength for NaCl admixed GPC mixes in comparison to control GPC mixes as evident from Fig. 7.2 to Fig. 7.5. A semi-crystalline peak related to halite (NaCl) was identified at 31.5º 2θ in the XRD patterns of all NaCl admixed fly ash and fly ash-GGBS based GPC mixes, which indicates the crystallization of sodium chloride in the GPC mixes [34,98].

From Fig. 7.21 to Fig. 7.28, it is observed that in case of fly ash based GPC mixes (control and NaCl admixed), the peak intensity related to albite mostly increased with increase in age. However, the variations in peak intensity related to sodalite, nepheline, and anorthoclase were mostly unsystematic with age. In case of fly ash-GGBS based GPC mixes, the peak intensity of anorthoclase, albite and C-S-H were mostly higher at later age. These observations indicate the formation of higher amount of aluminosilicate gels due to continuation of geopolymerization reaction with age in fly ash and fly ash-GGBS based GPC mixes that resulted in increase in compressive strength with age as evident from Fig. 7.2 to Fig. 7.5.

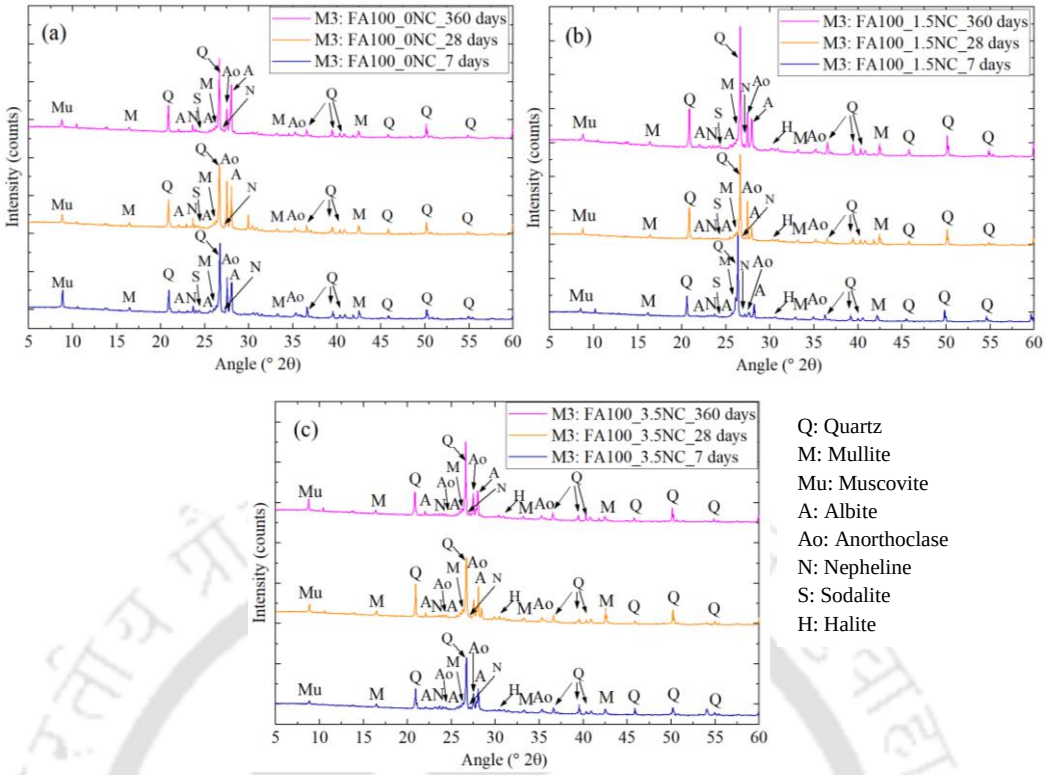

Fig. 7.21 XRD patterns of control and chloride admixed fly ash based GPC mixes (M3: FA100) at 7, 28, and 360 days: (a) 0% NaCl, (b) 1.5% NaCl, and (c) 3.5% NaCl.

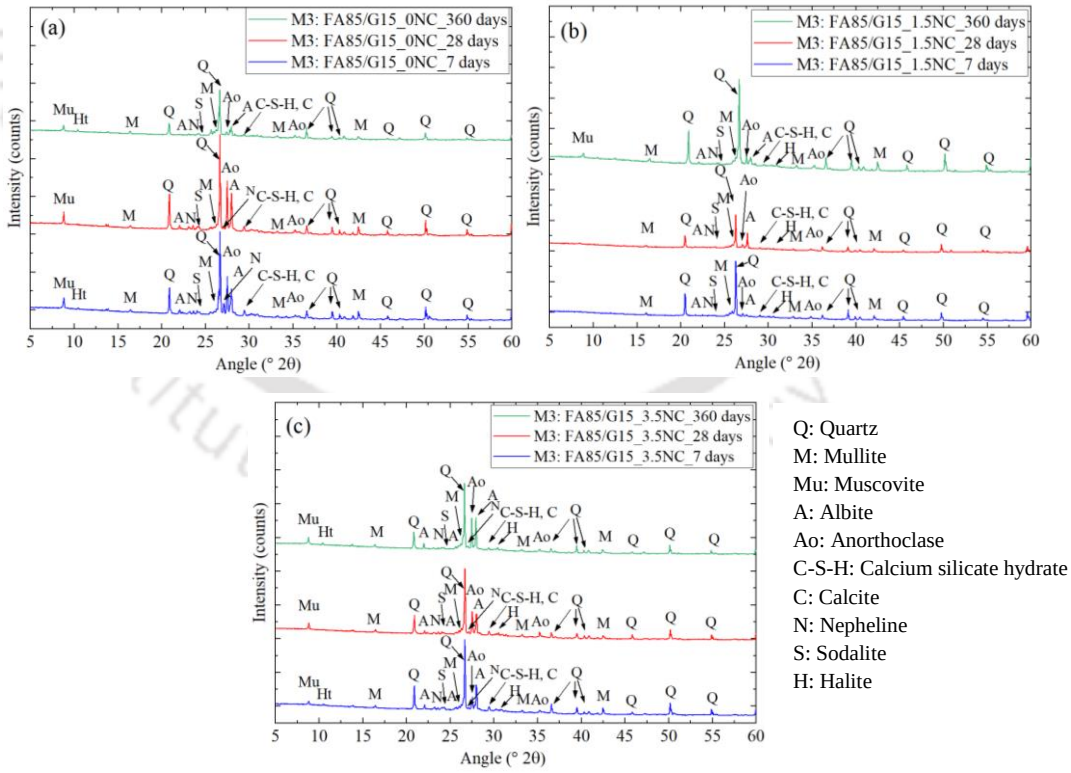

Fig. 7.22 XRD patterns of control and chloride admixed fly ash-GGBS based GPC mixes (M3: FA85/G15) at 7, 28, and 360 days: (a) 0% NaCl, (b) 1.5% NaCl, and (c) 3.5% NaCl.

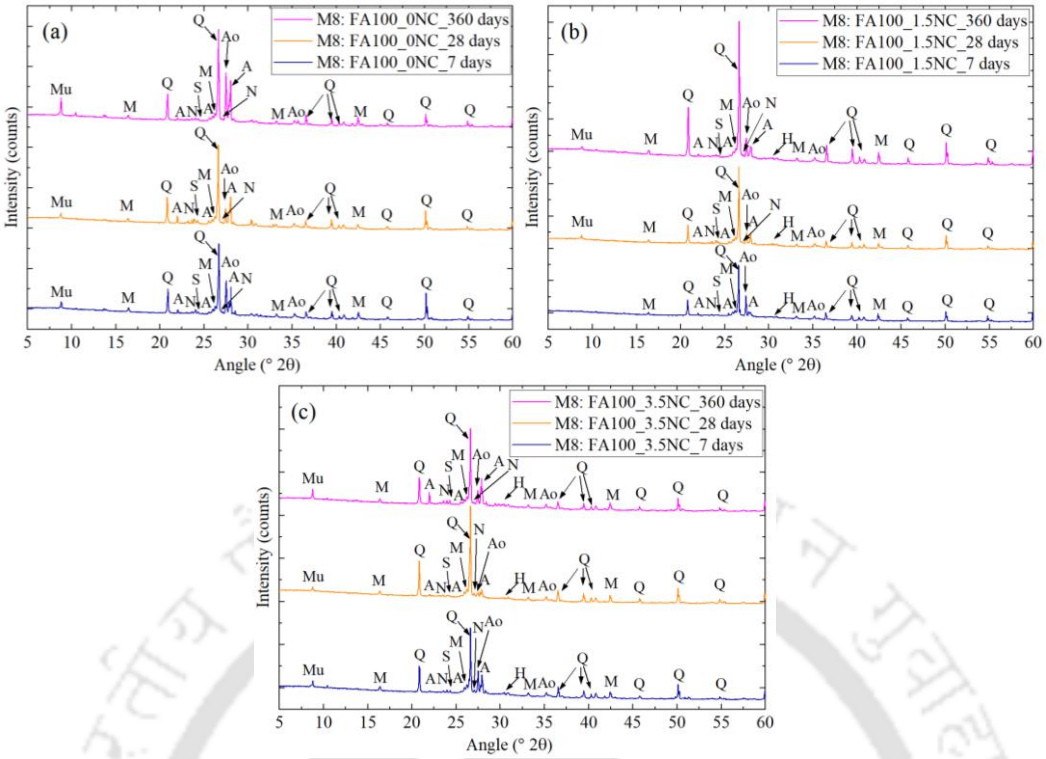

Fig. 7.23 XRD patterns of control and chloride admixed fly ash based GPC mixes (M8: FA100) at 7, 28, and 360 days: (a) 0% NaCl, (b) 1.5% NaCl, and (c) 3.5% NaCl.

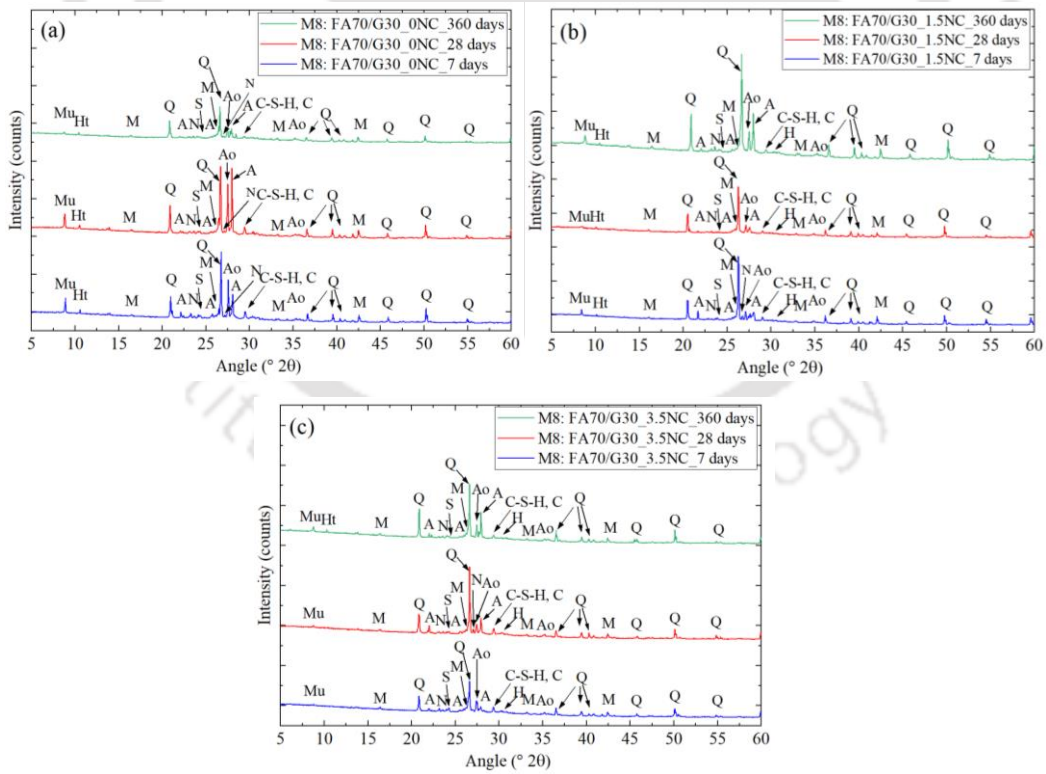

Fig. 7.24 XRD patterns of control and chloride admixed fly ash-GGBS based GPC mixes (M8: FA70/G30) at 7, 28, and 360 days: (a) 0% NaCl, (b) 1.5% NaCl, and (c) 3.5% NaCl.

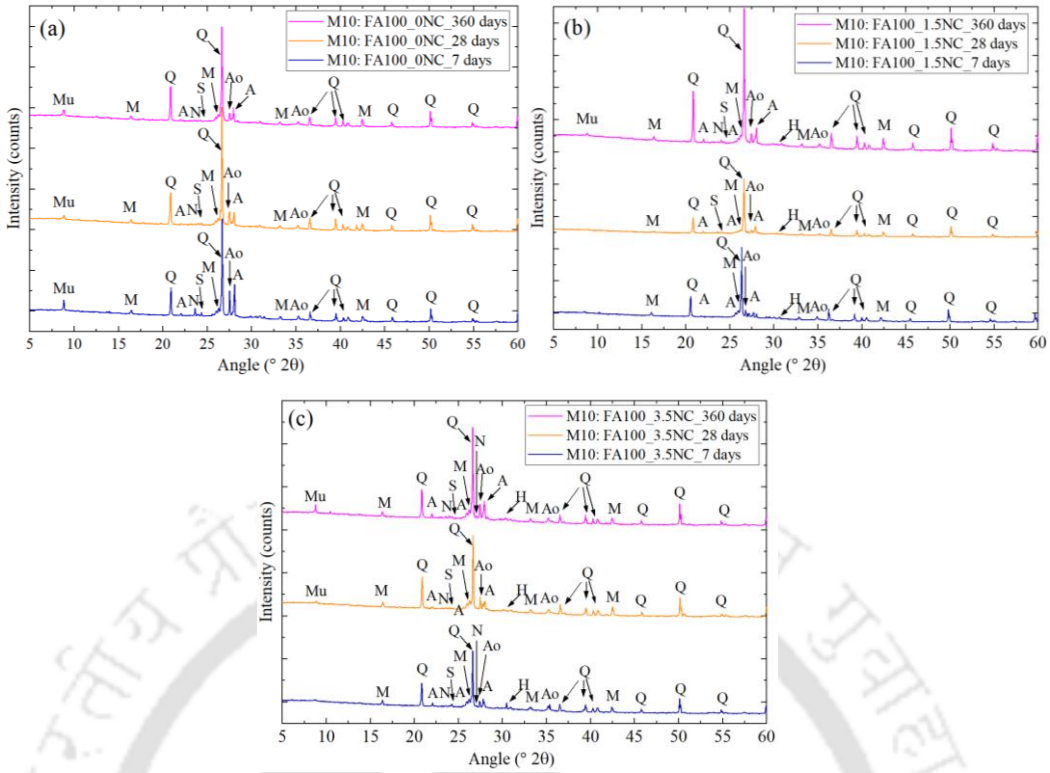

Fig. 7.25 XRD patterns of control and chloride admixed fly ash based GPC mixes (M10: FA100) at 7, 28, and 360 days: (a) 0% NaCl, (b) 1.5% NaCl, and (c) 3.5% NaCl.

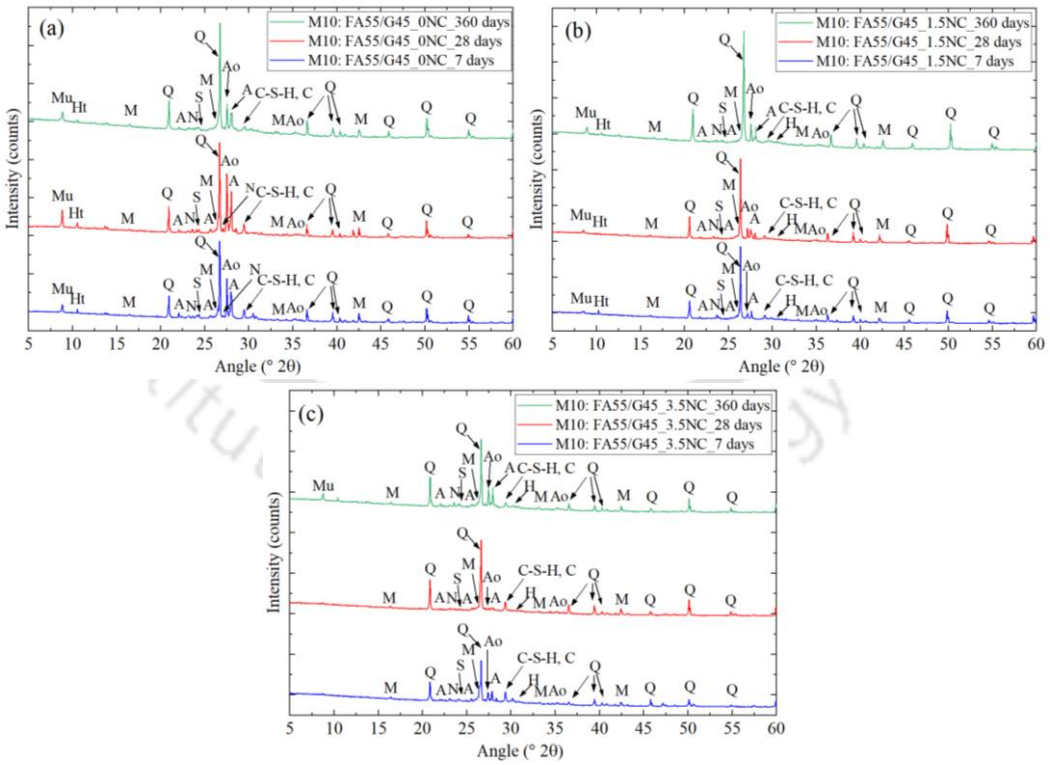

Fig. 7.26 XRD patterns of control and chloride admixed fly ash-GGBS based GPC mixes (M10: FA55/G45) at 7, 28, and 360 days: (a) 0% NaCl, (b) 1.5% NaCl, and (c) 3.5% NaCl.

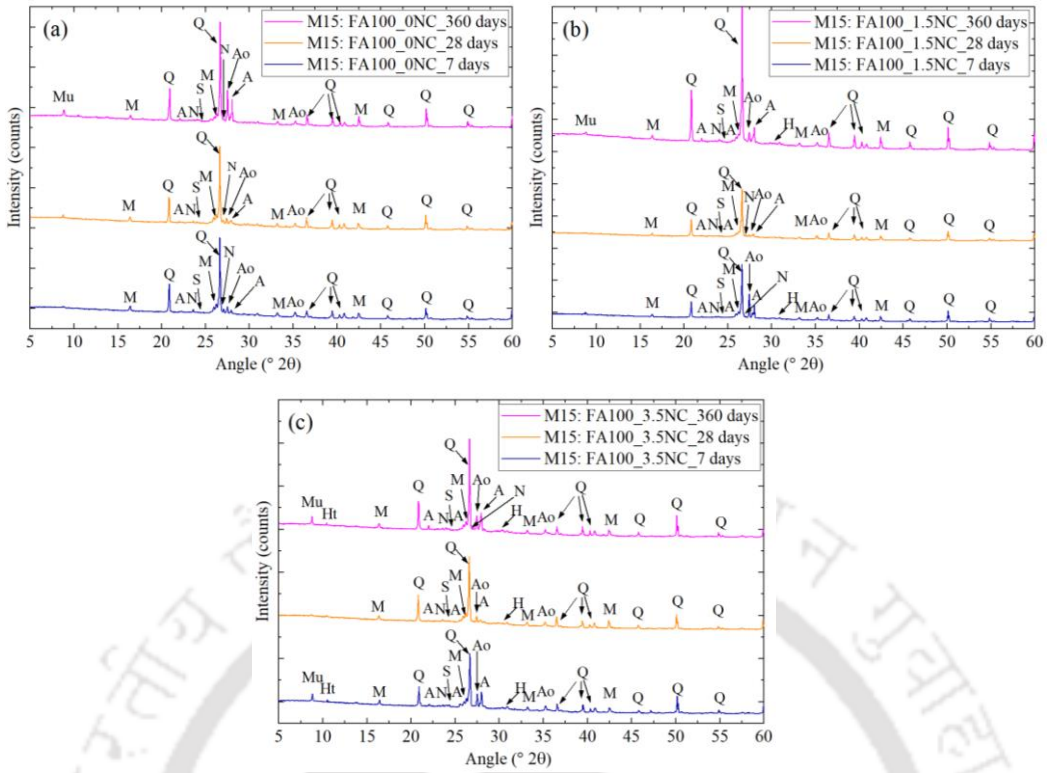

Fig. 7.27 XRD patterns of control and chloride admixed fly ash based GPC mixes (M15: FA100) at 7, 28, and 360 days: (a) 0% NaCl, (b) 1.5% NaCl, and (c) 3.5% NaCl.

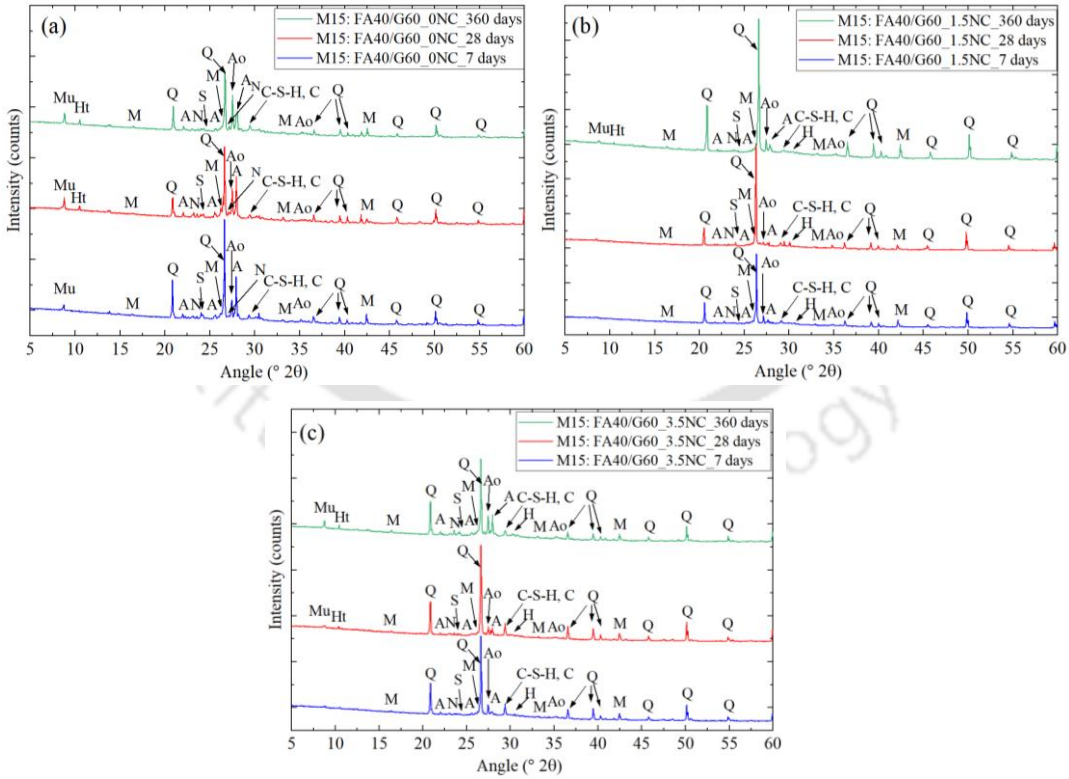

Fig. 7.28 XRD patterns of control and chloride admixed fly ash-GGBS based GPC mixes (M15: FA40/G60) at 7, 28, and 360 days: (a) 0% NaCl, (b) 1.5% NaCl, and (c) 3.5% NaCl.

7.6.1.2 XRD analysis of GPC at rebar level of cylindrical reinforced specimens

The XRD patterns of GPC powder collected from near the rebar level of cylindrical fly ash and fly ash-GGBS based GPC specimens at the age of 600 days are presented in Fig. 7.29 to Fig. 7.32. From these figures, it is observed that the peak intensity of sodalite, nepheline, anorthoclase, and albite were mostly higher in control and NaCl admixed fly ash-GGBS based GPC mixes (M3: FA85/G15, M8: FA70/G30, M10: FA55/G45, and M15: FA40/G60) as compared to their corresponding fly ash based GPC mixes (M3: FA100, M8: FA100, M10: FA100, and M15: FA100). Further, the peak related to formation of C-S-H gel was observed in the XRD patterns of all fly ash-GGBS based GPC mixes. These resulted in denser microstructure in fly ash-GGBS based GPC mixes that led to availability of lower amount of chloride ions near embedded rebar (Fig. 7.19). Thus, fly ash-GGBS based GPC specimens exhibited mostly less negative corrosion potential (E_{corr}) and lower corrosion current density (I_{corr}) as compared to fly ash based GPC specimens (Fig. 7.6 to Fig. 7.13). From Fig. 7.29 to Fig. 7.32, it is observed that the variations in peak intensity of sodalite, nepheline, anorthoclase, albite, and C-S-H gel were mostly unsystematic with increase in GGBS replacement level in the mixes. In few GPC mixes (M3: FA85/G15, M8: FA100, and M8: FA70/G30), there was no systematic variation in the peak intensity related to aluminosilicate gels with increase in concentration of admixed NaCl. However, in majority of the GPC mixes (M3: FA100, M10: FA100, M10: FA55/G45, M15: FA100, and M15: FA40/G60), the peak intensity related to sodalite, nepheline, anorthoclase, albite and C-S-H gel (in case of fly ash-GGBS based GPC) mostly decreased with increase in NaCl concentration. Therefore, the embedded steel bar in fly ash and fly ash-GGBS based GPC specimens mostly exhibited more negative E_{corr} and higher I_{corr} values with increase in concentration of NaCl (Fig. 7.6 to Fig. 7.13) as a result of presence of more amount of chloride ions near rebar level due to formation of less denser microstructure in the GPC mixes.

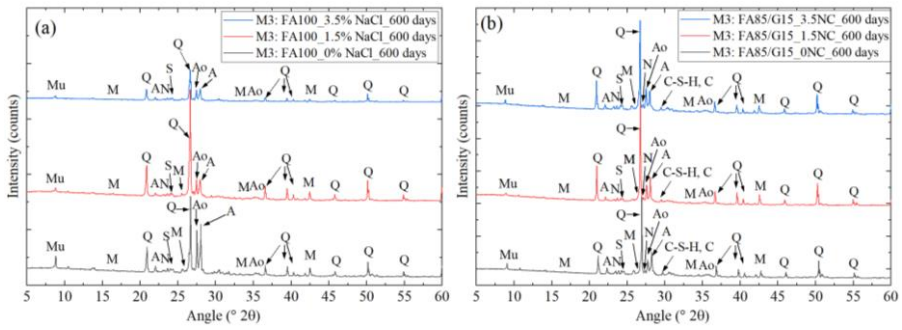

Fig. 7.29 XRD patterns obtained at rebar level of control and chloride admixed fly ash and fly ash-GGBS based GPC specimens: (a) M3: FA100 and (b) M3: FA85/G15.

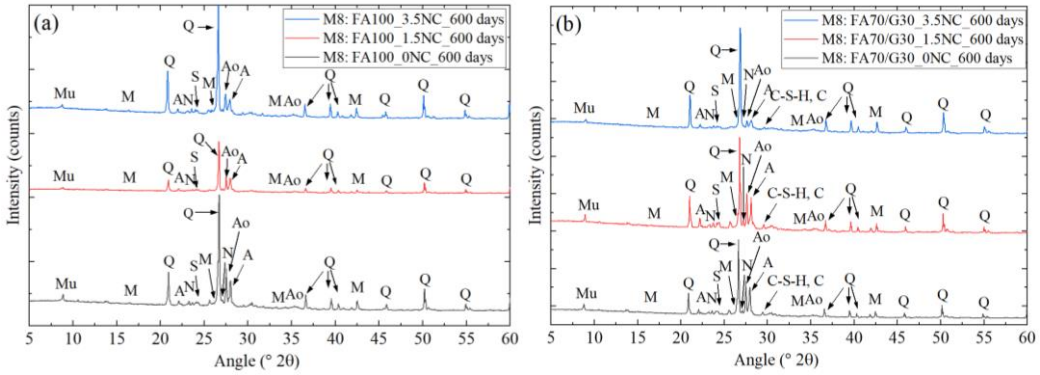

Fig. 7.30 XRD patterns obtained at rebar level of control and chloride admixed fly ash and fly ash-GGBS based GPC specimens: (a) M8: FA100 and (b) M8: FA70/G30.

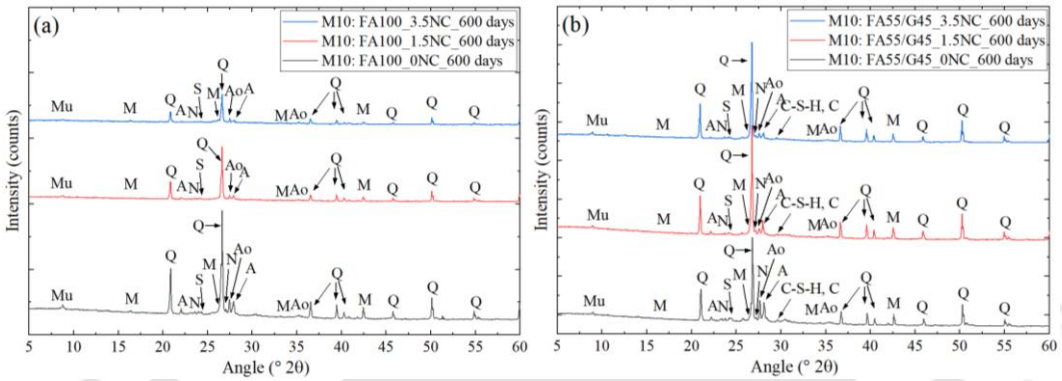

Fig. 7.31 XRD patterns obtained at rebar level of control and chloride admixed fly ash and fly ash-GGBS based GPC specimens: (a) M10: FA100 and (b) M10: FA55/G45.

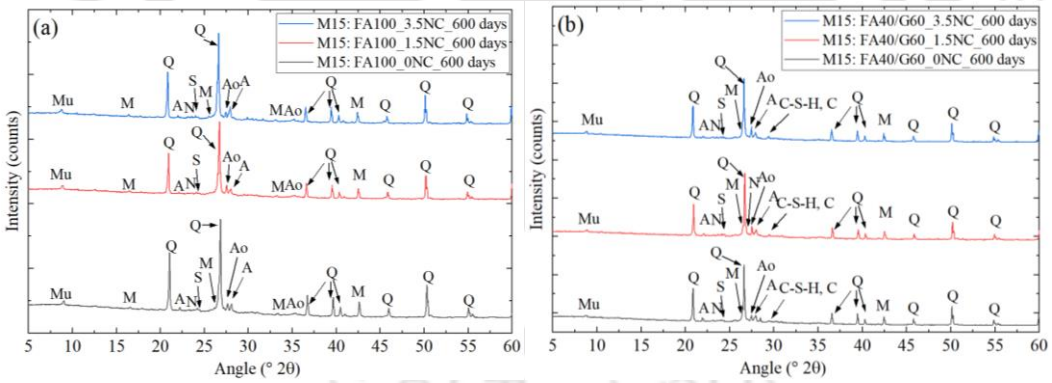

Fig. 7.32 XRD patterns obtained at rebar level of control and chloride admixed fly ash and fly ash-GGBS based GPC specimens: (a) M15: FA100 and (b) M15: FA40/G60.

7.6.2 EDS analysis of GPC mixes

7.6.2.1 EDS analysis of GPC mixes at different ages

Typical EDS spectra of control and chloride admixed fly ash and fly ash-GGBS based GPC mixes at the age of 7, 28, and 360 days are illustrated in Fig. 7.33 to Fig. 7.37 and Fig. B1 to B8 (in Appendix section). From these figures, the main elements identified are O, Si, Al, Ca, and Na. The elemental ratios such as atomic Na/Si, Al/Si, and Ca/Si ratios (average of five locations) of different fly ash and fly ash-GGBS based GPC mixes are depicted in Fig.

7.38 to Fig. 7.45. As observed from these figures, in case of fly ash based GPC mixes (control and NaCl admixed), the average atomic Na/Si, Al/Si, and Ca/Si ratios obtained are in the range of 0.18 - 0.44, 0.16 - 0.64, and 0.01 - 0.15 respectively. Similarly, in case of fly ash-GGBS based GPC mixes, the average atomic Na/Si, Al/Si, and Ca/Si ratios obtained are in the range of 0.13 - 0.56, 0.25 - 0.57, and 0.01 - 0.78 respectively. While comparing the average atomic ratios obtained from fly ash-GGBS based GPC mixes (M3, M8, M10, and M15) and their corresponding fly ash based GPC mixes, it is observed that GPC mixes made with 15% GGBS (M3) and 60% GGBS (M15) mostly exhibited higher atomic Na/Si ratio, and GPC mixes made with 30% GGBS (M8) and 45% GGBS (M10) mostly showed lower atomic Na/Si ratio as compared to their corresponding fly ash based GPC mixes. Similarly, the GPC mixes made with 15% GGBS (M3) and 30% GGBS (M8) mostly exhibited higher atomic Al/Si ratio, and GPC mixes made with 45% GGBS (M10) and 60% GGBS (M15) mostly showed lower atomic Al/Si ratio as compared to their corresponding fly ash based GPC mixes. Further, it is observed that all the fly ash-GGBS based GPC mixes exhibited higher atomic Ca/Si ratio as compared to their corresponding fly ash based GPC mixes at all ages, irrespective of admixed NaCl concentration. This indicates that in case of fly ash-GGBS based GPC mixes, the formation of calcium enriched binding gels such as N-(C)-A-S-H (in higher amount) and C-S-H resulted in higher compressive strength of fly ash-GGBS based GPC mixes as compared to their corresponding fly ash based GPC mixes. This observation is in line with the results obtained from XRD analysis, where higher peak intensity of albite (M8, M10, M15) and peak related to C-S-H gel (M3, M8, M10, and M15) were observed in fly ash-GGBS based GPC mixes in comparison to their corresponding fly ash based GPC mixes (Fig. 7.21 to Fig. 7.28).

While analysing the atomic ratios of fly ash-GGBS based GPC mixes, it is observed that the variations in atomic Na/Si, Al/Si, and Ca/Si ratios were unsystematic with increase in GGBS replacement level. In case of fly ash and fly ash-GGBS based GPC mixes, the variations in atomic Na/Si, Al/Si, and Ca/Si ratios were not systematic with increase in NaCl concentration in the mixes. The average atomic % of Cl ions in NaCl admixed fly ash and fly ash-GGBS based GPC mixes varied in the range of 0.26 - 1.0, and 0.20 - 1.40 respectively. This indicates the deposition and crystallization of NaCl in fly ash and fly ash-GGBS based GPC mixes, which might have altered the geopolymerization reaction and caused decrease in strength of NaCl added GPC mixes as evident from Fig. 7.2 to Fig.

7.5. From Fig. 7.38 to Fig. 7.45, there was no systematic variation in atomic ratios of fly ash and fly ash-GGBS based GPC mixes with increase in age.

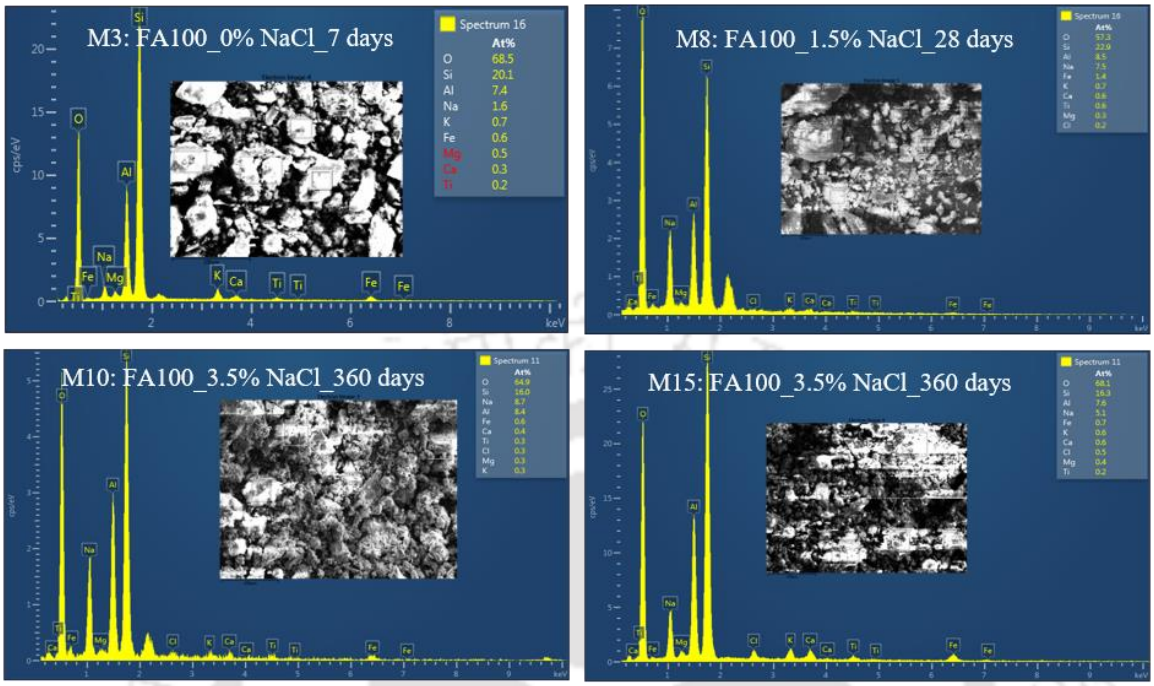

Fig. 7.33 EDS spectra of control and chloride admixed fly ash based GPC mixes at different ages.

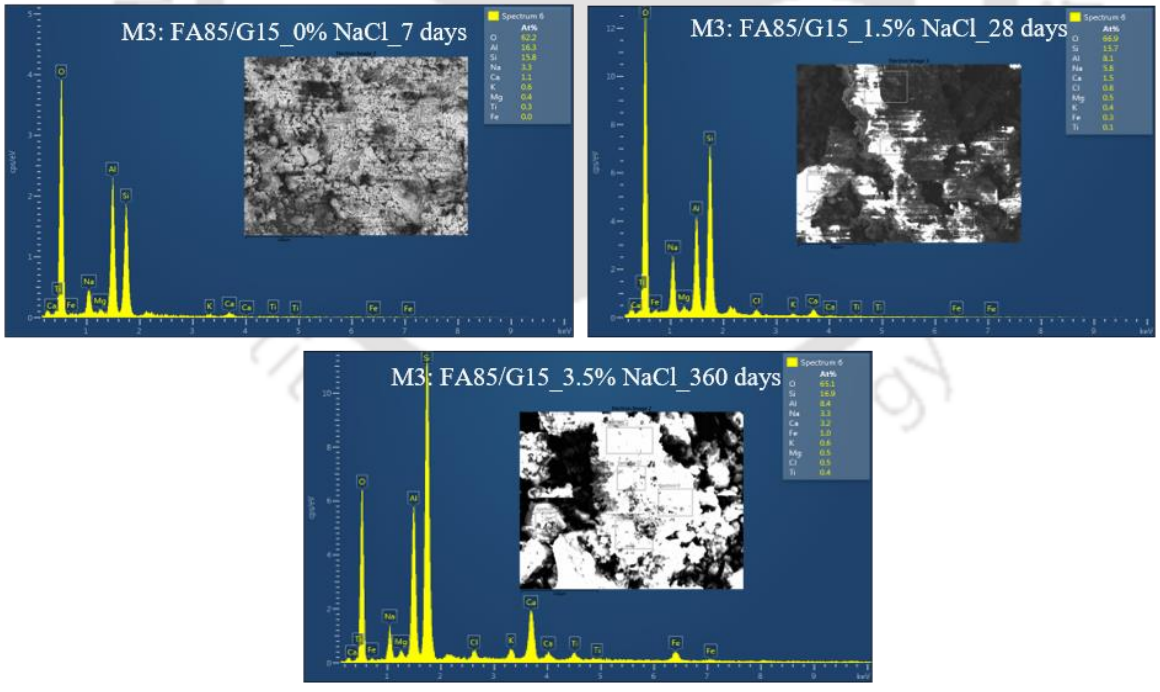

Fig. 7.34 EDS spectra of control and chloride admixed fly ash-GGBS based GPC mixes (M3: FA85/G15) at different ages.

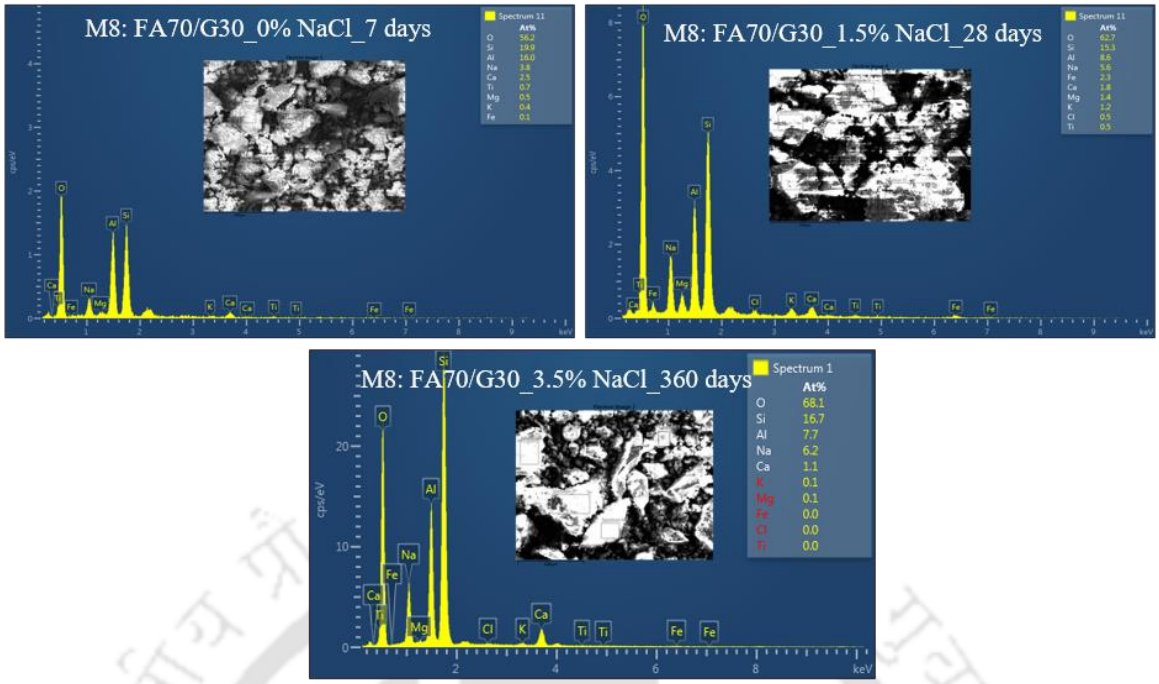

Fig. 7.35 EDS spectra of control and chloride admixed fly ash-GGBS based GPC mixes (M8: FA70/G30) at different ages.

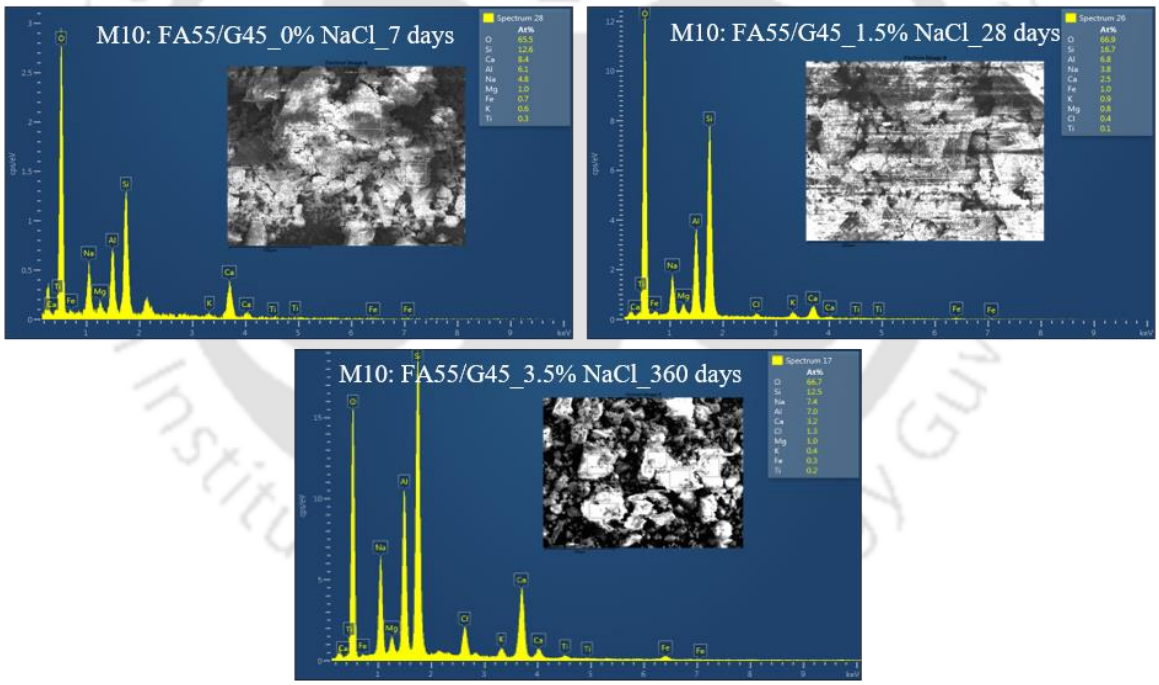

Fig. 7.36 EDS spectra of control and chloride admixed fly ash-GGBS based GPC mixes (M10: FA55/G45) at different ages.

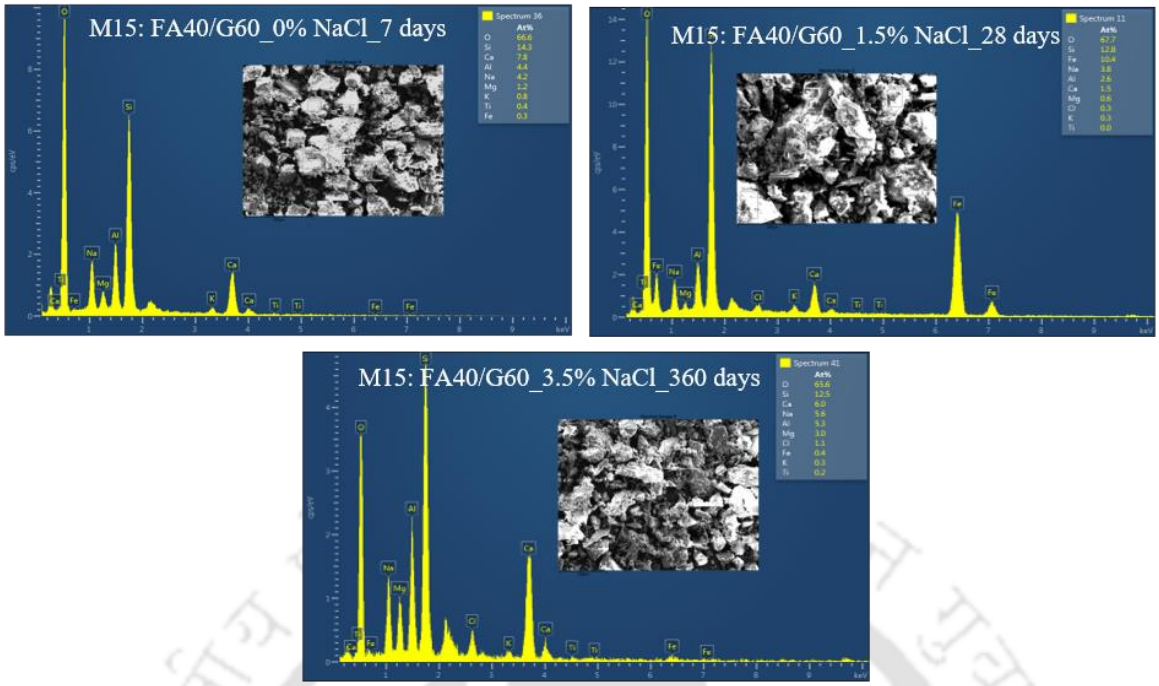

Fig. 7.37 EDS spectra of control and chloride admixed fly ash-GGBS based GPC mixes (M15: FA40/G60) at different ages.

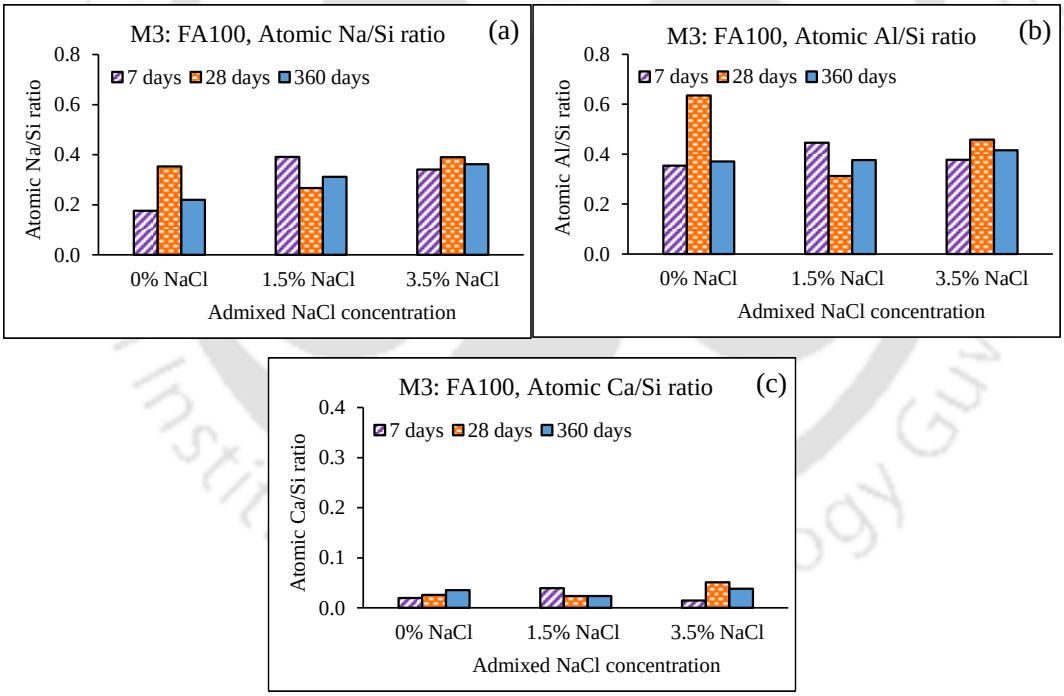

Fig. 7.38 Atomic ratios of control and chloride admixed fly ash based GPC mixes (M3: FA100): (a) atomic Na/Si ratio, (b) atomic Al/Si ratio, and (c) atomic Ca/Si ratio.

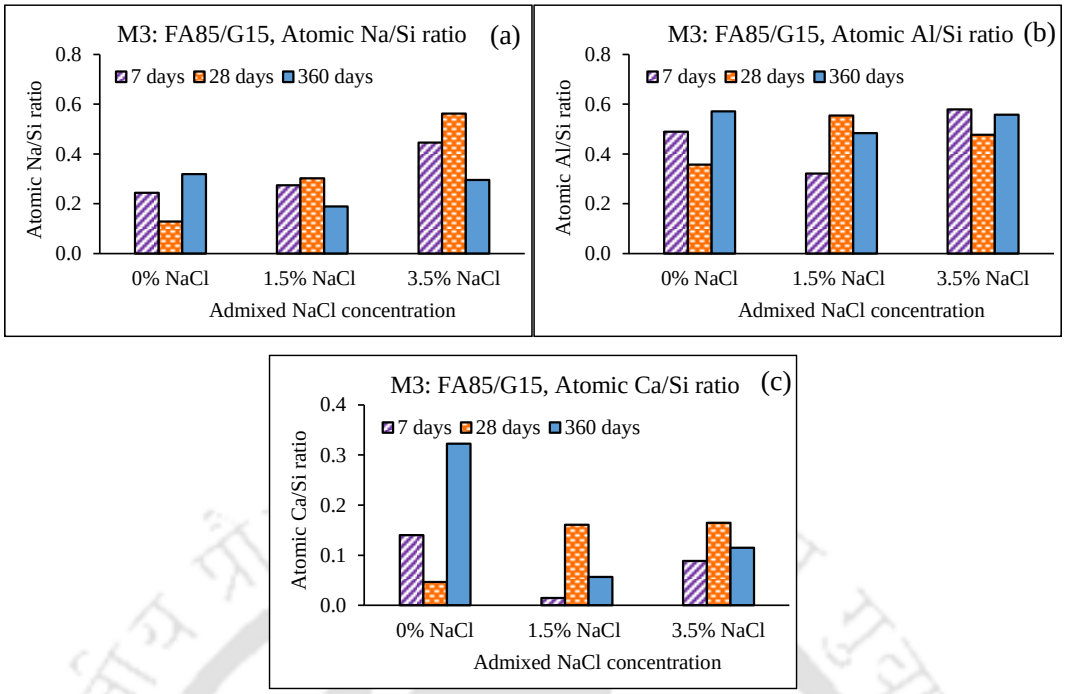

Fig. 7.39 Atomic ratios of control and chloride admixed fly ash-GGBS based GPC mixes (M3: FA85/G15): (a) atomic Na/Si ratio, (b) atomic Al/Si ratio, and (c) atomic Ca/Si ratio.

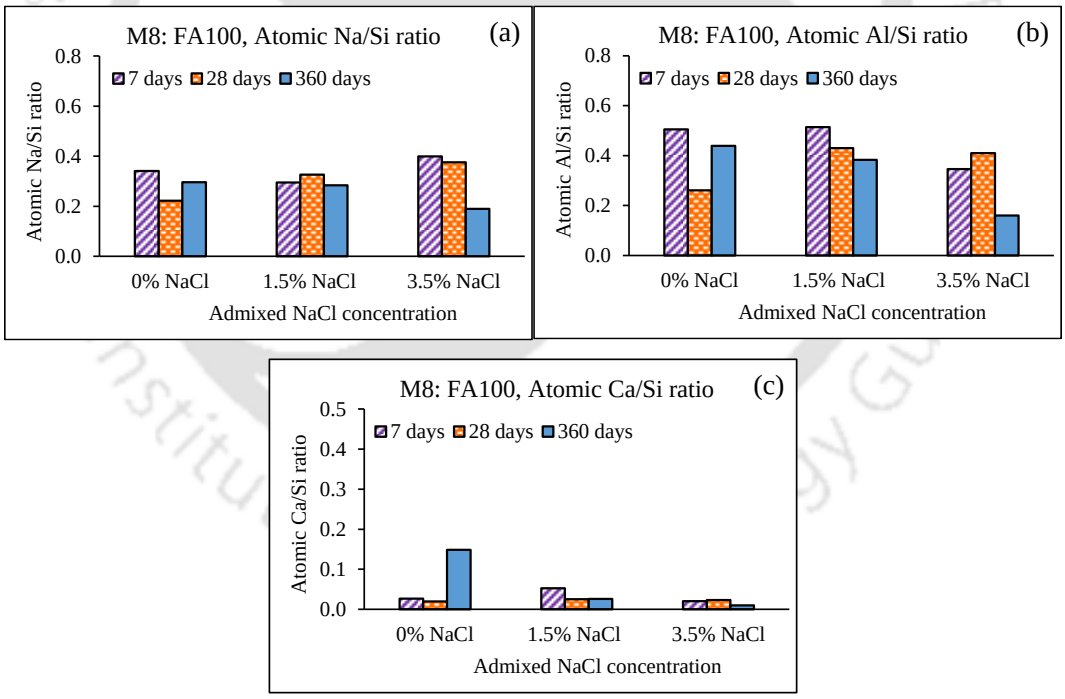

Fig. 7.40 Atomic ratios of control and chloride admixed fly ash based GPC mixes (M8: FA100): (a) atomic Na/Si ratio, (b) atomic Al/Si ratio, and (c) atomic Ca/Si ratio.

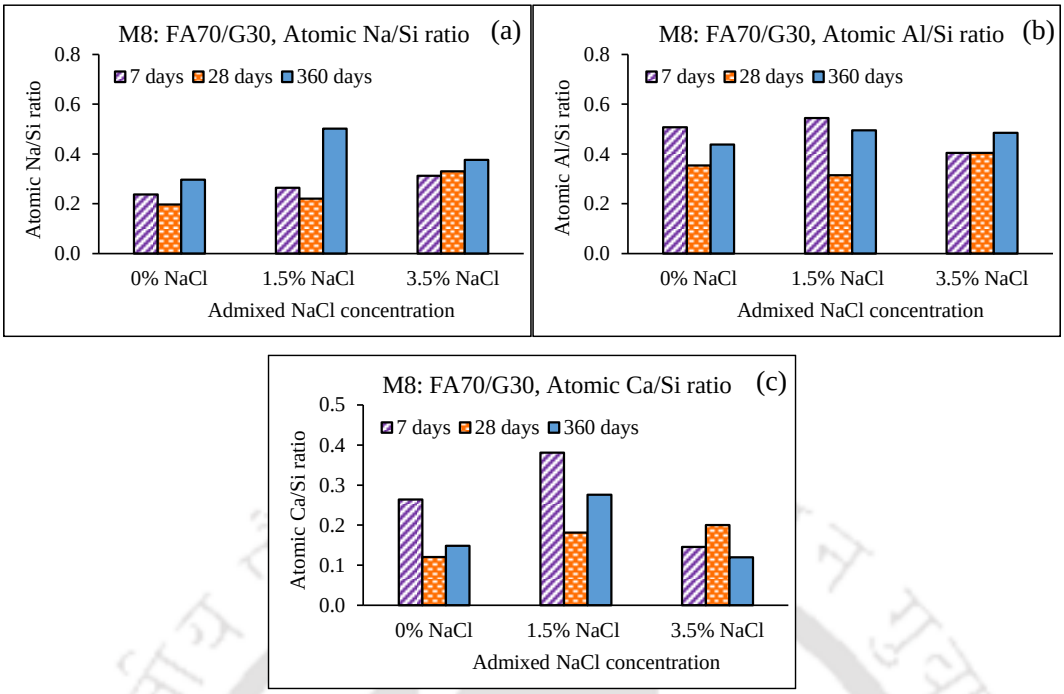

Fig. 7.41 Atomic ratios of control and chloride admixed fly ash-GGBS based GPC mixes (M8: FA70/G30): (a) atomic Na/Si ratio, (b) atomic Al/Si ratio, and (c) atomic Ca/Si ratio.

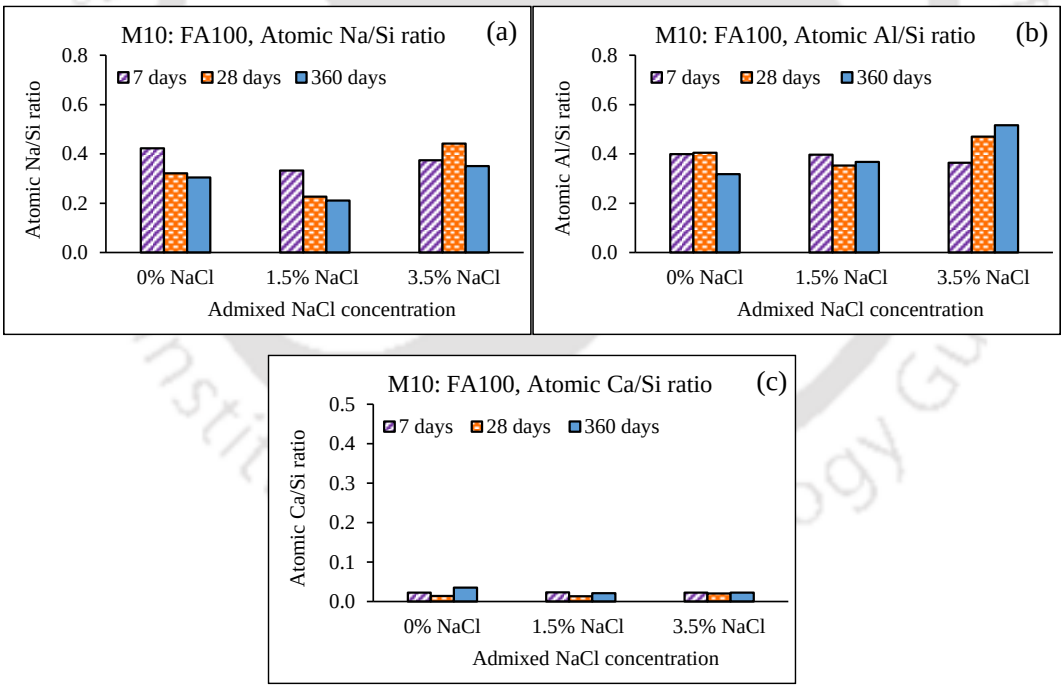

Fig. 7.42 Atomic ratios of control and chloride admixed fly ash based GPC mixes (M10: FA100): (a) atomic Na/Si ratio, (b) atomic Al/Si ratio, and (c) atomic Ca/Si ratio.

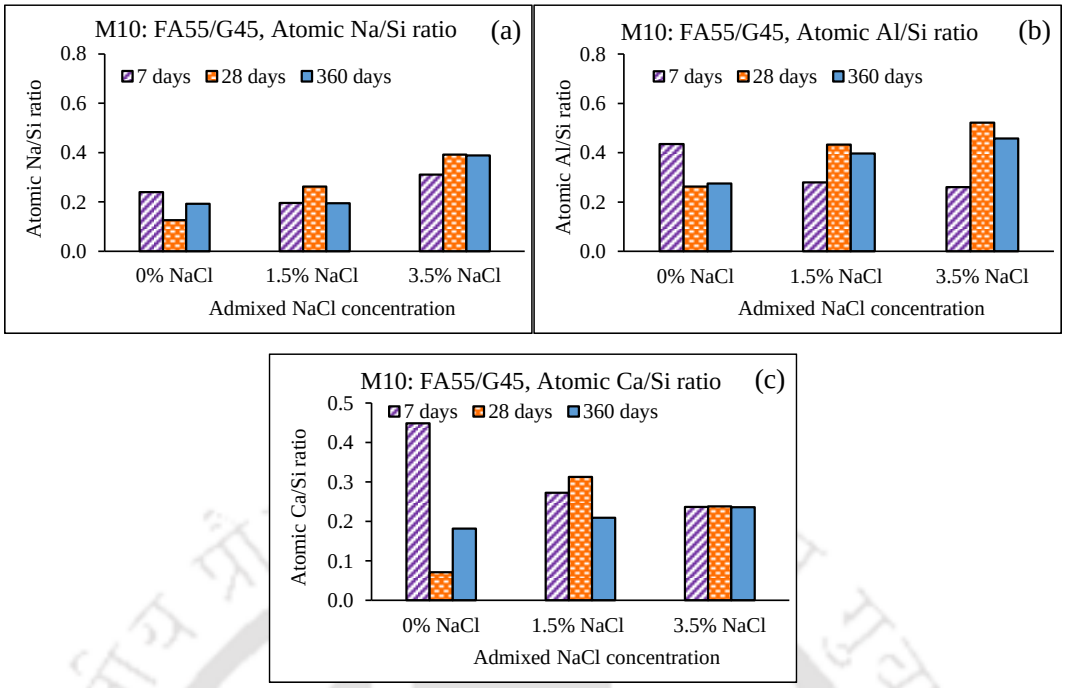

Fig. 7.43 Atomic ratios of control and chloride admixed fly ash-GGBS based GPC mixes (M10: FA55/G45): (a) atomic Na/Si ratio, (b) atomic Al/Si ratio, and (c) atomic Ca/Si ratio.

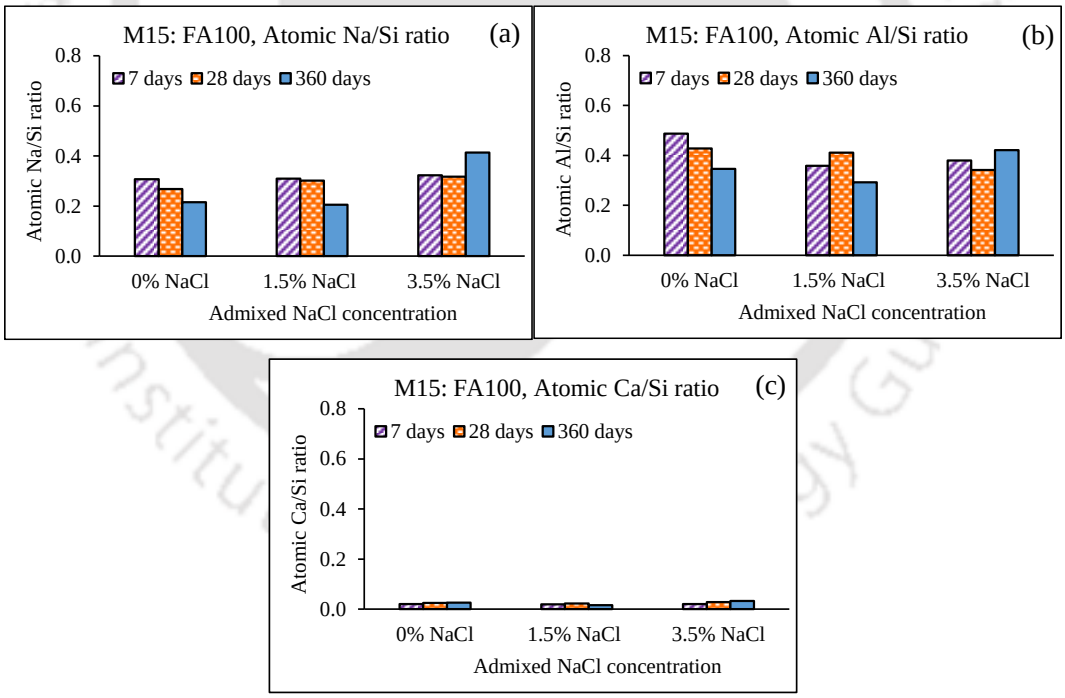

Fig. 7.44 Atomic ratios of control and chloride admixed fly ash based GPC mixes (M15: FA100): (a) atomic Na/Si ratio, (b) atomic Al/Si ratio, and (c) atomic Ca/Si ratio.

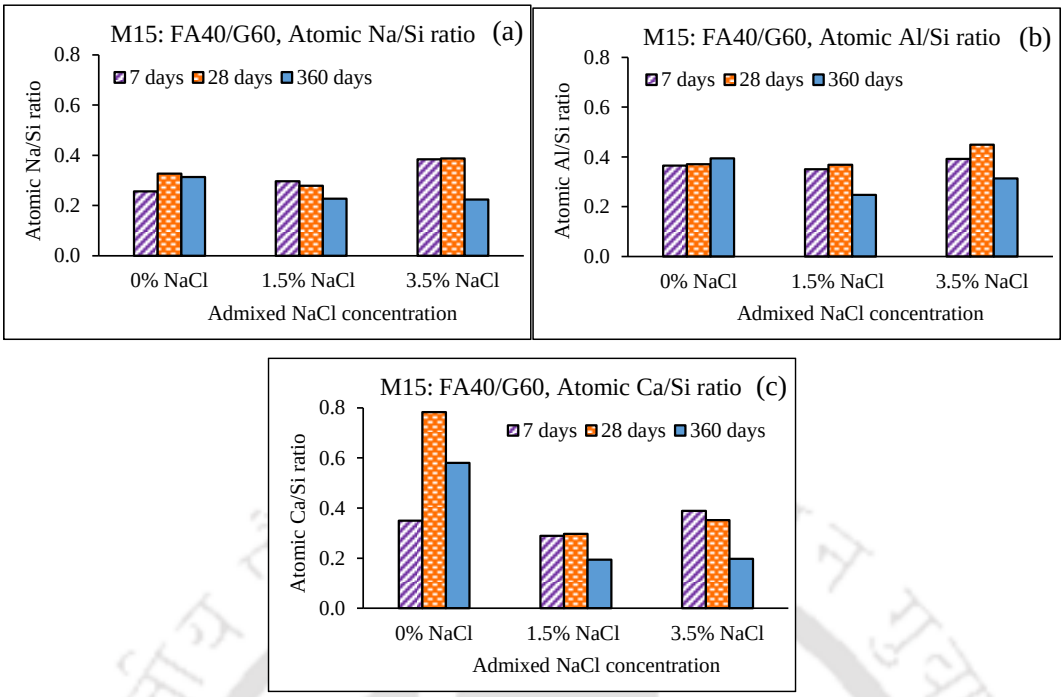

Fig. 7.45 Atomic ratios of control and chloride admixed fly ash-GGBS based GPC mixes (M15: FA40/G60): (a) atomic Na/Si ratio, (b) atomic Al/Si ratio, and (c) atomic Ca/Si ratio.

7.6.2.2 EDS analysis of GPC at rebar level of cylindrical reinforced specimens

Typical EDS spectra obtained near rebar level of control and chloride admixed fly ash and fly ash-GGBS based GPC specimens are illustrated in Fig. 7.46, and Fig. 7.47, and Fig. B9, and Fig. B10 (in Appendix section). Further, the average atomic ratios calculated from the EDS analysis at rebar level of fly ash and fly ash-GGBS based GPC specimens are depicted in Fig. 7.48 to Fig. 7.51. From these figures, it is observed that the fly ash-GGBS based GPC mixes M3 and M10 mostly exhibited lower atomic Na/Si and Al/Si ratios as compared to their corresponding fly ash based GPC mixes, whereas in mix M8 and M15, the variations in atomic Na/Si and Al/Si ratios were not systematic when compared with their corresponding fly ash based GPC mixes. Further, all fly ash-GGBS based GPC mixes showed higher atomic Ca/Si ratio in comparison to their corresponding fly ash based GPC mixes. As discussed earlier (Section 7.6.1.2), mostly higher peak intensity related to aluminosilicate gel and peak related to C-S-H gel were identified in the XRD patterns of fly ash-GGBS based GPC mixes. This indicates formation of higher amount of calcium-rich gels at rebar level of fly ash-GGBS based GPC mixes that led to formation of comparatively denser microstructure. This resulted in lower amount of chloride ions near rebar level leading to mostly less negative E_{corr} values (Fig. 7.6 to Fig. 7.9) and lower I_{corr}

values (Fig. 7.10 to Fig. 7.13) in fly ash-GGBS based GPC mixes in comparison to fly ash based GPC mixes.

While comparing the atomic ratios obtained at rebar level of GPC specimens made with different GGBS replacement levels, it is observed that the variations in atomic Na/Si, Al/Si, and Ca/Si ratios were unsystematic with increase in GGBS replacement level. The unsystematic variation in atomic ratios may be attributed to the effect of variations in other mix parameters such as W/GPS ratio, molarity of NaOH solution, binder content, and SS/SH ratio in the fly ash-GGBS based GPC mixes that might have led to alteration in the geopolymerization process at the age of 600 days. As observed from Fig. 7.48 to Fig. 7.51, the atomic Na/Si, Al/Si, and Ca/Si ratios varied unsystematically with increase in NaCl concentration in all fly ash and fly ash-GGBS based GPC mixes. These variations in atomic ratios in fly ash and fly ash-GGBS based GPC mixes with increase in admixed NaCl concentration may be attributed to the changes in the polycondensation process in the presence of chloride ions in GPC mixes thereby affecting the passivity of steel bar as a result of alteration in the electrolytic pore solution of GPC near steel reinforcement.

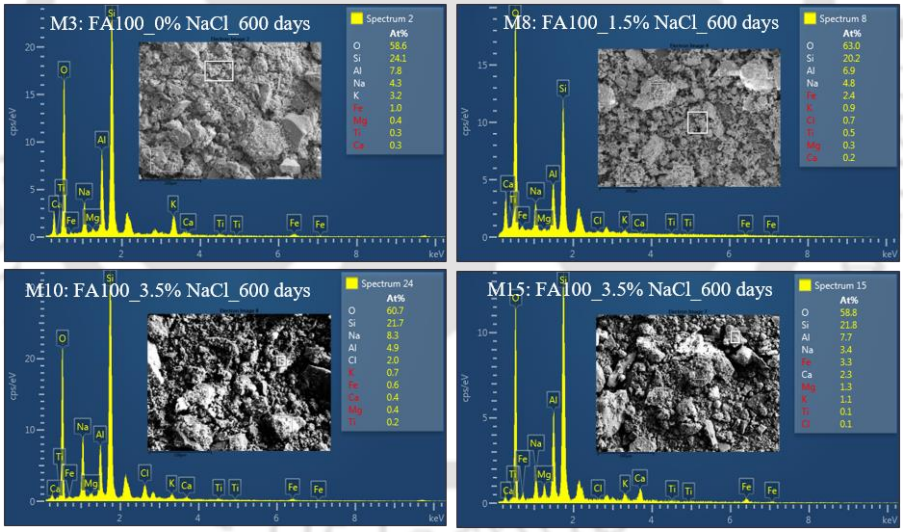

Fig. 7.46 EDS spectra obtained at rebar level of control and chloride admixed fly ash based GPC specimens.

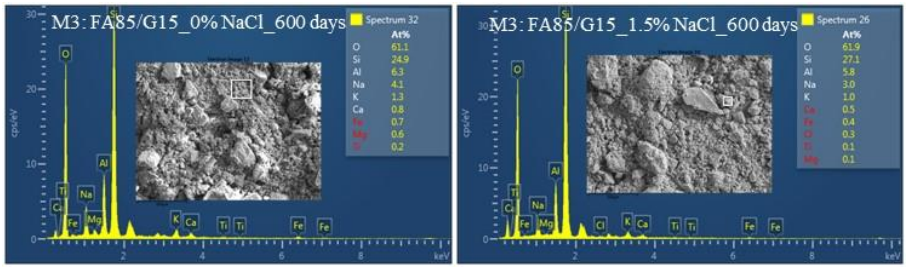

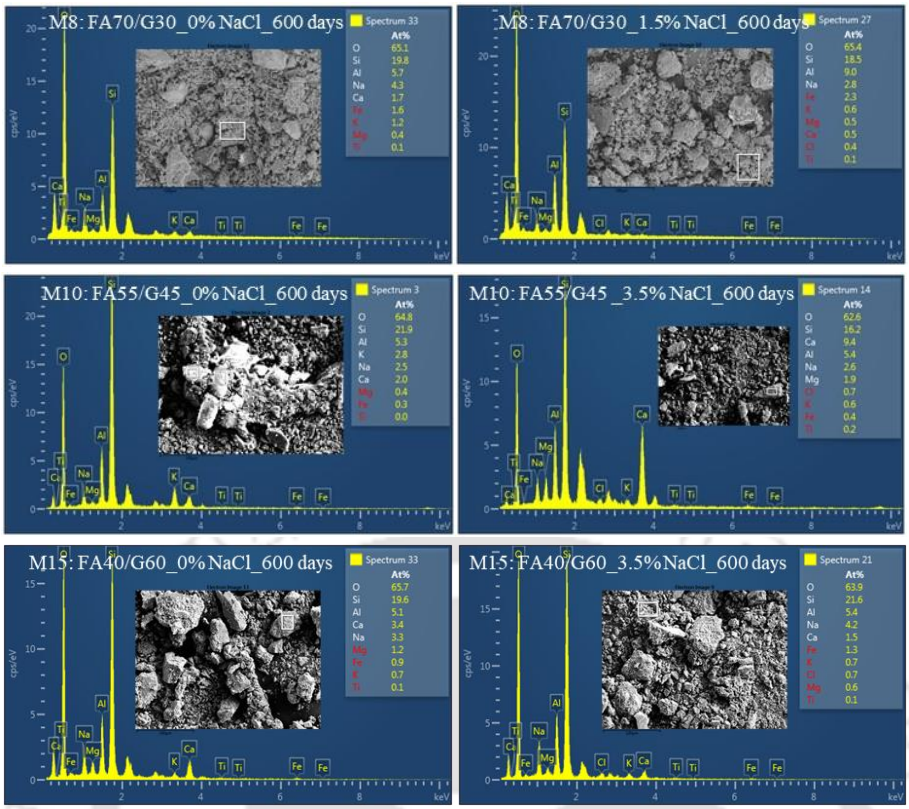

Fig. 7.47 EDS spectra obtained at rebar level of control and chloride admixed fly ash-GGBS based GPC specimens.

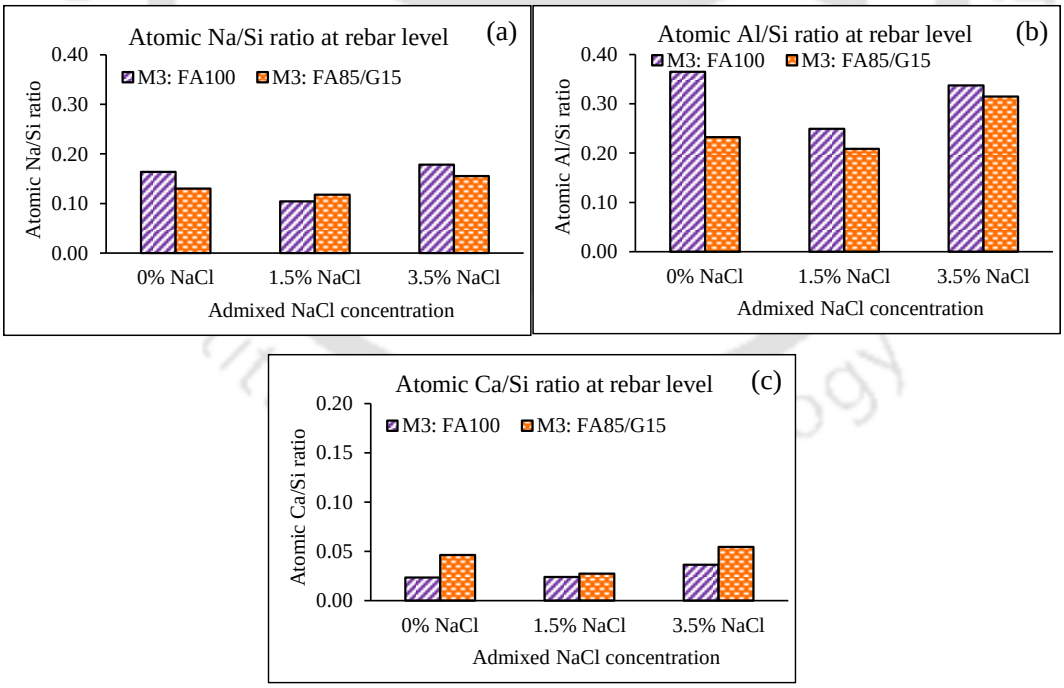

Fig. 7.48 Atomic ratios at rebar level of fly ash and fly ash-GGBS based GPC specimens (M3: FA100 and M3: FA85/G15): (a) atomic Na/Si ratio, (b) atomic Al/Si ratio, and (c) atomic Ca/Si ratio.

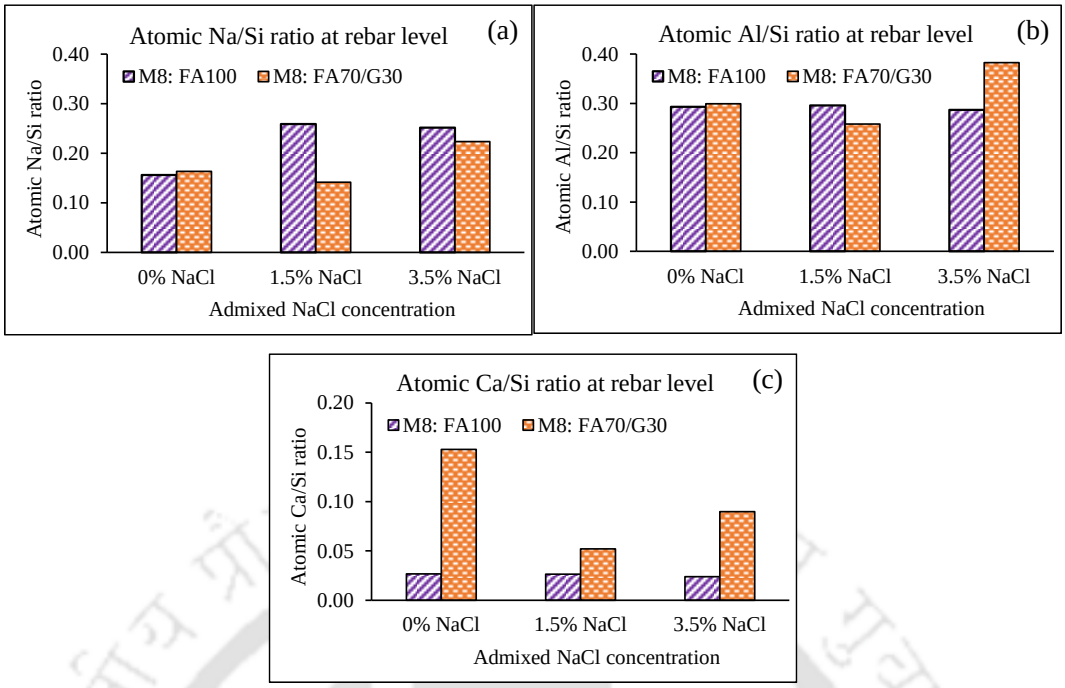

Fig. 7.49 Atomic ratios at rebar level of fly ash and fly ash-GGBS based GPC specimens (M8: FA100 and M8: FA70/G30): (a) atomic Na/Si ratio, (b) atomic Al/Si ratio, and (c) atomic Ca/Si ratio.

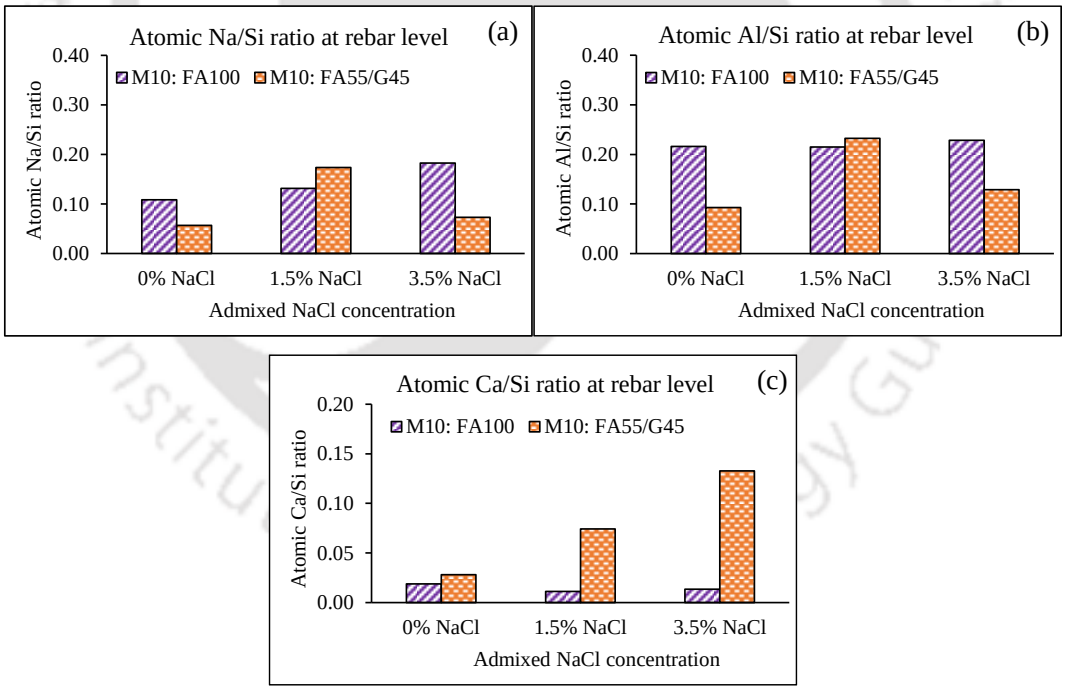

Fig. 7.50 Atomic ratios at rebar level of fly ash and fly ash-GGBS based GPC specimens (M10: FA100 and M10: FA55/G45): (a) atomic Na/Si ratio, (b) atomic Al/Si ratio, and (c) atomic Ca/Si ratio.

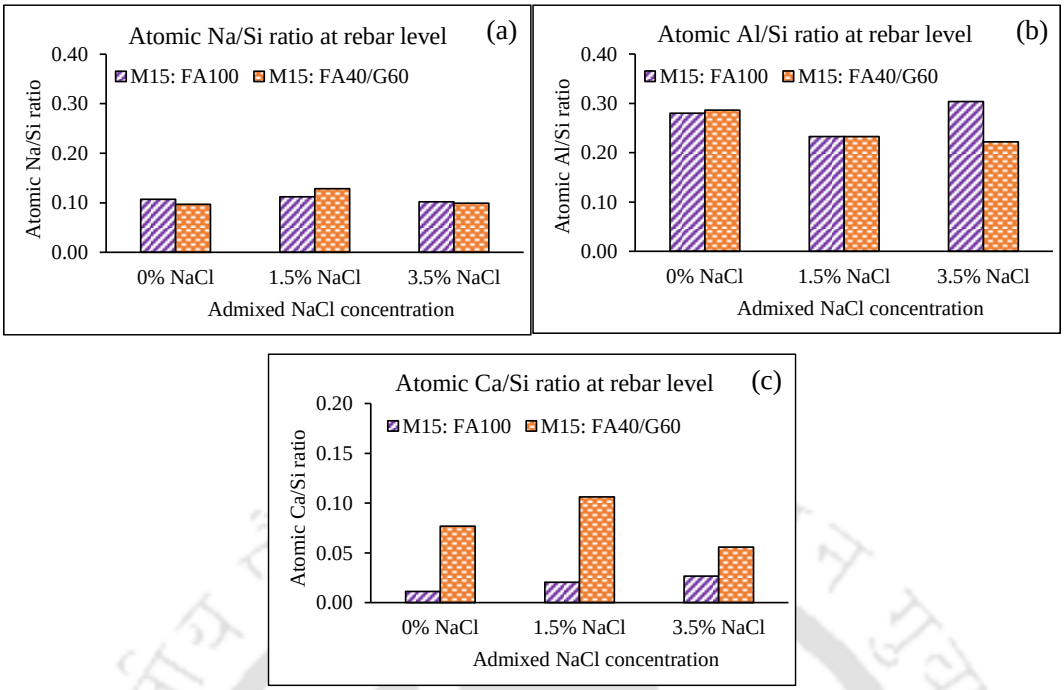

Fig. 7.51 Atomic ratios at rebar level of fly ash and fly ash-GGBS based GPC specimens (M15: FA100and M15: FA40/G60): (a) atomic Na/Si ratio, (b) atomic Al/Si ratio, and (c) atomic Ca/Si ratio.

7.6.3 FESEM analysis of GPC mixes

Typical FESEM images of control and chloride admixed fly ash and fly ash-GGBS based geopolymer concrete (GPC) mixes at the age of 7, 28, and 360 days are shown in Fig. 7.52 to 7.56. The remaining FESEM images are presented in Appendix section (Fig. B11 to Fig. B18). From the FESEM images, it is observed that the microstructure of GPC mixes mainly consists of (i) unreacted/partially reacted precursor materials, (i.e., unreacted/partially reacted fly ash particles in case of some fly ash based GPC, and unreacted/partially reacted fly ash and GGBS particles in case of some fly ash-GGBS based GPC), (ii) porous and dense geopolymer gels, (iii) crystalline needles i.e., short prismatic crystals of mullite, (iv) reticular structures of C-S-H (in case of fly ash-GGBS based GPC), (v) halite crystals in different shapes: cubical/octahedral crystals, and (vi) pores and microcracks etc. In case of fly ash based GPC mixes (Fig. 7.52, Fig. B11, Fig. B12, Fig. B14), the morphology at 7 and 28 days mostly shows the presence of partially reacted fly ash particles surrounded by porous type geopolymer gels (N-A-S-H type gels [98]). In addition, some short prismatic crystals of mullite (crystalline needles in M8: FA100_0% NaCl, Fig.7.52, M3: FA100_3.5% NaCl, Fig. B11, and M15: FA100_0% NaCl, Fig. B14, at the age of 28 days) were identified near partially reacted fly ash particles. In chloride admixed fly ash based GPC mixes, the presence of halite along with micro-pores were identified in geopolymer

gels (Fig. 7.52, M10: FA100_3.5% NaCl_28 days). This confirms the crystallization of NaCl in geopolymer gels that exerts internal stresses in the structure of geopolymer gel leading to expansion and formation of microcracks thereby resulting in strength reduction of fly ash based GPC mixes (Fig. 7.2 to Fig. 7.5). This can be corroborated with the peak related to halite identified in the XRD patterns (Section 7.6.1.1) and presence of Cl ions observed from the EDS analysis (Section 7.6.2.1).

From the FESEM images of fly ash-GGBS based GPC mixes (Fig. 7.53 to Fig. 7.56), the formation of comparatively denser geopolymer gels (N-(C)-A-S-H type gel) along with C-S-H gel (reticular structure) and some unreacted/partially reacted fly ash and GGBS particles were observed. The coexistence of denser geopolymer gels and C-S-H gel in fly ash-GGBS based GPC mixes was mainly responsible for higher compressive strength as compared to fly ash based GPC mixes. Further, the formation of comparatively denser microstructure was observed in fly ash-GGBS based GPC mixes made with higher GGBS content (Fig. 7.53 to Fig. 7.56, and Fig. B15 to Fig. B18). In case of both fly ash and fly ash-GGBS based GPC mixes, the morphology at the age of 360 days shows comparatively compact microstructure as compared to that at the age of 7 and 28 days (Fig. 7.52 to Fig. 7.56, and Fig. B11 to Fig. B18), which indicates continuation of geopolymerization reaction with age and resulted in strength enhancement at later ages (Fig. 7.2 to Fig. 7.5). In the FESEM images of some of the chloride admixed fly ash-GGBS based GPC mixes (Fig. 7.54 to Fig. 7.56), cubical/octahedral crystals of halite were identified, which indicates crystallization of sodium chloride that led to lower compressive strength in chloride admixed fly ash-GGBS based GPC mixes as compared to control fly ash-GGBS based GPC mixes.

Typical FESEM images at rebar level of fly ash and fly ash-GGBS based GPC specimens at the age of 600 days are presented in Fig. 7.57 and Fig. 7.58 respectively. The remaining FESEM images are shown in Appendix section (Fig. B19 and Fig. B20). Similar to the micrographs of fly ash based GPC mixes at different ages, the micrographs at rebar level of fly ash based GPC specimens mostly represents the formation of geopolymer gels along with the presence of small pores. Furthermore, the presence of octahedral halite crystals was identified in the morphology of 3.5% NaCl admixed fly ash based GPC mixes (M8: FA100_3.5% NaCl_600 days) (Fig. 7.57). The morphology at rebar level of fly ash-GGBS based GPC specimens indicates the coexistence of geopolymer gels, C-S-H gel and some partially reacted fly ash particles (M3 and M8) (Fig. 7.58 and Fig. B20). In addition, some

microcracks and presence of halite crystals were also identified in the morphology of chloride admixed fly ash-GGBS based GPC mixes (M3: FA85/G15_3.5% NaCl_600 days, M15: FA40/G60_3.5% NaCl_600 days) (Fig. 7.58).

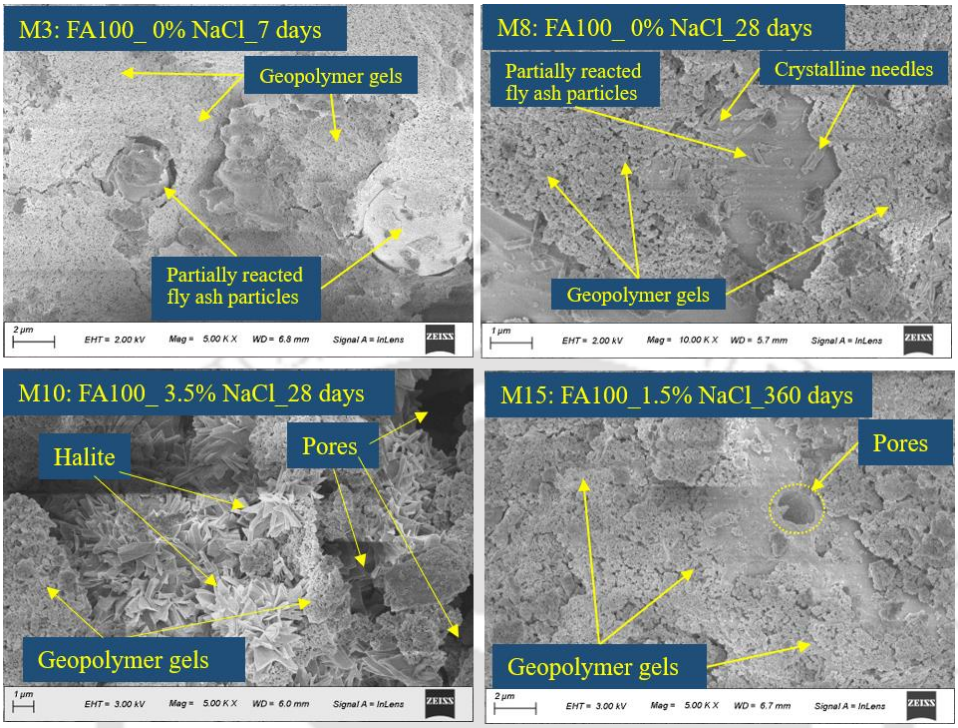

Fig. 7.52 FESEM images of control and chloride admixed fly ash based GPC at different ages.

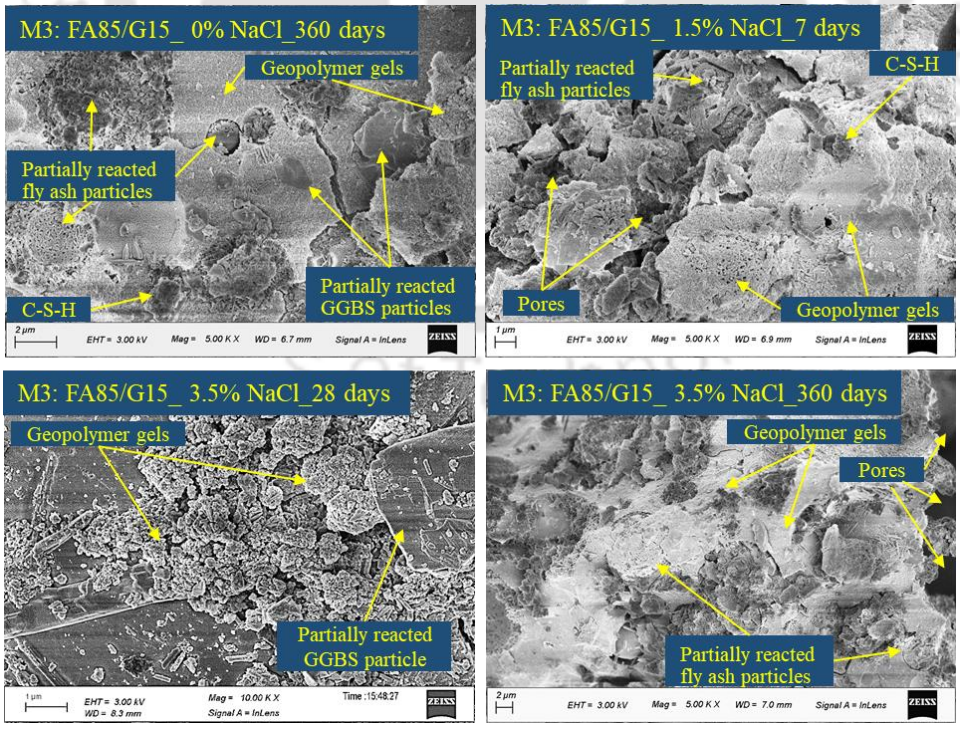

Fig. 7.53 FESEM images of control and chloride admixed fly ash-GGBS based GPC (M3: FA85/G15) at different ages.

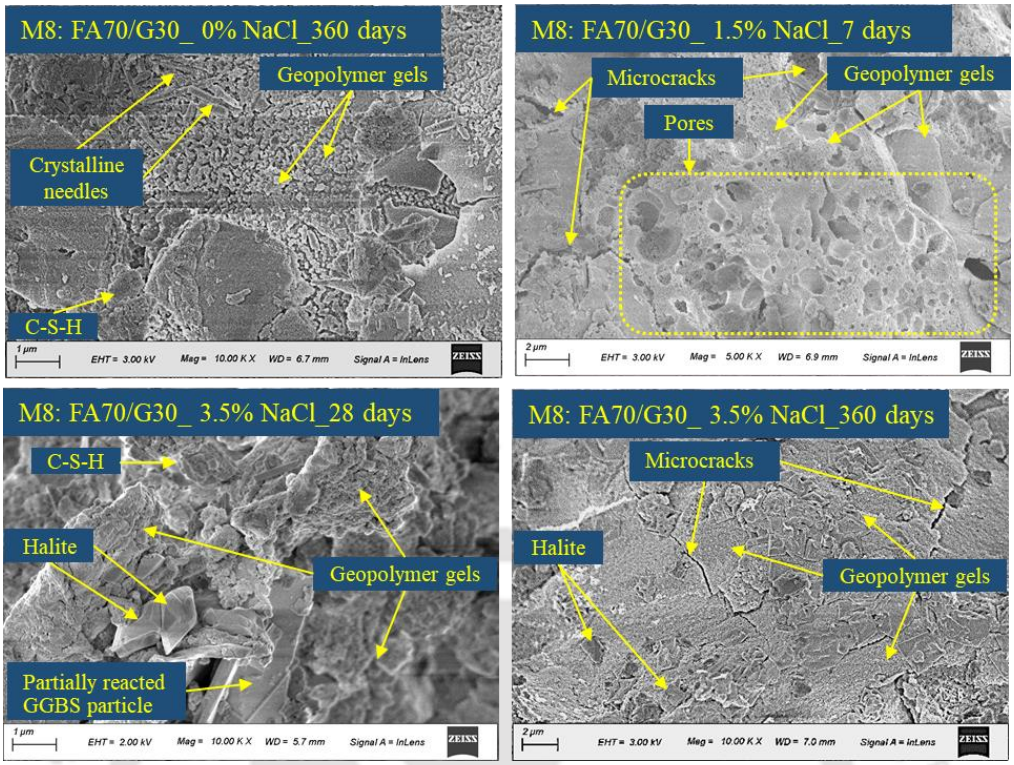

Fig. 7.54 FESEM images of control and chloride admixed fly ash-GGBS based GPC (M8: FA70/G30) at different ages.

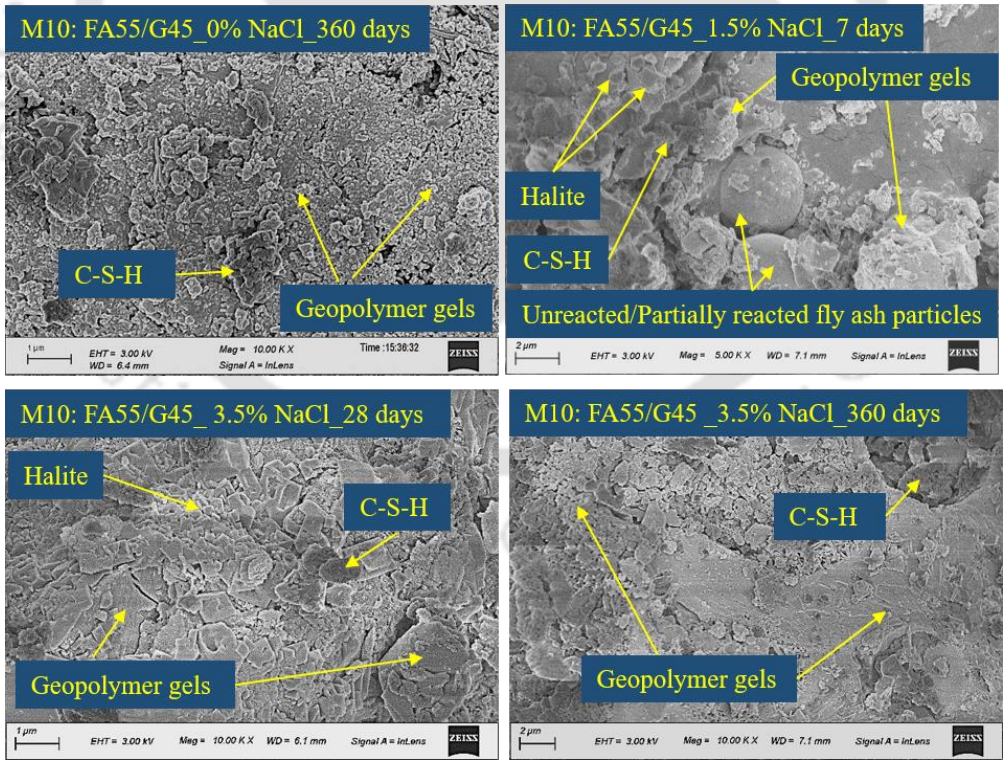

Fig. 7.55 FESEM images of control and chloride admixed fly ash-GGBS based GPC (M10: FA55/G45) at different ages.

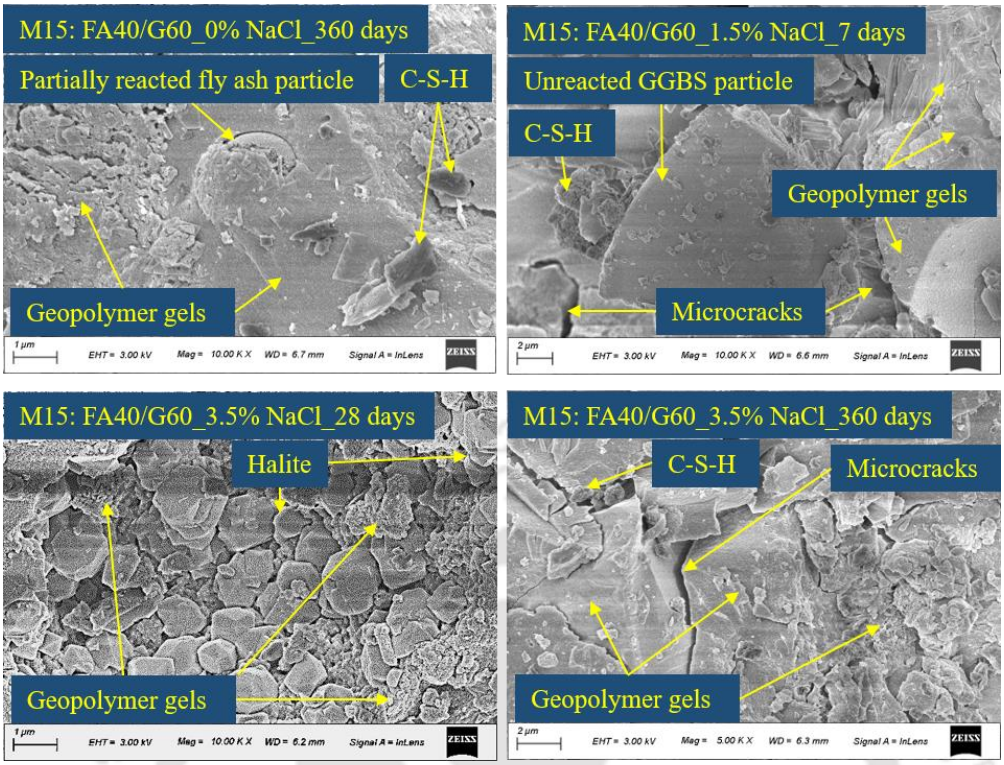

Fig. 7.56 FESEM images of control and chloride admixed fly ash-GGBS based GPC (M15: FA40/G60) at different ages.

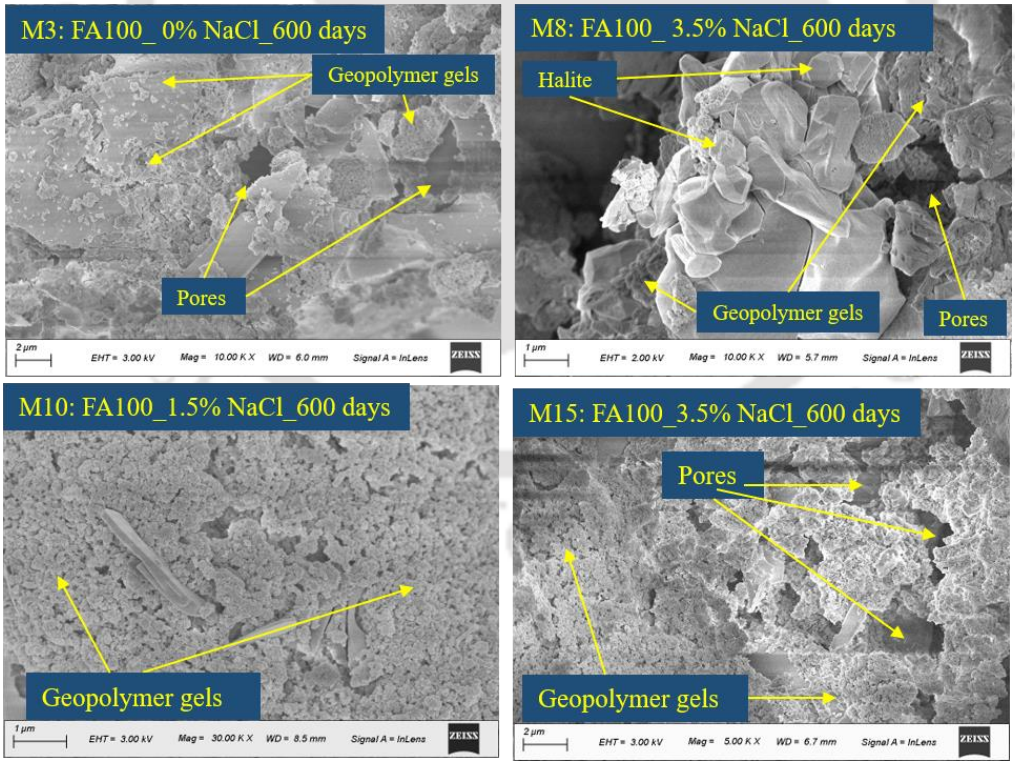

Fig. 7.57 FESEM images at rebar level of control and chloride admixed fly ash based GPC specimens at the age of 600 days.

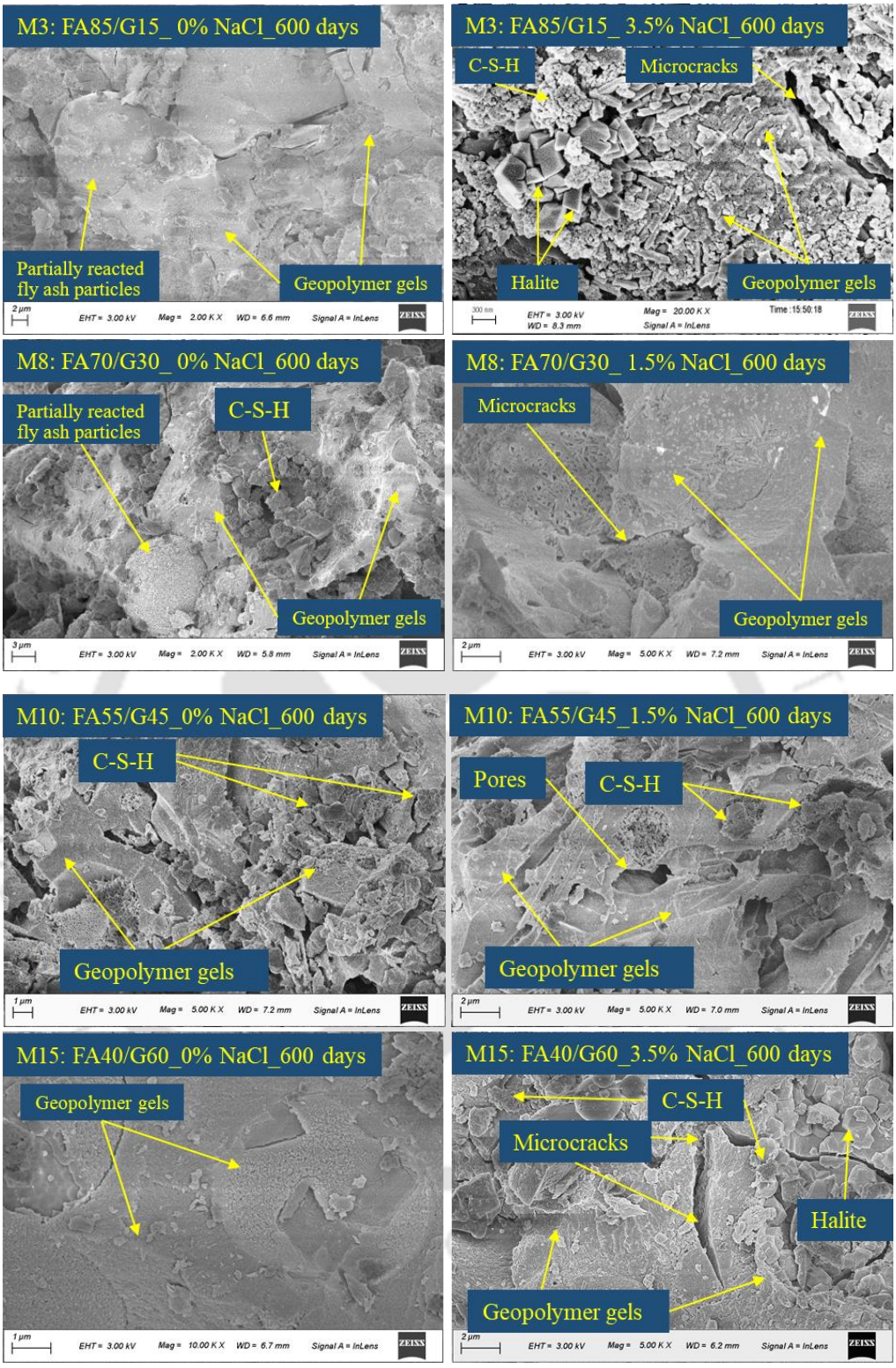

Fig. 7.58 FESEM images at rebar level of control and chloride admixed fly ash-GGBS based GPC specimens at the age of 600 days.

7.6.4 FTIR analysis of GPC mixes

The FTIR spectra of control, and chloride admixed fly ash and fly ash-GGBS based GPC mixes at the age of 7, 28 and 360 days are depicted in Fig. 7.59 to Fig. 7.66. As observed

from these figures, the asymmetric bending vibration of Si-O-Si bond was identified in the range of 460 cm^{-1} to 476 cm^{-1} in all fly ash based GPC mixes, and in the range of 451 cm^{-1} to 473 cm^{-1} in all fly ash-GGBS based GPC mixes at all ages. Further, the asymmetric bending vibration of Al-O bond was identified in the range of 778 cm^{-1} to 797 cm^{-1} in fly ash based GPC mixes and in the range of 774 cm^{-1} to 795 cm^{-1} in fly ash-GGBS based GPC mixes at all ages. This shows the presence of unreacted precursor materials in fly ash and fly ash-GGBS based GPC mixes [147].

From Fig. 7.59 to Fig. 7.66, the asymmetric stretching vibration of Si-O-Si(Al) bond identified in the range of 1034 cm^{-1} to 1094 cm^{-1} in all fly ash based GPC mixes, and 1008 cm^{-1} to 1066 cm^{-1} in all fly ash-GGBS based GPC mixes is attributed to the formation of geopolymer gels in GPC mixes [40,113]. These wavenumbers of Si-O-Si(Al) bond show shifting of peaks toward lower wavenumbers in fly ash-GGBS based GPC mixes in comparison to their corresponding fly ash based GPC mixes, which indicates the formation of more cross-linked aluminosilicate gels due to presence of GGBS that led to higher compressive strength in fly ash-GGBS based GPC mixes as compared to fly ash based GPC mixes (Fig. 7.2 to Fig. 7.5) [140]. In case of fly ash-GGBS based GPC mixes made with 30% GGBS and 60% GGBS, and their respective fly ash based GPC mixes (Fig. 7.61, Fig. 7.62, Fig. 7.65, and Fig. 7.66), there was unsystematic variation in wavenumber of Si-O-Si(Al) bond with increase in NaCl concentration. From Fig. 7.59, Fig. 7.60, Fig. 7.63, and Fig. 7.64, it is observed that the Si-O-Si(Al) bond mostly shifted to higher wavenumbers as NaCl concentration increased in fly ash-GGBS based GPC mixes made with 15% GGBS and 45% GGBS, and their corresponding fly ash based GPC mixes. This shows formation of comparatively lower amount of aluminosilicate gels leading to lower compressive strength in the GPC mixes admixed with higher concentration of NaCl (Fig. 7.2 to Fig. 7.5). From Fig. 7.59 to Fig. 7.66, there was unsystematic variation in wavenumber of Si-O-Si(Al) bond with increase in age in all fly ash and fly ash-GGBS based GPC mixes. The band in the range of 1400 cm^{-1} to 1454 cm^{-1} in all fly ash based GPC mixes, and in the range of 1414 cm^{-1} to 1480 cm^{-1} in all fly ash-GGBS based GPC mixes is related to stretching vibration of CO_3^{2-}, which is associated with carbonate groups [40,113]. The band identified in the range of 1600 cm^{-1} to 1642 cm^{-1} in fly ash based GPC mixes and 1629 cm^{-1} to 1642 cm^{-1} in fly ash-GGBS based GPC mixes is attributed to the bending vibration of H-O-H group. Further, the band identified from 3409 cm^{-1} to 3458 cm^{-1} in fly ash based

GPC mixes and 3416 cm^{-1} to 3471 cm^{-1} in fly ash-GGBS based GPC mixes is ascribed to the stretching vibration of -OH group [40].

The FTIR spectra obtained at rebar level of control and NaCl admixed fly ash and fly ash-GGBS based GPC specimens at the age of 600 days are shown in Fig. 7.67 to Fig. 7.70. From these figures, the asymmetric bending vibration of Si-O-Si bond (464 cm^{-1} to 477 cm^{-1}) and Al-O bond (778 cm^{-1} to 797 cm^{-1}) related to unreacted precursor materials, stretching vibration of CO_3^{2-} (1401 cm^{-1} to 1461 cm^{-1}), bending vibration of H-O-H group (1618 cm^{-1} to 1638 cm^{-1}) and stretching vibration of -OH group (3408 cm^{-1} to 3456 cm^{-1}) identified in the FTIR spectra obtained at rebar level of control and NaCl admixed GPC mixes are in the similar range of wavenumbers when compared with the FTIR spectra of GPC mixes obtained at different ages (Fig. 7.59 to Fig. 7.66). The asymmetric stretching vibration of Si-O-Si(Al) bond identified in the range of 1085 cm^{-1} to 1098 cm^{-1} in the FTIR spectra (Fig. 7.67 to Fig. 7.70) is ascribed to the formation of aluminosilicate gels at rebar level of fly ash and fly ash-GGBS based GPC mixes. Further, no significant difference was observed in the wavenumber of Si-O-Si(Al) bond with GGBS replacement level and concentration of NaCl in the GPC mixes.

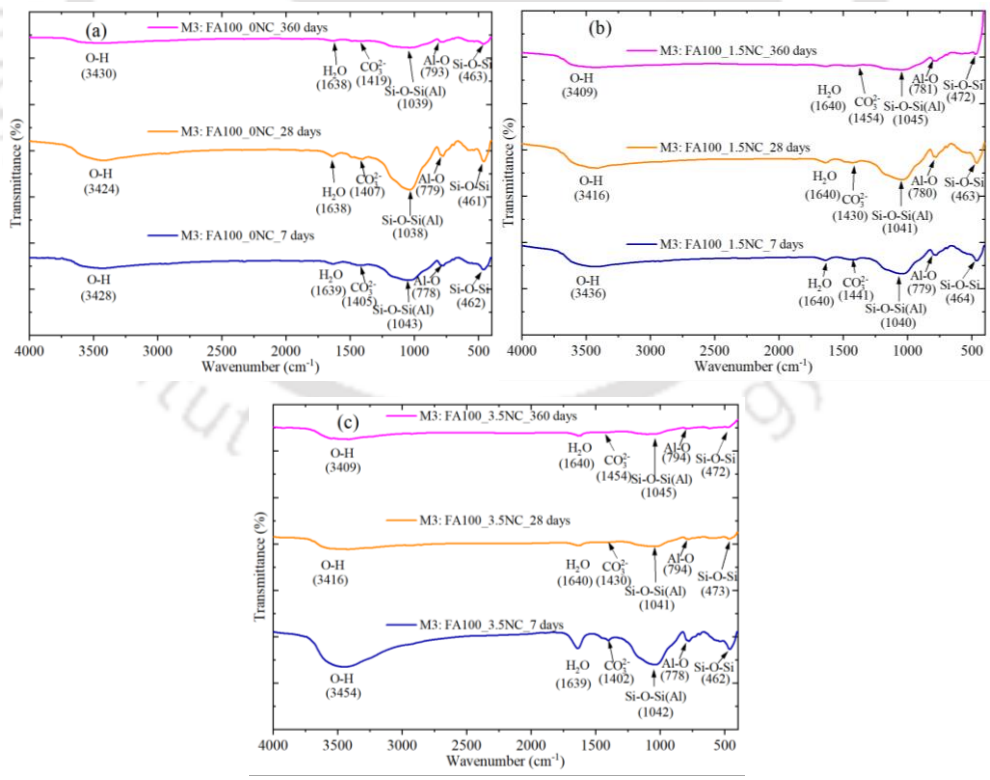

Fig. 7.59 FTIR spectra of fly ash based GPC mixes (M3: FA100) admixed with (a) 0% NaCl, (b) 1.5% NaCl, and (c) 3.5% NaCl, at different ages.

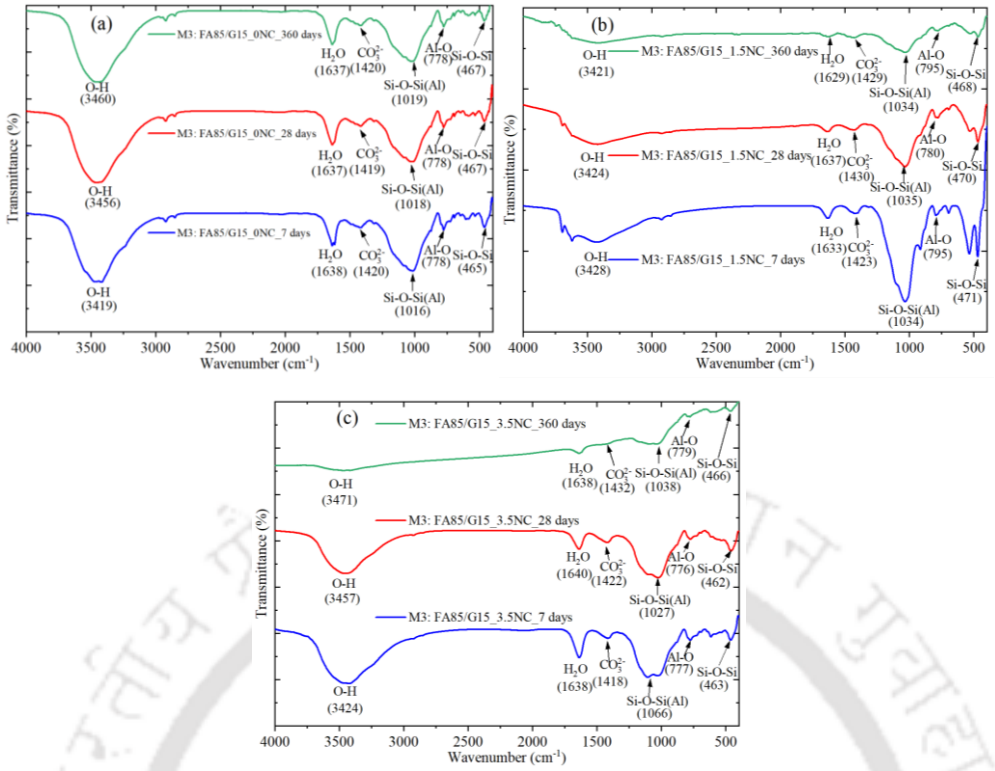

Fig. 7.60 FTIR spectra of fly ash-GGBS based GPC mixes (M3: FA85/G15) admixed with (a) 0% NaCl, (b) 1.5% NaCl, and (c) 3.5% NaCl, at different ages.

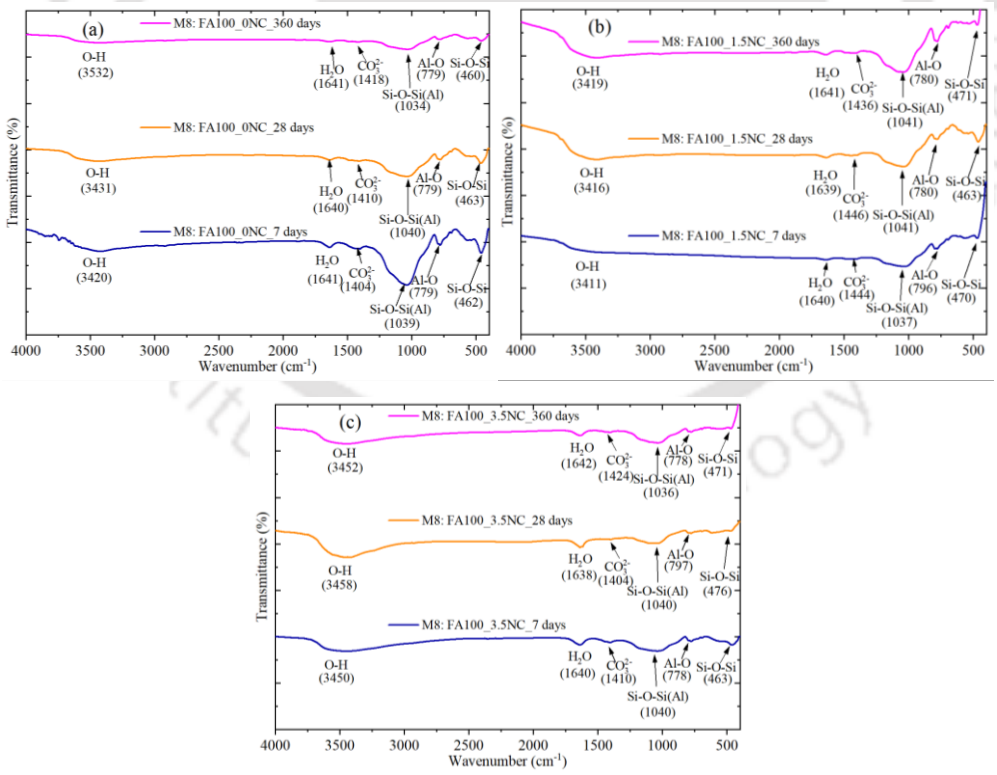

Fig. 7.61 FTIR spectra of fly ash based GPC mixes (M8: FA100) admixed with (a) 0% NaCl, (b) 1.5% NaCl, and (c) 3.5% NaCl, at different ages.

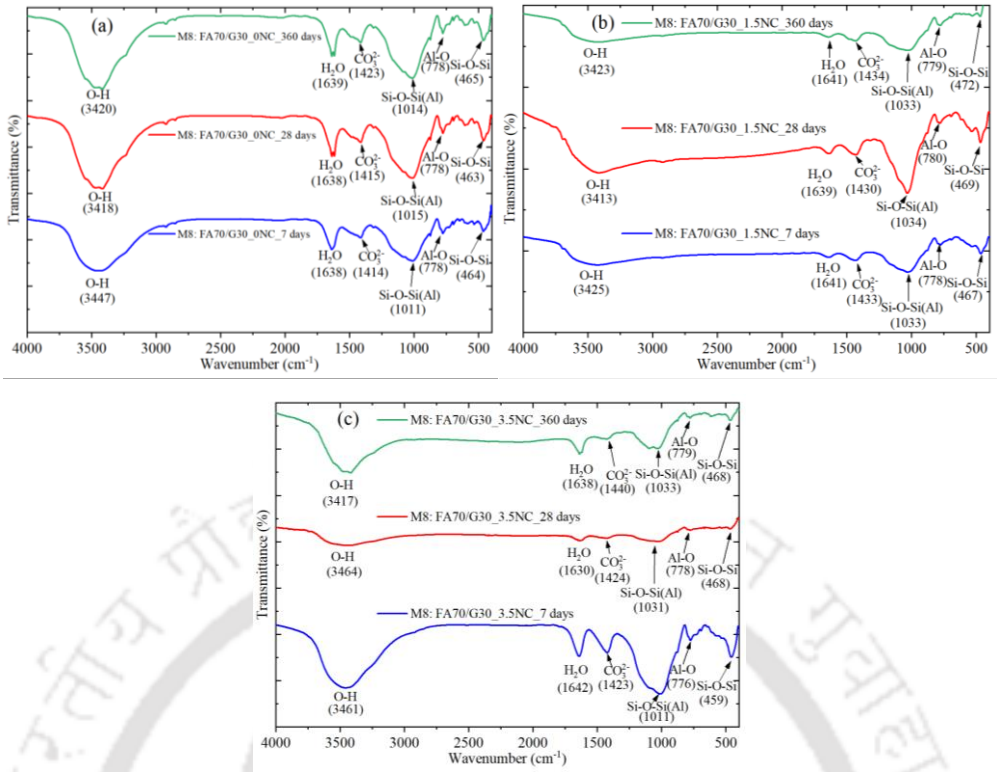

Fig. 7.62 FTIR spectra of fly ash-GGBS based GPC mixes (M8: FA70/G30) admixed with (a) 0% NaCl, (b) 1.5% NaCl, and (c) 3.5% NaCl, at different ages.

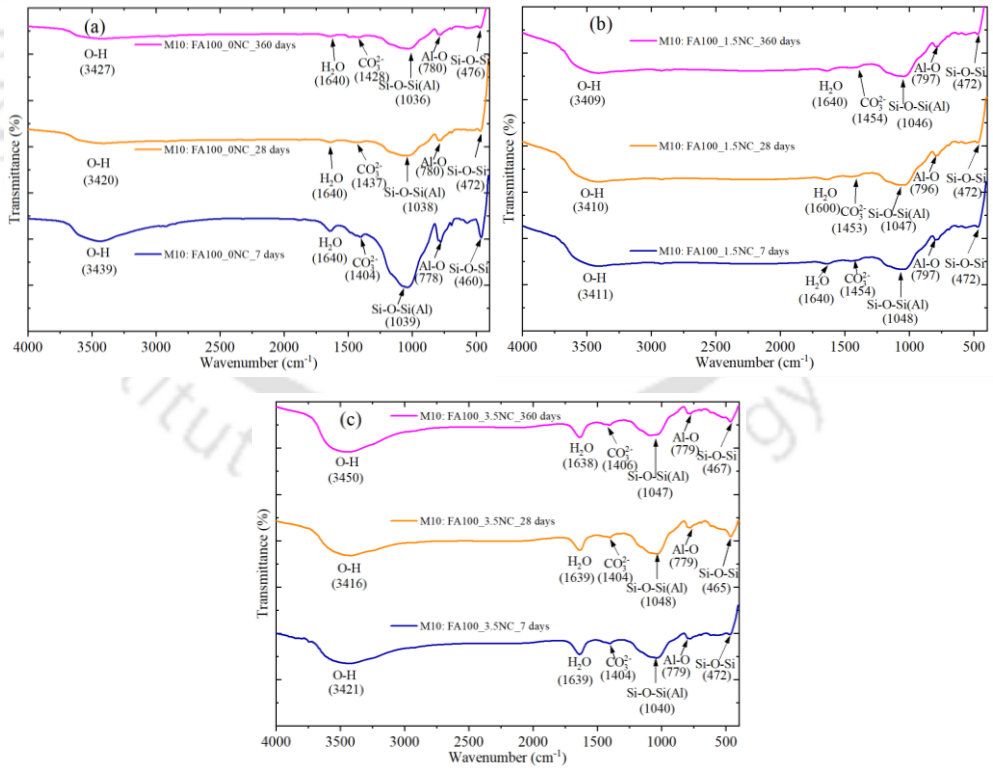

Fig. 7.63 FTIR spectra of fly ash based GPC mixes (M10: FA100) admixed with (a) 0% NaCl, (b) 1.5% NaCl, and (c) 3.5% NaCl, at different ages.

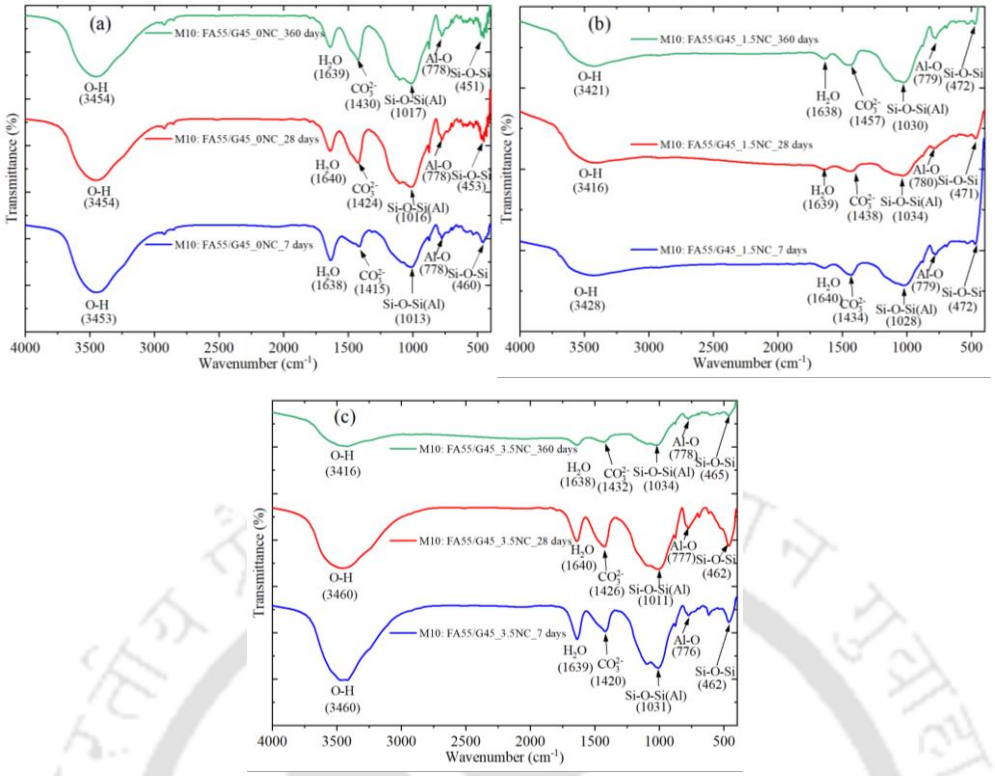

Fig. 7.64 FTIR spectra of fly ash-GGBS based GPC mixes (M10: FA55/G45) admixed with (a) 0% NaCl, (b) 1.5% NaCl, and (c) 3.5% NaCl, at different ages.

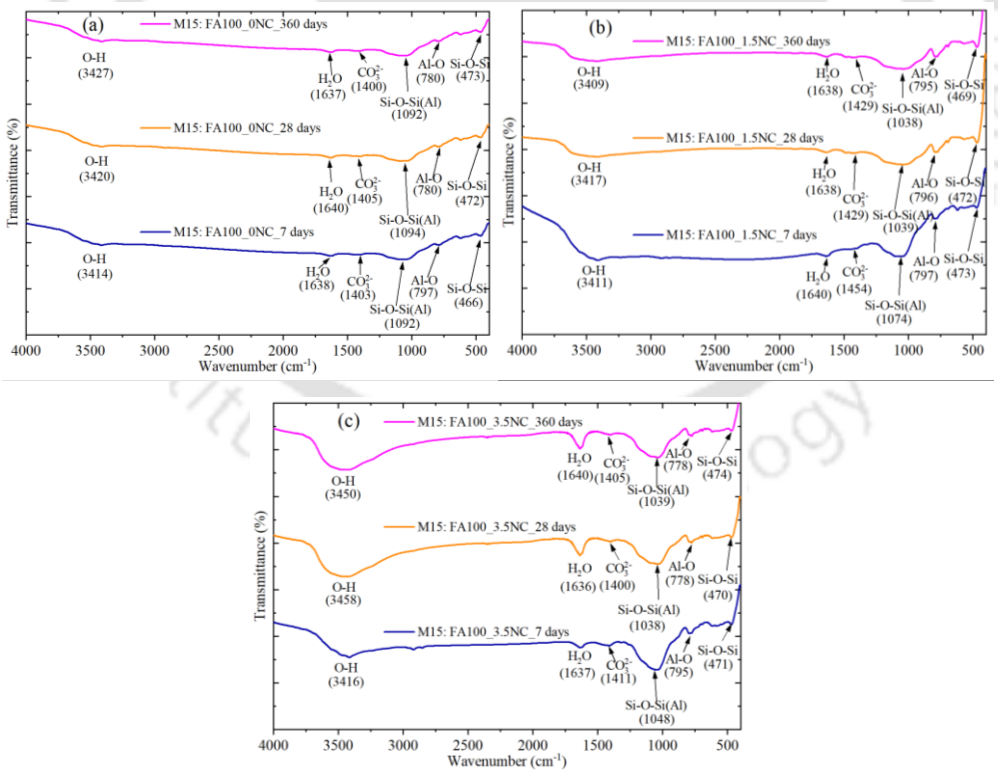

Fig. 7.65 FTIR spectra of fly ash based GPC mixes (M15: FA100) admixed with (a) 0% NaCl, (b) 1.5% NaCl, and (c) 3.5% NaCl, at different ages.

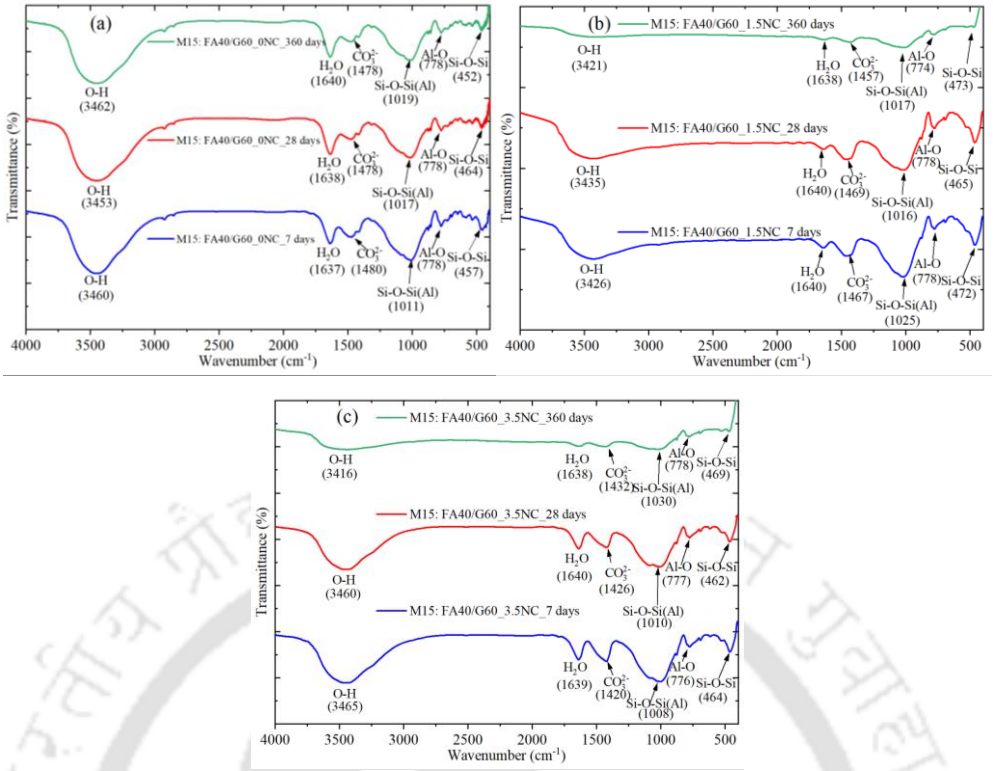

Fig. 7.66 FTIR spectra of fly ash-GGBS based GPC mixes (M15: FA40/G60) admixed with (a) 0% NaCl, (b) 1.5% NaCl, and (c) 3.5% NaCl, at different ages.

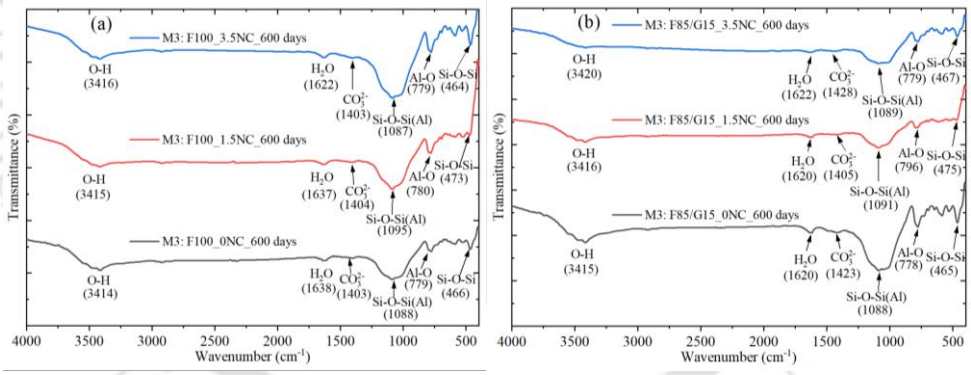

Fig. 7.67 FTIR spectra at rebar level of control and chloride admixed GPC specimens at the age of 600 days: (a) M3: FA100 and (b) M3: FA85/G15.

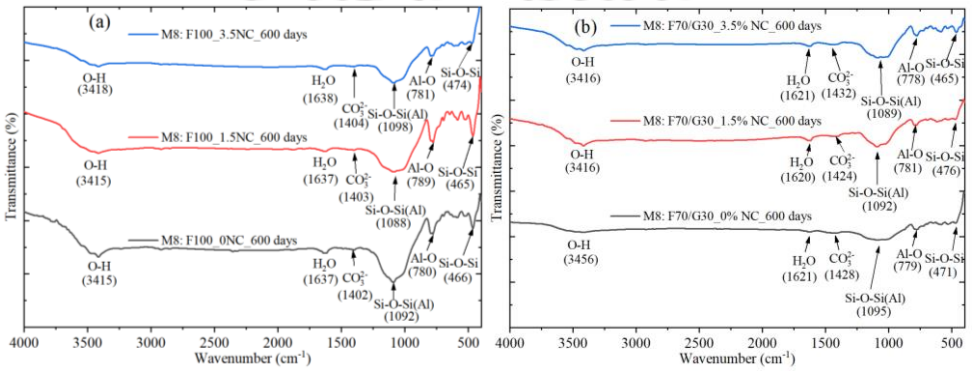

Fig. 7.68 FTIR spectra at rebar level of control and chloride admixed GPC specimens at the age of 600 days: (a) M8: FA100 and (b) M8: FA70/G30.

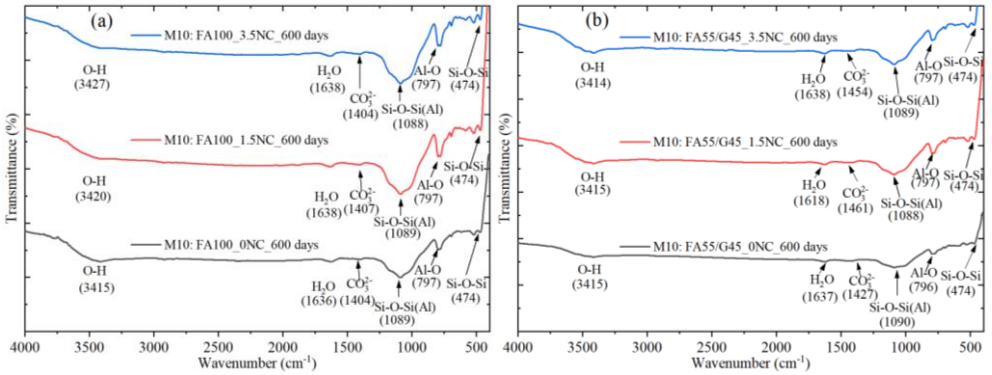

Fig. 7.69 FTIR spectra at rebar level of control and chloride admixed GPC specimens at the age of 600 days: (a) M10: FA100 and (b) M10: FA55/G45.

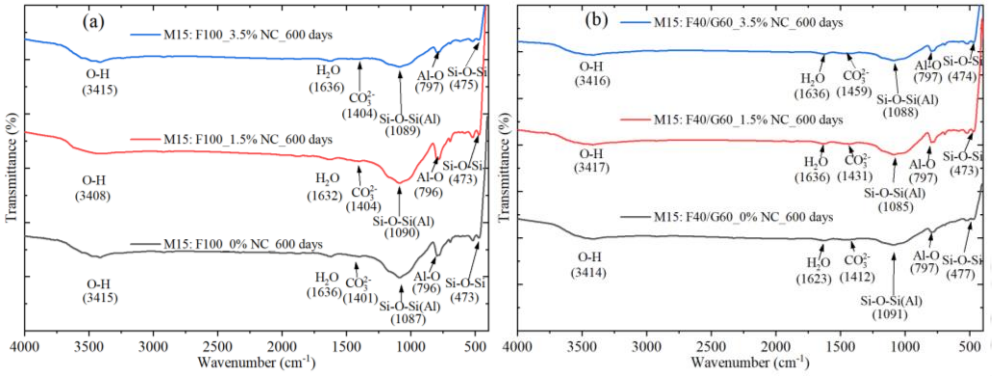

Fig. 7.70 FTIR spectra at rebar level of control and chloride admixed GPC specimens at the age of 600 days: (a) M15: FA100 and (b) M15: FA40/G60.

7.7 Summary

In this chapter, the influence of chloride ions on consistency, compressive strength, rebar corrosion, chloride content, and microstructural changes in fly ash and fly ash-GGBS based geopolymer concrete (GPC) were evaluated. The corrosion behaviour of steel reinforcement was evaluated through corrosion potential (E_{corr}) and corrosion current density (I_{corr}), and microstructural changes of GPC were examined at various ages and at rebar level through XRD, EDS, FESEM, and FTIR analyses. The obtained test results revealed that chloride ions had significant influence on consistency, strength, corrosion behaviour of rebar, and microstructure of GPC mixes. The addition of NaCl improved the consistency (slump value) of both fly ash and fly ash-GGBS based GPC mixes. However, the slump value of fly ash-GGBS based GPC mixes decreased with increase in GGBS content in the mixes. The GPC mixes exhibited lower compressive strength with increase in admixed NaCl concentration at all ages. Further, the GPC mixes mostly exhibited higher compressive strength with increase in GGBS replacement level. The steel rebar embedded in fly ash-GGBS based GPC specimens mostly exhibited less negative corrosion potential

(E_{corr}) and lower corrosion current density (I_{corr}) as compared to the corresponding fly ash based GPC specimens. The results of chloride analysis indicated very less extent of chloride binding in fly ash and fly ash-GGBS based GPC mixes. The fly ash-GGBS based GPC mixes mostly showed higher Cl^- binding capacity than their corresponding fly ash based GPC mixes at later ages, and at rebar level of reinforced GPC specimens due to physical adsorption of Cl^- ions on binding gels to a comparatively higher extent. In fly ash-GGBS based GPC mixes, the higher peak intensity of aluminosilicate gels and presence of C-S-H gel as identified from the XRD analysis, higher atomic Ca/Si ratio obtained from EDS analysis, and shifting of wavenumbers of Si-O-Si(Al) bond toward lower magnitude in FTIR analysis confirmed the improved performance of fly ash-GGBS based GPC mixes in terms of higher compressive strength, lower corrosion activity and lower chloride content as compared to fly ash based GPC mixes. The presence of halite crystals along with pores and microcracks as observed from the microstructure analysis (XRD and FESEM) of chloride admixed GPC mixes at different ages and at rebar level of cylindrical GPC specimens corroborated the obtained results of lower compressive strength, and higher corrosion activity in chloride admixed fly ash and fly ash-GGBS based GPC mixes.

Conclusions and Recommendations for Future Research Work

8.1 General

This chapter contains the conclusions obtained from the present research work. Based on the results obtained from the experimental work followed by discussion, the conclusions have been drawn on the investigation and optimization of the effect of various control parameters i.e., GGBS replacement level, water-to-geopolymer solids (W/GPS) ratio, molarity of NaOH solution, and sand-to-binder (S/B) ratio on fresh, hardened, and durability properties of geopolymer mortar (GPM) by Taguchi-Grey relational analysis (GRA) method. Further, the conclusions obtained from the investigation of effect of fly ash/GGBS blends and sand-to-binder (S/B) ratio on fresh, hardened, durability, and microstructural properties of GPM have been presented. The conclusions have been drawn on the investigation and optimization of influence of control parameters such as GGBS replacement level, W/GPS ratio, molarity of NaOH solution, binder content and sodium silicate solution to sodium hydroxide solution (SS/SH) ratio on setting time, workability and compressive strength of geopolymer concrete (GPC) by Taguchi-GRA method. In addition, the conclusions obtained on the influence of chloride ions on workability, compressive strength, rebar corrosion, and microstructural changes in fly ash and fly ash-GGBS based GPC have also been presented. Lastly, the significance of research outcome, and recommendations for future research work are presented in this chapter.

8.2 Conclusions obtained from optimization of performance of geopolymer mortar based on fresh, hardened, and durability properties

- The increase in GGBS replacement level, NaOH solution molarity and sand-to-binder (S/B) ratio resulted in shorter setting time (initial and final) of geopolymer mortar (GPM). However, the setting time increased with increase in W/GPS ratio. From ANOVA technique, for lower initial setting time, GGBS replacement had higher contribution (34.35%) as compared to S/B ratio (32.41%) followed by molarity of NaOH solution (25.94%) and W/GPS ratio (7.3%). Similarly, for lower final setting time, GGBS replacement had higher contributing effect (44.99%) as compared to molarity of NaOH solution (26.95%) followed by S/B ratio (23.42%) and W/GPS ratio (4.64%).

- The flowability as indicated by the flow index of the GPM mix decreased significantly with increase in S/B ratio. The S/B ratio had a dominant effect on the flowability of the GPM mix with substantially higher contributing effect of 82.81%, whereas the molarity of NaOH solution had the lowest effect on the flowability of GPM mixes, with a contributing effect of 1.72%, as compared to other control parameters.
- The compressive strength of geopolymer mortar (GPM) mixes mostly increased with increase in GGBS replacement level at all ambient curing ages. However, the compressive strength decreased with an increase in W/GPS ratio and S/B ratio. The effect of molarity of NaOH solution was not apparent at the early age (7 days); however, at later ages, the effect of greater extent of geopolymerization process at higher molarity of NaOH solution (14 M) resulted in higher compressive strength.
- From ANOVA technique, the GGBS replacement had highest contributing effect (32.74–84.75%) as compared to S/B ratio (8.86–38.29%) followed by W/GPS ratio (5.72–21.28%), and molarity of NaOH solution (0.67–16.8%) on the compressive strength of GPM mixes at different ages of ambient curing.
- The water absorption and volume of permeable voids of geopolymer mortar (GPM) decreased with increase in GGBS replacement level. Among all control parameters, GGBS replacement had dominant influence with highest contributing effect of 81.19% on water absorption and 81.73% on volume of permeable voids. However, the S/B ratio significantly influenced sorptivity of geopolymer mortar with contributing effect of 65.69% followed by W/GPS ratio with contributing effect of 21.43% as compared to other parameters.
- The GPM mixes made with lower GGBS replacement showed improved resistance against sulfate attack than higher GGBS replacement when compared with exposure to water. The reduction in compressive strength of GPM mixes made with higher GGBS replacement in case of exposure to sulfate solutions is ascribed to the decalcification of calcium-enriched gels that resulted in formation of higher amount of gypsum in the geopolymer matrix.
- From ANOVA technique, among all control parameters, the compressive strength of geopolymer mortar (GPM) was significantly influenced by S/B ratio with a contributing effect of 69.55% in case of exposure to 6% Na_2SO_4 solution. In case of exposure to 6%

$MgSO_4$ solution, the molarity of NaOH solution had highest contributing effect of 36.60% on compressive strength of GPM.

- The compressive strength of GPM exposed to H_2SO_4 and HCl solutions decreased significantly when compared with exposure to water, which is ascribed to the depolymerisation of geopolymer gels in the acidic environment. The maximum compressive strength loss was observed in the GPM mixes prepared with higher GGBS replacement (45%), whereas the minimum strength loss was observed in the GPM mixes prepared with lower GGBS replacement (15%) when exposed to acid solutions.
- The GGBS replacement level had significant effect on variation in compressive strength with contributing effect of 92.89%, and 94.07% in case of exposure to 0.62 mol/l H_2SO_4 and to 0.62 mol/l HCl solutions respectively; whereas the influence of W/GPS ratio, molarity of NaOH solution, and S/B ratio on variations in compressive strength of geopolymer mortar (GPM) were insignificant in case of exposure to 0.62 mol/l H_2SO_4 and 0.62 mol/l HCl solutions.
- From the results of multi-response optimization by Taguchi-GRA method, the GPM mix prepared with 45% GGBS, W/GPS ratio of 0.31, NaOH solution of 14 M and S/B ratio of 2 exhibited highest grey relational grade (GRG) as compared to other GPM mixes as it showed better performance in relatively more number of studied properties simultaneously.
- The variations in the peak intensity of compounds related to N-A-S-H and N-(C)-A-S-H gels formed in the geopolymer mortar mix (with highest GRG), as observed from the XRD analysis, were consistent with the variations in compressive strength with ambient curing age as well as with the variation in compressive strength between 6% Na_2SO_4 and 6% $MgSO_4$ solutions. The formation of gypsum, which is responsible for reduction in compressive strength of GPM in case of exposure to sulfate and H_2SO_4 solutions, was evident from the obtained results of XRD, FESEM, EDS, and FTIR analyses.
- The substantial reduction in compressive strength of geopolymer mortar in case of exposure to acid solutions is in line with the significant reduction: (a) in peak intensity of different compounds related to aluminosilicate gels as obtained from the XRD analysis, and (b) in atomic Na/Si ratio and Al/Si ratio as obtained from EDS analysis, which corroborates the depolymerization of aluminosilicate gels in GPM exposed to acidic environment.

- Based on the multi-response optimization by Taguchi-GRA method, the levels of mix parameters of the optimized geopolymer mortar mix as per maximum mean grey relational grade (GRG) were 45% GGBS, W/GPS ratio of 0.31, NaOH solution of 14 M and S/B ratio of 1.5. On the basis of the verification experiments, the optimized GPM mix exhibited adequate setting time, flow index, and water absorption properties, and higher compressive strength at all ages of ambient curing and in case of exposure to different sulfate and acid solutions when compared with the GPM mixes as per L_9 orthogonal array.

8.3 Conclusions obtained from effect of precursor materials and sand-to-binder ratio on strength development, durability and microstructure evolution of geopolymer mortar

- The results obtained from flowability of fresh geopolymer mortar (GPM) mixes showed that at constant sand-to-binder (S/B) ratio, the flow index of GPM mixes decreased from 126% to 108% with increase in amount of GGBS from 15% to 45% in the mixes. Further, the flow index of GPM mixes increased from 108% to 146% with increase in sand-to-binder ratio from 1.5 to 2.5 at a constant fly ash/GGBS blend.
- The compressive strength of GPM made from various fly ash/GGBS blends and S/B ratios mostly increased from 7 days to 180 days. This was supported by the XRD analysis where the intensity of peaks related to nepheline, albite and C-S-H mostly increased with increase in ambient curing age thereby indicating the formation of higher amount of N-A-S-H, N-(C)-A-S-H and C-S-H gel in the GPM mixes at later age of ambient curing.
- The rate of compressive strength enhancement was higher during the early age of ambient curing i.e., from 7 days to 28 days and then it gradually decreased with increase in ambient curing age from 28 days to 180 days. This was supported by the variations in atomic Na/Si, Al/Si, and Ca/Si ratios with age in geopolymer mortar mixes as observed from the EDS analysis.
- The geopolymer mortar mix prepared with higher GGBS content and lower S/B ratio i.e., fly ash/GGBS blend of FA55/G45 and S/B ratio of 1.5 exhibited highest compressive strength at all ages of ambient curing. This was corroborated by higher intensity of peaks related to nepheline, albite and C-S-H gel as obtained from the XRD analysis, and higher atomic Na/Si ratio and Ca/Si ratio as obtained from EDS analysis.

- The GPM mix made with higher GGBS content and lower S/B ratio (fly ash/GGBS blend: FA55/G45 and S/B ratio: 1.5) showed lower water absorption, volume of permeable voids, and sorptivity coefficient as compared to other mixes due to formation of relatively denser microstructure as a result of formation of relatively higher calcium-rich gels in this mix. The effect of S/B ratio on the sorptivity coefficient of GPM mixes was more significant than that of GGBS content.
- The visual observation of GPM specimens after exposure to different sulfate and acid solutions for 26 weeks indicated that the GPM mix made with lower GGBS content and lower S/B ratio i.e., fly ash/GGBS blend of FA85/G15 and S/B ratio of 1.5 had better resistance to different sulfate and acid solutions. Of the exposure solutions, H_2SO_4 solution produced more-intense surface damage and caused significant volumetric expansion in the GPM specimens.
- The GPM specimens had maximum gain in weight after exposure to 6% $MgSO_4$ solution, whereas maximum weight loss was observed in case of exposure to 0.62 mol/l HCl solution. The weight gain percentage of the GPM specimens exposed to sulfate solutions mostly decreased with the increase in GGBS content in the mixes. However, the weight loss percentage of the GPM mixes increased with increase in GGBS content and S/B ratio of the mixes in the case of exposure to acid solutions.
- The geopolymer mortar mix made with lower GGBS content and lower S/B ratio (FA85/G15, S/B1.5) had maximum gain in compressive strength in case of exposure to 6% $MgSO_4$ solution. However, the GPM mix made with higher GGBS content and lower S/B ratio (FA55/G45, S/B1.5) showed maximum strength loss when exposed to 6% $MgSO_4$ solution and 0.62 mol/l H_2SO_4 solution.
- Between acid solutions, the loss in compressive strength of GPM mixes was higher in case of exposure to H_2SO_4 solution as compared to HCl solution irrespective of GGBS replacement level, S/B ratio and concentration of acid solutions.
- The peak intensity related to aluminosilicate gels, i.e., N-A-S-H and N-(C)-A-S-H, and C-S-H gel, mostly increased with increase in GGBS content, and decreased with increase in S/B ratio of the geopolymer mortar when exposed to water and different sulfate solutions, which is in line with the variations in the obtained compressive strength of geopolymer mortar.

- The disappearance of phases related to nepheline, sodalite and C-S-H gel, and lower intensity peaks related to albite and anorthoclase in GPM specimens exposed to acid solutions when compared with that exposed to water as obtained from the XRD analysis, and mostly lower atomic ratios obtained from EDS analysis indicate the depolymerization of aluminosilicate gels and resulted in significant loss in compressive strength of geopolymer mortar after immersion in acid solutions.
- In case of exposure to different sulfate solutions and H_2SO_4 solution, the formation of more amount of gypsum in the GPM mixes made with higher GGBS content was confirmed from the XRD, EDS and FESEM analyses.
- The GPM mix made with lower GGBS amount i.e., 15% (FA85/G15) exhibited mostly higher atomic Na/Si, Al/Si and Ca/Si ratios when exposed to acid solutions, which indicates comparatively lower deterioration of aluminosilicate gels and hence, showed lower compressive strength loss when compared with GPM mixes made with higher GGBS content at constant S/B ratio. This was supported by the formation of relatively denser microstructure in this GPM mix as was evident from the FESEM analysis.
- Although the GPM mixes made with higher S/B ratio had lower compressive strength due to lower paste content in the mixes, the formation of lower amount of gypsum and leaching of lower amount of Na and Al in these mixes were responsible for relatively better performance against sulfate and acid solutions as compared to the GPM mixes made with lower S/B ratio.
- The shifting of Si-O-Si(Al) bond toward higher wavenumbers after exposure to 0.62 mol/l H_2SO_4 and 0.62 mol/l HCl solutions when compared with exposure to water indicated the increase in atomic Si/Al ratio due to weaker Al-O bonds in the aluminosilicate network, which is replaced by Si-O bonds in the acid exposure condition. Thus, the GPM mixes exhibited significantly lower compressive strength in case of exposure to H_2SO_4 and HCl solutions as compared that exposed to water.

8.4 Conclusions obtained from multi-response optimization for composition of geopolymer concrete based on fresh, and hardened properties

- From the results of ANOVA of signal-to-noise (S/N) ratio of the obtained properties, it was concluded that the GGBS replacement level (% by mass of binder) is the most influential parameter, which had dominant effect on setting time, and compressive strength of geopolymer concrete (GPC) under ambient condition. However, the W/GPS

ratio dominated the effect of other parameters on consistency (slump value) of fresh GPC mixes.

- The geopolymerization process of fly ash based GPC was accelerated under ambient curing condition due to the addition of GGBS, which resulted in lower setting time and higher early age compressive strength. Nevertheless, the presence of fly ash was equally important as that of GGBS from view point of adequate setting time, better workability and enhancement of compressive strength at later age of ambient curing.
- Although, the mean value of S/N ratio determined from Taguchi method provided the GPC mix with optimum level of parameters to achieve the individual properties with respect to "larger-the-better" function, the multi-response optimization approach using Grey relational analysis resulted in a single set of optimized level of parameters for all the properties simultaneously.
- The comparison of XRD patterns of raw fly ash and GGBS with that of GPC mixes indicated the formation of N-(C)-A-S-H gel along with C-S-H gel, which contributed to the compressive strength development of GPC mixes. Further, the XRD patterns indicated the formation of more amount of N-(C)-A-S-H gel with increase in GGBS replacement level leading to higher compressive strength of GPC at both 7 and 28 days.
- The comparison of FTIR spectra of raw fly ash and GGBS with that of GPC mixes showed the shifting in position of the peak attributed to Si–O–Si(Al) bond that indicated the occurrence of geopolymerization process of precursor materials leading to geopolymer gel formation in the GPC mixes. Further, the formation of N-A-S-H, N-(C)-A-S-H and C-S-H gels in the GPC mixes were confirmed from the FESEM micrographs. In addition, the variations in formation of aluminosilicate geopolymer gel with curing age were also evident from the micrographs.
- Based on the results of multi-response optimization approach by Taguchi-GRA method, the optimized GPC mix prepared with 55% fly ash, 45% GGBS, W/GPS ratio of 0.31, NaOH solution of 14 M, binder content of 450 kg/m^3 and SS/SH ratio of 1.5 in the verification experiment performed better among all the GPC mixes with respect to setting time, workability and compressive strength simultaneously.

8.5 Conclusions obtained from influence of chloride ions on workability, strength, rebar corrosion, and microstructure evolution of geopolymer concrete

- The slump value of control (0% NaCl) and NaCl admixed fly ash-GGBS based GPC mixes were lower than their corresponding fly ash based GPC mixes due to higher water demand of GGBS in fly ash-GGBS based GPC mixes as a result of its angular particle shape and larger surface area as compared to fly ash. Further, the NaCl admixed fly ash and fly ash-GGBS based GPC mixes showed improved consistency in comparison to control fly ash and fly ash-GGBS based GPC mixes.
- The control and chloride admixed fly ash-GGBS based GPC mixes mostly exhibited higher compressive strength as compared to their corresponding fly ash based GPC mixes at all ages . Further, the compressive strength of fly ash-GGBS based GPC mixes mostly increased with increase in GGBS replacement level, at all ages.
- The presence of NaCl in the mixes reduced the compressive strength of both fly ash and fly ash-GGBS based GPC mixes as compared to control mixes at all ages. Further, the compressive strength decreased with increase in admixed NaCl concentration in the GPC mixes.
- The reduction in compressive strength of fly ash and fly ash-GGBS based GPC mixes due to presence of NaCl decreased with increase in age. This indicates significant effect of NaCl in hindering the geopolymerization process at early age.
- In the presence of NaCl, the steel reinforcement embedded in fly ash-GGBS based GPC specimens mostly exhibited less negative corrosion potential (E_{corr}) and lower corrosion current density (I_{corr}) as compared to their corresponding fly ash based GPC specimens. This is attributed to the formation of more amount of geopolymer gels as a result of higher extent of geopolymerization reaction in the presence of GGBS in the GPC mixes. This resulted in comparatively denser microstructure in fly ash-GGBS based GPC mixes leading to availability of lower amount of chloride ions in the vicinity of rebar.
- In case of chloride admixed fly ash-GGBS based GPC mixes, the embedded steel bar mostly exhibited less negative corrosion potential and lower corrosion current density with increase in GGBS content. The effect of comparatively higher resistivity due to formation of denser microstructure in the mixes made with higher GGBS content resulted in availability of lower amount of chloride ions in the electrolytic pore solution of concrete surrounding the rebar that led to lower extent of corrosion.

- The steel bar embedded in fly ash as well as fly ash-GGBS based GPC specimens mostly exhibited more negative corrosion potential and higher corrosion current density with increase in admixed NaCl concentration as a result of higher conductivity in the presence of more amount of chloride ions in GPC.
- The fly ash-GGBS based GPC mixes showed lower free chloride content as compared to their corresponding fly ash based GPC mixes at all ages (7, 28, and 360 days), and at rebar level of GPC specimens at the age of 600 days. Further, the fly ash-GGBS based GPC mixes made with higher GGBS content mostly exhibited lower free chloride content as compared to that made with lower GGBS content at the age of 28 and 360 days, and at rebar level of GPC specimens at the age of 600 days.
- The fly ash-GGBS based GPC mixes mostly exhibited lower chloride binding capacity as compared to their corresponding fly ash based GPC mixes at the early age of 7 days whereas the opposite variation was observed at the age of 28 and 360 days, and at rebar level of GPC specimens at the age of 600 days. At later ages, the higher chloride binding capacity of fly ash-GGBS based GPC mixes may be attributed to the formation of more amount of calcium bearing binding gels that resulted in more physical adsorption of chloride ions. Further, the chloride binding capacity of fly ash-GGBS based GPC mixes mostly increased with increase in age.
- The chloride binding capacity at rebar level of fly ash and fly ah-GGBS based GPC specimens made with comparatively lower GGBS content (15% and 30%) mostly decreased with increase in NaCl concentration, whereas the opposite variation was observed in fly ah-GGBS based GPC specimens made with comparatively higher GGBS content (45% and 60%).
- The formation of peak related to C-S-H gel along with higher peak intensity related to aluminosilicate gels as observed from the XRD patterns of fly ash-GGBS based GPC mixes at different ages and at rebar level of fly ash-GGBS based GPC specimens indicated the formation of relatively denser microstructure in fly ash-GGBS based GPC mixes compared to fly ash based GPC mixes. This substantiates the results of compressive strength, corrosion parameters and chloride content where the fly ash-GGBS based GPC mixes showed higher compressive strength, lower corrosion activity, and lower free and total chloride content in comparison to fly ash based GPC mixes.

- The higher atomic Ca/Si ratio obtained from EDS analysis of fly ash-GGBS based GPC mixes at different ages and at rebar level of fly ash-GGBS based GPC specimens indicated the formation of calcium-rich gels in fly ash-GGBS based GPC mixes that corroborates the results obtained from XRD analysis.
- The XRD analysis at rebar level of fly ash and fly ash-GGBS based GPC specimens indicated that in majority of the GPC mixes, the peak intensity related to sodalite, nepheline, anorthoclase, albite and C-S-H gel (in case of fly ash-GGBS based GPC) mostly decreased with increase in concentration of NaCl. This observation is in line with the results of corrosion parameters and chloride content of NaCl admixed fly ash and fly ash-GGBS based GPC mixes.
- The presence of halite crystals identified from FESEM images of GPC mixes confirmed the crystallization of NaCl in geopolymer gels. This is also corroborated with the peak related to halite identified in the XRD patterns of GPC mixes.
- In control and NaCl admixed mixes, the shifting of wavenumbers of Si-O-Si(Al) bonds in the FTIR spectra between fly ash and fly ash-GGBS based GPC mixes, and comparatively denser microstructure of fly ash-GGBS based GPC mixes as observed from FESEM images corroborate the variation in compressive strength between fly ash and fly ash-GGBS based GPC mixes.

8.6 Significance of research outcome

In geopolymer composites, the geopolymerization process depends on several control parameters. As a construction material, the geopolymer mortar and concrete must satisfy different performance criteria such as adequate setting time and consistency, higher compressive strength, and better durability properties. The outcome of the present research work provides significant information about the influence of various control parameters such as GGBS replacement level, water-to-geopolymer solids (W/GPS) ratio, molarity of NaOH solution, and sand-to-binder (S/B) ratio on setting time, flowability, compressive strength, water absorption, apparent volume of permeable voids, sorptivity, and sulfate and acid resistance of fly ash-GGBS based geopolymer mortar (GPM), and arriving at the optimal combinations of mix parameters by Taguchi-grey relational analysis (GRA) method. This study also provides information about arriving at the optimal combination of mix parameters (GGBS replacement level, W/GPS ratio, molarity of NaOH solution, binder content, and mass ratio of Na_2SiO_3 to NaOH solution) for the composition of fly ash-GGBS

based geopolymer concrete (GPC) with respect to multiple properties i.e., setting time, workability, and compressive strength simultaneously using Taguchi-GRA method. The research outcome of the present study provides insight about the influence of chloride ions on consistency, strength development, chloride binding behaviour, and rebar corrosion in fly ash and fly ash-GGBS based geopolymer concrete. In addition, the present study also elucidated the correlation of strength development and rebar corrosion with microstructural changes in GPC mixes.

The findings of the present research work indicated that Taguchi-Grey relational analysis (GRA) method can be successfully implemented while investigating the effect of a wide range of control parameters on multiple properties of geopolymer mortar and concrete with minimum number of experiments. The obtained results of verification experiments on the proposed optimized geopolymer mortar mix and geopolymer concrete mix confirmed the effectiveness of Taguchi-GRA approach for determining the optimal combination of mix parameters for the production of geopolymer mortar and concrete. Based on the results obtained from the present research work, higher GGBS content and lower sand-to-binder (S/B) ratio can be recommended for the production of geopolymer composites for adequate setting time and flowability, higher compressive strength and lower water absorption properties. However, in case of sulfate and acidic exposure environment, geopolymer composites with lower GGBS content and higher S/B ratio can be recommended. The outcome form the present study indicated that the molarity of NaOH solution may not be an influential control parameter while considering multiple properties such fresh, hardened, and different durability properties of geopolymer composites simultaneously. The findings from the present study showed that the exposure to acid solutions produced surface damage in the specimens with more-intense damage, and significant volumetric expansion in the geopolymer mortar mixes exposed to H_2SO_4 solution, which resulted in significant strength loss when compared with exposure to HCl solution. Thus, in case of exposure of geopolymer composites to aggressive environment such as sulfuric acid as well hydrochloric acid exposure condition, the obtained outcome from the present study can be useful while selecting the levels of different mix parameters for the production of geopolymer composites. The obtained findings from the present study suggested that the fly ash-GGBS based geopolymer concrete made with higher GGBS content can perform better against chloride-rich environment in terms of improved strength, higher chloride binding, and protection against rebar corrosion as compared to fly ash based geopolymer

concrete. On the basis of the corroborations of variations in the strength development of geopolymer mortar and geopolymer concrete with age as well as in case of exposure to aggressive environment with the changes in microstructure analyzed through XRD, EDS, FESEM and FTIR analyses, the selection of different levels of mix parameters for the production of geopolymer composites can be decided based on the research outcome obtained from the present research work.

8.7 Recommendations for future research work

The recommendations for future research work are as follows:

- The present study can be extended to examine the influence of other precursor materials such as rice husk ash and silica fume on various fresh, mechanical, and durability properties of geopolymer mortar and concrete.
- The present investigation can be extended to assess the performance of geopolymer mortar and concrete against exposure to composite chloride-sulfate environment, and natural sewer environment.
- The present research work can also be extended to evaluate the effect of mix parameters on chloride diffusion, chloride binding, and rebar corrosion in geopolymer concrete exposed to chloride solutions with chloride ions associated with different cations.
- The present study can be extended to evaluate the performance of geopolymer mortar against sulfate attack for a longer exposure period.

References

[1] G. F. Huseien, J. Mirza, M. Ismail, S. K. Ghoshal, A. A. Hussein, Geopolymer mortars as sustainable repair material: A comprehensive review, Renewable and Sustainable Energy Reviews 80 (2017) 54–74.

[2] J. Shang, J. G. Dai, T. J. Zhao, S. Y. Guo, P. Zhang, B. Mu, Alternation of traditional cement mortars using fly ash-based geopolymer mortars modified by slag, Journal of Cleaner Production 203 (2018) 746–756.

[3] J. Davidovits, Global warming impact on the cement and aggregates industries, World Resource Review 6 (1994) 263–278.

[4] R. He, S. Zhang, X. Zhang, Z. Zhang, Y. Zhao, H. Ding, Copper slag: The leaching behavior of heavy metals and its applicability as a supplementary cementitious material, Journal of Environmental Chemical Engineering 9 (2021) 105132.

[5] K. Fang, J. Zhao, D. Wang, H. Wang, Z. Dong, Use of ladle furnace slag as supplementary cementitious material before and after modification by rapid air cooling: A comparative study of influence on the properties of blended cement paste, Construction and Building Materials 314 (2022) 125434.

[6] X. Zhang, C. Qian, Z. Ma, F. Li, Study on preparation of supplementary cementitious material using microbial CO_2 fixation of steel slag powder, Construction and Building Materials 326 (2022) 126864.

[7] H. Wang, T. Qi, G. Feng, X. Wen, Z. Wang, X. Shi, X. Du, Effect of partial substitution of corn straw fly ash for fly ash as supplementary cementitious material on the mechanical properties of cemented coal gangue backfill, Construction and Building Materials 280 (2021) 122553.

[8] V. Jittin, S. N. Minnu, A. Bahurudeen, Potential of sugarcane bagasse ash as supplementary cementitious material and comparison with currently used rice husk ash, Construction and Building Materials 273 (2021) 121679.

[9] J. M. Paris, J. G. Roessler, C. C. Ferraro, H. D. Deford, T. G. Townsend, A review of waste products utilized as supplements to Portland cement in concrete, Journal of Cleaner Production 121 (2016) 1–18.

[10] E. Aprianti, P. Shafigh, S. Bahri, J. N. Farahani, Supplementary cementitious materials origin from agricultural wastes - A review, Construction and Building Materials 74 (2015) 176–187.

[11] M. M. Hossain, M. R. Karim, M. K. Hossain, M. N. Islam, M. F. M. Zain, Durability of mortar and concrete containing alkali-activated binder with pozzolans: A review, Construction and Building Materials 93 (2015) 95–109.

[12] J. Kwasny, M. N. Soutsos, J. A. McIntosh, D. J. Cleland, Comparison of the effect of mix proportion parameters on behaviour of geopolymer and Portland cement mortars, Construction and Building Materials 187 (2018) 635–651.

[13] J. Davidovits, S. Quentin, Geopolymers: Inorganic polymeric new materials, 37 (1991) 1633–1656.

[14] A. Noushini, A. Castel, The effect of heat-curing on transport properties of low-calcium fly ash-based geopolymer concrete, Construction and Building Materials 112 (2016) 464–477.

[15] P. Cong, Y. Cheng, Advances in geopolymer materials: A comprehensive review, Journal of Traffic and Transportation Engineering 8 (2021) 283–314.

[16] P. W. Ken, M. Ramli, C. C. Ban, An overview on the influence of various factors on the properties of geopolymer concrete derived from industrial by-products, Construction and Building Materials 77 (2015) 370–395.

[17] X. Y. Zhuang, L. Chen, S. Komarneni, C. H. Zhou, D. S. Tong, H. M. Yang, W. H. Yu, H. Wang, Fly ash-based geopolymer: Clean production, properties and applications, Journal of Cleaner Production 125 (2016) 253–267.

[18] B. S. Thomas, J. Yang, A. Bahurudeen, S. N. Chinnu, J. A. Abdalla, R. A. Hawileh, H. M. Hamada, Geopolymer concrete incorporating recycled aggregates: A comprehensive review, Cleaner Materials 3 (2022) 100056.

[19] D. Hardjito, S. E. Wallah, D. M. J. Sumajouw, B. V. Rangan, On the development of fly ash-based geopolymer concrete, ACI Materials Journal 101 (2004) 467–472.

[20] M. Amran, S. Debbarma, T. Ozbakkaloglu, Fly ash-based eco-friendly geopolymer concrete: A critical review of the long-term durability properties, Construction and Building Materials 270 (2021) 121857.

[21] K. Kupwade-Patil, E. N. Allouche, Examination of chloride-induced corrosion in reinforced geopolymer concretes, Journal of Materials in Civil Engineering 25 (2013) 1465–1476.

[22] G. Nagalia, Y. Park, A. Abolmaali, P. Aswath, Compressive strength and microstructural properties of fly ash–based geopolymer concrete, Journal of Materials in Civil Engineering 28 (2016) 04016144.

[23] E. Özbay, M. Erdemir, H. I. Durmuş, Utilization and efficiency of ground granulated blast furnace slag on concrete properties - A review, Construction and Building Materials 105 (2016) 423–434.

[24] H. Xu, W. Gong, L. Syltebo, K. Izzo, W. Lutze, I. L. Pegg, Effect of blast furnace slag grades on fly ash based geopolymer waste forms, Fuel 133 (2014) 332–340.

[25] D. Khale, R. Chaudhary, Mechanism of geopolymerization and factors influencing its development: A review, Journal of Materials Science 42 (2007) 729–746.

[26] B. Singh, G. Ishwarya, M. Gupta, S. K. Bhattacharyya, Geopolymer concrete: A review of some recent developments, Construction and Building Materials 85 (2015) 78–90.

[27] A. Mehta, R. Siddique, An overview of geopolymers derived from industrial by-products, Construction and Building Materials 127 (2016) 183–198.

[28] J. S. J. V. Deventer, J. L. Provis, P. Duxson, Technical and commercial progress in the adoption of geopolymer cement, Minerals Engineering 29 (2012) 89–104.

[29] H. Rashidian-Dezfouli, P. R. Rangaraju, A comparative study on the durability of geopolymers produced with ground glass fiber, fly ash, and glass-powder in sodium sulfate solution, Construction and Building Materials 153 (2017) 996–1009.

[30] B. V. Rangan, Geopolymer concrete for environmental protection, Indian Concrete Journal 88 (2014) 41–59.

[31] P. Pavithra, M. S. Reddy, P. Dinakar, B. H. Rao, B. K. Satpathy, A. N. Mohanty, A mix design procedure for geopolymer concrete with fly ash, Journal of Cleaner Production 133 (2016) 117–125.

[32] M. Albitar, M. S. M. Ali, P. Visintin, M. Drechsler, Effect of granulated lead smelter slag on strength of fly ash-based geopolymer concrete, Construction and Building Materials 83 (2015) 128–135.

[33] P. Topark-Ngarm, P. Chindaprasirt, V. Sata, Setting time, strength, and bond of high-calcium fly ash geopolymer concrete, Journal of Materials in Civil Engineering 27 (2015) 04014198.

[34] C. Tennakoon, A. Shayan, J. G. Sanjayan, A. Xu, Chloride ingress and steel corrosion in geopolymer concrete based on long term tests, Materials and Design 116 (2017) 287–299.

[35] H. E. Elyamany, A. E. M. A. Elmoaty, A. M. Elshaboury, Setting time and 7-day strength of geopolymer mortar with various binders, Construction and Building Materials 187 (2018) 974–983.

[36] S. K. Nath, S. Kumar, Influence of iron making slags on strength and microstructure of fly ash geopolymer, Construction and Building Materials 38 (2013) 924–930.

[37] S. M. Laskar, S. Talukdar, Development of ultrafine slag-based geopolymer mortar for use as repairing mortar, Journal of Materials in Civil Engineering 29 (2017) 04016292.

[38] P. Nath, P. K. Sarker, Effect of GGBFS on setting, workability and early strength properties of fly ash geopolymer concrete cured in ambient condition, Construction and Building Materials 66 (2014) 163–171.

[39] A. M. Rashad, A comprehensive overview about the influence of different additives on the properties of alkali-activated slag - A guide for civil engineer, Construction and Building Materials 47 (2013) 29–55.

[40] J. G. Jang, H. K. Lee, Effect of fly ash characteristics on delayed high-strength development of geopolymers, Construction and Building Materials 102 (2016) 260–269.

[41] Z. Zhang, L. Li, X. Ma, H. Wang, Compositional, microstructural and mechanical properties of ambient condition cured alkali-activated cement, Construction and Building Materials 113 (2016) 237–245.

[42] V. Sata, A. Sathonsaowaphak, P. Chindaprasirt, Resistance of lignite bottom ash geopolymer mortar to sulfate and sulfuric acid attack, Cement and Concrete Composites 34 (2012) 700–708.

[43] M. B. Karakoç, I. Türkmen, M. M. Maraş, F. Kantarci, R. Demirboga, Sulfate resistance of ferrochrome slag based geopolymer concrete, Ceramics International 42 (2016) 1254–1260.

[44] A. M. Neville, Properties of concrete, Fifth edition, Pearson India Education Services Pvt. Ltd, 2012.

[45] M. M. Hossain, M. R. Karim, M. F. M. Zain, Acid and sulfate resistance of alkali-activated ternary blended composite binder, Journal of Materials in Civil Engineering 30 (2018) 04017276.

[46] R. Gopalakrishnan, K. Chinnaraju, Durability of ambient cured alumina silicate concrete based on slag/fly ash blends against sulfate environment, Construction and Building Materials 204 (2019) 70–83.

[47] W. G. V. Saavedra, D. E. Angulo, R. M. Gutiérrez, Fly ash slag geopolymer concrete: Resistance to sodium and magnesium sulfate attack, Journal of Materials in Civil Engineering 28 (2016) 04016148.

[48] H. A. Alcamand, P. H. R. Borges, F. A. Silva, A. C. C. Trindade, The effect of matrix composition and calcium content on the sulfate durability of metakaolin and metakaolin/slag alkali-activated mortars, Ceramics International 44 (2018) 5037–5044.

[49] M. O. Yusuf, Performance of slag blended alkaline activated palm oil fuel ash mortar in sulfate environments, Construction and Building Materials 98 (2015) 417–424.

[50] I. Ismail, S. A. Bernal, J. L. Provis, S. Hamdan, J. S. J. V. Deventer, Microstructural changes in alkali activated fly ash/slag geopolymers with sulfate exposure, Materials and Structures 46 (2013) 361–373.

[51] T. Bakharev, Durability of geopolymer materials in sodium and magnesium sulfate solutions, Cement and Concrete Research 35 (2005) 1233–1246.

[52] X. Guo, G. Xiong, Resistance of fiber-reinforced fly ash-steel slag based geopolymer mortar to sulfate attack and drying-wetting cycles, Construction and Building Materials 269 (2021) 121326.

[53] P. Chindaprasirt, P. Paisitsrisawat, U. Rattanasak, Strength and resistance to sulfate and sulfuric acid of ground fluidized bed combustion fly ash-silica fume alkali-Activated composite, Advanced Powder Technology 25 (2014) 1087–1093.

[54] H. E. Elyamany, A. E. M. A. Elmoaty, A. M. Elshaboury, Magnesium sulfate resistance of geopolymer mortar, Construction and Building Materials 184 (2018) 111–127.

[55] J. Zhang, C. Shi, Z. Zhang, Z. Ou, Durability of alkali-activated materials in aggressive environments: A review on recent studies, Construction and Building Materials 152 (2017) 598–613.

[56] A. Wang, Y. Zheng, Z. Zhang, K. Liu, Y. Li, L. Shi, D. Sun, The durability of alkali-activated materials in comparison with ordinary Portland cements and concretes: A review, Engineering 6 (2020) 695–706.

[57] P. S. Deb, P. K. Sarker, S. Barbhuiya, Sorptivity and acid resistance of ambient-cured geopolymer mortars containing nano-silica, Cement and Concrete Composites 72 (2016) 235–245.

[58] T. Bakharev, Resistance of geopolymer materials to acid attack, Cement and Concrete Research 35 (2005) 658–670.

[59] N. K. Lee, H. K. Lee, Influence of the slag content on the chloride and sulfuric acid resistances of alkali-activated fly ash/slag paste, Cement and Concrete Composites 72 (2016) 168–179.

[60] T. A. Aiken, J. Kwasny, W. Sha, M. N. Soutsos, Effect of slag content and activator dosage on the resistance of fly ash geopolymer binders to sulfuric acid attack, Cement and Concrete Research 111 (2018) 23–40.

[61] B. W. Jo, M. A. Sikandar, S. Chakraborty, Z. Baloch, Investigation of the acid and sulfate resistance performances of hydrogen-rich water based mortars, Construction and Building Materials 137 (2017) 1–11.

[62] R. R. Lloyd, J. L. Provis, J. S. J. V. Deventer, Acid resistance of inorganic polymer binders. 1. Corrosion rate, Materials and Structures 45 (2012) 1–14.

[63] M. Vafaei, A. Allahverdi, Durability of geopolymer mortar based on waste-glass powder and calcium aluminate cement in acid solutions, Journal of Materials in Civil Engineering 29 (2017) 04017196.

[64] L. Gu, T. Bennett, P. Visintin, Sulphuric acid exposure of conventional concrete and alkali-activated concrete: Assessment of test methodologies, Construction and Building Materials 197 (2019) 681–692.

[65] L. Gu, P. Visintin, T. Bennett, Evaluation of accelerated degradation test methods for cementitious composites subject to sulfuric acid attack; application to conventional and alkali-activated concretes, Cement and Concrete Composites 87 (2018) 187–204.

[66] M. H. Mahmoud, M. T. Bassuoni, Performance of concrete with alkali-activated materials and nanosilica in acidic environments, Journal of Materials in Civil Engineering 31 (2019) 04019009.

[67] A. Mehta, R. Siddique, Sulfuric acid resistance of fly ash based geopolymer concrete, Construction and Building Materials 146 (2017) 136–143.

[68] J. Ren, L. Zhang, R. S. Nicolas, Degradation of alkali-activated slag and fly ash mortars under different aggressive acid conditions, Journal of Materials in Civil Engineering 33 (2021) 04021140.

[69] F. Qu, W. Li, W. Dong, V. W. Y. Tam, T. Yu, Durability deterioration of concrete under marine environment from material to structure: A critical review, Journal of Building Engineering 35 (2021) 102074.

[70] B. Pradhan, Corrosion behavior of steel reinforcement in concrete exposed to composite chloride-sulfate environment, Construction and Building Materials 72 (2014) 398–410.

[71] C. Gunasekara, D. Law, S. Bhuiyan, S. Setunge, L. Ward, Chloride induced corrosion in different fly ash based geopolymer concretes, Construction and Building Materials 200 (2019) 502–513.

[72] M. Babaee, A. Castel, Chloride-induced corrosion of reinforcement in low-calcium fly ash-based geopolymer concrete, Cement and Concrete Research 88 (2016) 96–107.

[73] P. Chindaprasirt, W. Chalee, Effect of sodium hydroxide concentration on chloride penetration and steel corrosion of fly ash-based geopolymer concrete under marine site, Construction and Building Materials 63 (2014) 303–310.

[74] D. V. Reddy, J. B. Edouard, K. Sobhan, Durability of fly ash–based geopolymer structural concrete in the marine environment, Journal of Materials in Civil Engineering 25 (2013) 781–787.

[75] F. Tittarelli, A. Mobili, C. Giosuè, A. Belli, T. Bellezze, Corrosion behaviour of bare and galvanized steel in geopolymer and ordinary Portland cement based mortars with the same strength class exposed to chlorides, Corrosion Science 134 (2018) 64–77.

[76] C. Monticelli, M. E. Natali, A. Balbo, C. Chiavari, F. Zanotto, S. Manzi, M. C. Bignozzi, A study on the corrosion of reinforcing bars in alkali-activated fly ash mortars under wet and dry exposures to chloride solutions, Cement and Concrete Research 87 (2016) 53–63.

[77] S. K. Nath, S. Maitra, S. Mukherjee, S. Kumar, Microstructural and morphological evolution of fly ash based geopolymers, Construction and Building Materials 111 (2016) 758–765.

[78] U. Durak, S. İlkentapar, O. Karahan, B. Uzal, C. D. Atiş, A new parameter influencing the reaction kinetics and properties of fly ash based geopolymers: A pre-rest period before heat curing, Journal of Building Engineering 35 (2021) 102023.

[79] X. Chen, J. Zhang, M. Lu, B. Chen, S. Gao, J. Bai, H. Zhang, Y. Yang, Study on the effect of calcium and sulfur content on the properties of fly ash based geopolymer, Construction and Building Materials 314 (2022) 125650.

[80] A. A. Aliabdo, A. E. M. A. Elmoaty, H. A. Salem, Effect of water addition, plasticizer and alkaline solution constitution on fly ash based geopolymer concrete performance, Construction and Building Materials 121 (2016) 694–703.

[81] S. Saha, C. Rajasekaran, Enhancement of the properties of fly ash based geopolymer paste by incorporating ground granulated blast furnace slag, Construction and Building Materials 146 (2017) 615–620.

[82] I. Ismail, S. A. Bernal, J. L. Provis, R. S. Nicolas, S. Hamdan, J. S. J. V. Deventer, Modification of phase evolution in alkali-activated blast furnace slag by the incorporation of fly ash, Cement and Concrete Composites 45 (2014) 125–135.

[83] N. K. Lee, H. K. Lee, Reactivity and reaction products of alkali-activated, fly ash/slag paste, Construction and Building Materials 81 (2015) 303–312.

[84] T. Phoo-Ngernkham, A. Maegawa, N. Mishima, S. Hatanaka, P. Chindaprasirt, Effects of sodium hydroxide and sodium silicate solutions on compressive and shear bond strengths of FA-GBFS geopolymer, Construction and Building Materials 91 (2015) 1–8.

[85] M. A. Yazdi, M. Liebscher, S. Hempel, J. Yang, V. Mechtcherine, Correlation of microstructural and mechanical properties of geopolymers produced from fly ash and slag at room temperature, Construction and Building Materials 191 (2018) 330–341.

[86] Z. Li, S. Liu, Influence of slag as additive on compressive strength of fly ash-based geopolymer, Journal of Materials in Civil Engineering 19 (2007) 470–474.

[87] M. Chi, R. Huang, Binding mechanism and properties of alkali-activated fly ash/slag mortars, Construction and Building Materials 40 (2013) 291–298.

[88] M. Z. N. Khan, F. U. A. Shaikh, Y. Hao, H. Hao, Effects of curing conditions and sand-to-binder ratios on compressive strength development of fly ash geopolymer, Journal of Materials in Civil Engineering 30 (2018) 04017267.

[89] X. Lyu, N. Robinson, M. Elchalakani, M. L. Johns, M. Dong, S. Nie, Sea sand seawater geopolymer concrete, Journal of Building Engineering 50 (2022) 104141.

[90] P. S. Deb, P. Nath, P. K. Sarker, The effects of ground granulated blast-furnace slag blending with fly ash and activator content on the workability and strength properties of geopolymer concrete cured at ambient temperature, Materials and Design 62 (2014) 32–39.

[91] A. Rafeet, R. Vinai, M. Soutsos, W. Sha, Guidelines for mix proportioning of fly ash/GGBS based alkali activated concretes, Construction and Building Materials 147 (2017) 130–142.

[92] G. Fang, W. K. Ho, W. Tu, M. Zhang, Workability and mechanical properties of alkali-activated fly ash-slag concrete cured at ambient temperature, Construction and Building Materials 172 (2018) 476–487.

[93] B. Singh, M. R. Rahman, R. Paswan, S. K. Bhattacharyya, Effect of activator concentration on the strength, ITZ and drying shrinkage of fly ash/slag geopolymer concrete, Construction and Building Materials 118 (2016) 171–179.

[94] A. Wardhono, C. Gunasekara, D. W. Law, S. Setunge, Comparison of long term performance between alkali activated slag and fly ash geopolymer concretes, Construction and Building Materials 143 (2017) 272–279.

[95] D. Ravikumar, S. Peethamparan, N. Neithalath, Structure and strength of NaOH activated concretes containing fly ash or GGBFS as the sole binder, Cement and Concrete Composites 32 (2010) 399–410.

[96] I. I. Atabey, O. Karahan, C. Bilim, C. D. Atiş, The influence of activator type and quantity on the transport properties of class F fly ash geopolymer, Construction and Building Materials 264 (2020) 120268.

[97] M. M. Hossain, M. R. Karim, M. M. A Elahi, M. F. M. Zain, Water absorption and sorptivity of alkali-activated ternary blended composite binder, Journal of Building Engineering 31 (2020) 101370.

[98] I. Ismail, S. A. Bernal, J. L. Provis, R. S. Nicolas, D. G. Brice, A. R. Kilcullen, S. Hamdan, J. S. J. V. Deventer, Influence of fly ash on the water and chloride permeability of alkali-activated slag mortars and concretes, Construction and Building Materials 48 (2013) 1187–1201.

[99] Z. Bascarevic, M. Komljenović, Z. Miladinović, V. Nikolić, N. Marjanović, R. Petrović, Impact of sodium sulfate solution on mechanical properties and structure of fly ash based geopolymers, Materials and Structures 48 (2015) 683–697.

[100] N. Dzunuzovic, M. Komljenović, V. Nikolić, T. Ivanović, External sulfate attack on alkali-activated fly ash-blast furnace slag composite, Construction and Building Materials 157 (2017) 737–747.

[101] H. A. Khan, A. Castel, M. S. H. Khan, Corrosion investigation of fly ash based geopolymer mortar in natural sewer environment and sulphuric acid solution, Corrosion Science 168 (2020) 108586.

[102] J. C. Kuri, P. K. Sarker, F. U. A. Shaikh, Sulphuric acid resistance of ground ferronickel slag blended fly ash geopolymer mortar, Construction and Building Materials 313 (2021) 125505.

[103] M. Criado, I. Sobrados, J. M. Bastidas, J. Sanz, Corrosion behaviour of coated steel rebars in carbonated and chloride-contaminated alkali-activated fly ash mortar, Progress in Organic Coatings 99 (2016) 11–22.

[104] K. T. Nguyen, T. A. Le, K. Lee, Evaluation of the mechanical properties of sea sand-based geopolymer concrete and the corrosion of embedded steel bar, Construction and Building Materials 169 (2018) 462–472.

[105] C. Panagiotopoulou, S. Tsivilis, G. Kakali, Application of the Taguchi approach for the composition optimization of alkali activated fly ash binders, Construction and Building Materials 91 (2015) 17–22.

[106] B. Yuan, Q. L. Yu, H. J. H. Brouwers, Reaction kinetics, reaction products and compressive strength of ternary activators activated slag designed by Taguchi method, Materials and Design 86 (2015) 878–886.

[107] M. N. S. Hadi, N. A. Farhan, M. N. Sheikh, Design of geopolymer concrete with GGBFS at ambient curing condition using Taguchi method, Construction and Building Materials 140 (2017) 424–431.

[108] M. Shojaei, K. Behfarnia, R. Mohebi, Application of alkali-activated slag concrete in railway sleepers, Materials and Design 69 (2015) 89–95.

[109] ASTM C618-19, Standard specification for coal fly ash and raw or calcined natural pozzolan for use in concrete, ASTM International, West Conshohocken, PA, 2019.

[110] IS 4031 (Part 11): 1988, (Reaffirmed 2019), Methods of physical tests for hydraulic cement: Part 11 Determination of density, Bureau of Indian Standards, New Delhi, 2019.

[111] Y. Liu, W. Zhu, E. H. Yang, Alkali-activated ground granulated blast-furnace slag incorporating incinerator fly ash as a potential binder, Construction and Building Materials 112 (2016) 1005–1012.

[112] X. Gao, Q. L. Yu, H. J. H. Brouwers, Properties of alkali activated slag-fly ash blends with limestone addition, Cement and Concrete Composites 59 (2015) 119–128.

[113] Z. Zhang, Y. Zhu, T. Yang, L. Li, H. Zhu, H. Wang, Conversion of local industrial wastes into greener cement through geopolymer technology: A case study of high-magnesium nickel slag, Journal of Cleaner Production 141 (2017) 463–471.

[114] IS 383: 2021, Coarse and fine aggregate for concrete - specification, Bureau of Indian Standards, New Delhi, 2021.

[115] W. Ferdous, A. Manalo, T. Aravinthan, Bond behaviour of composite sandwich panel and epoxy polymer matrix: Taguchi design of experiments and theoretical predictions, Construction and Building Materials 145 (2017) 76–87.

[116] R. K. Roy, A primer on the Taguchi method, Second edition, Society of Manufacturing Engineers, 2010.

[117] C. Y. Chang, R. Huang, P. C. Lee, T. L. Weng, Application of a weighted Grey-Taguchi method for optimizing recycled aggregate concrete mixtures, Cement and Concrete Composites 33 (2011) 1038–1049.

[118] Y. Kuo, T. Yang, G. W. Huang, The use of a grey-based Taguchi method for optimizing multi-response simulation problems, Engineering Optimization 40 (2008) 517–528.

[119] J. L. Mercy, S. Prakash, A. Krishnamoorthy, S. Ramesh, D. A. Anand, Multi response optimisation of mechanical properties in self-healing glass fiber reinforced plastic using grey relational analysis, Measurement 110 (2017) 344–355.

[120] O. L. C. Narong, C. K. Sia, S. K. Yee, P. Ong, A. Zainudin, N. H. M. Nor, M. F. Hassan, Optimisation of EMI shielding effectiveness: Mechanical and physical performance of mortar containing POFA for plaster work using Taguchi Grey method, Construction and Building Materials 176 (2018) 509–518.

[121] ASTM C1437-20, Standard test method for flow of hydraulic cement mortar, ASTM International, West Conshohocken, PA, 2020.

[122] ASTM C403/C403M-16, Standard test method for time of setting of concrete mixtures by penetration resistance, ASTM International, West Conshohocken, PA, 2016.

[123] ASTM C109/C109M-21, Standard test method for compressive strength of hydraulic cement mortars (Using 2-in. or [50 mm] cube specimens), ASTM International, West Conshohocken, PA, 2021.

[124] ASTM C642-13, Standard test method for density, absorption, and voids in hardened concrete, ASTM International, West Conshohocken, PA, 2013.

[125] ASTM C1585-20, Standard test method for measurement of rate of absorption of water by hydraulic-cement concretes, ASTM International, West Conshohocken, PA, 2020.

[126] IS 4031 (Part 5): 1988, (Reaffirmed 2019), Methods of physical tests for hydraulic cement: Part 5 Determination of intial and final setting times, Bureau of Indian Standards, New Delhi, 2019.

[127] ASTM C191-19, Standard test methods for time of setting of hydraulic cement by vicat needle, ASTM International, West Conshohocken, PA, 2019.

[128] IS 1199 (Part 2): 2018, Fresh concrete - Methods of sampling, testing and analysis: Part 2 Determination of consistency of fresh concrete, Bureau of Indian Standards, New Delhi, 2018.

[129] ASTM C143/C143M-20, Standard test method for slump of hydraulic-cement concrete, ASTM International, West Conshohocken, PA, 2020.

[130] IS 516 (Part 1/Sec 1): 2021, Hardened concrete - Methods of test: Part 1 Testing of strength of hardened concrete, Section 1: Compressive, flexural and split tensile strength, Bureau of Indian Standards, New Delhi, 2021.

[131] ASTM C876-15, Standard test method for corrosion potentials of uncoated reinforcing steel in concrete, ASTM International, West Conshohocken, PA, 2015.

[132] S. Puligilla, P. Mondal, Role of slag in microstructural development and hardening of fly ash-slag geopolymer, Cement and Concrete Research 43 (2013) 70–80.

[133] J. N. Y. Djobo, A. Elimbi, H. K. Tchakouté, S. Kumar, Mechanical properties and durability of volcanic ash based geopolymer mortars, Construction and Building Materials 124 (2016) 606–614.

[134] M. Vafaei, A. Allahverdi, P. Dong, N. Bassim, Acid attack on geopolymer cement mortar based on waste-glass powder and calcium aluminate cement at mild concentration, Construction and Building Materials 193 (2018) 363–372.

[135] M. B. Haha, G. L. Saout, F. Winnefeld, B. Lothenbach, Influence of activator type on hydration kinetics, hydrate assemblage and microstructural development of alkali activated blast-furnace slags, Cement and Concrete Research 41 (2011) 301–310.

[136] H. Ye, A. Radlińska, Fly ash-slag interaction during alkaline activation: Influence of activators on phase assemblage and microstructure formation, Construction and Building Materials 122 (2016) 594–606.

[137] M. Vafaei, A. Allahverdi, P. Dong, N. Bassim, M. Mahinroosta, Resistance of red clay brick waste/phosphorus slag-based geopolymer mortar to acid solutions of mild concentration, Journal of Building Engineering 34 (2021) 102066.

[138] X. Zhao, C. Liu, L. Zuo, L. Wang, Q. Zhu, M. Wang, Investigation into the effect of calcium on the existence form of geopolymerized gel product of fly ash based geopolymers, Cement and Concrete Composites 103 (2019) 279–292.

[139] J. Kwasny, T. A. Aiken, M. N. Soutsos, J. A. McIntosh, D. J. Cleland, Sulfate and acid resistance of lithomarge-based geopolymer mortars, Construction and Building Materials 166 (2018) 537–553.

[140] A. Rafeet, R. Vinai, M. Soutsos, W. Sha, Effects of slag substitution on physical and mechanical properties of fly ash-based alkali activated binders (AABs), Cement and Concrete Research 122 (2019) 118–135.

[141] G. M. Rao, T. D. G. Rao, Final setting time and compressive strength of fly ash and GGBS-based geopolymer paste and mortar, Arabian Journal for Science and Engineering 40 (2015) 3067–3074.

[142] A. A. Siyal, K. A. Azizli, Z. Man, H. Ullah, Effects of parameters on the setting time of fly ash based geopolymers using Taguchi method, Procedia Engineering 148 (2016) 302–307.

[143] M. Z. N. Khan, F. U. A. Shaikh, Y. Hao, H. Hao, Synthesis of high strength ambient cured geopolymer composite by using low calcium fly ash, Construction and Building Materials 125 (2016) 809–820.

[144] M. Olivia, H. Nikraz, Properties of fly ash geopolymer concrete designed by Taguchi method, Materials and Design 36 (2012) 191–198.

[145] A. Nazari, H. Khanmohammadi, M. Amini, H. Hajiallahyari, A. Rahimi, Production geopolymers by Portland cement: Designing the main parameters' effects on compressive strength by Taguchi method, Materials and Design 41 (2012) 43–49.

[146] M. J. A. Mijarsh, M. A. M. Johari, Z. A. Ahmad, Synthesis of geopolymer from large amounts of treated palm oil fuel ash: Application of the Taguchi method in investigating the main parameters affecting compressive strength, Construction and Building Materials 52 (2014) 473–481.

[147] K. Kupwade-Patil, E. N. Allouche, Impact of alkali silica reaction on fly ash-based geopolymer concrete, Journal of Materials in Civil Engineering 25 (2013) 131–139.

[148] A. A. Siyal, K. A. Azizli, Z. Man, L. Ismail, M. I. Khan, Geopolymerization kinetics of fly ash based geopolymers using JMAK model, Ceramics International 42 (2016) 15575–15584.

[149] S. Puligilla, P. Mondal, Co-existence of aluminosilicate and calcium silicate gel characterized through selective dissolution and FTIR spectral subtraction, Cement and Concrete Research 70 (2015) 39–49.

[150] G. S. Ryu, Y. B. Lee, K. T. Koh, Y. S. Chung, The mechanical properties of fly ash-based geopolymer concrete with alkaline activators, Construction and Building Materials 47 (2013) 409–418.

[151] M. Eiamwijit, K. Pachana, S. Kaewpirom, U. Rattanasak, P. Chindaprasirt, Comparative study on morphology of ground sub-bituminus FBC fly ash geopolymeric material, Advanced Powder Technology 26 (2015) 1053–1057.

[152] S. Kumar, F. Kristaly, G. Mucsi, Geopolymerisation behaviour of size fractioned fly ash, Advanced Powder Technology 26 (2015) 24–30.

[153] X. Guo, H. Shi, W. A. Dick, Compressive strength and microstructural characteristics of class C fly ash geopolymer, Cement and Concrete Composites 32 (2010) 142–147.

[154] X. Ma, Z. Zhang, A. Wang, The transition of fly ash-based geopolymer gels into ordered structures and the effect on the compressive strength, Construction and Building Materials 104 (2016) 25–33.

[155] M. S. Reddy, P. Dinakar, B. H. Rao, Mix design development of fly ash and ground granulated blast furnace slag based geopolymer concrete, Journal of Building Engineering 20 (2018) 712–722.

[156] J. Xie, J. Wang, R. Rao, C. Wang, C. Fang, Effects of combined usage of GGBS and fly ash on workability and mechanical properties of alkali activated geopolymer concrete with recycled aggregate, Composites Part B 164 (2019) 179–190.

[157] S. Y. Oderji, B. Chen, S. T. A. Jaffar, Effects of relative humidity on the properties of fly ash-based geopolymers, Construction and Building Materials 153 (2017) 268–273.

Appendix A

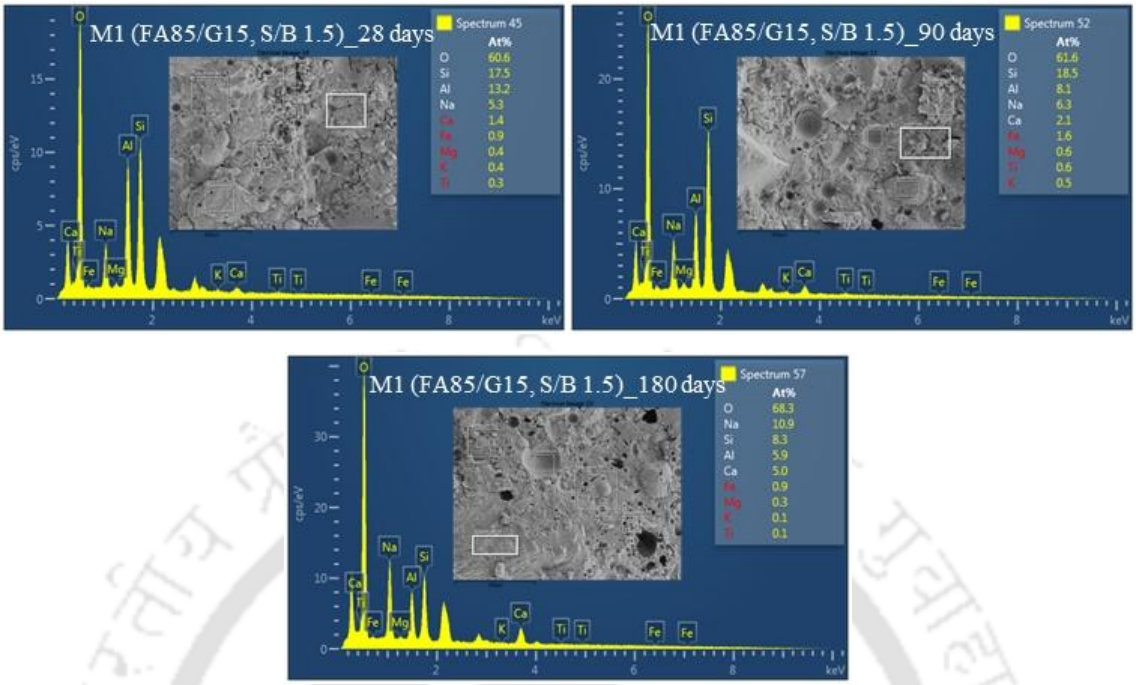

Fig. A1 EDS spectra of geopolymer mortar (GPM) mix M1 (FA85/G15, S/B 1.5) at different ages of ambient curing.

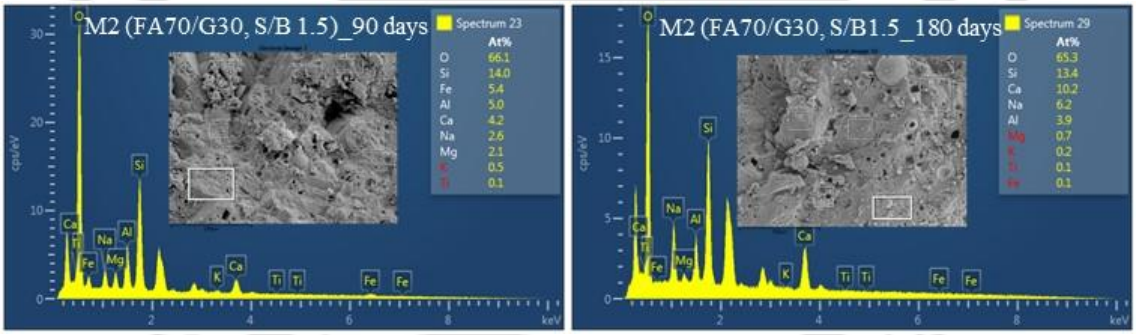

Fig. A2 EDS spectra of geopolymer mortar (GPM) mix M2 (FA70/G30, S/B 1.5) at different ages of ambient curing.

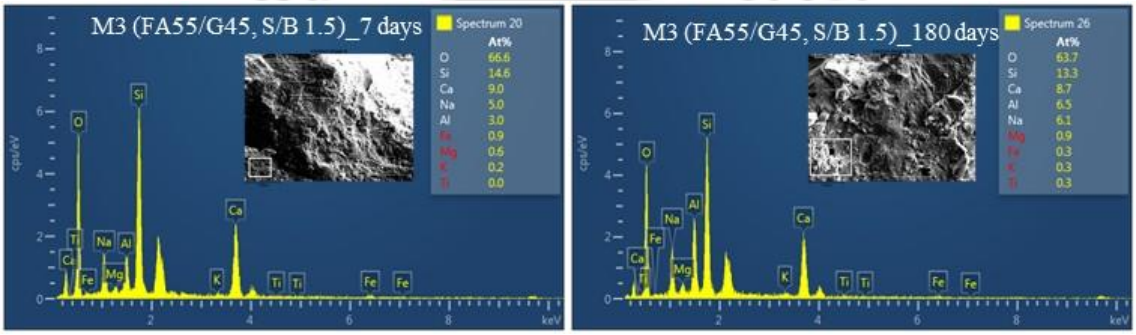

Fig. A3 EDS spectra of geopolymer mortar (GPM) mix M3 (FA55/G45, S/B 1.5) at different ages of ambient curing.

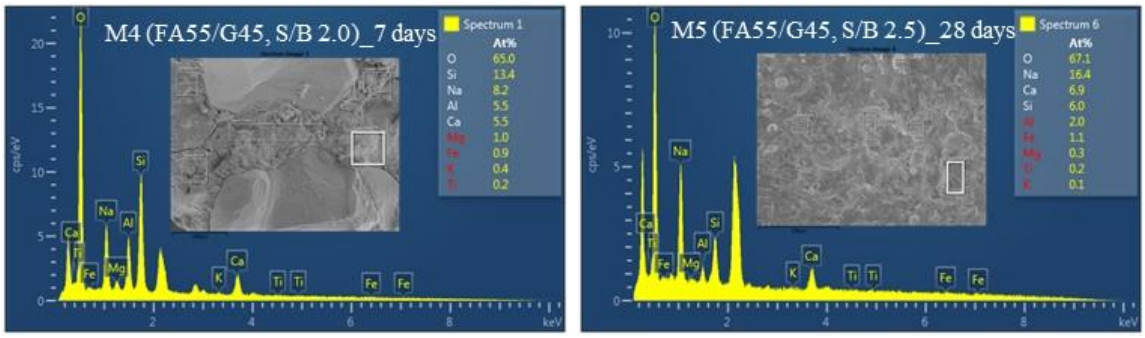

Fig. A4 EDS spectra of geopolymer mortar (GPM) mixes (M4: FA55/G45, S/B 2.0, M5: FA55/G45, S/B 2.5) at different ambient curing ages.

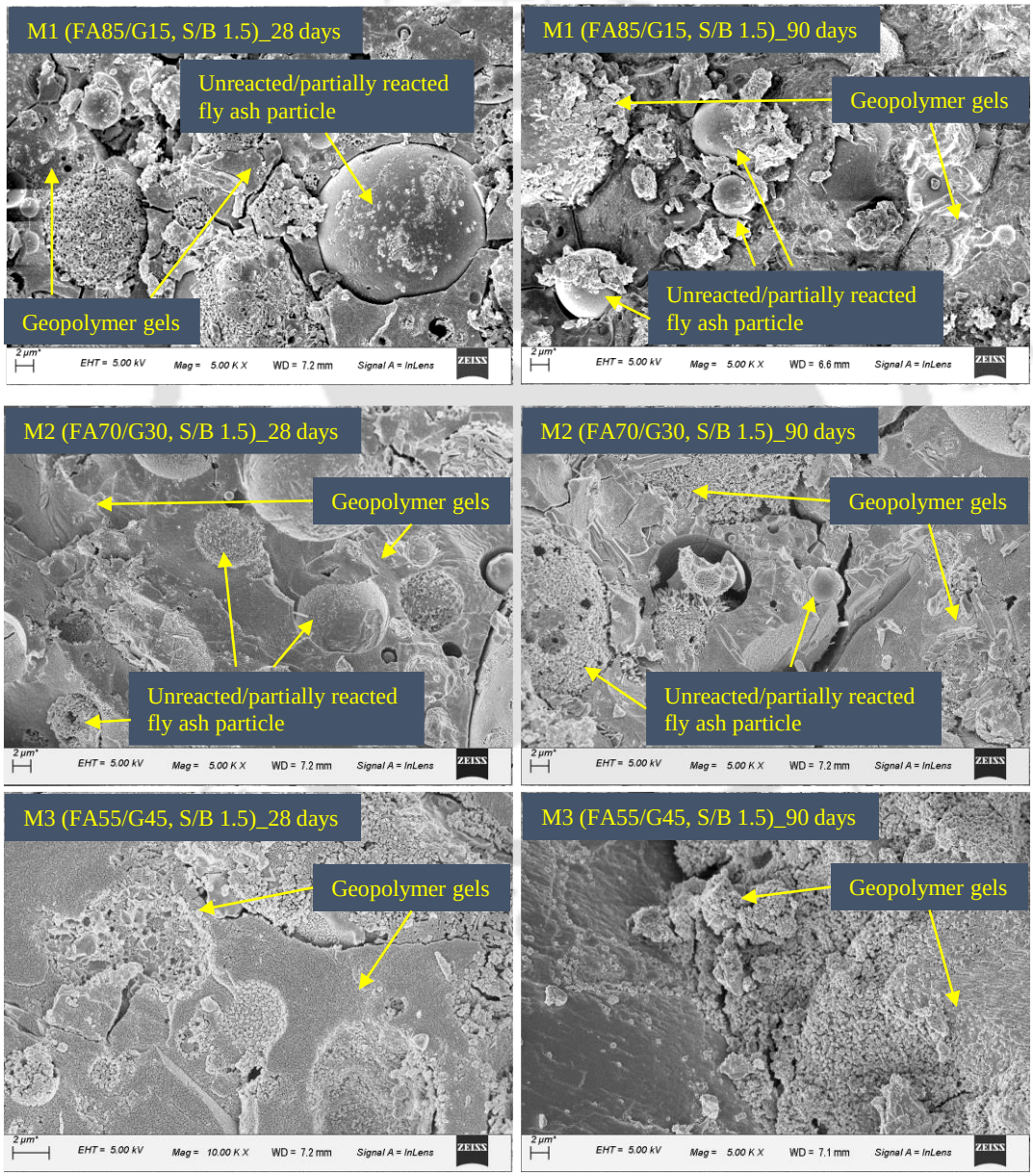

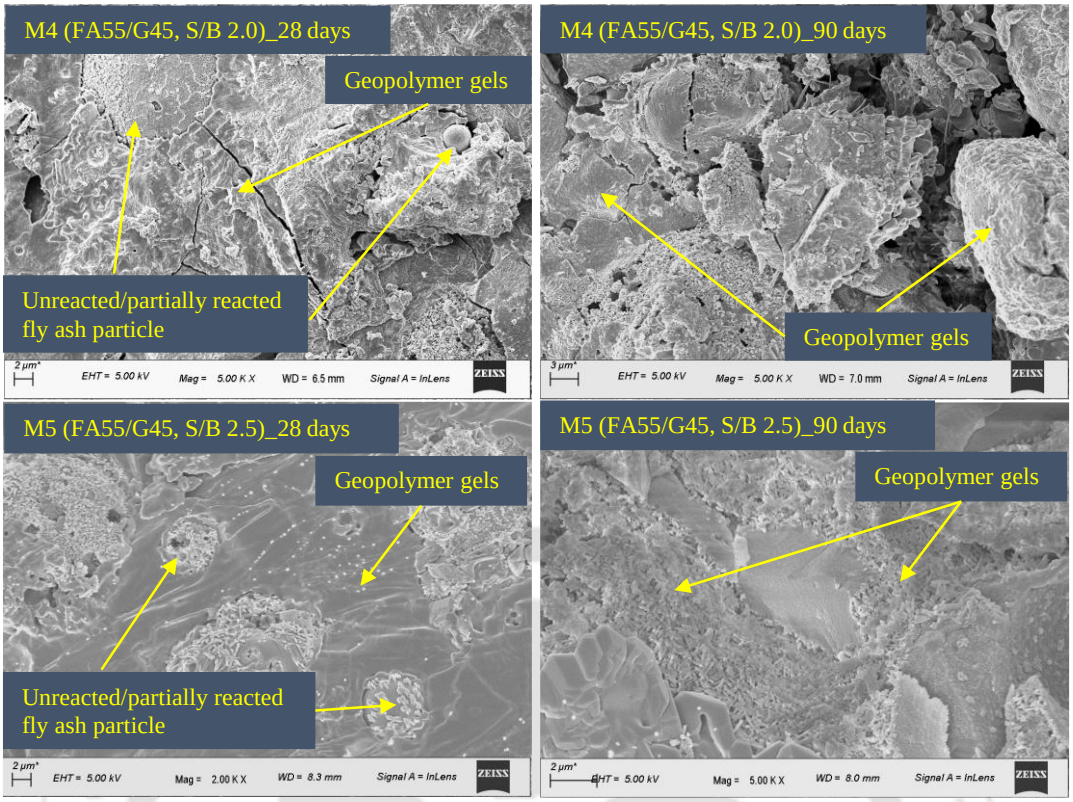

Fig. A5 FESEM images of geopolymer mortar (GPM) mixes at 28 and 90 days of ambient curing.

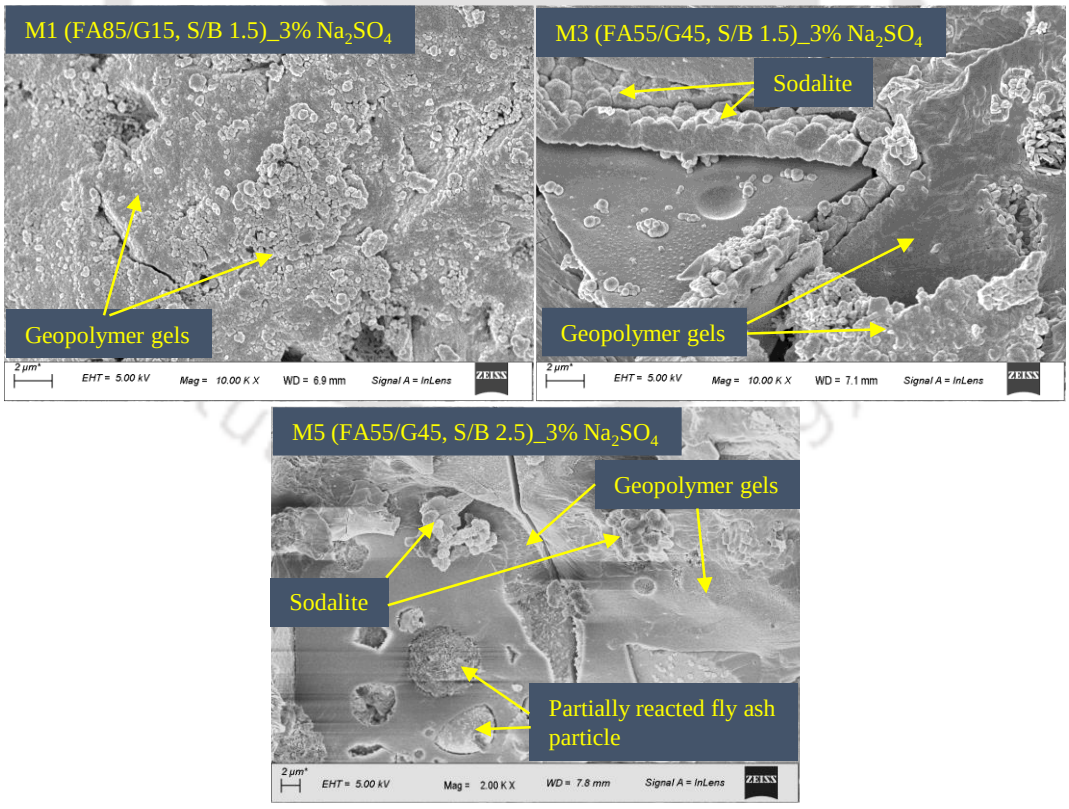

Fig. A6 FESEM images of geopolymer mortar (GPM) mixes exposed to 3% Na_2SO_4 solution for 26 weeks.

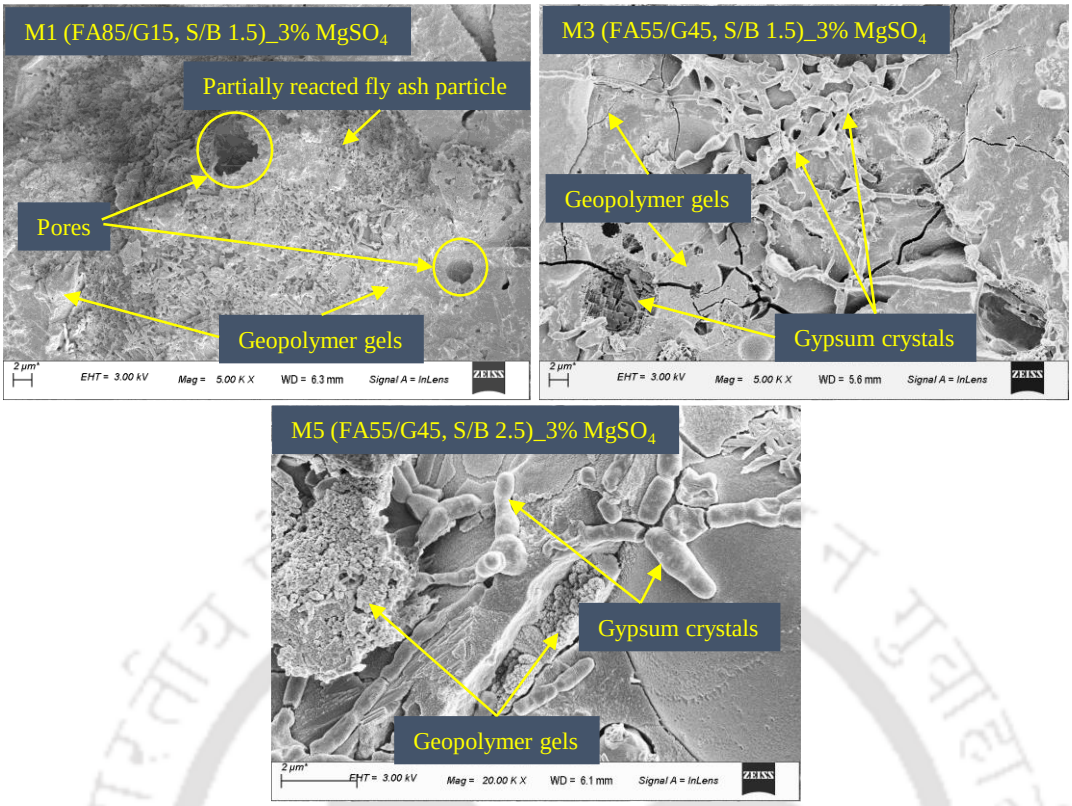

Fig. A7 FESEM images of geopolymer mortar (GPM) mixes exposed to 3% $MgSO_4$ solution for 26 weeks.

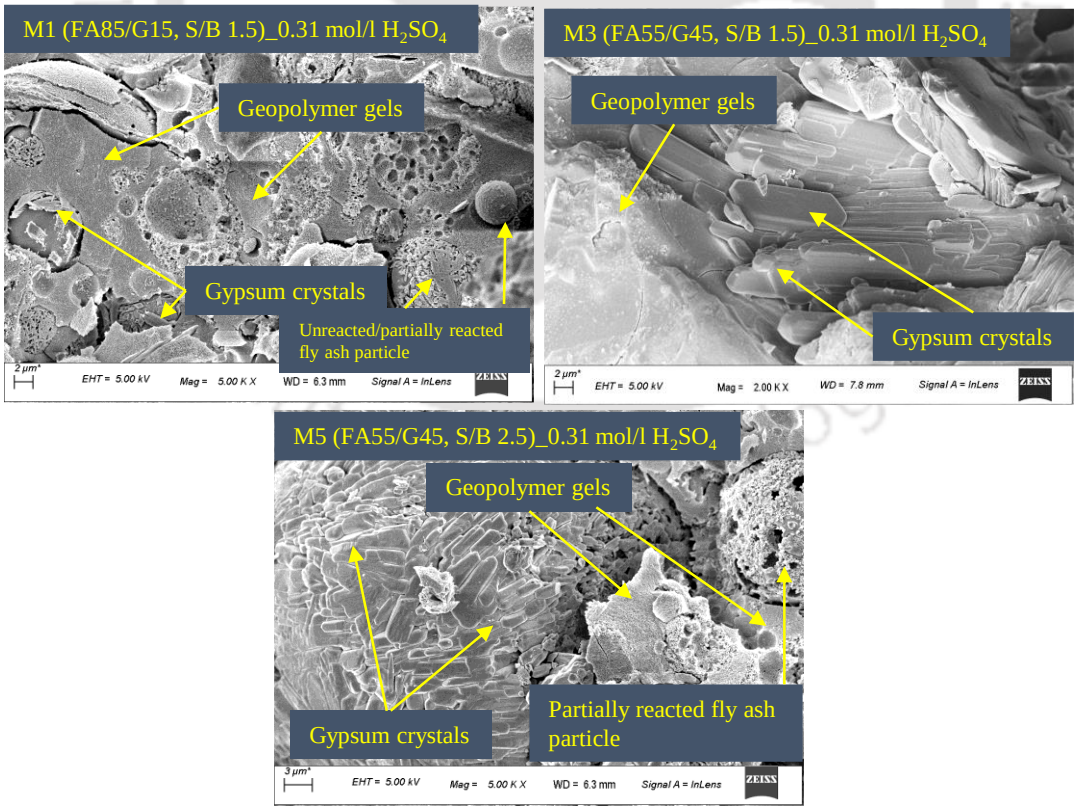

Fig. A8 FESEM images of GPM mixes after 26 weeks of immersion in 0.31 mol/l H_2SO_4 solution.

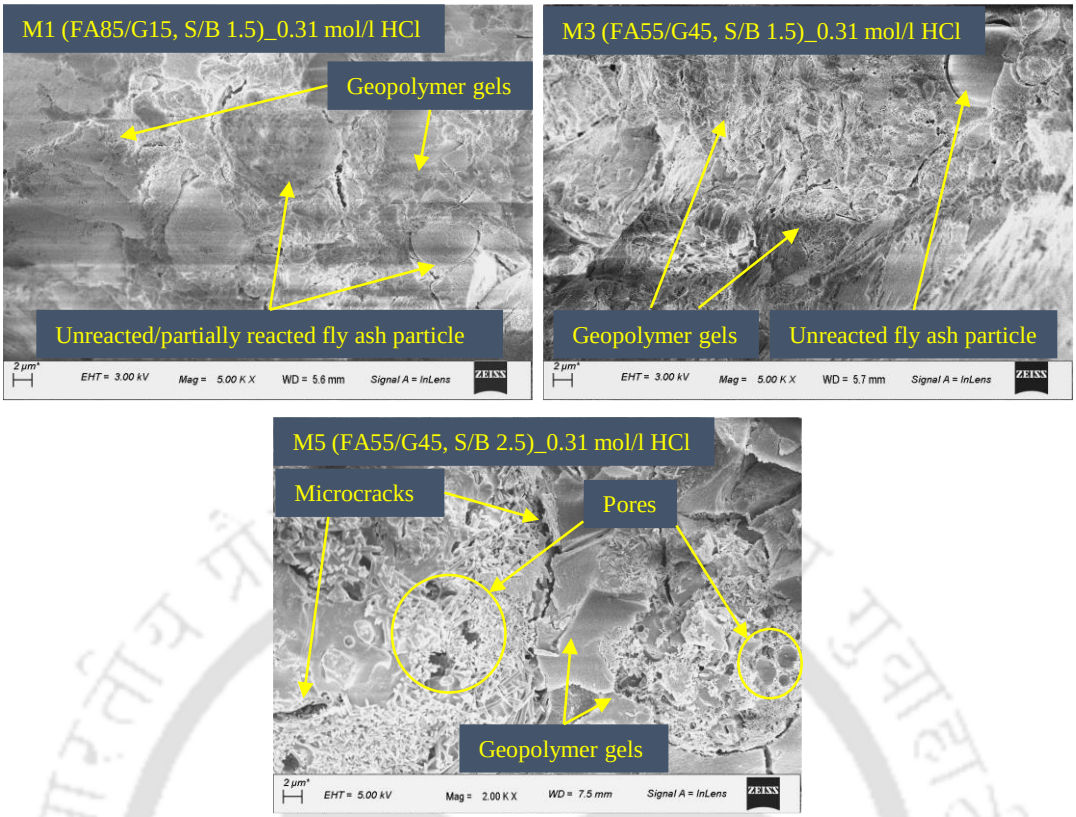

Fig. A9 FESEM images of GPM mixes after 26 weeks of immersion in 0.31 mol/l HCl solution.

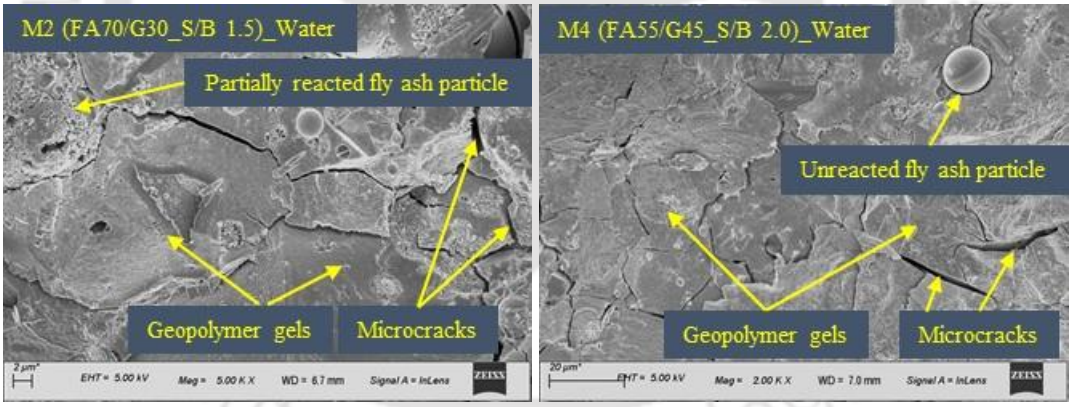

Fig. A10 FESEM images of geopolymer mortar mixes (M2 and M4) exposed to water for 26 weeks.

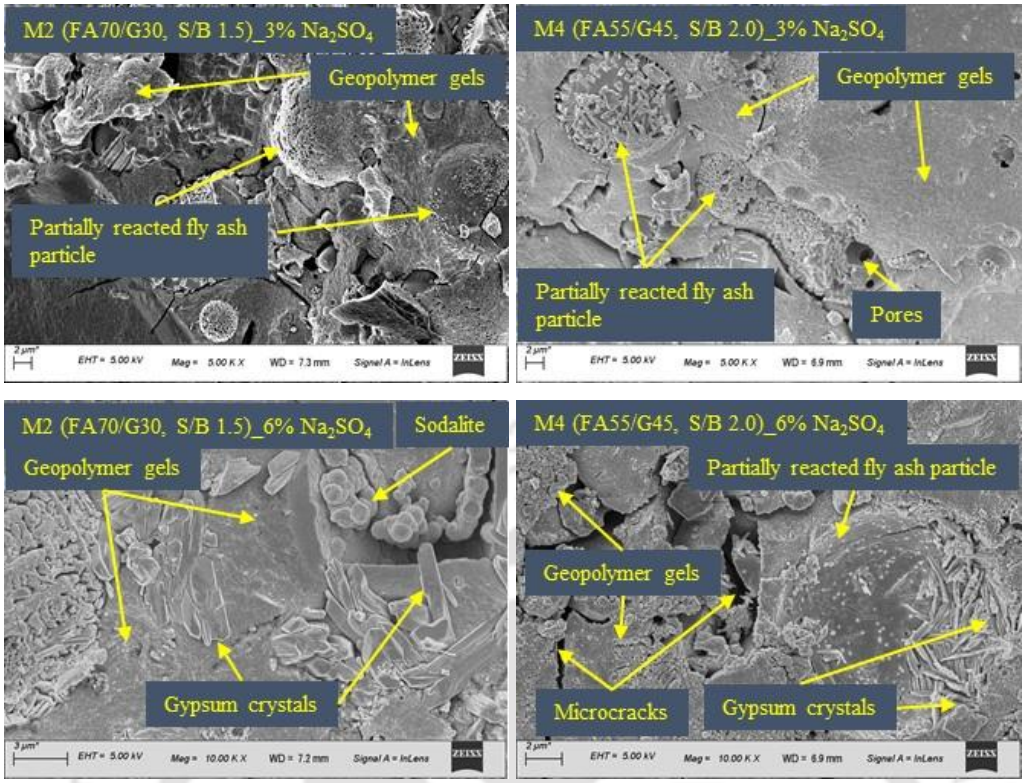

Fig. A11 FESEM images of geopolymer mortar mixes (M2 and M4) exposed to Na_2SO_4 solutions for 26 weeks.

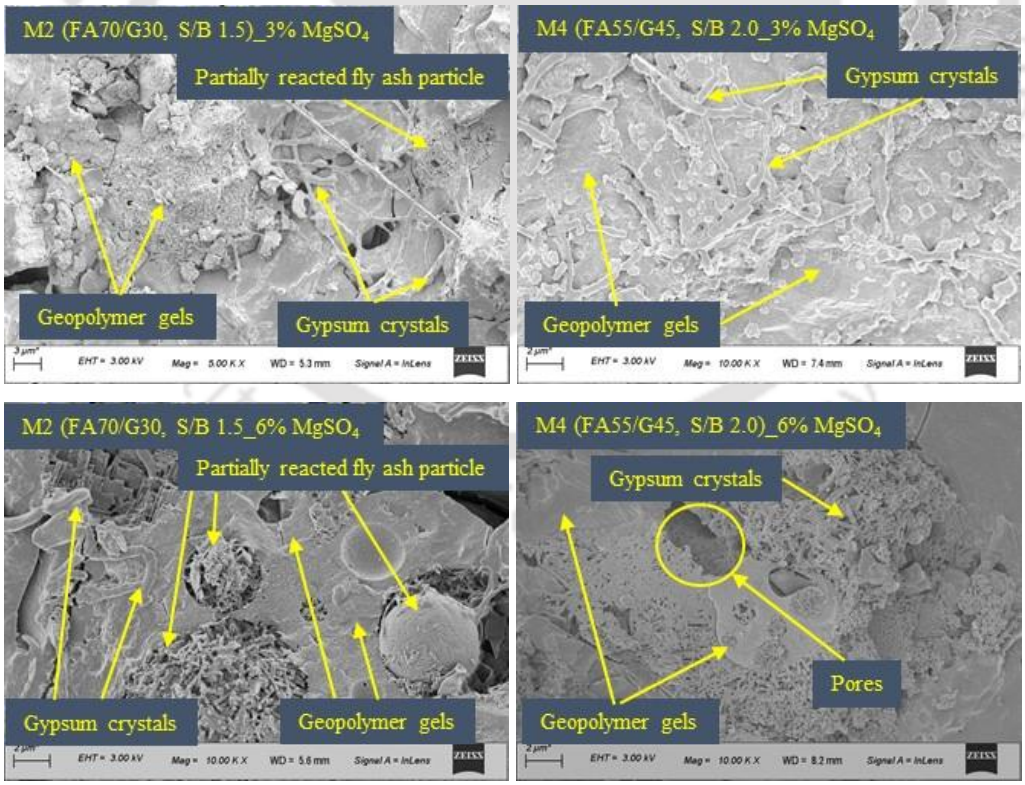

Fig. A12 FESEM images of geopolymer mortar mixes (M2 and M4) exposed to $MgSO_4$ solutions for 26 weeks.

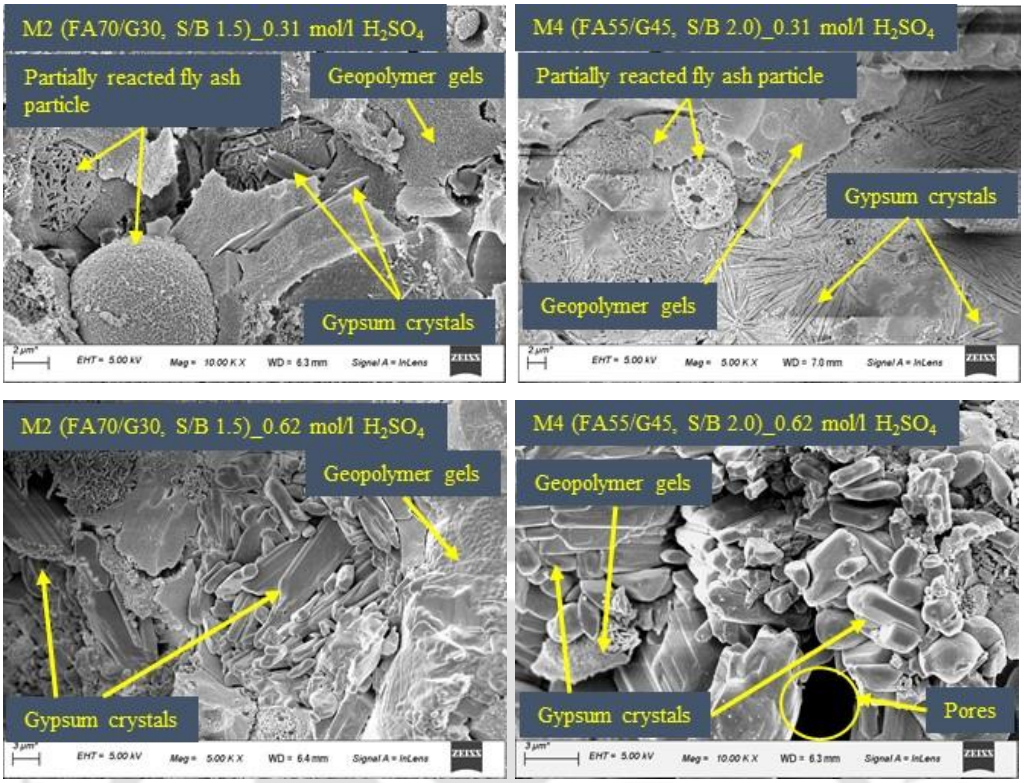

Fig. A13 FESEM images of geopolymer mortar mixes (M2 and M4) exposed to H_2SO_4 solutions for 26 weeks.

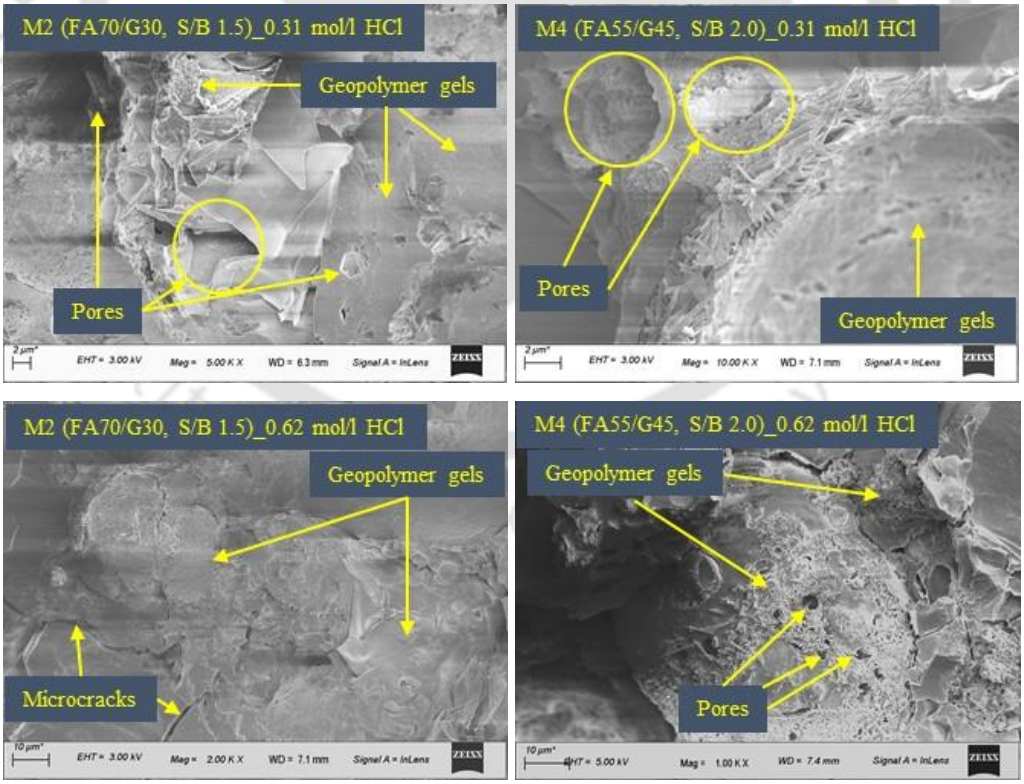

Fig. A14 FESEM images of geopolymer mortar mixes (M2 and M4) exposed to HCl solutions for 26 weeks.

Appendix B

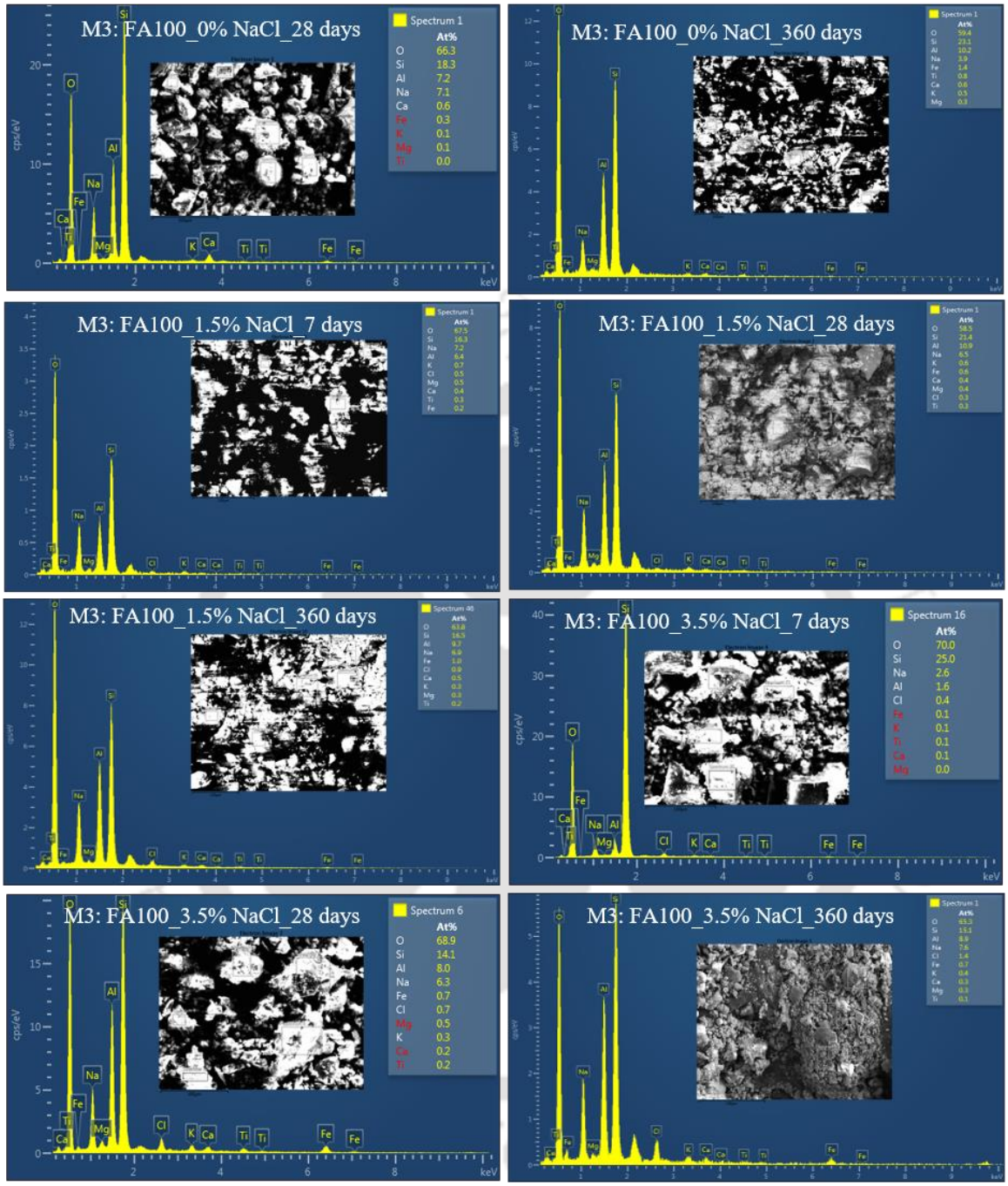

Fig. B1 EDS spectra of control and chloride admixed fly ash based GPC mix M3 (FA100) at different ages.

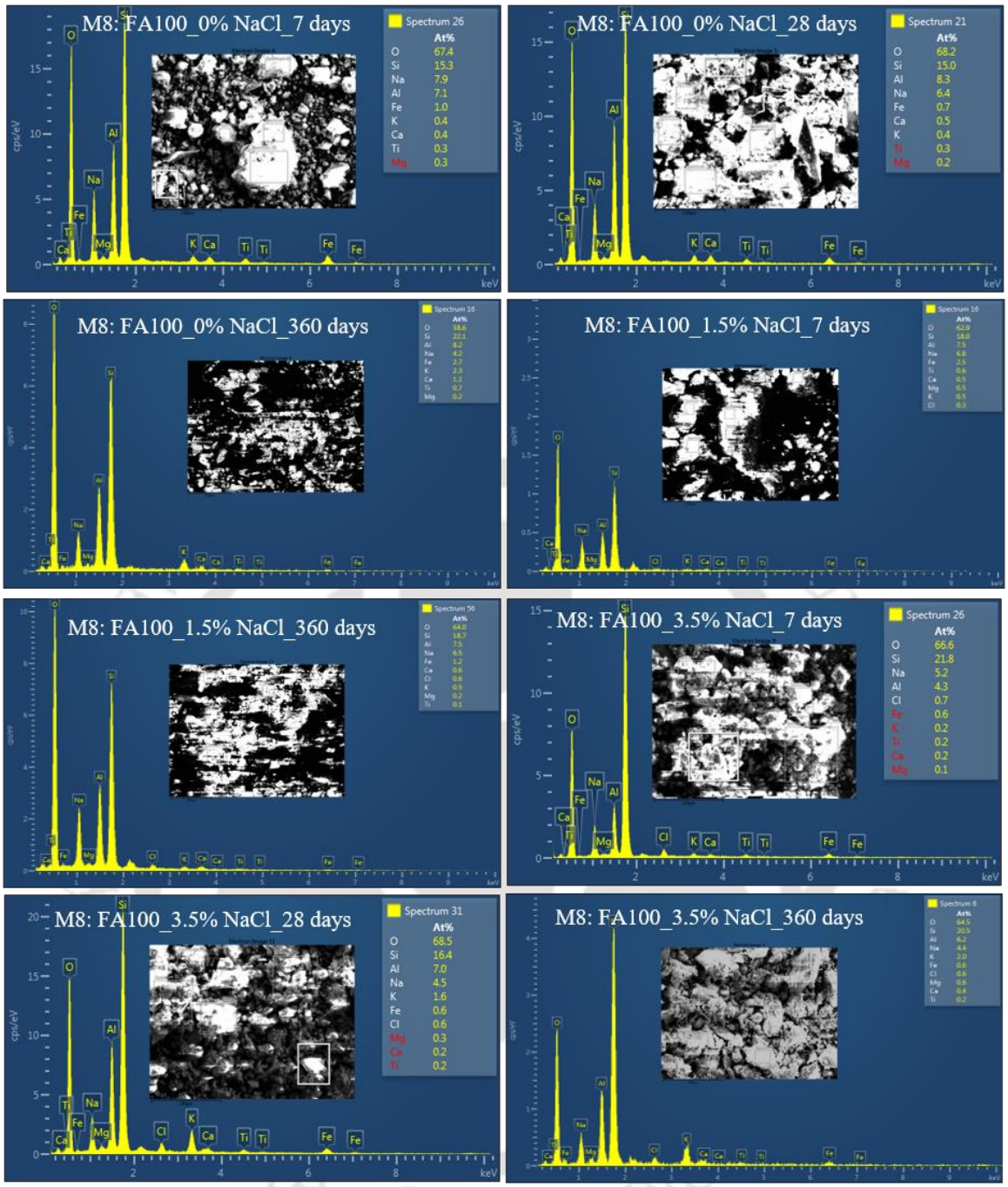

Fig. B2 EDS spectra of control and chloride admixed fly ash based GPC mix M8 (FA100) at different ages.

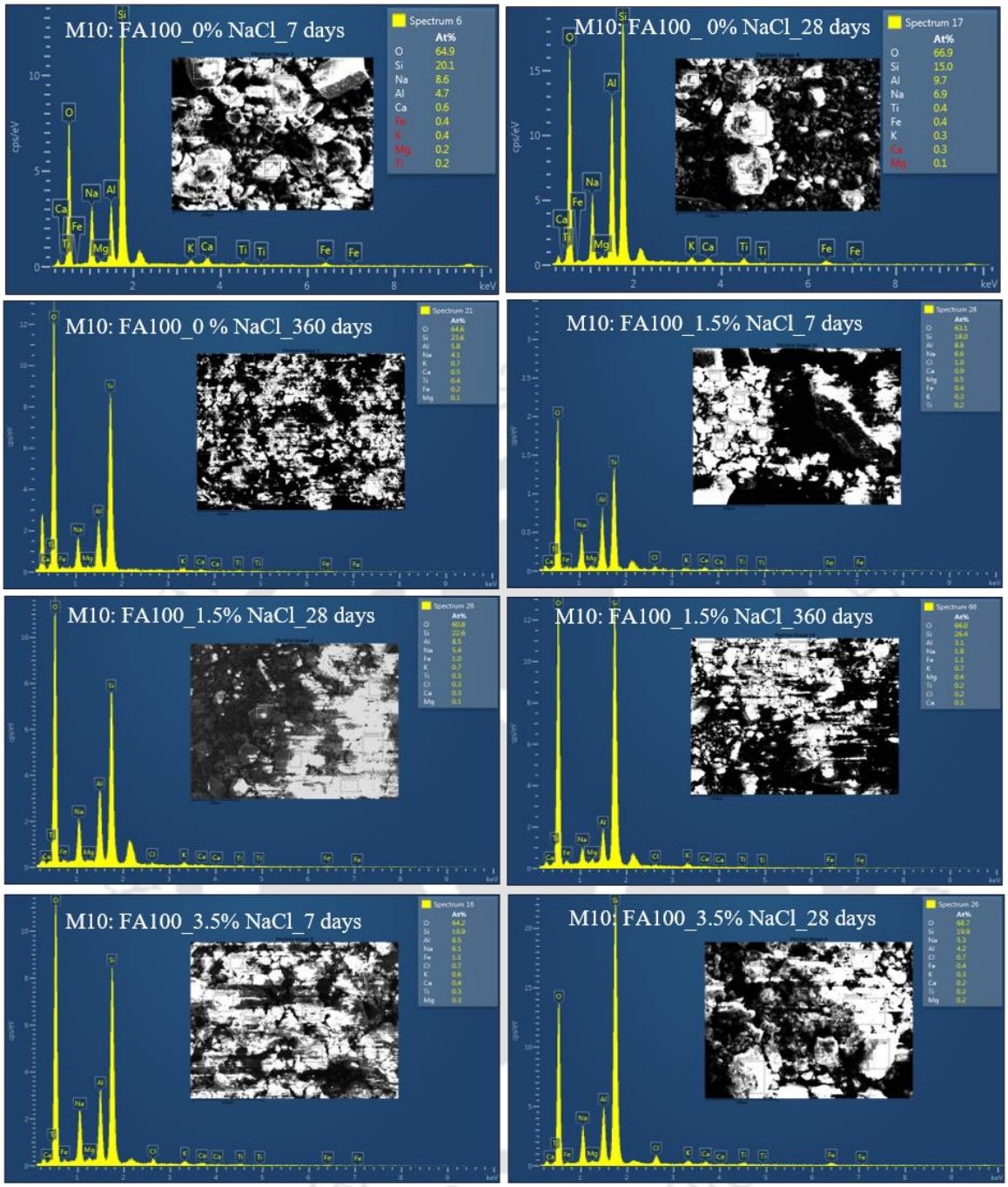

Fig. B3 EDS spectra of control and chloride admixed fly ash based GPC mix M10 (FA100) at different ages.

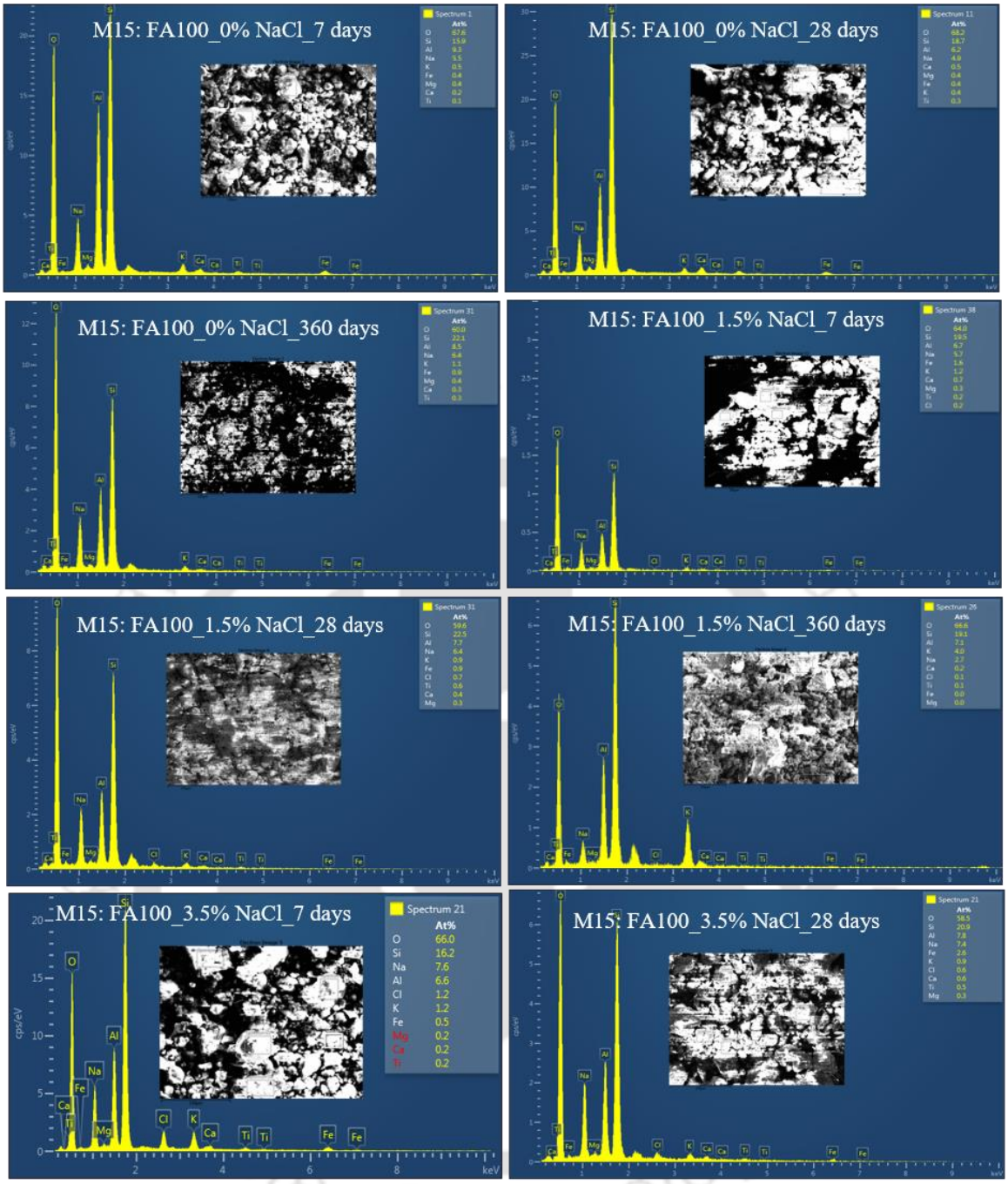

Fig. B4 EDS spectra of control and chloride admixed fly ash based GPC mix M15 (FA100) at different ages.

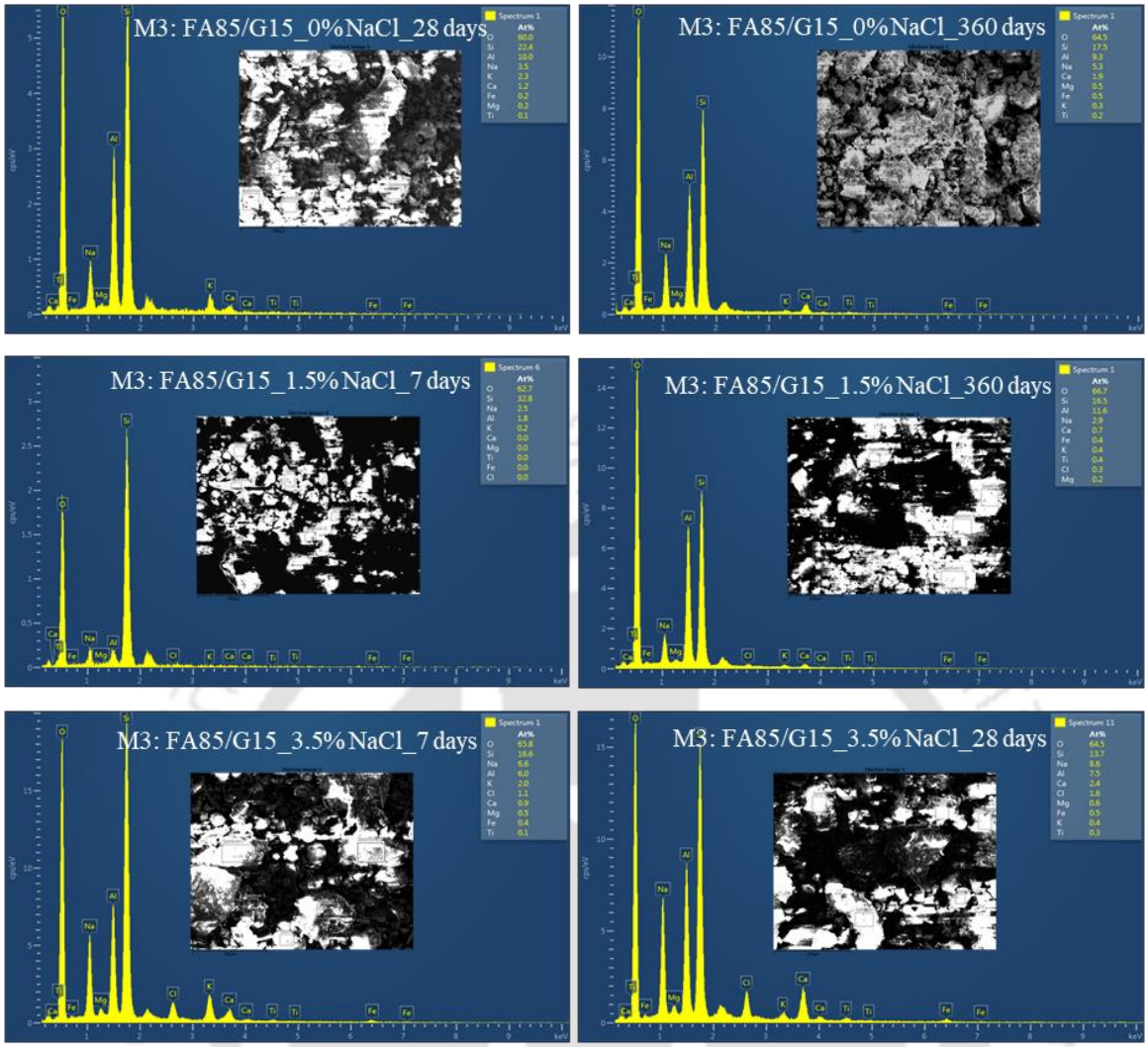

Fig. B5 EDS spectra of control and chloride admixed fly ash-GGBS based GPC mixes (M3: FA85/G15) at different ages.

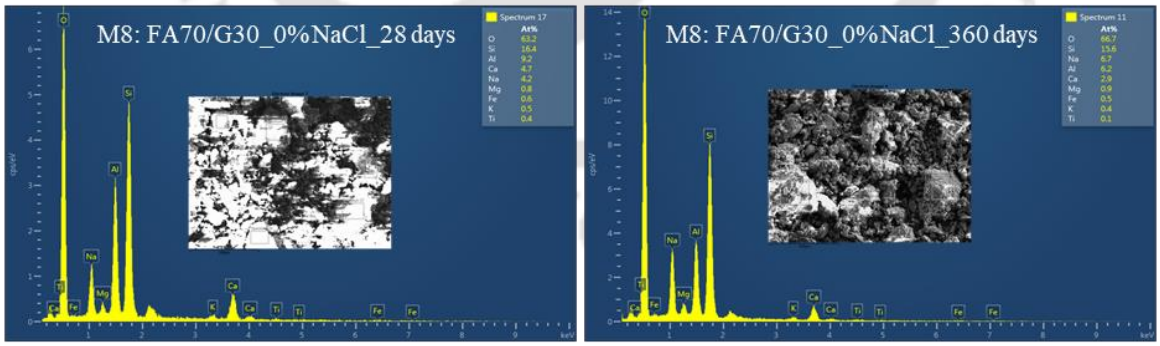

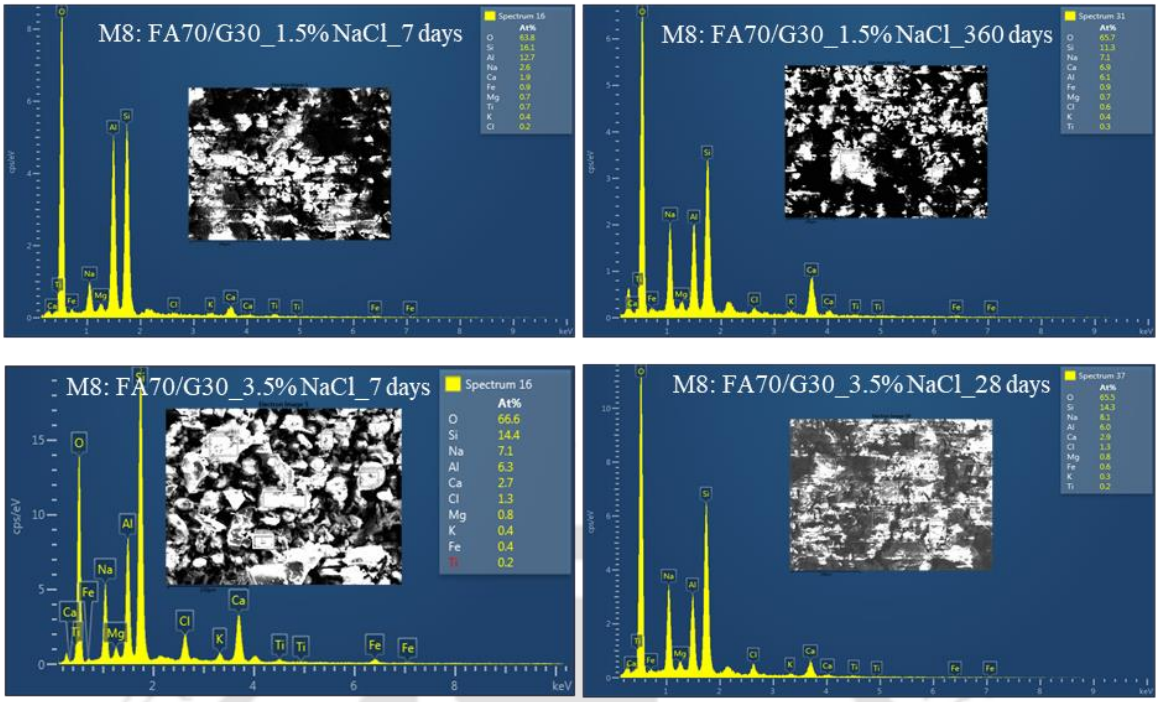

Fig. B6 EDS spectra of control and chloride admixed fly ash-GGBS based GPC mixes (M8: FA70/G30) at different ages.

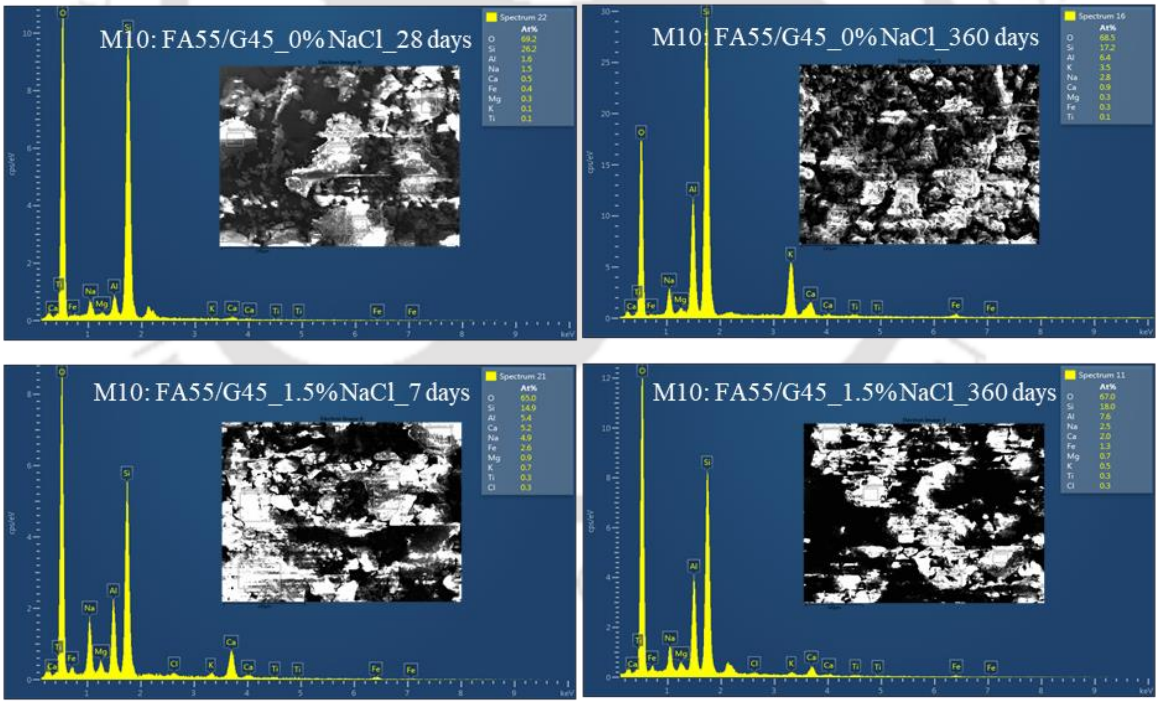

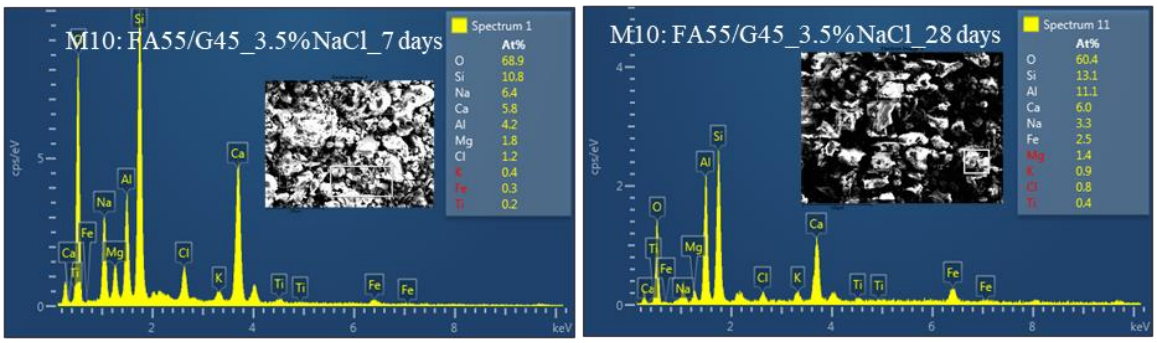

Fig. B7 EDS spectra of control and chloride admixed fly ash-GGBS based GPC mixes (M10: FA55/G45) at different ages.

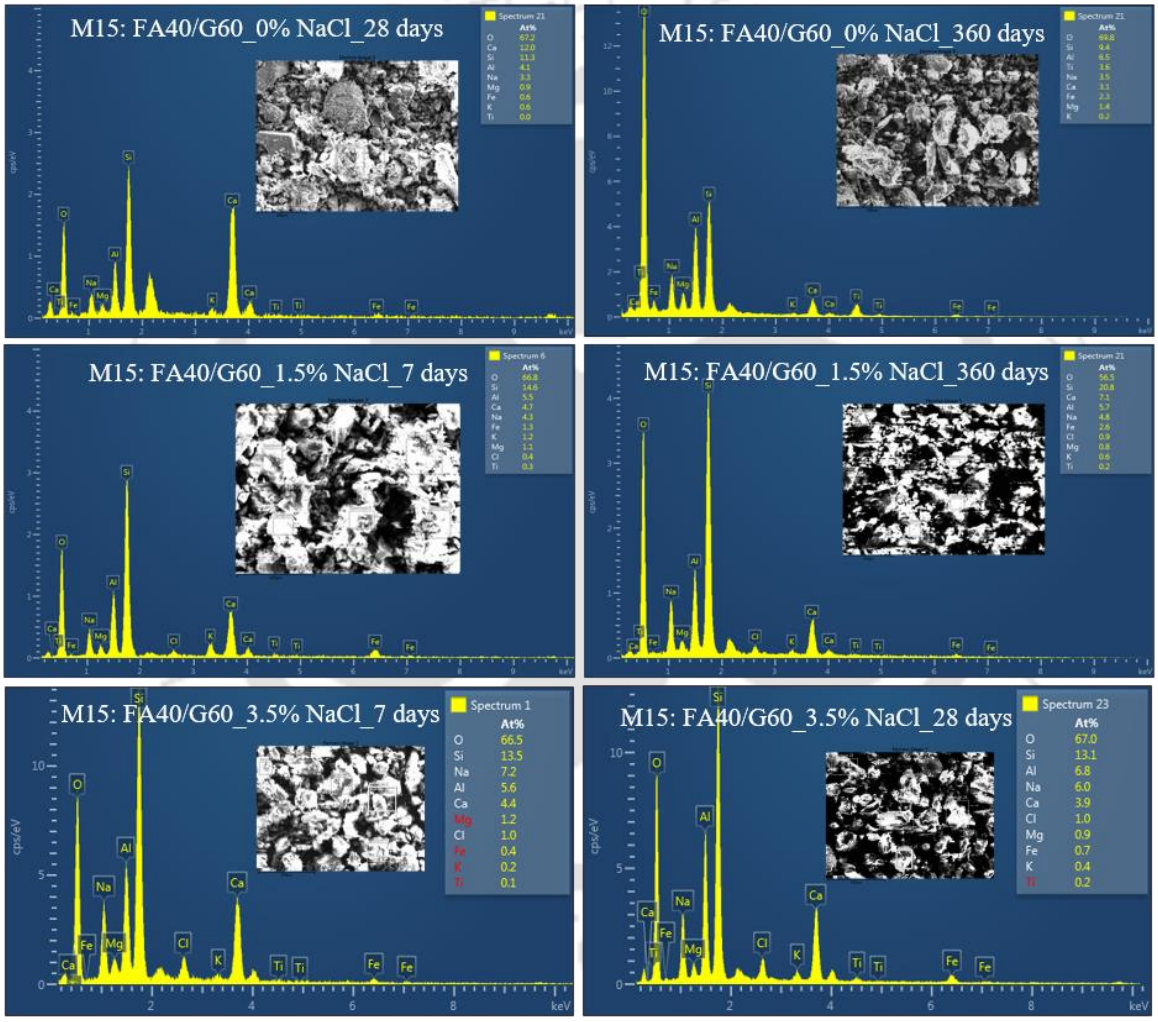

Fig. B8 EDS spectra of control and chloride admixed fly ash-GGBS based GPC mixes (M15: FA40/G60) at different ages.

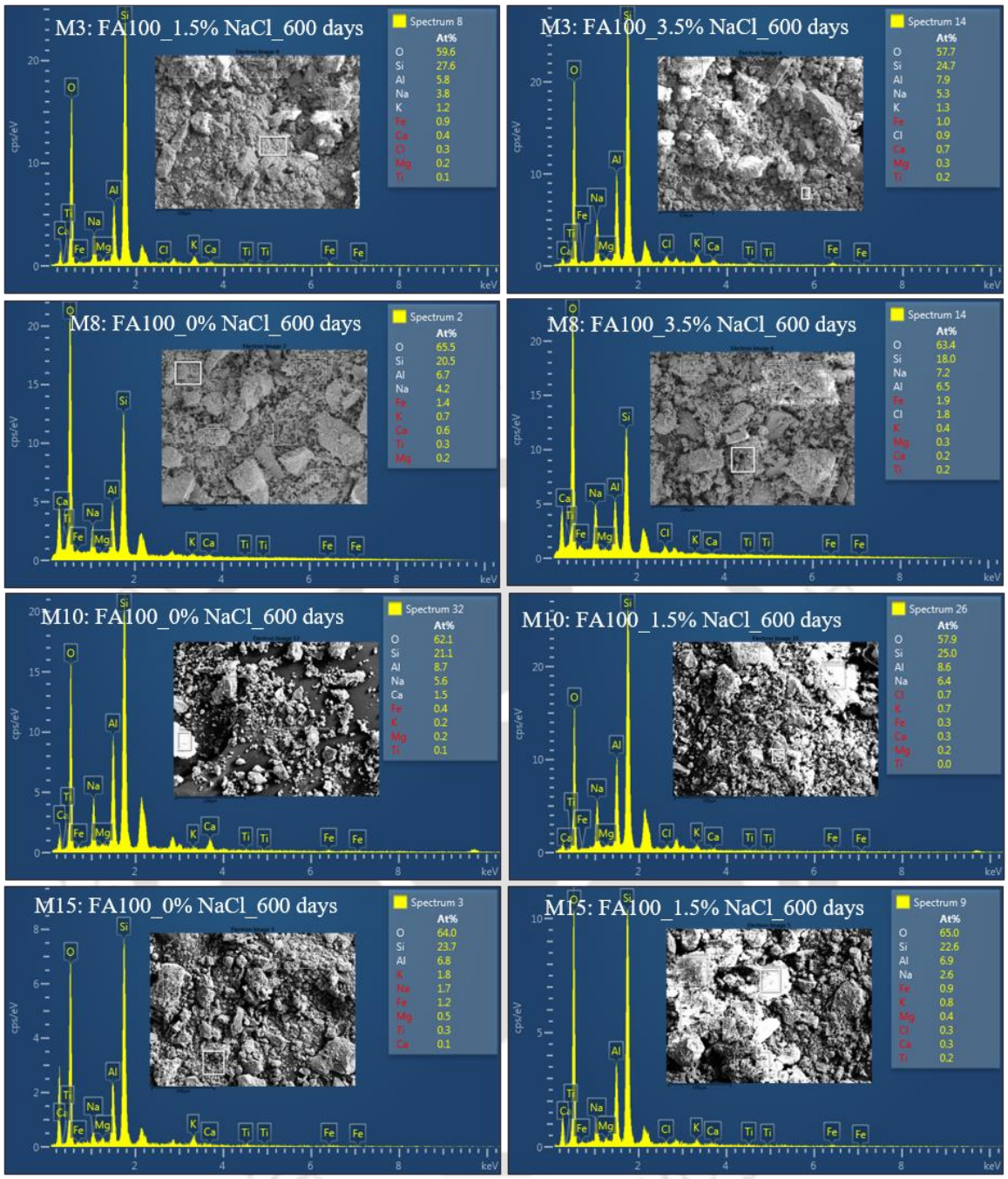

Fig. B9 EDS spectra obtained at rebar level of control and chloride admixed fly ash based GPC specimens (M3, M8, M10, and M15).

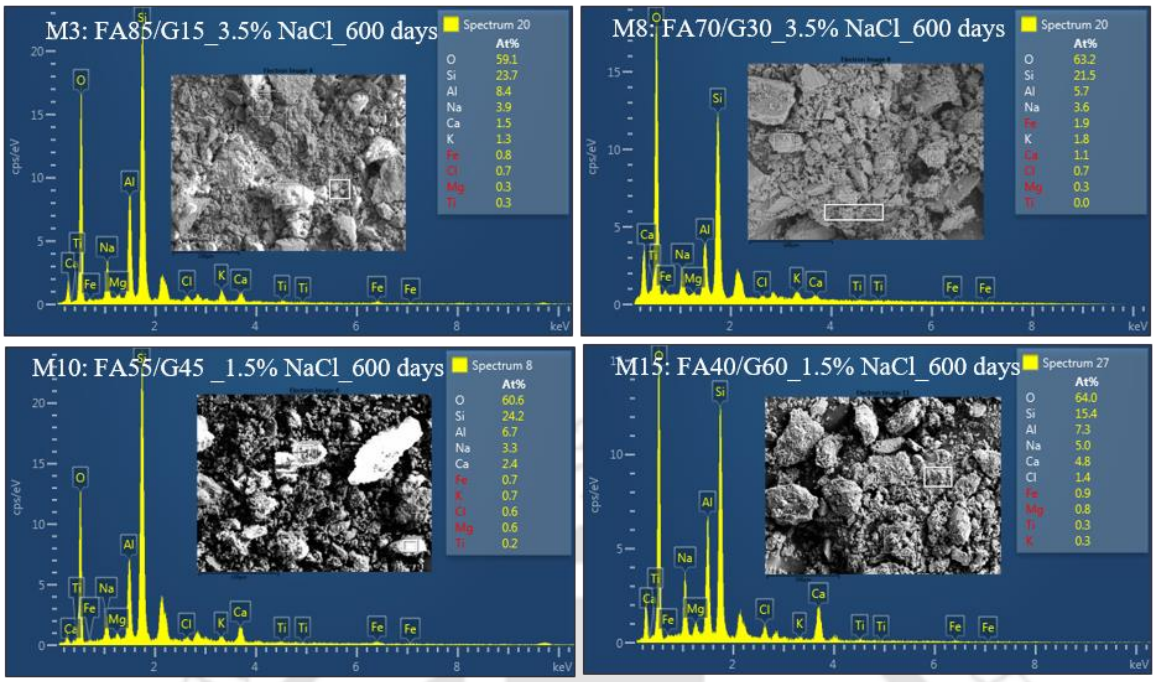

Fig. B10 EDS spectra obtained at rebar level of control and chloride admixed fly ash-GGBS based GPC specimens (M3, M8, M10, and M15).

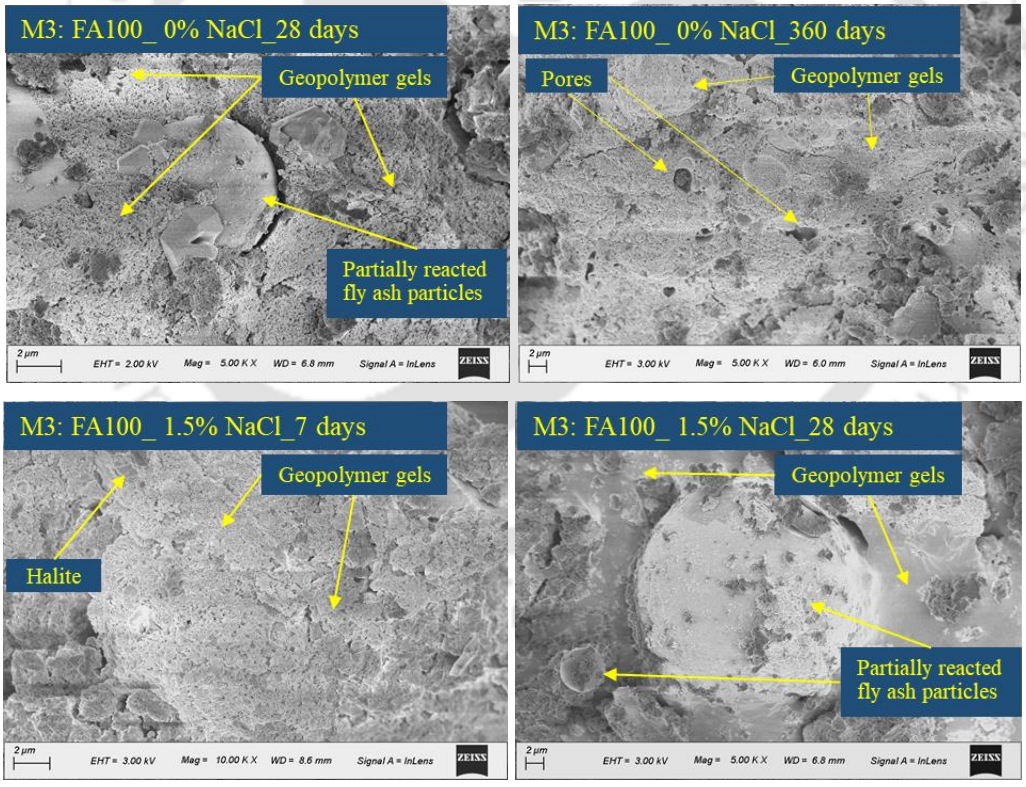

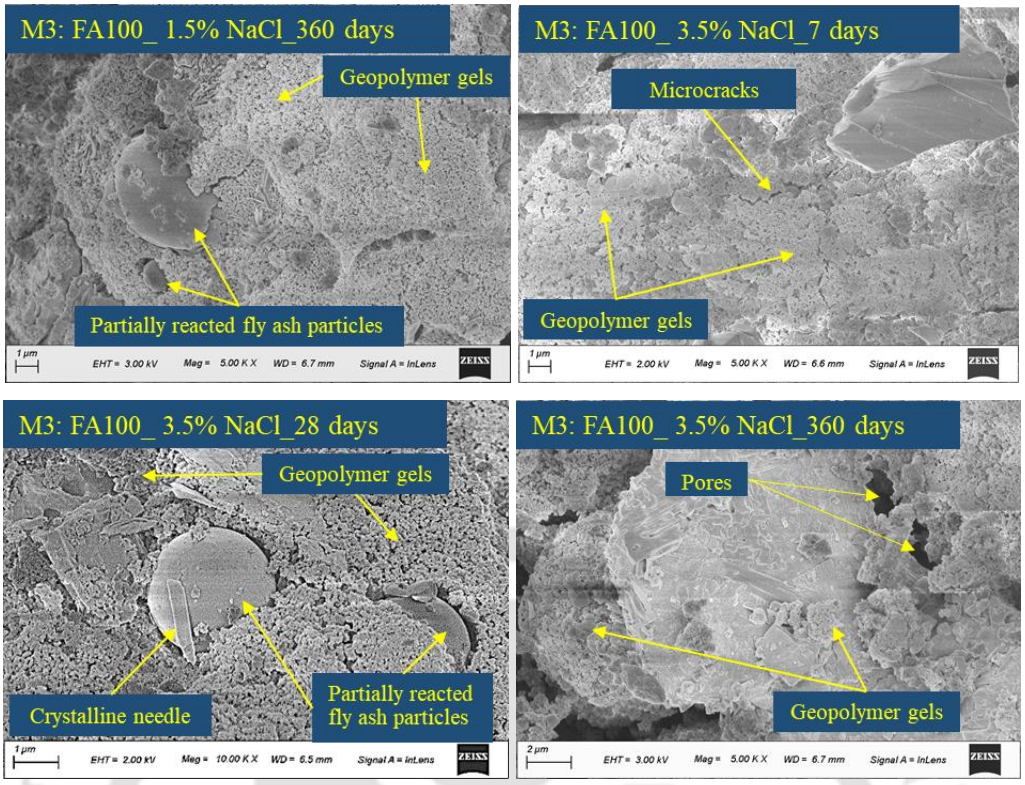

Fig. B11 FESEM images of control and chloride admixed fly ash based GPC (M3: FA100) at different ages.

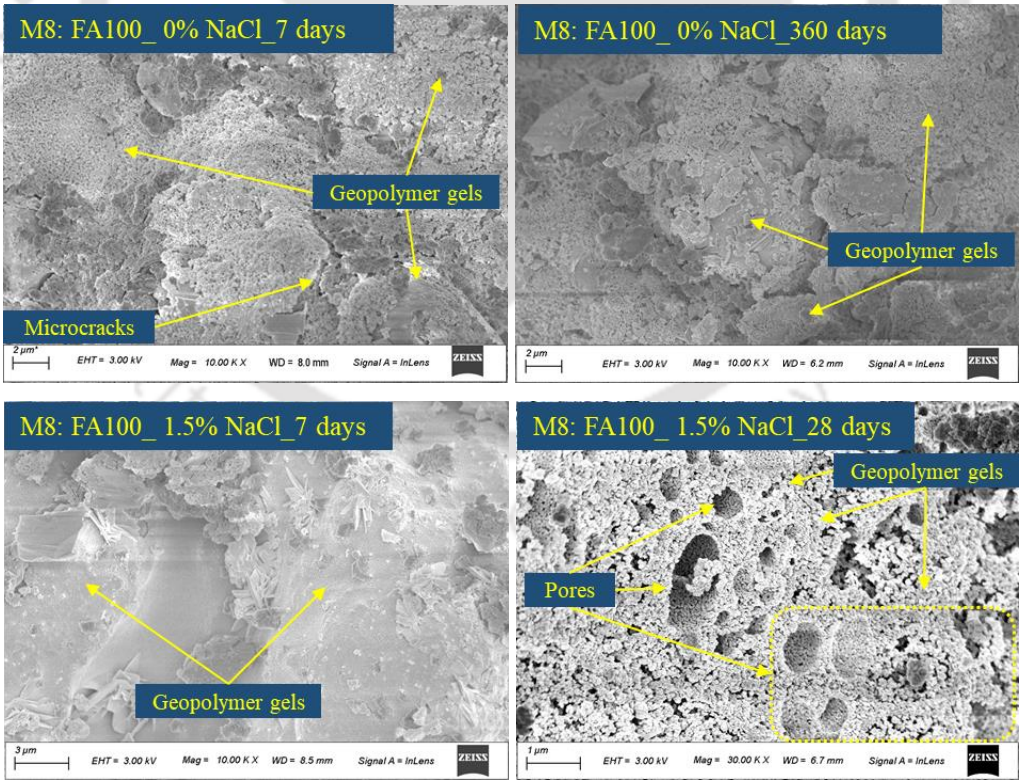

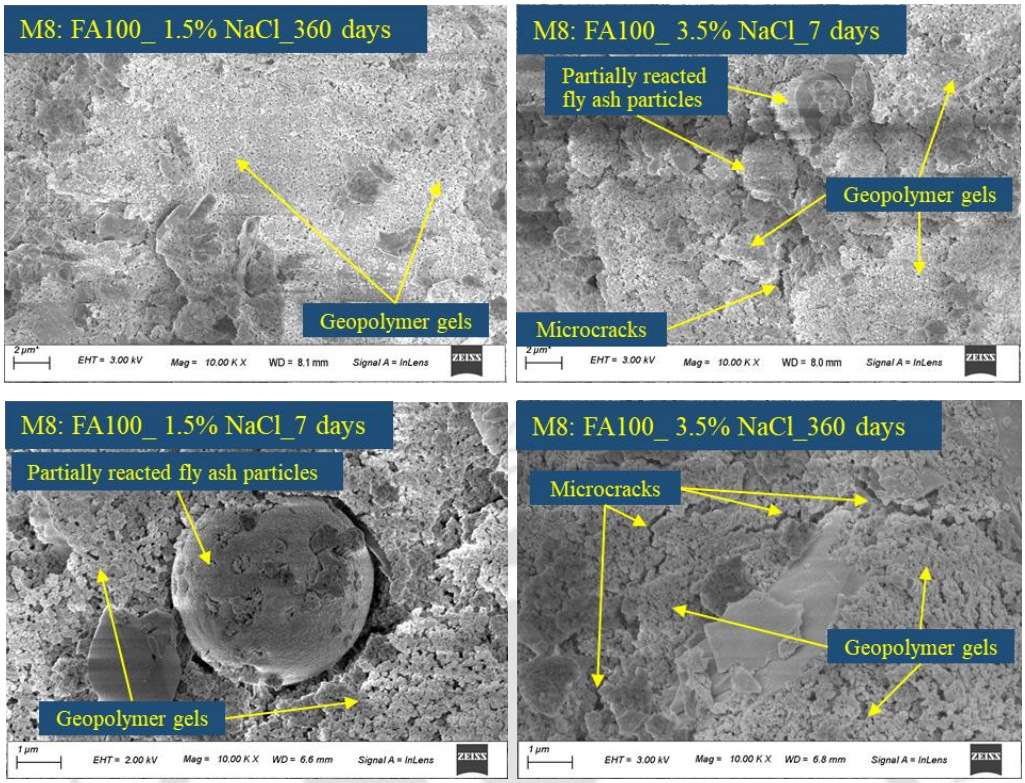

Fig. B12 FESEM images of control and chloride admixed fly ash based GPC (M8: FA100) at different ages.

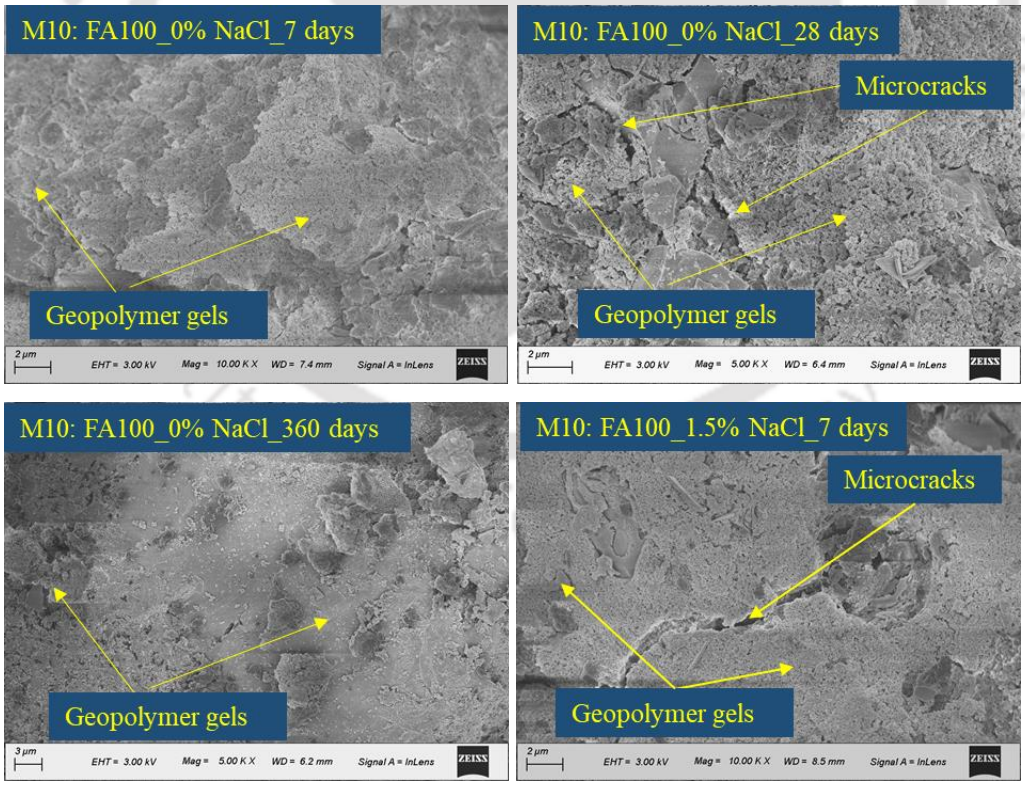

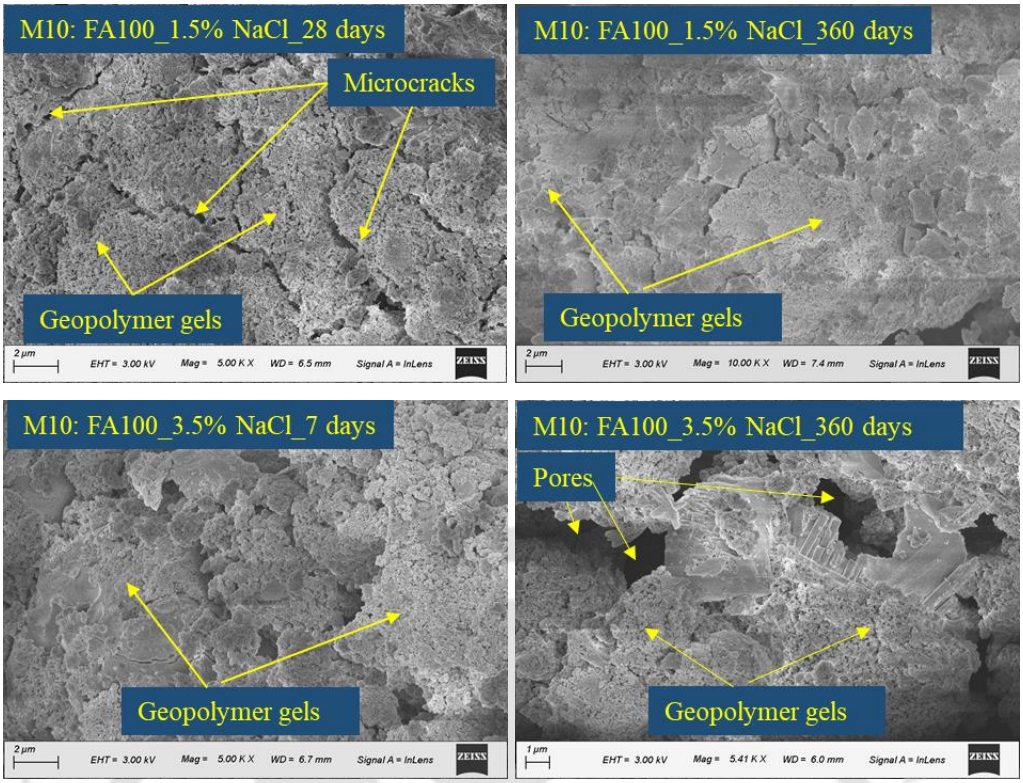

Fig. B13 FESEM images of control and chloride admixed fly ash based GPC (M10: FA100) at different ages.

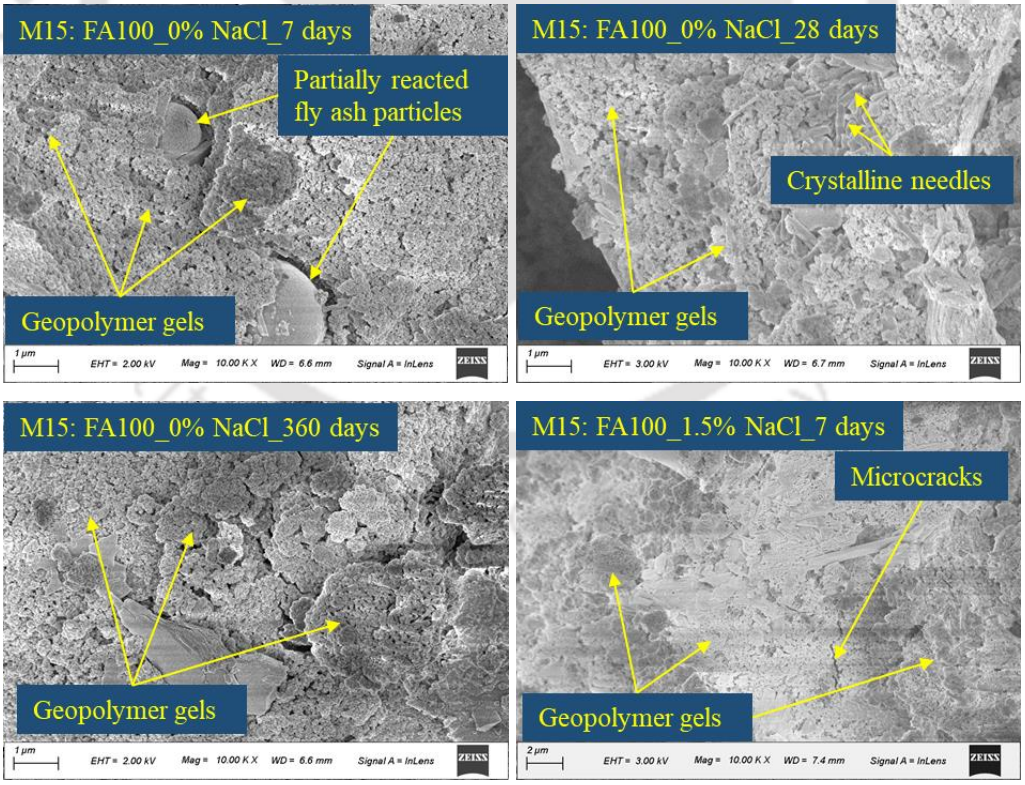

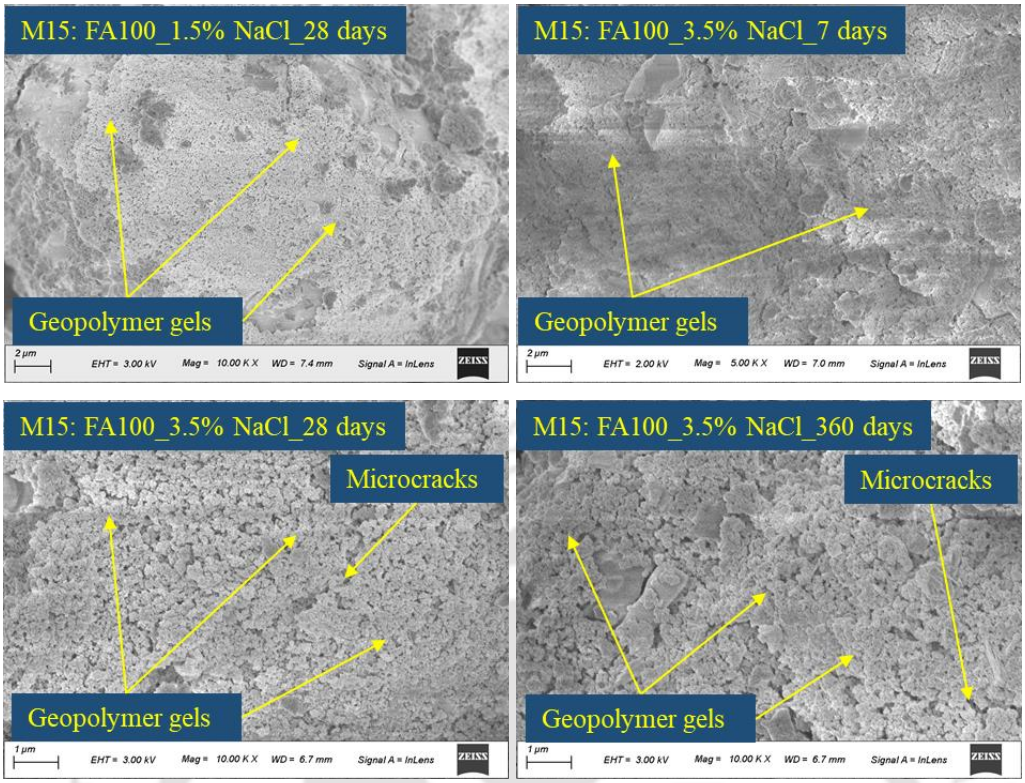

Fig. B14 FESEM images of control and chloride admixed fly ash based GPC (M15: FA100) at different ages.

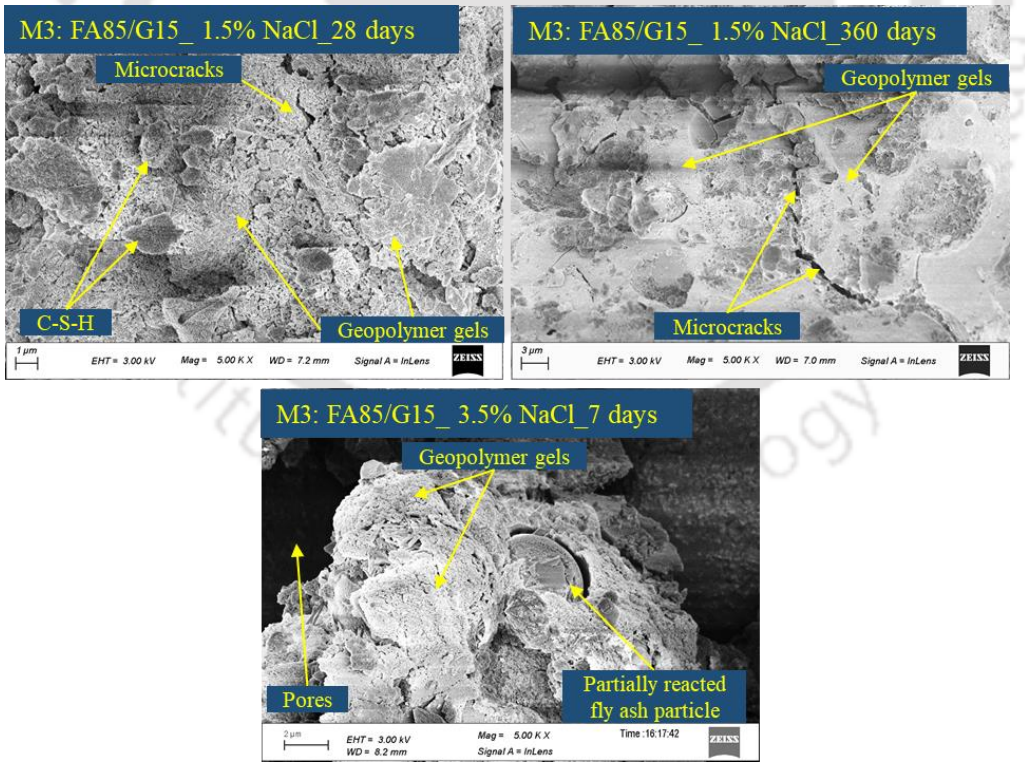

Fig. B15 FESEM images of control and chloride admixed fly ash-GGBS based GPC (M3: FA85/G15) at different ages.

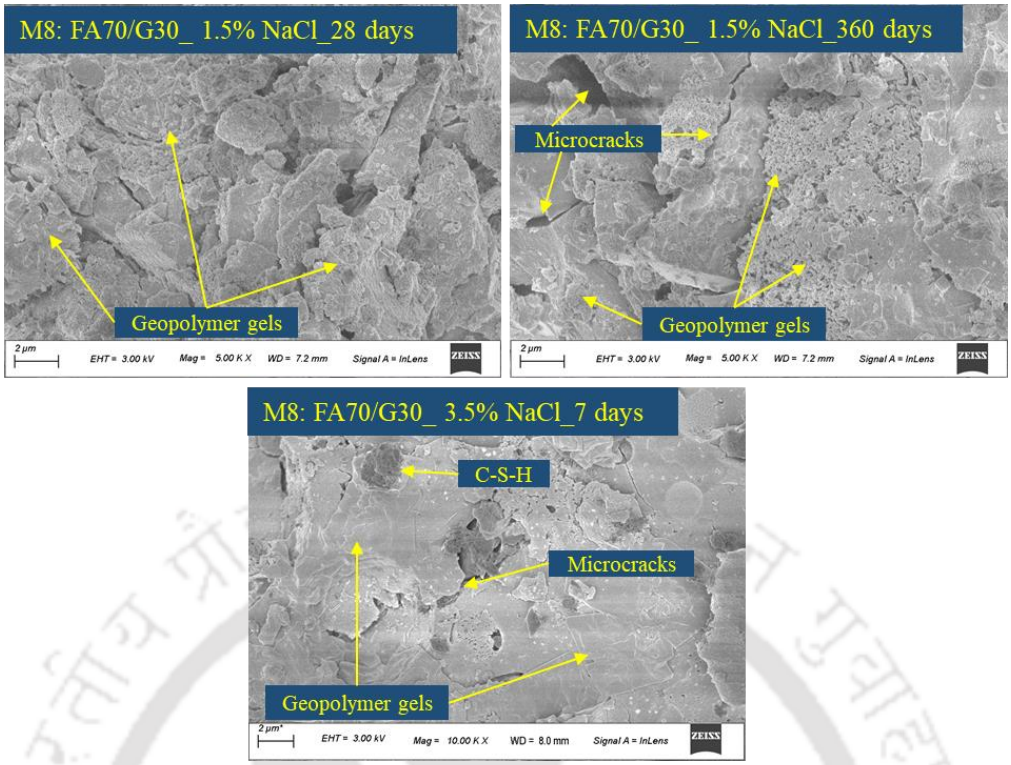

Fig. B16 FESEM images of control and chloride admixed fly ash-GGBS based GPC (M8: FA70/G30) at different ages.

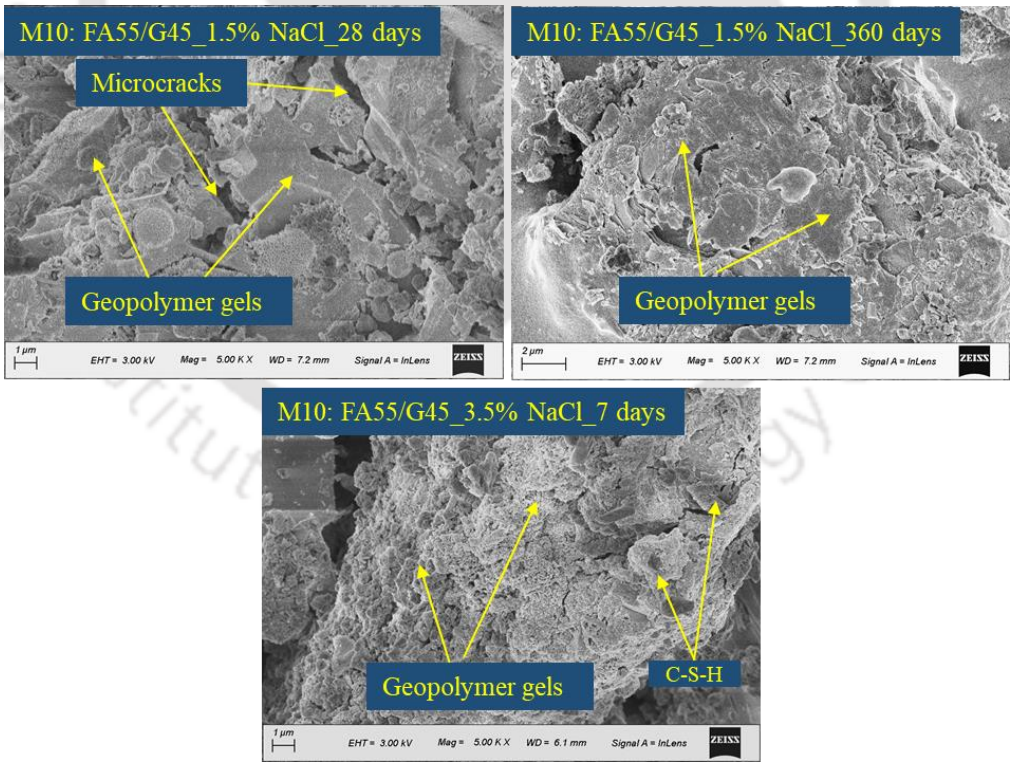

Fig. B17 FESEM images of control and chloride admixed fly ash-GGBS based GPC (M10: FA55/G45) at different ages.

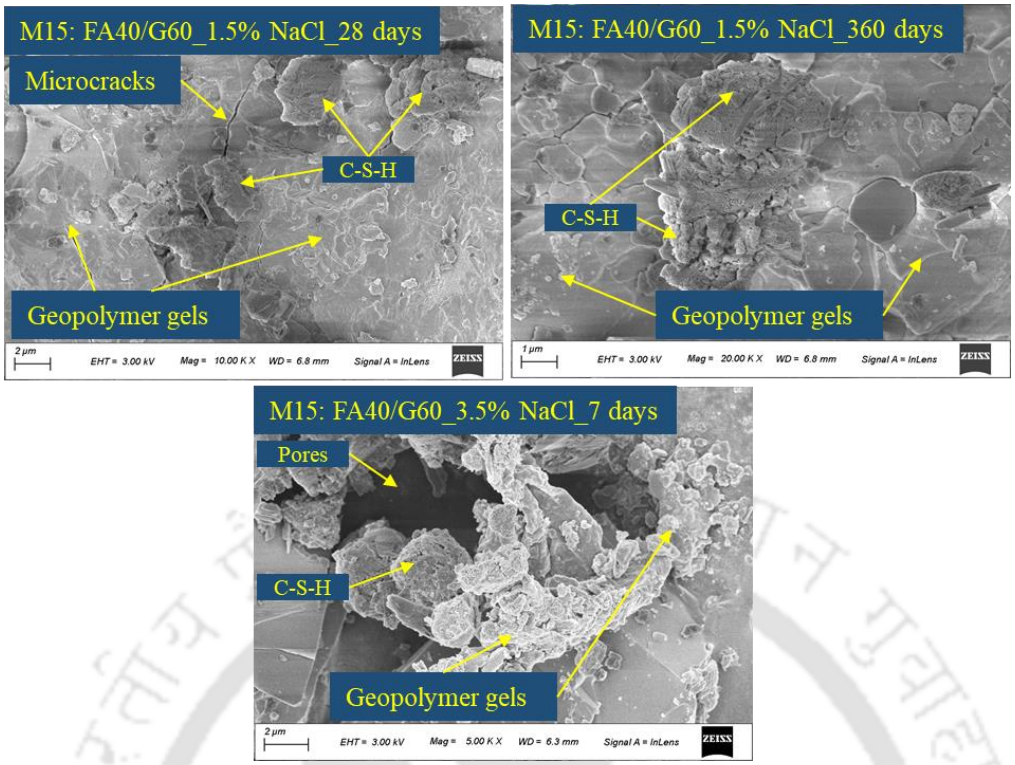

Fig. B18 FESEM images of control and chloride admixed fly ash-GGBS based GPC (M15: FA40/G60) at different ages.

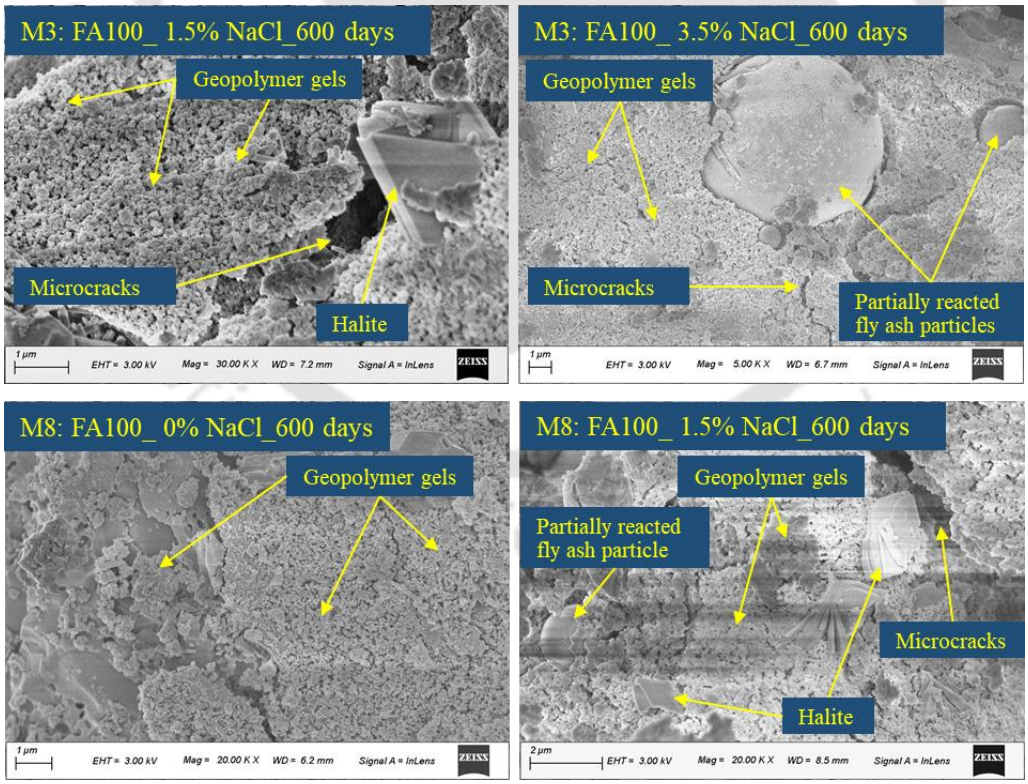

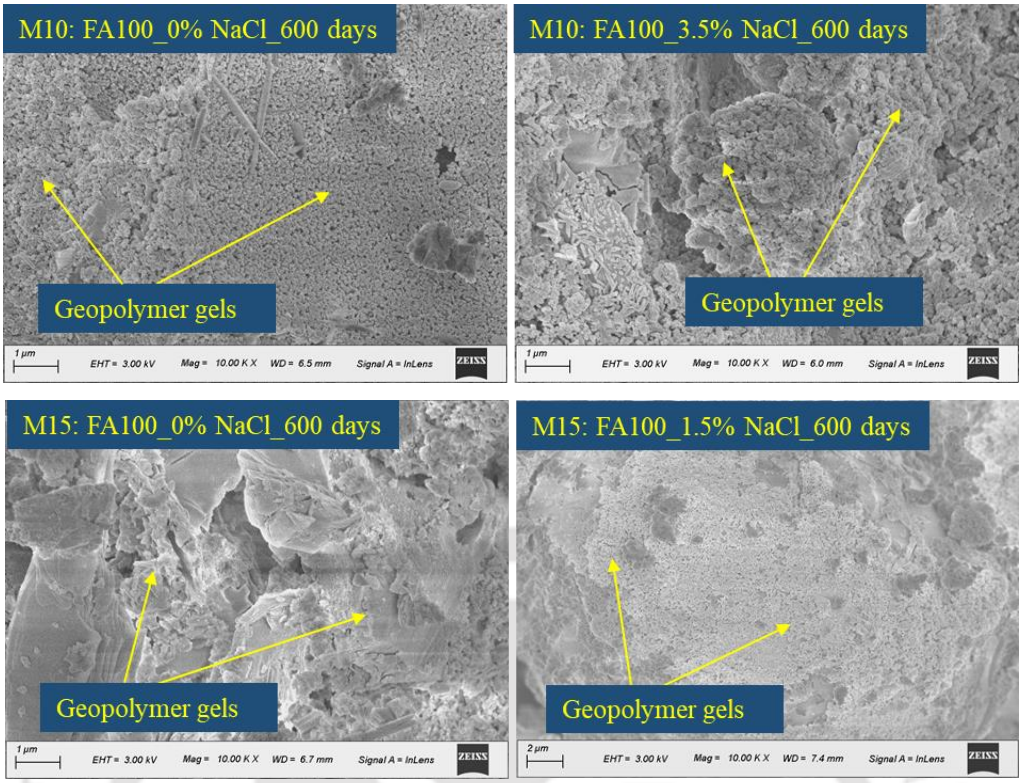

Fig. B19 FESEM images at rebar level of control and chloride admixed fly ash based GPC specimens (M3, M8, M10, and M15) at the age of 600 days.

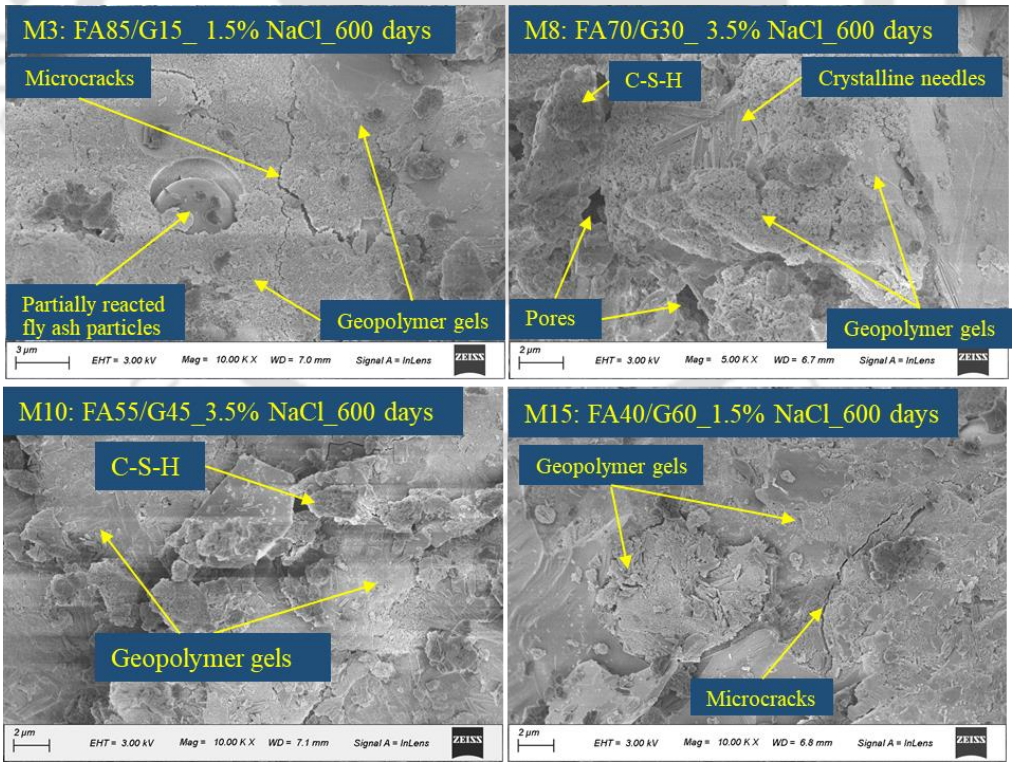

Fig. B20 FESEM images at rebar level of control and chloride admixed fly ash-GGBS based GPC specimens (M3, M8, M10, and M15) at the age of 600 days.

List of Publications

Publications from Ph.D. Thesis

Journals:

[1] J. K. Prusty and B. Pradhan (2022) "Investigation on effect of precursor materials and sand-to-binder ratio on strength development, acid resistance and microstructure evolution of geopolymer mortar", *Construction and Building Materials*, Vol. 346, 128501.

[2] J. K. Prusty and B. Pradhan (2022) "Effect of source materials and sand-to-binder ratio on durability performance and microstructural changes of geopolymer mortar subjected to sulfate and acid environment", *Journal of Materials in Civil Engineering, ASCE,* Vol. 34, 04022282.

[3] J. K. Prusty and B. Pradhan (2022) "Optimizing the performance of geopolymer mortar based on flowability, strength and durability properties", *Advances in Civil Engineering Materials, ASTM International*, Vol. 11, 372-397.

[4] J. K. Prusty and B. Pradhan (2022) "Influence of chloride ions on strength and microstructure of geopolymer concrete containing fly ash, and blend of fly ash-GGBS", *Materials Today: Proceedings*, Vol. 65, 925-932.

[5] J. K. Prusty and B. Pradhan (2020) "Multi-response optimization using Taguchi-Grey relational analysis for composition of fly ash-ground granulated blast furnace slag based geopolymer concrete", *Construction and Building Materials*, Vol. 241, 118049.

[6] J. K. Prusty and B. Pradhan (2020) "Effect of GGBS and chloride on compressive strength and corrosion performance of steel in fly ash-GGBS based geopolymer concrete", *Materials Today: Proceedings*, Vol. 32, 850-855.

Conferences:

[1] J. K. Prusty and B. Pradhan (2021) "Influence of chloride ions on strength and microstructure of geopolymer concrete containing fly ash, and blend of fly ash-GGBS", *International Conference on Advances in Construction Materials and Structures (ICCMS 2021)* (Virtual Mode), Kerala, India, December 15-17.

[2] J. K. Prusty and B. Pradhan (2020) "Effect of GGBS and chloride on compressive strength and corrosion performance of steel in fly ash-based geopolymer concrete", *3rd International Conference on Innovative Technologies for Clean and Sustainable Development (ITCSD2020)*, Chandigarh, India, February 19-21.

[3] J. K. Prusty and B. Pradhan (2020) "A study on strength and corrosion of steel reinforcement in chloride contaminated fly ash-GGBS based geopolymer concrete", *Second ASCE India*

Conference on "Challenges of Resilient and Sustainable Infrastructure Development in Emerging Economies" (CRSIDE2020), Kolkata, India, March 2-4.

[4] J. K. Prusty and B. Pradhan (2018) "Properties of fly ash and fly ash-GGBS based geopolymer concrete – A review", *Research Scholars Symposium on Advances in Concrete Science and Technology*, Indian Institute of Technology Bombay, India, December 13.

[5] J. K. Prusty and B. Pradhan (2016) "Geopolymer concrete with agro-industrial products as partial replacement of source materials – a review", *Proceedings of International Conference on Recent Advances in Mechanics and Materials (ICRAMM - 2016)*, VSS University of Technology, Burla, Odisha, India, December 17-18.

Manuscript submitted from Ph.D. Thesis

[1] J. K. Prusty and B. Pradhan (2022) "Evaluation of durability and microstructure evolution of chloride added fly ash and fly ash-GGBS based geopolymer concrete", *Construction and Building Materials*. (Under review)

[2] J. K. Prusty and B. Pradhan (2022) "Role of slag substitution in microstructural changes during strength development and rebar corrosion in chloride-rich geopolymer concrete", *Magazine of Concrete Research*. (Under review)

Other Publications

[1] N. S. Teklegiorgis, B. Pradhan, **J. K. Prusty**, and J. K. Das (2022) "Effect of sodium nitrite as corrosion inhibitor against chloride-induced corrosion of steel rebar in geopolymer concrete containing fly ash and GGBS", *Journal of Materials in Civil Engineering, ASCE*, Vol. 34, 04022007.